University of Dundee

DOCTOR OF PHILOSOPHY

Investigating the role that Interleukin-10's receptor binding properties play in defining its biological activities

Gorby, Claire

Award date:
2021

Link to publication

Investigating the role that Interleukin-10's receptor binding properties play in defining its biological activities

Claire Gorby

This thesis is submitted for the degree of Doctor of Philosophy (PhD) to the University of Dundee

March 2021

Contents

List of Figures

List of Tables

Abbreviations

7-ADD	7- Aminoactinomycin D		**GP130**	Glycoprotein 130
ACSL	Acyl-CoA-Synthetase		**GPCR**	G protein-coupled receptor
ACSS	Acetyl-CoA-Synthetase		**GSH**	Reduced Glutathione
AF	Alexa Fluor		**GSSG**	Glutathione Disulphide
Aga	a-Agglutinin		**GWAS**	Genome-Wide Association Study
AK4	Adenylate Kinase 4		**GZMB**	Granzyme B
ALDOC	Aldolase C		**HAVCR-2**	Hepatitis A Virus Cellular Receptor 2
AMP	Adenosine Mono-phosphate		**HEPES**	4-(2-hydroxyethyl)-1-piperazineethanesulfonic acid
AMPK	5' AMP-Activated Protein Kinase		**hGH**	Human Growth Hormone
APC	Antigen Presenting Cell		**HK**	Hexokinase
BAP	Biotin Acceptor Peptide		**HLA-DR**	Human Leukocyte Antigen-DR isotype
BSA	Bovine Serum Albumin		**IBD**	Inflammatory Bowel Disease
CAR	Chimeric antigen receptor		**iCASP9**	Inducible Caspase-9
CCL	Chemokine Ligand		**ICD**	Intracellular Domain
CD	Cluster of Differentiation		**IFN**	Interferon
CDR	Complementarity-determining region		**IFNAR**	Interferon alpha/beta receptor
COX	Cytochrome C Oxidase		**Ig**	Immunoglobulin
CXCL	Chemokine (C-X-C motif) Ligand		**IL**	Interleukin
DC	Dendritic Cell		**IL-1RAP**	Interleukin 1 Receptor Accessory Protein
DMSO	Dimethyl Sulfoxide		**IPTG**	Isopropyl β- d-1-thiogalactopyranoside
DNA	Deoxyribonucleic Acid		**ITA**	Isothermal Assembly
dNTPs	Deoxyribonucleotide Triphosphate		**JAK**	Janus Kinase
DTT	Dithiothreitol		**kDa**	Kilo Dalton
EBV	Epstein-Barr Virus		**KEGG**	Kyoto Encyclopaedia of Genes and Genomes
EC$_{50}$	Half maximal Effective Concentration		**KLRG1**	Killer cell lectin-like receptor subfamily G1
ECD	Extracellular Domain		**LAG-3**	Lymphocyte Activation Gene 3
ECFP	Enhanced Cyan Fluorescent Protein		**LB**	Lysogeny Broth
EDTA	Ethylenediaminetetraacetic Acid		**LFQ**	Label Free Quantification
EGFP	Enhanced Green Fluorescent Protein		**LIF**	Leukaemia inhibitory factor
EM	Electron Microscopy		**LPS**	Lipopolysaccharide
EN	Enhancer		**M-CSF**	Macrophage Colony-Stimulating Factor
EndoF	Endoglycosidase F		**MACS**	Magnetic Activated Cell Sorting
EOMES	Eomesodermin		**MARCO**	Macrophage Receptor with Collagenous Structure
EPO	Erythropoietin		**MCT4**	Monocarboxylate transporter 4
FBS	Foetal Bovine Serum		**MARCH1**	Membrane-Associated RING-CH 1
FCCP	Carbonyl cyanide-4 (trifluoromethoxy)phenylhydrazone		**MGAT5**	Alpha-1,6-mannosylglycoprotein 6-beta-N-acetylglucosaminyltransferase
FcR	Fragment Crystallisable Receptor		**MHC**	Major Histocompatibility Complex
FERM	4.1R Ezrin Radixin Moesin		**MI**	Minimiser
FPLC	Fast Protein Liquid Chromatography		**mRNA**	Messenger Ribonucleic Acid
FRET	Fluorescence Resonance Energy Transfer		**mTORC**	Mammalian Target of Rapamycin Complex
GF	Gel Filtration		**MVP**	Major Vault Protein
GFP	Green Fluorescent Protein		**NAD/NADH**	Nicotinamide Adenine Dinucleotide/+ Hydrogen
GHR	Growth Hormone Receptor		**NDUFB**	NADH Dehydrogenase [ubiquinone] 1 Beta Subcomplex

NFIL3	Nuclear Factor Interleukin 3 Regulated	**TNFRSF**	Tumour Necrosis Factor Receptor Superfamily
NFkB	Nuclear factor-κB	**TOX**	Thymocyte Selection Associated High Mobility Group Box
Ni-NTA	Nickel Nitrilotriacetic Acid	**TPI1**	Triosephosphate Isomerase 1
NK	Natural Killer	**TPO**	Thrombopoietin
OGT	O-GlcNAc transferase	**Treg**	T Regulatory Cell
OXPHOS	Oxidative Phosphorylation	**TYK2**	Tyrosine Kinase 2
PAM3CSK4	Pam3CysSerLys4	**γC**	Common Gamma Chain
PAMP	Pathogen-Associated Molecular Patterns	**γC**	Common Gamma Chain
PBE	Phosphate-buffered saline/EDTA		
PBMC	Peripheral blood mononuclear cell		
PBS	Phosphate-buffered saline		
PBSA	Phosphate-buffered saline/BSA		
PCR	Polymerase Chain Reaction		
PD-1	Programmed cell Death protein 1		
PEG	Polyethylene glycol		
PFA	Paraformaldehyde		
PI3K	Phosphoinositide 3-kinase		
PMSF	Phenylmethylsulfonyl Fluoride		
RCC	Renal cell carcinoma		
RNA	Ribonucleic Acid		
ROS	Reactive Oxygen Species		
RPM	Revolutions Per Minute		
RPMI	Roswell Park Memorial Institute		
RTqPCR	Reverse Transcription Quantitative PCR		
SA/SAV	Streptavidin		
SCID	Severe Combined Immuno-deficiency		
SDS-PAGE	Sodium Dodecyl Sulphate Polyacrylamide Gel Electrophoresis		
SH2	Src Homology 2		
SLC	Solute Carrier Transporters		
SNP	Single Nucleotide Polymorphism		
SOCS	Suppressor of Cytokine Signalling		
SPR	Surface Plasmon Resonance		
STAT	Signal Transducer and Activator of Transcription		
TAE	Tris base/Acetic acid/EDTA		
TCR	T Cell Receptor		
Th	T Helper Cell		
TIGIT	T Cell Immunoreceptor with Ig and ITIM Domain		
TIM-3	T Cell Immunoglobulin and Mucin Domain- 3		
TIRF	Total Internal Reflection Fluorescence Microscopy		
TMEM126B	Transmembrane protein 126B		
TNF-α	Tumour Necrosis Factor alpha		
TNFAIP	Tumour Necrosis Factor Alpha-Induced Protein		

Acknowledgements

Firstly, I would like to thank my supervisor Ignacio Moraga. He has provided support, advice and encouragement and taught me how to think like a scientist. I am grateful that his door was always open and for his unending patience while guiding me through my PhD.

I would like to thank all the members of the Moraga lab, for their patience when teaching me techniques, their help with experimental protocols and their constructive feedback on thesis drafts. Thank you to Liz Pohler for always knowing the answer to any problem that arose and for keeping the lab's cultures, experiments and members functioning. Liz's encouragement and her constant supply of chocolate was always greatly appreciated. Paul Fyfe was very patient teaching me about protein production and answering my never-ending questions about the gel filtration columns and for this I am very grateful. I would like to thank Stephan Wilmes for answering all my TIRF microscopy, cloning and flow cytometry questions and importantly providing the mulled wine for the divisional Christmas parties. Thank you to Jonathan Martinez-Fabregas for helping me perform experiments and for all of the time he gave up answering my questions with a smile. Thank you also to Alison McFarlane and Ariane Wilmes, both of whom made the lab such a friendly, fun and welcoming environment.

I would like to thank our collaborators in the University of Lille and the University of Osnabruck for their support in performing experiments and their advice and suggestions about the project, particularly Junel Sotolongo-Bellon, Adeline Cozzani, Dr. Suman Mitra and Prof. Jacob Piehler.

Thank you to the members of my thesis committee, Prof. Simon Arthur and Dr. Yogesh Kathulu for their great advice and feedback on my project at every stage.

Thank you very much to the many members of the Division of Cell Signalling and Immunology, especially to the lab management and technical team, particularly Jackie, Nancy and Courtney, without whom no experiments would be possible. I would like to thank members of the Cantrell lab particularly Andy Howden for giving up much of his time to show me how to design and prepare proteomic

Declarations

Candidate

The candidate is the author of the thesis. Unless otherwise stated, all references cited have been consulted by the candidate. The work of which the thesis is a record has been done by the candidate and has not been previously accepted for a higher degree

…………………………..
Claire Gorby

Supervisor

The conditions of the relevant ordinances and regulations have been fulfilled

.………………………….
Dr. Ignacio Moraga

Summary

Interleukin-10 (IL-10) is a key immuno-regulatory cytokine with potent anti-inflammatory effects. IL-10 contributes to immuno-suppression by inhibiting the presentation of antigen and decreasing the production of pro-inflammatory cytokines from innate cells such as dendritic cells and macrophages which in turn can suppress the activity of adaptive T cells. However, much is still unknown about the precise mechanisms through which this cytokine exerts its effects. This thesis used protein engineering techniques to explore the molecular mechanisms underpinning IL-10's activities.

IL-10 occurs naturally as a dimeric molecule which binds two receptor subunits: IL-10Rα and IL-10Rß. It has very poor affinity for the IL-10Rß receptor subunit and is unable to bind IL-10Rß in the absence of IL-10Rα (Walter, 2014). Using error-prone yeast display we were able to generate a variant of IL-10 which could directly bind to the IL-10Rß subunit, with affinities in the low micromolar range. This variant was recombinantly expressed in both the monomeric and dimeric conformations. Using these engineered variants in combination with the wild type monomeric and dimeric IL-10, allowed us to examine the contribution of both receptor affinity and stoichiometry to IL-10's activities.

Single particle imaging of the receptor subunits on the surface of live cells showed that increased affinity for IL-10Rß enhanced heterodimerisation of IL-10Rα and IL-10Rß for both the monomeric and dimeric variants. This increased receptor complex assembly translated into increased STAT1 and STAT3 activation by the high affinity monomer compared to the wild type monomer. The high affinity dimer showed a similar maximal STAT activation compared to the wild type dimer however, it also showed favourable activity at lower concentrations. This resulted in enhanced biological activities by the high affinity dimer compared to the wild type at sub-saturating concentrations e.g., enhanced suppression of LPS-induced IL-6 secretion.

In order to view differences between the variants on a more global level, RNA sequencing was performed on human primary monocytes and CD8 T cells, treated with the monomeric and dimeric wild type and high affinity variants. The

high affinity monomer had enhanced regulation of almost all transcripts compared to the wild type monomer however, it failed to reach dimeric expression levels. The wild type dimer showed poorer gene regulation when used at low doses, particularly when looking at suppression of pro-inflammatory cytokines and chemokines in monocytes. The high affinity dimer showed enhanced regulation of subsets of genes at low doses compared to the wild type, suggesting that improved receptor affinity could be used to overcome dose-dependent limitations. These data demonstrate that both stoichiometry and affinity play a large role in IL-10's activities.

A structure of the complete IL-10/IL-10Rα/IL-10Rß complex is lacking, hindering our understanding of the molecular interactions in this cytokine-receptor complex. We used our high affinity variants to attempt crystallisation of the receptor complex. While a stable complex was successfully purified by gel filtration, no crystals were generated. However, work done here lays the foundation for future attempts using alternate technologies such as cryogenic electron microscopy.

IL-10 has also been shown, under certain conditions, to enhance the tumour targeting ability of CD8 T cells (Naing et al., 2018) however much is still unknown about this process. We used proteomics as well as RNA sequencing to examine the action of IL-10 in human CD8 T cells. This study showed that IL-10 can downregulate exhaustion markers in these cells. In addition, it highlighted downregulation of several enzymes in glycolysis as well as an upregulation of several mitochondrial components, indicating that IL-10 may be regulating metabolic processes in CD8 T cells. While these results are only considered preliminary, they highlight key areas for future work.

Publications

Work carried out in this thesis contributed to the following publication:
Gorby, C., Sotolongo Bellon, J., Wilmes, S., Warda, W., Pohler, E., Fyfe, P. K., Cozzani, A., Ferrand, C., Walter, M. R., Mitra, S., Piehler, J. & Moraga, I. 2020. Engineered IL-10 variants elicit potent immunomodulatory effects at low ligand doses. Sci Signal, 13

Chapter 1. Introduction

1.1 Cytokines

Cytokines are a diverse family of ligands containing interleukins, interferons, chemokines, and growth factors, which critically contribute to the regulation of mammalian physiology. A unique feature of cytokines is their ability to elicit highly pleiotropic activities. Most cytokines trigger a wide range of biological responses, making the study of this family of ligands very challenging.

Cytokines are implicated in the pathologies of diseases such as asthma, arthritis and psoriasis (Foster et al., 2002, McInnes and Schett, 2007, Baliwag et al., 2015). Cytokine deficiencies can also cause severe pathologies such as Severe Combined Immunodeficiency (SCID) and Crohn's disease (Kovanen and Leonard, 2004, Correa et al., 2009). These observations highlight the importance of cytokines in human health. However, due to the complexity of the responses elicited by these ligands, our ability to translate them into the clinic is very limited, stressing the need for a more detailed molecular understanding of cytokine signalling and responses.

In this thesis I will focus specifically on interleukin-10 (IL-10), however I will first outline some general principles shared by all cytokines to better illustrate the complexity of this family of ligands.

1.1.1 Cytokine-receptor interactions

Cytokine receptors are single-pass transmembrane proteins. Their extracellular domain binds the cytokine and determines affinity. The cytoplasmic domain of most receptors is constitutively associated with a kinase, allowing signalling to occur via the Janus Kinase (JAK)/Signal Transducer and Activator of Transcription (STAT) pathway (Figure 1.1). JAK/STAT signalling will be discussed in greater detail below. Cytokine receptors themselves can be sub-divided into several families based on their structure and the cytokines they bind. Some cytokines are homodimeric where, following ligand binding, the receptor

subunit forms a complex with another identical subunit to induce signalling, e.g. erythropoietin (EPO) and human growth hormone (hGH) receptors. The majority of cytokine receptors, however, are heterodimeric, being composed of different receptor subunits. In addition, many receptor subunits can function in more than one cytokine receptor complex. For example, the glycoprotein 130 (gp130) receptor is a component of the IL-6, IL-27, LIF and oncostatin M cytokine receptor complexes (Silver and Hunter, 2010) The IL-10, IL-22, IL-26 receptors and type III interferons share the IL-10 receptor beta chain (IL-10Rß) subunit (Yoon et al., 2010) and the common gamma chain (γc) receptor functions in the IL-2, IL-4, IL-7, IL-15 and IL-21 systems (Pulliam et al., 2016). Cytokine receptor complexes usually have a receptor subunit which is specific for a particular cytokine. The cytokine IL-6 binds to the specific IL-6Rα chain in a complex with the shared gp130 receptor. IL-2 binds it's particular IL-2Rα and IL-2ß chains in a multiplex with the shared γc receptor (Pulliam et al., 2016) and IL-10 binds to its distinct IL-
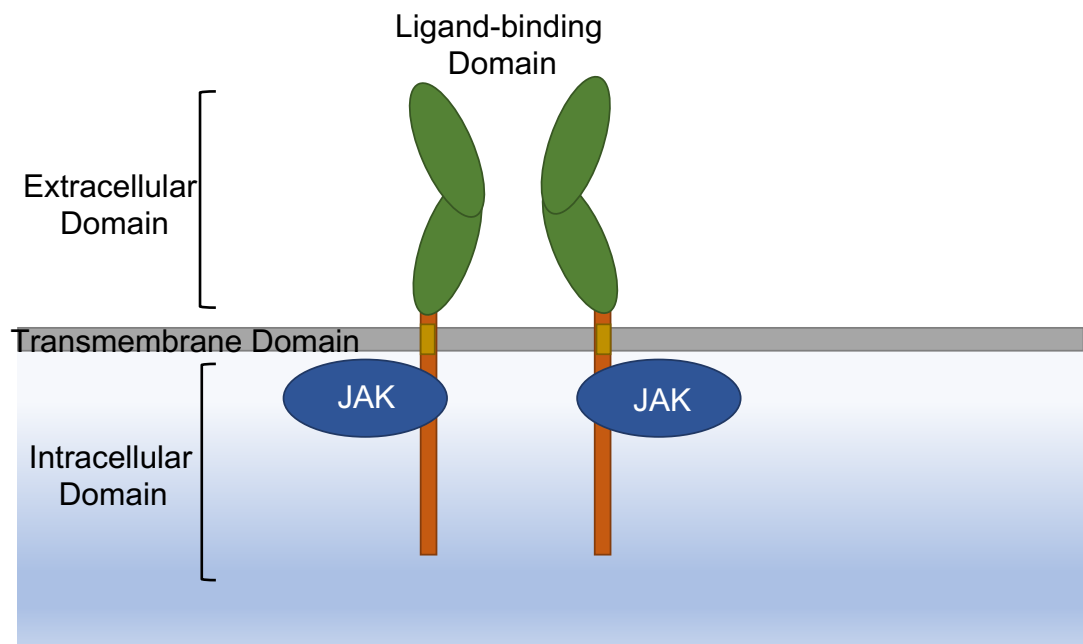
Figure 1.1 Schematic of cytokine receptor structure. Cytokine receptors are composed of an extracellular domain which binds to the ligand. They span the membrane with a transmembrane domain. The intracellular domain can vary in length depending on the cytokine. The intracellular domain is usually constitutively associated with a Janus kinase (JAK) which allows downstream signalling to occur.

10Rα subunit along with the shared IL-10Rß component (Walter, 2014).

Cytokines utilise a limited set of receptors and signalling molecules to carry out diverse functions in multiple cell types. This deceptively simple system of molecules is governed by complex biophysical interactions between the cytokine and its receptor as well as interactions between the receptor and intracellular

signalling molecules. These interactions determine the biological response. Variables such as receptor stoichiometry, geometry and affinity as well as regulation of receptor and kinase expression levels are crucial facets of how cytokines carry out their functions (Moraga et al., 2014).

1.1.2 Stoichiometry of the cytokine-receptor complex

In order for intracellular signalling to occur, the cytokine receptors must dimerise or oligomerise. There is debate in the field as to whether dimerisation of receptor subunits is induced upon cytokine binding or whether receptors are pre-formed dimers in the absence of ligand (Atanasova and Whitty, 2012). Several homo-dimeric receptor systems have been thought to exist as pre-formed dimers where ligand binding induces a conformational shift to allow the intracellular kinase domains to interact. One example of this is the EPO receptor (EPO-R) system where the crystal structure of the extracellular domains in the absence of ligand showed EPO-R dimers (Livnah et al., 1999). Pre-formed receptor complexes have also been suggested for other systems such as growth hormone receptor (GH-R) and thrombopoietin receptor (TPO-R) (Brown et al., 2005, Matthews et al., 2011).

Opposing this is the model of ligand-induced receptor assembly whereby cytokine receptors diffuse within the plasma membrane as monomers and the full complex is only assembled upon binding of the cytokine. In many cytokine systems the cytokine has preferential affinity for one receptor subunit which suggests a step-wise binding pattern. Experiments using single particle fluorescence imaging have allowed visualisation of individual receptors on the surface of live cells and these studies have shown that receptor subunits act as monomers in the absence of ligand in several cytokine-receptor systems such as type I interferons (IFNs), IL-13, IL-4 and EPO (Moraga et al., 2015a, Wilmes et al., 2015, Richter et al., 2017, Wilmes et al., 2020).

It is possible that cytokine receptors transition between both a monomeric and a dimeric state in the absence of ligand, depending on the local concentration of the receptors at the cell surface, forming an equilibrium rather than two opposing systems (Atanasova and Whitty, 2012). In addition, the techniques used to

analyse receptor systems can themselves introduce artefacts. For example, the use of crystal structures, while informative, use very high concentrations of receptor proteins which would not be reached under normal conditions on the cell surface. Similarly, the use of artificial systems such as tagged receptors usually requires large overexpression. However, in both the pre-assembled and ligand-induced assembly models, some form of cytokine-induced receptor reorganisation is essential for signal transduction. While binding patterns vary between cytokines, it is accepted that the binding event allows the formation of an activated receptor complex which brings the cytoplasmic domains of the receptors into close proximity, allowing phosphorylation by receptor-associated kinases (Atanasova and Whitty, 2012, Schreiber and Walter, 2010).

1.1.3 Geometry of the cytokine-receptor complex

The role that cytokine-receptor binding topology plays in activating signalling is complex and remains an area of interest in the field. Initially it was thought that only receptor dimerisation was needed to induce signalling, regardless of the conformation of the receptor extracellular domains. Work using chimeric receptors reinforced this idea. Studies where the extracellular domain (ECD) of EPO-R was replaced with the ECD of epidermal growth factor receptor or the tyrosine kinase receptor c-kit showed that these hybrid receptors could induce signalling similar to the wildtype receptor when bound to their respective ligand. This suggested that once dimerisation was achieved, the precise geometry of the ECD was permissible to change (Ohashi et al., 1994).

However, other studies have demonstrated that the geometry of the receptor complex can critically contribute to internal signalling. Studies have used dimeric coiled-coils to replace the ECD of both the EPO-R and TPO-R to further understanding of how receptor orientation impacts signalling (Staerk et al., 2011, Seubert et al., 2003). For EPO-R only one dimeric conformation allowed full activity with a second conformation giving only partial activity (Seubert et al., 2003). However, for the TPO-R there were several orientations which could induce biological activity, suggesting that this system was more permissible to changes in orientation (Staerk et al., 2011). Nevertheless, different conformations of TPO-R did also induce unique downstream effects, highlighting that receptor

geometry could be used to fine-tune the signalling output. More recently studies have demonstrated that surrogate ligands for the EPO-R could induce differential signalling patterns and this was dependent on the orientation of the receptor topology (Moraga et al., 2015b, Mohan et al., 2019).

The use of synthekines, molecules designed to activate non-native pairings of receptor heterodimers, has also been able to give us insight into the role that receptor topology plays in cytokine signalling. Novel synthekines were able to activate unique combinations of STATs and induce biological responses (Moraga et al., 2017). However, the authors of this study did note that the amplitude of signalling induced by the synthekines was reduced compared to their parent cytokines. This underlines the importance of the binding topology in signal potency.

Together these examples illustrate the importance of receptor geometry in the cytokine response. However, the geometry of the complex is just one facet of regulation of the cytokine response. The affinity and the stability of the cytokine-receptor interaction also critically contribute to the signalling outcome.

1.1.4 Affinity, stability and kinetics of the cytokine-receptor complex

The stability of the cytokine-receptor complex can determine the specificity of the cytokine as well as the signalling patterns it induces. The ligand-receptor affinity is a key factor in the stability of the complex. An example of this is seen in the type I IFN family. This family of cytokines all utilise the same receptor complex (IFNAR1 and IFNAR2), however different family members can induce different potencies of biological effects (Piehler et al., 2012). Studies have attempted to delineate the root of these differences by generating ligands with altered affinity for IFNAR1 and IFNAR2. A study which generated IFNα2 mutants with differential binding affinity ratios to the receptor subunits showed that the antiproliferative and antiviral activity of the mutants correlated with the overall complex stability, rather than the affinity for a specific receptor (Kalie et al., 2008).

Other examples of the influence of complex stability on biological activity include the IL-4, IL-13 and IL-6 cytokine systems. Both IL-4 and IL-13 can bind the same

receptor complex (IL-4Rα and IL-13Rα) however they can induce cytokine-specific effects (Junttila et al., 2008). This is dependent on the affinity for the cytokines for IL-4Rα which in turn determines the sensitivity of particular cell types for each cytokine based on the expression of IL-4Rα (Junttila et al., 2008). A recently published study from our laboratory using engineered variants of IL-6 with differential gp130 binding affinities showed that reduced receptor binding affinity and hence less stable complexes, could affect the intracellular trafficking of the receptor complexes. This in turn lead to reduced STAT1 phosphorylation, highlighting how changes in affinity can translate into differential signalling patterns (Martinez-Fabregas et al., 2019).

These examples illustrate the potential for alterations of cytokine signalling patterns using variants with differential binding stabilities and kinetics. Other factors such as actin cytoskeleton compartments, intracellular JAK interactions and endosome recycling can also impact stability (Moraga et al., 2015a, You et al., 2016, Wilmes et al., 2015).

1.2 JAK/STAT signalling

Although there are a broad range of cytokines activating multiple receptor combinations, they rely on a limited range of intracellular signalling molecules to induce biological responses. Specific gene induction programmes triggered by JAK/STAT activation allow cytokines to carry out their diverse range of functions and are central to the activity of both innate and adaptive immune cells. Other signalling pathways have also been described for cytokine systems such as mitogen-activated protein kinases (MAPKs) and phosphoinositide 3-kinase (PI3K)/Akt pathways. Knowledge of the exact contribution of these alternate pathways to IL-10 activities is lacking and outside the scope of this thesis, therefore, this section will focus on the role of JAK/STAT signalling in cytokine biology.

1.2.1 JAKs

Associated with the cytoplasmic tail of the cytokine receptor are tyrosine kinases called JAKs. There are four JAKs: JAK1, JAK2, JAK3 and TYK2. JAKs have

conserved domains which allow them to carry out their function (Figure 1.2). At the N terminus of the JAK is the FERM (band four-point-one, ezrin, radixin and moesin) homology domain which facilitates interaction with the cytoplasmic tail of the cytokine receptor (Yamaoka et al., 2004). This is adjacent to an SH2 (scr-homology 2)-like domain, followed by a regulatory pseudokinase domain (Lupardus et al., 2014). The C terminus of JAKs contain the catalytic tyrosine
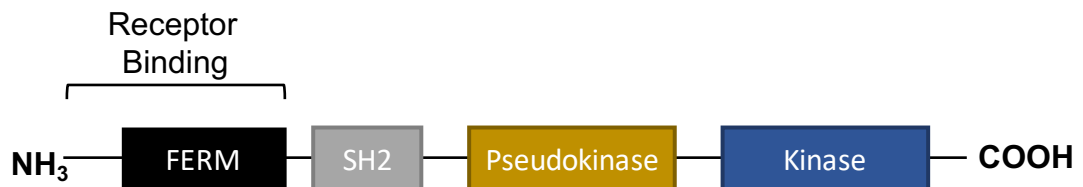
Figure 1.2 Schematic of JAK domains. JAKs can be divided into several domains based on their function and structure. The FERM domain at the N terminus binds to the receptor. The kinase domain is located at the C terminus.

kinase domain (Alicea-Velazquez and Boggon, 2011).

Different cytokine receptors have specific JAKs associated with them. Upon the receptor subunits coming into close proximity the associated JAKs phosphorylate each other on their tyrosine residues via their kinase domain (Jatiani et al., 2010). The JAKs are then in an active formation and phosphorylate the receptor's intracellular tyrosine residues. This provides a docking site for the STAT molecules.

JAKs are important for signal transduction but also for receptor expression patterns. Many cytokine receptor surface expression levels are controlled by JAKs, for example Tyk2 is required for stable surface expression of IFNAR1 (Ragimbeau et al., 2003). As well as regulating receptor expression, JAKs can modulate the stability of the cytokine-receptor complex. In the growth hormone receptor, interactions between two JAK2 molecules were shown to contribute to signalling (Brooks et al., 2014). Interactions between JAK1 and TYK2 were shown to stabilise the IFNAR complex in the IFN system (Wilmes et al., 2015). A recent study also showed that oncogenic mutations in JAK2 can facilitate receptor dimerisation of type I cytokine receptors in the absence of ligand (Wilmes et al., 2020). This highlights the intrinsic role that JAKs play in cytokine-receptor complex formation, as well as in signal propagation.

1.2.2 STATs

There are seven STATs in mammals: STAT1, STAT2, STAT3, STAT4, STAT5A, STAT5B, STAT6 and they reside in the cytosol in their inactivate state. Similar to JAKs, the specific STAT activated depends on the cytokine. STATs bind the receptor via their SH2 domain and become phosphorylated. This allows dimerisation of the STATs, either as homodimers or heterodimers. Upon dimerisation STATs can then translocate to the nucleus where they bind to DNA and induce transcription of gene expression programmes (O'Shea et al., 2013).

Cytokines can activate multiple STATs and can modulate the levels to which these STATs are activated. This can be affected by the amount of available STATs within the cell or previous exposure to other cytokines. For example, IL-10 can activate both STAT1 and STAT3, with STAT3 modulating the bulk of IL-10's anti-inflammatory activities (Williams et al., 2004). However, macrophages which have been primed with IFN-γ have a bias towards STAT1 activation and can suppress the ability of IL-10 to inhibit Major Histocompatibility Complex class II (MHC II) expression (Herrero et al., 2003).

The stability of the cytokine-receptor complex can also affect STAT activation. Engineered IL-6 variants with differential affinities for gp130 had altered STAT1/STAT3 ratios, with STAT1 activation more sensitive to changes in affinity (Martinez-Fabregas et al., 2019). This study suggested that low affinity STATs require more stable cytokine-receptor complexes and larger doses to reach maximal signalling. This generated competition between STATs and altered the biological response. This is in agreement with other studies in the IFN system which showed that a mutation of one tyrosine residues in the IFNAR2 intracellular domain (ICD) could abolish both STAT1 and STAT2 activation, suggesting competition for receptor binding (Zhao et al., 2008).

1.3 Interleukin-10

IL-10 is a pleiotropic cytokine with many central immune-regulatory functions. It is the founding member of the IL-10 family of cytokines which include IL-19, IL-20, IL-22, IL-24, IL-26 and IL-28 (Ouyang and O'Garra, 2019). IL-10 is the most well characterised member of this family and was initially discovered in 1989,

termed secreted cytokine synthesis inhibitory factor (CSIF) due to its ability to inhibit secretion of IFNγ, IL-2 and other cytokines from Th1 cells (Fiorentino et al., 1989). IL-10 activates a hetero-tetrameric receptor complex, comprising two IL-10Rα and two IL-10Rß subunits (Figure 1.3). Upon assembly of this receptor complex, JAK1 and TYK2, associated with IL-10Rα and IL-10Rß respectively, are activated (Moore et al., 2001). This provides docking sites for STATs and their subsequent activation, dimerisation and nuclear translocation. IL-10 has been shown to activate STAT1, STAT3 and, in some cell types, STAT5 (Wehinger et al., 1996). IL-10 receptor binding and signalling patterns will be
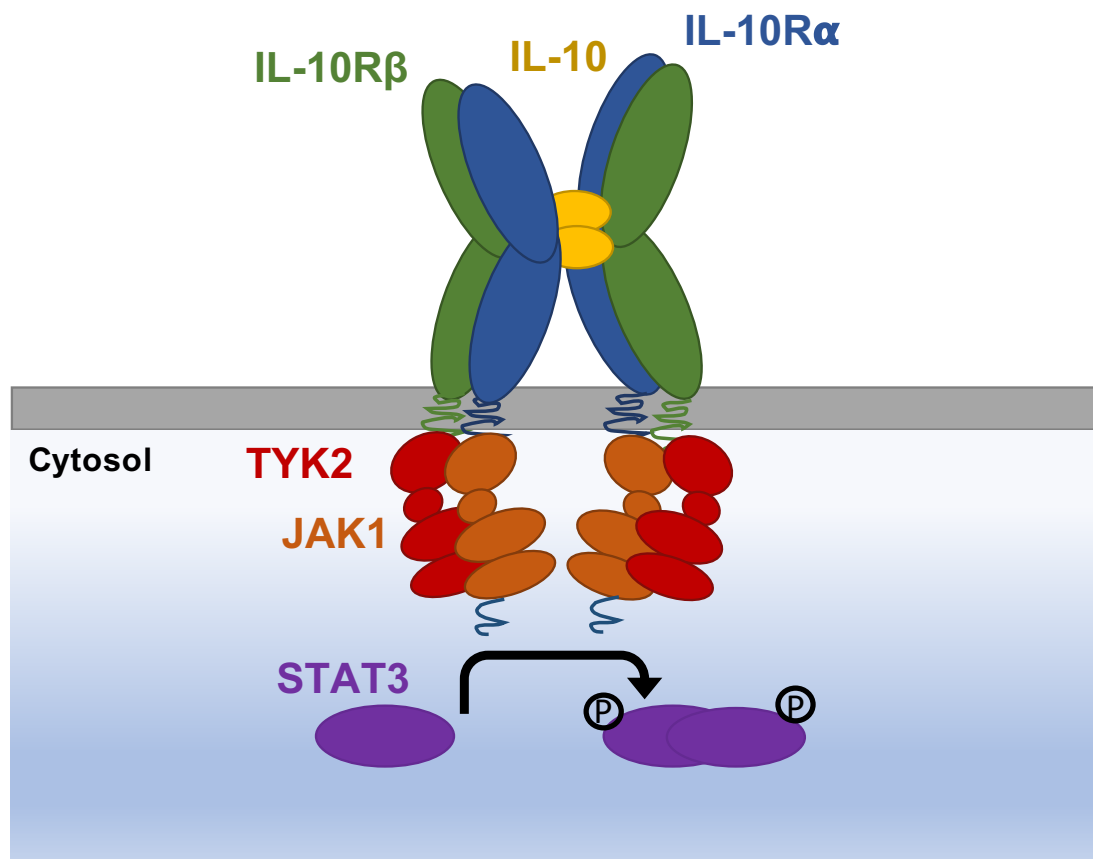
Figure 1.3 Illustration of the IL-10 cytokine receptor complex. As a dimer, IL-10 binds two IL-10Rα and two IL-10Rß subunits. The kinases JAK1 and TYK2 are associated with the intracellular tails of IL-10Rα and IL-10Rß respectively. These are activated upon receptor dimerisation, phosphorylating the intracellular domain of IL-10Rα. This provides a docking site for STAT3 which is then itself phosphorylated. STAT3 dimerises and translocated to the nucleus.

discussed in detail below.

IL-10 has been intensely studied since its discovery with huge progress being made characterising its effects on immune cell subsets. However, there are gaps in our knowledge of the molecular mechanisms underpinning some of IL-10's activities as well as an incomplete structural understanding of how IL-10 binds its receptor complex. In the following sections I will outline what is known about IL-

10 signalling, its anti-inflammatory effects and its immunostimulatory effects. I will also detail what is known about the structure of the IL-10 receptor complex.

1.3.1 Interleukin-10 dimer and monomer

IL-10 is a 36kDa homodimer comprised of two identical 160 amino acids polypeptides forming a domain-swapped dimer, similar to the structure of IFNγ (Zdanov et al., 1995). Each peptide chain consists of 6 alpha helices, A-F, and interconnect in a manner whereby helices E and F of one chain associate with helices A, B, C and D of the other chain (Zdanov et al., 1995) (Figure 1.4a). There are two disulphide bonds which connect the D-E loop to the N-terminus and helix C, however they do not link the two polypeptide chains together.
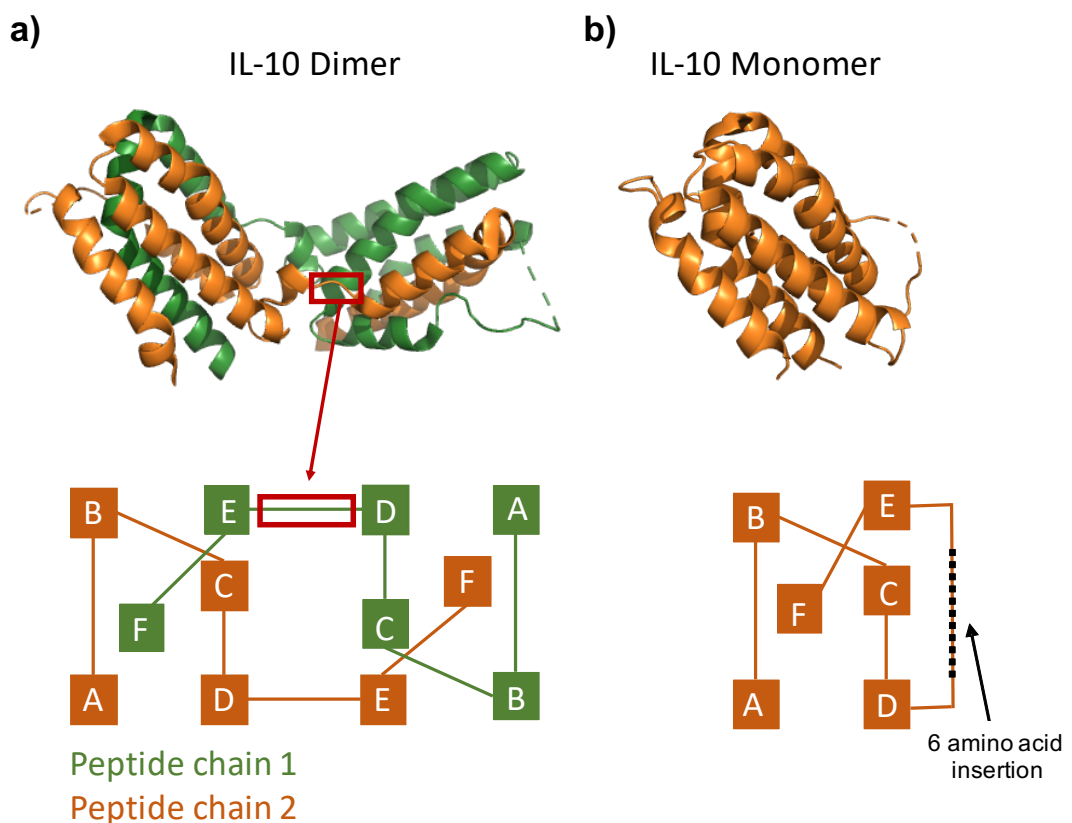
Figure 1.4 IL-10 dimer and IL-10 peptide chain configuration. (a) Structural ribbon diagram of dimeric IL-10 (PDB 2H24) (Yoon et al., 2006). Dimeric IL-10 is composed of two interlinked peptide chains of six alpha helices each. Helices E and F of one chain associate with helices A-D of the other chain to form a dimer (adapted from Walter, 2014). **(b)** Structural ribbon diagram of monomeric IL-10 (PDB 1LK3) (Josephson et al., 2002). A 6 amino acid extension between helices D and E allows the formation of an IL-10 monomer.

While IL-10 exists as a dimer, it was shown that IL-10 monomers can form in non-physiological conditions such as at low pH or high temperature (Syto et al., 1998). This study also showed that there was a correlation between the biological activity of IL-10 and the percentage of dimer present. To further investigate the properties

of the IL-10 monomer, a stable monomeric form of IL-10 was generated (Josephson et al., 2000b). It was created by inserting a flexible 6 amino acid linker between alpha helices D and E which allowed helices E and F to fold into the cleft created by helices A-D (Figure 1.4b). Their study showed that the IL-10 monomer bound to IL-10Rα with a 1:1 stoichiometry. The IL-10 monomer had weaker biological activity than the wild type as shown by proliferation of cells transfected with either the human or murine IL-10Rα. It also had 9-18 fold less activity than the dimer, depending on the cell line used, however at high concentrations the monomer could reach the maximal activity induced by the dimer. In addition, it was shown that the IL-10 monomer could not supress tumour necrosis factor alpha (TNF-α) secretion in a lipopolysaccharide (LPS)-stimulated macrophage cell line (Westerhof et al., 2012). Interestingly, the monomer is more thermally stable than the dimer.

More recently, a more stable IL-10 dimer was generated (Minshawi et al., 2020). Here they used two IL-10 monomers subunits, linking the C terminus of one monomer and the N terminus of the second. This IL-10 variant had increased temperature and pH stability compared to the native dimer. Additionally, the stable IL-10 variant had improved biological activities at low concentrations compared to the wild type dimer. Together, these works demonstrate that the activity of IL-10 is dependent on its structure and stability.

1.3.2 IL-10 receptors

As mentioned previously IL-10 binds two receptor subunits, IL10Rα and IL-10Rß. As a dimeric molecule, IL-10 binds two IL-10Rα and two IL-10Rß subunits, to form a complete signalling complex (Figure 1.3). Both receptor chains are needed for IL-10's activity.

Human IL-10Rα is composed of three domains: an extracellular domain which binds IL-10, a transmembrane domain and an intracellular domain which is constitutively associated with JAK1 (Walter, 2014). IL-10Rα's extracellular domain is formed of two ß-sandwich domains which are at an angle of 90 degrees to each other (Figure 1.5). The structure of IL-10 bound to the extracellular domain of IL-10Rα has been solved (Josephson et al., 2001) (Figure 1.5). IL-10

binds to IL-10Rα along the helix A, the AB loop and helix F and has high affinity for IL-10Rα, in the picomolar range.
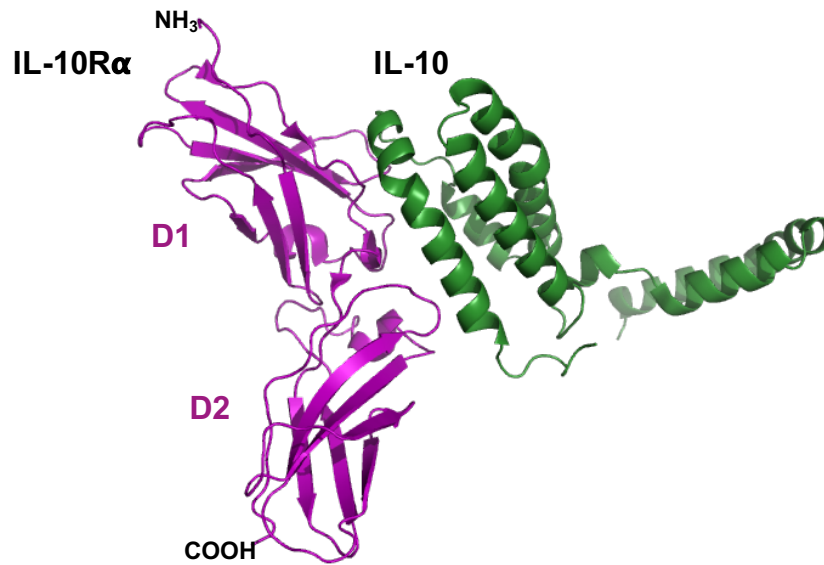
Figure 1.5 Structure of IL-10 bound to soluble IL-10Rα. IL-10Rα (magenta) has two domains, D1 at the N terminus (amino acids 1-98) and D2 at the C terminus (amino acids 105-205). One chain of IL-10 is shown in green (PDB 1J7V) (Josephson et al., 2001).

While IL-10Rα is specific for IL-10, IL-10Rß is termed a "promiscuous" cytokine receptor as it is shared between several other cytokines such as IL-22, IL-26 and IFN-lambda. It has a similar extracellular structure to IL-10Rα, forming two ß-sandwich domains (Yoon et al., 2010) (Figure 1.6). However, it has a much shorter intracellular domain of only 83 residues, which is constitutively associated with TYK2. In contrast to IL-10Rα, IL-10 has very weak affinity for IL-10Rß with interactions in the millimolar range. Due to this weak affinity, a crystal structure of IL-10 in complex with both IL-10Rα and IL-10Rß has not been solved. However, a model has been developed based on mutagenesis studies and computational modelling (Yoon et al., 2010, Yoon et al., 2006). Residues that were involved in IL-10Rß binding mapped to the A and D helices of IL-10 (Yoon et al., 2006). Structure-based alignment of the IL-10 receptor complex with the IFN-lambda receptor complex also identified these helices as the IL-10Rß binding site. However, without a complete structure of the complete IL-10 ternary complex the exact mechanisms of how IL-10 engages both receptor subunits is still unknown.
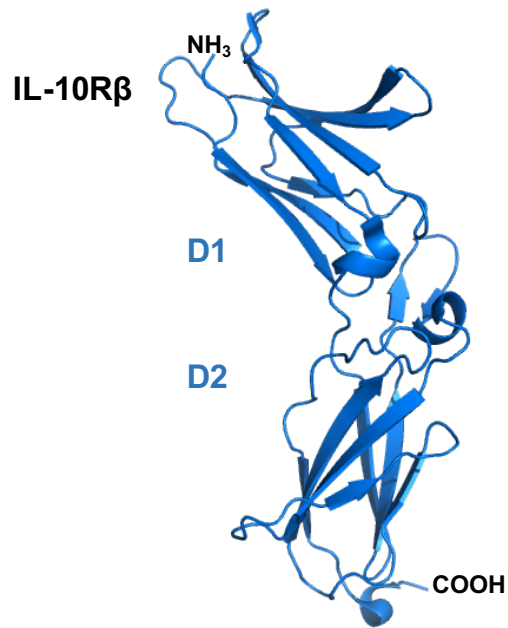
Figure 1.6 Structure of the IL-10Rß ectodomain. The structure of IL-10Rß was solved by Yoon et. al. 2010. (PDB 3LQM). Similar to IL-10Rα, IL-10Rß contains two domains, D1 at the N terminus (amino acids 23-111) and D2 at the C terminus (amino acids 114-216).

1.3.3 IL-10 receptor-complex assembly

Much is still unknown about how this receptor complex is assembled, in part due to the lack of structural knowledge of the IL-10/IL-10Rß interaction. As mentioned previously, IL-10 has high affinity for IL-10Rα and much weaker affinity for IL-10Rß (Walter, 2014). This means that IL-10Rα acts as the determining chain for IL-10 responsiveness and cells lacking IL-10Rα do not respond to IL-10 (Nagalakshmi et al., 2004). While IL-10Rß has much weaker affinity for IL-10, it is crucial for IL-10 signalling, most likely due to its association with TYK2. This model of a high affinity binding receptor and a low affinity signalling receptor has been discussed previously in the literature and is seen in other cytokine/receptor systems (Schreiber and Walter, 2010).

The exact mechanisms of the IL-10 receptor complex assembly are unknown, however two models have been proposed based on structural studies. A model of preformed IL-10 receptor dimers (Figure 1.7) was proposed where FRET analysis showed interactions between IL-10Rα and IL-10Rß in the absence of ligand (Krause et al., 2006). Another study supported this by demonstrating that the extracellular domain of IL-10Rα can be conformationally changed by co-

expression with IL-10Rß and that this was mediated by IL-10Rß's intracellular domain (Wilbers et al., 2017).
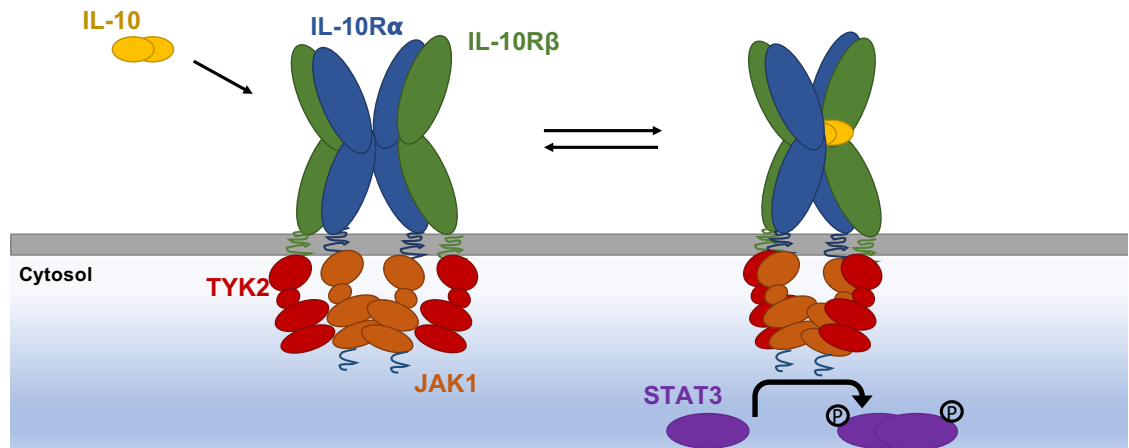
Figure 1.7 A model of the preformed IL-10 receptor complex. In this model IL-10Rα and IL-10Rß are dimerised in the absence of IL-10 stimulation, with JAK1 and TYK2 inactive. Upon IL-10 binding to this preformed receptor complex becomes activated, allowing intracellular phosphorylation by the associated JAK1 and TYK2. This allows the phosphorylation and dimerisation of STAT3.

Another proposed mechanism is that of ligand-induced receptor assembly (Figure 1.8). Due to its high affinity for IL-10Rα it has been proposed that this is the first chain bound by IL-10 followed by subsequent binding of IL-10Rß. It has been shown that IL-10Rß has increased affinity for the IL-10/IL-10Rα complex, compared to IL-10 alone, supporting a stepwise assembly mechanism (Logsdon et al., 2002, Yoon et al., 2005).
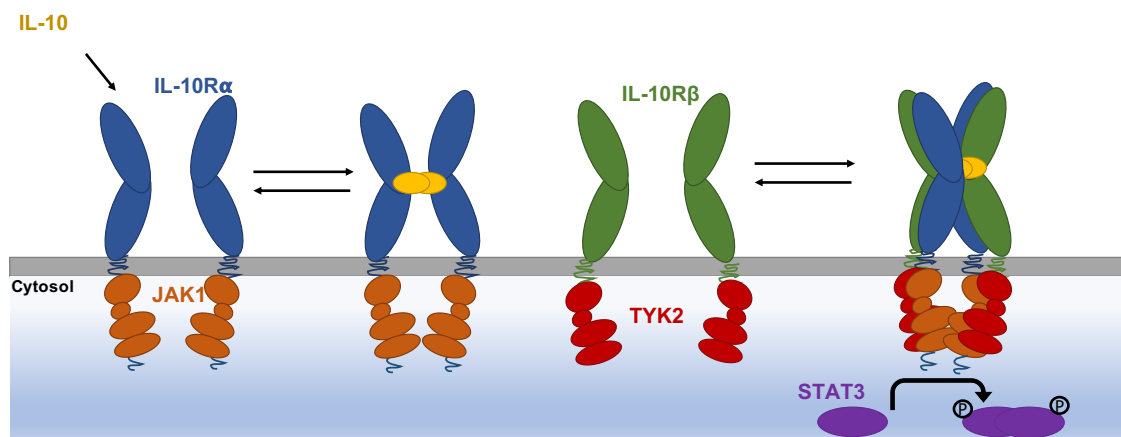
Figure 1.8 A model of ligand-induced assembly by IL-10. This model postulates that IL-10Rα and IL-10Rß are not associated in the absence of IL-10. It has been proposed that IL-10 first binds to the high affinity IL-10Rα subunit, followed by IL-10Rß. Signalling will only occur upon assembly of the complete receptor complex with IL-10. Other permutations of receptor stoichiometry are possible in addition to that shown here.

A further study demonstrated that IL-10Rα binding induces conformational changes in IL-10 which mediate IL-10Rß binding (Yoon et al., 2006). This could also be evidence for sequential receptor binding by IL-10. However other

permutations of complex assembly are possible, such as IL-10 binding one IL-10Rα followed by one IL-10Rß and then associating with the second chains. The exact pattern of receptor assembly is still unknown.

1.4 IL-10 Signalling
1.4.1 JAK/STAT signalling by IL-10

The JAK/STAT activation pathway has been well characterised for the IL-10 system. As mentioned previously, IL-10 activates JAK1 and TYK2, associated with IL-10Rα and IL-10Rß respectively. Macrophages from mice deficient in JAK1 are unresponsive to IL-10 demonstrating its key function in IL-10 signalling (Rodig et al., 1998). The role of TYK2 however is still unclear. Some studies have shown that TYK2 is dispensable for known IL-10 responses such as inhibition of LPS-induced TNF-α from macrophages (Wilbers et al., 2017, Karaghiosoff et al., 2000). However, it has been shown to potentially play a role in modulating the amplitude of the response, with TYK2 knock out macrophages and dendritic cells (DCs) showing reduced STAT3 phosphorylation and impaired suppressor of cytokine signalling 3 (SOCS3) upregulation in macrophages but not DCs (Wilbers et al., 2017). This supports an earlier study which showed that macrophages from TYK2 knock out mice had reduced STAT1 and STAT3 phosphorylation, requiring high concentrations of IL-10 to restore STAT3 phosphorylation (Shaw et al., 2006). Upon activation of these constitutively associated tyrosine kinases, tyrosine residues Y446 and Y496 on the IL-10Rα cytoplasmic tail are phosphorylated (O'Farrell et al., 1998). These then act as docking sites for STAT binding. It has also been shown that IL-10 requires the presence of serine residues in the IL-10Rα cytoplasmic domain for the suppression of TNF-α, suggesting a docking site for additional signalling proteins, however this has not been explored in detail (Riley et al., 1999).

STAT3 is the dominant factor activated by IL-10. Mice lacking STAT3 are embryonic lethal (Takeda et al., 1997) however conditional or cell-specific STAT3 deficiencies have helped elucidate the role of this molecule in IL-10 signalling. When IL-10 was administered to a mouse macrophage cell line lacking the tyrosines needed for STAT3 recruitment, no inhibition of proliferation was seen, compared to the control (O'Farrell et al., 1998). A similar result was seen when a

truncated STAT3 was used. However, this truncated STAT3 mutant was still able to inhibit LPS-induced TNF-α secretion whereas the tyrosine mutant could not, suggesting that certain IL-10 mediated effects had differential STAT3 requirements (O'Farrell et al., 1998). In contrast, a subsequent study demonstrated that IL-10 did not inhibit LPS-induced TNF-α secretion in STAT3 deficient macrophages (Riley et al., 1999). The key role of STAT3 in IL-10 mediated anti-inflammatory activities was also highlighted in an elegant study in which they generated mice with a STAT3 deficiency in macrophages and neutrophils (Takeda et al., 1999). These mice presented with inflammatory symptoms and macrophages and neutrophils did not display IL-10 mediated downregulation of LPS induced TNF-α secretion. Together these studies demonstrate the key role that STAT3 plays in downstream IL-10 activities.

IL-10 can also activate STAT1 and STAT5 (Wehinger et al., 1996). While the role of STAT3 is well understood, less is known about IL-10's activation of STAT1 and STAT5. Phosphorylation of STAT1 was detected in macrophages, monocytes and T cells following IL-10 stimulation (Shaw et al., 2006, Herrero et al., 2003, Finbloom and Winestock, 1995). In contrast to these studies, work by Wilbers et al. could not detect STAT1 phosphorylation by IL-10 in bone marrow derived macrophages, dendritic cells or neutrophils (Wilbers et al., 2017). This study also showed that cells from STAT1 deficient mice responded normally to IL-10 with macrophages and dendritic cells showing inhibition of LPS induced TNF-α in addition to inducing a survival signal in mast cells. Studies on the murine IL-10 receptor showed that mutations of tyrosine residues in the IL-10Rα chain prevented activation of STAT3 but not STAT1, suggesting differential binding sites or indirect recruitment to the receptor (Weber-Nordt et al., 1996). Macrophages from mice deficient in STAT1 are able to respond to IL-10 by suppression of TNF-α production, confirming that STAT1 is not needed for this IL-10 response (Riley et al., 1999). These conflicting reports on IL-10's ability to activate STAT1 may be explained in part by the influence of IFNγ on IL-10-induced STAT1. It has been demonstrated that IFNγ can bias IL-10 towards STAT1 activation rather than STAT3, leading to differential gene expression (Herrero et al., 2003). Similarly, priming with IFNα has also been shown to increase IL-10 STAT1 activation (Sharif et al., 2004). The presence of other cytokines in the studies described above may play a role in the balance between

STAT1 and STAT3 activation by IL-10, particularly in macrophages. This also highlights that, while studies of purified cell populations are necessary to deduce cytokine functions, they may not accurately reflect the activities of the cytokine when in a multi-faceted immune environment.

Very little work has been done examining the role that STAT5 plays in IL-10's biological activities. STAT5 phosphorylation in response to IL-10 was first seen in BaF3 cells transfected with the murine IL-10 receptor (Wehinger et al., 1996). However, a similar response was not detected in neutrophils (Cassatella et al., 1999). STAT5 activation was not detected in macrophages when stimulated with IL-10 but it was detected in mast cells, however only at the maximal concentration tested (Wilbers et al., 2017). Although in depth examination of STAT5 phosphorylation by IL-10 in different immune cell subsets is lacking, it can be assumed from the work described above that STAT5 plays a limited role in responses to IL-10.

1.4.2 Alternate IL-10 signalling pathways

Activation of the JAK/STAT pathway is primarily used as a readout of IL-10 activity. However other signalling pathways have been implicated in IL-10 activity such as phosphatidylinositol-3-kinase (PI3K) and AMP-activated protein kinase (AMPK) signalling pathways. The use of PI3K inhibitors in human primary macrophages decreased expression of several IL-10-inducible genes e.g. ARNT2. However, not all IL-10-regulated genes were affected following PI3K inhibition, an example being SOCS3 (Antoniv and Ivashkiv, 2011). Downstream of PI3K, protein kinase B (Akt) was shown to regulate expression of several IL-10 inducible genes (Antoniv and Ivashkiv, 2011). Inhibition of PI3K partially suppressed the ability of IL-10 to inhibit IL-1ß however it did not impact the suppression of TNF-α. In addition, inhibition of PI3K did not significantly affect STAT3 or STAT1 phosphorylation, suggesting that these are non-reliant pathways (Antoniv and Ivashkiv, 2011). These results outline a distinct but selective role for PI3K/Akt signalling in the IL-10 response.

AMPK has been shown to be activated in response to IL-10 (Sag et al., 2008). Macrophages from mice deficient in AMPKα1 have reduced expression of

SOCS3 and other IL-10-inducible genes (Zhu et al., 2015). This study also showed that AMPK was involved in the activation of PI3K by IL-10 as well as mammalian target of rapamycin complex 1 (mTORC1) activation. Cells from AMPKα1 deficient mice showed reduced STAT3 phosphorylation and blocking AMPK signalling prevented STAT3 phosphorylation by IL-10 (Zhu et al., 2015). However, other STAT3 activating cytokines such as IL-6 do not rely on AMPK for STAT3 activation. This suggests that although AMPK can regulate STAT3 phosphorylation, other signalling pathways also play a role.

1.5 Anti-inflammatory effects of IL-10

IL-10's anti-inflammatory and immune-suppressive effects have been intensely studied and its potency as an immunoregulatory cytokine has led to repeated attempts to translate it into the clinic. IL-10's main immune-regulatory functions are the suppression of antigen presentation and inhibition of pro-inflammatory cytokine production. These anti-inflammatory activities are primarily directed against myeloid cells such as macrophages, monocytes and dendritic cells which in turn lead to a decrease in T cell recruitment and activation, however IL-10 can also directly inhibit CD4 T cell subsets as discussed below.

1.5.1 IL-10 mediated inhibition of antigen presentation

IL-10 can potently inhibit antigen presentation and expression of costimulatory molecules by monocytes, macrophages and DCs (Mittal and Roche, 2015). The exact mechanisms through which it does this are still unclear however several explanations have been put forward. DCs constitutively express low levels of MHC on their cell surface which are upregulated along with co-stimulatory molecules by detection of pathogen associated molecular pattern molecules (PAMPs) via toll-like receptors (TLRs) ((Iwasaki and Medzhitov, 2004). IL-10 has been shown to negatively regulate TLR signalling which in turn supresses antigen presentation in DCs (Mittal and Roche, 2015). Monocytes and macrophages upregulate antigen presenting molecules after being primed with IFNγ (Keskinen et al., 1997). IL-10 can also negatively regulate IFNγ signalling, leading to inhibition of antigen presentation (Mittal and Roche, 2015). In addition, IL-10 can enhance the degradation of MHC and costimulatory molecules in monocytes by

increasing expression of the ubiquitin ligase membrane-associated RING-CH 1 (MARCH1) targeting these proteins (Thibodeau et al., 2008).

This effective inhibition of antigen presentation has many knock-on effects for the adaptive immune response. In the absence of sufficient T-cell receptor (TCR) ligation by peptide/MHC molecules, T cells are unable to activate, leading to a reduction in effector T cells. While this can have negative impacts on the adaptive immune system's ability to respond to pathogens it is also an important mechanism for self-tolerance and resolution of the immune response.

1.5.2 Regulation of cytokine secretion by IL-10

Another key facet of IL-10's anti-inflammatory capabilities is its suppression of pro-inflammatory cytokine and chemokine secretion from a variety of cell types. As described above, the inhibition of LPS-induced TNF-α secretion from monocytes and macrophages by IL-10 is frequently used as a readout of IL-10 activity. IL-10 was demonstrated to inhibit IL-1α, IL-6 and TNF-α at both the protein and mRNA level in LPS stimulated macrophages (Fiorentino et al., 1991). IL-10 can also inhibit the action of these cytokines by inducing the production of soluble TNF-α receptor and IL-1 receptor antagonist (Sabat et al., 2010). Production of soluble TNF-α receptor was observed upon IL-10 stimulation in monocytes (Joyce et al., 1994). The upregulation of IL-1 receptor antagonist occurs via stabilisation of mRNA (Cassatella et al., 1994). This blockade of inflammatory mediators in multiple cell types leads to the creation of an immune-suppressive environment, preventing the activation of cells and inhibiting their effector functions.

IL-10 has also been shown to inhibit IL-12 and IL-23 production (Schuetze et al., 2005, D'Andrea et al., 1993). These cytokines are needed for the development of Th1 and Th17 cells, respectively, and so through its action on innate cells IL-10 can hinder adaptive cell immunity. IL-10 also acts directly on T cells to inhibit production of cytokines, such as its ability to inhibit IFNγ secretion from Th1 cells (Del Prete et al., 1993).

IL-10 can inhibit several chemokines, leading to a reduction in cell recruitment and contributing to an anti-inflammatory environment. IL-10 was shown to reduce levels of the chemokines CCL2, CCL3 and CCL4 in the serum (Olszyna et al., 2000). It can also reduce the half-life of IL-8 mRNA in neutrophils (Kasama et al., 1994). The regulation of cytokines and chemokines, particularly those that are pro-inflammatory, is a hallmark activity of IL-10 and allows it to dampen both the innate and adaptive immune responses.

1.5.3 Clinical use of IL-10 as an anti-inflammatory therapeutic

The above sections give a brief overview of IL-10's anti-inflammatory capabilities. The regulatory effect mediated by IL-10 and its key role in immune homeostasis is clear when examining IL-10 deficient phenotypes. Mice deficient in IL-10 develop chronic enterocolitis (Kuhn et al., 1993). Mutations in IL-10 or in either the IL-10Rα or IL-10Rß gene can be found in subsets of human patients with early-onset colitis (Glocker et al., 2009, Begue et al., 2011, Kotlarz et al., 2012). These patients have increased pro-inflammatory cytokine production from peripheral blood mononuclear cells (PBMCs), supporting IL-10's role in controlling inflammatory cytokine secretion (Glocker et al., 2009). The link between defects in IL-10 and colitis were further highlighted in a genome-wide association study (GWAS) which found significant association between ulcerative colitis and a single nucleotide polymorphism (SNP) in IL-10 (Franke et al., 2008). Because of IL-10's potency in controlling inflammation it was hoped that it could be used therapeutically in the treatment of inflammatory auto-immune diseases such as inflammatory bowel disease (IBD), rheumatoid arthritis and psoriasis. Harnessing the therapeutic potential of IL-10 has proved difficult, with only limited success in subsets of patients. I will outline the strategies used in IL-10 treatment, the outcomes seen and highlight hypotheses discussed in the literature as to why this promising therapeutic did not translate well into the clinic.

In mouse studies, intraperitoneal introduction of splenic T cells from IL-10 transgenic mice provided protection against the development of colitis (Hagenbaugh et al., 1997). When given to mice, genetically engineered IL-10 producing bacteria reduced colitis symptoms in an induced model and could also protect against colitis in IL-10 knockout mice (Steidler et al., 2000). This

suggested that administration of IL-10 could have therapeutic benefits for patients with IBD. However, several studies failed to prove efficacy with different variants of IL-10 being tested. In PBMCs isolated from healthy volunteers following recombinant IL-10 (Tenovil) administration, reduced levels of the pro-inflammatory cytokines TNF-α and IL-1ß levels were observed following ex vivo LPS stimulation (Huhn et al., 1997). In addition, it was well tolerated and non-toxic (Wang et al., 2019). An initial trial in Crohn's disease patients showed that administration of recombinant IL-10 increased remission rates compared to a placebo (Fedorak et al., 2000). A subsequent larger study however showed no significant difference between recombinant IL-10 treated and placebo groups (Schreiber et al., 2000). Interestingly there was some clinical improvement in the 8 µg/kg treatment group compared to the placebo group although not remission. In those that responded there was a decrease in NFκB p65 activation. A further study assessing the effect of recombinant IL-10 in the prevention of recurrence of Crohn's disease after surgery showed no efficacy (Colombel et al., 2001).

The failure of IL-10 to act effectively as an anti-inflammatory agent in clinical trials for IBD may be due to the low concentrations of IL-10 reaching the gastrointestinal tract. This is supported by the comparatively better clinical response of psoriasis patients to IL-10 therapy where subcutaneous injection results in modest but significant improvements compared to those seen in Crohn's disease patients (Al-Robaee et al., 2008, McInnes et al., 2001). IL-10 has a short half-life of 1-5 hours (Huhn et al., 1997) meaning that sufficient concentrations may not reach the site of inflammation when administered systemically. Supporting this theory, the use of genetically engineered bacteria which can secrete IL-10 and deliver it directly to the gastrointestinal tract have shown promising results (Braat et al., 2006, Steidler et al., 2000). This was first shown using the bacteria *Lactococcus lactis* (Steidler et al., 2000) and more recently using *Bifidobacterium bifidum* bacteria (Mauras et al., 2018), highlighting the advantage of targeted delivery of IL-10 to mucosal sites. Further work is needed to design alternative strategies for IL-10 therapy in order to fully harness the potent anti-inflammatory potential of this cytokine.

1.6 Immuno-stimulatory effect of IL-10

While IL-10's anti-inflammatory effects have been well characterised, it also possesses several stimulatory effects on certain immune cell subsets. It can enhance IgG and IgM secretion from B cells (Heine et al., 2014) and has a stimulatory effect on mast cells (Polukort et al., 2016), however these features are outside of the scope of this thesis. Several studies in recent years have highlighted the ability of IL-10 to enhance the function of cytotoxic effector CD8 T cells, leading to its use in clinical trials as a cancer therapeutic, however the molecular basis of these properties is still being investigated (Oft, 2014).

1.6.1 Effect of IL-10 on CD8 T cell cytotoxicity

In contrast to its inhibitory effect on CD4 T cells, IL-10 has been shown to enhance the effector functions of CD8 T cells under certain conditions. This was first described in 1991 when recombinant IL-10 was shown to enhance IL-2 mediated CD8 proliferation (Chen and Zlotnik, 1991). IL-10 can also prevent T cell apoptosis occurring after IL-2 withdrawal (Taga et al., 1993). A study examining the effect of recombinant IL-10 administration to Crohn's disease patients reported an increase in IFNγ when whole blood cells isolated from patients who had been treated with a high dose of IL-10 were stimulated with phytohemagglutinin (PHA) ex-vivo (Tilg et al., 2002). An increase in IFNγ was also seen when recombinant IL-10 was given alongside LPS in healthy humans (Lauw et al., 2000). This induction of IFNγ by IL-10 prompted further study into potential stimulatory properties of this cytokine on CD8 T cells. In addition to an upregulation of IFNγ, IL-10 was also shown to upregulate granzyme B (Mumm et al., 2011).

The ability of IL-10 to enhance CD8 cytotoxic functions has led to investigation of its use as a cancer therapeutic. The role of endogenous IL-10 in cancer is multi-faceted. Because of its potent anti-inflammatory properties, it was assumed that IL-10 levels would correlate negatively with tumour growth by generating an immuno-suppressive environment through inhibition of antigen presenting cells. Indeed, several studies have shown correlation between increased IL-10 levels and poor outcomes in cancer patients for example in melanoma (Boyano et al.,

2000). In addition, it was shown that melanoma cells can produce and secrete IL-10 (Sato et al., 1996), suggesting that this may be a mechanism of immune evasion by cancerous cells. However, there are also studies which highlight a protective and/or anti-tumour effect mediated by IL-10. Mice deficient in IL-10 were sensitive to tumour induction whereas mice which overexpressed IL-10 showed protection against the same tumour induction (Mumm et al., 2011). A PEGylated version of IL-10 has been used to investigate whether IL-10 can provide a therapeutic benefit in tumour killing by CD8 T cells, both in mice and in humans. PEGylation of the cytokine increases its size, thereby increasing its half-life and allowing it to be retained in circulation longer (Eliason, 2001). PEGylated IL-10 has been used in clinical trials and has been termed Pegilodecakin. A phase I trial demonstrated that it met safety and tolerability standards when administered to patients with solid tumours (Naing et al., 2016). A further in depth study was performed to assess how IL-10 influenced the CD8 T cell immune response in cancer patients (Naing et al., 2018). In this study they found that PEGylated IL-10 increased levels of IFNγ, granzyme B and IL-18 in patient serum as well as enhancing activity of CD8 T cells expressing immune checkpoint markers such as PD-1 and LAG-3. In addition, they saw increased T cell clonal expansion which correlated with decreased tumour burdens in patients that had responded positively to the treatment. When combined with anti-PD-1 therapy, PEGylated IL-10 gave a favourable response in eight out of nineteen patients. While these patients had already been treated with other therapies meaning that direct comparisons are hard to make, these data show a potential therapeutic use for IL-10 in cancer treatment when combined with immune checkpoint inhibitors.

This is not to say that IL-10 consistently plays a stimulatory role in CD8 T cells; it can inhibit CD8 T cells proliferation and induce anergy (Groux et al., 1998). However, these results were dependent on activation of CD8 T cells by antigen presenting cells (APCs). When a CD3 monoclonal Ab (mAb) was used these inhibitory effects were reduced, suggesting that this was a secondary effect of inhibition of APCs, rather than a direct CD8 effect (Groux et al., 1998). In addition, IL-10 has been shown to inhibit CD8 function in chronic viral infections by increasing glycan branching and interfering with TCR activation (Smith et al., 2018). The timing of when the CD8 T cells are exposed to IL-10 as well as the

activation state of the cells may also play a role in balancing inhibitory or stimulatory effects.

Together these studies outline the complexity associated with examining the effect of IL-10 on CD8 T cells and highlight the need for further investigation into this subject.

1.7 Protein engineering of cytokines

In recent years protein engineering has become more common as a way of generating useful tools for the investigation of protein-receptor interactions as well as developing modified cytokines with alterative or improved activities. Examples include using engineered cytokines to enhance binding affinities, to improve structural studies, to augment signalling properties and even to alter cell targets (Spangler et al., 2015). Here I will discuss methods used in the literature to engineer cytokines with a particular focus on yeast display methodologies.

Protein engineering can broadly be divided into two types: site-directed rational design and directed evolution. Rational design involves generating mutated proteins based on their known structure and protein interactions. Rational design of cytokines has the caveat of requiring detailed structural knowledge of the cytokine and its interactions with the receptor. In directed evolution, the protein of interest is subject to random mutagenesis followed by a selection process to enhance the presence of favourable mutations. This approach has the benefit of not requiring detailed structural knowledge of the protein interactions. A common method used for random mutagenesis in directed evolution is error-prone PCR (Cadwell and Joyce, 1992). This technique uses Taq polymerase under conditions which reduce its fidelity in order to introduce mutations into the gene of interest. The concentration of $MgCl_2$ is usually increased, $MnCl_2$ is added and the extension time is elongated. $MnCl_2$ affects the fidelity of Taq polymerase. (Beckman et al., 1985) and $MgCl_2$ acts as a cofactor for the polymerase, but at higher concentrations can result in decreased specificity of the polymerase and thus introduce mutations. During this process it is important to fine-tune the frequency of the mutations in order to balance the generation of mutations which

introduce premature stop codons or misfolded proteins, while also still generating enough variability for powerful selection.

Once site-specific mutations or random mutations have been generated in the gene of interest, protein engineering then uses a selection mechanism to isolate favourable mutations, usually based on binding assays. There are several approaches which can be used for selection such as phage, bacterial or yeast display. For cytokine engineering, yeast display has been widely used due to its eukaryotic secretory apparatus which allows it to form disulphide bonds and glycosylate proteins (Spangler et al., 2015). The yeast display the cytokine variants on the cell surface. Large libraries of mutants can then be incubated with the receptor of interest and those with favourable binding patterns can be isolated using magnetic activated cell sorting and flow cytometry. Directed evolution provides artificial selection pressures on the library to remove unfavourable variants e.g. those that do not bind at a certain concentration.

There are several examples of cytokines which have been moldulated using protein engineering techniques to alter the trafficking of the cytokine, the affinity of the cytokine for its receptor and the specificity of the cytokine. A series of studies were undertaken to improve the affinity of IFN-α2 for IFNAR1. Firstly, alanine mutations were used to identify the region on IFN-α2 which binds to IFNAR1 (Roisman et al., 2005). This identified three amino acids which, when substituted for alanine, increased the binding affinity and in turn increased biological activity. In a subsequent study these three mutations were combined to generate the "HEQ" IFN-α2 mutant which had comparable IFNAR1 binding affinity to IFNß and also similar anti-proliferative activity levels, far exceeding the wildtype (Jaitin et al., 2006). However, it only showed slightly increased antiviral activities. As this HEQ mutant had only alanine substitutions at the identified binding site positions, a phage library was used to generate mutants with further optimised amino acids at these positions (Kalie et al., 2007). The library contained all amino acid combinations at these positions which were then screened against IFNAR1, producing a mutant with 60-fold increased IFNAR1 affinity. This mutant displayed largely increased antiproliferative activity which had a superior anti-tumour effect compared to wild type IFN-α2 in an *in vivo* tumour model. These high affinity mutants were also used in structural studies to elucidate the IFN

ternary complex (Thomas et al., 2011). These studies highlight how protein engineering can be harnessed to provide information about cytokine-receptor activity at a myriad of levels: structural, signalling and biological activities.

Attempts have been made to modulate the binding of IL-2 to its receptor complexes using error-prone PCR and yeast display, in order to improve its clinical efficacy (Levin et al., 2012). IL-2 can bind two receptor complexes: a high affinity ternary receptor complex containing two specific receptors, IL-2Rα and IL-2Rß, and the shared receptor γc or an intermediate complex of just IL-2Rß and γc (Wang et al., 2009). In this study a variant of IL-2 with 200-fold increased affinity for IL-2Rß was generated (Levin et al., 2012). This allowed the variant to signal through the IL-2Rß/γc complex to the same amplitude as for the high affinity ternary complex, ultimately allowing it to act in CD8 T cells but limiting its effect on regulatory T cells. This resulted in an enhanced anti-tumour response and decreased toxicity compared to wildtype IL-2, improving the therapeutic efficacy of the cytokine. This study is an elegant example of how protein engineering at the cytokine/receptor interface can be used to alter the specificity of the cytokine.

This thesis uses protein engineering techniques to affinity mature the cytokine IL-10 for its receptor complex.

1.8 Aims and Objectives

As outlined above, IL-10 is a potent immuno-regulatory cytokine which has been intensely studied for more than 30 years. However, there are still gaps in our knowledge of how this critical cytokine functions: how it interacts with its low affinity receptor subunit, the role stoichiometry plays in its activities, why it has translated poorly as a therapeutic for autoimmune disorders and finally, the molecular mechanisms underpinning its enhancement of CD8 activities.

The first aim of this thesis was to use protein engineering techniques to generate a variant of IL-10 in both a monomeric and dimeric conformation, which had increased affinity for the IL-10Rß subunit. This gave us insight into the IL-10/IL-10Rß binding interactions as well as providing us with ligands for use in *in vitro* systems.

The second aim of the thesis was to use these variants to examine the effect of affinity and stoichiometry on IL-10's activities at multiple levels of cytokine biology: receptor binding, receptor complex assembly, early signalling events and gene transcription. This provided us with information on how this cytokine functions at a molecular level and how changes at the receptor interface translate into biological activities.

Due in part to its weak affinity for IL-10Rß, complete structural knowledge of the IL-10/IL-10Rα/IL-10Rß complex is lacking. The third aim of this thesis was to use the high affinity IL-10 variants as tools to further crystallisation attempts of this complex.

IL-10 has been shown to enhance the cytotoxicity of CD8 T cells under certain conditions. While this effect has been well characterised at the cellular level, insight into the precise molecular mechanisms governing this effect are lacking. The final aim of the thesis was to use proteomics to observe changes induced by IL-10 in human CD8 T cells during activation. This highlighted a potential role for metabolic regulation by IL-10, opening avenues for future work in this area.

Chapter 2. Materials and Methods

2.1 Cell Culture

2.1.1 Growth media and buffers

Complete RPMI (cRPMI): RPMI-1640 with L-glutamine (Gibco) supplemented with 10% foetal bovine serum (FBS) (Gibco), penicillin/streptomycin (100 U/mL) (Gibco).

Hi5 media: Lonza Insect Xpress with glutamine (SLS) supplemented with gentamicin (10 µg/mL) (Gibco).

SF9 media: SF9 III (Thermo) supplemented with gentamicin (10 µg/mL) (Gibco).

PBE: Phosphate buffered saline, pH 7.2 (made in-house by SLS Central Technical Services, University of Dundee), 0.5% BSA (Sigma), 2 mM EDTA (SLS Central Technical Services)

PBSA: Phosphate buffered saline, pH 7.2, (SLS Central Technical Services), 0.5% BSA (Sigma)

All cells were handled in laminar flow cell culture hoods. Cells were cultured in incubators maintained at 37ºC, 5% CO_2 with the exception of insect cells *Trichoplusiani ni* (Hi5) (ThermoFisher) and *Spodoptera frugiperda* (SF9) (ThermoFisher) which were cultured with agitation (120 rpm) at 27-28ºC.

2.1.2 Isolation of PBMCs

Human buffy coats were supplied by the Scottish National Blood Transfusion Service (Licence agreement number 16-20, held by Dr. Ignacio Moraga). Peripheral blood mononuclear cells (PBMCs) were isolated by density gradient centrifugation (Lymphoprep, StemCell Technologies) following the manufacture's protocol. Briefly, buffy coats were diluted 1:2 with pre-warmed RPMI. 25 mL of Lymphoprep was added to 50 mL falcon tubes (Eppendorf) and 25 mL of diluted buffy coat was layered on top of the Lymphoprep with care taken not to mix the layers. The mixture was centrifuged at 800 g for 30 minutes with no brake applied. After centrifugation the buffy coat layer was removed using sterile pastettes into a new falcon tube with care taken not to remove any red blood cells. These cells

were then washed twice with 50 mL of RPMI each time by centrifugation at 1200 rpm for 5 minutes with brake applied. The total cells were then resuspended in 50 mL cRPMI and a sample was taken for counting by flow cytometry (Beckmann Coulter Cytoflex S).

2.1.3 CD8 T isolation

From the isolated human PBMCs, CD8 T cells were isolated using two methods, the method used for each experiment is highlighted in the relevant figure legend of the results chapters.

Negative cell selection was performed using the MojoSort CD8 T cell kit (Biolegend #480012) according to manufacturer's protocols.

The second method, used in the majority of experiments, is positive CD8 T cell isolation. Here PBMCs were resuspended in 500 µL cold PBE and 15 µL of anti-FITC CD8 antibody (Biolegend) was added. Cells were incubated at 4ºC in the dark for 15 minutes. Then, cells were washed with 10 mL PBE by centrifugation at 1200 rpm, 5 minutes. Supernatant was removed and cells were resuspended in 500 µL PBE and 70 µL of anti-FITC microbeads (Miltenyi #130-048-701) were added. Cells were incubated at 4ºC in the dark for 15 minutes and washed as before. An LS column (Miltenyi #130-042-401) was placed in a QuadroMACS Separator (Miltenyi) and equilibrated by passing 3 mL of cold PBE through the column. Cells were resuspended in 500 µL of cold PBE and added to the column to magnetically separate the labelled CD8 T cells. Cells were washed on the column three times with 3 mL of PBE. The column was removed from the magnet and 5 mL of PBE was added to elute the cells using the plunger supplied with the kit. Eluted cells were counted by flow cytometry to visualise FITC CD8 staining. CD8 isolation gave populations that were >90% pure.

2.1.4 Activation of T cells

T cells were activated within a PBMC culture using the following protocol, adapted from the laboratory of Professor Doreen Cantrell (Division of Cell Signalling & Immunology, University of Dundee). Cells were plated at a density of 0.1-0.5 x

10^6 cells/mL in cRPMI. IL-2 (20 ng/mL) (Proleukin, Novartis #709421) and anti-CD3 (100 ng/mL) (Human UltraLEAF, Biolegend #317326) were added to the culture to activate the T cells present. This culture media was maintained for three days. On day three cells were centrifuged and media was removed and replaced with cRPMI/IL-2 (20 ng/mL) for a further two to three days to allow the activated population to expand. If cells were to be simulated for a dose response or a kinetic study then cells were placed in cRPMI with no IL-2 overnight before the experiment was performed to remove any background stimulation due to IL-2.

For purified CD8 T cell cultures, the cells were activated in cRPMI with ImmunoCult Human CD3/CD28 T Cell Activator (1/1000 dilution) (StemCell #10971) and IL-2 (20 ng/mL) (Proleukin, Novartis) for three days. On day three, the cells were removed from this media and resuspended in cRPMI/IL-2 as above and cultured for a further 2-3 days.

For examination of the effect of IL-10 on T cell activation, IL-10 (recombinantly expressed in the lab as detailed below) was added to the culture medium in addition to anti-CD3 and IL-2 as described above at the start of culture. On day three when the media was changed, fresh IL-10 was also added to the culture. The concentrations of IL-10 added to the media are listed in the relevant figure legends of the results sections.

2.1.5 Isolation and culture of human monocytes

A similar positive selection protocol as used for CD8 T cell isolation was used to isolate monocytes from buffy coats. Here an anti-CD14 FITC antibody was used (Biolegend) and the protocol above was followed. A >90% pure population was obtained.

After isolation of CD14$^+$ cells, the cells were cultured in cRPMI plus M-CSF (20 ng/mL) (Biolegend #574804) for two days before stimulation. For experiments using IL-10 stimulation, the cells were treated with IL-10 for either 8 or 24 hours as detailed in figure legends.

2.1.6 CAR T Cell generation and cytotoxicity assay

The generation of the CAR T cells and the cytotoxicity cell assay was carried out by W. Warda, A Cozzani, C. Ferrand and S. Mitra, Institut pour la Recherche contre le Cancer de Lille, University of Lille (France). The IL-10 proteins used were made by the author of this thesis and sent to the University of Lille for use in this experiment.

Lentiviral construct and genetically modified Chimeric Antigen Receptor (CAR) T-cell transduction: The IL-1RAP (Interleukin-1 Receptor Accessory Protein) CAR lentiviral construct was generated as previously described (Warda *et al*., 2019). Briefly, this vector carries a 3rd generation CAR, an iCASP9 (inducible Caspase 9) suicide gene and a delta CD19 surface gene. The mock control vector doesn't contain the CAR sequence.

Peripheral blood mononuclear cells (PBMCs) were isolated by Ficoll gradient density centrifugation using Ficoll-Paque (Velizy-Villacoublay) with anonymous blood samples collected from healthy donors at a French blood center (Besançon, France). Donors provided written informed consent; the study was conducted in accordance with the ethical guideline (declaration of Helsinki) and approved by the local ethical the CPP-Est committee (France).

Human tumor Monomac-6 cell line was obtained from DSMZ German collection of microorganisms and cell culture GmbH and stored in a master cell bank. The cells were cultivated in cRPMI 1640. Activated cells were established from healthy donors and transduced with lentiviral supernatant encoding the IL-1RAP CAR or Mock sequence. At day 5 post-activation, cells were put in the different culture conditions: IL-2 (500 UI/mL) with or without IL-10 variants at 25 nM for 3 days. Then, IL-1RAP CAR T cells, Mock T cells and un-transduced T cells were used for the cytotoxicity assays.

For CAR T cell cytotoxicity assay, prior to the co-culture, effector cells (un-transduced T cells, Mock T cells and IL1RAP CAR T cells) were labeled with e-Fluor v450 (eBioscience, #65-0842-85). Then effector cells were co-cultured with Monomac-6 cell line at different Effector: Target (E:T) ratios (1:1; 2:1 and 4:1).

After 5 hours, cells were stained with 7-Aminoactinomycine D (7-AAD; BD Bioscience, #559925) and the percentage of alive Monomac-6 cells was determined by flow cytometry using a FACS Canto II (BD Bioscience).

2.2 Flow Cytometry

All antibodies, clones and suppliers are listed in Table 2.1

Target	Clone	Fluorophore	Dilution	Catalogue Number	Supplier
CD3	UCHT1	BV-510	1:100	300448	Biolegend
CD4	A161A1	PE	1:100	357404	Biolegend
CD8a	HIT8a	AF700	1:100	300920	Biolegend
CD8a	HIT8a	FITC	1:100	300906	Biolegend
CD9	HI9A	FITC	1:50	312103	Biolegend
CD14	63D3	FITC	1:100	367116	Biolegend
CD57	HNK-1	PE/Cy7	1:100	359623	Biolegend
CD69	FN50	APC	1:50	310909	Biolegend
CD71	A015	FITC	1:50	334103	Biolegend
cMyc-tag	9B11	AF647	1:100	2233S	CST
GranzymeB	GB11	FITC	1:100	515403	Biolegend
HA-tag	6E2	AF647	1:100	3444S	CST
HLA-DR	L243	PE	1:100	307605	Biolegend
HLA-DR	L243	APC	1:100	307609	Biolegend
KLRG1	2F1	BV-711	1:100	138427	Biolegend
LAG3	11C3C65	AF647	1:100	369303	Biolegend
PD-1	EH12.2H7	AF488	1:50	329935	Biolegend
pSTAT1 (Y701)	58D6	AF647	1:100	8009S	CST
pSTAT3 (Y705)	13A3-1	AF488	1:100	651006	Biolegend
TIGIT	A1515G3	PE	1:100	372703	Biolegend
TIM3	F38-2E2	BV-510	1:100	345029	Biolegend

Table 2.1 Antibodies used for flow-cytometry.

2.2.1 Cell surface staining

For live cell surface staining of cell surface molecules, the following protocol was used. T cells and non-adherent monocytes were removed from culture by centrifugation and resuspension in PBSA. Adherent monocytes were detached using Accutase (Sigma) at room temperature for 5 to 10 minutes. Cells were kept

at 4ºC or on ice during live cell surface marker staining and staining was done in 96-well V-bottom plates (Greiner) unless otherwise stated. Cells were resuspended in 150 µL PBS and centrifuged at 1200 rpm for 5 minutes. FcR blocking was performed for 10 minutes at 4ºC using human FcR blocking reagent (Miltenyi #130-059-091) diluted 1/5 in PBE to a volume of 50 µL per well. Cells were washed as above in 150 µL PBE and resuspend in 50 µL of antibody mixture, diluted in PBSA. Antibody incubation was for 30 to 60 minutes at 4ºC in the dark. Cells were washed twice in PBSA before resuspension in 100 µL PBSA per well for analysis on the CytoFlex S flow cytometer (Beckman Coulter).

2.2.2 Intracellular staining

For intracellular staining cells were first fixed using a 2% final concentration of paraformaldehyde (Thermo) for 10 minutes at room temperature. Cells were then centrifuged at 1600 rpm for 5 minutes and resuspended in 150 µL PBS for washing. After another centrifugation step cells could then be resuspended in PBSA and stored at -80ºC for analysis at a later point or else permeabilised. Permeabilisation was done by resuspending the cells in 500 µL 100% ice-cold methanol (VWR) in deep-well V-bottom blocks (Greiner) for a minimum of 30 minutes. For granzyme B staining a different method of permeabilisation was used to enhance antibody staining due to reaction of the antibody to methanol. Here cells were incubated in 0.1% Triton-X100 (Sigma) in PBS for 10 minutes at room temperature.

In both cases, cells were then washed in PBSA and FcR blocked as described above. After FcR blocking, cells were incubated in 50 µL of antibody mixture diluted in PBSA for an hour at room temperature before washing and analysis on the flow cytometer as previously described.

2.2.3 Fluorescent Cell Barcoding

Fluorescent cell barcoding as described in (Krutzik et al., 2011) was used to combine 16 different samples together for antibody staining. This increased reproducibility of the antibody staining and helped to reduce experimental error

and costs. Briefly, two dyes Dylight 800 (Thermo Scientific #10561664) and Pacific Blue (Thermo Scientific #P10163) were prepared at four concentrations each and mixed in 4 different ratios, providing a panel of 16 unique staining combinations with which individual samples could be identified. The top concentration of each dye was 100 µg/mL, DyLight800 was serially diluted one in four and Pacific Blue was diluted one in three in DMSO (Sigma). 10 µL of the barcoding dye set were added per well directly to the 500 µL of methanol used for cell permeabilisation, after 30 minutes of permeabilisation. The plate was vortexed briefly to ensure complete mixing and 500 µL of PBS was added per well to maintain the pH close to 7. The cells incubated on ice for 35 minutes. 1 mL of PBSA was added per well to quench the dyes and cells were pelleted at 1600 rpm for 5 minutes. Each well was resuspended in 50 µL of PBSA and each of the 16 wells of the shared barcode set were pooled together i.e., one pool of cells for each barcode dye set. Pooled cells were washed in PBSA and FcR blocked. Cells were then resuspended in an appropriate final volume to allow each pool to be divided equally between several wells for antibody staining. Antibody staining and analysis were done as described above. Compensation controls for barcoding were cells stained with the top concentration of either DyLight 800 or Pacific Blue (100 µg/mL).

2.2.4 Mitotracker staining

For analysis of mitochondrial mass MitoTracker Green FM (ThermoFisher #M7514) was used (provided by the Hundal laboratory, University of Dundee). For analysis of mitochondrial membrane potential MitoTracker Red FM was used (ThermoFisher #M22425). CD8 T cells were purified and activated as described above. Cells were then stained at day 6, 8 and 10 after activation. FCCP (carbonyl cyanidep-trifuoromethoxyphenylhydrazone) (provided by the Hundal laboratory, University of Dundee) was used as a positive control. A final concentration of 5 µM FCCP was added to the cell culture media of the controls and incubated at 37ºC for 45 minutes. The cells were then centrifuged and resuspended in media containing the MitoTracker dye. Both dyes were used at a final concentration of 100 nM in RPMI without FBS. Cells were incubated at 37ºC for 20-30 minutes. The cells were then centrifuged at 1200 rpm and the MitoTracker media was removed. Fresh cRPMI was added to each sample and the cells were centrifuged

to remove any remaining dye. This wash step was repeated a total of three times to reduce any background non-specific signal. Cells were then FcR blocked and live stained for CD8 as described above.

2.2.5 Compensation and data analysis

For all experiments appropriate compensation was applied to correct for spectral overlap. In some cases, a compensation matrix was created by staining cells with one of each of the fluorochromes to be used as well as an unstained cell sample. This was needed for compensations involving the fluorescent barcodes as described above. For all other experiments a compensation matrix was created by staining positive and negative beads (Beckman Coulter) with each of the fluorochromes. In all cases the compensation matrix was created using the CytExpert software on the CytoFlex S (Beckman Coulter).

All data acquisition and gating was done using CytExpert software.

2.3 Molecular Cloning
2.3.1 Expression Vectors

All bacterial growth media and agar plates were provided by SLS Central Technical Services, University of Dundee.

During this project, several vectors for bacterial, insect and yeast protein expression were used. For yeast surface display a previously modified pCTCON2 vector, pCT302, (Chao et al., 2006) was used, modified for the generation of a BamHI/NotI cloning site. This plasmid introduces a c-myc tag on the C-terminus of the displayed protein, allowing for its identification via flow cytometry and has a resistance marker for ampicillin.

For insect expression of proteins two similar plasmids were used; the first was a previously modified version of pACgp67-A vector (BD Biosciences) (Levin et al., 2012), altered to introduce a BamHI/NotI cloning site (pACgp67BN BH3). This plasmid introduces an N-terminal gp67 signal sequence and a hexa-histidine tag on the C-terminus of the expressed protein, allowing for its isolation via Ni-NTA.

This plasmid also has a BH3 site for chemical biotinylation of the protein expressed. This BH3 site is a C-terminal biotin acceptor peptide (BAP)-LNDIFEAQKIEWHW.

The second plasmid used for insect cell expression was pACgp67 BN, differing only from the above by the removal of the BH3 site.

For bacterial expression of proteins, the pET21 vector was used. This vector introduces a hexa-histidine tag at the N-terminus of the expressed protein and has a Lac promoter for inducible expression.

2.3.2 Restriction digest, ligation and isothermal assembly

Plasmids were digested at the appropriate cloning sites using restriction digest enzymes from New England Biolabs (BamHI, NotI, NdeI). Digests used 10x CutSmart buffer (NEB) and followed the manufacturer's protocol for digestion (1 hour at 37ºC).

Synthesised gene blocks (IDT) were used for generation of double-stranded DNA for insertion into expression vectors.

Ligation was done using T4 Ligase (NEB) with T4 ligase buffer (NEB) according to the manufacturer's protocol (1 hour at room temperature) and then used to transform DH5α bacteria.

Isothermal assembly (ITA) was used in some cases to ligate plasmid and insert DNA. Gene blocks for ITA had overhanging 5' and 3' ends of 20-25 nucleotides corresponding with the vectors they were to be cloned into. Here an ITA master mix (see below) of 15 µL was added to 10-100 ng of purified cut plasmid and an equivalent of in-frame insert. The mixture was incubated at 50ºC for 1 hour and then used to transform DH5α bacteria.

5x isothermal assembly buffer:

1M Tris-HCl pH 7.5, 1M MgCl$_2$, 10mM dNTP mix, 1M DTT, PEG-8000 20 mg NAD.

Isothermal assembly master mix:

320uL 5x isothermal assembly buffer, 1 μL T5 exonuclease, 20uL Phusion polymerase, 160 uLTaq ligase, 700uLH$_2$O. Used in 15uL aliquots.

2.3.3 Bacterial Transformation

For cloning and expression of vectors, the *E. Coli* strain DH5α was used. For bacterial protein expression strain BL21 (DE3) was used. The same transformation protocol was used for both. Frozen bacterial stocks were partially thawed on ice for 10 minutes. The appropriate amount of plasmid DNA was added to the partially thawed bacteria and incubated on ice for a further 10 minutes. Bacteria were then heat-shocked by incubating at 45ºC for 45 seconds and then returned to ice for a further 2 minutes. 1 mL of SOCS recovery media (SLS Central Technical Services) was then added and the bacteria were placed at 37ºC for 30 minutes to allow recovery.

For single colony growth the bacteria were then centrifuged at 7000 rpm for 3 minutes and supernatant was removed. Bacteria were resuspended in 100 μL of SOCS media and plated on the appropriate agar plate depending on antibiotic resistance (usually LB/ampicillin agar plates).

For protein expression using BL21, the transformed bacteria were added to 10 mL of terrific broth/ampicillin media and grown overnight at 37ºC.

2.3.4 Gel electrophoresis, gel extraction, PCR purification and miniprep

For separation of restriction digest products or to visualise PCR products, agarose gel electrophoresis was used. For all gels a 1% agarose mixture was made by dissolving agarose (Invitrogen) in 1X TAE buffer (SLS Central Technical Services) by heating. Gel red (Biotium) was added to the agarose solution at 1 in 10,000 dilution as a nucleic acid dye. Samples were run at 110 V for 35 minutes to 1 hour depending on the size of the product.

For extraction of DNA and/or PCR purification, the Promega Wizard Gel and PCR Clean-Up Kit was used following manufacturer's protocol.

For extraction of plasmid from bacteria the Promega Wizard Miniprep Kit was used following manufacturer's protocol.

2.3.5 Sequencing

All sequencing was performed by the in-house facility, MRC PPU DNA Sequencing and Services. Samples were submitted in 20 µL aliquots at concentrations ranging from 25-30 ng/µL, dilute in H_2O. For primers used in sequencing please refer to table 2.2. Sequences were analysed using SnapGene Software, version 4.2.11.

Primer Name	Sequence	Purpose
AML-6	CGAGCTAAAAGTACAGTGGG	Sequencing pCT
Bac Fw	TATTCCGGATTATTCATACCGTC	Sequencing pAC
Bac Rv	CAACAATTGCATTCATTTTATGTTTCAGG	Sequencing pAC
T7 Term	TATGCTAGTTATTGCTCAG	Sequencing pET
R5A11Dimer Nde Fw	GACATATGTCCGAGAACAGTTGCACGCACTTTC	Cloning into pET vector
R5A11Dimer BamHI Rv	GAGGATCCCTAGTTGCGGATTTTCATC GTCATATAGGC	Cloning into pET vector
NdeI WTD Fw	GACATATGTCTGAGAACAGCTGCACCCACTTCC	Cloning into pET vector
BamHI WTD Rv	GAGGATCCCTAGTTTCGTATCTTCATTGTCATGTAGGCT	Cloning into pET vector

Table 2.2 Primers used for sequencing and cloning

2.4 Protein production (insect cells)

Proteins produced via insect cell expression include monomeric wild type IL-10 (Josephson et al., 2000a), monomeric high affinity variants, IL-10Rα ectodomain (amino acids 22-235) and IL-10Rβ ectodomain (amino acids 20-220).

2.4.1 Buffers

10 X HBS: 100 mM HEPES, 1.5 M Sodium Chloride, 0.2% Sodium Azide, pH 7.2
Precipitation buffer: 1 mM $NiCl_2$, 5 mM $CaCl_2$, 60 mM Tris pH 8.0
Wash buffer: 20 mM imidazole in HBS, pH 7.2
Elution buffer: 200 mM imidazole in HBS, pH 7.2

2.4.2 Generation of virus and amplification

To generate a P0 virus, transfection of SF9 (*Spodoptera frugiperda*) cells was performed as follows. Cells were seeded in a 6 well plate (1 well per transfection) at a density of 1×10^6 cells/mL, 2 mL per well. Cells were left to adhere for a minimum of 30 minutes. 2 µL of BestBac 2.0 linearized virus (Expression Systems) was mixed with 2 µg of DNA (pACgp67 plasmid) and incubated for 5 minutes. In a separate vial, 10 µL of TransIT (GeneFlow) was added to 100 µL of SF9 III media (Thermo). This solution was added to the DNA solution and incubated for 15-20 minutes. 1.8 mL of SF9 III media was then added to the vial. Media was removed from the adherent cells and replaced with the transfection mixture. Cells were incubated statically at 28ºC for 5 to 8 hours after which the transfection media was replaced with 3 mL SF9 III media, and the plate was sealed with saran wrap to prevent evaporation. Cells were left for 7 to 10 days at 28ºC, static. For each transfection a positive mCherry control was done in parallel to determine transfection efficiency via fluorescence.

On day 7 to 10 the media containing the virus was removed from the cells and centrifuged at 2000 rpm for 5 minutes and the supernatant transferred to a clean tube as P0 virus. 30 µL of this P0 virus was added to 30 mL of suspension SF9 cells at a cell density of 2×10^6/mL. Cells were counted daily and media added to maintain cell density at 2×10^6/mL until cell division stopped (usually day 3). The cells were then left for 7 days to amplify the virus. After that, the cells were centrifuged as above and the supernatant removed to a clean tube as the viral P1.

A titration of the P1 virus was done by infecting suspension Hi5 cells (*Trichoplusiani ni*) (2 x 10^6/mL, 2 mL/well in a 6 well plate) over a variety of volumes of the virus, usually 0 µL, 1 µL, 2 µL, 4 µL, 6 µL, 8µL of P1 virus per 2 mL Hi5s. Cells were incubated for 2 days before the supernatant was harvested for analysis of protein production.

To observe if protein was produced a "protein miniprep" was done. Here 1.8 mL of culture supernatant was buffered with 200 µL of 10X HBS and incubated with 25µL Ni-NTA resin (Thermo) for a minimum of 3 hours at room temperature on rotation. The media was then centrifuged at 5000 rpm for 1 minute and the supernatant removed. The Ni-NTA was washed with 1.5 mL 10 mM imidazole and centrifuged again. Protein was eluted with 25 µL of 200 mM imidazole and this was run on an SDS-PAGE gel, followed by staining with Coomassie Blue to observe if protein was present.

2.4.3 Infection of insect cells for protein production

For production of protein, Hi5 cells were used. Cells were maintained at a density of 2 x 10^6 cells/mL in Insect-XPRESS media (Lonza), supplemented with gentamycin (10 µg/mL, Thermo). Cells were infected with virus at the appropriate dilution depending on the viral titre as determined above. Usually this was in the range of 1-2 mL of P1 virus per litre of Hi5 cells. Cells were infected with P1 virus and left to incubate with gentle shaking (120 rpm) for 2 days.

2.4.4 Protein purification via His-tag

Cells which had been infected with virus were centrifuged in 1L bottles at 2,000 rpm, 15 minutes and supernatant was transferred to a clean beaker. 50 mL of precipitation buffer was added to this and the solution was left with spinner at 120 rpm for 15 minutes to remove components of the media which inhibit the action of the Ni-NTA resin. The solution was then centrifuged at 6000 rpm for 15 minutes and supernatant was removed to a clean beaker. 2 mL of Ni-NTA agarose resin (Thermo) was added per litre of media and placed with a spinner at 120 rpm for a minimum of 3 hours at room temperature.

The media was then filtered through a glass Buchner funnel to collect the Ni-NTA resin. The resin was washed with 20 mM imidazole/HBS before removal of the resin to a poly-prep column (Biorad). The protein of interest was eluted from the Ni-NTA resin by addition of 200 mM imidazole/HBS to the column. 10 fractions of 0.5 mL each were collected. Absorbance at 280 nm (A_{280}) was measured to determine which fractions contained the protein of interest and these fractions were then concentrated in a centrifugal filter unit (Merck). Protein concentration was determined using the formula below. Extinction coefficients were calculated using the online programme ProtParam (ExPASy) (Wilkins et al., 1999).

Concentration (molarity) = A_{280nm} / Extinction Coefficient

Concentration (mg/mL) = (A_{280nm} / Extinction Coefficient) x Molecular Weight

2.4.5 Size exclusion chromatography

After isolation via his-tag, proteins were purified via Fast Protein Liquid Chromatography (FPLC) and separated on the basis of size. For all proteins except IL-10 dimers an Enrich SEC 650 1x300 column (Biorad) was used. For the IL-10 dimer proteins a SuperDex 75 increase 10/300 column (Cytiva) was used. HBS was used as the equilibration buffer for the columns. For Enrich column the flow rate was 1 mL/min. For SuperDex 75 the flow rate was 0.5 mL/minute. 0.5 mL fractions were collected for both.

2.4.6 Protein Sterilisation

After purification and concentration, proteins for cell stimulation were sterilised and aliquoted. Centrifugal filter units with a 0.22 μm filter were used to sterilise the proteins (Merck). Proteins were then aliquoted in sterile PCR tubes and snap frozen in liquid nitrogen. Aliquots were stored at -80ºC until use.

2.4.7 Protein biotinylation

IL-10Rβ was biotinylated via its C-terminal Biotin Acceptor Peptide (BAP)-LNDIFEAQKIEWHW. This involved incubation of the protein with BirA ligase

(1:100) in an excess of biotin overnight at 4ºC as described in (Spangler et al., 2019). BirA ligase was recombinantly produced by Dr. I. Moraga.

IL-10Rα had poor expression when expressed with the biotin acceptor peptide and so biotinylation was performed using NHS-ester activated biotinylation. EZ-Link NHS Biotin (Thermo #20217) was used according to the manufacturer's protocol.

The proteins were purified via FPLC after biotinylation as described above to separate the biotinylated protein from the excess of biotin. To confirm biotinylation an aliquot of protein was incubated with an excess of streptavidin (Thermo) and run on a non-reducing SDS-PAGE gel. Proteins which were biotinylated displayed a shift upwards on the gel.

2.5 Protein Production (Bacterial)

Human wild type dimeric IL-10 and high affinity dimeric IL-10 variants (amino acids 26 to 178) were produced using bacterial protein production.

2.5.1 Buffers

Resuspension buffer: 50 mM Tris-HCl pH 8.0, 25% (w/v) sucrose, 1 mM Na EDTA, 10 mM DTT, 0.2 mM PMSF.
2x Lysis buffer: 100 mM Tris-HCl pH 8.0, 2% (v/v) TritonX-100, 200 mM NaCl, Benzonase 10 µL, 10 mM DTT, 5 mM $MgCl_2$, 0.2 mM PMSF.
Wash buffer 1: 50mM Tris-HCl pH 8.0, 0.5% Triton X-100, 100 mM NaCl, 1 mM Na EDTA, 1 mM DTT, 0.2 mM PMSF.
Wash buffer 2: 50 mM Tris-HCl pH 8.0, 1 mM Na EDTA, 1 mM DTT, 0.2 mM PMSF.
Refolding Buffer: 50 mM Tris-HCl, pH 8.0, 50 mM NaCl, 5 mM EDTA, 2 mM reduced glutathione (GSH) and 0.2 mM oxidized glutathione (GSSG).

2.5.2 Lysis and Inclusion body isolation

Transformation of BL21 bacteria was done as described in section 2.3.3. The 10 mL overnight culture was added to 1 litre of terrific broth/ampicillin media (SLS Central Technical Services) and grown until the OD_{600} reached 0.5-0.7. The bacteria were then induced using 1 mM final concentration of Isopropyl β-d-1-thiogalactopyranoside (IPTG, Formedium) and incubated at 37ºC for 3 to 5 hours. Cultures were centrifuged at 6000 g for 15 minutes and the supernatant was discarded. Cell pellets were resuspended in 25 mL of resuspension buffer per litre of original culture and frozen at -80ºC until needed.

Lysis was done by adding 25 mL of 2X lysis buffer (1X final concentration) to the cells previously resuspended in 25 ml of resuspension buffer and incubating for 20 minutes at room temperature on a rotator. 10 mM EDTA (final concentration) was then added to the suspension and cells were sonicated (10 cycles of 15 seconds on/off, 15 microns, Soniprep150) in an ice-bath. The solution was centrifuged at 7000 g for 15 minutes (4ºC) and resuspended in 50-100 mL of wash buffer 1. Sonication was repeated as above and cells were centrifuged and resuspended in 50-100 mL of wash buffer 1. This washing and sonication step was repeated a total of three times until the preparation appeared white. The preparation was then washed once in wash buffer 2 (detergent-free).

The pellet containing the protein of interest as inclusion bodies was solubilised in 10 mL of 6M GuHCl per litre of original culture for 30 minutes. The solution was clarified by a high speed centrifugation and the supernatant was removed for refolding.

2.5.3 Refolding, dialysis and purification of proteins

The solubilised solution was added dropwise into refolding buffer (10 mL of solution into 200 mL of buffer) at 4ºC and incubated with gentle spinning overnight at 4ºC. The next day the solution was filtered to remove any precipitant present. Dialysis membranes (14,000 Da cut off, Sigma) were used to dialyse 200 mL of solution into 2 L of HBS. This dialysis was replaced daily for 5-7 days. After dialysis, the protein was isolated by incubating with Ni-NTA resin for 1 hour and purification continued as described in 2.4.4.

2.5.4 Endotoxin removal

The removal of endotoxin from bacterially produced proteins was done as follows at 4ºC. 1 mL of Ni-NTA agarose was added to a poly-prep column and washed with 10 mL of HBS. The protein was added to the column and the flow through was collected and A_{280} measured to ensure all protein had bound the column. Any unbound protein was re-added to the column and elute was checked until the flow through had no protein detectable. The column was washed with 50 column volumes of ice-cold HBS/150 mM NaCl/20 mM imidazole/ 0.1% Triton-X114 to remove endotoxin. The column was then washed with 20 column volumes of HBS/20 mM imidazole. The endotoxin-free protein was eluted using 4 column volumes of HBS/200 mM imidazole.

The protein was buffer exchanged into HBS using PD-10 columns (GE Healthcare) following the manufacturer's protocol.

Endotoxin levels were measured using Pierce LAL Chromogenic Endotoxin Quantitation Kit (Thermo) following the manufacturer's protocol. For all proteins, endotoxin levels were below detection levels of the kit.

2.6 De-glycosylation and crystal screening
2.6.1 De-glycosylation

In order to de-glycosylate IL-10Rα the protein was treated with kifunensine (Carbosynth) and endoglycosidase F (EndoF). Kifunensine was added to the insect cell media at the same time as the P1 virus was added. A range of kifunensine concentrations were used as outlined in the relevant results section. EndoF was recombinantly produced by Dr. I. Moraga. After purification of the kifunensine-treated protein, EndoF was added to the protein at a concentration of 50 µg/mL. This was incubated overnight at 4ºC before purification via gel filtration.

2.6.2 Crystal screens

Screening of different conditions in order to generate crystals of the high affinity IL-10/IL-10 receptor complex was undertaken as part of this thesis. Commercial screens were used to test a wide range of variables such as pH, salts and polyethylene glycol (PEG) concentrations. Screens used in this thesis were: ProPlex (Molecular Dimensions), JCSG Core Suites I, II, III, IV (Quiagen) and PurePEGS (Molecular Dimensions). ProPlex screens a range of pHs as well as PEG molecular weights and concentrations. The JCSG Core Suites use a variety of salts, buffers and precipitants. PurePEGS uses PEGs over a range of molecular weights. 60 µL volumes were used in the reservoirs.

Protein complexes were concentrated to a range of 3-10 mg/mL in HBS for use in the screens and were filtered through a 0.2 µm clarification spin column (Generon). Sitting drop wells were used for the screens in MRC 96-well 2 drop plates (Molecular Dimensions), to allow simultaneous screening of different complexes. A Mosquito Xtal3 (SPT Lab Tech) was used to dispense 100 nL volumes in a 1:1 ratio. Plates were sealed with an adhesive sheet and stored either in a communal temperature controlled room (21ºC) or in an incubator (18ºC). Plates were checked regularly for crystal growth using a light microscope.

2.7 Yeast surface display library for affinity maturation of IL-10 for IL-10Rβ
2.7.1 Buffers

All media was prepared by Central Technical Services, SLS.
YPD media: 20 g dextrose, 20 g peptone, 10 g yeast extract in deionized H2O to a volume of 1 litre and sterilised by filtration.
E buffer: 1.2 g Tris base, 92.4 g sucrose, 0.2 g MgCl$_2$ in deionized H2O to a volume of 1 litre, pH to 7.5 and sterilised by filtration
SDCAA media: 20 g dextrose, 6.7 g Difco yeast nitrogen base, 5 g Bacto casamino acids, 5.4 g Na2HPO4, 8.56 g NaH2PO4_H2O in deionized H2O to a volume of 1 litre and sterilised by filtration
SGCAA media: Prepared as for SDCAA, but use 20 g galactose instead of dextrose

2.7.2 Error-prone PCR

For error-prone PCR a monomeric form of IL-10 as designed by the Walter group (Josephson et al., 2000a) was used as a template. Error-prone PCR introduces random mutations into the gene, the rate of which can be altered by changing amounts of $MgCl_2$ and $MnCl_2$ in the reaction mixture. The reaction was set up as outlined in Table 2.3 below with primers listed in Table 2.4.

Reagent	Volume (µL)	Final concentration
10X Taq Polymerase Buffer (magnesium free)	5	1X
ddH$_2$0	29.5	N/A
MgCl$_2$ (100 nM)	3.5	7 mM
Primer Mix (25 µM)	1	200 nM each
Template DNA (8 ng/µL)	1	N/A
dNTPs (10 mM each)	1	200 µM each
dCTP/dTTP (40 mM each)	1	800 µM each
MnCl$_2$ (1 mM)	7.5	0.15 mM
Taq Polymerase	0.5	N/A

Table 2.3 Error Prone PCR

Primer Name	Sequence	Purpose
IL-10 Error Fw	TCCGAGAACAGTTGCACGCAC	Error-prone PCR (Taq Polymerase)
IL-10 Error Rv	GTTGCGGATTTTCATCGTCATATAGGC	Error-prone PCR (Taq Polymerase)
IL-10 Error Amp Fw	GTAGCGGTGGGGGCGGTTCTCTGGAAG TTCTGTTCCAGGGTCCGAGCGGCGGAT CCTCCGAGAACAGTTGCACGCAC	Amplify error-prone PCR product (Phusion PCR)
IL-10 Error Amp Rv	AGATCTCGAGCAAGTCTTCTTCGGAGAT AAGCTTTTGTTCGCCACCAGAAGCGGC CGCGTTGCGGATTTTCATCGTCATATAG GC	Amplify error-prone PCR product (Phusion PCR)

Table 2.4 Error PRC Primers

The cycle for the PCR reaction was: 94ºC melt for 3 minutes, 30 cycles of (94ºC for 30 seconds, 60ºC annealing for 30 seconds, 72ºC for a 1 minute extension) 5' polish at 72ºC for 5 minutes. A sample of the PCR reaction (5 µL) was run on a 1% agarose gel to check the size of the product which was around 500 base pairs. The error-prone PCR product was amplified by standard Phusion PCR

(NEB) and the product was cleaned up to remove any primer-dimers using the Promega Wizard PCR clean-up kit.

The pCT plasmid (as described in section 2.3.1) was restriction digested at the BamHI/NotI cloning site to remove the insert present (had previously contained the sequence of Leukaemia Inhibitory Factor (LIF)) and run on a 1% agarose gel. The upper band of the linearized plasmid was extracted and purified.

A test ligation of a sample of the error-prone PCR product with the cut plasmid was done and DH5α bacteria were transformed. Colonies were picked and the plasmid was mini-prepped. The isolated DNA was sent for sequencing to confirm the error rate for the PCR which was 4-5 mutation per gene.

2.7.3 Electroporation

Saccharomyces cerevisiae strain EBY100 was grown on a YPD plate at 30ºC overnight. 5 mL of YPD was inoculated with 5-10 colonies of EBY100 and grown with agitation at 30ºC overnight. The following day 100 mL of YPD was inoculated with the 5 mL culture and grown to an OD_{600} of 1.3 in a baffled flask. 1 mL of Tris-DTT (2.5M DTT in 1M Tris, pH 8.0) was added to the culture and left shaking at 30ºC for 15 minutes.

The culture was divided into two 50 mL falcon tubes and centrifuged at 2500 g for 3 minutes, resuspended in 25 mL of E buffer and centrifuged again. Each pellet was resuspended in 1 mL of E buffer and centrifuged again. One pellet was then resuspended in 300 µL of E buffer plus a total of 275 µL of IL-10 error PCR product and linearized pCT vector in a 5:1 ratio, PCR product: vector. This suspension was then used to resuspend the other pellet and the solution was aliquoted into chilled electroporation cuvettes (2 mm, VWR) and kept on ice. Electroporation was done at 500 V LV, resistance none, 0.025 µF. Each aliquot was rescued with 2 x 1 mL of YPD. All electroporated aliquots were combined into a baffled flask and made up to 50 mL of YPD media. This was placed at 30ºC for 1 hour. The culture was then centrifuged at 2500 g for 3 minutes and resuspended in 10 mL SDCAA.

In order to determine the size of the yeast library a titration of the yeast was done and several dilutions of the library were plated on SDCAA agar plates and grown for 3 days at 30ºC.

The 10 mL of the library was added to 500 mL of SDCAA (+ chloramphenicol) and grown at 250 rpm, 30ºC overnight.

The following day 10^{10} cells (as determined by OD_{600}) were removed and placed into fresh SDCAA and grown overnight.

On day three, 10^{10} cells were removed and centrifuged. They were resuspended into SGCAA (induction media) and grown at 20ºC for 2 days in order to allow the yeast to display the protein on the cell surface.

2.7.4 Yeast library screening

All screening rounds started with a negative selection to remove any yeast which bound streptavidin in the absence of biotinylated protein. This involved incubating the yeast with 100 µL fluorescently labelled streptavidin (AlexaFlour647 (AF647), made by Dr. I. Moraga) for 1 hour at 4ºC. The yeast were then washed twice with cold PBE and centrifuged at 2500 g for 3 minutes. Anti-AF647 magnetic microbeads were added (Miltenyi #130-091-395) and incubated for 1 hour at 4ºC. After another wash, Magnetic Activated Cell Sorting (MACS) was performed using LS columns (Miltenyi) in a QuadroMACS Separator according to manufacturer's protocol. Briefly, the yeast suspension was added to the column and flow through was collected. The column was then washed three times with 3 mL of PBE. This flow through was collected. The column was then removed from the magnet and 5 mL of PBE was used to elute any yeast bound to the column. The flow through contained yeast which did not show non-specific streptavidin binding and so were taken forward for the positive selection round.

The first round of positive selection was done to recover all positive binders in the library and also to reduce the complexity of the library. 250 µL of streptavidin microbeads (Miltenyi #130-048-101) were incubated with 400 nM of biotinylated IL-10Rß for 15 minutes. This was then incubated with the yeast at 4ºC for 2 hours. The yeast was washed as before and MACS was performed. This time the yeast

which were eluted were kept as these yeast displayed affinity for IL-10Rß and the flow through was discarded. The yeast were returned to culture and grown at 30ºC for 1 day in SDCAA media and changed into SGCAA media at 20ºC for induction for 2 days. This growth protocol was followed for the entire screening process.

The second screening round selected those yeast which displayed the c-myc tag on the cell surface. The c-myc tag is expressed on the C terminus of the yeast-displayed IL-10. By selecting for c-myc expression we were removing any yeast which displayed truncated IL-10. A negative clearing step was performed as before. The flow through yeast were incubated with anti-cmyc tag AF647 antibody (CST, #2233S) for 2 hours at 4ºC, followed by 20 minutes incubation with anti-AF647 microbeads. The yeast were washed and MACS separation was performed with the eluted yeast being taken forward for culture.

The third screening round began to select for yeast which displayed IL-10 variants with affinity for the IL-10Rβ and all subsequent rounds were performed following a similar protocol with decreasing concentrations of IL-10Rβ. The yeast were incubated with a known concentration of recombinantly expressed biotinylated IL-10Rβ for two hours. They were then washed and incubated with streptavidin-AF647 for 15 minutes and the wash was repeated followed by incubation with anti-AF647 beads for 20 minutes. This meant that the yeast-displayed IL-10 which could bind IL-10Rβ could be isolated by magnetic activated cell sorting (MACS) and visualised using flow cytometry. Each round of selection used decreasing IL-10Rβ concentrations. IL-10Rα (non-biotinylated) was also used in early selection rounds to stabilise binding as described in the results section.

Once the concentration of IL-10Rβ needed for binding was decreased sufficiently compared to wild type monomeric IL-10, the yeast were spread on SDCAA plates and single colonies were isolated and used for dose response experiments to determine the EC50 values of the mutants.

Yeast colonies displaying promising mutant IL-10 variants were subject to Zymoprep (Zymoreserach) to isolate the pCT plasmid which was then heat shocked into DH5α competent cells. Plasmids were then mini-prepped and sent

for sequencing to observe where mutations had occurred in the monomeric IL-10 gene. These genes were then cloned into the baculovirus expression vector pACgp67BN and recombinantly expressed as described above.

2.8 Yeast surface display library for selection of nanobodies recognising the IL-10/IL-10R complex

2.8.1 Media and buffers

All media was prepared by Central Technical Services, SLS.

YGLC-glucose/galactose: 3.8 g of –Trp drop-out media supplement, 6.7 g Yeast Nitrogen Base, 10.4 g Sodium Citrate, 7.4 g Citric Acid Monohydrate, 20 g glucose or galactose in deionized H2O to a volume of 1 litre and sterilised by filtration

2.8.2 Yeast library preparation

The nanobody yeast library as described in (McMahon et al., 2018) was used to isolate nanobodies capable of binding the high affinity IL-10 molecule R5A11M in complex with IL-10Rβ/IL-10Rα. The yeast library was thawed from frozen stocks into 500 mL of YGLC-glucose media and incubated overnight at 30ºC. The following day 1×10^{10} cells were placed into fresh YGLC-glucose media to remove dead cells and incubated overnight. Cells were then placed in 500 mL of YGLC-galactose media for 48 hours at 20ºC to induce expression of the nanobody protein on the yeast cell surface. Expression of the protein was confirmed by staining for HA-tag AF647 (CST, #3444S) by flow cytometry, expressed on the C terminus of the nanobody.

2.8.3 Yeast library screening

Screening was carried out initially with R5A11M/IL-10 receptor complex biotinylated alternately on IL-10Rα or IL-10Rβ and subsequently with biotinyalted IL-10Rα or IL-10Rβ alone. This is described in more detail in Chapter 6. Screening was carried out with anti-AF647 beads (Miltenyi) and MACS separation as for the previous library. Details of the concentrations of biotinylated protein are outlined in the results chapter.

Single colonies were isolated by spreading on YGLC-glucose plates and picking single colonies. The plasmids were isolated from these clones as described for the previous library.

2.9 Secreted Cytokine Analysis

2.9.1 ELISA

For analysis of IL-6 from supernatants of stimulated human monocytes an ELISA kit for human IL-6 was used (Biolegend). Samples for IL-6 quantification were diluted 1 in 6. Manufacturer's protocols were followed with the following exception: half-volume flat bottom plates (Greiner) were used and so the volume of all reagents added per well was halved. Fluorescence was measured at 450 nm on a CLAIROstar plate reader and standard curves were fitted using the CLAIROstar analysis software.

2.9.2 Bioplex

Biorad's bioplex assay was used to measure levels of IL-6, TNF-α, GM-CSF and IL-13 from murine BMDMs after stimulation (cells were isolated by S. Laba in collaboration with the Simon Arthur laboratory, University of Dundee). Cells were stimulated with PAM3CSK at 1 µg/mL for 8 hours in the presence or absence of varying concentrations of IL-10 wild type and high affinity variants. Supernatant was removed and frozen at -80ºC. Manufacturer's guidelines were followed for the bioplex assay (Biorad). Plates were read on a Luminex 200 instrument. Data was analysed using Excel and GraphPad Prism.

2.10 Proteomics

2.10.1 Cell pellet preparation

CD8 T cells were submitted for proteomic analysis. CD8 T cells were activated and grown in a PBMC culture in the presence of IL-10 (100 nM) as described above. CD8 T cells were isolated by negative selection after 6 days of activation as described above. After cell stimulation and isolation was complete, a sample of the cells were stained for analysis by flow cytometry to determine the live cell count using Biolegend's Zombie Aqua dye following manufacturer's protocol. For

all proteomic samples live count was >90%. The purity of the population's cell type was also determined by flow cytometry by staining for CD8a (AlexaFlour700, Biolegend). The population was >90% positive for the correct cell type.

Cell pellets were frozen as follows, all steps were done on ice or at 4ºC: cells were centrifuged at 1500 rpm for 5 minutes and media was removed. Cells were resuspended in 600 µL of cold HBSS (Gibco) and this was transferred to a pre-chilled Eppendorf. A further 600 µL of HBS was added to the original falcon tube which held the cells to ensure maximum cell recovery and this was added to the Eppendorf. This was centrifuged at 8000 rpm for 10 seconds. The tubes were turned 180 degrees to face the opposite way in the centrifuge and centrifuged again at 8000 rpm for 10 seconds. Supernatant was removed and the pellet was resuspended in 1 mL of HBSS. 10 µL was taken for a cell count estimate. The rest of the samples were centrifuged as before and the supernatant was removed. The pellets were snap frozen in liquid nitrogen and stored at -80ºC until lysis.

2.10.2 Lysis and protein digest

Cell lysis and protein digest was done with the assistance of Dr. A. Howden in the Cantrell laboratory, University of Dundee. Filter tips, pure H_2O and clean glassware were used during sample processing to minimise protein contamination. For cell lysis, digestion and preparation for mass spectrometry, the SP3 method was followed as described in (Howden et al., 2019).

Briefly, samples were resuspended in lysis buffer (4% SDS, 10 mM TCEP, 50 mM TEAB) and vortexed before shaking for 5 minutes at room temperature. Samples were then boiled for 5 minutes while shaking and cooled before sonicating, 15 cycles of 30 seconds on/off (Bioruptor). Benzonase was added to the samples to remove any nucleotides and incubated for 15 minutes at 37ºC. Protein quantification was determined by EZQ Protein Quantification Kit (Thermo) following manufacturers protocol. A final concentration of 20 mM iodoacetic acid was added to each sample and incubated in the dark for 1 hour to alkylate the cysteines and prevent disulphide bond formation. 200 µg of SP3 (Single-Pot Solid-Phase-enhanced Sample Preparation) beads were added to each sample. Acetonitrile/10% formic acid was added to allow binding of proteins to the bead

surface and incubated for 8 minutes with gentle shaking. Supernatant was removed by placing on a magnetic rack and 1 mL of 70% ethanol was used to wash the beads. This was repeated with 100% acetonitrile and beads were air dried for 15 seconds. Digest buffer was added (0.1% SDS, 50 mM TEAB 1 M CaCl2) along with 1 µg LysC per 100 µg protein and incubated overnight at 37ºC shaking to digest the proteins to peptides.

On day two, 1 µg trypsin was added per 100 µg protein and incubated overnight as before. On day 3, acetonitrile was added to the samples before placing on a magnetic rack to remove supernatant. Acetonitrile was added again for 30 seconds before air drying for 15 seconds. Peptides were eluted from the beads by addition of 189 µL of 2% DMSO and sonication (5 minutes, 30 seconds off/on). Samples were placed on magnetic racks and the supernatants containing the peptides were removed and placed into protein low-bind tubes. The samples were centrifuged at max speed in a table-top centrifuge to remove any non-magnetic bead debris and the supernatant was stored at -20ºC overnight. The following day 21 µL of 50% formic acid (5% final concentration) was added. Samples were dried using a SpeedVac (GeneVac) and resuspended in 300 µL 0.1% TFA/1% DMSO.

2.10.3 Fractionation

Samples were fractionated before mass spectrometry to reduce sample complexity in order to increase protein identify. Peptides were fractionated on the basis of their hydrophobicity. The Pierce High-pH Reversed Phase Peptide Fractionation Kit (Thermo) was used according to the manufacturer's protocol. 8 fractions per sample were generated and dried down before mass spectrometry analysis.

2.10.4 Mass Spectrometry Analysis

Mass spectrometry was performed by the FingerPrints Proteomics facility at the University of Dundee as follows. 1 µg of peptide from each fraction was analysed on an Ultimate 3000 RSLCnano system (Thermo Scientific) coupled to a Q Exative HF-X Mass Spectrometer (Thermo Scientific). Samples were injected in

0.1% formic acid. Peptides were trapped on an Acclaim PepMap 100 (C18, 100 µM x 2 cm) and subsequently separated on an Easy-Spray PepMap RSLC C18 column (75 µM x 50 cm) (Thermo Scientific). The mobile phase consisted of 0.1% formic acid (solvent A) and 80% acetonitrile in 0.08% formic acid (solvent B). A constant flow rate of 0.3 µL/min was used. The sample was then transferred to the mass spectrometer via an Easy-Spray source with temperature set at 50ºC and a source voltage of 1.9 kV. A Top 40 method was used for the Q Exative HF-X.

2.10.5 Data analysis

Peptides were searched using MaxQuant Software Version 1.5.8.3 with the assistance of Dr. A. Howden. Proteins were identified using the UniProt database Human2017. Search parameters for fixed modifications included carbamidomethylation of cysteines and variable modifications included methionine oxidation and acetylation of amino termini. Data was filtered to remove any proteins that were identified as contaminants, reverse and only identified by site. Label Free Quantification (LFQ) values were used to compare treatments and further data analysis was done in Excel.

Fold change was calculated by dividing IL-10 treated LFQ values by non-IL-10 treated LFQ values in each donor group. The average fold change was calculated over three donors and the $\log_2$ of this was calculated. For calculation of significance, the $\log_2$ of the fold change between IL-10 stimulated LFQ values and non-IL-10 treated LFQ values for each donor was calculated separately and a two-sample equal variance two tailed t test was used to generate the p value.

2.11 Surface Plasmon Resonance

Surface plasmon resonance (SPR) was used to determine the binding affinity of the recombinantly produced monomeric IL-10 wild type and variants to IL-10Rβ in the presence or absence of IL-10Rα. This was done with the assistance of Dr. P.K. Fyfe. Biotinylated IL-10Rβ was immobilised onto the chip surface via streptavidin. The chips used were Series S Sensor A Chip SA (GE Healthcare). A Biacore T100 (T200 Sensitivity Enhanced) was used for measurement.

Monomeric variants were flowed over the chip in a solution of HBS/ 0.5% BSA/ 0.05% Tween-20. For measurement of IL-10Rβ affinity in the presence of IL-10Rα monomeric IL-10 variants were incubated IL-10Rα and this complex was then flowed over the chip. Serial 1:3 dilutions of ligands were used. Biacore T200 Evaluation Software 3.0 was used for curve fitting for affinity curves and surface bound kinetic curves.

2.12 RNA Sequencing
2.12.1 Cell Stimulation and RNA extraction

The monocytes and CD8 T cells used for RNA sequencing were isolated from human PBMCs purchased from StemCell Technologies. Human primary monocytes from three donors were isolated as described above. Cells were rested in M-CSF containing media (20 ng/mL, Biolegend) for two days. On day two IL-10 wt and variants were added to the cells for 24 hours. Non-adherent cells were removed from media by centrifugation while adherent cells were removed by incubation with Accutase (Sigma) at room temperature for 5-10 minutes. Adherent and non-adherent cell populations were combined and cells were washed in Hank's balanced salt solution (HBSS, Gibco) and snap frozen for storage.

CD8 T cells were isolated by positive selection from three donors as described above. Cells were activated as described above in the presence of IL-10 wt and variants. On day 6 of activation/expansion cells were centrifuge, washed in HBSS and snap frozen for storage.

RNA was isolated using the RNeasy Kit (Qiagen) according to manufacturer's protocol. All RNA A_{260}/A_{280} ratios were above 1.9. 1 µg of RNA per sample was sent to Novogene for RNA sequencing.

2.12.2 RNA sequencing (Novogene)

Transcriptomic analysis was done by Novogene as follows; Sequencing libraries were generated using NEBNext® UltraTM RNALibrary Prep Kit for Illumina® (NEB, USA) following manufacturer's recommendations and index codes were

added to attribute sequences to each sample. Briefly, mRNA was purified from total RNA using poly-T oligo-attached magnetic beads. Fragmentation was carried out using divalent cations under elevated temperature in NEBNext First StrandSynthesis Reaction Buffer (5X). First strand cDNA was synthesized using random hexamer primer and M-MuLV Reverse Transcriptase (RNase H-). Second strand cDNA synthesis was subsequently performed using DNA Polymerase I and RNase H. Remaining overhangs were converted into blunt ends via exonuclease/polymerase activities. After adenylation of 3' ends of DNA fragments, NEBNext Adaptor with hairpin loop structure were ligated to prepare for hybridization. In order to select cDNA fragments of preferentially 150~200 bp in length, the library fragments were purified with AMPure XP system (Beckman Coulter, Beverly, USA). Then 3 µl USER Enzyme (NEB, USA) was used with size-selected, adaptor-ligated cDNA at 37 °C for 15 minutes followed by 5 minutes at 95 °C before PCR. Then PCR was performed with Phusion High-Fidelity DNA polymerase, Universal PCR primers and Index (X) Primer. At last, PCR products were purified (AMPure XP system) and library quality was assessed on the Agilent Bioanalyzer 2100 system.

2.12.3 Data Analysis

Primary data analysis for quality control, mapping to reference genome and quantification was conducted by Novogene as outlined below.

Quality control: Raw data (raw reads) of FASTQ format were firstly processed through in-house scripts. In this step, clean data (clean reads) were obtained by removing reads containing adapter and poly-N sequences and reads with low quality from raw data. At the same time, Q20, Q30 and GC content of the clean data were calculated. All the downstream analyses were based on the clean data with high quality.

Mapping to reference genome: Reference genome and gene model annotation files were downloaded from genome website browser (NCBI/UCSC/Ensembl) directly. Paired-end clean reads were mapped to the reference genome using HISAT2 software. HISAT2 uses a large set of small GFM indexes that collectively cover the whole genome. These small indexes (called local indexes), combined

with several alignment strategies, enable rapid and accurate alignment of sequencing reads.

Quantification: HTSeq was used to count the read numbers mapped of each gene, including known and novel genes. And then RPKM of each gene was calculated based on the length of the gene and reads count mapped to this gene. RPKM, (Reads Per Kilobase of exon model per Million mapped reads), considers the effect of sequencing depth and gene length for the reads count at the same time and is currently the most commonly used method for estimating gene expression levels.

Statistical analysis was done by the author in Excel. The fold change was calculated by dividing the IL-10 stimulated expression levels by the unstimulated control within each donor. The average fold change was calculated across the three donors and the $\log_2$ of this average was then calculated. To calculate significance, the $\log_2$ of the fold change between IL-10–stimulated and IL-10–unstimulated expression levels of each donor was calculated separately and a two sample equal variance two tailed t test was used to generate the p value. The negative $\log_{10}$ of this p value was then plotted against the previously calculated $\log_2$ average fold change. Genes which were significantly ($p \leqq 0.05$) changed greater than 0.6 or less than -0.6 $\log_2$ fold change in the wild type IL-10 dimer (WTD) 50 nM condition were taken as a set list of genes against which all other IL-10 stimulations were compared, regardless of the level of significance in the other IL-10 stimulations. A list of these genes and their fold change can be found in the Appendix tables 1 and 2. Upregulated genes were denoted as genes $\geqq 0.6$ $\log_2$ fold change and downregulated genes were denoted as genes $\leqq -0.6$ $\log_2$ fold change. For comparison of WTD to other IL-10 variant stimulations the average $\log_2$ fold changes of the variant/unstimulated was divided by the average $\log_2$ fold change of WTD/unstimulated. Genes with an RPKM of less than 1 in two or more donors were excluded from analysis so as to remove genes with abundance near detection limit.

Functional annotation of genes (KEGG pathways, GO terms) was done using DAVID Bioinformatics Resource functional annotation tool (Huang da et al., 2009a, Huang da et al., 2009b).

2.13 Real Time Quantitative PCR
2.13.1 RT-qPCR Reactions

RNA was isolated using RNeasy Kit (Qiagen) following manufacturer's protocol. 50 ng RNA per sample was reverse transcribed to cDNA using iScript cDNA synthesis kit (Biorad). This was used as template for qPCR. SYBR premix Ex-Taq (Clontech) was used for the reaction and primers were used at 10 µM final concentration. A CFX96 Touch Real-Time PCR Detection System (Biorad) was used.

2.13.2 Primers

All primers used are listed in table 2.5. Sequence for granzyme B primer was acquired from (Morissette et al., 2007). All primers were ordered from IDT.

Primer Name	Sequence (5'- 3')	Purpose
Granzyme B Fw	TGGGGGACCCAGAGATTAAAA	qPCR
Granzyme B Rv	TTTCGTCCATAGGAGACAATGC	qPCR
GAPDH Fw	ACCCACTCCTCCACCTTTGA	qPCR
GAPDH Rv	CTGTTGCTGTAGCCAAATTGGT	qPCR
18S Fw	GGCCCTGTAATTGGAATGAGTC	qPCR
18S Rv	CCAAGATCCAACTACGAGCTT	qPCR

Table 2.5 Primers used for qPCR

2.13.3 qPCR Data Analysis

GAPDH and 18S were used as housekeeping genes for normalisation. Each sample was done in duplicate. Fold induction was calculated from the Cq values as follows;

$$Relative\ Fold\ Induction = \frac{E_u^{(cq\ uc - cq\ us)}}{E_r^{(cq\ rc - cq\ rs)}}$$

Where E is the efficiency of qPCR, u is the mRNA of interest, c is the non-IL-10 treated control, s is the sample and r is the housekeeping gene.

2.14 Total internal reflection microscopy (TIRF)

All TIRF experiments were conducted by <u>Junel Sotolongo Bellón, University of Osnabrück</u> using wild type and high affinity proteins made by the author in University of Dundee.

Receptor homo- and heterodimerisation was quantified by two-colour single-molecule co-tracking as described previously (Moraga et al., 2015b, Wilmes et al., 2015, Wilmes et al., 2020). Receptor dimerisation experiments were performed in HeLa cells transiently expressing IL-10Rα and IL-10Rβ with N-terminally fused variants of monomeric ECFP and EGFP, respectively. Cell surface Labelling was achieved using anti-GFP nanobodies Minimizer (MI) and Enhancer (EN), respectively, site-specifically conjugated with photostable fluorophores via an engineered cysteine residue. For quantification of receptor heterodimerisation, IL-10Rα and IL-10Rβ were labelled with MI^{Rho11} (ATTO Rho11, ATTO-TEC GmbH) and EN^{AT643} (ATTO 643, ATTO-TEC GmbH), respectively. For quantification of homodimerisation, either IL-10Rα was labelled with MI^{Rho11} and MI^{AT643}, or IL-10Rβ was labelled with EN^{Rho11} and EN^{AT643}. Over-expression of the corresponding other receptor subunit was ensured by labelling with EN^{AT488} or MI^{AT488} (ATTO 488, ATTO-TEC GmbH), respectively. Time-lapse dual-colour imaging of individual IL-10Rα and IL-10Rβ in the plasma membrane was carried out by total internal reflection fluorescence microscopy with excitation at 561 nm and 640 nm and detection with a single EMCCD camera (Andor iXon Ultra 897, Andor) using an image splitter (QuadView QV2, Photometrics). Molecules were localised using the multiple-target tracing (MTT) algorithm (Serge et al., 2008). Receptor dimers were identified as molecules that co-localised within a distance threshold of 150 nm for at least 10 consecutive frames as described in detail previously (Moraga et al., 2015b, Wilmes et al., 2015, Wilmes et al., 2020).

Chapter 3. Generation and biophysical characterisation of IL-10 variants with increased affinity for IL-10Rβ

Background

IL-10 carries out its diverse functions by binding a cell surface receptor comprised of two receptor chains: IL-10Rα and IL-10Rß. In a first step, IL-10 binds to two IL-10Rα subunits with high affinity (picomolar range) (Yoon et al., 2012). Two IL-10Rß chains are then thought to be recruited to the IL-10/IL-10Rα complex in a second step to form the signalling active IL-10 complex. In contrast to its strong affinity for IL-10Rα, IL-10 binds with very weak affinity to IL-10Rß (high micromolar to low millimolar range) (Yoon et al., 2006). Thus, the assembly of the active IL-10 receptor signalling complex is likely rate limited by IL-10's affinity for IL-10Rß. How this IL-10/IL-10Rß low affinity interaction contributes to IL-10's biological activities is poorly understood. To address this question, we have engineered IL-10 variants with increased affinity for the IL-10Rß subunit. We envisioned that these engineered variants would provide us with key molecular insights into the role that complex stability plays in IL-10 biology.

In order to generate high affinity variants, error-prone PCR and yeast surface display was used. Yeast surface display is a powerful methodology which has been harnessed previously for the affinity maturation of cytokines (Mendoza et al., 2017, Martinez-Fabregas et al., 2019, Levin et al., 2012). The secretory apparatus of yeast allows it to display a diverse range of proteins due to its ability to glycosylate proteins and form disulphide bonds (Spangler et al., 2015). Yeast libraries also have the advantage of being amenable to magnetic activated cell sorting (MACS), meaning that large libraries can been screened rapidly and preliminary binding characterisation can be done on-yeast without the need for recombinant protein expression (Spangler et al., 2015, Gai and Wittrup, 2007). IL-10 engineering is challenging due to the dimeric nature of this cytokine. To overcome this limitation, we used a monomeric version of IL-10, previously reported by the Walter group, as a template for our engineering platform (Josephson et al., 2000b).

Aims:

- Generate high affinity variants of IL-10 with increased affinity for IL-10Rβ.
- Recombinantly express wild type and high affinity monomeric and dimeric IL-10 variants.
- Measure binding affinity of recombinant IL-10 variants for IL-10Rβ by surface plasmon resonance (SPR).

3.1 Selection of IL-10 variants with increased affinity for IL-10Rβ using yeast surface display

We used yeast surface display to enhance the binding affinity of monomeric IL-10 for IL-10Rß. First, we confirmed that monomeric IL-10 could be displayed in a native conformation on the yeast surface. Error-prone PCR was then carried out to introduce random mutations into the IL-10 monomer gene to create the library. Selection rounds were performed to select for variants with high affinity for IL-10Rß before sequencing and characterisation of individual yeast clones.

3.1.1 IL-10 monomer can be correctly displayed on the yeast cell surface

Display of ligands on the yeast surface can sometimes alter their original structure and topology leading to misfolded proteins and loss of function. Thus, in a first step, we transfected *Saccharomyces cerevisiae* strain EBY100 with the IL-10 monomer (WTM) to examine its ability to bind both IL-10 receptor subunits in the context of the yeast surface. WTM was displayed as a fusion protein at the C-terminus of the yeast cell surface protein agglutinin (Aga2) which was under the control of a galactose inducible promotor. The yeast were grown in SDCAA (media with glucose as the carbon source) at 30ºC for 24 hours before being changed into SGCAA (media with galactose as the carbon source) and grown at 20ºC for 48 hours to induce the surface display of the WTM. The lower temperature for induction provides slower growing conditions for the yeast, ensuring correct processing of the protein. Both media used lack tryptophan, which allows selection for the transfected clones. Expression of WTM in the yeast surface was monitored using an anti-c-myc tag antibody, that recognizes a c-myc tag encoded at the C-terminus of WTM (Figure 3.1a). Yeast were then incubated with 100 nM of either biotinylated IL-10Rß or biotinylated IL-10Rα, followed by fluorescently labelled streptavidin (AF647) to visualise receptor binding as illustrated in Figure 3.1b. As expected WTM was able to bind IL-10Rα, however it did not bind IL-10Rß, even in the presence of non-biotinylated IL-10Rα (Figure 3.1c). Together these data confirmed that monomeric IL-10 was displayed on the yeast surface and maintained the expected receptor binding properties i.e., high affinity for IL-10Rα and poor affinity for IL-10Rß.
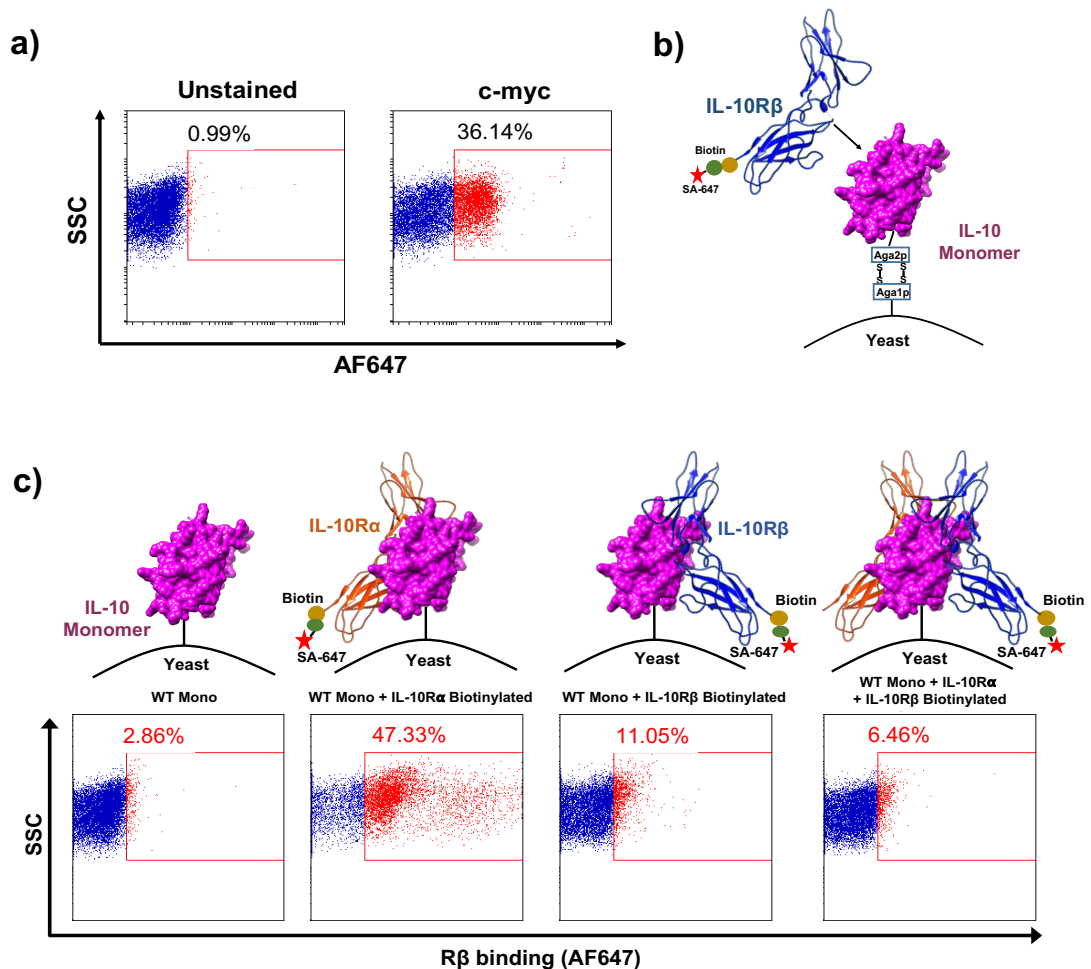
Figure 3.1 Confirmation of WTM yeast display. (a) Yeast displaying the WTM were stained using AF647 anti-c-myc tag antibody to confirm the induction of protein expression on the yeast cell surface. An unstained control is included. **(b)** WTM (purple) was displayed as a fusion protein to the yeast cell surface protein Aga2. The yeast was then incubated with biotinylated IL-10Rß (blue). Binding of IL-10Rß could be detected by flow cytometry using AF647-labelled streptavidin. **(c)** Detection of binding of IL-10Rα (100 nM) and IL-10Rß (100 nM) to yeast displayed WTM. Panel one shows yeast in the absence of receptor as an unstained control. Panel two shows IL-10Rα (biotinylated) binding. Panel three shows IL-10Rβ (biotinylated) binding in the absence of IL-10Rα. Panel four shows IL-10Rβ (biotinylated) binding in the presence of IL-10Rα (non-biotinylated).

3.1.2 Error-prone PCR and generation of an IL-10 monomer yeast display library

Currently we lack a crystal structure of IL-10 binding its beta receptor, precluding us from undertaking a structure-guided library designing approach to affinity mature IL-10. Thus, we used error-prone PCR to insert mutations into the WTM gene in a random and unbiased fashion. Error-prone PCR uses Taq polymerase which has a low fidelity rate which can be further decreased by increasing concentrations of $MgCl_2$, addition of $MnCl_2$ and adjusting the amount of nucleotides added (Cadwell and Joyce, 1992). A final concentration of 7 mM

MgCl$_2$ and 0.15 mM MnCl$_2$ was used in the PCR along with 800 µM each of dCTP and dTTP and a dNTP mixture of 200 µM. To determine the mutation rate, a sample of the PCR product was ligated with the yeast pCT vector and used to transform DH5α *Escherichia coli* cells. The resulting colonies were then screened. Mutations were introduced at a rate of 7-9 nucleotides substations per kilobase (or 4 to 5 mutations per gene) as shown by alignments in Figure 3.2.

```
WT       TCCGAGAACAGTTGCACGCACTTTCCGGGCAACCTTCCTAACATGCTTCGCGACCTGCGA   60
Clone1   TCCGAGAACAGTTGCACGCACTTTCCGGGCAACCTTCCTAACATGCTTCGCGACCTGCGA   60
Clone2   TCCGAGAACAGTTGCACGCACTTTCCGGGCAACCTTCCTAACATGCTTCGCGACCTGCGT   60
Clone3   TCCGAGAACAGTTGCACGCACTTTCCGGGCAACCTTCCTAACATGCTTCGCGACCTGCGA   60
Clone4   TCCGAGAACAGTTGCACGCACTTTCCGGGCAACCTTCCTAACATGCTTCGCGACCTGCGA   60
         ************************************************************

WT       GATGCGTTCTCTCGAGTGAAAACTTTCTTTCAGATGAAAGATCAGTTGGATAATTTGCTC   120
Clone1   GATGCGTTCTCTCGAGTGAAAACTTTCTTTCAGATGAAAGATCAGTAGGATAATTTGCTC   120
Clone2   GATGCGTTCTCTCGAGTGAAAACTTTCTTTCAGTTGAAAGATCAGTAGGATAATTTGCTC   120
Clone3   GATGCGTTCTCTCGAGTGAAAACTTTCTTTCAGATGAAAGATCAGTTGGATAATTTGCTC   120
Clone4   GATGCGTTCTCACGAGTGAAAACTTTCTTTCAGATGAAAGATCAGTTGGATAATTTGCTC   120
         *********** *********************** *********** *************

WT       CTCAAGGAGTCCCTTCTCGAAGACTTTAAAGGATACCTGGGGTGCCAGGCGCTTAGCGAG   180
Clone1   CTCAAGGAGTCCCTTCACGAAGACTTTAAAGGATACCTGGGGTGCCAGGCGCTTAGCGAG   180
Clone2   CTCAAGGAGTCCCTTCTCGAAGACTTTAAAGGATACCTGGGGTGCCAGGCGCTTAGCGAG   180
Clone3   CTCAAGGAGTCCCTTCTCGAAGACTTTAAAGGATACCTGGGGTGACAGGCGCTTAGCGAG   180
Clone4   CTCAAGGAGTCCCTTCTCGAAGACTTTAAAGGATACCTGGGGTGCCAGGCGCTTAGCGAG   180
         *************** ************************** **** *************

WT       ATGATACAGTTCTATCTGGAGGAAGTGATGCCCCAAGCAGAAAATCAAGATCCCGATATT   240
Clone1   ATAAATACAGTTCTATCTGGAGGAAGTGATGCCCCAAGCAGAAAATCAAGATCCCGATATT   240
Clone2   ATGATACAGTTCTATCTGGAGGAAGTGATGCCCCAAGCAGAAAATCAAGATCCCGATATT   240
Clone3   ATGATACAGTTCTATCTGGAGGAAGTGATGCCCCAAGCAGAAAATCAAGATCCCGATATT   240
Clone4   ATGATACAGTTCTATCTGGAGGAAGGGATGCCCCAAGCAGAAAATCAAGACCCGATATT   240
         ** ***************** ****** ************************* *********

WT       AAGGCCCATGTCAACAGCCTTGGCGAAAATTTGAAAACTCTCAGACTCCGACTTCGCCGA   300
Clone1   AAGGCCCATGTCAACAGCCTTGGCGAAAATTTGAAAACTCTCAGACTCCGTCTTCGCCGA   300
Clone2   AAGGCCCATGTCAACAGCCTTGGCGAAAATTTGAAAACTCTCAGACTCCGACTTCGCCGA   300
Clone3   AAGGCCCATGTCAACAGCCTTGGCGAAAATTTGAAAACTCTCAGACTCCGACTTCGCCGA   300
Clone4   AAGGCCCATGTCAACAGCCTTGGCGAAAATTTGAAAACTCTCAGACTCCGACTTCGCCGA   300
         ************************************************** *********

WT       TGCCACAGGTTTTTGCCATGTGAGAATGGGGGTGGTTCCGGGGGTAAGTCCAAGGCCGTT   360
Clone1   TGCCACAGGTTTTTGCCATGTGAGAATGGGGGTGGTTCCGGGGGTAAGTCCAAGGCCGTT   360
Clone2   TGCCTCAGGTTTTTGCCATGTGAGAATGGGGGTGGTTCCGGGGGTAAGTCCAAGGCCGTT   360
Clone3   TGCCACAGGTTTTTGCCATGTGAGAATGGGGGTGGTTCCGGGGGTAAGTCCAAGGCCGTT   360
Clone4   TGCCACAGGTTTTTGCCATGTGAGAATGGGGGTGGTTCCGGGGGTAAGTCCAAGGCCGTT   360
         **** *******************************************************

WT       GAGCAGGTGAAAAACGCTTTCAACAAACTGCAAGAAAAGGGGGATCTACAAAGCGATGTCA   420
Clone1   GAGCAGGTGAAAAACGCTTTCAACAAACTGCAAGAAAAGGGGGATCTACAAAGCGATGTCA   420
Clone2   GAGCAGGTGAAAAACGCTTTCAACAAACTGCAAGAAAAGGGGGATCTACAAAGCGATGTCA   420
Clone3   GAGCAGGTGCAAAACGCTTTCAACAAACAGCAAGAAAAGGGGGATCTACACAGCGATGTCA   420
Clone4   GAGCAGGTGAAAAACGCTTTCAACAAACTGCAAGAAATGGGGGATCTACAAAGCGATGTCA   420
         ********* ***************** ******** ************** *********

WT       GAGTTCGACATATTTATAAACTACATAGAAGCCTATATGACGATGAAAATCCGCAA   476
Clone1   GAGTTCGACATGTTTATAAACTACATAGAAGCCTATATGACGATGAAAATCCGCAA   476
Clone2   GAGTTCGACATATTTATAAACTACATAGATGCCTATATGACGATGAAAATCCGCAA   476
Clone3   GAGTTCGACGTATTTATAAACTACATAGAAGCCTATATGACGATGAAAATCCGCAA   476
Clone4   GAGTTCGACATATTTATAAACTACATAGAAGCCTATATGACGATGAAAATCCGCAA   476
         ********* * **************** ***************************
```

Figure 3.2 Error-prone PCR. Sequence alignment (DNA) of wild type IL-10 monomer with four clones used to confirm the error rate of the PCR. WT sequence is in bold and mutations are highlighted in red. Each clone contained 4-5 mutations.

This was an optimal number as too high a rate increases the chances of either nonsense mutations or mutations which may affect the folding or expression of the protein, however too few mutations would result in a poorly diverse library. The PCR product was then amplified and electroporated into yeast along with the linearized pCT vector in order to generate the IL-10 monomer yeast display library.

3.1.3 Screening of the IL-10 monomeric yeast display library

We successfully generated an IL-10 yeast library with approximately 2×10^8 display variants. This was estimated by titrating a sample of the electroporated culture on SDCAA plates. The library underwent several rounds of screening with the first two rounds used to ensure proper functioning of the library and the subsequent rounds used to affinity mature IL-10 for IL-10Rß. A summary of the conditions used for each screening round is shown in Figure 3.3a.

a)

Round 1: SAV-IL-10Rβ clearing
Round 2: Selection for c-myc expression
Round 3: 1 µM IL-10Rβ plus 100 nM IL-10Rα
Round 4: 300 nM IL-10Rβ plus 100 nM IL-10Rα
Round 5: 50 nM IL-10Rβ plus 100 nM IL-10Rα
Round 6: 500 nM IL-10Rβ
Round 7: 100 nM IL-10Rβ
Round 8: 20 nM IL-10Rβ

[IL-10Rβ]

b)

SA-647

IL-10 Monomer

Yeast

MACS Column

Pre-Separation   Flow Through   Eluate

0.92%   0.89%   4.85%

SSC

AF647
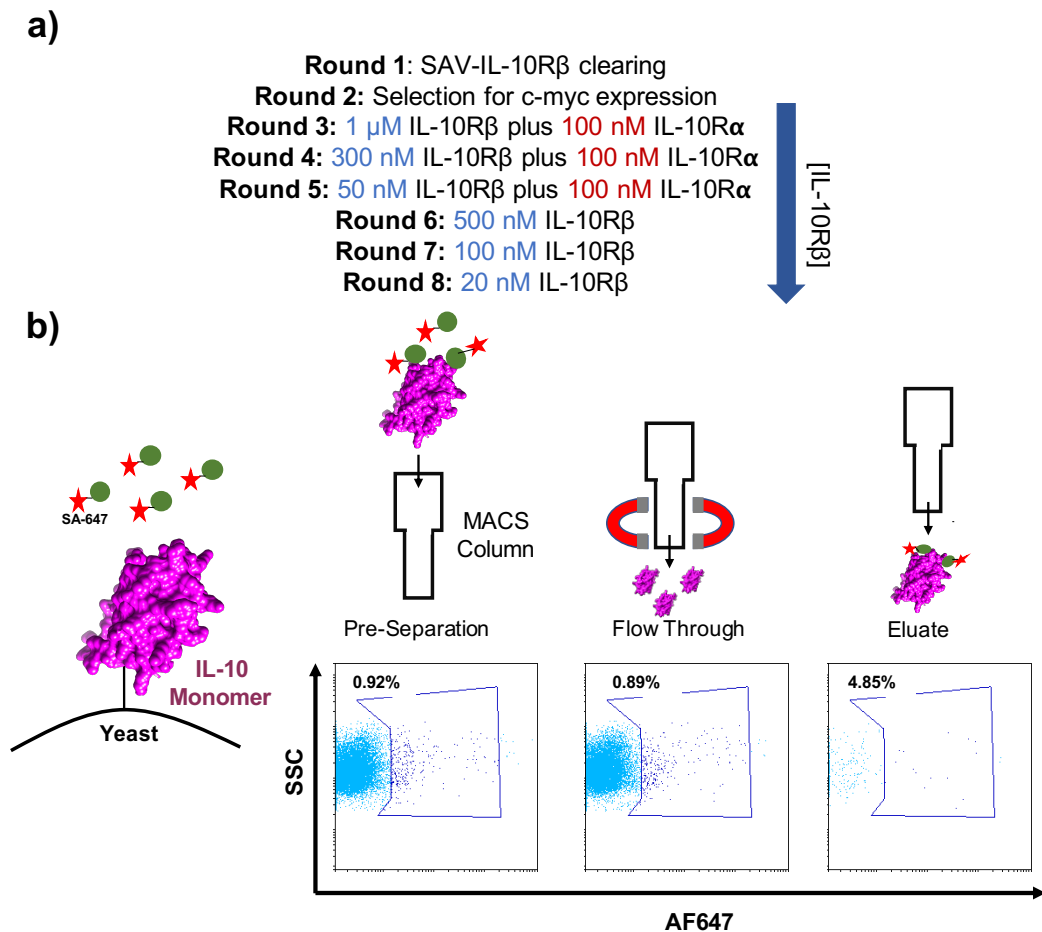
Figure 3.3 Screening of the IL-10 yeast library. (a) Schematic outlining the conditions used in each selection round. Concentrations of IL-10Rß were decreased as selection progressed. IL-10Rα was not biotinylated. **(b)** Representative FACS plots for negative selection of streptavidin binders. For negative selection the yeast were incubated with 500 nM fluorescently labelled streptavidin (SA647) followed by incubation with anti-AF647 magnetic beads. Panel one shows the yeast after incubation with SA647, before MACS. The flow through (panel two) contained yeast negative for streptavidin binding and these were brought forward for positive selection. Panel three contains the eluate, yeast which were positive for streptavidin binding which were discarded. This negative selection process was repeated at the beginning of each round of selection.

Each screening round started with a negative selection clearing step, followed by a positive selection step. The negative selection was performed by incubating the yeast with 500 nM fluorescently labelled streptavidin (SA-AF647) (Figure 3.3b).

The mixture was washed and then incubated with anti-AF647 microbeads. Magnetic activated cell sorting (MACS) technology was used. The yeast were added to the MACS column and the column was washed several times. The flow through contained yeast which did not bind streptavidin. The column was then removed from the magnet and any yeast which displayed an affinity for streptavidin in the absence of biotinylated protein were removed in the eluate. The flow through was then taken forward for positive selection.

Round 1:

The first positive selection round had the aim of recovering all positive binders in the library while also reducing the complexity of the library. Streptavidin microbeads (SAV) were pre-incubated with 400 nM biotinylated IL-10Rß. These microbeads have very high avidity as each bead has thousands of streptavidin molecules bound to it and each streptavidin molecule has the capability of binding between 1 to 4 biotinylated IL-10Rß proteins (Figure 3.4a).
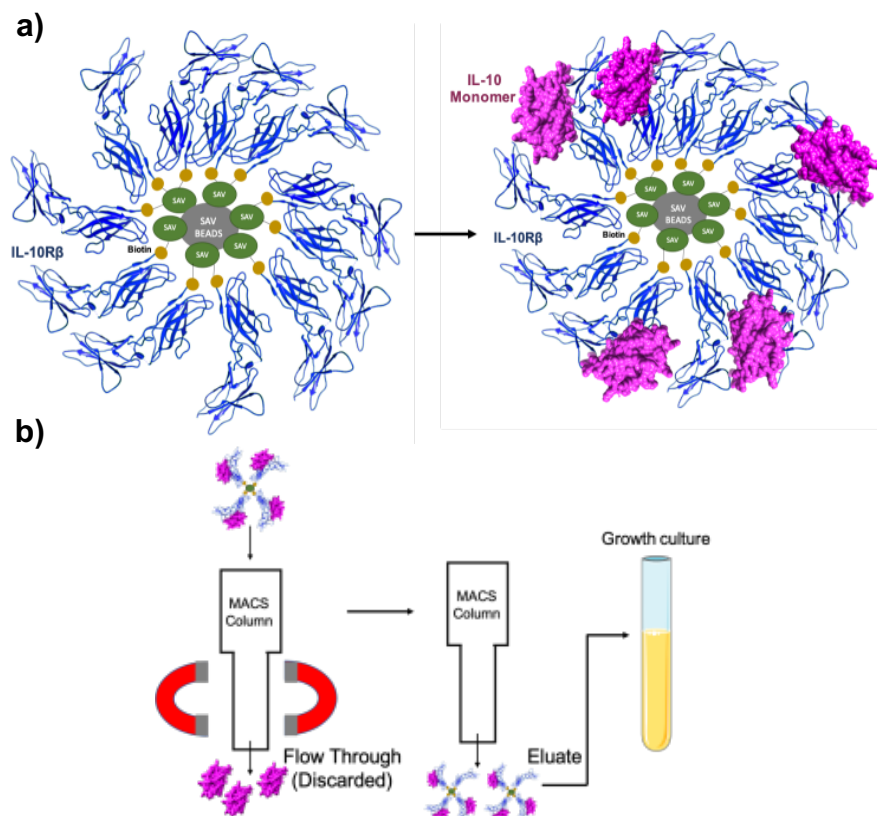
Figure 3.4 Magnetic activated cell sorting of yeast library. (a) Each streptavidin microbead (SAV) can bind many biotinylated proteins i.e. biotinylated IL-10Rß. The streptavidin/IL-10Rß complexes are then incubated with the yeast-displayed IL-10 proteins. **(b)** The yeast/IL-10Rß/SAV mixture is added to the MACS column and placed within a magnetic field. Yeast which display IL-10 variants incapable of binding IL-10Rß flow through and are discarded. The column is removed from the magnet and yeast which display IL-10 variants bound to IL-10Rß are eluted and placed in culture for further growth.

This significantly reduces the amount of reagent needed in this round where large numbers of yeast were used. After incubation of the streptavidin microbeads with the biotinylated protein they were then added to the yeast flow through from the negative selection. Another round of MACS was performed (3.4b). Here the eluted yeast were kept as these displayed IL-10 variants capable of IL-10Rß binding. The yeast were grown in SDCAA (glucose) media for 24 hours and then transferred to SGCAA (galactose) media for 2 days before the next round of selection.

Round 2:

The second round was a selection for the c-myc tag which was expressed at the C-terminus of the yeast-displayed IL-10. This ensured that any IL-10 displayed on the yeast was full length. Again, a negative selection clearing step was performed first to remove any streptavidin binders, as was done for round 1. Following this, the yeast in the flow through were incubated with an Alexa Fluor 647 (AF647) anti-c-myc antibody, followed by incubation with anti-AF647 magnetic beads (Figure 3.5a). The population had roughly 18% of yeast positive for c-myc before MACS (Figure 3.5b). Yeast which were negative for c-myc were removed in the flow through as shown in Figure 3.5c. The eluted fraction was enriched for yeast positive for c-myc (Figure 3.5d). This population was then cultured as described above before beginning the affinity maturation selection rounds.
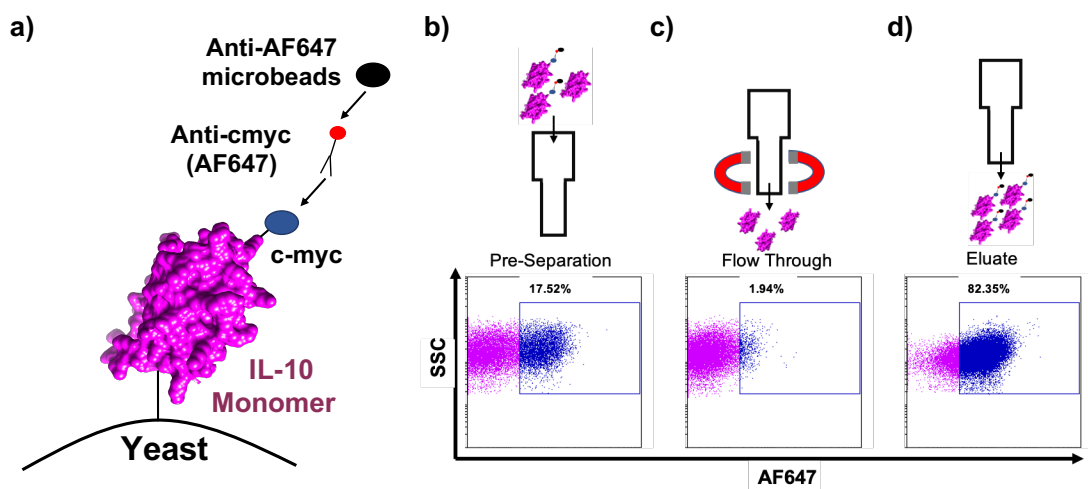
Figure 3.5 Positive selection for c-myc. (a) c-myc tag is expressed at the C-terminus of the yeast-displayed IL-10 monomer. The yeast are incubated with an anti-c-myc antibody (AF647) followed by incubation with anti-AF647 microbeads. **(b)** Visualisation of yeast positive for c-myc before MACS. **(c)** Yeast negative for c-myc are removed in the flow through. **(d)** Yeast positive for c-myc are recovered in the eluate.

3.1.4 Affinity maturation of IL-10 for IL-10Rß

Once the complexity of the library was reduced and it was confirmed that the IL-10 variants being displayed were full length, affinity maturation selection could then be commenced. Conditions for each selection round are shown in Figure 3.3a. As before, each round started with a negative selection step to remove any yeast which could bind streptavidin in the absence of biotinylated protein. The flow through was taken forward for positive selection. In the positive selection step, the yeast were pre-incubated with a known concentration of biotinylated IL-10Rß before addition of fluorescently labelled streptavidin (AF647) (Figure 3.6a).
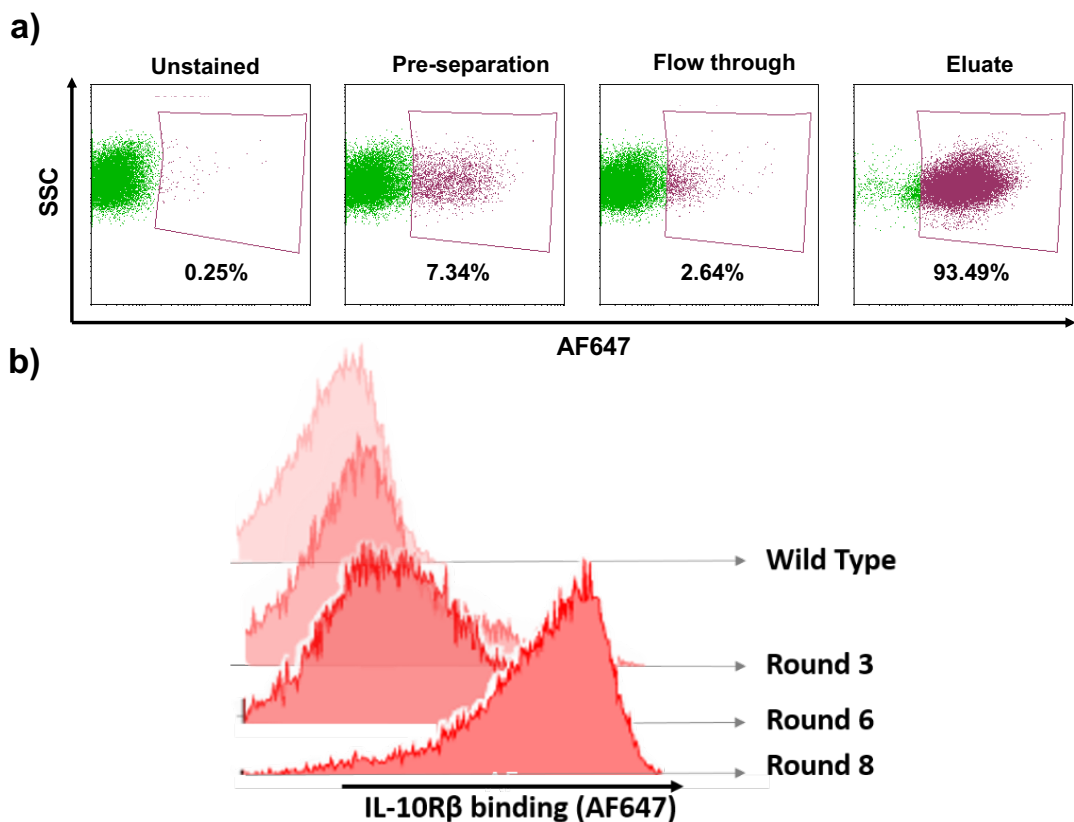
Figure 3.6 Affinity maturation of IL-10 for IL-10Rß using yeast display (a) Example of the positive selection used in each affinity maturation round. The yeast isolated in the flow through of the negative streptavidin MACS are washed and incubated with biotinylated IL-10Rß. This is followed by incubation with SA647 and anti-AF647 beads. MACS is performed again. The eluate contains yeast capable of binding IL-10Rß. **(b)** Representative histograms of IL-10Rß binding (AF647) of yeast displayed wild type IL-10, round 3 selection, round 6 selection and round 8 selection. Yeast from each round were incubated with 1 µM IL-10Rß, followed by staining with SA647. As the library selection proceeds the IL-10Rß staining improves.

This was then incubated with anti-AF647 microbeads for a second round of MACS. The yeast which bound IL-10Rß were recovered in the eluate. The eluted yeast were grown and induced over three days as previously described before

commencing the next round of selection. This positive selection procedure commenced with a 1 μM concentration of biotinylated IL-10Rβ as well as 100 nM non-biotinylated IL-10Rα to stabilise the surface complex and recover low affinity binders. Each selection round used decreasing concentrations of IL-10Rβ as shown in Figure 3.3a and by round 6 the yeast-displayed IL-10 variants were able to bind IL-10Rβ without the need for IL-10Rα. After 8 rounds of selection the library was able to bind nanomolar concentrations of IL-10Rß. Figure 3.6b shows a representative histogram of IL-10Rβ binding by the library throughout the selection rounds, visualised by flow cytometry using fluorescently labelled streptavidin (AF647). The shift in fluorescence demonstrates the biasing of the library towards variants which display enhanced affinity for IL-10Rβ.

3.1.5 Characterisation of yeast-displayed high affinity clones

After 8 selection rounds, single yeast colonies were grown by spreading on SDCAA (glucose) agar plates. An initial screen was done to select colonies which displayed enhanced IL-10Rß binding. 24 single yeast colonies (12 from round 7 and 12 from round 8) were grown in SDCAA (glucose) media for 24 hours and induced in SGCAA (galactose) media for 2 days. These cultures were then incubated with 100 nM IL-10Rß (biotinylated) followed by addition of streptavidin-AF647. Comparative binding between the 24 colonies was assessed by flow cytometry. 6 colonies (A1, A8, A11, B5, B10, B11) showed promising binding patterns (Figure 3.7a). These colonies were sent for DNA sequence analysis. Two unique variants were identified: A11 and B11, indicating convergency of the library. Sequence comparison with the wild type IL-10 monomer showed mutations at several points in the sequence, many of which were conserved between the variants indicating possible areas of importance for IL-10Rβ binding e.g. N36Y, N110I. (Figure 3.7b).

To get an estimation of the apparent binding affinity of the IL-10 variants for IL-10Rß an on-yeast binding dose response study was performed. A11 and B11 showed a large increase in affinity for IL-10Rß compared to the WT (Figure 3.7c). In order to confirm that the variants maintained binding to IL-10Rß in the presence of IL-10Rα the dose response was repeated using biotinylated IL-10Rβ as well as a constant concentration of IL-10Rα (non-biotinylated) to mimic the natural

stepwise binding pattern of IL-10. Figure 3.7c shows that there was a decrease in IL-10Rß binding in the presence of IL-10Rα. This suggested that the introduced mutations may be contributing to competition for binding between IL-10Rß and IL-10Rα receptor subunits on the yeast surface, perhaps due to a change in the binding topology of the complex.

a)

b)

WT	N36	D73	I87	N110	N115	K117	R128	N172
A11	Y			I		N		H
B11	Y	V	M	I	K		W	

c)
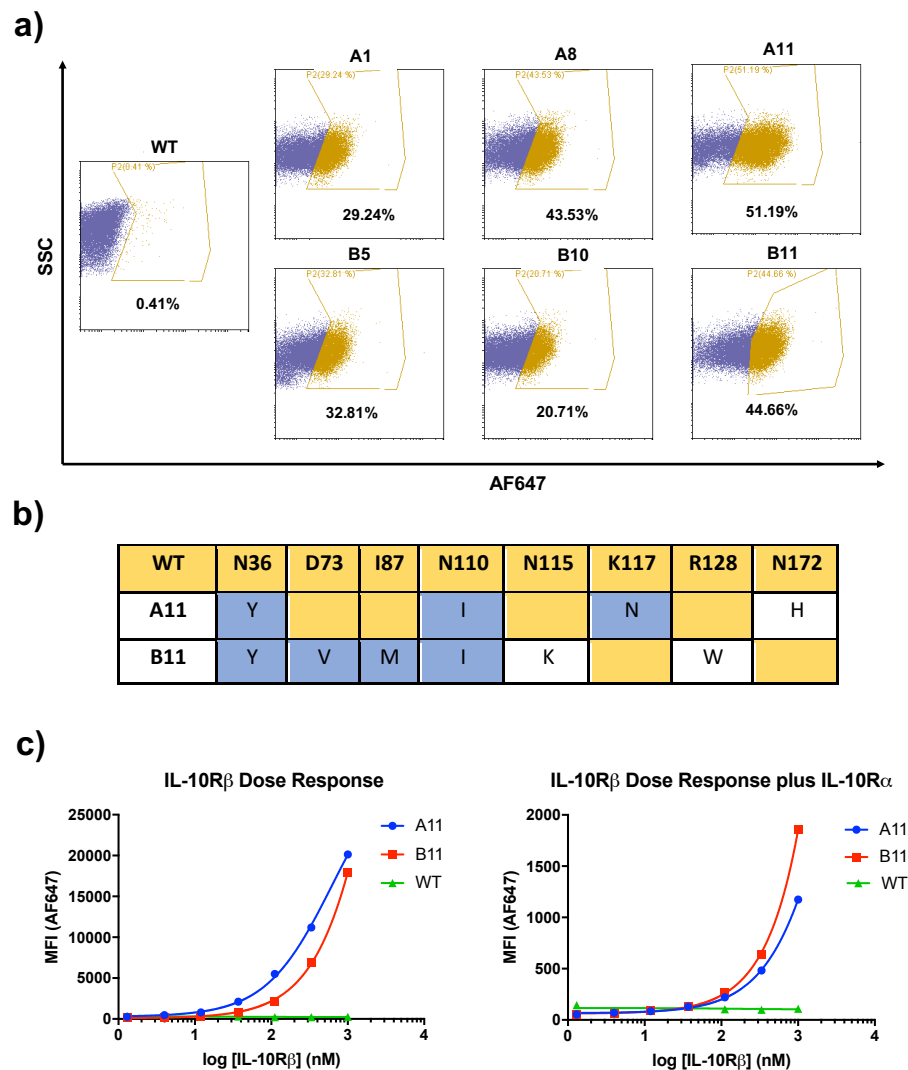
Figure 3.7 Selection and screening of colonies. (a) 24 individual colonies from round 7 and round 8 of selection were incubated with 100 nM of biotinylated IL-10Rß followed by incubation with SA647. Binding of the yeast colonies to IL-10Rß is indicated by increased AF647 fluorescence. WT monomeric yeast on the left is compared to the 6 colonies which showed enhanced affinity for IL-10Rß. **(b)** Table for amino acid changes found in high affinity variants. Wild type sequence is shown in yellow and is based on the amino acid sequence reported for IL-10 on the UniProt database (P22301), with the addition of the 6 amino acid linker at position 134 allowing the formation of the monomer. Conserved changes between mutants are shown in blue. Individual mutations are shown in white. **(c)** Yeast displayed IL-10 mutants A11 and B11 and wild type monomer were incubated with three-fold serial dilutions of biotinylated IL-10Rβ, top concentration 1 µM. Receptor binding was visualised and quantified using AF647 labelled streptavidin. Panel 2 shows yeast treated as in panel 1 with un-biotinylated IL-10Rα added at a constant concentration of 100 nM.

In order to retain the natural affinity for IL-10Rα we returned to the 5ᵗʰ round of selection, the last round where a constant concentration of IL-10Rα had been used during the screening (Figure 3.3a). From this round we plated and isolated colonies and screened them against IL-10Rß in the presence of non-biotinylated IL-10Rα. The dose responses are shown in Figure 3.8a. All R5 clones showed weaker responses to IL-10Rß alone compared to A11 and B11, however their IL-10Rß binding was significantly improved upon the addition of IL-10Rα, mimicking

a)

IL-10Rβ Dose Response — IL-10Rβ Dose Response plus IL-10Rα

b)

WT	F33	N36	N73	I87	Q88	N100	N110	N115	K117	R120	H127	R128	F129	N172	I174
A11		Y					I		N					H	
B11		Y	V	M			I	K				W			
R5A2	L						I		N						L
R5B2		H				I	I		N						
R5A4		Y							N			N			
R5B4							I			D	S				
R5A8		Y			L				N						
R5A11		I					I		N				L		

Round 8: A11, B11

Round 5: R5A2, R5B2, R5A4, R5B4, R5A8, R5A11

c)

WT IL-10 — Helix A, Helix D — IL-10Rβ binding site

R5A11 — N110I, K117N, F129L, N36I
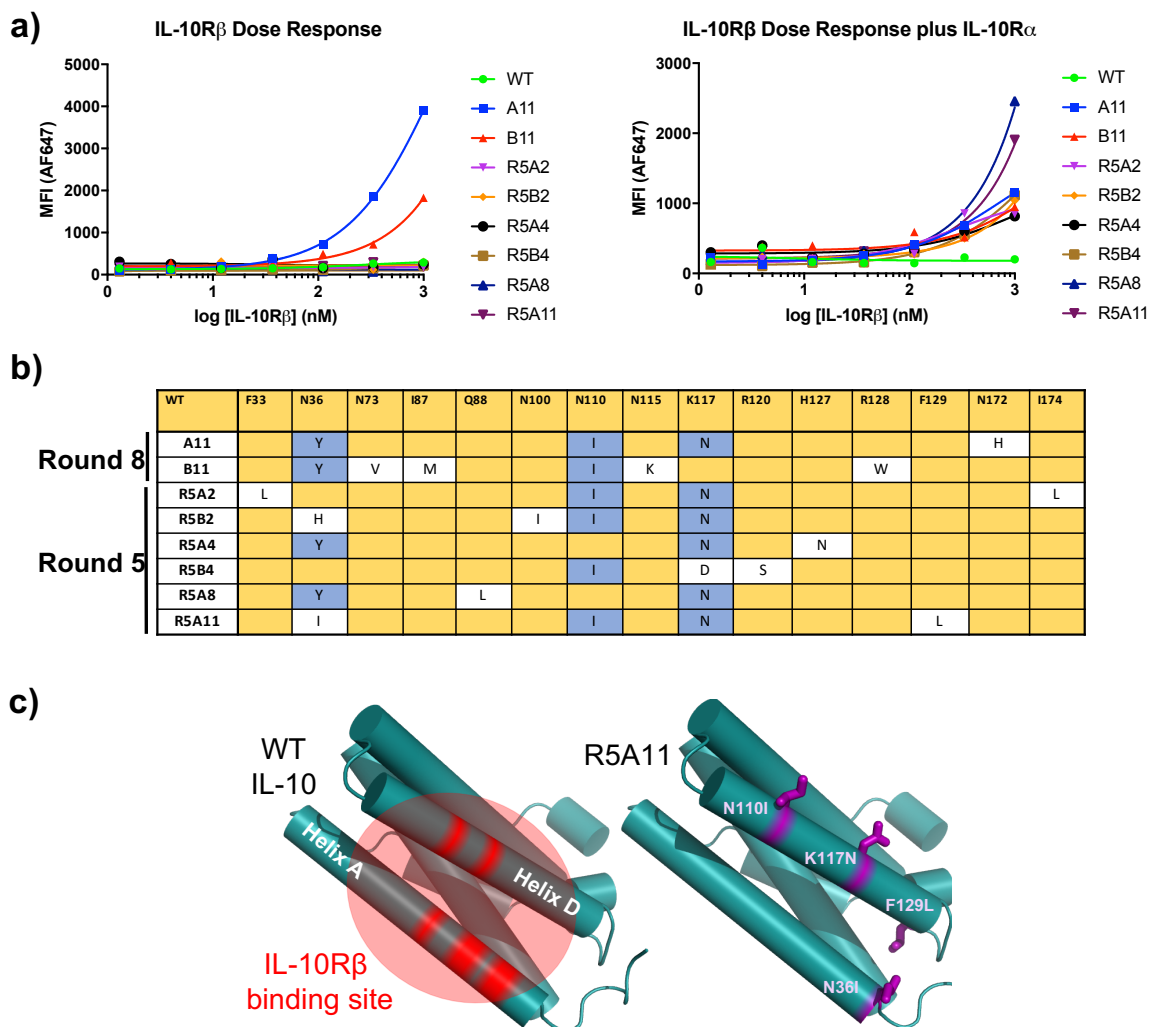
Figure 3.8 Round 5 colonies (a) Yeast displayed IL-10 mutants A11 and B11 and wild type monomer along with variants from round 5 (R5) were incubated with three-fold dilutions of biotinylated IL-10Rβ, top concentration 1 µM. Receptor binding was visualised and quantified using AF647 labelled streptavidin. Panel 2 shows yeast treated as in panel 1 with un-biotinylated IL-10Rα added at a constant concentration of 100 nM. **(b)** Table for amino acid changes found in high affinity variants. Wild type sequence is shown in yellow and is based on the amino acid sequence reported for IL-10 including on the UniProt database (P22301) with the addition of the 6 amino acid linker at position 134 allowing the formation of the monomer. Conserved changes between mutants are shown in blue. Individual mutations are shown in white. (**c**) Cartoon representation of wild type IL-10 and R5A11 with the predicted IL-10Rβ binding site in red and mutations highlighted in purple.

a natural IL-10 binding pattern. These round 5 variants were sequenced and their mutations are displayed in Figure 3.8b.

Many of the mutations are conserved between both round 5 and round 8 variants, in particular mutations at N36, N110 and K117. The majority of these conserved mutations occurred along the A and D helices of IL-10, highlighted in Figure 3.8c. This is the area previously predicted to be the IL-10Rβ binding site (Mendoza et al., 2017, Yoon et al., 2010), validating the selection process. In summary, several high affinity IL-10 variants were successfully generated using a yeast display affinity maturation library. These variants were taken forward for further characterisation.

3.2 Recombinant expression of wild type and mutant IL-10 in monomeric and dimeric form

After screening of the yeast library clones, we had several high affinity variants to take forward for further biophysical analyses. We chose to take forward A11, B11 and R5A11 based on their IL-10Rß binding patterns. We firstly needed to recombinantly express these proteins in addition to the wild type IL-10. The monomeric IL-10 variants were cloned into the baculovirus system and expressed in insect cells as described in the Materials and Methods. Proteins contained a His tag at the C-terminus and were purified by batch binding using Ni-NTA agarose beads and eluted in a high concentration imidazole buffer. Size exclusion chromatography was then used to further purify the proteins. The chromatograms for size exclusion chromatography for the A11 and B11 variants are shown in Figure 3.9a.

In addition to the monomeric variants, we wanted to express the variants in the natural dimeric conformation. This would allow us to use wild type dimeric IL-10, wild type monomeric IL-10, high affinity dimeric variants and high affinity monomeric variants in further characterisation studies. By having both the monomeric and dimeric forms of IL-10 we could examine how receptor stoichiometry as well as receptor affinity influence IL-10 activities. Of the variants we chose R5A11 to express in the dimeric conformation due to its apparent enhanced ability to bind IL-10Rß in the presence of IL-10Rα, mimicking the natural binding pattern of IL-10 as well as its favourable expression profile.

In order to recombinantly express the dimeric forms of the high affinity variants, the 6 amino acid linker between helices D and E was removed during cloning into the recombinant expression vectors to allow the protein to form its domain swapped dimer conformation. However, using insect cell expression for the dimeric versions of the proteins gave poor yields. The wild type IL-10 dimer had previously been expressed in bacterial cells via inclusion bodies (Zdanov et al., 1995) and so this was the approach taken forward. As shown in Figure 3.9b, when R5A11 and wild type IL-10 were recombinantly expressed and run in a gel filtration column there was a clear distinction between the monomeric and dimeric versions.
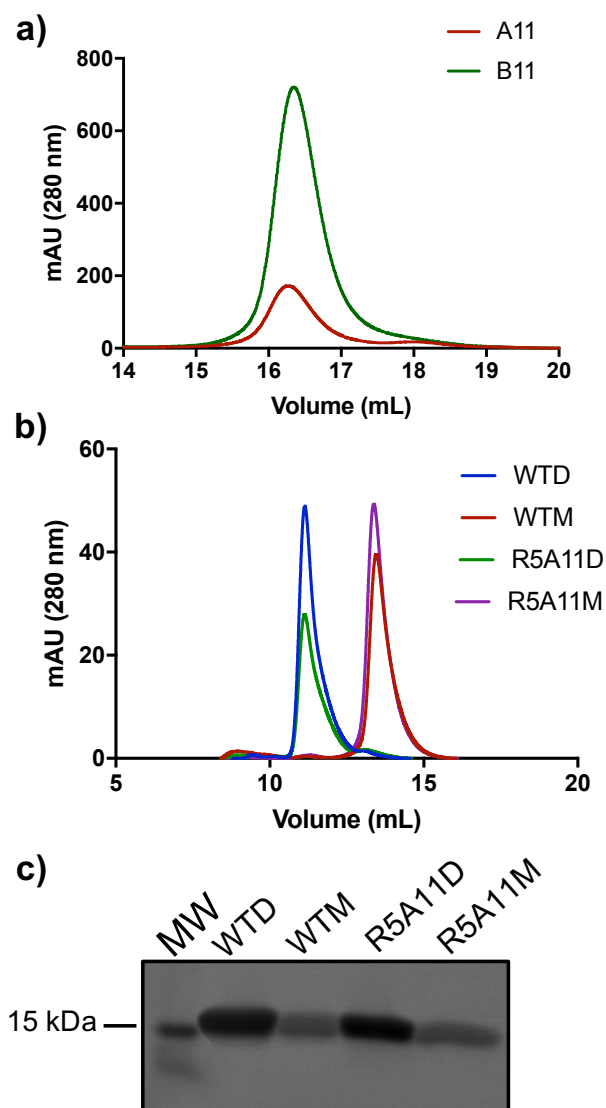
Figure 3.9 Recombinant expression of wild type and high affinity IL-10 monomeric and dimeric variants. (a) Gel filtration chromatogram for monomeric high affinity variants A11 and B11. Proteins were run on an S200 column. **(b)** Gel filtration chromatogram for wild type and variant monomer and dimer. Proteins were run on a S75 column **(c)** A sample of the gel filtration-purified proteins were run on a 10% SDS-PAGE gel. Lane one contains the molecular weight marker (MW).

When run on a reducing SDS-PAGE gel, dimeric and monomeric proteins ran at the same molecular weight as expected (Figure 3.9c). We used these monomeric and dimeric high affinity variants to compare against the monomeric and the dimeric wild type IL-10 in further biophysical and bioactivity studies.

3.3 Engineered IL-10 variants bind IL-10Rβ with nanomolar affinities

To validate the apparent binding affinities seen in the on-yeast binding titration experiments, surface plasmon resonance (SPR) was performed using the recombinantly produced cytokines. SPR studies were done using the monomeric version of IL-10 (wild type and high affinity variants). The monomeric versions were chosen as they provided a monovalent ligand flow on the Biacore chip. This gave a 1:1 ratio of ligand: receptor binding, allowing binding curves to be fitted. The dimeric forms of IL-10 are bivalent ligands and rebinding may have occurred if these were used, leading to inaccurate K_D measurements.

3.3.1 Affinity measurement of wild type and variant IL-10 binding to IL-10Rß

Biotinylated IL-10β was immobilised onto the chip surface through attachment to streptavidin molecules on the chip surface. Monomeric wild type and high affinity IL-10 variants were then flowed across the chip in solution (Figure 3.10a). At the range of doses used here (13-0.06 μM) we could not detect substantial binding of wild type monomeric IL-10 (WTM) to IL-10Rβ, in agreement with IL-10's previously reported weak affinity for IL-10Rβ (Figure 3.10b, c). The upper concentration of all variants was determined and limited by recombinant protein yield. High affinity variants A11, B11 and R5A11 were tested for IL-10Rβ binding under the same conditions as the wild type. All variants were capable of binding IL-10Rβ at the concentrations tested (Figure 3.10b, c). High affinity variants bound with a K_D value in the low micromolar range (Figure 3.10b). This confirmed the on-yeast dose response studies, validating that our IL-10 variants were capable of enhanced IL-10Rβ binding compared to wild type. Although R5A11 did not display binding affinity for IL-10Rß in the absence of IL-10Rα in the on-yeast dose responses, it showed comparable affinity with A11 and B11 in SPR. This discrepancy may be due to increased steric hinderance when the proteins are displayed on the yeast surface or poor sensitivity of the yeast dose response studies at the concentrations used.
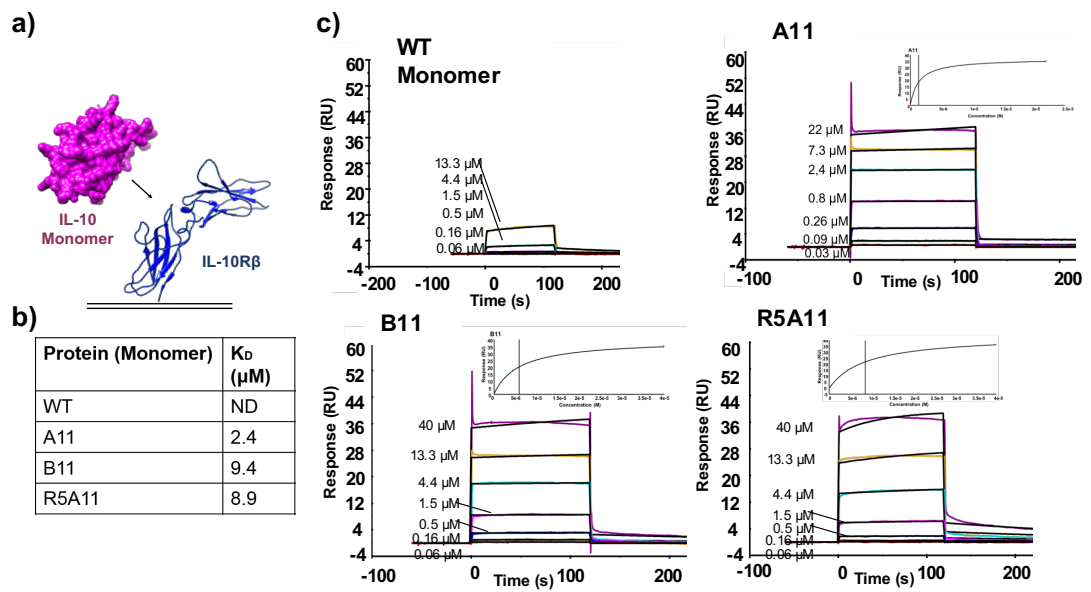
Figure 3.10 Measurement of binding affinity of monomeric variants to IL-10Rß (a) For SPR measurement IL-10Rβ is immobilised on the chip surface via a biotin-streptavidin interaction and IL-10 variants are flowed across the chip in solution. **(b)** K_D values for IL-10Rβ binding for wild type and high affinity variants. ND= no data measured. **(c)** Kinetic charts for IL-10Rβ binding for wild type and high affinity IL-10 with inserts for equilibrium analysis. Concentrations used are shown on curves.

3.3.2 High affinity IL-10 variants retain cooperative receptor binding patterns

IL-10 displays cooperative binding to its receptor subunits whereby its affinity for IL-10Rβ is increased once pre-bound to IL-10Rα (Walter, 2014). To confirm that the affinity matured IL-10 variants retained this cooperative binding property we repeated SPR measurements using the IL-10 wild type and high affinity variants pre-bound to soluble IL-10Rα (Figure 3.11a). We could not detect significant binding of the wild type IL-10 monomer/IL-10Rα complex to IL-10Rβ, again mimicking what was seen in yeast-displayed wild type IL-10 (Figure 3.11b, c). All the high affinity variants tested exhibited enhanced binding to IL-10Rβ when pre-bound to IL-10Rα, with K_D values in the nanomolar range: A11= 23 nM, B11= 170 nM, R5A11= 50 nM (Figure 3.11b, c). This confirmed that the high affinity variants maintained a cooperative binding pattern and suggested that the canonical IL-10 receptor complex binding topology had not been perturbed by the mutations introduced. This was in contrast to what was observed in the yeast where A11 and B11 had reduced binding affinity to IL-10Rß when IL-10Rα was present. This

may be due to increased steric hinderance when the proteins were displayed on the yeast surface.
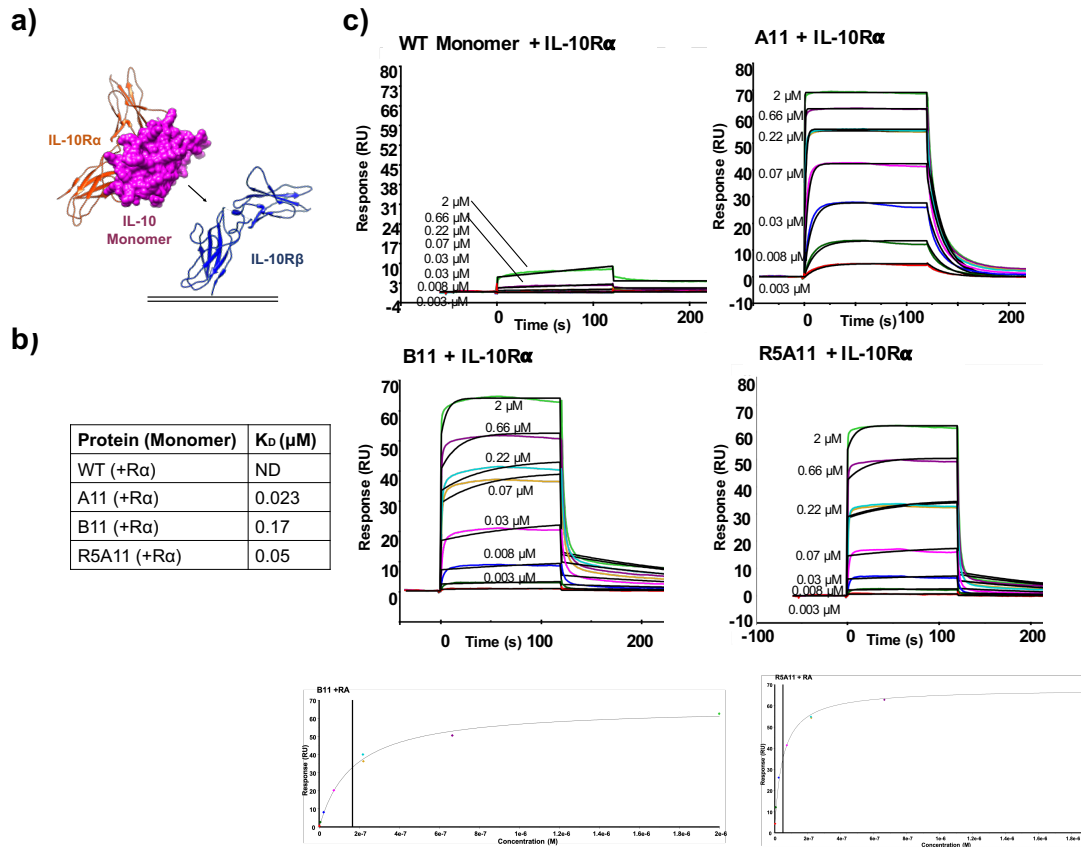
Figure 3.11 Measurement of binding affinity of monomeric variants to IL-10Rß in the presence of IL-10Rα **(a)** IL-10Rβ is immobilised on the chip surface and IL-10 variants pre-bound to IL-10Rα are flowed across the chip surface in solution. Concentrations used are shown on curves. **(b)** K_D values for IL-10Rβ binding when IL-10 proteins are pre-bound to IL-10Rα. **(c)** Kinetic curves for IL-10Rβ binding in the presence of IL-10Rα. Affinity curves are included for B11 and R5A11 due to the poor fit of the kinetic curves.

3.4 Discussion

Protein engineering techniques have previously been used to successfully affinity mature cytokines for their receptors, for example in the cases of IFN-α2, IFN-λ, IL-13 and IL-2 (Mendoza et al., 2017, Moraga et al., 2015a, Levin et al., 2012, Kalie et al., 2007). These affinity matured variants act as tools with which to investigate how early events in cytokines' interactions with their receptors can shape the cellular response. Thus far no attempt had been made to enhance IL-10's receptor affinity, despite its poor affinity for IL-10Rβ. This may be due to the dimeric nature of the cytokine which makes manipulation by protein engineering difficult. By using the monomeric version of IL-10 generated previously (Josephson et al., 2000b) as a template we overcame this difficulty. We could then investigate the biophysical properties of high affinity IL-10 in both a monomeric and dimeric conformation.

Amino acid mutations in high affinity IL-10 variants give insight into the IL-10/IL-10Rß binding interface

Here we used error-prone PCR and yeast surface display to affinity mature monomeric IL-10 for IL-10Rß. When the sequences of the high affinity variants were compared to wild type IL-10 many of the mutated residues were highly conserved. In particular residues N36, N110 and K117 were mutated in nearly all variants. The majority of the conserved mutations occurred on the outward facing amino acids, suggesting that the structure of the cytokine remained intact with no changes to the hydrophobic core. Without a structure of IL-10 bound to IL-10Rß no definitive conclusions can be drawn about the nature of the mutations and how they enhance binding. However, by comparing the sites where the mutations arise with previously published models of IL-10Rß binding we can see that these conserved mutation sites occurred primarily along the A and D helices of IL-10 which has been reported to be the IL-10Rß binding site (Pletnev et al., 2005). Previous studies used IL-10Rß alanine mutants as well as computational docking models to examine the IL-10/IL-10Rß binding interface (Yoon et al., 2010, Yoon et al., 2006). Here helices A and D were identified as a probable IL-10Rß binding site, in particular M40, a hydrophobic residue, was identified as the centre of the interface which interacts with Y82 on loop 3 of IL-10Rß. This is close to N36 which

was mutated to tyrosine in variants A11 and B11 and to isoleucine in R5A11. Both tyrosine and isoleucine have hydrophobic side chains, similar to methionine at position 40, suggesting that this conversion to a hydrophobic residue may be important for binding. In addition, N110 is converted to isoleucine in all high affinity variants from our library. This residue is beside S111 which was previously shown to make contact with Y56 on IL-10Rß (Yoon et al., 2010). This conversion of a polar residue to a hydrophobic residue may allow tighter binding through expansion of the hydrophobic pocket where IL-10Rß docks.

Other studies have modelled IL-10/IL-10Rß binding by using IL-10Rß's property as a shared cytokine receptor between IL-10, IL-22 and IFN-λ. Modelling of the IL-10/IL-10Rß binding interface based on the binding of IFN-λ3/IL-10Rß also predicted binding sites on helices A, C and D of IL-10 (Mendoza et al., 2017). Despite the lack of conservation between the sequences of IFN-λ3, IL-22 and IL-10 which map to the IL-10Rß binding site, Mendoza et al. showed that they do share common hydrophobic areas which contact the tyrosine residues of IL-10Rß predicted to be involved in binding (Y59, Y82, Y140), again highlighting the importance of these hydrophobic areas for IL-10Rß binding.

Previous work on the human growth hormone (hGH) has shown that increased affinity can arise from "energetic remodelling" of the complex due to a combinatorial effect of several mutations (Pal et al., 2005, Spangler et al., 2015). Shotgun alanine scanning of hGH demonstrated that it was an additive effect of several interactions which form the site I interaction between hGH and its receptor. Therefore, while analysis of the positions of the mutations arisen in the high affinity variants can give insight into the IL-10Rß binding site we must be cautious about assigning the increased affinity to any one residue substitution without a crystal structure of the mutant IL-10/IL-10 receptor complex to inform us of the specific cytokine-receptor interactions.

Another aspect to consider when examining the effect of amino acid substitutions to IL-10 receptor affinity is the viral IL-10 homolog produced by the Epstein-Barr virus, ebvIL10, which has 84% amino acid sequence similarity with human IL-10 (Moore et al., 1990). The main differences in sequence are at the N terminus, the AB loop and the CD loop. EbvIL-10 mimics human IL-10's anti-inflammatory

properties in its ability to inhibit proinflammatory cytokine production and antigen presentation from monocytes (de Waal Malefyt et al., 1991). However, it is unable to stimulate proliferation of mast cells or the upregulation of MHC II on murine B cells, suggesting that its differences at the amino acid levels translate into functional differences (Vieira et al., 1991, Go et al., 1990). In addition it was shown that ebvIL10 has much lower affinity for IL-10R1 than human IL-10 (Liu et al., 1997). Work by Ding et al. showed that, similar to human IL-10, ebvIL-10 does not bind to IL-10Rß alone (Ding et al., 2001). This work also demonstrated that the poor responses of ebvIL-10 could be restored to human IL-10 levels by increasing levels of IL-10Rα on the cell surface. It was later shown that this is due to the ebvIL-10 displaying monomeric IL-10Rα binding properties at low IL-10Rα levels, which is restored to dimeric binding at high IL-10Rα levels (Yoon et al., 2012). The altered amino acid residues in ebvIL-10 compared to human IL-10 resulted in a change in binding energy and kinetics to IL-10Rα however, replacing single ebvIL-10 amino acids with human IL-10 amino acids did not substantially enhance binding to IL-10Rα, suggesting that it is not a single substitution responsible for the binding activities (Yoon et al., 2012). The mutation of alanine to isoleucine at position 105 in ebvIL-10 was shown to have the greatest effect on biological activities, with its replacement restoring it to activity similar to human IL-10 immuno-stimulatory effects (Ding et al., 2000). In the same study this mutation also significantly changed the binding affinity of IL-10 for IL-10R, in contrast to what was reported by Yoon et al. This may be due to the use of murine IL-10Rα in the study by Ding et al. When comparing the mutations in our high affinity IL-10 to ebvIL-10 the N110I substitution is in close proximity to the I105A substitution. This supports the idea that an isoleucine residue in this area may confer an advantage. However, while position 110 is on helix D, 105 is in the CD loop region and so the ability to draw comparisons is limited.

Conclusions and future perspectives

Here we have successfully demonstrated the generation and biophysical characterisation of IL-10 variants with increased affinity for IL-10Rß. This increased receptor affinity has several implications for the study of IL-10. Firstly, it indicates that R5A11 may be a good candidate for attempts to crystallise the IL-10/IL-10R complex as the improved affinity may mean that a more stable

complex would be able to form. Secondly, the increased receptor affinity may have implications for downstream signalling. IL-10Rα and IL-10Rß are constitutively associated with JAK1 and TYK2 respectively. The interaction of the receptors activates these kinases and allows the phosphorylation of intracellular domains on IL-10Rα, providing docking sites for STAT molecules and their subsequent phosphorylation, dimerisation and activation. The ability of R5A11 to more effectively bind IL-10Rß may enhance formation of these active complexes and lead to increased STAT activation. Previous studies have shown that changes in the stability and thus the lifetime of cytokine-receptor complexes can alter the potency of intracellular signalling as well as downstream biological activities (Martinez-Fabregas et al., 2019). In the IL-6 system it was shown that by using IL-6 variants with a range of binding affinities for gp130, graded responses could be generated such as differential pSTAT1: pSTAT3 ratios. This in turn led to differential cell responses i.e. biasing of Treg/Th17 differentiation (Martinez-Fabregas et al., 2019). This link between cytokine receptor binding stability and biological output has also been investigated in systems such as type I interferons, IL-4 and IL-13 (Moraga et al., 2015a, Roisman et al., 2005, Junttila et al., 2012), however thus far reports using IL-10 are lacking. These high affinity IL-10 variants in both monomeric and dimeric conformations provide unique tools with which to probe the molecular basis of IL-10's activity. This will be further explored in subsequent chapters.

Chapter 4. Investigating the link between IL-10 receptor binding affinity and biological functions

Background

This chapter will describe the use of the previously generated high affinity IL-10 variant R5A11 to examine how changes in receptor binding affinity alter known IL-10 biological effects. R5A11 and wild type IL-10 were used in both their monomeric and dimeric conformations. This allowed us to also assess the contribution that receptor stoichiometry played in the IL-10 response.

IL-10 is a key anti-inflammatory and immuno-regulatory cytokine. It can potently suppress the ability of innate cells such as macrophages and dendritic cells to present antigen and produce pro-inflammatory cytokines. This in turn inhibits the activity of the adaptive arm of the immune response, particularly Th1 cells. IL-10 can also act directly to suppress adaptive cell responses, for example, by its action on Th17 cells (Huber et al., 2011). The central role that IL-10's anti-inflammatory activities play in the regulation of the immune response is seen in patients deficient in IL-10 or with defects in the receptor. These patients develop auto-immune diseases such as Crohn's disease and colitis (Correa et al., 2009, Zhu et al., 2017), emphasising the importance of effective IL-10 production and response. Despite promising *in vitro* activity, IL-10 based therapies have so far shown poor clinical efficacy in the treatment of auto-immune diseases, hindered by IL-10's short half-life and difficulties in targeted delivery (Saraiva et al., 2020)

In recent years several studies have highlighted another key IL-10 activity. It has been shown that, under certain conditions, IL-10 can enhance the cytotoxicity of CD8 T cells, leading to enhanced tumour cell targeting (Mumm et al., 2011). A PEGylated version of IL-10 is currently in clinical trials as a cancer therapeutic, with initial studies showing promising results (Naing et al., 2019).

We hypothesised that an IL-10 variant with enhanced receptor binding affinity has the potential to improve the efficacy of the IL-10 response. In this chapter I outline how we used the high affinity IL-10 variant R5A11 to assess the contribution of

receptor binding affinity as well as receptor complex stoichiometry to IL-10 biology. Monocytes and CD8 T cells isolated from human buffy coats were used for experiments in this chapter. IL-10's ability to potently suppress pro-inflammatory responses in monocytes has been well characterised (Moore et al., 2001). The ability of IL-10 to enhance CD8 cytotoxicity has also been described in detail in recent studies (Mumm and Oft, 2013). This, along with their ability to be easily isolated and cultured, made these cells ideal for studying how high affinity changes influence IL-10 activities in both an innate and an adaptive cell setting. Wild type IL-10 was used in its native conformation as a dimer (WTD) and also as a monomer (WTM). R5A11 was used in dimeric (R5A11D) and monomeric (R5A11M) forms (Figure 4.0).

Results discussed in this chapter form the basis for the publication "Engineered IL-10 variants elicit potent immunomodulatory effects at low ligand doses", Gorby et al., 2020.
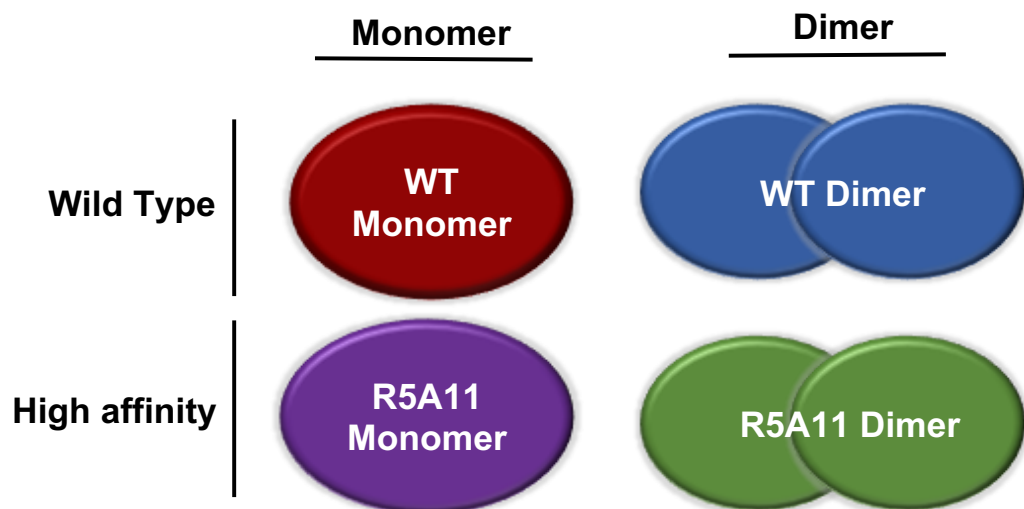
Figure 4.0 Schematic of IL-10 variants used. Four variants of IL-10 were used in this study. Wild type IL-10 was used in its natural dimeric conformation (WTD) and in a monomeric conformation (WTM) as described by (Josephson et al., 2000b). The high affinity IL-10 variant R5A11 was also used in dimeric (R5A11D) and monomeric conformations (R5A11M).

Aims:

- Assess the effect of receptor affinity on assembly of the IL-10 receptor complex
- Examine early signalling events (i.e., STAT activation) by wild type and high affinity IL-10 monomers and dimers.
- Test the known IL-10 cellular response to high affinity variants (inhibition of antigen presentation, granzyme B production).
- Analyse gene expression in monocytes and CD8 T cells after stimulation with WT and high affinity variants.

4.1 Increased affinity for IL-10Rß enhances assembly of the complete IL-10 receptor complex

All experiments in this section (4.1) were conducted by <u>Junel Sotolongo Bellón in the lab of Jacob Piehler at University of Osnabrück</u>. The Piehler lab has extensive experience with multi-colour single-molecule fluorescence TIRF imaging of cytokine receptors. The wild type and high affinity IL-10 variants were produced and provided by the author in the University of Dundee.

IL-10 carries out its biological functions by binding to IL-10Rα and IL-10Rβ on the cell surface, forming a hexameric complex, i.e. one IL-10 dimer, bound to two copies of IL-10Rα and two copies of IL-10Rβ. According to the law of mass action, IL-10 would first bind IL-10Rα via the receptor's high-affinity binding site. In a subsequent step, IL-10Rβ is recruited into the complex leading to a dynamic equilibrium of receptor complex assembly and dissociation. This equilibrium is largely defined by the affinity of IL-10 toward IL-10Rβ, as this is the weakest interaction in the complex. As our engineered IL-10 variants had increased affinity for IL-10Rβ we wanted to investigate how this change in affinity would affect the assembly of the signalling complex in the context of the plasma membrane of live
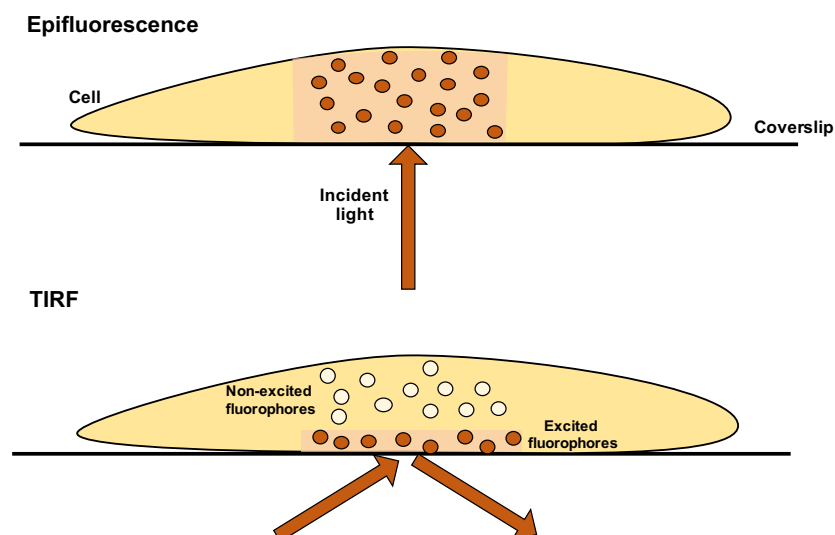
Figure 4.1 TIRF microscopy. Simplified representation of the differential excitation of fluorophores by traditional epifluorescence versus TIRF microscopy. Using epifluorescence, the incident light travels straight through the coverslip into the sample and all fluorophores in this path are excited. Using TIRF microscopy, the incident light is reflected back off the coverslip. This generates an evanescent wave at the solid-liquid interface with is the same frequency as the exciting beam. Only fluorophores within this range are excited, reducing background signal. Figure adapted from (Mattheyses et al., 2010).

cells. We took advantage of Total Internal Reflection Fluorescence (TIRF) microscopy to do this (Figure 4.1).

TIRF microscopy allows selective excitation of fluorophores proximal to the basal membrane of adherently growing cells which significantly reduces background signals. Using super-resolution imaging algorithms, individual fluorescence emitters can be localised with high spatial accuracy (~20nm), allowing single molecule co-localisation and co-tracking experiments of fluorescently labelled cell surface receptors.

4.1.1 Labelling of IL-10Rα and IL-10Rß for single molecule co-localisation studies

For visualisation of IL-10Rα and IL-10Rβ engineered versions of the receptors were expressed in HeLa cells as follows (Figure 4.2a). IL-10Rα and IL-10Rß were tagged at their N-terminus with non-fluorescent variants of either monomeric ECFP (enhanced cyan fluorescent protein) or EGFP (enhanced green fluorescent protein) respectively, each of which carry a Y66F mutation. This mutation impairs chromophore formation and thus these variants are non-fluorescent. ECFP and EGFP were used as GFP and CFP have low intrinsic affinities which may affect dimerisation. These tags were designed to be specifically recognised by either one of two different anti-GFP nanobodies; minimiser (MI) or enhancer (EN), for IL-10Rα and IL-10Rß respectively (Figure 4.2a). These anti-GFP nanobodies were previously generated using a phagemid library (Kirchhofer et al., 2010). The nanobodies (NBs) were conjugated to the photostable organic fluorophores ATTO Rho11 and ATTO 643 (referred to in the figures as Rho11 and AT643 respectively). This allowed simultaneous dual-colour single molecule tracking of IL-10Rα and IL-10Rβ in the plasma membrane of live cells with high spatio-temporal accuracy as shown previously in other cytokine receptor systems such as IL-6, IL-13, erythropoietin and thrombopoietin (Martinez-Fabregas et al., 2019, Moraga et al., 2015a, Wilmes et al., 2020, Moraga et al., 2015b).

In the dimeric conformation we expected that IL-10 would interact with two molecules of IL-10Rα and two molecules of IL-10Rß while the monomeric variants would recruit one IL-10Rα and one IL-10Rß chain, fitting the previously

reported cytokine-receptor stoichiometry (Josephson et al., 2000b). A schematic of receptor assembly is shown in Figure 4.2b. As this is a dynamic system,
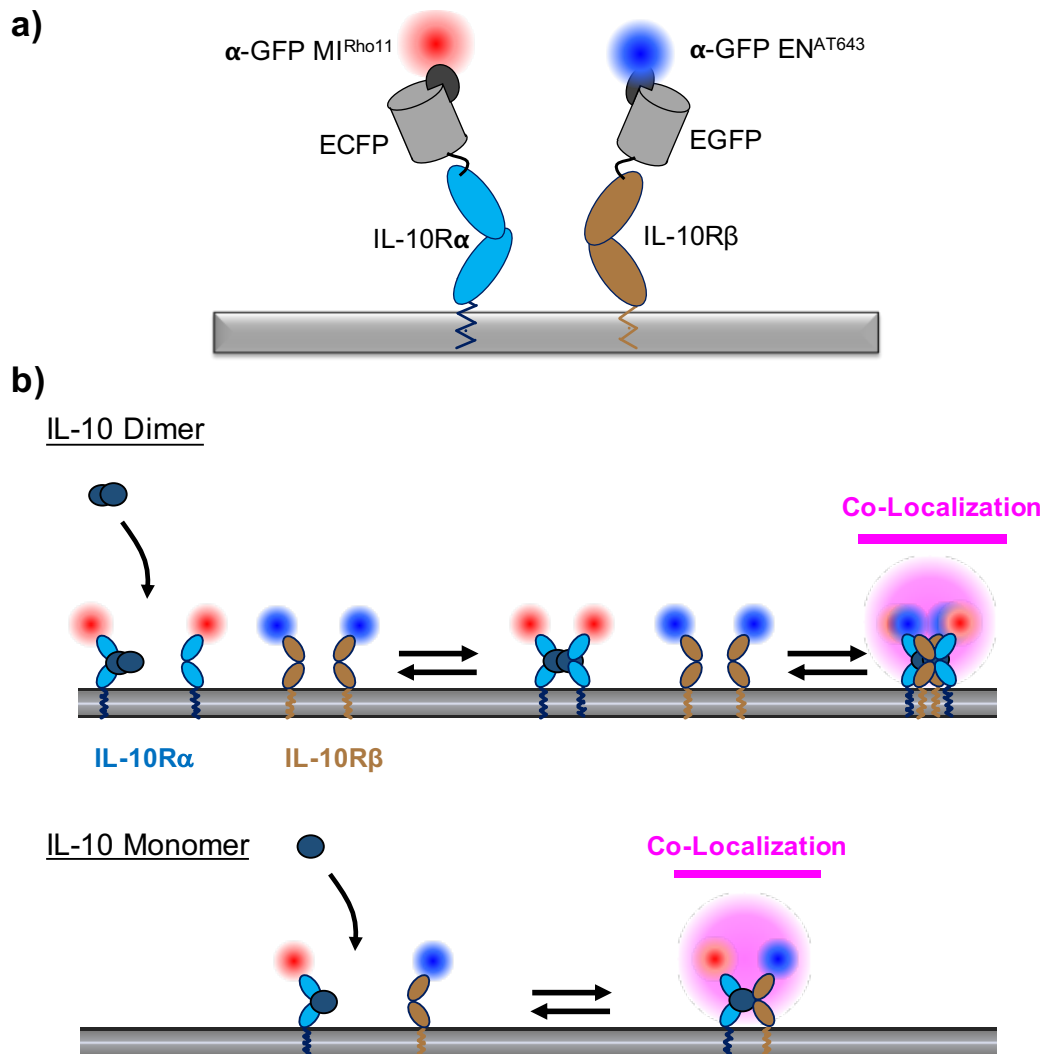
Figure 4.2 Labelling strategy for probing receptor co-localisation. (a) Schematic of receptor labelling. IL-10Rα is tagged with an ECFP non-fluorescent variant. This is recognised by an anti-GFP nanobody conjugated to the fluorophore Rho11. IL-10Rß is tagged with an EGFP non-fluorescent variant which is recognised by an anti-GFP nanobody conjugated to the fluorophore AT643. **(b)** Quantifying receptor dimerisation in the plasma membrane by dual-colour single molecule co-localisation and co-tracking. IL-10Rα and IL-10Rß were labelled with nanobodies MI^{Rho11}, EN^{AT643} respectively allowing visualisation of single receptor molecules and co-localisation events. This experiment was performed and analysed by J. Sotolongo Bellón, University of Osnabrück.

several permutations of the dimeric complex assembly are possible e.g. 1:2:1, 1:1:2 for IL-10:IL-10Rα:IL-10Rß. However, for illustration of the labelling strategy only one configuration is shown.

After quantitative cell surface labelling, single-molecule co-localisation of IL-10Rα and IL-10Rß can be taken as a readout for interaction of the two receptor chains. In order to effectively remove density-dependent random encounter co-

localisations, only persistent co-localisation (threshold 150nm for ≥ 10 consecutive steps ≈ 320ms) of receptor chains was taken as readout for receptor complex assembly. This labelling and evaluation strategy was applied to both the monomeric and the dimeric variants of IL-10 (Figure 4.2b).

4.1.2 High affinity IL-10 variants display enhanced IL-10 receptor dimerisation

Cells expressing both receptor subunits were treated with saturating doses of the respective IL-10 variants, ensuring that each high-affinity IL-10Rα subunit would be occupied by the ligand. Only cells showing a mild excess of IL-10Rß were considered for analysis (Figure 4.3a), so that maximal receptor assembly would only be limited by the affinity of IL-10 towards IL-10Rß, not the availability of IL-10Rα, as recently shown for the Type I interferon system (Wilmes et al., 2015). Both receptor subunits diffused randomly in the plasma membrane as shown in Figure 4.3b. In absence of IL-10 stimulation, no heterodimers of IL-10Rα and IL-10Rß could be detected. After IL-10 stimulation, a significant fraction of dimers was observed, as shown in Figure 4.3b.
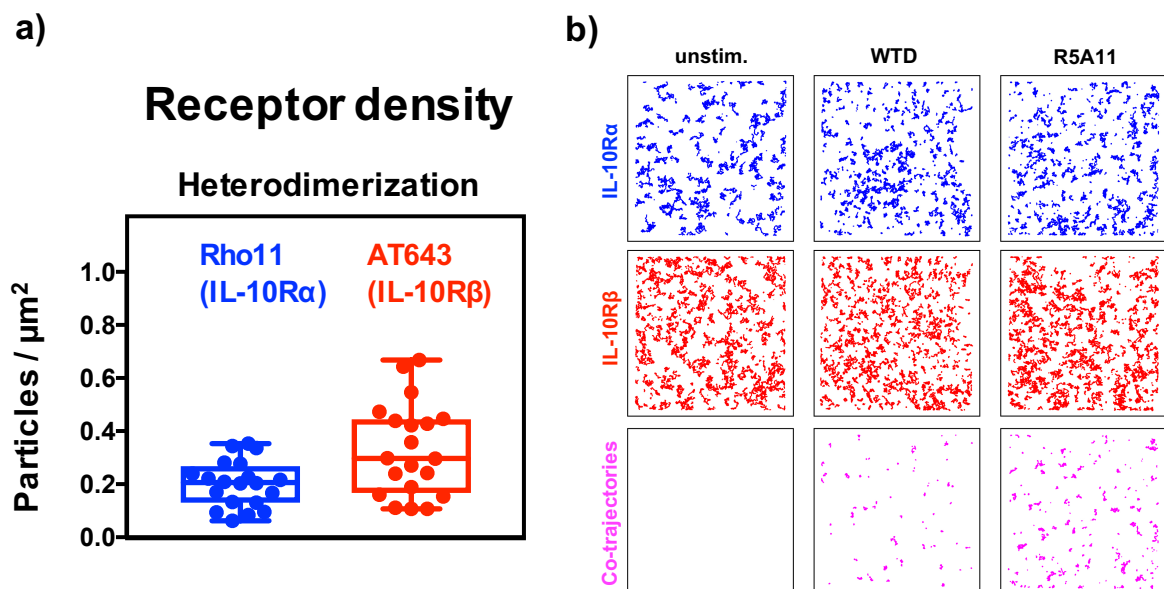
Figure 4.3 Visualisation of hetero- and homodimerisation of IL-10 receptor subunits.
(a) Cell surface receptor density of ectopically expressed IL-10Rα (blue) and IL-10Rß (red). Each dot represents one cell. **(b)** Trajectories of IL-10Rα (blue), IL-10Rß (red) and co-localized IL-10Rα:IL-10Rß (magenta) in the absence of IL-10 (left column) and in the presence of WTD (middle column) and R5A11D (right column), respectively. This experiment was performed and analysed by J. Sotolongo Bellón, University of Osnabrück.

Interestingly, the R5A11 dimer (R5A11D) induced a significantly higher level of receptor heterodimers compared to WTD (Figure 4.4a, panel 1). We also compared the wild type IL-10 monomer (WTM) with the monomeric high affinity variant (R5A11M). Similar to the dimeric variants, WTM induced lower levels of heterodimerisation than R5A11M (Figure 4.4b, panel 1).

Next, we quantitatively examined the homodimerisation of the two receptor subunits. In order to do this either receptor chain was stochastically labelled with both dyes, showing a 1:1 ratio as demonstrated in Figure 4.4c. Because of this binomial distribution of stochastic receptor labelling, only half of the formed dimers would be picked up by co-tracking analysis and quantification was mathematically corrected for this. For homodimerisation of IL-10Rα no significant difference was seen between WTD and R5A11D (Figure 4.4a, panel 2). In contrast, R5A11D induced significantly more homodimerisation of IL-10Rß compared to WTD (Figure 4.4a, panel 3), in agreement with its higher affinity for IL-10Rß. As expected, no homodimerisation events were detected for the monomeric cytokines, verifying their monomeric nature (Figure 4.4b, panel 2-3).

In summary, the high affinity variants of IL-10 in both monomeric and dimeric conformations displayed enhanced heterodimerisation of the IL-10 receptor subunits when compared to wild type IL-10.
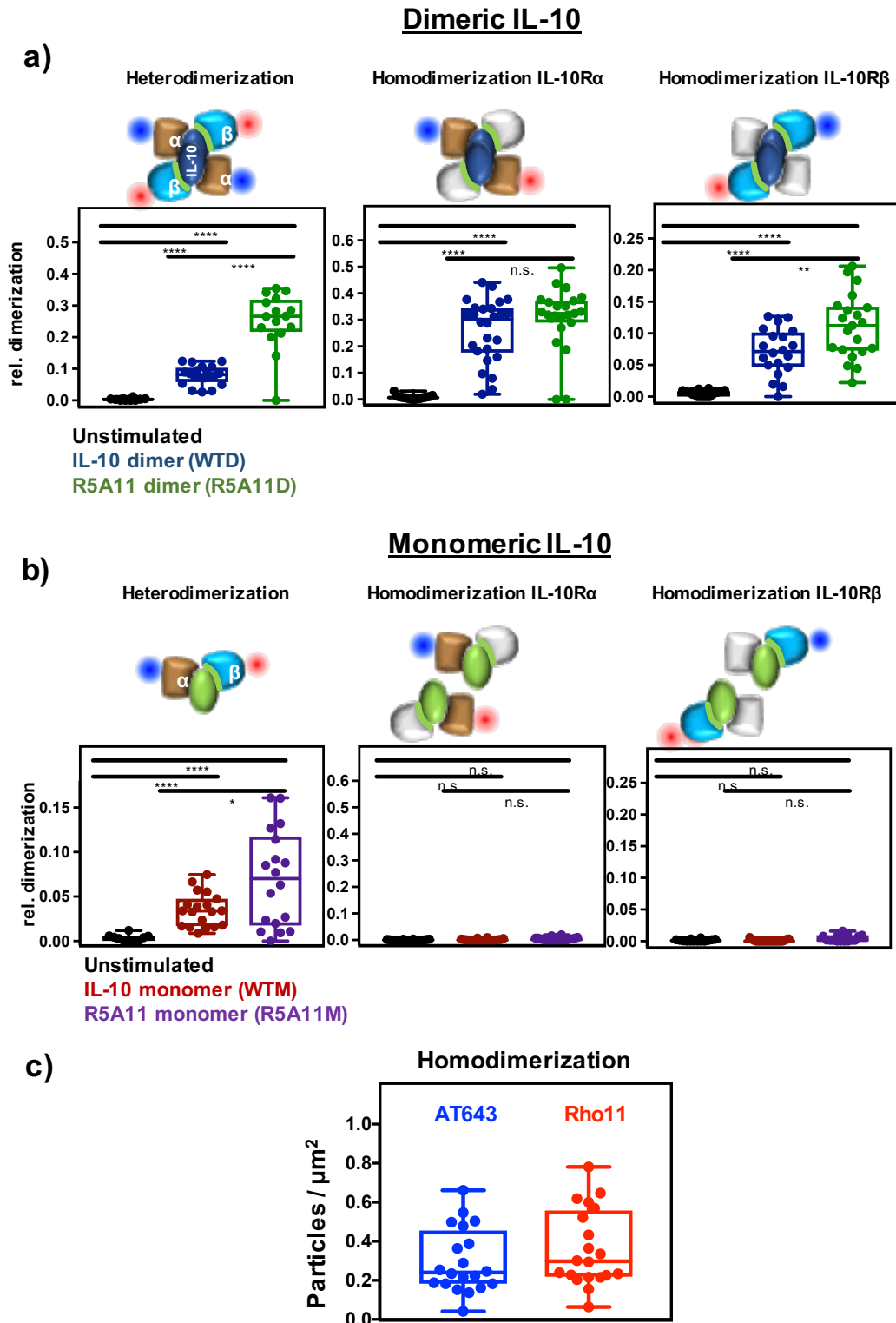
Figure 4.4 Quantification of hetero- and homodimerisation of IL-10 receptor subunits
(a) Heterodimerisation of IL-10Rα and IL-10Rß (left), and homodimerisation of IL-10Rα (centre) and IL-10Rß (right) induced by dimeric IL-10 variants, quantified by co-locomotion analysis. Each data point represents one cell. **(b)** Homo- and heterodimerisation of IL-10Rα and IL-10Rß induced by monomeric IL-10 variants quantified by co-locomotion analysis. **(c)** Cell surface density for homodimerisation experiments. Each data point represents a cell. P value is calculated by two-tailed student's t test. *P < 0.05, **P ≤ 0.01, ***P ≤ 0.001, ****P ≤ 0.0001. n.s., not significant. This experiment was performed and analysed by J. Sotolongo Bellón, University of Osnabrück.

4.2 High affinity IL-10 regulation of innate (monocyte) immune responses

As R5A11 showed enhanced assembly of the receptor complex we next wanted to see how this would affect other aspects of IL-10 biology. We examined the effect of receptor affinity and receptor stoichiometry on IL-10's ability to activate STATs, the IL-10 transcriptome and known IL-10 biological activities. As IL-10 has very well characterised activities in innate cells we chose monocytes to work with. The response of these cells to IL-10 has been previously studied in depth, giving us a broad range of literature to work from. These cells are also easily isolated from human buffy coats, allowing us to examine the effect of our high affinity variants in primary human cells.

4.2.1 Increased affinity enhances STAT activation in monocytes

IL-10's activation of the JAK/STAT pathway is the primary way in which signals from the receptor complex are transmitted within the target cell. JAK1 and TYK2 are associated with IL-10Rα and IL-10Rß respectively. Upon ligand stimulation these kinases are activated and phosphorylate tyrosines in the intracellular domain of the receptor tails. This provides a docking site for STAT molecules and allows their dimerisation and activation upon Tyr phosphorylation by JAKs. Once dimerised, STATs translocate to the nucleus to induce gene expression programmes. Both STAT1 and STAT3 have been shown to be activated in response to IL-10 (Finbloom and Winestock, 1995). In order to assess how increased receptor affinity affected early signalling events, phospho-flow cytometry was used to measure tyrosine phosphorylation of STAT1 and STAT3
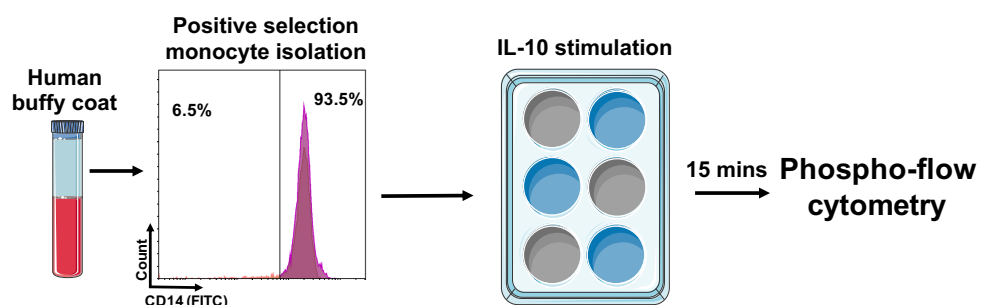
Figure 4.5 Isolation and treatment of monocytes for STAT activation. Monocytes (CD14^{+}) were isolated by positive selection (MACS) from human buffy coats. The cells were then stimulated with IL-10 wild type and variants over a range of concentrations for 15 minutes before fixation.

in human monocytes. Monocytes were isolated from human buffy coats stimulated with a range of IL-10 concentrations for 15 minutes (Figure 4.5). Cells were stimulated with wild type and high affinity monomers and dimers over a large range of concentrations, from 200 nM to 12.8 pM.

Dose response curves were generated from these experiments with the $\log_{10}$ of the concentration of the IL-10 variants on the x-axis and the pSTAT response (normalised) on the y-axis. The curves are sigmoidal in nature as the response reaches saturation at high concentrations where, despite increased cytokine concentration, no increase in STAT activation is seen. This allows us to compare the EC_{50} of the IL-10 variants, giving an insight into the relative potency of the variants. The dose response curves for pSTAT1 and pSTAT3 are shown in Figure 4.6a-b respectively. We first compared the WTD dose response curves with those of the high affinity dimer, R5A11D. At high concentrations for both WTD and R5A11D there was an apparent decrease in pSTAT1 activity which was not seen for pSTAT3. In addition, R5A11D showed a non-significant but enhanced pSTAT1 response at high concentrations compared to WTD. When we examined the ability of WTD and R5A11D to activate STAT3 we saw that R5A11D phosphorylated STAT3 to a very similar level as WTD at saturation. Despite showing an almost identical pattern of STAT3 activation to WTD at high concentrations, R5A11D appeared to show enhanced STAT1 and STAT3 phosphorylation at low concentrations, leading to a shift in the dose response curves. When the EC_{50} values were plotted, R5A11D had a non-significant but consistently lower EC_{50} for both pSTAT1 and pSTAT3 compared to WTD, suggesting enhanced activity by the high affinity variant (Figure 4.6c-d).

We next examined STAT activation by the monomeric variants to gain an understanding of the role that receptor stoichiometry plays in STAT signalling. The wild type monomer (WTM) activated both STAT1 and STAT3 poorly, with less than 25% of maximal STAT1 activity and 35% of STAT3 activity compared to WTD at saturating levels (Figure 4.6a-b). This also led to apparently higher EC_{50} levels than WTD for both STAT1 and STAT3 (Figure 4.6c-d). When we compared WTM to the high affinity monomer (R5A11M) we saw that the increase in affinity greatly enhanced the ability of the monomer to activate both STAT1 and

STAT3. At saturating concentrations, R5A11M activated STAT1 to a similar extent to WTD and STAT3 reached 80% of the dimeric activity (Figure 4.6a-b).
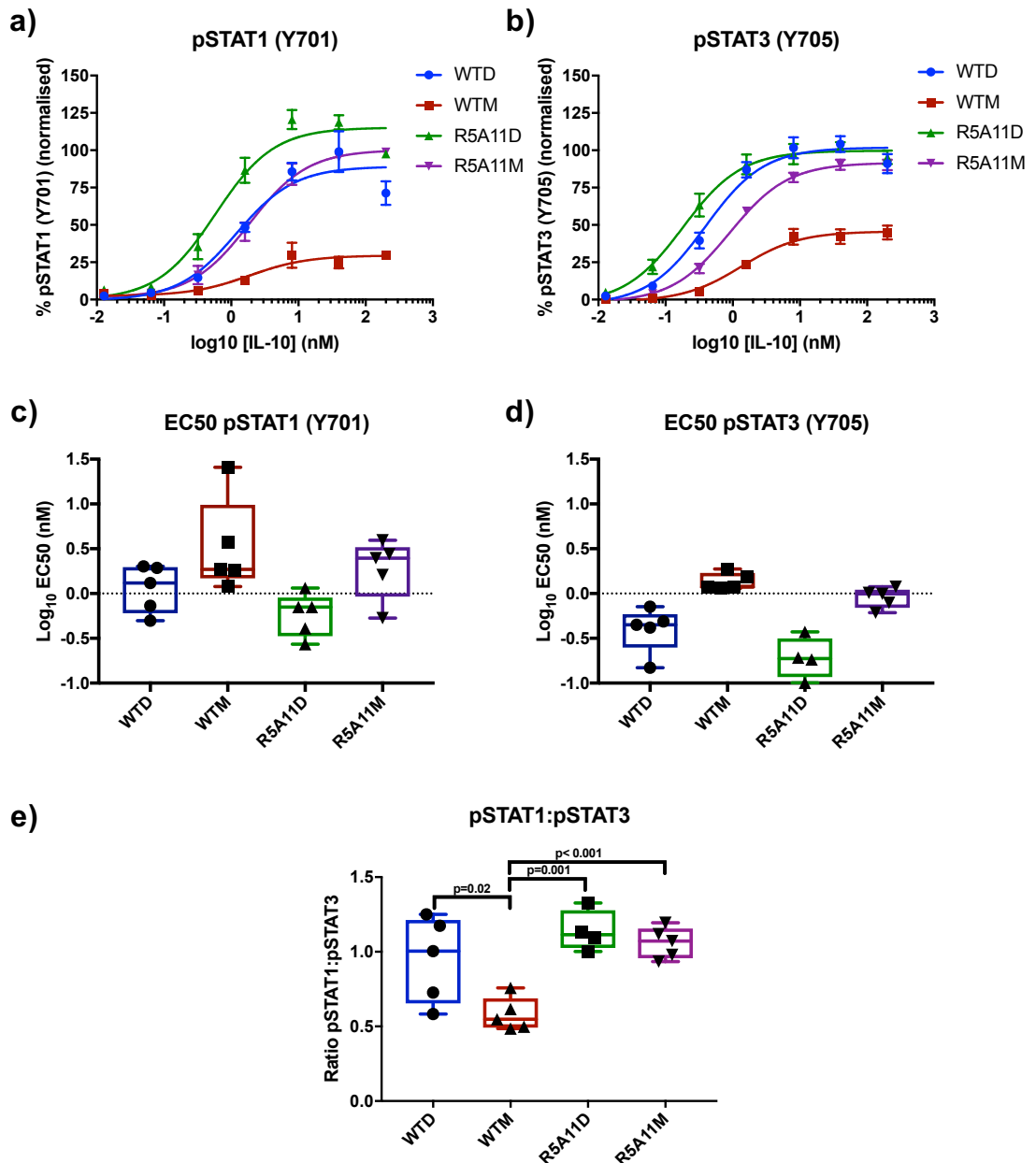
Figure 4.6 STAT1 and STAT3 activation by high affinity IL-10 variants. (a-b) Human CD14 positive monocytes were stimulated with IL-10 variants over a range of concentrations for 15 minutes. Phosphorylation of STAT1 and STAT3 was measured by flow cytometry. Data shown is the mean of 5 biological replicates with error bars showing the standard error of the mean. Each replicate is normalised by assigning the highest MFI value of the top concentration as 100% and the lowest MFI value of the bottom concentration as 0%. **(c-d)** Log_{10} EC_{50} values for pSTAT1 and pSTAT3 from the corresponding dose response curves in (a-b). **(e)** Ratio of pSTAT1 to pSTAT3 in monocytes upon IL-10 variant stimulation. Ratio was calculated by taking the percentage activation of pSTAT1 and pSTAT3 at 40 nM and dividing the pSTAT1 by pSTAT3 values. P values were calculated using paired t tests.

Although the STAT response was similar to the level of the dimeric cytokine at saturating concentrations, there appeared to be a shift in the dose response

curves at low concentrations, particularly for STAT3. This was reflected when the EC_{50} values were plotted, with apparently higher EC_{50} values for R5A11M for STAT1 and STAT3 than WTD (Figure 4.6c-d).

We also noted that WTM had increased STAT3 activity compared to STAT1. When the ratios of pSTAT1 to pSTAT3 levels were examined it was clear that WTM showed a bias towards STAT3 activation, whereas WTD, R5A11D and R5A11M had 1:1 ratios (Figure 4.6e). This will be examined further in the discussion.

In summary, increased affinity significantly enhances the ability of monomeric IL-10 to activate STAT1 and STAT3 at high concentrations. Increased affinity in the dimeric form of IL-10 does not enhance the STAT activation at saturation, however, it does appear to improve the EC_{50} of the response, suggesting enhanced activity at low concentrations compared to WTD.

4.2.2 Changes in receptor affinity and stoichiometry do not affect the kinetics of the IL-10 response in monocytes

We next wanted to see if the change in affinity for IL-10Rß by the R5A11 variants would impact the kinetics of the IL-10 response. Human monocytes were isolated as described previously. Cells were stimulated for the denoted time periods between 15 minutes and 3 hours and phosphorylation of STAT1 and STAT3 was examined. The pSTAT1 and pSTAT3 response peaked at 15 mins after stimulation and decreased thereafter with levels returning to basal after 2 hours for pSTAT1 and 3 hours for pSTAT3 (Figure 4.7). The amplitudes of signalling match with those seen in the dose response studies. WTM again showed poor activation of both pSTAT1 and pSTAT3. While the amplitudes of the response appeared to differ between the variants there was no significant changes in the kinetics between either high affinity vs wild type or dimeric vs monomeric molecules, concluding that changes in affinity for IL-10Rß do not affect the duration of the STAT response.
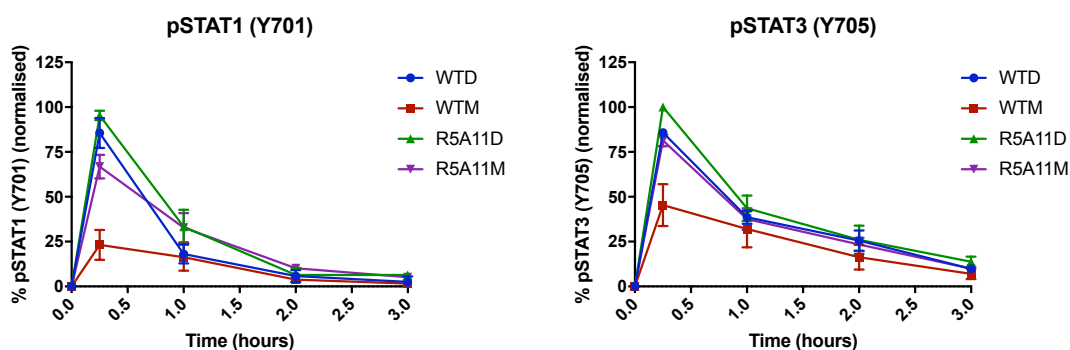
Figure 4.7 Kinetics of pSTAT1 and pSTAT3 response to IL-10 variants in monocytes.
Monocytes were stimulated with 50 nM IL-10 for the indicated time periods before fixation. Data shown is the mean of four biological replicates with error bars depicting the standard error of the mean. Each biological replicate is normalised by assigning the highest MFI value at 15 minutes as 100% and the lowest MFI value of an untreated control as 0%.

4.2.3 Increased affinity enhances known IL-10 biological activities at low concentrations in monocytes

Activation of STATs is the primary signalling step in the IL-10 response. As we observed differences in the amplitude of STAT phosphorylation between the IL-10 variants we next wanted to see if this would translate into any differences in cellular responses. To investigate this, we examined two well characterised IL-10 responses in monocytes: suppression of antigen presentation molecules and inhibition of pro-inflammatory cytokine production.

Human leukocyte antigen-DR (HLA-DR) is a cell surface receptor, analogous to major histocompatibility class II (MHC-II) in mice. It is a molecule which allows presentation of processed antigens to CD4 T helper cells, via interaction with the T cell receptor (TCR). This is a key step in the activation of the adaptive immune response. A key characteristic of IL-10 is its ability to inhibit antigen presentation by innate cells, dampening the immune response. IL-10 reduces MHC II via regulation at the protein level, reducing exocytosis of MHC II and also inhibiting the recycling mechanisms used to return these molecules to the cell surface (Koppelman et al., 1997). Measurement of surface HLA-DR expression on human monocytes was used as a proxy to examine the ability of our high affinity variants to modulate the innate immune response. Monocytes (CD14+) were isolated from human buffy coats and rested for two days as shown in in Figure 4.8a. Cells were placed in media containing either WTD, WTM, R5A11D or

R5A11M at a saturating dose of 50 nM for 24 hours. After 24 hours of treatment, cell surface HLA-DR was measured by flow cytometry. All data were normalised to a non-IL-10 treated control within each donor. Figure 4.8b shows that, as expected, WTD induced a decrease of almost 50% in HLA-DR compared to non-IL-10 treated controls. In line with its ability to activate STAT signalling at levels equivalent to WTD at saturating concentrations, R5A11D also showed a 50% decrease in cell-surface HLA-DR. WTM induced only a 20% reduction in HLA-DR molecules, in keeping with its poor STAT activation. R5A11M showed a 30% inhibition of HLA-DR, demonstrating a better response than WTM but not reaching dimeric levels of inhibition, despite having similar STAT activation as the dimeric variants at this saturating concentration.
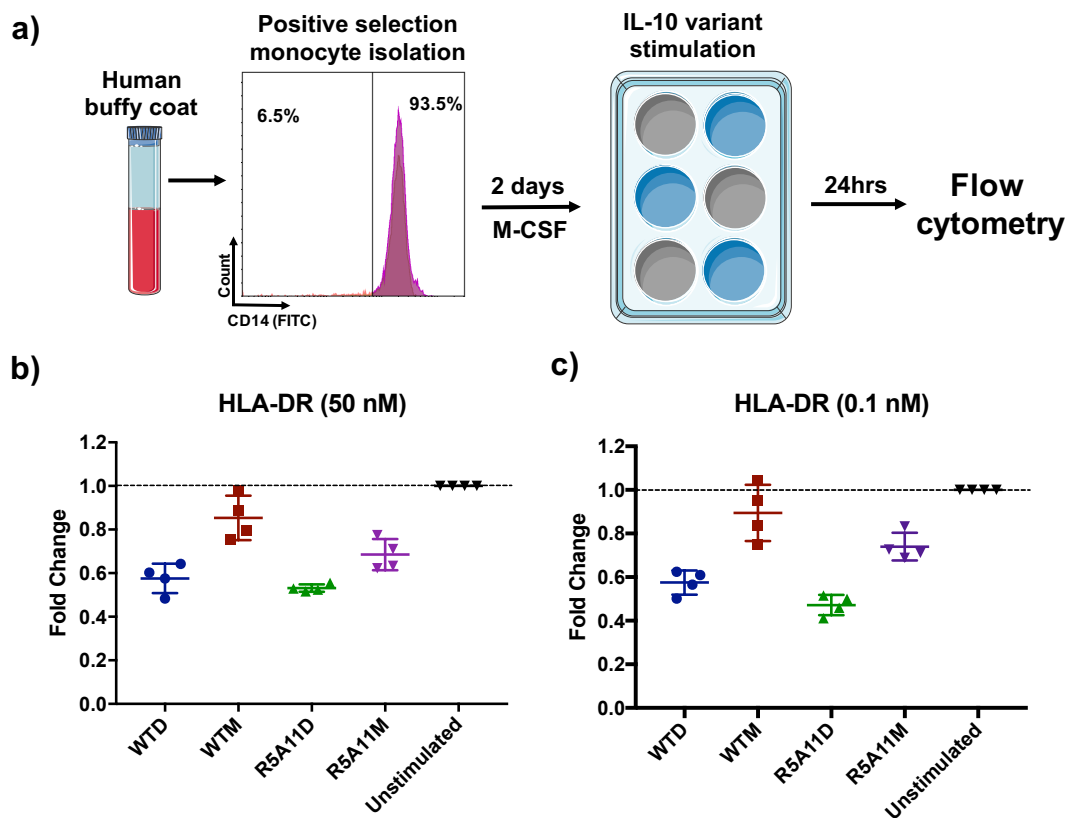
Figure 4.8 Measurement of cell surface HLA-DR upon IL-10 stimulation. CD14^{+} monocytes were isolated from human buffy coats by positive selection and rested for 2 days in media containing M-CSF (20 ng/mL). The cells were then stimulated with IL-10 variants for 24 hours at either a high concentration ((b) 50 nM) or a low concentration ((c) 0.1 nM) for 24 hours. HLA-DR was measured on the cell surface of live cells by flow cytometry. Each point represents one biological replicate (n=4). Fold change is calculated by dividing the MFI of each IL-10 treated sample by an untreated control from the same donor.

As R5A11D appeared to show enhanced STAT activation compared to WTD at sub-saturating concentrations, we tested inhibition of HLA-DR using a low dose of 0.1 nM of the IL-10 variants. Figure 4.8c shows that at this low concentration

R5A11D appeared to display slightly stronger inhibition of HLA-DR compared to WTD. Again, R5A11M and WTM failed to reach the levels of inhibition induced by the dimeric cytokines. These results are in keeping with the trends seen in STAT1 and STAT3 activation by the IL-10 variants and suggest that the high affinity dimeric IL-10 may provide an advantage over the wild type at low doses.

A key feature of IL-10's anti-inflammatory activities is its ability to suppress secretion of pro-inflammatory cytokines from a myriad of cell types such as monocytes, dendritic cells and Th1 cells. IL-10 was shown to potently inhibit LPS and PMA-induced IL-6 secretion from monocytes at the level of RNA (Takeshita et al., 1996). We decided to use this known response to IL-10 to further examine if the high affinity variant R5A11D displayed a dose-dependent advantage over the wild type IL-10 (WTD). CD14$^+$ monocytes isolated from human buffy coats were stimulated with LPS in the absence or presence of WTD or R5A11D at varying concentrations for 8 hours before the supernatant was collected and IL-6 secretion was measured.

Upon LPS stimulation a large increase in IL-6 secretion was seen which could be potently inhibited by co-incubation with either WTD or R5A11D at 50 nM (Figure 4.9a). When a low dose of IL-10 was used, 0.01 nM, R5A11D inhibited significantly more IL-6 secretion compared to WTD (Figure 4.9b). This corresponds to its stronger STAT activation at low doses. Again, this suggests that increased affinity provides an advantage to IL-10 when used at low doses, in keeping with what was seen at the level of STAT activation.
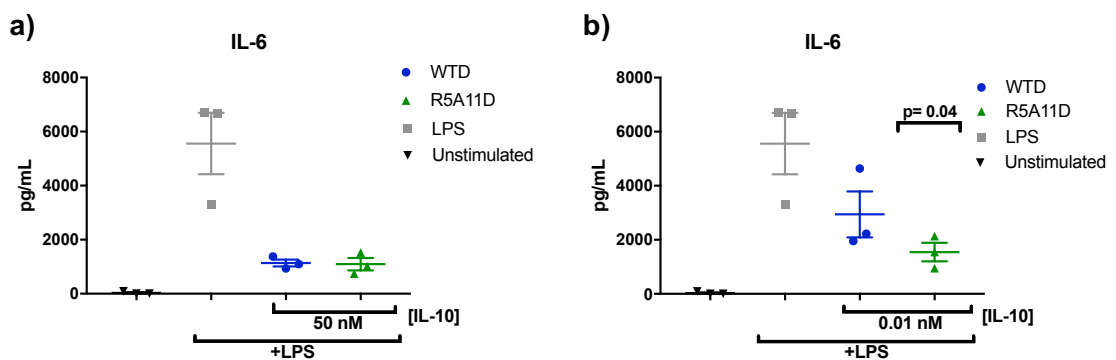
Figure 4.9 WTD and R5A11D inhibition of LPS-induced IL-6 secretion. CD14$^+$ human monocytes were stimulated with LPS (100 ng/mL) alone or with WTD or R5A11D at the denoted concentrations for 8 hours. (a)= 50 nM, (b)= 0.01 nM. An ELISA was used to measure IL-6 secretion. Each point represents one biological replicate (n=3) and error bars indicate the standard error of the mean. P value was calculated by two-tailed ratio paired t-test.

4.3 Comparison of transcriptional activity induced by IL-10 and high affinity variants in monocytes

Our comparisons between the IL-10 variants had so far focussed on two classical markers of IL-10 activity in monocytes: suppression of antigen presentation and pro-inflammatory cytokine production. We wanted to gain a broader understanding of how the differences in affinity, receptor complex assembly and STAT activation would regulate monocyte activity. The phosphorylation of STAT1 and STAT3 by IL-10 allows the dimerisation and translocation of these transcription factors to the nucleus where they can induce gene transcription programmes. We decided to use RNA sequencing to examine in depth the transcriptional activity induced by our IL-10 variants in human monocytes. This gave us a global view of this cytokine's regulation of monocyte activity and allowed us to compare the effect of our variants in an unbiased fashion. The effect of IL-10 on monocytes and myeloid cells has been well characterised however the sensitivity of these activities to changes in ligand concentration and/ or receptor binding affinity is less well understood. We envisioned that our transcriptomic studies would further our understanding of IL-10 biology under different ligand conditions.

Monocytes (CD14$^+$) were isolated from human PBMCs (StemCell Technologies) (3 donors) and rested for two days in M-CSF containing media before 24 hours of stimulation with IL-10 variants as shown in Figure 4.10.
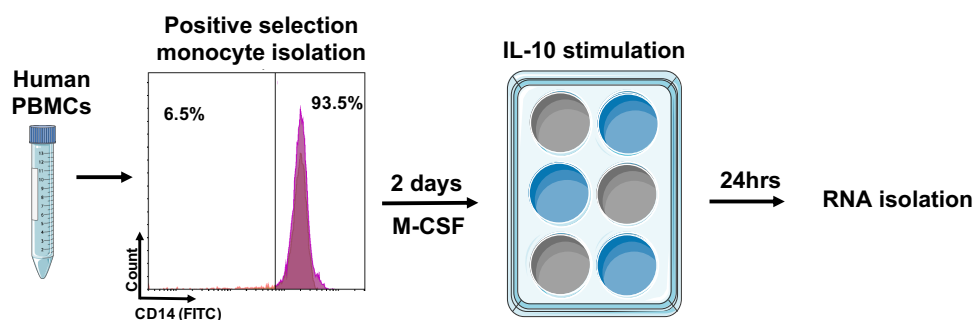
Figure 4.10 Isolation and treatment of monocytes for RNA sequencing. Monocytes (CD14$^+$) were isolated by positive selection from human PBMCs (n=3) and rested in M-CSF containing media (20 ng/mL) for two days. The cells were then stimulated with IL-10 wild type and variants for 24 hours. WTD and R5A11D were used at 50 nM and 0.1 nM each. WTM and R5A11M were used at 50 nM each.

All variants (WTD, R5A11D, WTM, R5A11M) were used at a saturating concentration of 50 nM. In addition, WTD and R5A11D were used at a low

concentration of 0.1 nM due to the previously demonstrated apparent enhanced activity displayed by R5A11D compared to WTD at this concentration. Each biological replicate contained an untreated control against which the IL-10 variants could be compared.

Cells were stimulated and RNA was isolated by the author. RNA sequencing and primary data analysis for quality control, mapping to reference genome and quantification was conducted by an external company (Novogene) as detailed in the "Materials & Methods" chapter. Statistical analysis and comparison of gene regulation between the IL-10 variants was done by the author.

4.3.1 Characterising the transcriptional effect of WTD on human monocytes

First, we wanted to fully characterise the effect of high concentration (50 nM) WTD on monocytes so as to generate a template of IL-10 regulated genes against which we could compare the other ligand and concentration conditions. We compiled a list of those genes whose expression was changed by WTD (50 nM) compared to unstimulated cells more than 1.5 fold or less than 0.67 fold (>0.6 $\log_2$ fold change or <-0.6 $\log_2$ fold change). This list can be found in Appendix Table 1. We excluded any genes which were non-significantly regulated (p value > 0.05). This filtering of data is described in more detail in the "Materials & Methods" chapter. There was a strong transcriptional regulation by WTD with 1825 genes significantly changed compared to unstimulated controls, as shown in the volcano plot in Figure 4.11a. Of these 41% were upregulated genes (741) and 59% were downregulated (1084) compared to non-IL-10 treated controls (Figure 4.11b).

Cytokines and chemokines can act as key drivers of inflammation. The ability of IL-10 to supress production of pro-inflammatory cytokines and chemokines as well as their receptors is an important aspect of its immune-suppressive capabilities. We saw downregulation of IL-24, IL-18 and IL-8 transcripts by WTD in our study (Figure 4.12a). IL-24 is an IL-10 family member cytokine with diverse effects. Of note is its ability to induce secretion of pro-inflammatory cytokines such as IL-6 and TNF-α in PBMC cultures (Caudell et al., 2002). It has also been implicated in several autoimmune diseases such as psoriasis and inflammatory

bowel disease (Chen et al., 2018). IL-18 has been shown to stimulate granulocytes such as mast cells to produce histamines and can also act in concert with IL-12 to induce IFNγ secretion from T cells (Yasuda et al., 2019). Many TNF-associated genes such as TNFAIP3, TNFRSF18 and TNFRSF4 were also downregulated. Together this significant downregulation of pro-inflammatory cytokines by WTD supports IL-10's known role in limiting the inflammatory response by monocytes.

a)

WTD vs Unstimulated (50 nM)

b)
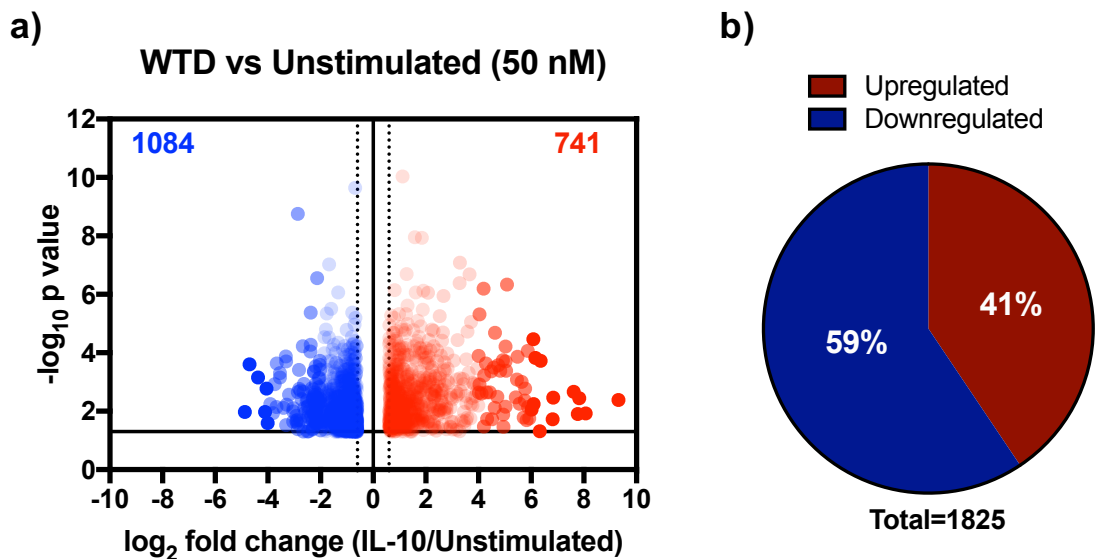
Figure 4.11 Regulation of monocyte gene transcription by WTD. (a) Volcano plot of monocytes genes significantly upregulated by WTD > 0.6 $\log_2$ fold change (red) and significantly downregulated by WTD <-0.6 $\log_2$ fold change (blue) compared to non-IL-10 treated cells. Fold change was calculated by dividing WTD 50 nM values by unstimulated values for each donor. The average fold change was calculated for three donors and the $\log_2$ of this value is plotted. P values were calculated by two-tailed two sample equal variance t test of the $\log_2$ fold change of WTD 50 nM/ unstimulated genes for each donor. Genes which were not significantly changed or were <0.6 >-0.6 $\log_2$ fold change were excluded. **(b)** Proportion of genes significantly up or down regulated by WTD in monocytes.

IL-8 transcripts were also downregulated by WTD. IL-8, also known as CXCL8, is a potent chemo-attractant for neutrophils (Yoshimura et al., 1987) again confirming the immune-suppressive role of IL-10. Several other chemokine transcripts were also downregulated by WTD such as CXCL10 and CXCL11 (Figure 4.12a). These are both pro-inflammatory chemo-attractants, known to effect cells such as activated T cells and NK cells (Vazirinejad et al., 2014, Metzemaekers et al., 2017).

However not all cytokines and chemokines were inhibited by WTD. We observed a large upregulation of IL-7 and its receptor (Figure 4.12a). IL-7 plays a role in the maintenance of survival of T cells, suggesting that WTD may be modulating

the T cell response via changes in monocyte cytokine secretion. WTD also induced the upregulation of IL-21R in monocytes. IL-21 has previously been shown to enhance phagocytosis of opsonised targets in human monocytes (Vallieres and Girard, 2017).
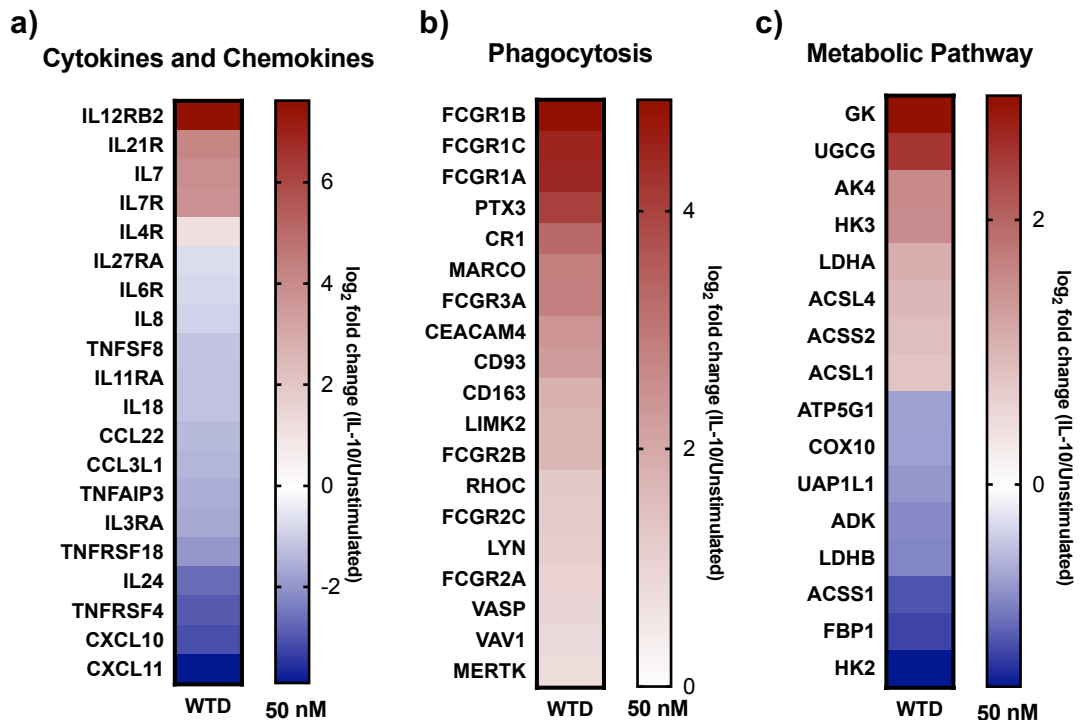
Figure 4.12 Regulation by WTD 50 nM of genes previously reported to be changed upon IL-10 stimulation in monocytes. (a) Heatmap of regulation of genes encoding cytokines, chemokines and their receptors by WTD. **(b)** Regulation of genes associated with phagocytosis by WTD. **(c)** Regulation of genes associated with metabolic pathways by WTD. For all genes the $\log_2$ fold change was calculated by dividing values for WTD 50 nM by untreated controls for each donor. Values plotted are the average of three biological replicates.

Phagocytosis is one of the primary functions of monocytes. The phagocytosis of bacteria or damaged/infected cells limits infections. It also induces further pro-inflammatory responses by monocytes such as antigen presentation and the production of cytokines and chemokines which activate other facets of the immune system. IL-10 has been shown to enhance the phagocytic activity of monocytes. Previous studies have demonstrated the upregulation of genes encoding receptors and signalling molecules involved in phagocytosis as well as scavenger functions by IL-10. For example, it has been observed that monocytes incubated with IL-10 showed increased expression of FC gamma receptor 1 (FCγR1) and complement receptors 1 and 3 (CR1, CR3) which resulted in increased uptake of opsonised particles (Capsoni et al., 1995). Similar results were observed in monocyte derived macrophages where IL-10 stimulated macrophages had enhanced levels of phagocytosis (Schulz et al., 2019). A

previous study characterised gene expression in IL-10-treated CD14^{+} cells isolated from human PBMCs (Jung et al., 2004). They identified the IL-10 mediated upregulation of genes encoding cell surface receptors for phagocytosis and scavenger functions and also genes associated with phagocytosis signalling. We compared these previously reported genes to our WTD regulated genes and found many similar expression patterns. These are shown in Figure 4.12b. The FC gamma receptors FCGR1, 2 and 3 (also known as CD64, CD32 and CD16), the complement receptor 1 (CR1) as well as the scavenger receptor MARCO were all upregulated upon WTD treatment. Genes known to be involved in phagocytosis signalling such as LYN, a Src family member associated with FcγR1, and the Rho GTPase RhoC were also upregulated by WTD stimulation. In line with what was previous reported VASP, a regulator of actin dynamics known to mediate FcγR phagocytosis was upregulated (Garcia-Garcia and Rosales, 2002). Overall, these data support the previously reported ability of IL-10 to enhance phagocytosis in monocytes.

IL-10 has also been shown to regulate the metabolic state of myeloid cells. IL-10 downregulates glycolysis and promotes oxidative phosphorylation in macrophages as well as enhancing the removal of damaged mitochondria (Ip et al., 2017). We examined the genes significantly regulated by WTD in our study and found many genes involved in metabolic regulation (Figure 4.12c). Genes associated with fatty acid metabolism, ACSL1, ACSL4 and ACSS2 were significantly upregulated upon IL-10 stimulation (Figure 4.12c). ACSL1 and ACSL4 are isoforms of long chain fatty acid CoA ligases (Tang et al., 2018) which catalyse the conversion of long chain fatty acids into acyl CoA. ACSS2 is acetyl coenzyme A synthase and converts short chain fatty acids into acetyl CoA. Several other genes involved in metabolic pathways were also regulated by IL-10 such as hexokinase-2 (HK2) and hexokinase-3 (HK3) which convert glucose to glucose-6-phosphate, a rate limiting step in glycolysis (Figure 4.12c). We saw an upregulation of hexokinase-3 but a strong downregulation of hexokinase-2. The opposing regulation of these two kinases by WTD is interesting given their similar function. In addition to its role in glycolysis, HK2 has been shown to regulate apoptosis via association with the mitochondria and suppression of cytochrome C (Mathupala et al., 2006). HK3 is less well studied but one report suggested that it may play a role in mitochondrial integrity by reducing ROS

production and maintaining membrane potential (Wyatt et al., 2010). WTD also induced the downregulation of another key enzyme in glycolysis, lactate dehydrogenase B (LDHB), the enzyme which catalyses the conversion of pyruvate to lactate. Lactate has been shown to have immune-modulatory functions with high levels of lactate inhibiting *in vitro* monocyte migration and pro-inflammatory cytokine release (Goetze et al., 2011). Although these results will need to be confirmed by alternative methods such as qPCR and investigated at the protein level, it suggests that IL-10 may be inducing metabolic changes in monocytes, consistent with the previous study by Ip et al.

Together this demonstrated that our WTD treatment could robustly reproduce known IL-10 activities in monocytes i.e. downregulation of pro-inflammatory cytokines and chemokines, upregulation of phagocytosis-associated genes and modulation of key metabolic enzymes. This gave us a template against which we could then compare the abilities of our variants to induce these known IL-10 activities.

4.3.2 WTD loses its ability to induce key anti-inflammatory transcriptional activities at low doses

As mentioned previously, a leading hypothesis for the failure of IL-10 therapies in the clinic is the low local concentration of IL-10 in the gut upon systemic administration. We wanted to examine how sensitive the different activities exhibited by IL-10 were to changes in ligand concentration. For that, we compared expression levels of genes significantly up and downregulated by WTD at 50 nM (1825 genes) to their corresponding regulation by WTD at 0.1 nM. The majority of the genes regulated by WTD at 50 nM were induced to a similar level at the low concentration, indicating that the IL-10 response is very robust. However, roughly a quarter of genes (490 genes) regulated by WTD showed poorer expression levels when the low concentration was used.

To gain a more in depth view of the genes being differentially regulated by WTD at different doses we directly compared regulation of the three sets of genes outlined previously: cytokines and chemokines, phagocytosis-related genes and genes involved in metabolic pathways (Figure 4.13). Genes encoding pro-

inflammatory cytokines and chemokines showed poorer downregulation by WTD at the low dose (Figure 4.13a). This was particularly evident for very highly downregulated genes such as IL-24 and CXCL11 (Figure 4.13b). This trend was not seen for genes associated with phagocytosis (Figure 4.13c). Here there was almost identical regulation by WTD at 50 nM and 0.1 nM, with genes such as CR1 and LYN showing resilience to changes in concentration (Figure 4.13d). Examining genes associated with metabolic pathways we saw that the majority were unaffected by a change in concentration (Figure 4.13e), although there were exceptions such as ACSS1 and AK4 which showed somewhat poorer regulation by low dose WTD (Figure 4.13f).
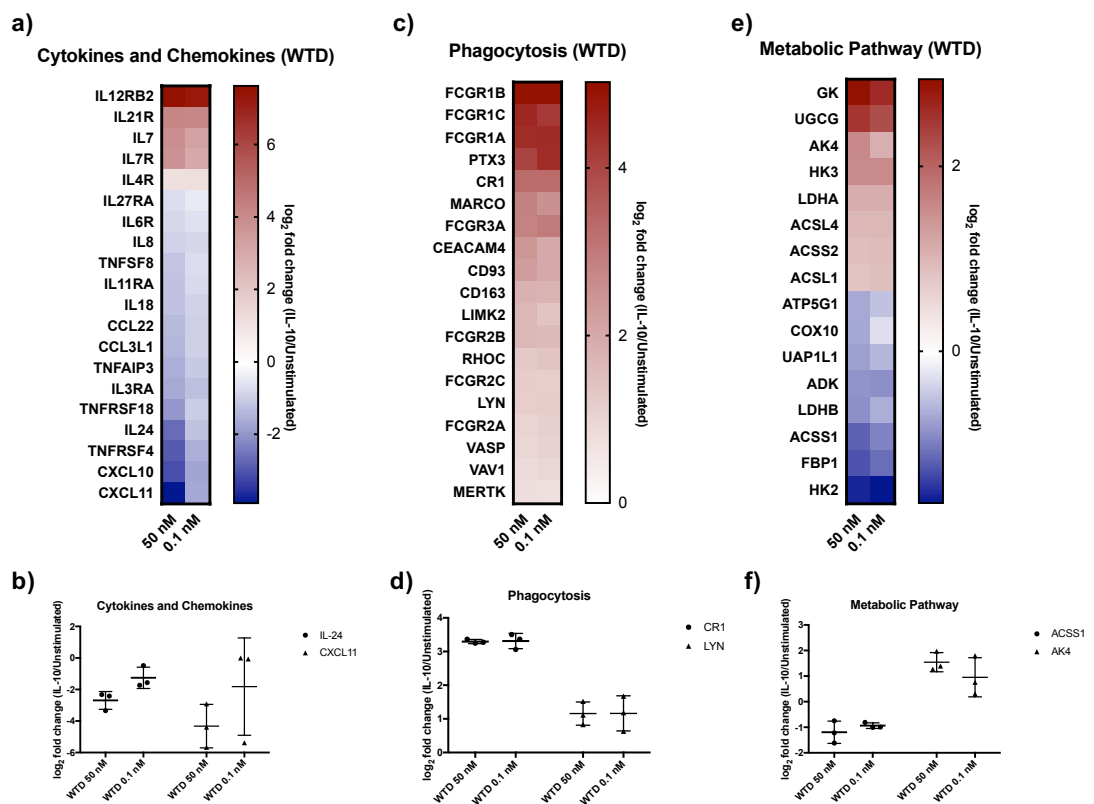
Figure 4.13 Comparison of WTD activity at 50 nM and 0.1 nM. (a) Heatmap of regulation of genes encoding cytokines, chemokines and their receptors by WTD at 50 nM and 0.1 nM. **(b)** Log$_2$ fold change for IL-24 and CXCL11 stimulated with WTD at 50 nM and 0.1 nM. **(c)** Heatmap of expression of genes associated with phagocytosis by WTD at 50 nM and 0.1 nM. **(d)** Log$_2$ fold change for CR1 and LYN stimulated with WTD at 50 nM and 0.1 nM. **(e)** Regulation of genes associated with metabolic pathways by WTD at 50 nM and 0.1 nM. **(f)** Log$_2$ fold change for ACSS and AK4 stimulated with WTD at 50 nM and 0.1 nM. For all genes the log$_2$ fold change was calculated by dividing values for WTD 50 nM or 0.1 nM by untreated controls for each donor. Heatmap values are the average of three biological replicates (a, c, e). For dot plots, each point represents one biological replicate (b, d, f).

This provided us with insight into how changes in dose affected IL-10's activities at the transcriptional level. The majority of genes were unaffected or only slightly impeded by using a low dose of IL-10. However, of note is that many of the

inflammatory cytokines, chemokines and receptors showed much weaker regulation at the low concentration. An inability to perform these activities at low doses could significantly impede IL-10's anti-inflammatory functions. This supports the hypothesis that IL-10's inability to inhibit inflammation in the clinic may be due to a dose-dependent effect.

4.3.3 High affinity dimeric IL-10 displays enhanced transcriptional activity at low doses compared to wild type IL-10 in monocytes

We next wanted to compare the activity of WTD with our high affinity dimeric variant R5A11D. As described above, we stimulated cells with both WTD and R5A11D at 50 nM and 0.1 nM each, allowing us to compare their activities at high and low concentrations. We took genes shown to be significantly regulated by WTD at 50 nM (1825 genes) and compared the activity of these genes across the other treatments. As before, we focussed on sets of genes with known regulation by IL-10: proinflammatory cytokines and chemokines, phagocytosis and metabolic pathways.

We first compared the activity of WTD and R5A11D at 50 nM. Pro-inflammatory cytokines and chemokines overall showed similar levels of regulation by WTD and R5A11D (Figure 4.14a), with some exceptions such as TNFRSF18 and IL18 showing weaker downregulation by R5A11D (Figure 4.14b). Genes involved in phagocytosis also showed largely similar patterns of regulation between the two variants (Figure 4.14c-d). When looking at metabolic pathway genes we saw that many of the genes downregulated by WTD showed poorer downregulation by R5A11D e.g. COX10, ATP5G1 (Figure 4.14e-f).

R5A11D showed consistently stronger responses than WTD in STAT activation and biological activities when both were used at low concentrations. We next wanted to investigate whether this increased receptor assembly and increased STAT activation would result in an enhanced transcriptional response. Comparing the WTD and R5A11D 0.1 nM treatments, both displayed similar proportions of genes up and downregulated by IL-10 (Figure 4.15a) however examining the numbers of genes significantly regulated, R5A11D had 1389 genes which reached significance (76% of those regulated by WTD 50 nM),

whereas WTD 0.1 nM had 1226 genes significantly regulated (67% of those regulated at 50 nM), again showing that at low concentrations WTD performed more poorly. We compared expression levels of genes induced by WTD and R5A11D at 0.1 nM. Figure 4.15b shows that R5A11D had decreased expression of only 6% of genes compared to WTD and enhanced expression of 19% of genes, with the majority of genes (75%) remaining unchanged.
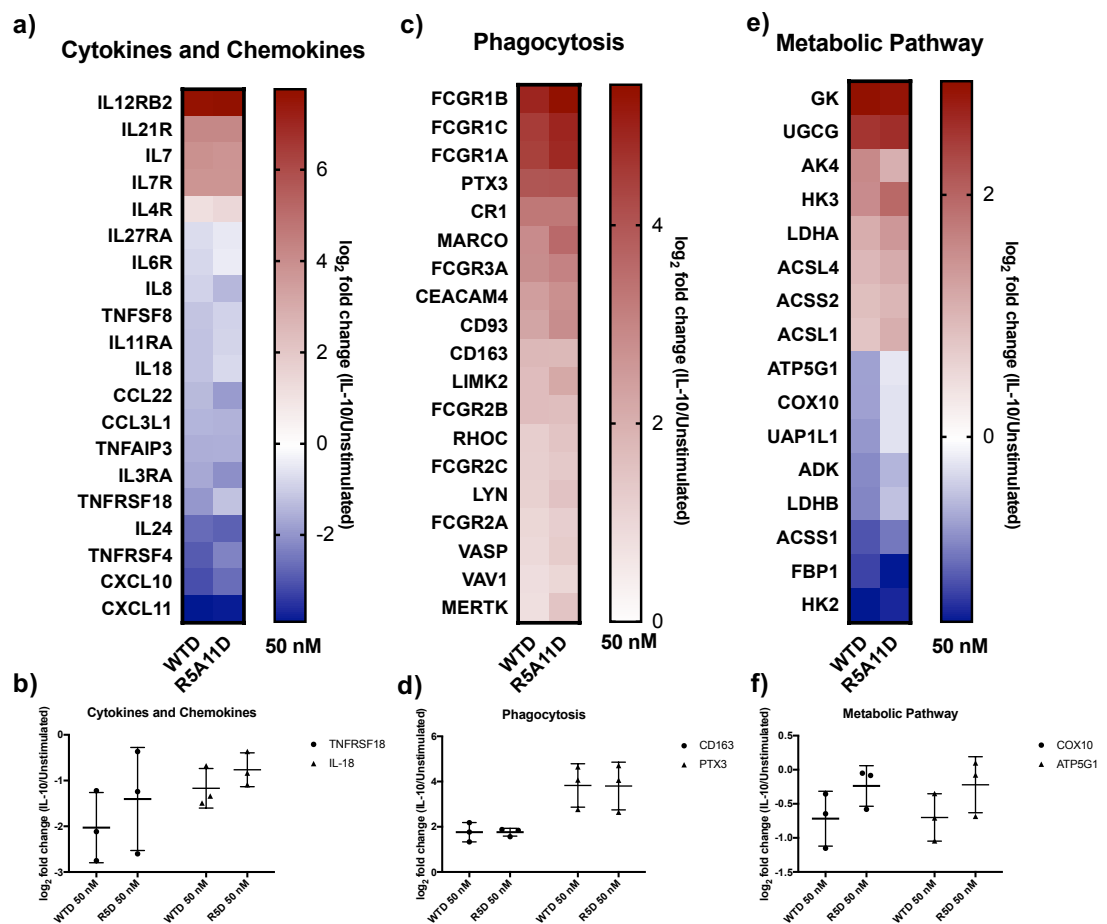
Figure 4.14 Comparison of gene regulation by WTD and R5A11D at 50 nM. (a) Heatmap of regulation of genes encoding cytokines, chemokines and their receptors by WTD and R5A11D at 50 nM. **(b)** Log_2 fold change for TNFRSF18 and IL-18 stimulated with WTD and R5A11D at 50 nM. **(c)** Regulation of genes associated with phagocytosis by WTD and R5A11D at 50 nM. **(d)** Log_2 fold change for CD163 and PTX3 stimulated with WTD and R5A11D at 50 nM. **(e)** Regulation of genes associated with metabolic pathways by WTD and R5A11D at 50 nM. **(f)** Log_2 fold change for COX10 and ATP5G1 stimulated with WTD and R5A11D at 50 nM. For all genes the log_2 fold change was calculated by dividing values for WTD 50 nM or R5A11D 50 nM by untreated controls for each donor. Heatmap values are the average of three biological replicates (a, c, e). For dot plots, each point represents one biological replicate (b, d, f).

We next examined regulation of the three sets of genes outlined before. R5A11D showed stronger downregulation of many cytokine and chemokine genes than WTD at 0.1 nM (Figure 4.15c). As outlined previously, WTD showed poorer regulation of these genes at the low dose compared to the high dose. Unlike WTD, regulation of these genes by R5A11D did not appear to be affected by a

change in dose. For phagocytosis and metabolic pathways, we saw an overall enhanced regulation by R5A11D compared to WTD at 0.1 nM, with some exceptions. From the three sets of genes examined, cytokines and chemokines appear the most changed between WTD and R5A11D, suggesting that the sensitivity of these genes to changes in concentration can be rescued to some extent by an increase in receptor affinity (Figure 4.15c).

To take a more unbiased sample of genes we examined expression levels of the top 10 most up or downregulated genes by WTD at 0.1nM. Figure 4.15d shows that the majority of these highly up and downregulated genes had enhanced regulation by R5A11D compared to WTD. Together this suggests that increased affinity can enhance IL-10's transcriptional activity when used at low doses.
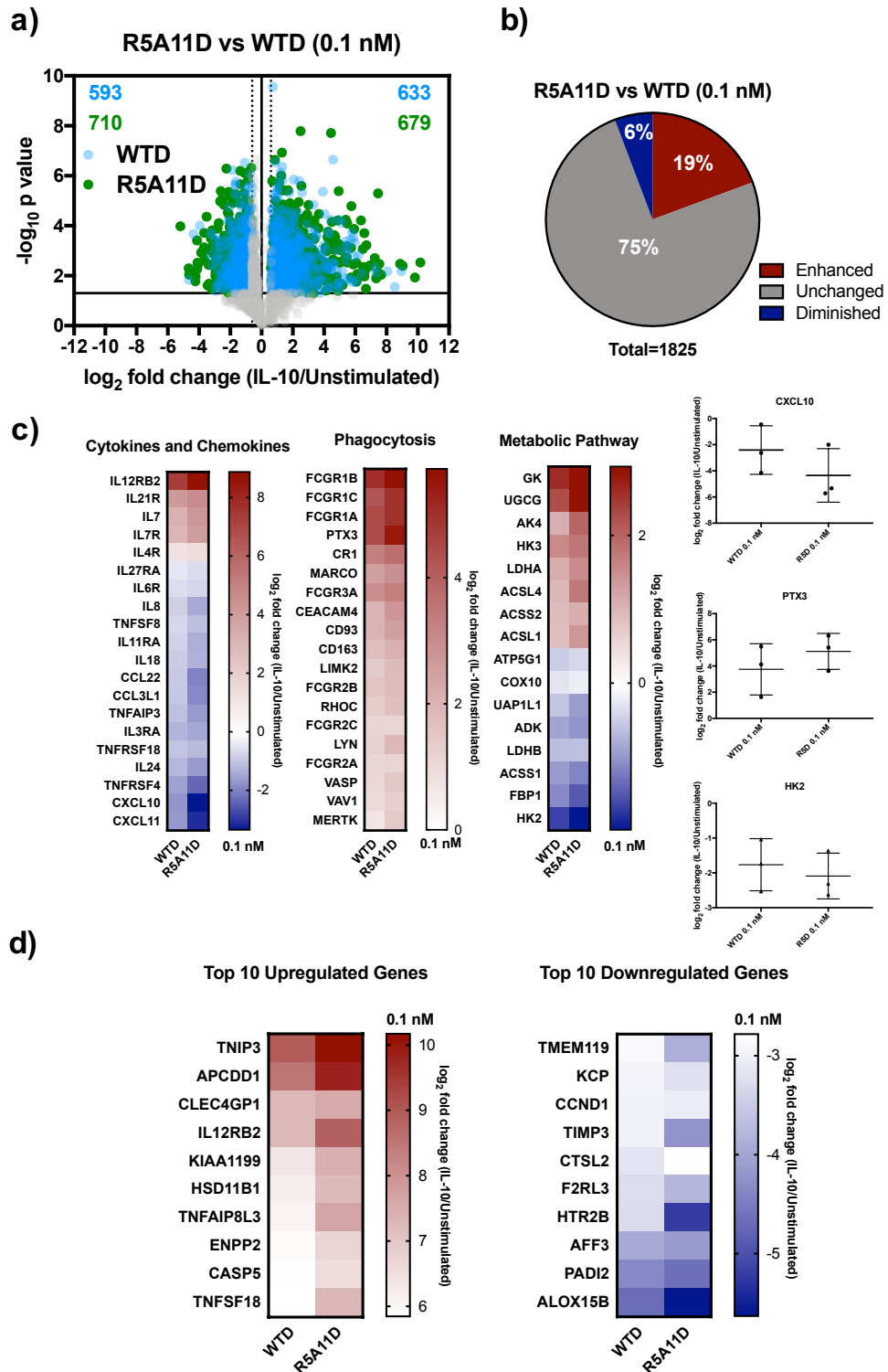
Figure 4.15 Comparison of gene regulation by R5A11D and WTD at 0.1 nM. (a) Volcano plot of genes regulated by WTD (blue) and R5A11D (green) at 0.1 nM each. Only genes which had been shown previously to be significantly regulated by WTD at 50 nM are plotted. Numbers of significant genes up and downregulated by each treatment are shown on the plot in their respective colours. **(b)** Percentage activity of R5A11D compared to WTD at 0.1 nM. The log_2 fold change of R5A11D/unstimulated was divided by the log_2 fold change of WTD/unstimulated. Enhanced expression denotes genes which had expression increased in R5A11D by more than 1.5 fold compared to WTD. Decreased expression denotes genes with less than 0.67 fold change. **(c)** Comparison of gene regulation by WTD and R5A11D at 0.1 nM for genes associated with proinflammatory cytokines and chemokines, phagocytosis and metabolic pathways, with values for individual replicates plotted for CXCL10, PTX3 and HK2 shown. **(d)** Heatmap of top 10 up and down regulated genes by WTD at 0.1 nM are compared to R5A11D 0.1 nM. For all genes shown the average of three biological replicates is plotted.

4.3.4 Monomeric IL-10 variants induce poorer transcriptional responses in monocytes compared to dimeric variants

Our previous work had shown that WTM displayed poor STAT activation while R5A11M showed STAT activation of 80-100% of the dimeric levels at saturating concentrations. We next wanted to see if this improvement in STAT activation translated into an increased transcriptional response. Cells were stimulated with a high concentration (50 nM) of both the wild type monomer (WTM) and high affinity monomer (R5A11M). When we compared the activity of WTM to WTD, WTM induced poorer regulation of 85% of genes (Figure 4.16a). This is in line with its very low levels of STAT activation. R5A11M showed much better transcriptional activity than WTM however it still showed poorer activity than WTD, with diminished regulation of 40% of genes (Figure 4.16b). These patterns of activity did not seem to be specific to a particular set of genes or pathways. When comparing cytokines and chemokines, phagocytosis and metabolic pathways across the conditions, we saw consistently poorer responses in the monomeric variants compared to WTD, with R5A11M showing an enhanced response over WTM but a poorer response compared to WTD (Figure 4.16c). Examples of this include genes such as IL-24, MARCO and ACSS1 (Figure 4.16d). This demonstrates that although increased affinity can greatly enhance activity of the monomeric IL-10, the transcriptional response does not reach dimeric levels. This suggests that stoichiometry contributes to IL-10's activity beyond STAT activation.
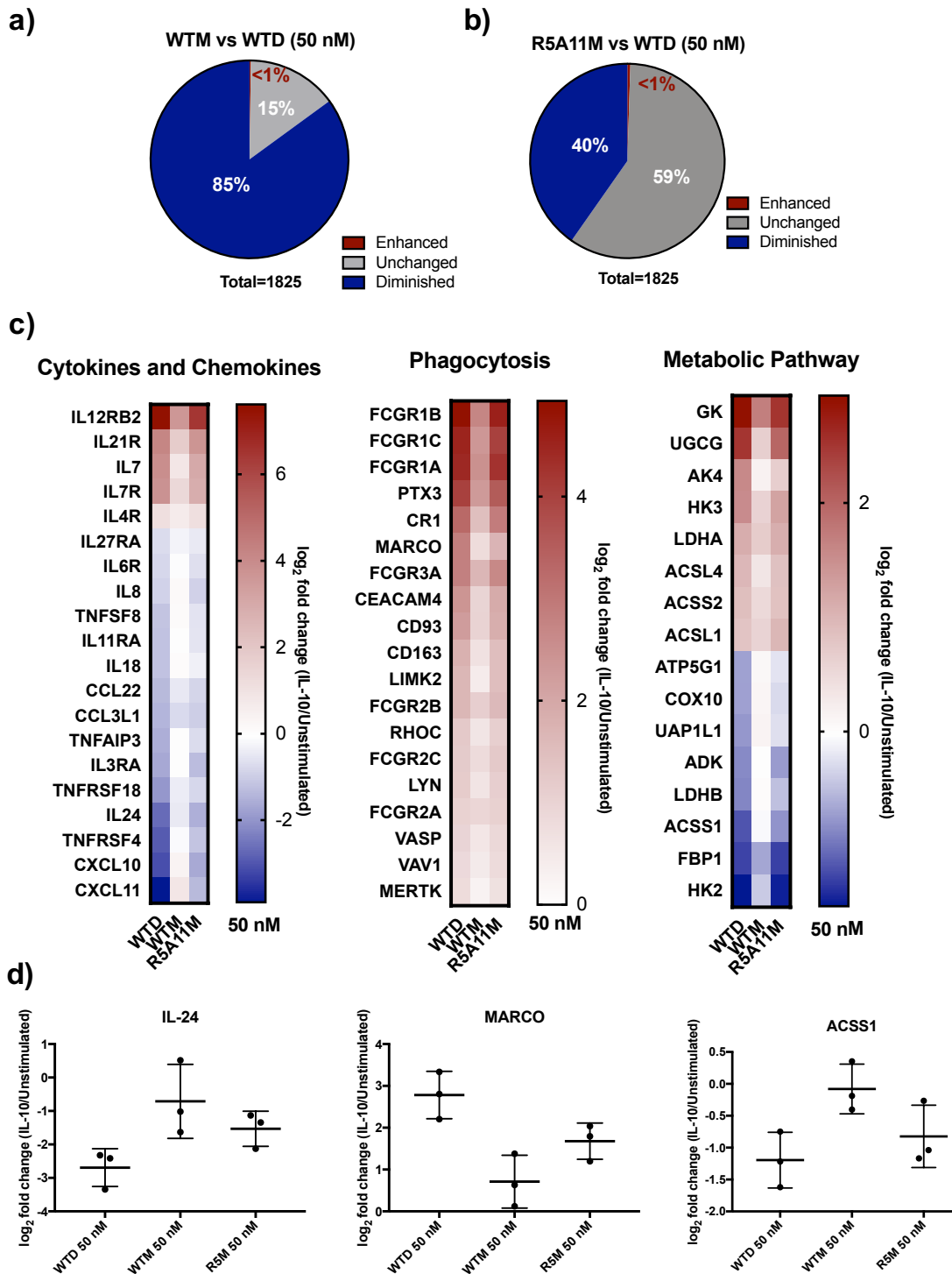
Figure 4.16 Comparison of monomeric transcriptional activity. (a) Comparison of regulation of monocyte genes by WTM and WTD at 50 nM. The $\log_2$ fold change of WTM/unstimulated was divided by the $\log_2$ fold change of WTD/unstimulated. Enhanced expression denotes genes which had expression increased in WTM by more than 1.5 fold compared to WTD. Decreased expression denotes genes with less than 0.67 fold change. **(b)** Comparison of regulation of monocyte genes by R5A11M and WTD at 50 nM. Gene regulation was determined as in (a). **(c)** Heatmap of $\log_2$ fold change for WTD, WTM, R5A11M at 50 nM compared to unstimulated cells for genes associated with proinflammatory cytokines and chemokines, phagocytosis and metabolic pathways. All values shown are the average of three biological replicates. **(d)** $\log_2$ fold change for IL-24, MARCO and ACSS1 for WTD, WTM and R5A11M at 50 nM.

4.4 High affinity IL-10 regulation of adaptive (CD8 T cell) immune responses

IL-10Rß affinity and receptor stoichiometry had profound effects on the response of monocytes to IL-10. We wanted to see if this held true in adaptive immune cells. As mentioned previously, IL-10 enhances the cytotoxicity of CD8 T cells, leading to its potential use as a cancer therapeutic (Emmerich et al., 2012). We chose to assess the effect of IL-10 on these cells due to their relevancy for human health.

4.4.1 Increased affinity enhances STAT activation in CD8 T cells

As was done in monocytes, we first examined differences in STAT activation by the IL-10 variants. Peripheral blood mononuclear cells (PBMCs) were isolated from human buffy coats and CD8 T cells were activated within this population. Media supplemented with anti-CD3 was used along with IL-2 to activate these cells for three days after which the media was changed to that with IL-2 alone to allow further expansion of activated populations for two more days as shown in Figure 4.17. Cells were then rested in media with no IL-2 overnight to reduce background levels of STAT activation. The cells were stimulated with the IL-10 variants (WTD, R5A11D, WTM, R5A11M) over a range of concentrations for 15 minutes before fixation in order to examine STAT1 and STAT3 activation.
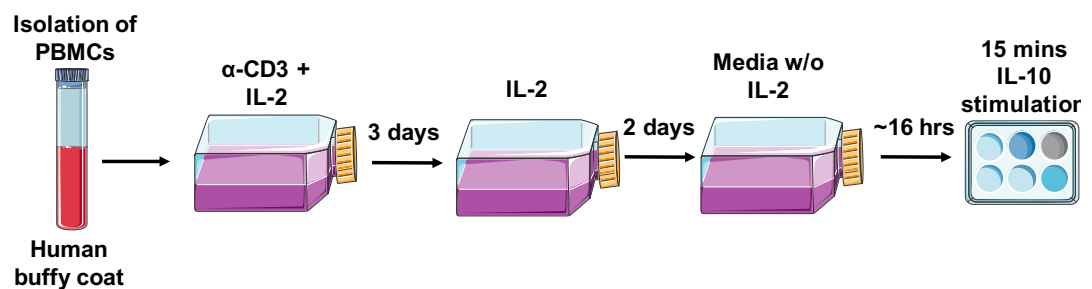
Figure 4.17 Activation and stimulation of CD8 T cells in a PBMC culture. PBMCs were isolated from human buffy coats and activated for three days using anti-CD3 (100 ng/mL) and IL-2 (20 ng/mL). Media was replaced to media containing only IL-2 for a further 2 days. Cells were then left overnight in media with no added IL-2 before a 15 minute stimulation with serially diluted IL-10 variants.

The dose response curves for CD8 cells are shown in Figure 4.18a-b. First comparing WTD with R5A11D, we saw patterns similar to those seen in monocytes. R5A11D and WTD showed comparable patterns of STAT activation at saturation however R5A11D displayed an apparent enhanced activity at very low doses, leading to a non-significant but decreased EC_{50} for both STAT1 and

STAT3 (Figure 4.18c-d). Similar to the results in monocytes, we saw that R5A11D had higher although non-significant, pSTAT1 levels at high concentrations.
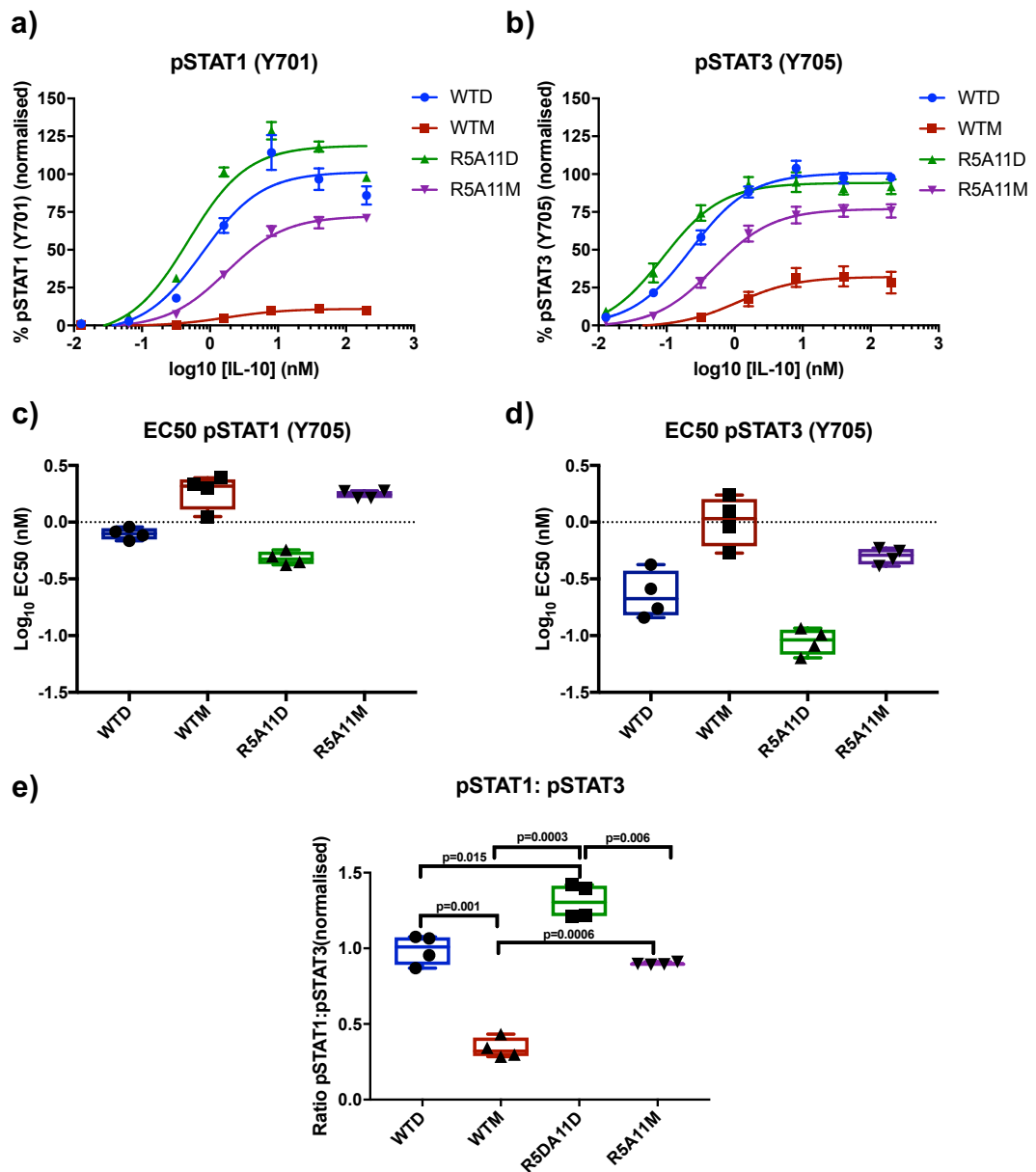
Figure 4.18 STAT1 and STAT3 activation by high affinity IL-10 variants. (a-b) Activated human CD8 cells in a PBMC culture were stimulated with IL-10 variants for 15 minutes. Phosphorylation of STAT1 and STAT3 was measured by flow cytometry. Data shown is the mean of 4 biological replicates. Each replicate is normalised by assigning the highest MFI value of the top concentration as 100% and the lowest MFI value of the bottom concentration as 0%. Error bars represent the standard error of the mean. **(c-d)** Log_{10} EC50 values for pSTAT1 and pSTAT3 from the corresponding dose response curves in (a-b). **(e)** Ratio of pSTAT1 to pSTAT3 in CD8 cells upon IL-10 variant stimulation. Ratio was calculated by taking the percentage activation of pSTAT1 and pSTAT3 at 40 nM and dividing the pSTAT1 by pSTAT3 values. P values were calculated using paired t tests.

When looking at the monomeric IL-10 variants we again saw similar results to those in monocytes. WTM displayed very poor activation of STAT1, reaching only 10% of the dimeric activity even at high concentrations. It also had very poor

STAT3 activity at 25% of WTD activation levels (Figure 4.18a-b). This resulted in an apparent much higher EC_{50} values for WTM compared to the dimeric variants (Figure 4.18c-d). When we compare this to the high affinity monomer, R5A11M, it showed greatly enhanced STAT activation, reaching 70% of the dimeric activity at saturation (Figure 4.18a-b). However, it performed much poorer than the dimers at low concentrations, leading to higher EC_{50} values (Figure 4.18c-d).

When we examined the differences between the variants in activating STAT1 and STAT3 we saw that WTM had a clear bias for STAT3 activity, with a low pSTAT1:pSTAT3 ratio as was seen in monocytes (Figure 4.18e). WTD and R5A11M had a 1:1 ratio but interestingly R5A11D showed a significantly higher ratio.

Results seen in CD8 T cells are broadly in keeping with those seen in monocytes. Increased affinity greatly enhanced activation of STAT1 and STAT3 at saturating concentrations by the monomeric variant. The high affinity dimer showed an apparent improved activity compared to the wild type at low concentrations but acted similarly at saturation. This suggests that STAT activation by IL-10 follows broadly similar patterns in both monocytes and CD8 T cells.

4.4.2 Changes in receptor affinity and stoichiometry do not affect the kinetics of the IL-10 response in CD8 T cells

As receptor affinity and stoichiometry played a role in the activation of STAT1 and STAT3 in CD8 T cells, we next wanted to see if they would induce any change in the kinetics of STAT activation. CD8 T cells in a PBMC population were stimulated with the IL-10 variants at a constant concentration for specified times between 15 minutes and 3 hours. As shown in Figure 4.19, activation of both STAT1 and STAT3 peaked at 15 minutes. STAT1 was dephosphorylated faster than STAT3, with levels returning to basal after 1 hour. While the amplitude of STAT activation varied between the IL-10 variants, the kinetics of the response was consistent. As was seen in the dose response studies, R5A11D activated more STAT1 compared to the other variants. WTM had a poor STAT1 and STAT3

activation. However, dephosphorylation happened at an identical rate for all variants.
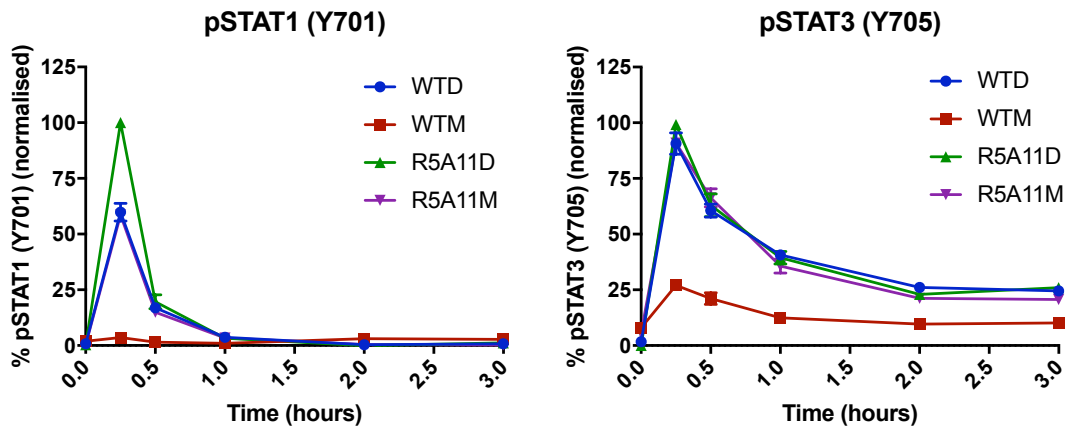
Figure 4.19 Kinetics of pSTAT1 and pSTAT3 response to IL-10 variants in CD8 T cells. CD8 T cells in a PBMC population were stimulated with IL-10 variants at a constant concentration of 50 nM for the specified time periods before fixation. Three biological replicates were used. Error bars represent the standard error of the mean. Data was normalised by assigning the highest value at 15 mins as 100% and the lowest value of an untreated control as 0%.

In summary, as was seen in monocytes, changes in receptor affinity or stoichiometry do not alter the kinetics of the IL-10 response. When compared to monocytes, dephosphorylation of STAT1 occurred at a faster rate in CD8 T cells, suggesting differential mechanisms regulating the resolution of the response in these cells.

4.4.3 High affinity dimeric variant R5A11D enhances granzyme B production in CD8 T cells at low cytokine concentrations

Several studies in recent years have investigated the effect of IL-10 on cytotoxic CD8 T cells. It has been shown that IL-10 can enhance the cytotoxicity of these cells, leading to greater rates of tumour clearance in both mice and human patients (Naing et al., 2019). It does this, in part, by increasing the production of cytotoxic effector molecules such as granzyme B and IFNγ. This was demonstrated *in vitro* in PBMCs and also in patients treated with PEGylated IL-10 (Chan et al., 2015, Naing et al., 2018). We used this known IL-10 response in CD8 T cells to see if the improved STAT activation by R5A11D in CD8 T cells translated into an improvement in biological activity. Human CD8 T cells were activated in a PBMC population as shown in Figure 4.20. Cells were activated in

the absence or presence of IL-10 variants. Two different concentrations of IL-10 variants were used: 50 nM and 0.1 nM. Granzyme B protein levels were then measured after the 6 days of activation using flow cytometry.
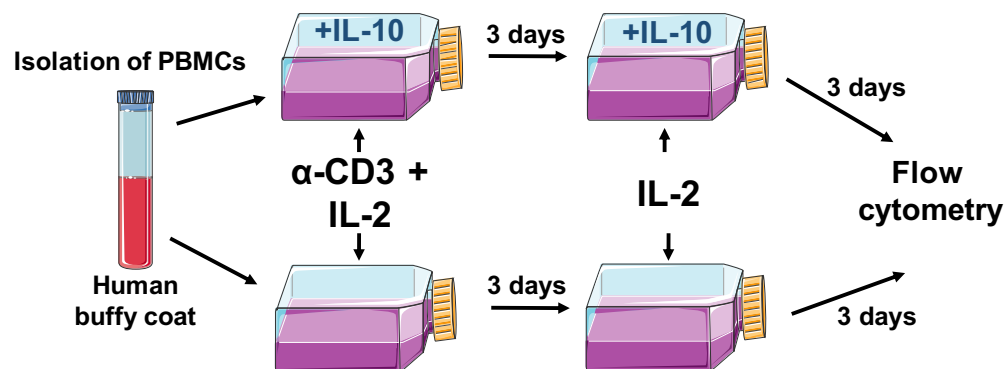
Figure 4.20 Activation and stimulation of CD8 T cells in a PBMC culture in the presence of IL-10 variants. PBMCs were isolated from human buffy coats and activated for three days using anti-CD3 (100 ng/mL) and IL-2 (20 ng/mL). Media was replaced to that containing IL-2 only for a further 2 days. IL-10 variants WTD, R5A11D, WTM, R5A11M, were added to the media at the start of culture and again at day 3, each at 50 nM and 0.1 nM final concentration. Cells from each donor were also activated in the absence of IL-10 as a control.

At a high concentration of IL-10 (50 nM), both WTD and R5A11D induced a 2.5-fold upregulation of granzyme B compared to cells grown without IL-10 stimulation (Figure 4.21). WTM induced a very poor granzyme B upregulation, with many donors showing no increase. This is in line with WTM's poor STAT activation and its poor activity in monocytes. R5A11M showed a variable response: in half the donors tested granzyme B was upregulated to a similar level as seen in the dimeric molecules. However, half of the donors showed a poor response, similar to WTM. When the low dose of IL-10 was used R5A11D induced significantly more granzyme B compared to WTD, in keeping with its enhanced STAT activation at this concentration (Figure 4.21).
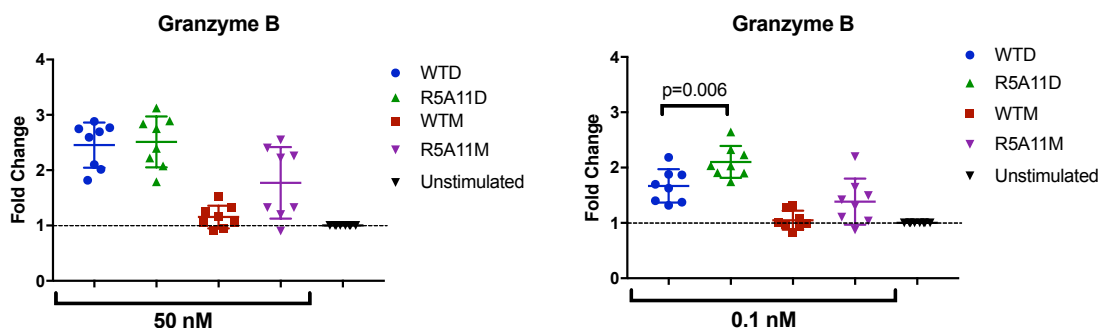
Figure 4.21 Comparison of granzyme B upregulation by IL-10 variants. CD8 T cells were activated in a PBMC population using anti-CD3 and IL-2 for three days followed by IL-2 for 3 days. IL-10 wild type and variants were added to the media at the above concentrations at day 1 and day 3 of activation. Granzyme B protein was measured at day 6 by flow cytometry after permeabilisation. Each point represents one biological replicate (n=8). Fold change was calculated by dividing the granzyme B MFI of treated cells by non-IL-10 treated control cells within. P value was calculated by two tailed paired t test.

4.5 Characterisation of the transcriptional activity induced by IL-10 and high affinity variants in CD8 T cells

Our analysis of transcriptional regulation in monocytes by our high affinity variants supported our previous observations that increased affinity provided an advantage at low doses. It also highlighted that, although the high affinity monomer showed STAT activation levels similar to those induced by the dimeric variants, this did not linearly translate into similar levels of gene regulation. We had shown that, in CD8 T cells, R5A11D also displayed enhanced activity at low doses compared to WTD. We wanted to see if this advantageous effect held true at a global level of cell regulation and so we used RNA sequencing to characterise the response of human CD8 T cells to our IL-10 variants. As mentioned previously recent studies have shown that IL-10 can enhance the cytotoxicity and tumour-targeting activity of CD8 T cells both *in vitro* and i*n vivo*. However, much less is known about the molecular mechanisms which underpin the effect. We envisioned that our transcriptional data would provide an unbiased comparison of the transcriptional activities of our high affinity variants and offer new insights into the molecular basis through which IL-10 carries out its pleiotropic effects.

Human CD8 positive T cells were isolated from human PBMCs (StemCell Technologies) from three donors and activated using anti-CD3/CD28 and IL-2 over 6 days as shown in Figure 4.22. IL-10 wild type and high affinity monomeric and dimeric variants were added to the media at day one of activation and again at day three. The monomeric variants (WTM, R5A11M) were used at the high dose of 50 nM and the dimeric variants (WTD, R5A11D) were used at 50 nM and a low dose of 0.1 nM as well. Cells were also activated in a similar manner but left without IL-10 stimulation within each donor group to act as controls.

Cells were stimulated and RNA was isolated by the author. RNA sequencing and primary data analysis for quality control, mapping to reference genome and quantification was conducted by an external company, Novogene as detailed in the "Materials & Methods" chapter. Statistical analysis and comparison of gene regulation between the IL-10 variants was done by the author.
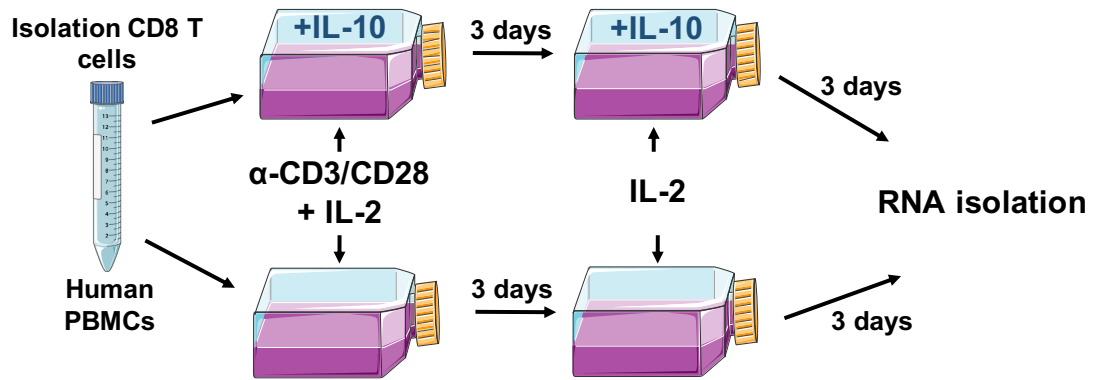
Figure 4.22 Activation and stimulation of purified CD8 T cells presence of IL-10 variants for RNA sequencing. CD8 T cells were isolated from PBMCs (n=3) and activated for three days using anti-CD3/CD28 beads and IL-2 (20 ng/mL). Media was replaced to IL-2 only for a further 2 days. IL-10 variants were added to the media at day 1 and again at day 3 when the media was changed. IL-10 variants used were WTD, R5A11D, WTM, R5A11M. WTD and R5A11D were used each at 50 nM and 0.1 nM final concentration and WTM and R5A11M were used at 50 nM. Cells from each donor were also activated in the absence of IL-10 as a control.

4.5.1 Characterising the transcriptional effect of WTD on human CD8 T cells

A similar analysis methodology was used on the RNA sequencing data from CD8 T cells as was done for monocytes. First, we examined the effect of WTD on CD8 T cell gene transcription programmes. We generated a list of gene transcripts whose expression was significantly changed by WTD more than 1.5 fold or less
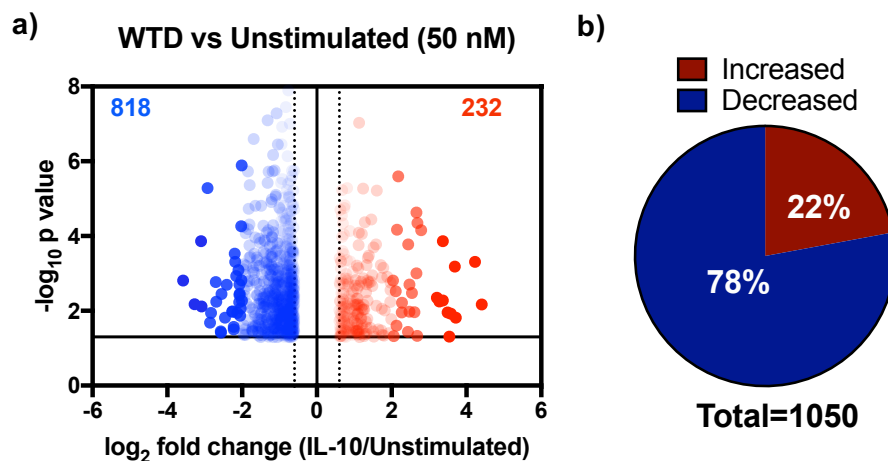
Figure 4.23 Regulation of CD8 transcription by WTD. (a) Volcano plot of CD8 genes significantly upregulated by WTD >0.6 log$_2$ fold change (red) and significantly downregulated by WTD <-0.6 log$_2$ fold change compared to non-IL-10 treated cells. Fold change was calculated by dividing WTD 50 nM by unstimulated values for each donor. The average fold change was calculated for three donors and the log$_2$ of this value is plotted. P values< 0.05 were calculated by two-tailed two sample equal variance t test of the log$_2$ fold change of WTD 50 nM/ unstimulated genes for each donor. Genes which were not significantly changed were <0.6 >0.6 log$_2$ fold change were excluded. N=3. **(b)** Proportion of genes significantly up or down regulated by WTD in CD8 T cells.

than 0.67 fold compared to unstimulated cells (>0.6 log$_2$ fold change or <-0.6 log$_2$ fold change). This list can be found in Appendix Table 2.

There were 1050 genes significantly up or down regulated by WTD (Figure 4.23a). 78% of these significantly regulated genes were downregulated by WTD (Figure 4.23b).

When looking at subsets of downregulated genes we saw the significant inhibition of the classical exhaustion markers EOMES, TOX and TIGIT by WTD as well as HAVCR-2 (encoding the protein TIM-3) although this did not reach significance (Figure 4.24a). This led us to speculate that WTD may regulate the exhaustion state of CD8 T cells. An in depth profile of exhausted CD8 T cells at both the transcriptional, epigenetic and protein level was previously characterised using RNA sequencing and mass cytometry (Bengsch et al., 2018). We used their list of genes shown to be up and downregulated in exhausted CD8 T cells by this study to compare the exhaustion signature in our WTD treated cells. We could detect 97 genes regulated by WTD that also appeared in the exhaustion signature previously published (this list is shown in Appendix Table 3). When we compared regulation of these genes, they could be grouped into four clusters: cluster 1 comprises genes upregulated in exhausted T cells and by WTD treatment, cluster 2 are genes upregulated in exhausted T cells and downregulated by WTD, cluster 3 are genes downregulated in exhausted T cells and upregulated by WTD and cluster 4 are genes downregulated in both exhausted and IL-10 treated cells (Figure 4.24b). A sample of genes from each cluster is shown in Figure 4.24c. Cluster 2 is the largest cluster, showing genes which are upregulated in exhausted cells but downregulated by WTD. This suggests that IL-10 may be preventing, to some extent, T cell exhaustion suggesting a potential mechanism by which IL-10 enhances the activity of CD8 T cells.
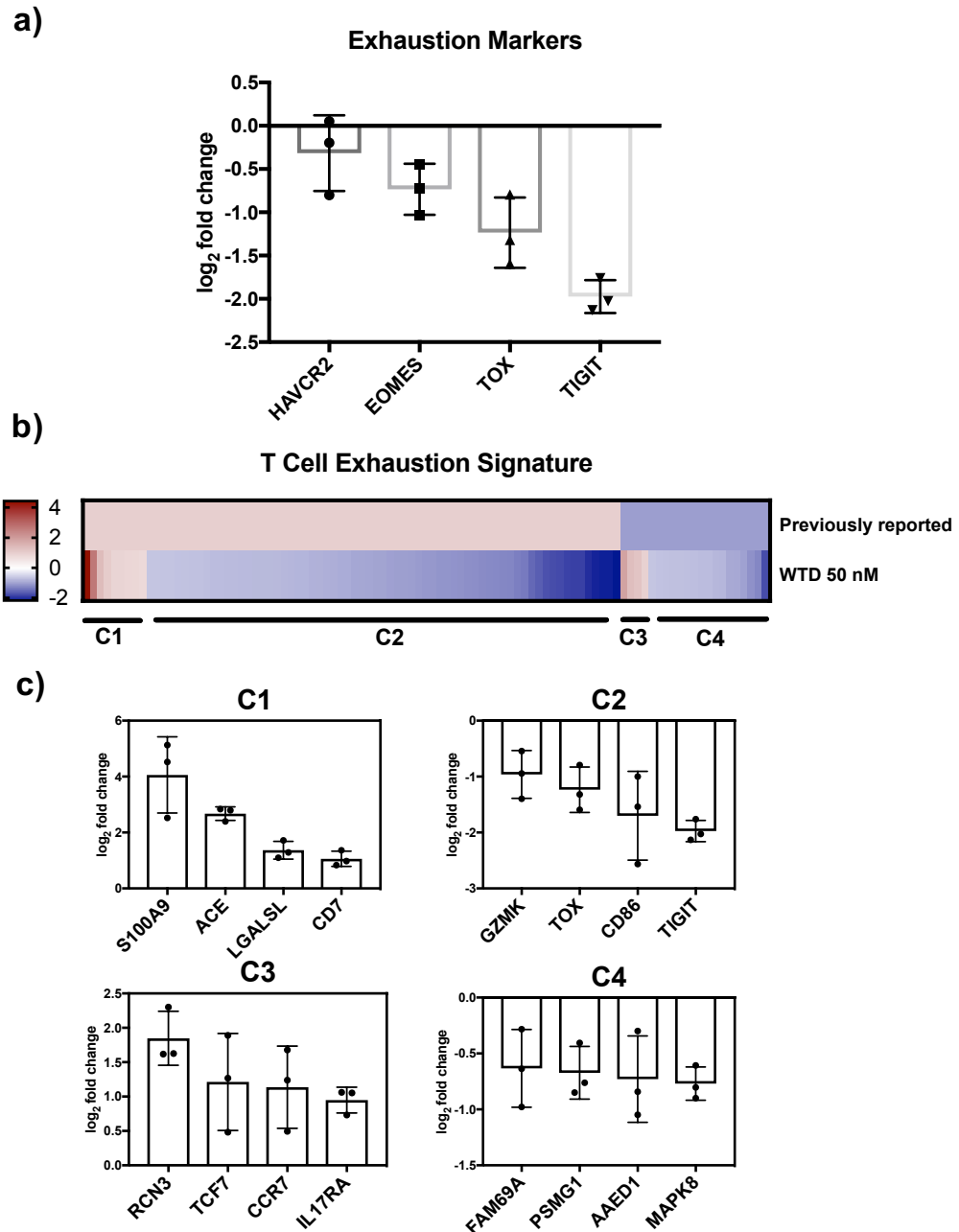
Figure 4.24 Regulation of exhaustion-associated genes by WTD. (a) Log2 fold change of exhaustion markers downregulated by WTD (50 nM) compared to unstimulated. Each point represents one biological replicate and error bars indicate the standard deviation. **(b)** Heatmap of genes previously reported to be present in exhausted T cells. A list of exhaustion specific genes from (Bengsch et al., 2018) was used as a comparison for genes significantly up or down regulated by WTD 50 nM. Previously reported genes were given a nominal value of 1 for upregulated genes and -1 for downregulated genes. Log2 fold change for WTD 50 nM was plotted. The gene names and their log2 fold change can be found in Appendix Table 3. **(c)** The log2 fold change induced by WTD (50 nM) for a sample of genes from each cluster is shown. Each point represents one biological replicate.

We also noted a significant downregulation in the levels of the IL2RA gene (Figure 4.25a), which could also be confirmed at the level of protein expression by flow cytometry of similarly treated cells (Figure 4.25b). IL-2 is a key regulator of T cell function and was used in our study as a growth factor for CD8 T cells,

along with stimulation of the T cell receptor. We speculated whether a decrease in IL2RA was moderating the response of these cells to IL-2.
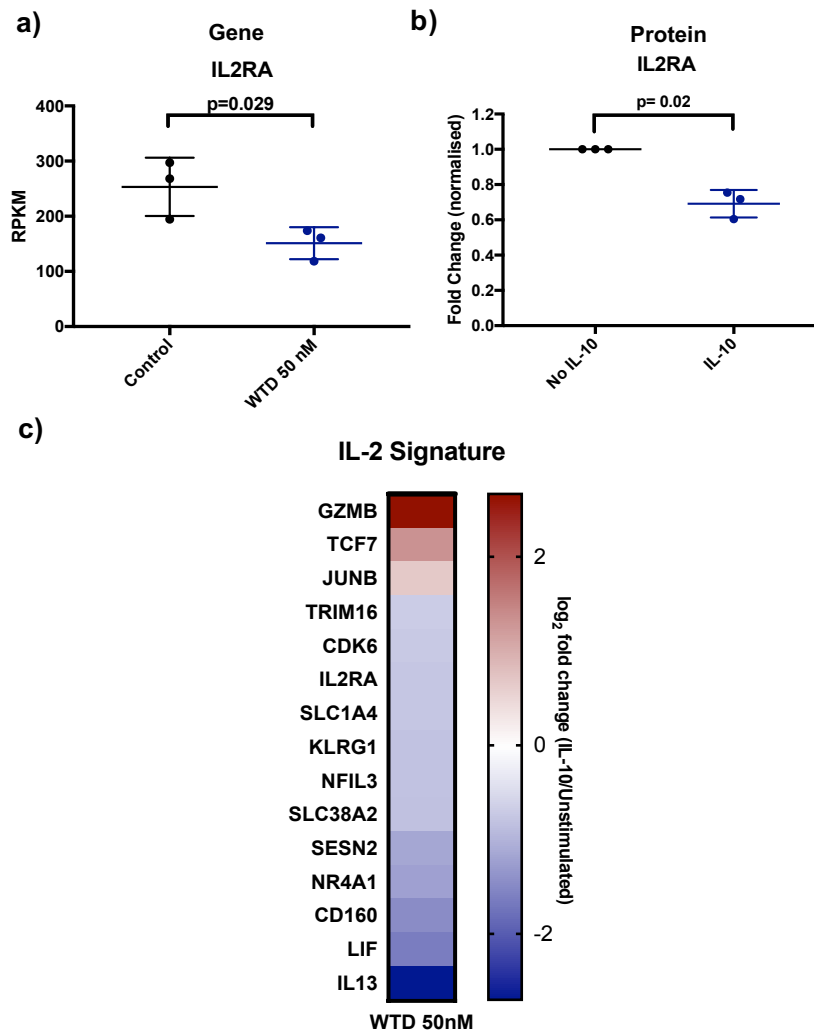
Figure 4.25 Modulation of IL-2 receptor and IL-2 associated genes in CD8 T cells by WTD. (a) Expression of IL2RA RNA measured by RNA sequence analysis. Each point represents one biological replicate. P value was calculated by a paired t test. **(b)** IL2RA protein levels measured by flow cytometry. CD8 T cells were activated in a PBMC population for three days using anti-CD3 and IL-2 in the presence or absence of IL-10 (WTD, 50nM), followed by two days expansion with IL-2 in the presence or absence of IL-10. Fold change was calculated by dividing IL2RA levels of IL-10 stimulated by non-IL-10 stimulated control values for each donor. Each point represents one biological replicate. P value was calculated by paired t test. **(c)** Heatmap showing the log$_2$ fold change induced by WTD at 50 nM for genes previously reported to be regulated by IL-2 in CD8 T cells (Rollings et al., 2018).

The effect of IL-2 on the CD8 T cell proteome was previously examined using quantitative high resolution mass spectrometry (Rollings et al., 2018). We compared the many proteins in their study which were shown to be modulated by IL-2 to transcripts significantly regulated by WTD in our study. Figure 4.25c shows that WTD treatment downregulated several IL-2 regulated genes such as IL-13, LIF, SLC1A4 and NFIL3 but enhanced expression of GZMB. While a direct comparison between gene regulation and protein expression cannot be made as

changes at the level of RNA do not always translate into changes at the level of protein, it suggests that IL-10 could be limiting the sensitivity to IL-2 via a downregulation in IL2RA levels, perhaps delaying or protecting these cells from exhaustion. Much further work will need to be done to investigate this hypothesis further.

4.5.2 WTD loses potency at low concentrations in CD8 T cells

Together these data gave us an insight into how IL-10 modulates CD8 T cell activity. This list of 1050 significantly regulated genes then acted as a template against which we could compare our other IL-10 variants and doses. As was done in monocytes, we wanted to see if these genes were sensitive to changes in WTD concentration. We compared regulation of these genes by WTD at 50 nM and also at 0.1 nM. As shown in Figure 4.26a, 813 genes showed activity of 75% or less at low dose WTD compared to high dose WTD. Of this large set of dose-dependent genes, 77% of those were genes that were downregulated by IL-10. We identified several genes involved in the IL-2 or exhaustion response such as IL-13, LIF and TOX which were poorly regulated by WTD at 0.1 nM (Figure 4.26b). This poorer regulation of subsets of genes at low doses is in keeping with the results seen in monocytes, supporting the idea that IL-10 loses efficacy at sub-saturating concentrations.
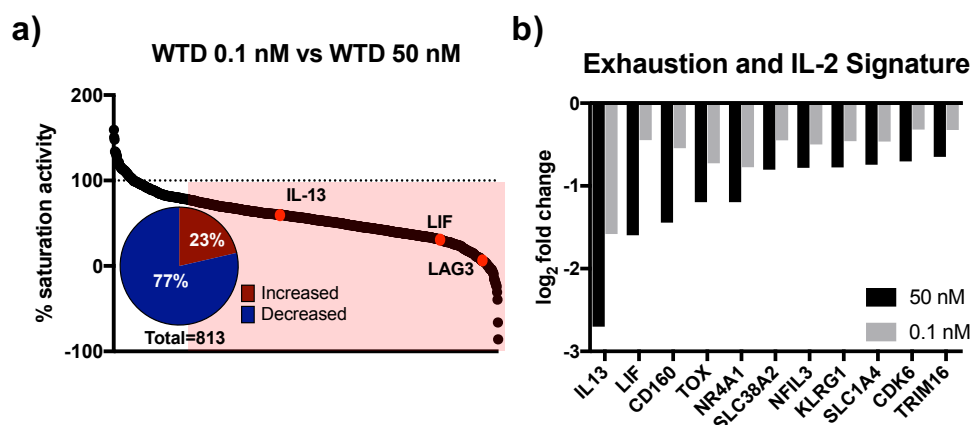
Figure 4.26 Comparison of WTD activity at 0.1 nM vs 50 nM. (a) Percentage activity of low dose WTD compared to high dose WTD. Points within the red box are those which show <75% activity at low dose compared to high dose WTD (813 genes). The percentage activity was calculated by dividing the $\log_2$ fold change of WTD 50 nM/US by the $\log_2$ fold change WTD 0.1 nM/US and multiplying by 100. Insert shows the percentage of those 813 genes which were up or downregulated by WTD compared to unstimulated controls. **(b)** Average $\log_2$ fold change for exhaustion and IL-2 related genes at 50 nM and 0.1 nM WTD.

4.5.3 High affinity dimeric IL-10 displays enhanced transcriptional activity at low doses compared to wild type IL-10 in CD8 T cells

In monocytes, R5A11D showed improved gene regulation at low concentrations compared to WTD. When we compared the activity of R5A11D at 0.1 nM with WTD at 0.1 nM we saw that this held true in CD8 T cells. Firstly, we compared the distribution of significantly regulated genes. Figure 4.27a shows that for both WTD and R5A11D at 0.1 nM, the majority of genes were downregulated. R5A11D showed more significantly downregulated genes than WTD at 0.1 nM (480 genes compared to 235). When we compared expression levels of genes, we saw that R5A11D displayed a large advantage over WTD at 0.1 nM, with 39% of genes showing enhanced regulation by R5A11D and only 8% showing better activity by WTD (Figure 4.27b).

Again, to take an unbiased sample of genes we looked at the expression of the top 10 up and down regulated genes by WTD at 0.1 nM and compared this to R5A11D at 0.1 nM (Figure 4.27c). Similar to what was seen in monocytes, the majority of these highly regulated genes showed enhanced expression by R5A11D. This held true when we looked at subsets of genes such as CD markers and cytokines and chemokines (Figure 4.27d-f). This data supports what was seen in monocytes, confirming that R5A11D displays enhanced activity at low doses compared to WTD.

4.5.4 Monomeric IL-10 variants induce poorer transcriptional responses in CD8 T cells compared to dimeric variants

As the WTM had a decreased transcriptional response in monocytes we wanted to see if this also held true in CD8 T cells. WTM consistently showed poor STAT activation at all doses tested in CD8 T cells, as well as a poor upregulation of granzyme B. STAT activation could be enhanced greatly by increased affinity as shown by R5A11M however upregulation of granzyme B by R5A11M was variable between the donors tested. We hoped that by comparing the transcriptional response of CD8 T cells to WTD, WTM and R5A11M we could determine the contribution of receptor stoichiometry and affinity to the CD8 IL-10 response.
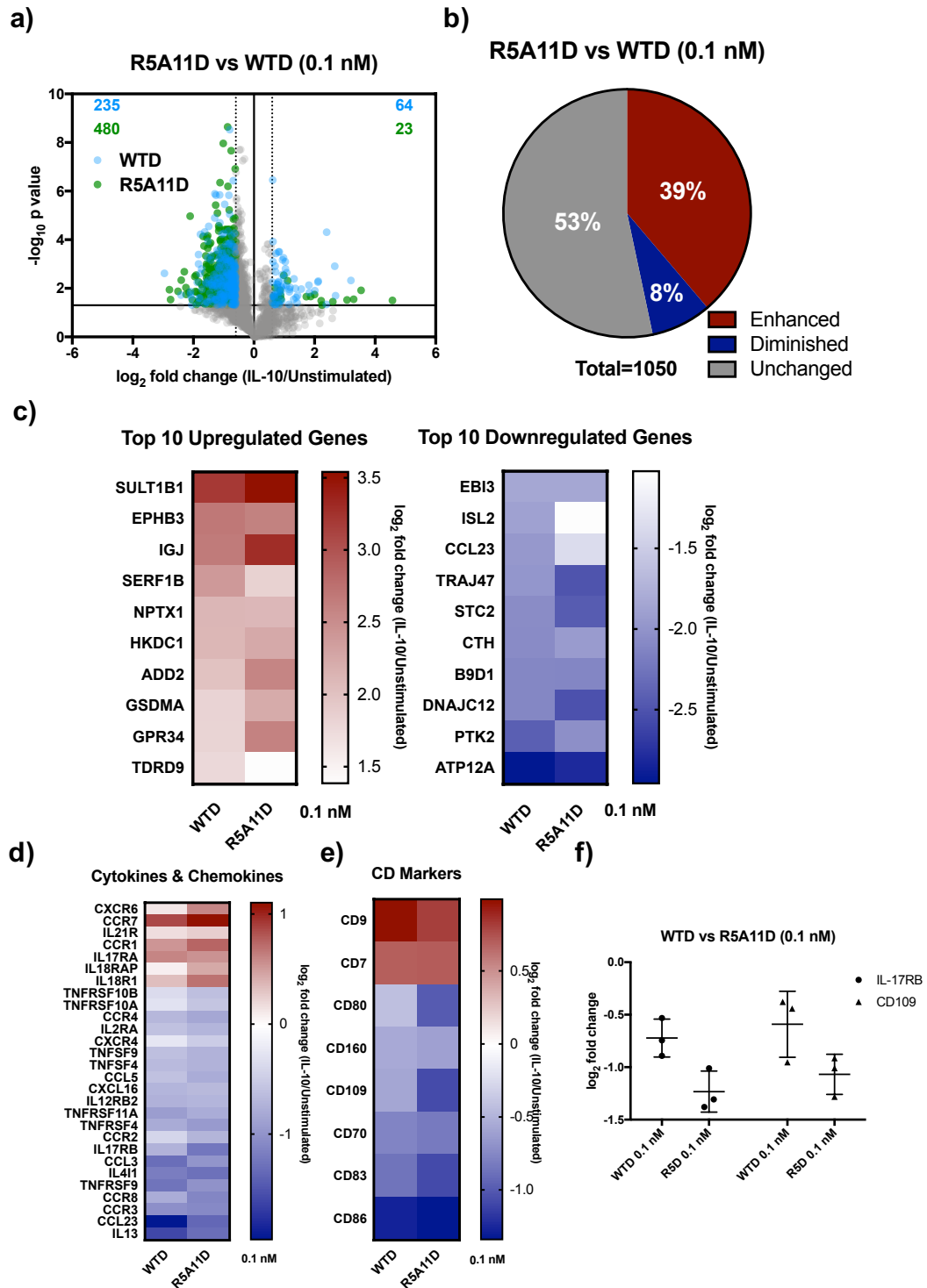
Figure 4.27 Comparison of R5A11D and WTD at 0.1 nM. (a) Volcano plot of genes regulated by WTD (blue) and R5A11D (green) at 0.1 nM each. Only genes which had been shown previously to be significantly regulated by WTD at 50 nM are plotted. Numbers of significant genes up and downregulated by each treatment are shown on the graph in their respective colours. **(b)** Percentage activity of R5A11D compared to WTD at 0.1 nM. The $\log_2$ fold change of R5A11D/unstimulated was divided by the $\log_2$ fold change of WTD/unstimulated. Enhanced expression denotes genes which had expression increased in R5A11D by more than 1.5 fold compared to WTD. Decreased expression denotes genes with less than 0.67 fold change. **(c)** Heatmap of top 10 up and down regulated genes by WTD at 0.1 nM compared to R5A11D 0.1 nM. **(d)** Heatmap of inflammatory cytokines and chemokine genes regulated by WTD and R5A11D at 0.1 nM. each **(e)** Regulation of genes encoding CD markers by WTD and R5A11D at 0.1 nM. **(f)** $\log_2$ fold change of IL-17RB and CD109 by WTD and R5A11D at 0.1 nM.

When cells were stimulated with WTM we saw a very poor response compared to WTD activity at the same concentration with 96% showing a diminished response (Figure 4.28a). R5A11M showed better regulation than WTM, with 42% of genes showing similar levels of regulation to WTD however over half of the genes (58%) had diminished activity (Figure 4.28b). This pattern of activity appeared consistent across groups of genes such as cytokine and chemokines and CD markers (Figure 4.28c-d). In nearly all genes analysed R5A11M enhanced expression compared to WTM however it failed to reach dimeric levels of activity, suggesting that stoichiometry as well as receptor affinity plays a crucial role in determining the amplitude of the IL-10 response.
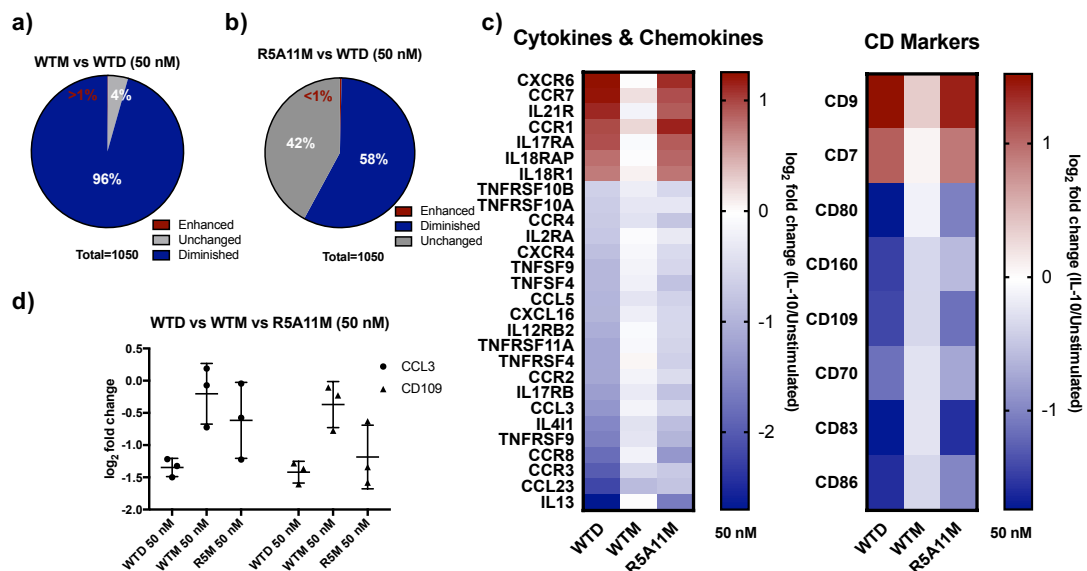
Figure 4.28 Comparison of monomeric transcriptional activity. (a) Comparison of regulation of CD8 T cell genes by WTM and WTD. The log$_2$ fold change of WTM/unstimulated was divided by the log$_2$ fold change of WTD/unstimulated. Enhanced expression denotes genes which had expression increased in WTM by more than 1.5 fold compared to WTD. Decreased expression denotes genes with less than 0.67 fold change. **(b)** Comparison of regulation of monocyte genes by R5A11M and WTD. Gene regulation was determined as in (a). **(c)** Heatmap of log$_2$ fold change for WTD, WTM, R5A11M compared to unstimulated cells for cytokines and chemokine genes and genes encoding CD markers. **(d)** Log$_2$ fold change of CCL3 and CD109 by WTD, WTM and R5A11M at 50 nM.

4.6 High affinity IL-10 enhances target cell killing by CAR T cells *in vitro*

Work in this section was carried out in <u>the University of Lille by W. Warda, A Cozzani, C. Ferrand and S. Mitra</u> as they had previously developed the CAR T cell model used here targeting acute myeloid leukemic cells (Warda et al., 2019). The IL-10 proteins were made by the author of this thesis and sent to the University of Lille for use in this experiment.

Our high affinity dimeric IL-10 (R5A11D) proved advantageous over its wild type counterpart (WTD) in receptor assembly, STAT activation and transcriptional activity. We also noted that it induced higher levels of the cytotoxic effector molecule granzyme B. IL-10 has been shown to boost the cytotoxicity of CD8 T cells both *in vitro* and *in vivo*, leading to enhanced tumour targeting and clearing (Mumm and Oft, 2013). Chimeric antigen receptor (CAR) T cells are another promising immune-therapeutic in cancer treatment which has already translated into the clinic for treatment of blood cancers such as acute lymphoblastic leukaemia (ALL). Due to IL-10's known ability to enhance the anti-tumour response of CD8 T cells we speculated whether this could be applied to CAR T cells. In addition, we wanted to investigate if R5A11D would show enhanced efficacy over WTD in this clinically-relevant scenario.

A CAR T cell model targeting acute myeloid leukemic cells was used to address these questions. In this CAR T cell model, cells were generated which target the interleukin-1 receptor accessory protein (IL-1RAP) (Warda et al., 2019). IL-1RAP is expressed on leukemic stem cells but absent on normal haematopoietic stem cells, making it a promising therapeutic target. They demonstrated that generation of anti-IL1RAP CAR T cells showed efficacy in targeted killing in an *in vitro* setting using either an IL-1RAP expressing cell line and primary cells as well as *in vivo* efficacy in a murine model. We used anti-IL-1RAP CAR T cells as a model to investigate if changes in IL-10 receptor affinity affected targeted killing by T cells.

4.6.1 Activation, transduction and culture of anti-IL-1RAP CAR T Cells

The protocol developed by Warda et al. was used here to generate anti-IL-1RAP CAR T cells as shown in Figure 4.29a. Briefly, PBMCs were isolated from healthy donors and activated using anti-CD3/CD28 for 2 days. These cells were then transduced with supernatant containing lentivirus which encoded either the anti-IL-1RAP CAR or a mock CAR with no anti-IL-1RAP. A sample of cells were also left un-transduced as a control. The cells were grown for 5 days after transduction in media containing IL-2. The cells were then transferred into three IL-10 different
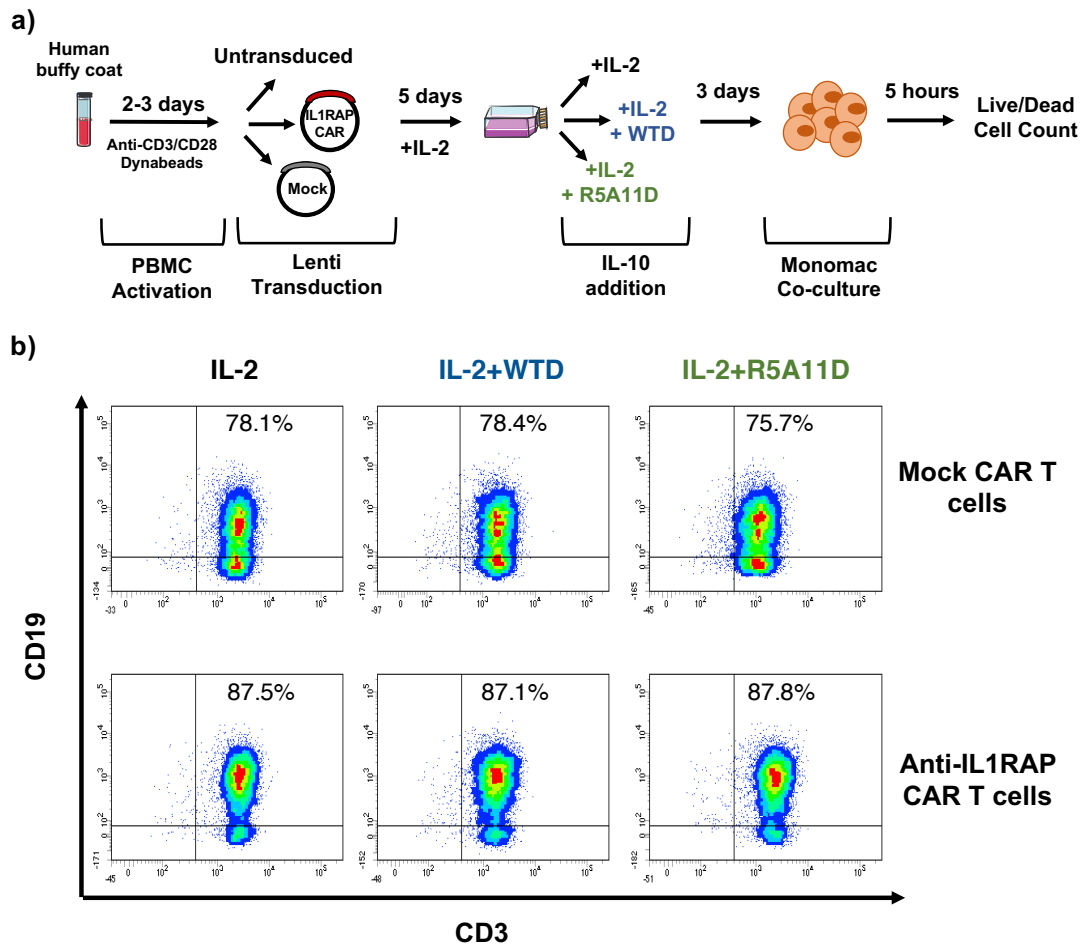
Figure 4.29 Generation and IL-10 stimulation of anti-IL-1RAP CAR T cells. (a) Schematic of CAR T cell cytotoxicity assay. Total T cells in PBMC culture were activated with anti-CD3/CD28 Dynabeads for 2-3 days. The cells were then transduced with lentivirus-containing supernatant (un-transduced, mock CAR vector, anti-IL-1RAP CAR vector). Cells were cultivated for three days in media devoid of IL-10 or containing WTD (25 nM) or R5A11D (25 nM). The target cells, Mono-Mac-6 cells (IL-1RAP positive leukemic cell line), were co-cultured at various Effector: Target (E:T) ratios. After 5 hours, the percentage of alive Mono-Mac-6 cells were measured by 7-AAD staining using flow cytometry. **(b)** Representative dot plots of CAR expression profiles on anti-IL-1RAP CAR T cells and Mock T cells cultured in the presence of IL-2 with or without WTD or R5A11D (25nM) for 3 days. **This experiment was performed and analysed by A. Cozzani, University of Lille.**

culture conditions: WTD (25 nM), R5A11D (25 nM) or no IL-10. IL-2 was also present in the media of all cultures.

The cells were kept in these conditions for a further 3 days before killing activity was tested.

Figure 4.29b shows efficacy of the Lentiviral transduction. The plots show expression of CD3 as well as CD19. A truncated CD19 is included in both the mock and the anti-IL-1RAP CAR T cell vectors as a selection marker. Both mock and anti-IL-1RAP CAR T cell vectors showed high rates of transduction.

4.6.2 R5A11D has a greater rate of target cell killing than WTD

After the CAR T cells had been cultured under the different IL-10 conditions they could then be tested for target cell killing activity. The cells were co-cultured with Mono-Mac-6 cells, a human leukemic cell line which is positive for IL-1RAP. Cells were cultured at three Effector: Target ratios; 1:1, 2:1, 4:1 as well as a target cell only control (0:1). Killing activity was determined by assessing the viability of the Mono-Mac-6 cells after 5 hours co-culture. Viability was normalised within each donor as a percentage of the live cells in the 0:1 effector: target cell condition.
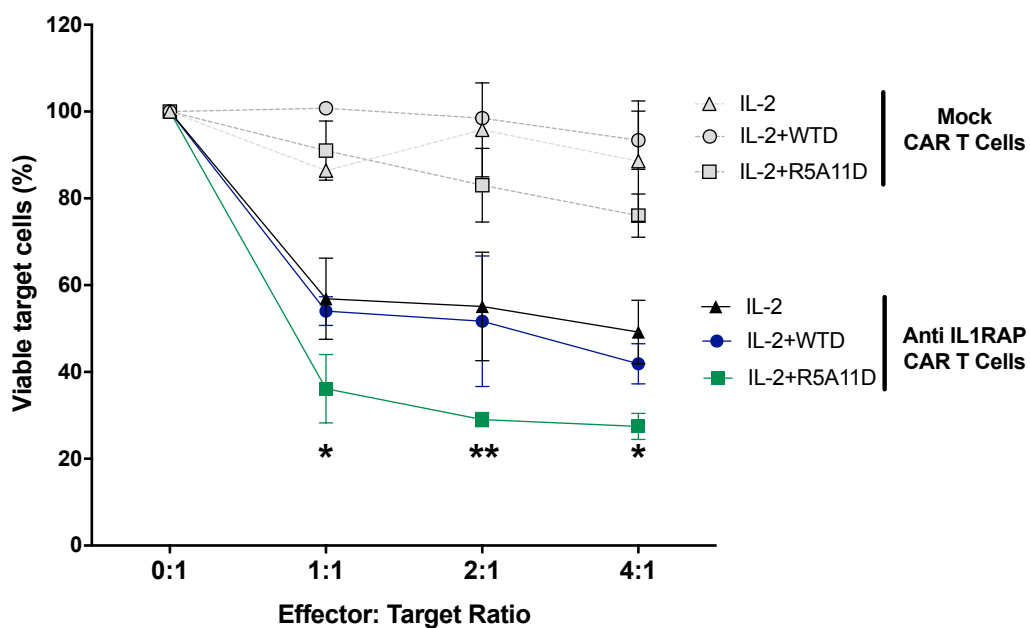
Figure 4.30 Effect of WTD and R5A11D on anti-IL-1RAP CAR T cell target killing. Target cells viability after 5 hours co-culture with effector cells at the denoted Effector: Target cell ratios. Viability was measured by 7-ADD staining by flow cytometry and the percentage of live cells was calculated. Data are presented as mean ±SEM, n=3. *p<0.001, **p<0.0001 (IL-2 alone or IL-2+WTD vs. IL-2+R5A11D). **This experiment was performed and analysed by A. Cozzani, University of Lille.**

Figure 4.30 shows that the anti-IL-1RAP CAR T cells showed greater killing capabilities than the mock T cells, confirming the efficacy of the anti-IL-1RAP CAR vector.

When we examined the effect of IL-10 on target cell killing, R5A11D showed enhanced killing compared to either IL-2 alone or WTD at all Effector: Target cell ratios tested. This confirms that in an *in vitro* environment R5A11D can enhance the cytotoxicity of CAR T cells compared to WTD.

4.7 Discussion

In this chapter I have outlined how we used our high affinity IL-10 variants to examine the effect of receptor affinity and receptor stoichiometry on IL-10's activities. We took a step-wise approach, studying how changes in early events, i.e., receptor assembly and STAT activation, affected downstream activities such as transcriptional regulation and known IL-10 biological effects. Using human primary monocytes and CD8 T cells provided us with insights into the molecular basis of IL-10's activity in these cells which are highly relevant for human health.

Increased affinity for IL-10Rß enhanced the stability of the IL-10/IL-10 receptor complex

Once recombinantly expressed, we were able to use our high affinity variants in both monomeric and dimeric conformations to assess the contribution of receptor affinity to cytokine-receptor complex stability in the IL-10 system. By examining homodimerisation of the receptor subunits we clarified that our monomeric variants were indeed acting as monomers and confirmed the 1:1 stoichiometry of IL-10 monomer/IL-10Rα previously reported by the study in which the monomeric IL-10 molecule was generated (Josephson et al., 2000b). In their study they did not examine binding of monomeric IL-10 to IL-10Rß, however from visualisation of the assembly of the receptor complex in our body of work we see that monomeric IL-10 also binds one molecule of IL-10Rß, forming a 1:1:1 complex stoichiometry between IL-10 monomer: IL-10Rα: IL-10Rß.

Both the high affinity monomeric and dimeric variants showed a significant improvement in receptor heterodimerisation compared to the wild type monomer and dimer respectively. The increase in homodimerisation of IL-10Rß by R5A11D was significant compared to WTD homodimerisation, consistent with the increase in receptor affinity. Of note is that R5A11D and WTD showed similar levels of IL-10Rα homodimerisation, in keeping with the idea that the engineered R5A11D variant would exclusively improve binding to IL-10Rß and not disrupt binding to IL-10Rα. This validates our yeast selection model and supports the idea that the introduced mutations occur specifically on the IL-10Rß binding interface.

The use of TIRF microscopy to visualise single molecules of the receptor on the surface of live cells also allowed us to examine the state of the receptors in the absence of IL-10 i.e. whether the receptor complex was pre-assembled. This question of whether cytokine receptors exist as pre-assembled inactive complexes or if they are monomeric and randomly diffusing in the plasma membrane has been highly contested in the field. For several homo-dimeric molecules such as erythropoietin receptor (EpoR) and the growth hormone receptor (GHR), preassembled receptor complexes have been reported. Crystals of EpoR in the absence of ligand showed dimerisation of the receptor (Livnah et al., 1999). For the GHR, a tagged receptor subunit could be co-immunoprecipitated with the wild type receptor (Gent et al., 2002). One study has provided evidence for pre-assembled IL-10 receptor complexes in the absence of the cytokine (Krause et al., 2006). In this study fluorescence resonance energy transfer (FRET) was used to show that IL-10Rα and IL-10Rß existed as a dimer in the absence of IL-10. However, these models lack a comprehensive explanation as to why a preformed dimer would not be able to signal. In addition, artefacts may be introduced by the methodologies used, such as the very high concentrations used for crystallisation. FRET uses over-expression of the receptor subunits. Physiological levels of cytokine receptors on the cell surface are usually only a few hundred copies per cells (Moraga et al., 2014). This means that the receptor affinities and interaction rates are fine-tuned to these expression levels. Overexpression of receptor components may shift the equilibrium of monomers and dimers towards dimers even in the absence of ligand. The use of TIRF microscopy allows examination of interactions at physiologically relevant receptor densities as well as co-tracking analysis to ensure that only true dimerisation events are captured. Single particle fluorescence imaging studies have been invaluable in determining the stoichiometry of cytokine receptor complexes and to date have shown a model of ligand-induced dimerisation for many cytokines such as IL-4 and Type I IFNs (Richter et al., 2017, Wilmes et al., 2015). We have used this technique here to show that the IL-10 receptor does not exist as a preformed dimer in the absence of ligand stimulation in our hands.

IL-10 receptor stoichiometry is a key determinant of the potency of downstream activities

STAT activation is one of the first events triggered by cytokine-receptor binding and acts as a key translator of events at the cytokine-receptor interface into biological outputs. Here we were able to use our high affinity monomeric and dimeric variants for comparison with their wild type counterparts to examine the role of IL-10 receptor affinity and stoichiometry in STAT activation. WTM showed very poor activation of STAT1 and STAT3, even at very high doses (200 nM). WTM has previously been shown to bind IL-10Rα 60 times weaker than WTD (Josephson et al., 2000b). This was also seen in our studies of receptor complex assembly where WTM had poorer heterodimerisation of the receptor complex than WTD, suggesting that stoichiometry plays an integral role in amplitude of the IL-10 response. When we examined the activity of R5A11M which retains a monomeric conformation but has increased IL-10Rß binding affinity, we saw a large increase in the ability of a monomeric IL-10 to activate STATs, with activity of 70-100% of WTD at high concentrations. This implied that deficiencies in receptor stoichiometry could be supplemented by increased receptor affinity. However, this ability of R5A11M to reach dimeric levels of activity did not extend past STAT activation. R5A11M showed a consistently weaker transcriptional response as well as poorer biological activity compared to the dimeric variants in both monocytes and CD8 T cells, even when used at high concentrations. Together this suggests that the receptor stoichiometry of the IL-10 complex contributes to the potency of the IL-10 response beyond STAT activation.

This is supported by the fact that the dimeric viral homolog of IL-10 produced by the Epstein-Barr virus (vIL-10) has significantly lower affinity for IL-10Rα than WTD but can still suppress pro-inflammatory cytokine production and antigen presentation at levels equivalent to WTD (Liu et al., 1997). This suggests that receptor stoichiometry can supplement weak receptor affinity. Interestingly, previous work has shown that, in cells with low levels of IL-10Rα, vIL-10 acts like a monomer due to its poor ability to assemble a complex of one vIL-10 with two IL-10Rα subunits (Yoon et al., 2012). This co-opting of receptor stoichiometry biases by the virus highlights the advantage that the dimeric cytokine shows over the monomeric version, despite increased affinity. However, R5A11M did show much greater transcriptional activity than WTM, indicating that this high affinity version could be advantageous in situations where a monomeric conformation is

preferable e.g., generation of a fusion protein with other cytokines or chemical modification such as PEGylation.

A possible explanation for the enhanced activity of dimeric variants over monomeric variants may be the differences in the number of phospho-tyrosines activated. Previous work in our laboratory demonstrated that, in the IL-6 system, differential receptor binding capability triggered differential phosphorylation of the intracellular tyrosines of gp130 (Martinez-Fabregas et al., 2019). Those variants which only triggered partial tyrosine phosphorylation showed biased STAT3 activation over STAT1. The study outlined that the number of phospho-tyrosines is a determinant in the cytokine's signalling capabilities. In the IL-10 system WTM also showed a biased STAT3 response compared to STAT1 in both CD8 T cells and monocytes, suggesting that similar mechanisms may be at play here. The dimeric variants may activate different patterns of phospho-tyrosines in the IL-10 receptor subunits compared to the monomeric variants, triggering additional signalling pathways. However, further work will need to be done to fully understand the reasons behind the weaker biological activities of the monomeric variants.

Increased receptor affinity enhances IL-10's activity at low doses

The translation of IL-10 therapies into the clinic has been very poor. Its use as a treatment for Crohn's disease showed efficacy in only limited numbers of patients. One of the key factors in the poor response to IL-10 treatment discussed in the literature may be the very low local concentrations of IL-10 in the gut when it is given systemically. In mouse studies, it was reported that IL-10 concentrations can reach between 1-5ng/ml depending on the stimuli used (Elcombe et al., 2013, Yamaguchi et al., 2000). In humans, similar results are observed. In therapies where 25 µg/kg of IL-10 were used, IL-10 serum levels at 3 hours were around 20 ng/mL and fell to 3 ng/mL at 6 hours, returning to basal levels at 24 hours (Chernoff et al., 1995). Interestingly, studies have shown that a targeted delivery of IL-10 can enhance efficacy such as the use of IL-10-producing lactobacillus (Braat et al., 2006), agreeing with the idea that low local IL-10 concentrations significantly hinder IL-10 therapies. Another barrier to IL-10 treatment is the short half-life of the cytokine. IL-10 has a half-life of 3-5 hours *in*

vivo meaning that treatments using IL-10 require frequent administration with high doses, usually in the range of 10-20 µg/kg of body weight with daily injection. A PEGylated version of IL-10 has shown enhanced tumour killing in human cancer patients in early clinical trials (Naing et al., 2019). PEGylation of the cytokine increases its size, leading to a longer retention in circulation by delaying its filtration by the kidneys (Alvarez et al., 2012). Together this highlights that effective IL-10 responses *in vivo* require high and sustained concentrations.

We showed that our high affinity dimeric IL-10 variant displayed enhanced efficacy at low doses. The low dose of IL-10 used was 0.1 nM, equivalent to roughly 3.6 ng/mL. This corresponds to the amount of IL-10 present in serum after 6 hours of high dose IL-10 injection in the study outlined above. Therefore, this low dose represents the equivalent serum IL-10 levels seen after systemic administration of this cytokine. We demonstrated that, at this concentration, WTD showed significantly reduced transcriptional activity across a large portion of its genes. In particular at the low dose WTD showed poorer regulation of inflammatory cytokines and chemokines compared to the high dose in monocytes. The crucial anti-inflammatory activities of IL-10 are compromised by these dose-dependent effects, perhaps contributing in part to the poor efficacy of IL-10 treatments for Crohn's disease. This in turn supports the assumption that R5A11D may demonstrate a therapeutic advantage over WTD as the majority of its activities are not affected by use at this low concentration.

R5A11D also showed advantage over WTD in improving the target cell killing activity of CAR T cells *in vitro* when used at a high dose of 40 nM. WTD showed no significant difference compared to the control. This improvement in activity at a high dose was unexpected as in all other tests R5A11D only showed advantage at low doses and, in some cases, performed poorer than WTD at high doses. In experiments comparing doses we were looking directly at primary effects on the cell i.e. protein production or gene transcription. Target cell killing by CAR T cells comes from a variety of factors such as secretion of granzymes, cytokine release and Fas ligand activation. It may be that the enhanced activity of R5A11D on CD8 T cells is more visible in these secondary effects. Small changes in gene expression may lead to amplification of secondary effects. Another possible explanation is that high doses of IL-10 are needed to improve CAR T cell killing

activity. After three days of incubation the levels of WTD in the media may not have been sufficient to induce an effect however R5A11D could still act effectively at low doses. While the mechanism underpinning this enhanced CAR T cell killing is unclear, it demonstrates another possible therapeutic use for R5A11D.

High affinity variants may show a disadvantage at high concentrations due to a "bell-shaped" response

While R5A11D showed consistently improved activities compared to WTD at low doses, the results at high doses were more variable. In cell-based assays R5A11D appeared to act similarly to WTD at 50 nM however we did observe that many genes showed stronger regulation by WTD rather than R5A11D at 50 nM, for example those involved in metabolism such as AK4 and COX10. One potential explanation for poorer activity by R5A11D at high concentrations may be the higher affinity for IL-10Rß. WTD is unable to bind IL-10Rß in the absence of IL-10Rα however R5A11D can bind IL-10Rß alone. At high concentrations of R5A11D this may mean that single chains of IL-10Rß are bound by R5A11D without IL-10Rα being present, sequestering them and inhibiting dimerisation-induced signalling (Figure 4.31). Bell shaped binding curves have previously been reported for cytokine-receptor systems such as hGH and EPO where homo-dimeric receptor assembly is seen. In hGH, high concentrations led to decreased activity as individual receptors are occupied by individual cytokines with no secondary interactions between the receptor chains (Whitty and Borysenko, 1999, Pearce et al., 1999). Similar bell shaped curves were seen in EPO when EPO-Rs were triggered with an agonist antibody, indicating that each receptor was bound separately and thus couldn't form an active dimeric complex (Middleton et al., 1999). It may be that the ability of R5A11D to bind IL-10Rß in the absence of IL-10Rα means that it displays characteristics similar to a homo-dimeric receptor system at high concentrations such as a bell shaped curve. Even though R5A11D could promote dimerisation of IL-10Rß it has been shown that dimerisation of IL-10Rß or IL-10Rα alone is not sufficient to trigger signalling. IL-10Rß KO mice develop colitis and defective Treg and anti-inflammatory macrophage responses (Shouval et al., 2014). Mice deficient in IL-10Rα showed

increased pro-inflammatory cytokine production and enhanced colitis susceptibility (Pils et al., 2010).
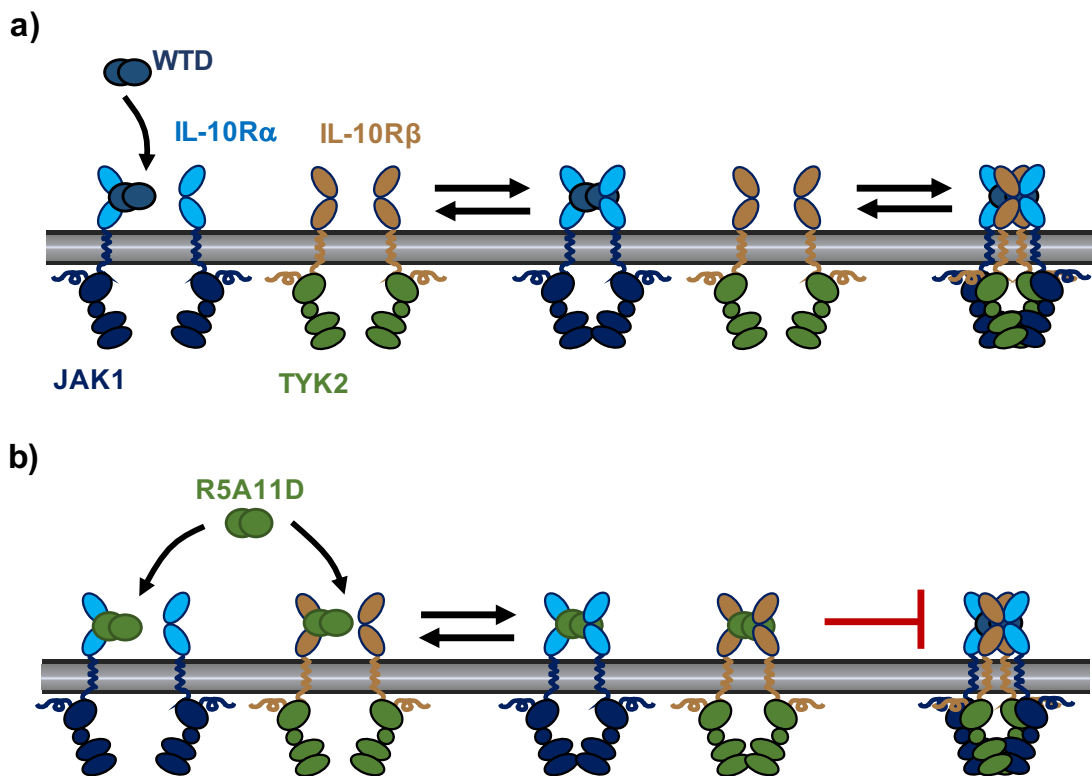
Figure 4.31 Schematic of potential differential receptor binding patterns for WTD and R5A11D. (a) WTD binds to IL-10Rα and recruits IL-10Rß in a second step as it is unable to bind IL-10Rß in the absence of IL-10Rα. The assembly of the WTD/IL-10Rα/IL-10Rß complex is the activate conformation, allowing signalling to occur. **(b)** R5A11D can bind both IL-10Rα and IL-10Rß alone. At high concentrations it is possible that R5A11D may bind to both IL-10Rα and IL-10Rß, preventing the hetero-dimerisation of the receptor complex.

Examination of alternative signalling pathways by high affinity variants

In this thesis I focussed on activation of the JAK/STAT pathway by IL-10. This is the most well studied downstream signalling pathway for IL-10 and the majority of IL-10's responses have been shown to be STAT3-dependent. Because of IL-10's well characterised JAK/STAT activation this was the best way to compare activities of our high affinity variants. R5A11D showed enhanced STAT activation at low concentrations and more potent biological responses compared to WTD. However, IL-10 has been also been shown to activate AMPK, PI3K and mTORC1 in macrophages (Zhu et al., 2015, Antoniv and Ivashkiv, 2011). In one study AMPK activation occurred even in the presence of a JAK inhibitor and a PI3K inhibitor (Zhu et al., 2015). In addition, STAT3 phosphorylation was inhibited in

AMPKα1 deficient macrophages and these macrophages were also unable to inhibit LPS-induced pro-inflammatory cytokine production (Zhu et al., 2015). This suggests that AMPK may play a role in IL-10 signalling.

The use of a PI3K inhibitor in human primary macrophages demonstrated that some IL-10 inducible genes required PI3K activation however other genes such as SOCS3 were PI3K independent (Antoniv and Ivashkiv, 2011). In contrast to AMPK, STAT activation was not broadly affected by inhibition of PI3K. In addition to the activation of PI3K, IL-10 has been shown to activate p70 S6 kinase which could be inhibited by rapamycin, an mTORC inhibitor (Crawley et al., 1996). The use of rapamycin resulted in an inhibition of proliferation of D23 cells but did not disrupt anti-inflammatory activities in monocytes, suggesting that different facets of the IL-10 response may be under the control of different signalling pathways (Crawley et al., 1996).

Activation of alternate signalling pathways by our IL-10 variants was not examined during this project. Differential activation of AMPK, PI3K or mTORC by our IL-10 variants may help to further explain differences in biological responses. Further work will need to be done to explore this hypothesis such as examining levels of STAT3 phosphorylation in combination with inhibitors of AMPK, PI3K and mTORC.

Conclusions and future perspectives

Our study has shown that increased affinity for IL-10Rß has wide ranging effects on the activities of this well studied cytokine. Increased affinity can alter receptor complex assembly, STAT activation, transcriptional programmes and known biological activities.

Despite R5A11M displaying poorer responses than the dimeric cytokine, its large improvement in activity compared to WTM means it is an ideal candidate for further study. A monomeric conformation can be advantageous over the dimeric conformation in many ways. It provides a simpler system for structural studies as the 1:1:1 IL-10:IL-1Rα:IL-10Rß stoichiometry means structural modelling may prove less complex. It also opens up avenues for further manipulation of the

cytokine, for example by generating fusion proteins with other cytokines. As mentioned previously, manipulation of IL-10 is difficult due to its dimeric nature and the wild type monomeric IL-10 variant has weak biological activity, limiting its use. The enhanced activity of R5A11M in a monomeric conformation would allow for its easy manipulation through PEGylation, forming linkers with other cytokines and other modifications.

Our high affinity dimer, R5A11D, displayed enhanced activities at low concentrations, suggesting that it may provide a therapeutic advantage over WTD. Ideally, we would assess this *in vivo*, for example in mouse models of colitis. However, this proved difficult as we were using human IL-10 and its receptors in all our studies. Human IL-10 and mouse IL-10 share 73% amino acid similarities and human IL-10 can induce activity in mouse cells however mouse IL-10 does not function in human cells (Windsor et al., 1993). Human and mouse IL-10Rα have 60% amino acid similarity and IL-10Rß is 69% similar between the species (Liu et al., 1994, Gibbs and Pennica, 1997). As R5A11D was affinity matured against the human IL-10Rß we did not know if this enhanced affinity would translate into enhanced affinity for the murine IL-10Rß. A preliminary *in vitro* assay using murine macrophages demonstrated that, while both WTD and R5A11D could suppress TLR-induced cytokine production from these cells, R5A11D did not display an advantage over WTD at any concentration tested (Figure 4.32) (This experiment was conducted in collaboration with S. Laba in the Arthur laboratory, University of Dundee). This suggests that the amino acid mutations which give R5A11D enhanced affinity for the human IL-10Rß do not confer an advantage in the mouse system. This is not unsurprising given the differences in sequences between the mouse and human systems however, it does limit our ability to test the efficacy of R5A11D *in vivo*. The use of human CAR T cells demonstrated the ability of R5A11D to enhance IL-10 responses in a clinically relevant setting, suggesting that further study into the translational applications of this high affinity cytokine may be merited, however how this will be done poses many questions.

As well as highlighting differences between the engineered variants, our RNA sequencing study indicated potential regulation of exhaustion markers and the IL-2 response by IL-10 in CD8 T cells. The effect of IL-10 on CD8 T cells is still

poorly understood and these results highlight areas for further study which will be examined in the next chapter.
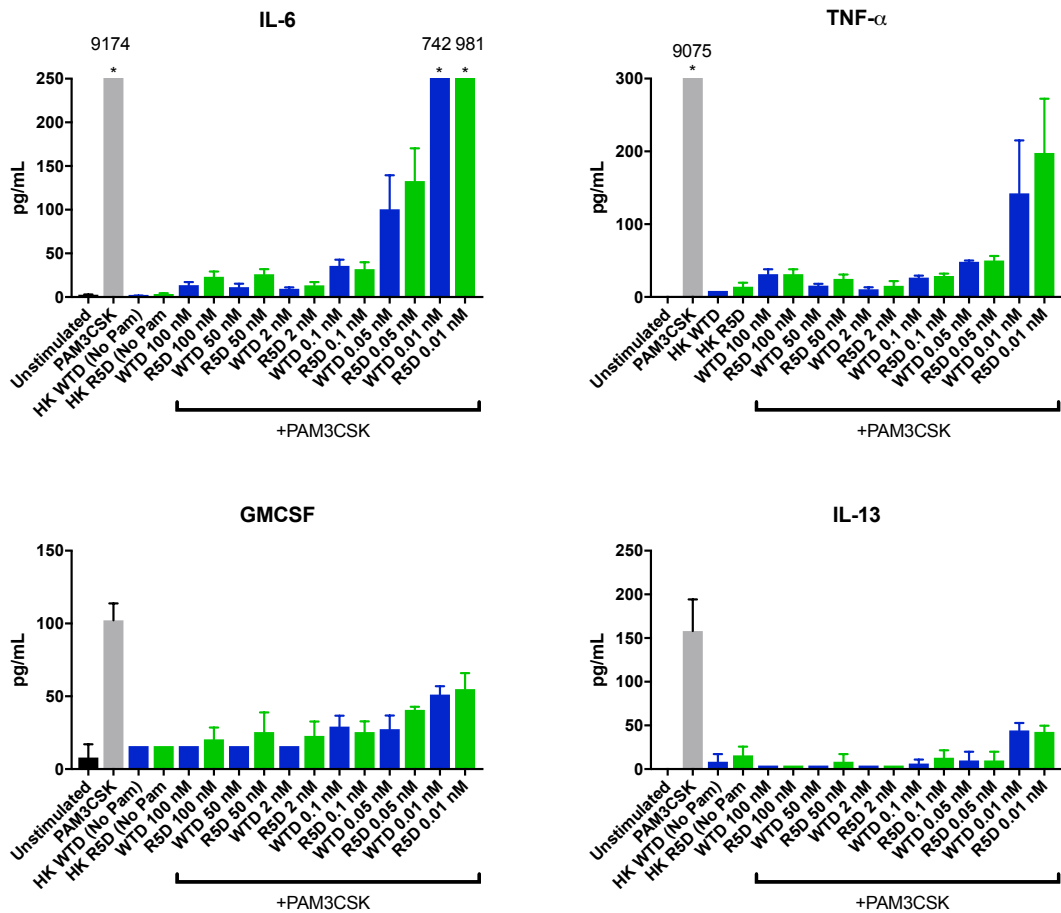
Figure 4.32 Comparison of efficacy of WTD and R5A11D in murine cells. Murine BMDMs were stimulated with the PAM3CSK (1µg/mL) ± WTD and R5A11D at the concentrations listed above for 8 hours. Supernatants were harvested and cytokine secretion was measured using a bioplex assay. HK= heat-killed controls where WTD and R5A11D were boiled for 30 minutes. Asterisks indicate values outside of the range of the graph and in these cases the values are shown in text above the corresponding bar. N=4. **This experiment was done with the help of S. Laba in the Arthur laboratory group, University of Dundee.**

Chapter 5. Examining the molecular basis of IL-10's effect on CD8 T cells

Background

As discussed in Chapter 4, IL-10 has been shown to enhance the cytotoxicity of CD8 T cells, improving their tumour targeting abilities and leading to clinical trials using a PEGylated recombinant human IL-10 in the treatment of cancer (Naing et al., 2019). Supporting this, it has also been shown that IL-10 deficient mice are more susceptible to induced cancers and children with IL-10 receptor deficiencies have higher rates of B cell lymphomas with less tumour infiltrating CD8 T cells (Neven et al., 2013). Work shown in Chapter 4 demonstrated that stimulation with wild type IL-10, as well as our high affinity variants, increased granzyme B production in human CD8 T cells. Our transcriptomic analysis of IL-10 treated CD8 T cells also showed the downregulation of exhaustion markers such as TOX and TIGIT suggesting that IL-10 may limit the transition of CD8 T cells into an exhausted phenotype. In addition, we observed an IL-10-mediated downregulation of IL-2Rα as well as a reduction in mRNA levels for many IL-2 dependent genes such as IL-13 and LIF. It is possible that this regulation of exhaustion and IL-2 responses may contribute to the enhanced cytotoxicity of IL-10 treated CD8 T cells. However, at this point this model remains very speculative and more work is required to address how IL-10 enhances CD8 T cells cytotoxic activities.

To understand in greater detail how IL-10 tunes CD8 cytotoxic activities, we studied how classical markers of T cell activation were regulated by IL-10 treatment. We also performed unbiased proteomics studies to better understand how IL-10 regulates CD8 T cells activities. Our proteomic study highlighted significant metabolic proteins altered upon IL-10 stimulation. Key proteins involved in glycolysis were downregulated by IL-10. In addition, we saw large subsets of mitochondrial proteins upregulated by IL-10, specifically those involved in the electron transport chain. These results suggested that IL-10 could modulate the metabolic response of CD8 T cells which may contribute towards enhanced cytotoxicity. Together this provides a preliminary model of the IL-10

response in CD8 T cells and gives a solid foundation upon which further studies can be based.

Aims:

- Characterise the IL-10-treated CD8 T cell phenotype
- Use proteomics to gain an understanding of how IL-10 enhances the cytotoxic functions of CD8 T cells
- Validate proteomic hits using orthogonal experimental approaches

5.1 Phenotyping of CD8 T cells activated in the presence of IL-10

There are many conflicting reports about the effect of IL-10 in CD8 T cells. It has been reported that IL-10 can affect CD8 T cell proliferation, activation, exhaustion and memory cell development (Smith et al., 2018, Blackburn and Wherry, 2007, Walk et al., 2012, Taga and Tosato, 1992). Other reports have shown opposing results, indicating that IL-10 does not negatively impact CD8 T cell activation or exhaustion (Rowbottom et al., 1999, Emmerich et al., 2012). These disparities may arise due to different methods of activation, different growth conditions and the addition of IL-10 at different time points during culture. We first wanted to gain a more accurate understanding of the phenotype of IL-10 treated CD8 T cells. As our previous work was performed using CD8 T cells activated in the presence of IL-10 and IL-2 we chose to use the same conditions going forward for further phenotyping. We examined the early activation marker CD69 and the late activation marker CD71. We also measured levels of several exhaustion markers as well as granzyme B production.

CD8 T cells were activated within a PBMC environment using anti-CD3 and IL-2 ± IL-10 for three days, followed by IL-2 ± IL-10 for a further 3 days to allow the population to expand. This activation protocol is referred to as "TCR (T Cell Receptor) stimulated" in the results below. IL-10 was added to the media at day 1 and again at day 3 when the media was changed (Figure 5.1).
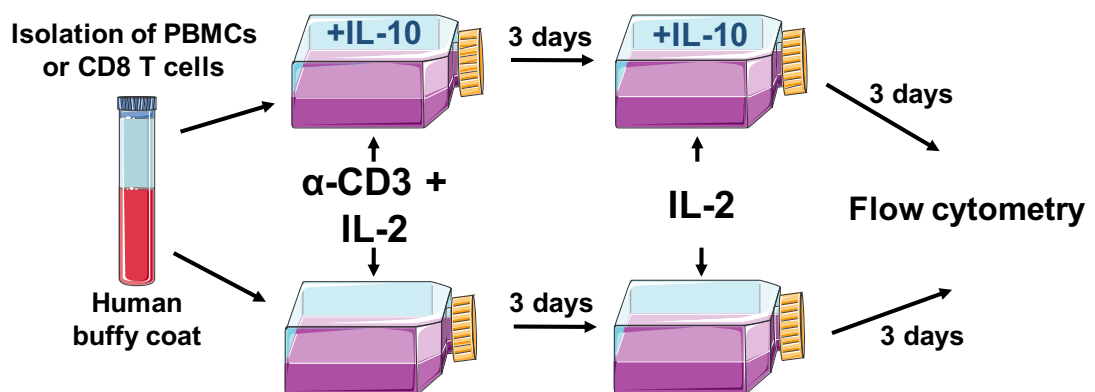
Figure 5.1 Activation and IL-10 stimulation of CD8 T cells. CD8 T cells were activated either in a PBMC population or in a purified CD8 T cell population. For CD8 T cells in a PBMC population cells were activated with anti-CD3 and IL-2 ± IL-10 (50-100 nM) for three days followed by three days in media containing IL-2 ± IL-10. For isolated CD8 T cells, activation was performed using anti-CD3/CD28 and IL-2 ±IL-10 (50-100 nM) for three days followed by three days in media containing IL-2 ± IL-10. Cells were harvested on day 6 for analysis by flow cytometry.

Purified CD8 T cells were also used to uncouple the direct effect of IL-10 on the cells from any secondary effect via other cells in the PBMC population. In these purified populations the cells required activation with anti-CD3/CD28 beads plus the presence of IL-2. IL-10 was added at day 1 and day 3 as was done for the PBMC population. This activation and growth protocol was used throughout the experiments outlined in this chapter to gain an insight into how the presence of IL-10 during activation and expansion would affect the CD8 T cell phenotype.

5.1.1 IL-10 does not inhibit CD8 T cell proliferation

The effect of IL-10 on T cell proliferation is highly contested in the literature. Reports have shown that it can inhibit the proliferation of both CD4 and CD8 T cells while others have shown that it does not effect CD8 T cell proliferation (Groux et al., 1998). It is difficult to uncouple the direct effect of IL-10 on T cells from secondary effects of IL-10 on other cells in the immunological environment. Work by Giroux et al. demonstrated that the negative effect of IL-10 on T cell proliferation may be a result of the inhibitory effect of IL-10 on antigen presenting cells, limiting their ability to activate T cells. We wanted to investigate an IL-10 mediated effect on proliferation in our system. We activated T cells within a PBMC culture for 6 days as described above. While this chapter focuses on CD8 T cells we also examined CD4 T cell proliferation within the same PBMC population as a control. Figure 5.2 shows that in the IL-10 treated population there were significantly less CD4 T cells compared to the non-IL-10 treated group. In contrast to this, IL-10 had little to no effect on the proliferation of CD8 T cells.
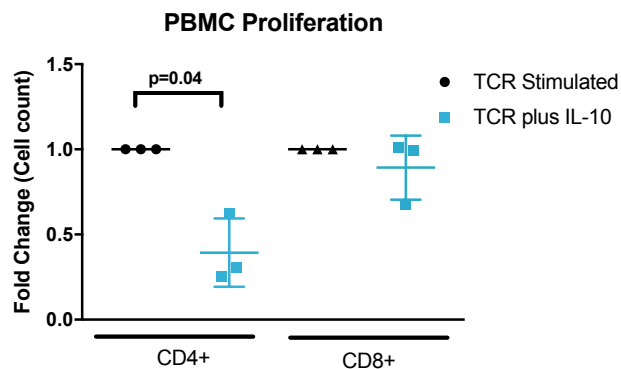
Figure 5.2 Examination of T cell proliferation upon activation in the presence of IL-10. PBMCs were activated using anti-CD3 and IL-2 ± IL-10 (100 nM) for three days followed by three days with IL-2 ± IL-10. CD4 and CD8 T cells were counted on day 6 by flow cytometry. Fold change was calculated by dividing the number of IL-10 treated cells by non-IL-10 treated controls. N=3. Error bars represent the SD. P values were calculated using paired t test.

5.1.2 IL-10 does not inhibit activation of CD8 T cells

We chose to add IL-10 to the cell media throughout activation rather than at only one point to mimic a physiological setting where cells may be exposed to IL-10 over long time periods e.g., during persistent viral infections. This was done to give us an insight into how the presence of IL-10 would affect activation of the cells. CD69 is an early activation marker in T cells (Sancho et al., 2005). Figure 5.3a shows the cell surface levels of CD69 on CD8 T cells 24 hours after activation in both a PBMC culture and a purified CD8 T cell culture. There was no significant change in CD69 levels between IL-10 treated and non-IL-10 treated for either population, suggesting that at early stages of activation IL-10 does not hinder CD8 T cell activation.

We examined activation again at day 6, this time measuring levels of the late activation maker CD71 (Figure 5.3b). There were two large outliers in the data, one donor with greatly increased CD71 upon IL-10 stimulation and one donor with decreased CD71. However, overall, there was no significant difference in CD71 in IL-10 treated CD8 T cells in either a PBMC population or a purified population. Together these data show that under the above conditions, IL-10 does not significantly affect the classical markers of activation in CD8 T cells.
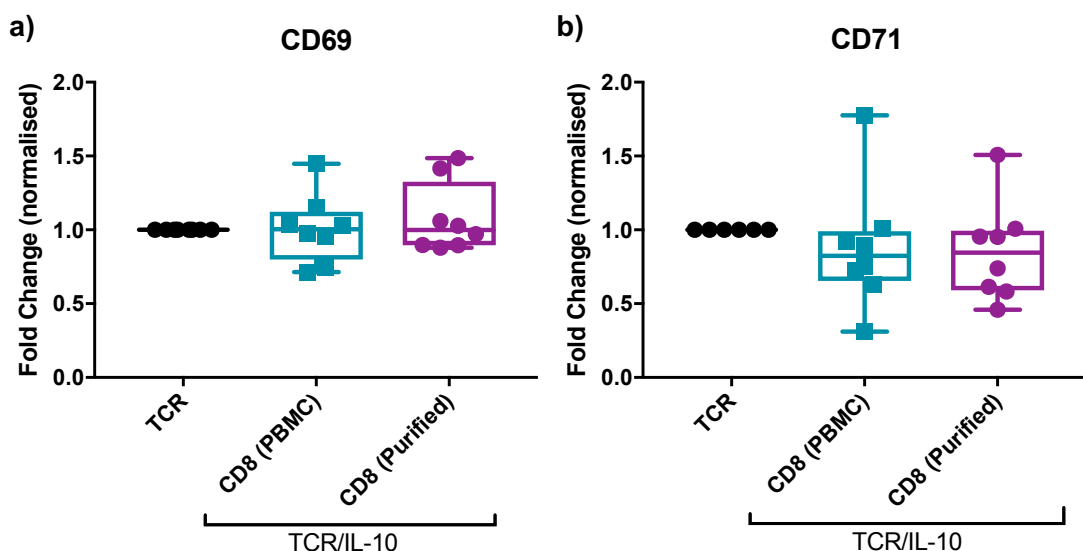
Figure 5.3 Effect of IL-10 on CD8 activation. (a) CD8 T cells in a PBMC population or in purified population were activated using anti-CD3 (PBMC population) or anti-CD3/CD28 (purified) and IL-2 in the presence or absence of IL-10 (100 nM). CD69 cell surface levels were measured 24 hours after activation by flow cytometry. **(b)** CD71 cell surface levels were measured by flow cytometry 6 days after activation. N=8. Error bars represent standard deviation. Fold change was calculated by dividing IL-10 treated MFI by non-IL-10 treated MFI for each donor.

5.1.3 IL-10 does not increase the level of classical exhaustion markers on CD8 T cells

As described in Chapter 4, we saw a decrease in mRNA levels of exhaustion markers such as TIGIT and TOX in our IL-10 treated CD8 T cells. Exhaustion of CD8 T cells has been implicated in cancer and viral progression. The role of IL-10 in T cell exhaustion is complex and it is difficult to uncouple the direct effect of IL-10 on CD8 T cells from indirect effects via other cells in the environment. We wanted to look at exhaustion markers at the level of protein to complement our transcriptomic study. We chose a panel of commonly used T cell exhaustion and inhibitory markers comprising of CD57, KLRG1, LAG3, PD-1, TIGIT and TIM3 and examined the cell surface levels of these exhaustion markers after 6 days of activation in the presence of IL-10. This experiment (Figure 5.4) was performed by Dr. J. Martinez-Fabregas, due to time constraints.
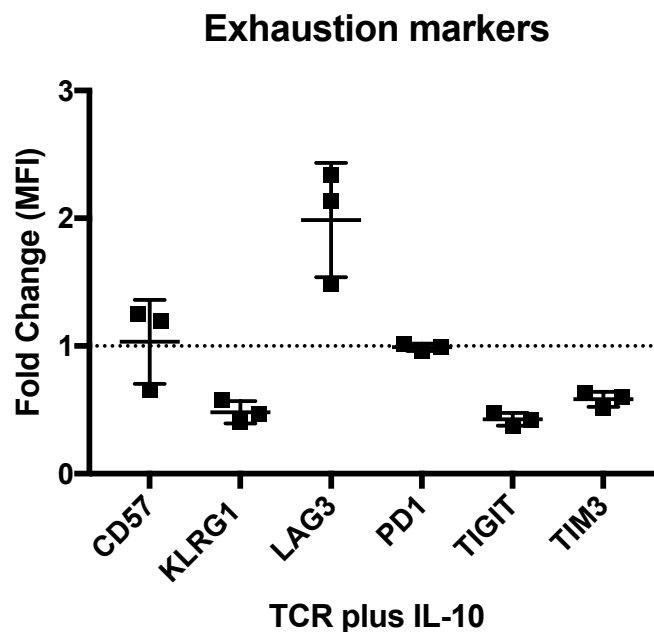
Figure 5.4 Effect of IL-10 on exhaustion markers. Purified CD8 T cells were activated with anti-CD3/CD28 and IL-2 in the presence or absence of IL-10 (50 nM) for three days followed by expansion in IL-2 ± IL-10 for three days. Cell surface expression levels of classic exhaustion markers were measured by flow cytometry on day 6. Error bars represent standard deviation. Fold change was calculated by dividing IL-10 treated MFI by non-IL-10 treated MFI for each donor. N=3. **Cell culture and flow cytometry for this experiment were performed by Dr. J. Martinez-Fabregas.**

As shown in Figure 5.4 we observed a 50% reduction in the levels of KLRG1, TIGIT and TIM3 after activation in the presence of IL-10 compared to non-IL-10 treated controls. PD-1 showed no change upon IL-10 treatment and CD57 had a small increase (~20%) in two donors and a decrease in the third donor.

Interestingly, we saw an increase in LAG3 expression after IL-10 treatment. Although LAG3 and PD-1 are inhibitory receptors which are implicated in T cell exhaustion (Du et al., 2020), it has been shown that treatment with PEGylated IL-10 expanded populations of LAG3^{+} PD-1^{+} CD8 T cells with increased functional responses (Naing et al., 2018). This suggests that, although PD-1 and LAG3 are exhaustion markers, expression of these markers does not preclude functionally active T cells. The substantial decrease in expression of TIGIT and TIM-3 aligns with our RNA sequencing data and supports the hypothesis that IL-10 does not directly induce exhaustion in CD8 T cells, however further functional assays will need to be performed to confirm this.

5.1.4 IL-10 upregulates granzyme B production in CD8 T cells

In Chapter 4 we showed an increase in granzyme B protein and mRNA in CD8 T cells stimulated with both wild type and mutant IL-10. As mentioned previously, IL-10 has been shown to boost the cytotoxicity of CD8 T cells, leading to enhanced tumour clearing in both mouse models and human patients (Naing et al., 2018, Emmerich et al., 2012). The studies showed that administration of IL-10 enhanced the presence of effector molecules such as granzyme B. We wanted to confirm these results in both purified and PBMC populations of CD8 T cells. We saw a large increase in granzyme B induced by IL-10 in CD8 T cells grown in a PBMC culture (Figure 5.5a), similar to the results from Chapter 4 Figure 5.5b shows that IL-10 also induced a significant increase in granzyme B in the purified population, confirming a direct effect. In our RNA sequencing study we noted a significant increase in granzyme B transcripts when the cells were stimulated with IL-10 and this was confirmed by RT-qPCR in separate donors. As shown in Figure 5.5c, IL-10 induced a five-fold upregulation of granzyme B mRNA compared to cells activated in the absence of IL-10, demonstrating that IL-10 enhances transcription of this cytotoxic effector molecule and confirming the results seen in our transcriptomic study. These high levels of granzyme B induced by IL-10 are in keeping with previously published reports (Mumm et al., 2011), supporting the role of IL-10 in enhancing the effector functions of CD8 T cells.
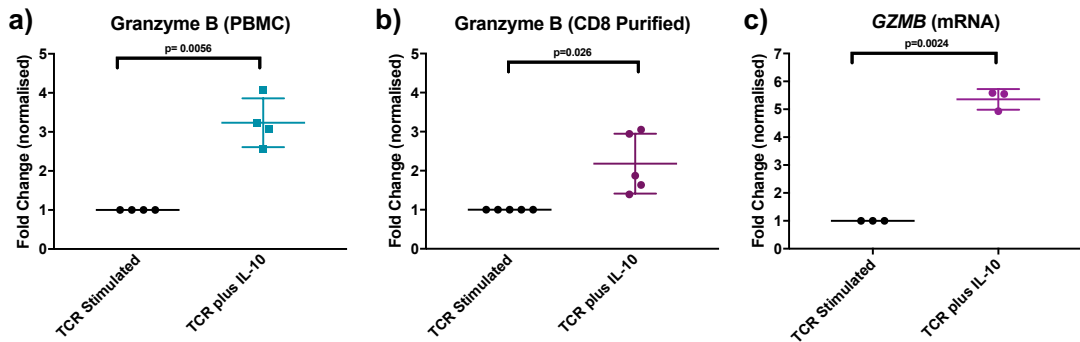
Figure 5.5 Effect of IL-10 on CD8 granzyme B production. (a) Granzyme B fold change in CD8 T cells activated in a PBMC population. Cells were activated in the presence or absence of IL-10 (50 nM) and granzyme B levels were measured by flow cytometry on day 6. Fold change was calculated by dividing the granzyme B MFI of IL-10 treated cells by that of untreated cells. N= 4. **(b)** Granzyme B fold change in CD8 T cells activated in a purified CD8 population. CD8 cells were isolated and activated for three days ± IL-10 (50 nM) followed by three days with IL-2 ± IL-10. Granzyme B levels were measured by flow cytometry on day 6. Fold change was calculated by dividing the granzyme B MFI of IL-10 treated cells by that of untreated cells. N=5. **(c)** Fold change of *GZMB* mRNA measured by RT-qPCR. Purified CD8 T cells were isolated and activated over 6 days as above, n=3. Error bars represent the standard deviation. P values were calculated by paired t test.

5.2 Examining the proteome of an IL-10 treated CD8 T cell

Thus far we had shown that CD8 T cells activated in the presence of IL-10 did not display inhibition of proliferation, or activation or a consistent upregulation of exhaustion markers. These cells also showed an increase in effector molecules, in line with published results. We next used quantitative mass spectrometry to gain insight into how IL-10 treatment regulated the CD8 T cell proteome. This gave us an unbiased and global overview of how IL-10 affects these cells and allowed us to compare how changes in the CD8 transcriptome induced by IL-10 translated into changes at the protein level.

As shown in Figure 5.6, CD8 T cells were activated within a PBMC population using anti-CD3 and IL-2 for three days, followed by expansion of the population with IL-2 for another three days. On day 6 CD8 T cells were isolated from the population by negative selection and samples were lysed and prepared for mass spectrometry. IL-10 was added to the culture media at the start of activation and again at day 3 when the media was changed. Three human donors were used and cells were also cultured in the absence of IL-10 as controls for each donor.
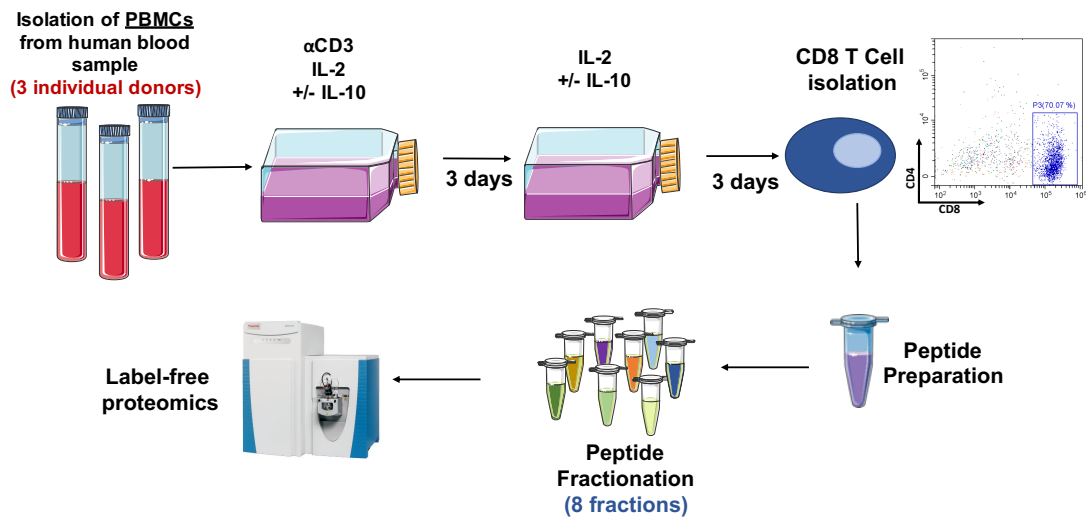
Figure 5.6 IL-10 treatment of CD8 T cells within a PBMC population for proteomic analysis. PBMCs were isolated from three human buffy coats. Cells were activated for three days using anti-CD3 and IL-2 in the presence or absence of IL-10 (100 nM). After three days the media was changed to IL-2 ± IL-10 for a further three days. On day 6, CD8 T cells were purified by negative selection before peptides were isolated. Cells were lysed and peptides were isolated as described in the Materials and Methods. The peptides were fractionated and analysed by mass spectrometry.

5.2.1 Overview of IL-10 treated CD8 T cell proteome

6643 proteins were detected in total, with 4868 detected in all three donors. The fold change was calculated by dividing the label free quantification (LFQ) values for the IL-10 treated cells by non-IL-10 treated (i.e. unstimulated) values within each donor group. The significance was calculated by two-tailed two sample equal variance t test of the $\log_2$ fold change of IL-10/ unstimulated genes for each donor. The fold change for all proteins and their corresponding p-value is plotted in Figure 5.7a. The majority of proteins were unchanged by IL-10 stimulation however 80 proteins were significantly upregulated by IL-10 stimulation (>0.6 $\log_2$ fold change) and 58 were significantly downregulated (<-0.6 $\log_2$ fold change). This corresponded to 7% of significantly regulated proteins being upregulated and 10% being downregulated (Figure 5.7b). This small shift in proteins whose expression is changed by IL-10 is in contrast to the large number of genes (>1000) which were significantly up or down regulated by IL-10. There are several possible explanations for this. Firstly, both the transcriptomic and the proteomic data come from cells harvested after 6 days of IL-10 treatment. This may mean that more time is needed to fully see the changes from mRNA translate into changes in protein. The discrepancy between mRNA and protein may also arise

due to the degradation or fast turnover of some proteins or as a result of the lower sensitivity of the proteomic technology compared to RNA sequencing.
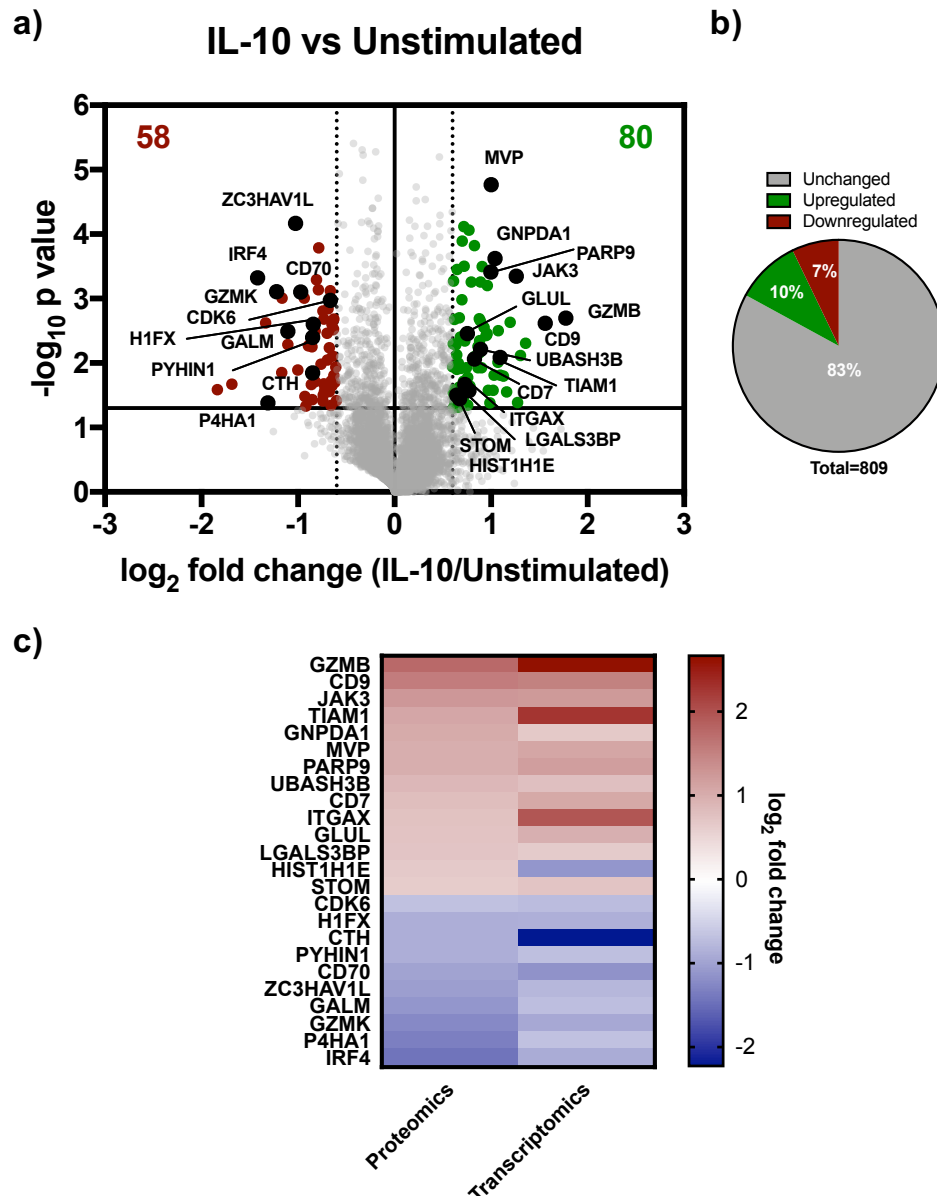
Figure 5.7 Proteome of CD8 T cells activated in the presence of IL-10. (a) Volcano plot of proteins significantly upregulated by IL-10 > 0.6 $\log_2$ fold change (green) and significantly downregulated by IL-10 <-0.6 $\log_2$ fold change (red) compared to non-IL-10 treated cells. Proteins marked in black are proteins significantly regulated in both the proteomics and transcriptomic datasets. Fold change was calculated by dividing IL-10 treated values by unstimulated values for each donor. The average fold change was calculated for three donors and the $\log_2$ of this value is plotted. P values were calculated by two-tailed two sample equal variance t test of the $\log_2$ fold change of IL-10/ unstimulated genes for each donor. Proteins which were not significantly changed or were >-0.6<0.6 $\log_2$ fold change are in grey. **(b)** Proportion of proteins significantly upregulated > 0.6 $\log_2$ fold change (green) or downregulated <-0.6 $\log_2$ fold change (red) by IL-10. Unchanged proteins are those which reached significance but fell within >-0.6<0.6 $\log_2$ fold change. **(c)** Comparison of $\log_2$ fold change of datapoints shared between proteomic and transcriptomic studies.

The proteins significantly regulated at the level of protein expression which were also significantly regulated at the level of mRNA from our transcriptomic dataset are highlighted within the volcano plot. Figure 5.7c shows the regulation of these shared proteins. With the exception of HIS1H1E, all shared datapoints between the proteomic and transcriptomic studies showed similar regulation by IL-10. Examining these proteins we see, as expected, granzyme B being upregulated, confirming our previous data. We also saw a significant upregulation of CD9 in our proteomic data. CD9 is a tetraspanin protein which is widely expressed by many immune cells including T cells, NK cells, dendritic cells and macrophages and has been implicated in many processes such as cell migration, adhesion and survival (Reyes et al., 2018). In CD8 T cells CD9 has been shown to play a role in T cell activation by modulating interactions at the immunological synapse and cells transduced with shCD9 showed reduced CD69 levels and reduced IL-2 secretion (Rocha-Perugini et al., 2014).

The Major Vault Protein (MVP) was highly upregulated in the proteome of all donors tested and was also highly upregulated in our transcriptomic dataset. MVP is involved in regulation of intracellular signalling and has been shown to be IFNγ-inducible (Steiner et al., 2006). JAK3 was also upregulated by IL-10 in our proteomic and transcriptomic datasets. While IL-10 does not activate JAK3 directly, JAK3 is essential for IL-2 signalling (Kirken et al., 1995). IL-2 was added to the culture media to enhance CD8 T cell proliferation and so the upregulation of JAK3 by IL-10 suggested the potential for IL-10 mediated regulation of IL-2 signalling.

5.2.2 IL-10 downregulates many proteins involved in glycolysis

We used GO and KEGG analysis on those proteins significantly up or downregulated by IL-10 to better understand how IL-10 regulated CD8 T cells biology. KEGG pathway analysis showed that the glycolysis/gluconeogenesis and fructose/mannose metabolism pathways were significantly represented in the downregulated group of proteins (Figure 5.8a). GO biological processes highlighted glycolytic processes, canonical glycolysis and gluconeogenesis enriched in the downregulated fraction (Figure 5.8b). The LFQ values of these

proteins are shown in Figure 5.8c with their fold change compared to non-IL-10 treated controls shown in Figure 5.8d.
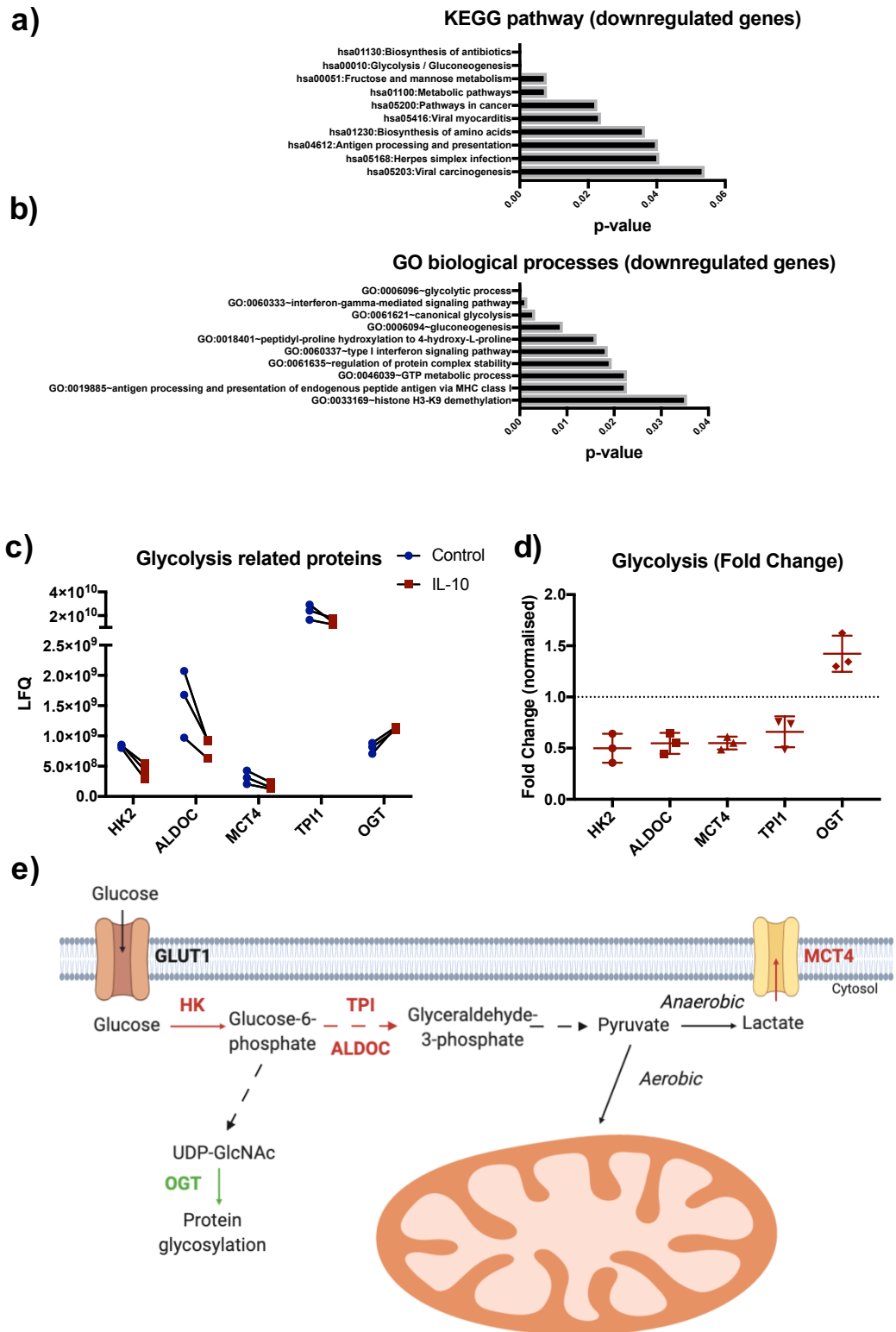
Figure 5.8 IL-10 regulation of glycolysis-associated proteins in CD8 T cells. (a-b) The 58 significantly downregulated proteins following IL-10 treatment were subject to KEGG and GO pathway analysis using DAVID online software (Huang da et al., 2009). Pathways are ranked by p value. **(c)** Glycolysis associated proteins LFQ values are plotted. **(d)** Fold change of LFQ values shown in (c), n=3. **(e)** Schematic displaying proteins upregulated by IL-10 (green) and downregulated by IL-10 (red) involved in glycolysis. Image generated using BioRender.

We saw a significant downregulation of hexokinase-2 (HK2), triosephosphate isomerase 1 (TPI1) and fructose bisphosphate aldolase C (ALDOC) by IL-10 treatment.

These are key proteins and enzymes in glycolysis, suggesting that IL-10 may be inhibiting this pathway in CD8 T cells. The metabolic processes these proteins are involved in are highlighted in Figure 5.8e. HK2 catalyses the conversion of glucose to glucose-6-phosphate, a rate limiting step in glycolysis. ALDOC and TPI1 are both involved in the conversion of glucose-6-phosphate to glyceraldehyde-3 phosphate which is then converted to pyruvate. In addition, we also observed a downregulation in the lactate transporter SLC16A3 (MCT4). Interestingly we saw upregulation of the enzyme OGT which catalyses the OGlcNAcylation of proteins. A study by Swamy et al. demonstrated that OGlcNAcylation is key for T cell expansion and function (Swamy et al., 2016). IL-10 mediated regulation of glycosylation has also been demonstrated in CD8 T cells where IL-10 induced N-glycan branching via MGAT5 which downregulated TCR signalling, leading to inhibition of CD8 T cells (Smith et al., 2018).

We next wanted to see if the apparent upregulation of the OGT enzyme by IL-10 corresponded to a change in the level of OGlcNAcylation of the cell. CD8 T cells in either a PBMC or a purified population were activated over 6 days in the presence or absence of IL-10 as above and OGlcNAcylation was measured on day 6. As seen in Figure 5.9a there was a small but significant decrease in OGlcNAc levels in IL-10 treated CD8 cells activated in a PBMC population. In the IL-10 treated purified CD8 population there was also a small decrease in two out of three donors however this was non-significant (Figure 5.9b). It is important to mention that separate donors were used for the PBMC and purified populations and experiments were carried out separately which may have led to differences in the amplitudes of the MFI signals between the two populations. The decrease in OGlcNAcylation, while only minimal, opposes the upregulation of OGT seen in the proteomic data.
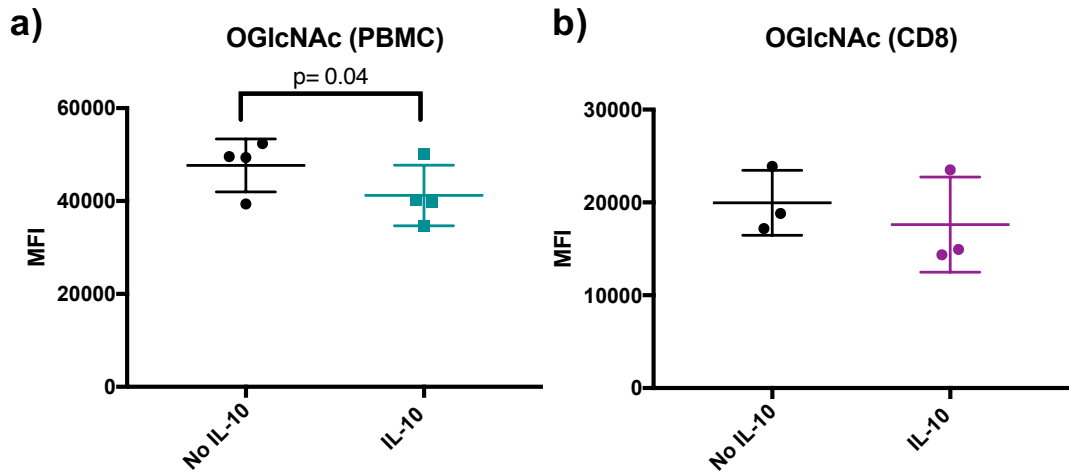
Figure 5.9 Effect of IL-10 on OGlcNAcylation in CD8 T cells. (a) PBMCs were activated using anti-CD3 and IL-2 ± IL-10 (50 nM) for three days followed by three days with IL-2 ± IL-10. OGlcNAc levels were measured on day 6 of activation using flow cytometry. P values were calculated by paired t test. N=4 **(b)** CD8 T cells were purified from a PBMC population and activated using anti-CD3/CD28 and IL-2 ± IL-10 (50 nM) for three days followed by three days with IL-2 ± IL-10. OGlcNAc levels were measured on day 6 of activation by flow cytometry. N=3.

5.2.3 IL-10 upregulates many mitochondrial proteins

GO cellular compartment analysis revealed that upregulated proteins were significantly associated with the mitochondria and specifically the inner mitochondrial membrane (Figure 5.10a). Several proteins comprising complex I in the mitochondrial electron transport chain were upregulated by IL-10 treatment, namely NDUFB9, NDUFB10, NDUFB11, NDUFB13 and TMEM126B (Figure 5.10b-c). Although they were upregulated NDUFB9, NDUFB11 and TMEM126B did not reach significance due to variation between donors as well as NDUFB11 and TMEM126B being undetected in the untreated samples in two donors. Complex I transfers electrons from NADH to the respiratory chain and is the largest component in oxidative phosphorylation. Inhibition of complex I in T cells has been shown to reduce proliferation, IFNγ production and degranulation (Yi et al., 2006). COX5A, a component of Complex IV in the mitochondrial electron transport chain was also upregulated by IL-10 (Figure 5.10b-c).

a)

GO cellular component enrichment (upregulated genes)

GO:0043025~neuronal cell body
GO:0005743~mitochondrial inner membrane
GO:0000502~proteasome complex
GO:0043209~myelin sheath
GO:0071437~invadopodium
GO:0043679~axon terminus
GO:0005925~focal adhesion
GO:0030027~lamellipodium
GO:0043231~intracellular membrane-bounded organelle
GO:0016020~membrane
GO:0005739~mitochondrion
GO:0043197~dendritic spine
GO:0005829~cytosol
GO:0005737~cytoplasm
GO:0070062~extracellular exosome

p-value

b)

Oxidative phosphorylation-related proteins

LFQ

NDUFB9 NDUFB11 NDUFB10 NDUFA13 TMEM126B COX5A

Control
IL-10

c)

Oxidative phosphorylation (Fold Change)

Fold Change (normalised)

NDUFB9 NDUFB11 NDUFB10 NDUFA13 TMEM126B COX5A

Figure 5.10 Regulation of oxidative-phosphorylation-associated proteins by IL-10 in CD8 T cells. (a) The 80 proteins upregulated by IL-10 were subject to GO cellular component analysis using the DAVID online software . Components are ranked by p value. **(b)** Oxidative-phosphorylation associated proteins LFQ values are plotted. N=3. **(c)** Fold change of LFQ values shown in (b). For NDUFB11 and TMEM126B only one point is shown as these proteins were not detected in the unstimulated samples for two donors.

As with those proteins involved in glycolysis, none of the mitochondrial proteins upregulated by IL-10 were shown to be significantly regulated by IL-10 at the mRNA level in the transcriptomic dataset, again suggesting post-translational modulation. This strong mitochondrial signature induced by IL-10 prompts many questions about what effect IL-10 could be having. Some potential hypotheses are that IL-10 may be increasing oxidative phosphorylation or altering reactive oxygen species (ROS) production which may enhance CD8 T cell activity. The proteins altered by IL-10 that are involved in metabolic processes are highlighted in Figure 5.11.
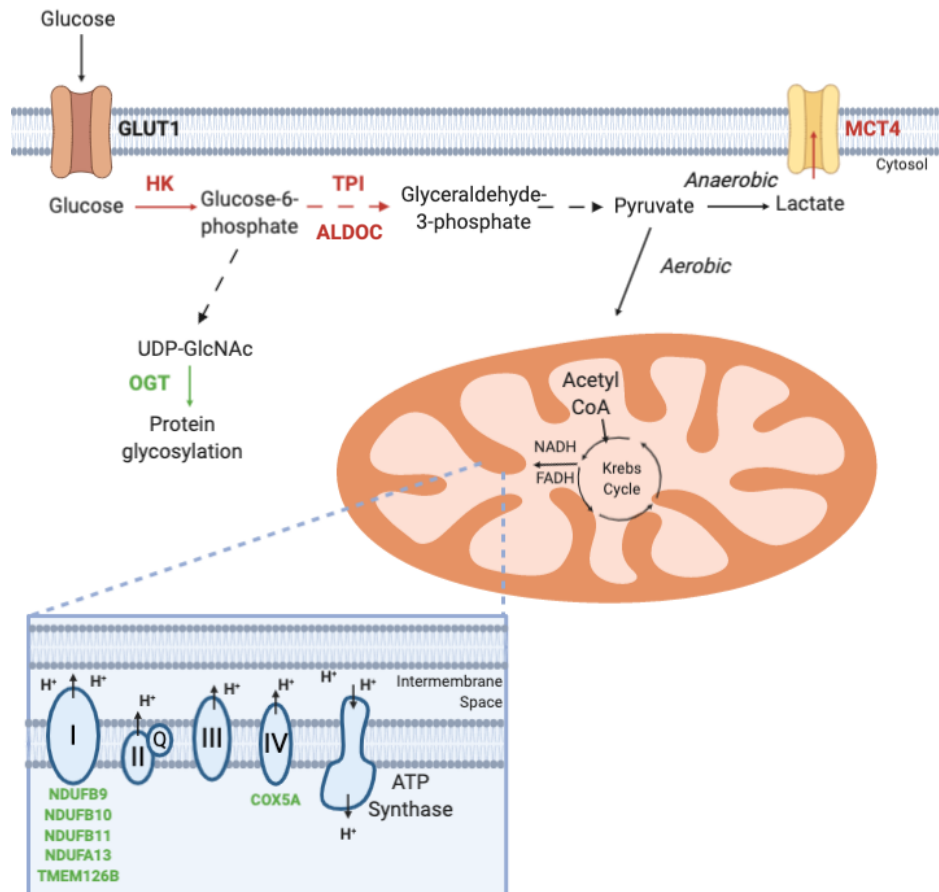
Figure 5.11 Schematic of IL-10 mediated regulation of metabolic processes in CD8 T cells. Simplified schematic of glycolysis and oxidative phosphorylation. Proteins upregulated by IL-10 are highlighted in green, proteins downregulated by IL-10 are highlighted in red. Image generated using BioRender.

Due to the large amount of mitochondrial complex I proteins altered by IL-10 in our proteomic dataset, we wanted to examine the effect of IL-10 on mitochondrial mass and membrane potential. Purified CD8 T cells were activated and cultured in the presence of IL-10 over ten days in a preliminary experiment. Mitochondrial mass and membrane potential were examined using MitoGreen and MitoRed stains respectively at two timepoints, day 6 and day 10. Day 6 is the same timepoint used for the proteomic study however we wanted to use a later timepoint in addition to this to gain more information about the longer effect of IL-10 on the cultures. At both timepoints a sample of non-IL-10 treated cells were incubated with the ionophore FCCP as a positive control. FCCP uncouples oxidative phosphorylation by transporting protons across the inner membrane (Benz and McLaughlin, 1983).

The reduction in MitoGreen staining seen upon FCCP treatment was unexpected. MitoGreen should be membrane potential independent (Figure 5.12a) (Ip et al.,

2017). However a study has shown that the fluorescence of this dye can vary with the production of reactive oxygen species (Doherty and Perl, 2017) and FCCP was previously shown to reduce high glucose-induced ROS production (Yu et al., 2006). Therefore, the reduction seen in the present study may be an artefact of this and further research will be required to confirm this. On day 10 there was a decrease seen in mitochondrial mass in the IL-10 treated cells compared to the non-IL-10 treated controls however this was minimal (15%) (Figure 5.12a).

a)

b)
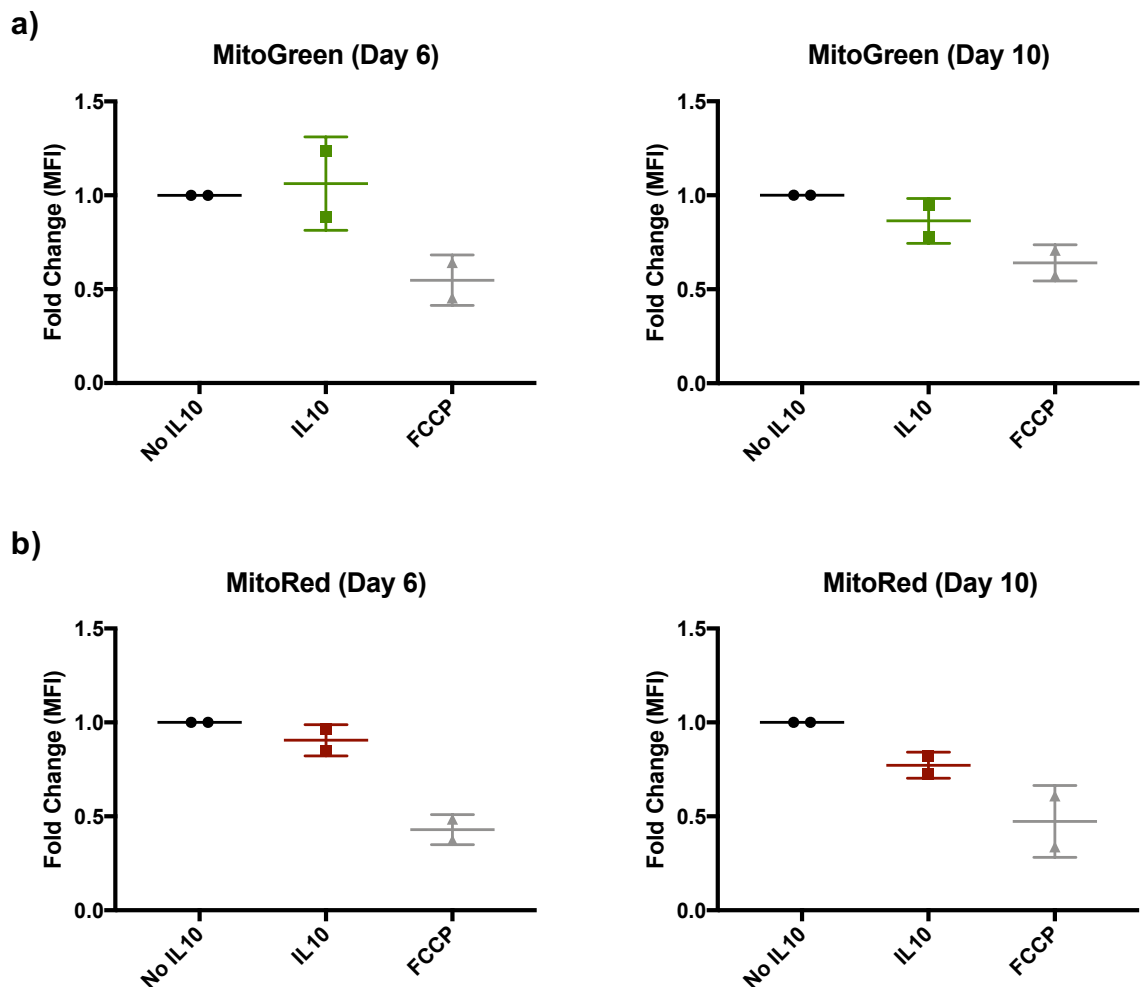
Figure 5.12 Examination of the effect of IL-10 on mitochondrial mass and membrane potential. CD8 T cells were purified from a PBMC population and activated using anti-CD3/CD28 and IL-2 ± IL-10 (50 nM) for three days followed by three days with IL-2 ± IL-10. For growth to day 10, cells were placed in fresh media with IL-2 and IL-10 on day 6 and day 8. Samples were taken at day 6 and day 10 for analysis by flow cytometry of mitochondrial mass using MitoGreen (a) and mitochondrial membrane potential using MitoRed (b). A sample of non-IL-10 treated cells were stimulated with FCCP (5 µM) for 45 minutes before mitotracker staining as a positive control for collapsing membrane potential. N=2.

As expected FCCP induced a reduction in MitoRed fluorescence, denoting a decrease in membrane potential (Figure 5.12b). A small reduction (10%) in

MitoRed fluorescence was seen in the IL-10 treated cells compared to the control cells on day 6 and this difference increased by day 10 to 25% (Figure 5.12b). While this experiment was only performed twice, it suggests that IL-10 may be decreasing the mitochondrial membrane potential. However further work will need to be done to confirm this.

5.3 Discussion

In this chapter I explored the effect of IL-10 on CD8 T cells. We confirmed previously published work demonstrating that IL-10 can enhance effector functions of CD8 T cells. IL-10 treatment of CD8 T cells did not inhibit activation or induce exhaustion. The proteomic study gave an in-depth view of how IL-10 affected protein regulation in CD8 T cells during activation. This highlighted a metabolic signature induced by IL-10 which had previously not been reported in CD8 T cells. The regulation of key metabolic pathways by IL-10 may provide an explanation for the molecular basis of how IL-10 increases the fitness of these cells, however much further work will need to be done to confirm these results.

Regulation of CD8 T cell exhaustion via IL-2Rα levels by IL-10 as a potential mechanism for enhancing cytotoxic activity

In Chapter 4 we used RNA sequencing to examine the effect of IL-10 on CD8 T cells. This, alongside the proteomic data presented in this chapter, gives us an in-depth insight into regulation of both RNA and protein in CD8 T cells by IL-10. One caveat in comparing these two datasets is the differences in CD8 T cell cultures used. For the proteomic dataset, CD8 T cells were activated and grown in a PBMC culture before isolation. In the RNA sequencing study, CD8 T cells were activated and grown in a purified population. Despite these differences both populations were activated for the same time length and IL-10 was added to the cultures at the same time points. This means that, although some differences will arise due to the culture conditions, both data sets describe how the presence of IL-10 during activation affects CD8 T cells.

In the RNA sequencing study, we showed that IL-10 significantly decreased levels of exhaustion marker transcripts TOX and TIM-3. Changes in these were not detected at the level of protein expression in our proteomic dataset. However, using flow cytometry, we saw that IL-10 did reduce cell surface levels of TIGIT, TIM-3 and KLRG1 compared to non-IL-10 treated activated controls. The discrepancies between RNA and protein levels may be explained by the differences in the sensitivity between proteomics and RNA sequencing.

The role of IL-10 in T cell exhaustion is complex. Several studies have shown that the presence of IL-10 can contribute to poor CD8 responses and T cell exhaustion. Sawant et al. demonstrated that IL-10/IL-35 producing Treg cells enhance exhaustion in T cells within the tumour microenvironment (Sawant et al., 2019). CD8 T cells from IL-10 deficient mice in LCMV infection had increased production of effector cytokines and these mice showed enhanced viral clearance, suggesting that IL-10 contributes to chronic viral persistence (Brooks et al., 2006).

In contrast to this, treatment of RCC patients with PEGylated IL-10 led to an increase in CD8 T cells expressing PD-1 and LAG-3 which positively correlated with tumour clearance (Naing et al., 2018). These cells had increased effector molecules and, despite high levels of PD-1 and LAG-3, they did not display an exhausted phenotype. Importantly these cells did not display TIM-3. The authors suggested that IL-10 treatment led to an expansion of tumour-specific activated PD-1/LAG-3 positive CD8 T cells which were key for tumour clearance. In addition, a study using IL-10 KO mice challenged with *Trypanosoma cruzi* showed that, in the absence IL-10, there was an increase in exhausted CD8 T cells, characterised by less proliferation and cytotoxic activities (Pino-Martinez et al., 2019).

These conflicting reports on the link between IL-10 and CD8 T cell exhaustion may be due differences in the length of exposure to IL-10, the timing of IL-10 administration, the sources of IL-10, the viral or cancer challenge used, the cytokine environment of the cells or the activation state of the cells. Our results suggest that the presence of IL-10 during activation may downregulate exhaustion in CD8 T cells, as shown by a decrease in exhaustion markers, an increase in granzyme B and no inhibition in proliferation. This may be a potential mechanism by which IL-10 enhances the cytotoxicity of CD8 T cells, by limiting their functional exhaustion.

In the RNA sequencing study, we saw that IL-10 downregulated IL-2Rα and this was confirmed by flow cytometry at the protein level. In our proteomic dataset, IL-2Rα was downregulated by ~25% in two donors but not detected in the third donor. This confirmation of IL-2Rα downregulation in 8 out of 9 individual donors

(3 for RNA sequence analysis, 3 for flow cytometry and 2 out of 3 for proteomics) in both purified and PBMC cultures suggests that this is a key feature of IL-10 stimulation in CD8 T cells. IL-2Rα is the key subunit in the IL-2 receptor which determines sensitivity to IL-2 and is upregulated by T cells upon activation. IL-2 was present in the T cell culture at every stage during activation to allow the growth and proliferation of the activated populations and so changes to sensitivity to IL-2 may be important in the IL-10-treated phenotype. We saw in our RNA sequencing study that known IL-2 regulated cytokines such as LIF and IL-13 were downregulated by IL-10 treatment and we proposed that this may be due to downregulation of IL-2Rα. In addition, comparison of an IL-2 treated and untreated activated CD8 T cell proteome by Rollings et al. showed increased levels of TIM-3 by IL-2 (Rollings et al., 2018), an inhibitory receptor that was also downregulated in our study by IL-10 treatment.

We hypothesise that this dampening of IL-2 signalling by IL-10 may be linked to the decrease in exhaustion markers. Links between IL-2 and CD8 T cell function have already been explored in the literature (Kalia et al., 2010). Here it was demonstrated that CD25^{lo} CD8 T cells tend towards a memory cell phenotype and are long lived whereas CD25^{hi} CD8 T cells are terminally differentiated with higher rates of apoptosis. Another study showed that removal of the IL-2Rß chain reduced inhibitory receptor levels on CD8 T cells, suggesting a positive role for IL-2 and/or IL-15 in T cell exhaustion (Beltra et al., 2016). Further work will need to be done to confirm the data seen in both our transcriptomic and proteomic data, however the initial results provide new insights into the regulation of CD8 T cell activities by IL-10.

IL-10 regulates key metabolic proteins in CD8 T cells

Our proteomic dataset showed regulation of several key metabolic proteins by IL-10 in CD8 T cells. Glycolysis is upregulated upon T cell activation expanding the capability for rapid protein production, allowing expansion of the population and production of effector molecules (van der Windt and Pearce, 2012). However, in our IL-10 treated cells we saw a downregulation of hexokinase-2, triosephosphate isomerase 1 and fructose-bisphosphate aldolase C, key enzymes in glycolysis. Work by the Cantrell lab has shown that IL-2 is a key

regulator of nutrient transporters and specifically plays a role in maintaining glucose uptake in activated CD8 T cells via regulation of glucose transporters (Ross et al., 2016). It is possible that the downregulation of IL-2Rα by IL-10 may contribute to a metabolic shift in CD8 T cells. We also saw a large upregulation of many components of the mitochondrial electron transport chain by IL-10, in particular those associated with complex I. This is a key step in ATP production during oxidative phosphorylation (OXPHOS) with complex I being the rate limiting step. Together these data support the importance of IL-10 in mediating regulation of significant components of CD8 T cell metabolism.

A study examining the metabolic effect of IL-10 on macrophages saw that IL-10 inhibited glycolysis and promoted OXPHOS (Ip et al., 2017). Here this was linked to IL-10's anti-inflammatory properties in macrophages. While we see regulation of key glycolysis and mitochondrial proteins which suggest that IL-10 may be mediating a similar metabolic shift in CD8 T cells, we link this to an increase in the effector functions of these cells. It has been shown that inhibition of glycolysis using 2-deoxyglucose promotes the generation of memory T cells and can enhance tumour targeting (Sukumar et al., 2013). In addition, studies have reported that increased OXPHOS can enhance memory T cell generation (van der Windt et al., 2012). We hypothesise that the IL-10 induced shift in metabolism in CD8 T cells may be increasing their cytotoxic potential by stabilising the cells and allowing them to continue to produce effector molecules but preventing over-activation and transition into exhaustion.

Conclusions and Future Perspectives

In this chapter I have demonstrated that IL-10 induces key changes in CD8 T cells. I confirmed previously published work showing that IL-10 can enhance production of the effector molecule granzyme B. I then used proteomics to gain insight into the molecular mechanisms that underpin this activity. This highlighted the potential role that IL-10 may play in regulation of IL-2 signalling and CD8 T cell metabolism. Much further work is needed to investigate this. Measurement of rates of glycolysis and OXPHOS using Seahorse assays are needed to confirm if the changes in metabolic pathways seen at the protein level are impacting the metabolic output of these cells. The many mitochondrial proteins regulated by IL-

10 merit further investigation into what changes, if any, IL-10 is inducing in CD8 T cell mitochondria. Further measurement of mitochondrial mass and membrane potential perhaps using isolated mitochondria is needed to confirm the preliminary results shown here. Investigation into ROS production in IL-10 treated CD8 T cells would also help to determine if IL-10 is positively or negatively affecting mitochondrial function. Another interesting aspect to consider for future work is the potential role of mTOR in the activities we are seeing. mTOR is a key regulator of metabolic programmes in CD8 T cells (Howden et al., 2019). Using rapamycin, an mTOR inhibitor, would allow us to assess the contribution of mTOR to IL-10's activities in CD8 T cells.

The results presented here reliably reproduce published work outlining the enhancement of CD8 T cell activities by IL-10. These results also provide a potential molecular mechanism for this enhancing effect, suggesting that IL-10 could regulate the response to IL-2 and the metabolism of CD8 T cells. While further studies are needed to confirm this hypothesis, these results provide a solid foundation upon which future work can be based.

Chapter 6. The use of high affinity IL-10 variants to enable structural characterisation of the receptor complex

Introduction

The crystal structures have been obtained for IL-10 and IL-10Rß as individual polypeptides, as well as for the IL-10/IL-10Rα complex (Walter and Nagabhushan, 1995, Josephson et al., 2001, Zdanov et al., 1995, Yoon et al., 2010, Hoover et al., 1999). Thus far however, the structure of IL-10 in complex with both IL-10Rα and IL-10Rß has remained unresolved. This is probably at least in part due to the weak affinity of IL-10 for IL-10Rß, making purification of a stable complex difficult (Yoon et al., 2010, Freeze and Kranz, 2010b, Pletnev et al., 2005). The availability of a complete structure for the assembled IL-10 cytokine-receptor complex remains an important step in allowing a full understanding of the early molecular events which trigger the IL-10 response.

The work to develop the high affinity IL-10 variant, R5A11, in both a monomeric (R5A11M) and dimeric (R5A11D) conformation (Chapter 3), provided us with unique tools with which it was hoped we would be able to generate stable IL-10/IL-10 receptor complexes which could then be used for crystallisation screens. This chapter describes the attempts to develop a platform for structural characterisation of these complexes.

Aims:
- Generate stable IL-10/IL-10Rα/IL-10Rß complexes using high affinity IL-10 monomer and dimer
- Attempt to de-glycosylate IL-10Rα and IL-10Rß
- Attempt crystallisation of high affinity IL-10/IL-10 receptor complexes
- Screen for nanobodies which bind the R5A11M/IL-10 receptor complex using yeast display

6.1 Generation of purified R5A11M/IL-10Rß and R5A11M/IL-10Rß/IL-10Ra complexes

The engineered monomeric high affinity variant (R5A11M) was shown to bind IL-10Rß with several fold higher affinity than its wild type counterpart by SPR (Chapter 3). To generate the binary complex R5A11M and IL-10Rß were incubated at 4 ºC in a 1:1 ratio before purification via gel filtration (S200 column). This complex eluted as a single peak, confirming that R5A11M can form a stable complex with IL-10Rß (Figure 6.1a). The R5A11M/IL-10Rα/IL-10Rß ternary complex was generated by incubation at 4 ºC of R5A11M with IL-10Rß and IL-10Rα in a 1:1:1 ratio followed by purification via gel filtration (S200 column). This complex eluted at a volume of 14.4 mL (Figure 6.1a).
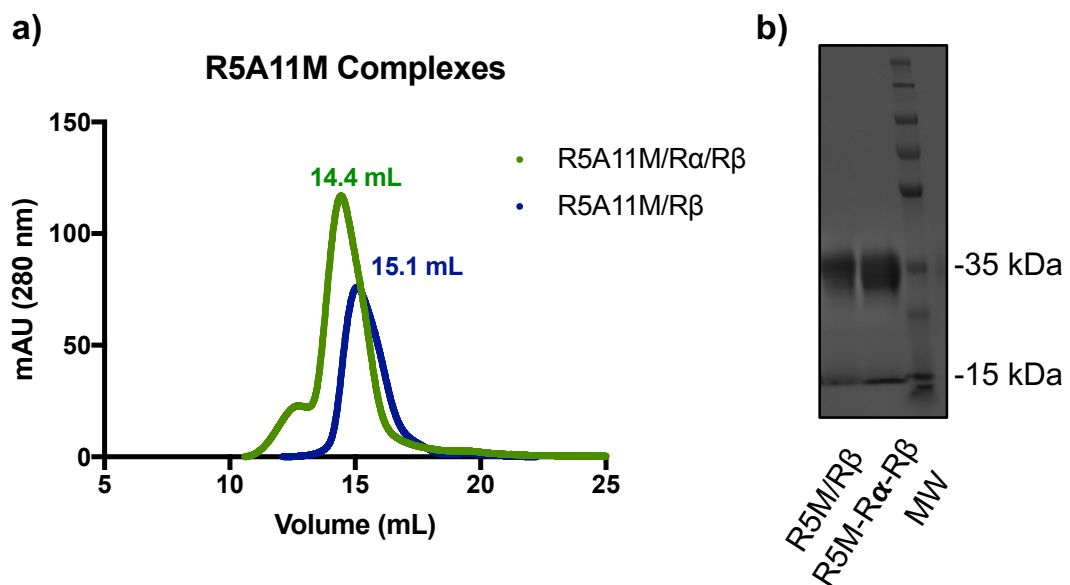
Figure 6.1 Formation of a stable complex of R5A11M with IL-10 receptor subunits. (a) R5A11M and IL-10Rß were incubated at a 1:1 ratio before purification via gel filtration. R5A11M, IL-10Rα and IL-10Rß were incubated at a 1:1:1 ratio before purification via gel filtration. Gel filtration was performed on an S200 column **(b)** A sample from the peak of each complex was run on a 12% SDS-PAGE gel. R5M= R5A11M. MW= molecular weight marker.

The earlier elution volume for the ternary complex was expected due to its increased size compared to the binary complex. Protein fractions from the ternary and binary IL-10-receptor complexes were run on an SDS-PAGE gel to determine the polypeptide species present within each peak (Figure 6.1b). However, while R5A11M runs as a band around 18 kDa, detection of the individual receptor ectodomains is complicated somewhat due to their similar molecular weights (IL-

10Rα at 24 kDa and IL-10Rß at 23.5 kDa respectively) and the multiple glycosylation sites on each subunit.

Crystal screens were set (ProPlex (Molecular Dimensions), JCSG Core Suite I, JCSG Core Suite II and JCSG Core Suite IV (Qiagen)) using both the binary and the ternary complex. Sitting MRC 96-well 2 drop plates were used. 100 nL volumes were dispensed in a 1:1 ratio of protein: crystallisation condition. Screens were placed in a temperature controlled room (~21ºC) and periodically checked however, no crystal were obtained.

6.1.1 De-glycosylation of receptor proteins

A common barrier to the generation of crystals for structure determination is the glycosylation of proteins as the presence of the sugars reduces the homogeneity of the protein (Nettleship, 2012). Human IL-10 is not glycosylated however both IL-10Rα and IL-10Rß contain several N-linked glycosylation sites (Hoover et al., 1999, Yoon et al., 2010, Pletnev et al., 2005). As an extension of the purification process, and to provide further samples for crystallisation, attempts were made to produce components devoid of glycosylation.

De-glycosylation of IL-10Rβ

A non-glycosylated mutant of the IL-10Rß ectodomain had previously been designed by the Walter group (Yoon et al., 2010). This mutant had asparagine to glutamine substitutions at four sites: N49Q, N68Q, N102Q, N161Q (Figure 6.2.a) and was used to generate a 2.14Å resolution structure of IL-10Rß (Yoon et al., 2010). This same IL-10Rß glycosylation mutant was generated for use in the IL-10 cytokine-receptor complexes going forward. As shown in Figure 6.2b when the glycosylation mutant was purified by gel filtration it eluted at a slightly higher volume than the wild type, suggesting a reduction in mass due to the lack of glycosylation. When run on an SDS-PAGE gel, the reduction in apparent mass from ~35 kDa to ~25 kDa indicated that the mutations had indeed removed the glycosylation sites present in the WT the protein (Figure 6.2c).

a)

IL-10Rβ Glycosylation Mutant

MVPPPENVRMNSVNFKNILQWESPAFAKG**Q**LTFTAQYLSY
RIFQDKCM**Q**TTLTECDFSSLSKYGDHTLRVRAEFADEHSD
WV**Q**ITFCPVDDTIIGPPGMQVEVLADSLHMRFLAPKIENEYE
TWTMKNVYNSWTYNVQYWK**Q**GTDEKFQITPQYDFEVLRNL
EPWTTYCVQVRGFLPDRNKAGEWSEPVCEQTTHDETVPS

b)

c)
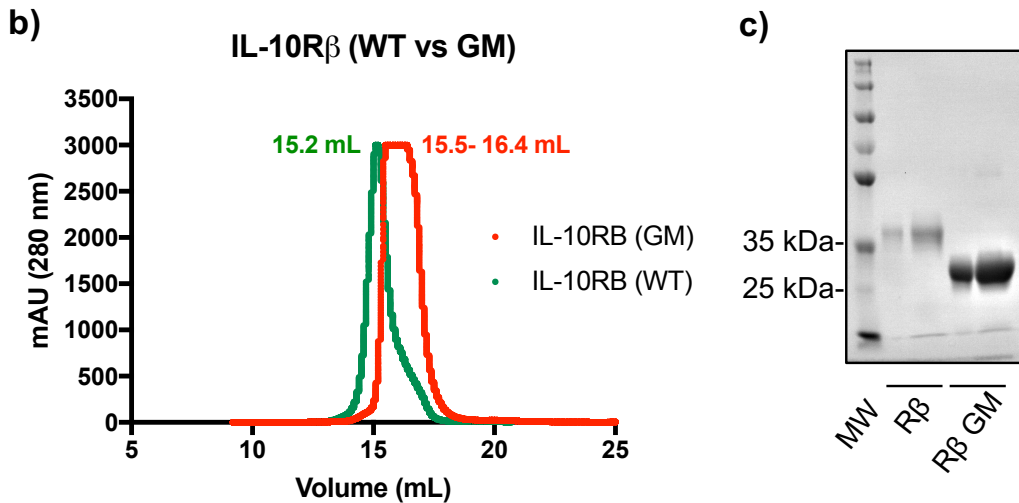
Figure 6.2 Expression of IL-10Rß glycosylation mutant. (a) Sequence of IL-10Rß glycosylation mutant with the N to Q substitutions highlighted in red. **(b)** Overlay of GF chromatograms for IL-10Rß wild type and glycosylation mutant, each run on an S200 column. **(c)** IL-10Rß wild type and glycosylation mutant run on a 10% SDS-PAGE gel. Both IL-10Rß WT and GM were run at 5 µL and 15 µL each (first and second lane of each proteins) MW= molecular weight marker.

De-glycosylation of IL-10Rα

Similarly to IL-10Rß, a glycosylation mutant of the IL-10Rα ectodomain had previously been generated by the Walter group where asparagine residues were mutated to glutamine at 6 positions (N29Q, N53Q, N89Q, N133Q, N156Q, N168Q) (Josephson et al., 2001). The production of this glycosylation mutant in both Hi5 cells and *Drosophila* S2 cells was attempted however adequate expression levels of the protein were not achieved. In order to de-glycosylate IL-10Rα, kifunensine was added to the insect cell culture when the protein was being expressed. Kifunensine inhibits the α-mannosidase enzyme, blocking the branching of the N-linked glycans, resulting in glycosylation limited to just simple high mannose residues (Elbein et al., 1990) (Figure 6.3a). After purification the protein was treated with endoglycosidase F (EndoF). This enzyme cleaves the oligosaccharide between two GlcNAc subunits which are adjacent to the asparagine residue of the protein, leaving only one GlcNAc residue on the protein

(Freeze and Kranz, 2010a) (Figure 6.3a). A titration of kifunensine over a range of 5-100 μM was performed to determine the optimal concentration needed (Figure 6.3b). As shown by the separation pattern in SDS-PAGE, the addition of kifunensine, followed by incubation with a constant concentration of EndoF (50 μg/mL) successfully reduced the glycosylation from the purified IL-10Rα. When purified by GF and compared to previous non-treated samples, both the glycosylated (WT) and Kifu/EndoF treated IL-10Rα eluted at similar volumes (15.4 mL and 15.5 mL respectively), suggesting that some glycosylation still remained (Figure 6.3c).
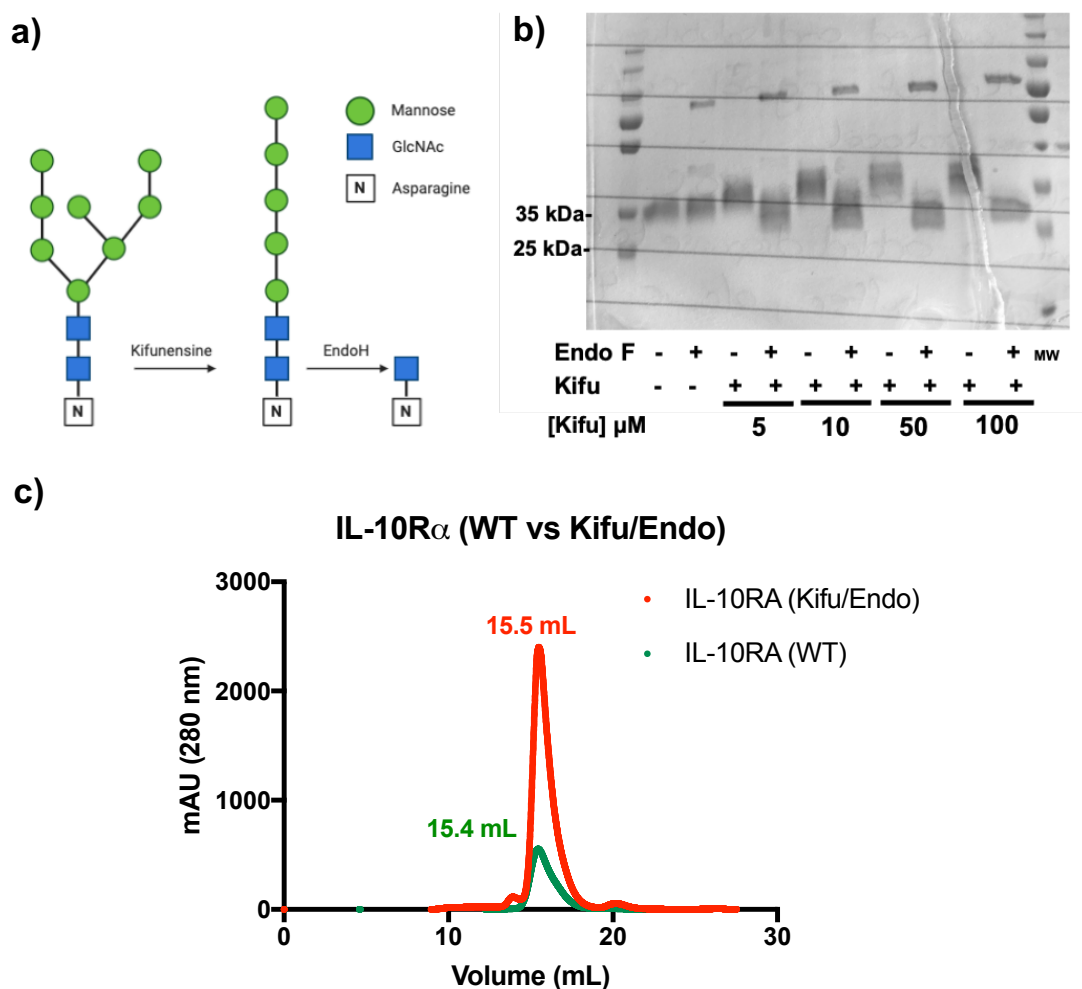
Figure 6.3 De-glycosylation of IL-10Rα. (a) Simplified cartoon representation of the effect of kifunensine and EndoH treatment on oligosaccharide residues adapted from (Freeze and Kranz, 2010b). Image generated using BioRender. **(b)** IL-10Rα was expressed in the presence of kifunensine (Kifu) followed by EndoF treatment. The concentration of kifunensine used increased from left to right (5 μM, 10 μM, 50 μM and 100 μM). Each concentration condition was then either treated (+) with EndoF or untreated (-). A constant concentration of EndoF was used (50 μg/mL). MW= molecular weight marker. **(c)** GF traces of IL-10Rα compared to a kifunensine/EndoH treated IL-10Rα. S200 columns were used for gel filtration.

6.2 Purification of R5A11D/IL-10Rα/IL-10Rß Complex

We had previously generated the high affinity IL-10 in the dimeric confirmation (R5A11D). We next attempted crystallisation of the dimeric variant as it was hoped that the symmetry of the dimeric complex would further improve the chances of crystallisation. We did not attempt crystallisation of the monomer with the de-glycosylated receptor subunits nor did we attempt to crystallisation of the dimer with the glycosylated receptor subunits due to time constraints.

As a dimer, R5A11D will bind two IL-10Rα and two IL-10Rß subunits in a 1:2:2 stoichiometry, different to the 1:1:1 stoichiometry of the monomer. R5A11D was complexed with the IL-10Rß glycosylation mutant alone to form the binary complex, as well as with the kifunensine/EndoH treated IL-10Rα and the IL-10Rß glycosylation mutant for ternary complex formation. Each complex was then purified by GF. As expected, a difference in the elution volumes was seen between the binary and the ternary complex, with the binary complex eluting at 14 mL and the ternary at 13.3 mL (Figure 6.4a).

Unlike the monomeric-receptor complexes, the dimeric-receptor complexes did not run as a monodispersed peak, with two distinct peaks seen in both the binary and the ternary complex. Overlaying the ternary complex GF trace with that of the individual receptor components highlights that the second peak resembles the elution volumes of the receptors (Figure 6.4b). To examine these peaks more closely each was analysed by SDS-PAGE. The early fraction which eluted at 13.4 mL (EF) corresponded to the R5A11D/IL-10Rα/IL-10Rß complex, while the late fraction (LF) which eluted at 15.9 mL contained the receptor subunits (Figure 6.4c). This fraction of unbound receptor was unexpected as the complex components were incubated according to the 1:2:2 IL-10:IL-10Rα:IL-10Rß ratio. It may be that some R5A11D was lost in the column due to non-specific binding, altering the ratio. In future, re-running the early fraction peak on a gel filtration column would be advised, in order to ensure that the complex is not dissociating. Additionally, our stock concentration of IL-10Rß is very high, meaning that very small volumes of it are needed in the complex relative to the other components.

This may mean that a small deviation in the volume of IL-10Rß added results in a substantial excess of protein in the complex.

a)

b)

c)
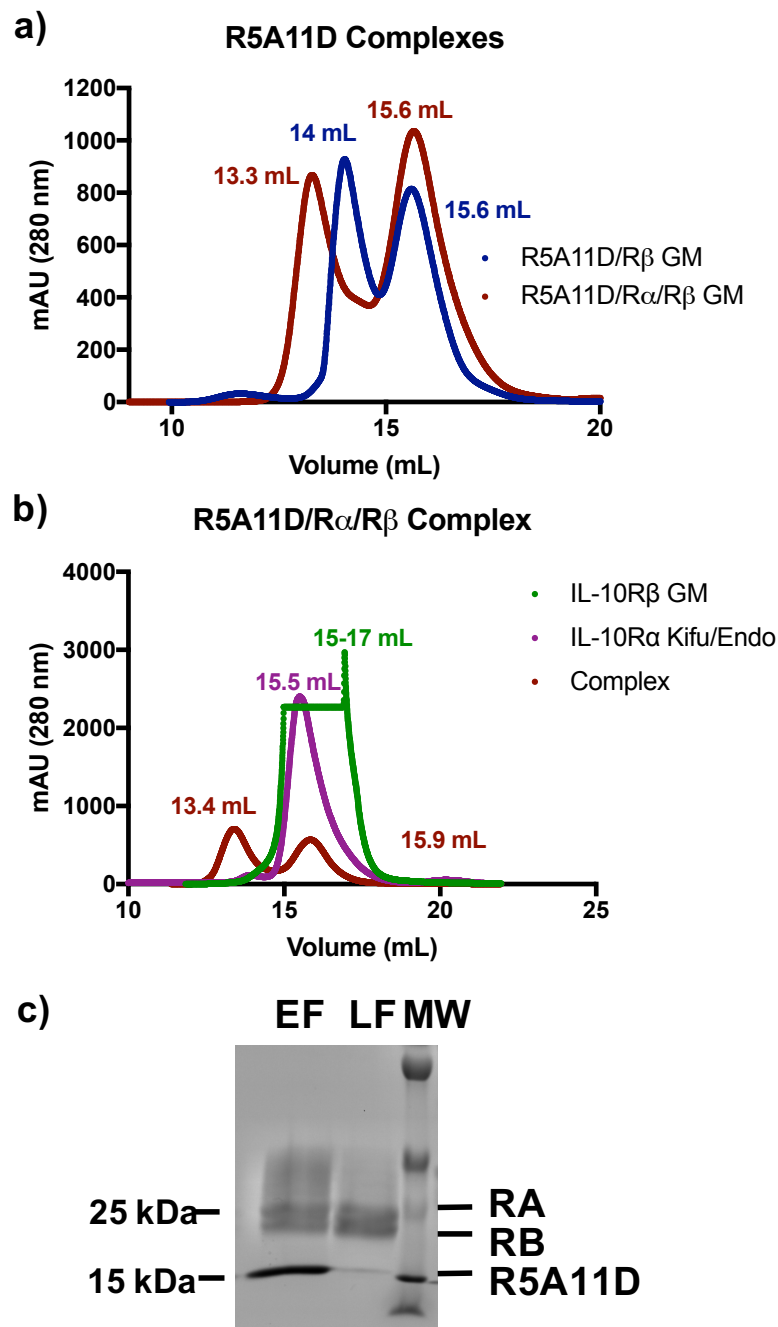
Figure 6.4 R5A11D/IL-10Rß/IL-10Rα complex. (a) Overlay of the GF traces of the binary and ternary complexes. Each complex was run on an S200 column, **(b)** GF trace of the R5A11D/IL-10Rα/IL-10Rß complex overlaid with the receptor subunits run on an S200 column. **(c)** A sample from the early fraction (EF) and late fraction (LF) separated by GF in (b) was run on a 10% SDS-PAGE gel. MW= molecular weight marker.

6.3 Crystallisation Screening of R5A11D complex

6.3.1 Initial rounds

Having demonstrated the ability to generate stable complexes which remained intact through GF as well as reducing the glycosylation of the receptors we next attempted to prepare crystals for structure determination. We performed crystallisation screening with samples of R5A11D/IL-10Rß and R5A11D/IL-10Rα/IL-10Rß. Concentrations of each complex ranging from 3-10 mg/mL were used in various commercially available screens: PurePEG, ProPlex (Molecular Dimensions), JCSG Core Suite I, JCSG Core Suite III and JCSG Core Suite IV (Qiagen). 60 µL of crystallisation conditions were used and sitting MRC 96-well 2 drop plates were used. 100 nL volumes were dispensed in a 1:1 ratio of protein: crystallisation condition. Screens were placed in a temperature controlled room (~21ºC) or in an incubator maintained at 18°C with humidity control however neither condition produced crystals.

6.3.2 Follow-up

Methylation of lysine residues has been shown to improve the success rate of crystallisation (Sledz et al., 2010). This process involves adding a methyl group to the exposed primary amines (i.e., lysine residues and the N-terminus of the protein). Why this process can enhance the generation of crystals is unclear however several explanations have been proposed such as the increase in hydrophobic surfaces or a reduction in the isoelectric point (Walter et al., 2006). We methylated a complex of R5A11D/IL-10Rα/IL-10Rß for use in screens however no crystals were observed.

All efforts thus far had used proteins in an HBS solution (100 mM HEPES, 1.5 M NaCl). We buffer exchanged a sample of R5A11D/IL-10Rß/IL-10Rα complex into a low salt buffer (10 mM HEPES, 50 mM NaCl) and set up screening plates using this protein solution. After 3 days incubation at 18ºC two small crystal fragments were visible in well 8E of the JCSG Core III suite (Figure 6.5). This well contained the following conditions: 0.2 M calcium acetate, 0.1 M sodium cacodylate, pH 6.5, 18% PEG8000. In an attempt to optimise this condition, we set up a screen using

variations of these conditions, varying the pH of sodium cacodylate, the molarity of calcium acetate and the percentage of PEG8000. Unfortunately, despite multiple attempts we could not repeat the generation of these crystal fragments, even when repeating the original screen conditions.
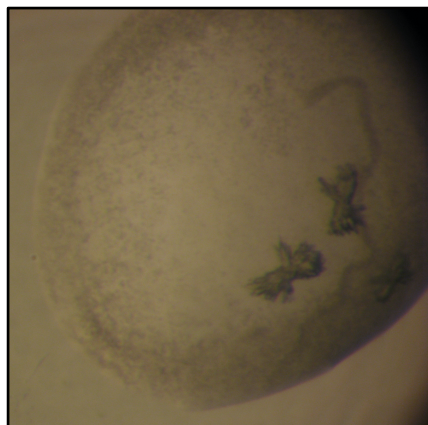
Figure 6.5 Crystallisation attempts of the IL-10 receptor complex. Image of fragments seen when the R5A11/IL-10Rα/IL-10Rß complex was placed in a low salt buffer in well 8E of JCSG Core III suite.

6.4 Generation of nanobodies which recognise the R5A11M/IL-10Rα/IL-10Rß complex

Work done in this section (6.5) was carried out by Rachael Brown during her honours project in the Moraga lab, supervised and assisted by the author of this thesis.

Due to our inability to crystallise high affinity IL-10 with its receptor components through the traditional pathway, we decided to generate nanobodies capable of binding the ligand-receptor complex. Nanobodies have previously shown efficacy in acting as chaperones in the crystallisation of protein complexes. A synthetic nanobody yeast display library, previously generated by McMahon et al., was used here to isolate nanobodies capable of recognising the high affinity IL-10 variant in complex with the receptor subunits (McMahon et al., 2018).

Conventional antibodies are comprised of two chains: a heavy chain and a light chain (Figure 6.6). Each chain has a constant domain and a variable domain and it is the variable domain that recognises the epitope and gives the antibody specificity. Camelids produce antibodies which consist only of heavy chains, with one variable domain and two constant domains (Muyldermans, 2013). The

variable heavy chain alone can be recombinantly expressed as a nanobody. Nanobodies retain the antigen binding site but have a greatly reduced size compared to antibodies, with a mass of approximately 15 kDa.
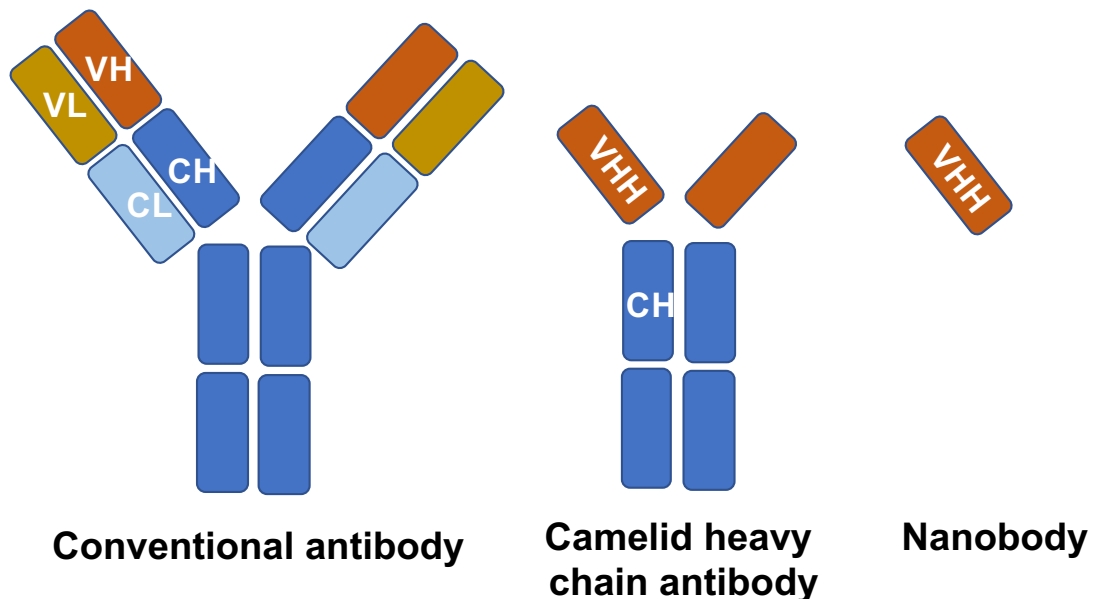
Figure 6.6 Antibody and nanobody structure. Conventional antibodies are comprised of heavy and light chains. These can be divided up into variable domains and constant domains. VL= variable light chain, VH= variable heavy chain, CL= constant light chain, VH= variable heavy chain. Camelid antibodies are comprised only of heavy chains with a variable domain (VHH) and a constant domain (CH). Nanobodies comprise the variable heavy chain only.

Their antigen specificity, small size and ease of expression means they have been used in many applications, both as research tools and as therapeutics (Muyldermans, 2013). Of interest to this thesis, nanobodies have been successfully used to stabilise ligand-G-protein coupled receptor (GPCR) complexes, allowing their crystallisation and structure determination (Manglik et al., 2017). Traditional production of nanobodies involves the costly and time-consuming process of immunising camelids. Pioneering work by the Kruse laboratory generated a synthetic yeast-display nanobody library which can be used to isolate nanobodies capable of binding a target antigen (McMahon et al., 2018). We took advantage of this technology to isolate nanobodies which recognise the R5A11M/IL-10Rα/IL-10Rß complex. We used the monomeric version of our high affinity IL-10 variant as the 1:1:1 IL-10: receptor stoichiometry represented a more efficient system to express and was a more economical use of protein than the dimeric system.

6.4.1 Nanobody library screening

The screening process used magnetic activated cell sorting (MACS) following a very similar process to the one used for the affinity maturation of IL-10 in Chapter 1 (Figure 6.7). Briefly, the yeast library displaying the nanobody variants on the yeast cell surface is incubated with the biotinylated protein of interest. This is followed by incubation with Alexa Fluor647 (AF647)-labelled streptavidin. Anti-AF647 magnetic beads are then used to isolate yeast which display nanobodies capable of binding the protein. This process is repeated with decreasing concentrations of protein until single clones with high affinity can be isolated. We generated two variations of the R5A11M/IL-10Rα/IL-10Rß complex for use in screening rounds: one where IL-10Rα was biotinylated and the second where IL-10Rß was biotinylated. These could then be alternated during the early selection rounds to ensure that the nanobodies were binding to an epitope within the complex, rather than just on the receptor subunit alone.
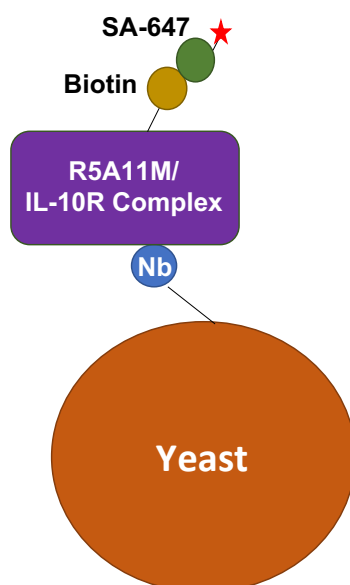
Figure 6.7 Isolation of nanobodies. Yeast displaying nanobodies on their cell surface were incubated with biotinylated R5A11M/IL-10 receptor complex. This could then be recognised by fluorescently labelled streptavidin. Nb= nanobody, SA-647= streptavidin labelled with the fluorochrome AlexaFluor647.

The conditions used for the screening rounds are outlined in Figure 6.8. The first round was a clearing selection round using streptavidin beads (SAV) bound to high concentrations of complex (400 nM) to recover all positive binders and reduce the complexity of the library. As was done for the IL-10 library, we also performed an additional negative clearing step at the start of each selection

round, incubating the yeast with Alexa Fluor647 (AF647)-labelled streptavidin in the absence of biotinylated protein in order to remove any yeast displaying nanobodies which were capable of binding streptavidin.
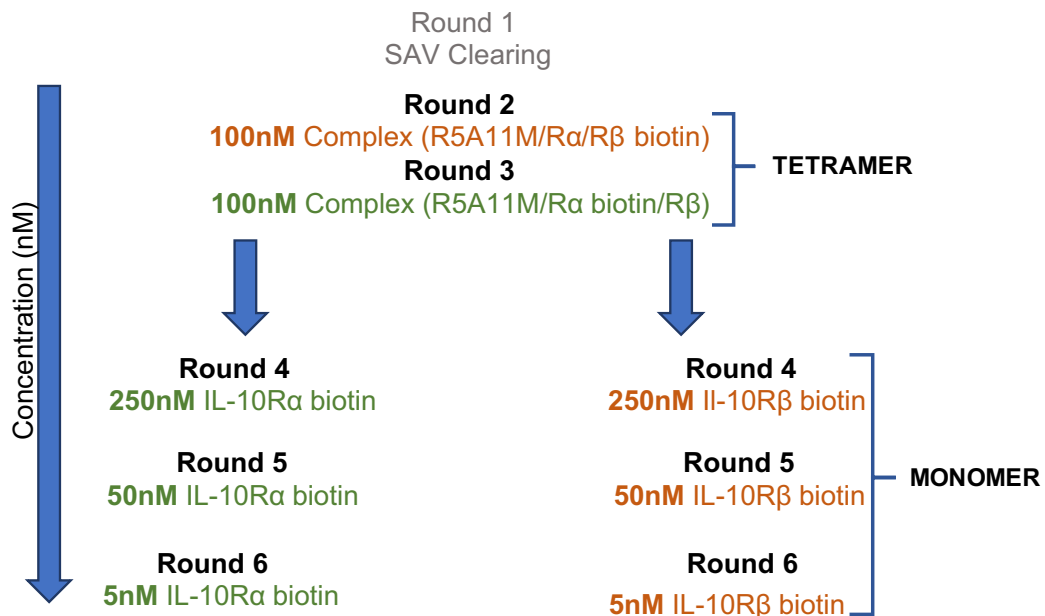
Figure 6.8 Screening conditions to isolate nanobodies capable of binding the R5A11M/IL-10 receptor complex. Selection rounds used decreasing concentrations of biotinylated protein to isolate high affinity nanobodies. For rounds two and three a tetramer was used: each streptavidin molecule was bound to four biotinylated R5A11M/IL-10Rß/IL-10Rα complexes. For rounds four to six, monomers were used: one streptavidin molecule binds one biotinylated protein.

For round 2 of positive selection, we used a 100 nM concentration of the complete IL-10/receptor complex (R5A11M/IL-10Rα/IL-10Rß) where IL-10Rß was biotinylated. In order to increase avidity, we used this complex as a tetramer with the fluorescently labelled streptavidin. This meant that each streptavidin molecule could bind to four IL-10 receptor complexes. The same concentration of tetramer was repeated for the third selection round however this round used a complex which was biotinylated at IL-10Rα. After this section round we then divided the library in two: one library would proceed with selection using IL-10Rß alone and the other would use IL-10Rα alone (Figure 6.8) as it was assumed that all single receptor binders were removed in the previous rounds. It was hoped that this would generate a wider range of nanobodies which could bind the complex over a variety of epitopes. A monomeric compound of the receptor bound to streptavidin was used i.e., 1:1 receptor: streptavidin stoichiometry with the concentrations shown in Figure 6.8. As the selection rounds progressed, the concentration of the biotinylated receptor subunits was decreased from 250 nM to 5 nM.

6.4.2 Isolation and identification of nanobody clones

After the final round at just 5nM IL-10 receptor concentration, individual yeast colonies were isolated by plating on glucose agar, following a similar protocol to that in Chapter 3. These clones were then used in a dose response experiment to determine the approximate on-yeast affinity of the nanobodies for the receptor complex. The yeast clones from the library which had used biotinylated IL-10Rα were denoted as "A" nanobodies and those from the biotinylated IL-10Rß library were denoted as "B" nanobodies. Two dose response experiments were performed using both A and B nanobodies. In one dose response experiment, the yeast clones were titrated against the R5A11M/IL-10Rα/IL-10Rß complex which was biotinylated at IL-10Rα (Figure 6.9a). In the second dose response, the yeast clones were titrated against the R5A11M/IL-10Rα/IL-10Rß complex which was biotinylated at IL-10Rß (Figure 6.9b). Several variants from each library displayed promising binding patterns: A7, A9, A12, B4, B9, B10 and B12.
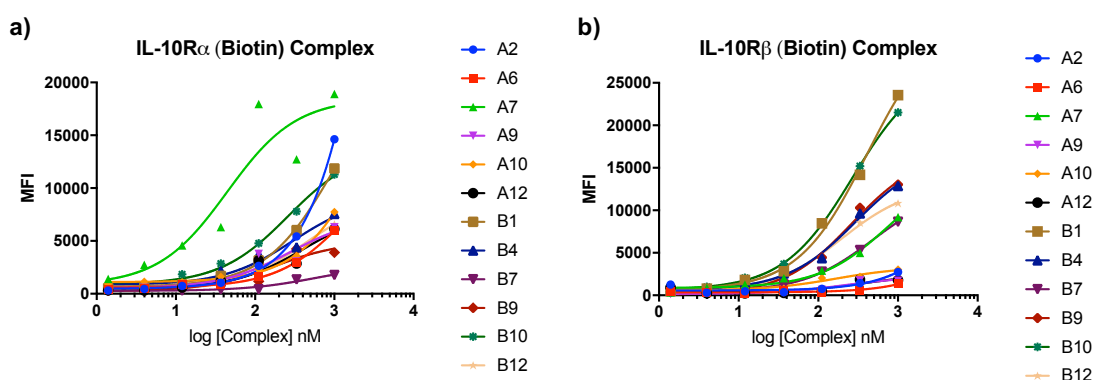
Figure 6.9 Dose response of nanobody clones. Yeast displaying the nanobody clones were incubated with decreasing concentrations of R5A11M/IL-10 receptor complex (top concentration of 1000 nM, 1/3 serial dilution). Complex binding was measured by fluorescence of AF647-labelled streptavidin by flow cytometry. **(a)** R5A11M/IL-10 receptor complex was biotinylated at IL-10Rα. **(b)** R5A11M/IL-10 receptor complex was biotinylated at IL-10Rß.

The plasmids encoding these nanobodies were isolated and sent for sequence identification. Figure 6.10 shows the alignment of the nanobody sequences. As expected, the variations between the nanobodies occured at three distinct sites, corresponding to the complementarity determining regions (CDRs) and not the backbone structure of the nanobody. Due to the combinatorial effect of the amino acid variations at the CDRs, no conclusion can be made about specific amino acid substitutions between the nanobody variants.

CDR1   CDR2

Nb   QVQLQESGGGLVQAGGSLRLSCAASGSISLYAEMGWYRQAPGKERELVAGITRGTTTYYA   60
B12   QVQLQESGGGLVQAGGSLRLSCAASGSIFGYYIMGWYRQAPGKERELVAAIAYGANTYYA   60
B9   QVQLQESGGGLVQAGGSLRLSCAASGTISRSPFMGWYRQAPGKERELVAAIATGTNTYYA   60
B4   QVQLQESGGGLVQAGGSLRLSCAASGTIFFAYVMGWYRQAPGKERELVAGIGRGANTNYA   60
B10   QVQLQESGGGLVQAGGSLRLSCAASGSISYIKYMGWYRQAPGKERELVAAIAYGGTTYYA   60
A12   QVQLQESGGGLVQAGGSLRLSCAASGSIFRLKFMGWYRQAPGKEREFVAGISGGATTNYA   60
A9   QVQLQESGGGLVQAGGSLRLSCAASGTISGLPYMGWYRQAPGKERELVAGISAGGSTYYA   60
A7   QVQLQESGGGLVQAGGSLRLSCAASGNIFALTFMGWYRQAPGKEREFVAAITQGGTTYYA   60
      ************************.*   ***************:**.*   * .* **

Nb   DSVKGRFTISRDNAKNTVYLQMNSLKPEDTAVYYCAADYV-QGKSRVIPHYYWGQGTQVTVSS   122
B12   DSVKGRFTISRDNAKNTVYLQMNSLKPEDTAVYYCAARGP-YYHRTENRYDYWGQGTQVTVSS   122
B9   DSVKGRFTISRDNAKNTVYLQMNSLKPEDTAVYYCAAIRP-TGISARSFHRYWGQGTQVTVSS   122
B4   DSVKGRFTISRDNAKNTVYLQMNSLKPEDTAVYYCAVYA-RRYQYSSYYLSYWGQGTQVTVSS   122
B10   DSVKGRFTISRDNAKNTVYLQMNSLKPEDTAVYYCAVGGVVSYDPYRSLHRYWGQGTQVTVSS   123
A12   DSVKGRFTISRDNAKNTVYLQMNSLKPEDTAVYYCAALQ-----YDSHALGYWGQGTQVTVSS   118
A9   DSVKGRFTISRDNAKNTVYLQMNSLKPEDTAVYYCAVVY-----RYYDRHWYWGQGTQVTVSS   118
A7   DSVKGRFTISRDNAKNTVYLQMNSLKPEDTAVYYCAVND-----YYGYTHPYWGQGTQVTVSS   118
      **********************************. .   ***********

CDR3

Figure 6.10 Sequences of nanobodies capable of bind the R5A11M/IL-10 receptor complex. Sequences of the nanobodies isolated from the synthetic library are aligned against the template nanobody sequence from (McMahon et al., 2018). The sequence variations between the nanobodies are highlighted in red.

Much further work will need to be done before these can be used for crystallisation attempts. Firstly, the nanobodies will need to be recombinantly expressed. Nanobodies have been expressed in both bacterial and mammalian systems giving us several options for expression. Once expressed, it would be pertinent to determine the binding affinity of the nanobodies to the cytokine-receptor complex using SPR to validate the on-yeast affinities. The nanobodies could then be bound to the complex alone or in combinations. As the sequences of R5A11M and R5A11D are identical apart from the glycine-serine linker, it may also be possible to use the nanobodies with the R5A11D-receptor complex. It is hoped that the nanobodies could act as chaperones to promote crystallisation as has been done for previous structural studies with GPCRs (Manglik et al., 2017).

6.5 Discussion

The generation of a high affinity IL-10 variant in both monomeric and dimeric conformations opened new avenues to further explore IL-10 biology. Here we used the high affinity variants to attempt crystallisation of the IL-10 receptor complex. Although crystallisation attempts were unsuccessful, we did succeed in generating stable complexes of IL-10 bound to both IL-10Rα and IL-10Rß. In addition, the use of a synthetic nanobody yeast display library allowed the

isolation of nanobodies with affinity for the R5A11M/IL-10 receptor complex. These will hopefully be used in future work to enhance the chances of generating crystals suitable for diffraction.

Crystallisation attempts

The stable complexes generated here failed to produce crystals, suggesting that it is not only the low affinity for IL-10Rß that is preventing crystallisation. Difficulties usually arise with crystallisation of proteins when ordered, heterogenous proteins cannot be obtained. Because of this, glycosylation of proteins often presents a barrier to crystallisation. This is due to the mobility and flexibility of the sugar residues which introduces structural and conformational disorder. In order to combat this we expressed a mutant of the IL-10Rß ectodomain which effectively removed N-linked glycosylation from this receptor subunit by the conversion of asparagine to glutamine residues at several sites, as previously described (Yoon et al., 2010). We were unable to express IL-10Rα with similar mutations at N-linked glycosylation sites. Why this failed is unknown however it may be due to differences in cell culture or in expression induction from that done by Josephson et al. A previous study which attempted crystallisation of the IL-10 receptor complex observed precipitation of the IL-10Rα protein upon de-glycosylation which was attributed to reduced solubility (Hoover et al., 1999), suggesting that there are intrinsic difficulties in the expression of a de-glycosylated IL-10Rα variant. Due to the myriad of factors which affect the crystallisation process it is often not possible to say why a particular protein fails to crystallise and so this explanation act only as a suggestion.

Conclusions and future work

The ability of nanobodies to aid in the crystallisation process remains untested for our complexes due to time constraints. While significant effort will be required to get these into a crystallisation campaign, specific nanobodies have been successfully identified for the complex.

Although crystallisation has historically been the favourable method for structure determination, the use of cryoEM is suitable for large complexes and so this may

be a favourable strategy to use going forward for examination of the complete IL-10 receptor complex. This technique has the advantage of not requiring crystals and using smaller amounts of sample, although access to specialised facilities is required. Since completion of this thesis, work has continued on this project by Dr. P.K Fyfe in collaboration with the Scottish Centre for Macro-molecular Imaging (SCMI, University of Glasgow). A limited number of cryoEM grids containing R5A11D in complex with IL-10Rα and IL-10Rß were prepared by the SCMI and the preliminary image collected is shown in Figure 6.11. Initial analysis suggests that there could be aggregates or that the particles are overlapping on the grid, however there are some standalone particles which appear promising. Much more optimisation will need to be undertaken however we are hopeful that our high affinity complex will yield more favourable results using cryoEM in the future.
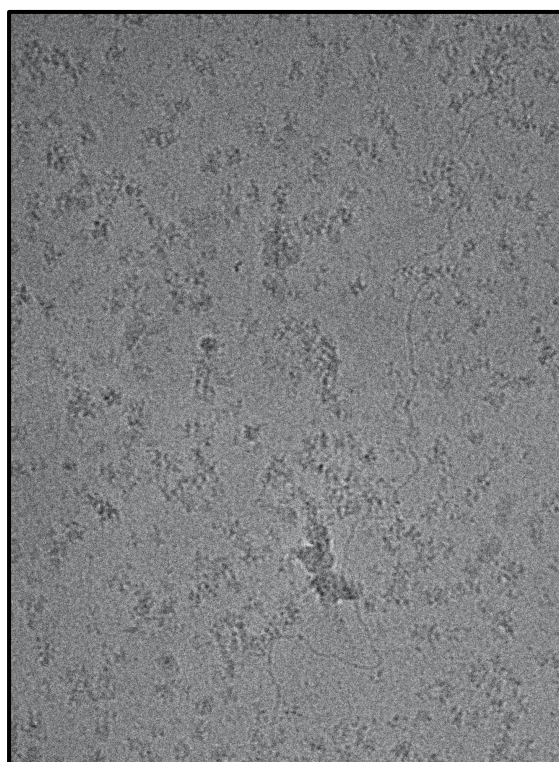
Figure 6.11 Preliminary cryoEM attempt of R5A11D/IL-10Rα/IL-10Rß complex. R5A11D in complex with IL-10Rα and IL-10Rß in a 1:2:2 ratio was purified via gel filtration (S200 column) by the author of the thesis. Quantifoil 2/2 grids were glow discharged twice at 25 mA for 30 seconds. 3.5 µL of sample was applied to the grid and backside blotting was performed in the Leica GP2 with 85% humidity at 18ºC. **Grids were set and images were collected by SCMI, University of Glasgow in collaboration with Dr. P.K Fyfe.**

Chapter 7. Conclusions and Future Perspectives

It has been over 30 years since IL-10 was first described and since then much work has been done to characterise the effects of this potent cytokine (Vieira et al., 1991). While its anti-inflammatory functions have been well described, there is still a dearth of knowledge of how this cytokine carries out its effects at a structural and molecular level. This lack of understanding was brought into sharp focus when attempts to use it as an anti-inflammatory therapeutic failed in the clinic despite promising *in vitro* studies (Saraiva et al., 2020). The primary aim of this thesis was to generate a high affinity variant of IL-10 for use in both structural and immunological studies to gain a better understanding of the molecular mechanisms this cytokine employs to carry out its activities.

In order to generate a high affinity variant of IL-10 we took advantage of previously described yeast display technologies (Spangler et al., 2015). This allowed us to engineer a variant of IL-10 which had increased affinity for the IL-10Rß subunit, without the structural knowledge of the IL-10/IL-10Rß interaction site. Identifying the sites where mutations occurs gave us insight into the IL-10/IL-10Rß binding interface. Mutations occurred primarily along the A and D helices, which is in keeping with previously published binding models and validates our selection process (Pletnev et al., 2005, Mendoza et al., 2017).

While the mutations shed light on the potential interaction of IL-10 with IL-10Rß, a full structure of the IL-10/IL-10Rα/IL-10Rß ternary complex is still lacking. Previous work suggested that the difficulty in generating a crystal structure was due to the weak affinity between IL-10 and IL-10Rß (Pletnev et al., 2005). The generation of an IL-10 variant with the capability of binding IL-10Rß, even in the absence of IL-10Rα, presented a unique opportunity to attempt to crystalise this complex. The R5A11 variant could form stable complexes with IL-10Rß alone and in combination with IL-10Rα. This is, to our knowledge, the first time an IL-10/IL-10Rß complex sufficiently stable to be purified by gel filtration has been reported. Although large amounts of purified complex could be generated, crystallisation of the complex was not achieved despite multiple screening attempts. In order to provide more options for future structural studies, we used the synthetic yeast display nanobody library generated by the Kruse laboratory

(McMahon et al., 2018) to isolate several nanobodies with the apparent capability to bind the high affinity IL-10/IL-10 receptor complex. Much further work will need to be done to confirm if the nanobodies bind the complex when recombinantly expressed. Future experiments would include the optimisation of recombinant expression of the nanobody variants and SPR to accurately determine the binding affinities. The nanobodies could then be bound to the complex, in the hope that they could act as crystallisation chaperones. Future work in this project will also include using cryoEM as an alternative approach for structure determination.

The generation of a high affinity IL-10 variant also allowed us to investigate the role that receptor affinity plays in this cytokine's biological activities. This work demonstrates that wild type IL-10 loses key activities at low concentrations, in particular its ability to regulate pro-inflammatory cytokines and chemokines. It has been speculated that low local concentrations of IL-10 when give systemically in clinical trials for Crohn's disease contributed to the lack of efficacy (Saraiva et al., 2020), which supports these results. Our high affinity variant was able to retain better activity at low concentrations. This improved affinity at sub-saturating concentrations held true at multiple levels of IL-10 activity: STAT activation, transcription and cellular effects such as decreased pro-inflammatory cytokine production. This improved efficacy suggests that this variant could provide a therapeutic advantage over wild type IL-10. However, without *in vivo* data, this can only be considered speculative.

Ideally future work would investigate if our high affinity variant out-performed wild type IL-10 *in vivo*. Experiments such as measuring levels of LPS-induced pro-inflammatory cytokine production in the serum of mice in the presence of IL-10 would provide good evidence for any differential dose-dependent effects between the wild type and high affinity variant. However, as our high affinity variant is based on the human IL-10 amino acid sequence, use of a murine system is problematic. A preliminary test showed that the wild type and high affinity variant had very similar activities in murine macrophage cultures. While human IL-10 can act in murine cells, it only has 73% amino acid similarity with murine IL-10 (Windsor et al., 1993), which may explain why the high affinity variant failed to show an advantage over wild type in the IL-10 system. Without the use of murine

models, *in vivo* experimental options are very limited. While the data presented here highlights the favourable activity of the high affinity variant over wild type, these results can only be viewed in the context of controlled cell culture environments, without the myriad of cell types, cytokines and growth factors which play large roles in an *in vivo* setting. As highlighted by clinical trials using IL-10 in the past, efficacy *in vitro* regularly does not translate well to an *in vivo* system. However, our use of human cells does avoid the common pitfall of discrepancies arising between murine models and human systems (Masopust et al., 2017). Culturing of human organoids, particularly those which recapitulate the gut environment, may be an option for use in future studies which would provide us with information about how the high affinity variant acts in a multi-faceted environment (Wallach and Bayrer, 2017).

The use of the high affinity variant in both monomeric and dimeric confirmations provided us with unique tools to also examine the contribution of stoichiometry to IL-10's molecular activities. Data presented in this thesis showed that, while the high affinity monomer outperformed the wild type monomer, it could not reach the levels of transcriptional activity seen in the dimeric molecules. This was unexpected as at saturating concentrations, the high affinity monomer activated STATs to approximately 80% of the dimeric level. This result suggests that the potency of the IL-10 response is not linearly associated with STAT activation. There are several possible explanations to this, for example, the ability of IL-10 to activate alternate signalling pathways such as PI3K and AMPK which were not examined in this thesis (Antoniv and Ivashkiv, 2011, Sag et al., 2008). It may be that these pathways are more sensitive to changes in receptor stoichiometry than the JAK/STAT pathways. Differing numbers of phospho-tyrosine activated between the monomers and dimers may also play a role, similar to what was seen in the IL-6/gp130 system (Martinez-Fabregas et al., 2019). Future work would include signalling analysis of non-JAK/STAT pathways activated by the IL-10 variants as well as examining internal phosphorylation of tyrosines on the IL-10 receptor.

Despite having a poorer response than the dimeric variants, the high affinity monomer still far outperformed the wild type monomer in receptor assembly, signalling and transcription and could still induce some level of biological

activities. This opens future opportunities for further engineering of this variant where a monomeric confirmation may be preferable, for example, generating fusion proteins with other cytokines and antibodies.

Work presented in this thesis also shed light on some of IL-10's less well understood effects, namely its enhancement of CD8 T cell activity. While the ability of IL-10 to improve the tumour targeting ability of CD8 T cells has been well characterised (Oft, 2014, Naing et al., 2019) the mechanisms underpinning this remain elusive and differing protocols used to activate and culture CD8 T cells make direct comparisons in the literature difficult. Using a combination of transcriptomics and proteomics we characterised in-depth the CD8 response to the presence of IL-10 during activation. Although IL-10 has been implicated in T cell exhaustion previously (Sawant et al., 2019), we saw a decrease in several markers of T cell exhaustion at both the protein and mRNA level in IL-10 treated CD8 T cells. Interestingly, we also observed a decrease in expression of IL-2Rα at both the mRNA and protein level. The data presented in this thesis suggests that IL-10 may be limiting the transition to an exhausted state, perhaps by decreasing the responsiveness of the cells to IL-2. However, expression of exhaustion markers is only one facet of exhausted T cells. In order to confirm this effect, additional characterisations will need to be carried out such as measuring cytokine section, proliferation and response to re-stimulation. In addition, the link between IL-2Rα expression and exhaustion will need to be studied further to investigate whether it is a correlation or a causation effect.

Our proteomic data also suggested a possible role for IL-10 in the metabolic regulation of CD8 T cells. In macrophages IL-10 has previously been shown to alter the cell's metabolic state (Ip et al., 2017) and it is possible that a similar mechanism is at play in CD8 T cells. As these results were seen in our proteomic dataset, further experimental work will be needed to investigate this. The use of a Seahorse analyser to measure rates of oxidative phosphorylation and glycolysis will be a key experiment in this project going forward.

In summary this thesis has generated novel high affinity monomeric and dimeric variants of IL-10, acting as tools with which to probe the molecular basis of IL-10 activities. This has furthered our understanding of the role of affinity and

stoichiometry in this cytokine's biological effects. The use of high throughput methodologies such as transcriptomics and proteomics has also highlighted potential new angles on the effect of IL-10 on CD8 T cells, laying the foundation for further characterisation of these responses.

References

AL-ROBAEE, A. A., AL-ZOLIBANI, A. A., AL-SHOBILI, H. A., KAZAMEL, A. & SETTIN, A. 2008. IL-10 implications in psoriasis. *Int J Health Sci (Qassim),* 2**,** 53-8.

ALICEA-VELAZQUEZ, N. L. & BOGGON, T. J. 2011. The use of structural biology in Janus kinase targeted drug discovery. *Curr Drug Targets,* 12**,** 546-55.

ALVAREZ, H. M., SO, O. Y., HSIEH, S., SHINSKY-BJORDE, N., MA, H., SONG, Y., PANG, Y., MARIAN, M. & ESCANDON, E. 2012. Effects of PEGylation and immune complex formation on the pharmacokinetics and biodistribution of recombinant interleukin 10 in mice. *Drug Metab Dispos,* 40**,** 360-73.

ANTONIV, T. T. & IVASHKIV, L. B. 2011. Interleukin-10-induced gene expression and suppressive function are selectively modulated by the PI3K-Akt-GSK3 pathway. *Immunology,* 132**,** 567-77.

ATANASOVA, M. & WHITTY, A. 2012. Understanding cytokine and growth factor receptor activation mechanisms. *Crit Rev Biochem Mol Biol,* 47**,** 502-30.

BALIWAG, J., BARNES, D. H. & JOHNSTON, A. 2015. Cytokines in psoriasis. *Cytokine,* 73**,** 342-50.

BECKMAN, R. A., MILDVAN, A. S. & LOEB, L. A. 1985. On the fidelity of DNA replication: manganese mutagenesis in vitro. *Biochemistry,* 24**,** 5810-7.

BEGUE, B., VERDIER, J., RIEUX-LAUCAT, F., GOULET, O., MORALI, A., CANIONI, D., HUGOT, J. P., DAUSSY, C., VERKARRE, V., PIGNEUR, B., FISCHER, A., KLEIN, C., CERF-BENSUSSAN, N. & RUEMMELE, F. M. 2011. Defective IL10 signaling defining a subgroup of patients with inflammatory bowel disease. *Am J Gastroenterol,* 106**,** 1544-55.

BELTRA, J. C., BOURBONNAIS, S., BEDARD, N., CHARPENTIER, T., BOULANGE, M., MICHAUD, E., BOUFAIED, I., BRUNEAU, J., SHOUKRY, N. H., LAMARRE, A. & DECALUWE, H. 2016. IL2Rbeta-dependent signals drive terminal exhaustion and suppress memory development during chronic viral infection. *Proc Natl Acad Sci U S A,* 113**,** E5444-53.

BENGSCH, B., OHTANI, T., KHAN, O., SETTY, M., MANNE, S., O'BRIEN, S., GHERARDINI, P. F., HERATI, R. S., HUANG, A. C., CHANG, K. M., NEWELL, E. W., BOVENSCHEN, N., PE'ER, D., ALBELDA, S. M. & WHERRY, E. J. 2018. Epigenomic-Guided Mass Cytometry Profiling Reveals Disease-Specific Features of Exhausted CD8 T Cells. *Immunity,* 48**,** 1029-1045 e5.

BENZ, R. & MCLAUGHLIN, S. 1983. The molecular mechanism of action of the proton ionophore FCCP (carbonylcyanide p-trifluoromethoxyphenylhydrazone). *Biophys J,* 41**,** 381-98.

BLACKBURN, S. D. & WHERRY, E. J. 2007. IL-10, T cell exhaustion and viral persistence. *Trends Microbiol,* 15**,** 143-6.

BOYANO, M. D., GARCIA-VAZQUEZ, M. D., LOPEZ-MICHELENA, T., GARDEAZABAL, J., BILBAO, J., CANAVATE, M. L., GALDEANO, A. G., IZU, R., DIAZ-RAMON, L., RATON, J. A. & DIAZ-PEREZ, J. L. 2000. Soluble interleukin-2 receptor, intercellular adhesion molecule-1 and interleukin-10 serum levels in patients with melanoma. *Br J Cancer,* 83**,** 847-52.

BRAAT, H., ROTTIERS, P., HOMMES, D. W., HUYGHEBAERT, N., REMAUT, E., REMON, J. P., VAN DEVENTER, S. J., NEIRYNCK, S., PEPPELENBOSCH, M. P. & STEIDLER, L. 2006. A phase I trial with transgenic bacteria expressing interleukin-10 in Crohn's disease. *Clin Gastroenterol Hepatol,* 4**,** 754-9.

BROOKS, A. J., DAI, W., O'MARA, M. L., ABANKWA, D., CHHABRA, Y., PELEKANOS, R. A., GARDON, O., TUNNY, K. A., BLUCHER, K. M., MORTON, C. J., PARKER, M. W., SIERECKI, E., GAMBIN, Y., GOMEZ, G. A., ALEXANDROV, K., WILSON, I. A., DOXASTAKIS, M., MARK, A. E. & WATERS, M. J. 2014. Mechanism of activation of protein kinase JAK2 by the growth hormone receptor. *Science,* 344**,** 1249783.

BROOKS, D. G., TRIFILO, M. J., EDELMANN, K. H., TEYTON, L., MCGAVERN, D. B. & OLDSTONE, M. B. 2006. Interleukin-10 determines viral clearance or persistence in vivo. *Nat Med,* 12**,** 1301-9.

BROWN, R. J., ADAMS, J. J., PELEKANOS, R. A., WAN, Y., MCKINSTRY, W. J., PALETHORPE, K., SEEBER, R. M., MONKS, T. A., EIDNE, K. A., PARKER, M. W. & WATERS, M. J. 2005. Model for growth hormone receptor activation based on subunit rotation within a receptor dimer. *Nat Struct Mol Biol,* 12**,** 814-21.

CADWELL, R. C. & JOYCE, G. F. 1992. Randomization of genes by PCR mutagenesis. *PCR Methods Appl,* 2**,** 28-33.

CAPSONI, F., MINONZIO, F., ONGARI, A. M., CARBONELLI, V., GALLI, A. & ZANUSSI, C. 1995. IL-10 up-regulates human monocyte phagocytosis in the presence of IL-4 and IFN-gamma. *J Leukoc Biol,* 58**,** 351-8.

CASSATELLA, M. A., GASPERINI, S., BOVOLENTA, C., CALZETTI, F., VOLLEBREGT, M., SCAPINI, P., MARCHI, M., SUZUKI, R., SUZUKI, A. & YOSHIMURA, A. 1999. Interleukin-10 (IL-10) selectively enhances CIS3/SOCS3 mRNA expression in human neutrophils: evidence for an IL-10-induced pathway that is independent of STAT protein activation. *Blood,* 94**,** 2880-9.

CASSATELLA, M. A., MEDA, L., GASPERINI, S., CALZETTI, F. & BONORA, S. 1994. Interleukin 10 (IL-10) upregulates IL-1 receptor antagonist production from lipopolysaccharide-stimulated human polymorphonuclear leukocytes by delaying mRNA degradation. *J Exp Med,* 179**,** 1695-9.

CAUDELL, E. G., MUMM, J. B., POINDEXTER, N., EKMEKCIOGLU, S., MHASHILKAR, A. M., YANG, X. H., RETTER, M. W., HILL, P., CHADA, S. & GRIMM, E. A. 2002. The protein product of the tumor suppressor gene, melanoma differentiation-associated gene 7, exhibits immunostimulatory activity and is designated IL-24. *J Immunol,* 168**,** 6041-6.

CHAN, I. H., WU, V., BILARDELLO, M., MAR, E., OFT, M., VAN VLASSELAER, P. & MUMM, J. B. 2015. The Potentiation of IFN-γ and Induction of Cytotoxic Proteins by Pegylated IL-10 in Human CD8 T Cells. *J Interferon Cytokine Res,* 35**,** 948-55.

CHAO, G., LAU, W. L., HACKEL, B. J., SAZINSKY, S. L., LIPPOW, S. M. & WITTRUP, K. D. 2006. Isolating and engineering human antibodies using yeast surface display. *Nat Protoc,* 1**,** 755-68.

CHEN, J., CASPI, R. R. & CHONG, W. P. 2018. IL-20 receptor cytokines in autoimmune diseases. *J Leukoc Biol,* 104**,** 953-959.

CHEN, W. F. & ZLOTNIK, A. 1991. IL-10: a novel cytotoxic T cell differentiation factor. *J Immunol,* 147**,** 528-34.

CHERNOFF, A. E., GRANOWITZ, E. V., SHAPIRO, L., VANNIER, E., LONNEMANN, G., ANGEL, J. B., KENNEDY, J. S., RABSON, A. R., WOLFF, S. M. & DINARELLO, C. A. 1995. A randomized, controlled trial of IL-10 in humans. Inhibition of inflammatory cytokine production and immune responses. *J Immunol,* 154**,** 5492-9.

COLOMBEL, J. F., RUTGEERTS, P., MALCHOW, H., JACYNA, M., NIELSEN, O. H., RASK-MADSEN, J., VAN DEVENTER, S., FERGUSON, A., DESREUMAUX, P., FORBES, A.,

GEBOES, K., MELANI, L. & COHARD, M. 2001. Interleukin 10 (Tenovil) in the prevention of postoperative recurrence of Crohn's disease. *Gut,* 49**,** 42-6.

CORREA, I., VENY, M., ESTELLER, M., PIQUE, J. M., YAGUE, J., PANES, J. & SALAS, A. 2009. Defective IL-10 production in severe phenotypes of Crohn's disease. *J Leukoc Biol,* 85**,** 896-903.

CRAWLEY, J. B., WILLIAMS, L. M., MANDER, T., BRENNAN, F. M. & FOXWELL, B. M. 1996. Interleukin-10 stimulation of phosphatidylinositol 3-kinase and p70 S6 kinase is required for the proliferative but not the antiinflammatory effects of the cytokine. *J Biol Chem,* 271**,** 16357-62.

D'ANDREA, A., ASTE-AMEZAGA, M., VALIANTE, N. M., MA, X., KUBIN, M. & TRINCHIERI, G. 1993. Interleukin 10 (IL-10) inhibits human lymphocyte interferon gamma-production by suppressing natural killer cell stimulatory factor/IL-12 synthesis in accessory cells. *J Exp Med,* 178**,** 1041-8.

DE WAAL MALEFYT, R., HAANEN, J., SPITS, H., RONCAROLO, M. G., TE VELDE, A., FIGDOR, C., JOHNSON, K., KASTELEIN, R., YSSEL, H. & DE VRIES, J. E. 1991. Interleukin 10 (IL-10) and viral IL-10 strongly reduce antigen-specific human T cell proliferation by diminishing the antigen-presenting capacity of monocytes via downregulation of class II major histocompatibility complex expression. *J Exp Med,* 174**,** 915-24.

DEL PRETE, G., DE CARLI, M., ALMERIGOGNA, F., GIUDIZI, M. G., BIAGIOTTI, R. & ROMAGNANI, S. 1993. Human IL-10 is produced by both type 1 helper (Th1) and type 2 helper (Th2) T cell clones and inhibits their antigen-specific proliferation and cytokine production. *J Immunol,* 150**,** 353-60.

DING, Y., QIN, L., KOTENKO, S. V., PESTKA, S. & BROMBERG, J. S. 2000. A single amino acid determines the immunostimulatory activity of interleukin 10. *J Exp Med,* 191**,** 213-24.

DING, Y., QIN, L., ZAMARIN, D., KOTENKO, S. V., PESTKA, S., MOORE, K. W. & BROMBERG, J. S. 2001. Differential IL-10R1 expression plays a critical role in IL-10-mediated immune regulation. *J Immunol,* 167**,** 6884-92.

DOHERTY, E. & PERL, A. 2017. Measurement of Mitochondrial Mass by Flow Cytometry during Oxidative Stress. *React Oxyg Species (Apex),* 4**,** 275-283.

DU, H., YI, Z., WANG, L., LI, Z., NIU, B. & REN, G. 2020. The co-expression characteristics of LAG3 and PD-1 on the T cells of patients with breast cancer reveal a new therapeutic strategy. *Int Immunopharmacol,* 78**,** 106113.

ELBEIN, A. D., TROPEA, J. E., MITCHELL, M. & KAUSHAL, G. P. 1990. Kifunensine, a potent inhibitor of the glycoprotein processing mannosidase I. *J Biol Chem,* 265**,** 15599-605.

ELCOMBE, S. E., NAQVI, S., VAN DEN BOSCH, M. W., MACKENZIE, K. F., CIANFANELLI, F., BROWN, G. D. & ARTHUR, J. S. 2013. Dectin-1 regulates IL-10 production via a MSK1/2 and CREB dependent pathway and promotes the induction of regulatory macrophage markers. *PLoS One,* 8**,** e60086.

ELIASON, J. F. 2001. Pegylated cytokines: potential application in immunotherapy of cancer. *BioDrugs,* 15**,** 705-11.

EMMERICH, J., MUMM, J. B., CHAN, I. H., LAFACE, D., TRUONG, H., MCCLANAHAN, T., GORMAN, D. M. & OFT, M. 2012. IL-10 Directly Activates and Expands Tumor-Resident CD8(+) T Cells without De Novo Infiltration from Secondary Lymphoid Organs. *Cancer Research,* 72**,** 3570-3581.

FEDORAK, R. N., GANGL, A., ELSON, C. O., RUTGEERTS, P., SCHREIBER, S., WILD, G., HANAUER, S. B., KILIAN, A., COHARD, M., LEBEAUT, A. & FEAGAN, B. 2000. Recombinant human interleukin 10 in the treatment of patients with mild to

moderately active Crohn's disease. The Interleukin 10 Inflammatory Bowel Disease Cooperative Study Group. *Gastroenterology,* 119**,** 1473-82.

FINBLOOM, D. S. & WINESTOCK, K. D. 1995. IL-10 induces the tyrosine phosphorylation of tyk2 and Jak1 and the differential assembly of STAT1 alpha and STAT3 complexes in human T cells and monocytes. *J Immunol,* 155**,** 1079-90.

FIORENTINO, D. F., BOND, M. W. & MOSMANN, T. R. 1989. Two types of mouse T helper cell. IV. Th2 clones secrete a factor that inhibits cytokine production by Th1 clones. *J Exp Med,* 170**,** 2081-95.

FIORENTINO, D. F., ZLOTNIK, A., MOSMANN, T. R., HOWARD, M. & O'GARRA, A. 1991. IL-10 inhibits cytokine production by activated macrophages. *J Immunol,* 147**,** 3815-22.

FOSTER, P. S., MARTINEZ-MOCZYGEMBA, M., HUSTON, D. P. & CORRY, D. B. 2002. Interleukins-4, -5, and -13: emerging therapeutic targets in allergic disease. *Pharmacol Ther,* 94**,** 253-64.

FRANKE, A., BALSCHUN, T., KARLSEN, T. H., SVENTORAITYTE, J., NIKOLAUS, S., MAYR, G., DOMINGUES, F. S., ALBRECHT, M., NOTHNAGEL, M., ELLINGHAUS, D., SINA, C., ONNIE, C. M., WEERSMA, R. K., STOKKERS, P. C., WIJMENGA, C., GAZOULI, M., STRACHAN, D., MCARDLE, W. L., VERMEIRE, S., RUTGEERTS, P., ROSENSTIEL, P., KRAWCZAK, M., VATN, M. H., GROUP, I. S., MATHEW, C. G. & SCHREIBER, S. 2008. Sequence variants in IL10, ARPC2 and multiple other loci contribute to ulcerative colitis susceptibility. *Nat Genet,* 40**,** 1319-23.

FREEZE, H. H. & KRANZ, C. 2010a. Endoglycosidase and glycoamidase release of N-linked glycans. *Curr Protoc Mol Biol,* Chapter 17**,** Unit 17 13A.

FREEZE, H. H. & KRANZ, C. 2010b. Endoglycosidase and glycoamidase release of N-linked glycans. *Curr Protoc Protein Sci,* Chapter 12**,** Unit12 4.

GAI, S. A. & WITTRUP, K. D. 2007. Yeast surface display for protein engineering and characterization. *Curr Opin Struct Biol,* 17**,** 467-73.

GARCIA-GARCIA, E. & ROSALES, C. 2002. Signal transduction during Fc receptor-mediated phagocytosis. *J Leukoc Biol,* 72**,** 1092-108.

GENT, J., VAN KERKHOF, P., ROZA, M., BU, G. & STROUS, G. J. 2002. Ligand-independent growth hormone receptor dimerization occurs in the endoplasmic reticulum and is required for ubiquitin system-dependent endocytosis. *Proc Natl Acad Sci U S A,* 99**,** 9858-63.

GIBBS, V. C. & PENNICA, D. 1997. CRF2-4: isolation of cDNA clones encoding the human and mouse proteins. *Gene,* 186**,** 97-101.

GLOCKER, E. O., KOTLARZ, D., BOZTUG, K., GERTZ, E. M., SCHAFFER, A. A., NOYAN, F., PERRO, M., DIESTELHORST, J., ALLROTH, A., MURUGAN, D., HATSCHER, N., PFEIFER, D., SYKORA, K. W., SAUER, M., KREIPE, H., LACHER, M., NUSTEDE, R., WOELLNER, C., BAUMANN, U., SALZER, U., KOLETZKO, S., SHAH, N., SEGAL, A. W., SAUERBREY, A., BUDERUS, S., SNAPPER, S. B., GRIMBACHER, B. & KLEIN, C. 2009. Inflammatory bowel disease and mutations affecting the interleukin-10 receptor. *N Engl J Med,* 361**,** 2033-45.

GO, N. F., CASTLE, B. E., BARRETT, R., KASTELEIN, R., DANG, W., MOSMANN, T. R., MOORE, K. W. & HOWARD, M. 1990. Interleukin 10, a novel B cell stimulatory factor: unresponsiveness of X chromosome-linked immunodeficiency B cells. *J Exp Med,* 172**,** 1625-31.

GOETZE, K., WALENTA, S., KSIAZKIEWICZ, M., KUNZ-SCHUGHART, L. A. & MUELLER-KLIESER, W. 2011. Lactate enhances motility of tumor cells and inhibits monocyte migration and cytokine release. *Int J Oncol,* 39**,** 453-63.

GROUX, H., BIGLER, M., DE VRIES, J. E. & RONCAROLO, M. G. 1998. Inhibitory and stimulatory effects of IL-10 on human CD8+ T cells. *J Immunol,* 160**,** 3188-93.

HAGENBAUGH, A., SHARMA, S., DUBINETT, S. M., WEI, S. H., ARANDA, R., CHEROUTRE, H., FOWELL, D. J., BINDER, S., TSAO, B., LOCKSLEY, R. M., MOORE, K. W. & KRONENBERG, M. 1997. Altered immune responses in interleukin 10 transgenic mice. *J Exp Med,* 185**,** 2101-10.

HEINE, G., DROZDENKO, G., GRUN, J. R., CHANG, H. D., RADBRUCH, A. & WORM, M. 2014. Autocrine IL-10 promotes human B-cell differentiation into IgM- or IgG-secreting plasmablasts. *Eur J Immunol,* 44**,** 1615-21.

HERRERO, C., HU, X., LI, W. P., SAMUELS, S., SHARIF, M. N., KOTENKO, S. & IVASHKIV, L. B. 2003. Reprogramming of IL-10 activity and signaling by IFN-gamma. *J Immunol,* 171**,** 5034-41.

HOOVER, D. M., SCHALK-HIHI, C., CHOU, C. C., MENON, S., WLODAWER, A. & ZDANOV, A. 1999. Purification of receptor complexes of interleukin-10 stoichiometry and the importance of deglycosylation in their crystallization. *Eur J Biochem,* 262**,** 134-41.

HOWDEN, A. J. M., HUKELMANN, J. L., BRENES, A., SPINELLI, L., SINCLAIR, L. V., LAMOND, A. I. & CANTRELL, D. A. 2019. Quantitative analysis of T cell proteomes and environmental sensors during T cell differentiation. *Nat Immunol,* 20**,** 1542-1554.

HUANG DA, W., SHERMAN, B. T. & LEMPICKI, R. A. 2009. Systematic and integrative analysis of large gene lists using DAVID bioinformatics resources. *Nat Protoc,* 4**,** 44-57.

HUBER, S., GAGLIANI, N., ESPLUGUES, E., O'CONNOR, W., JR., HUBER, F. J., CHAUDHRY, A., KAMANAKA, M., KOBAYASHI, Y., BOOTH, C. J., RUDENSKY, A. Y., RONCAROLO, M. G., BATTAGLIA, M. & FLAVELL, R. A. 2011. Th17 cells express interleukin-10 receptor and are controlled by Foxp3(-) and Foxp3+ regulatory CD4+ T cells in an interleukin-10-dependent manner. *Immunity,* 34**,** 554-65.

HUHN, R. D., RADWANSKI, E., GALLO, J., AFFRIME, M. B., SABO, R., GONYO, G., MONGE, A. & CUTLER, D. L. 1997. Pharmacodynamics of subcutaneous recombinant human interleukin-10 in healthy volunteers. *Clin Pharmacol Ther,* 62**,** 171-80.

IP, W. K. E., HOSHI, N., SHOUVAL, D. S., SNAPPER, S. & MEDZHITOV, R. 2017. Anti-inflammatory effect of IL-10 mediated by metabolic reprogramming of macrophages. *Science,* 356**,** 513-519.

IWASAKI, A. & MEDZHITOV, R. 2004. Toll-like receptor control of the adaptive immune responses. *Nat Immunol,* 5**,** 987-95.

JAITIN, D. A., ROISMAN, L. C., JAKS, E., GAVUTIS, M., PIEHLER, J., VAN DER HEYDEN, J., UZE, G. & SCHREIBER, G. 2006. Inquiring into the differential action of interferons (IFNs): an IFN-alpha2 mutant with enhanced affinity to IFNAR1 is functionally similar to IFN-beta. *Mol Cell Biol,* 26**,** 1888-97.

JATIANI, S. S., BAKER, S. J., SILVERMAN, L. R. & REDDY, E. P. 2010. Jak/STAT pathways in cytokine signaling and myeloproliferative disorders: approaches for targeted therapies. *Genes Cancer,* 1**,** 979-93.

JOSEPHSON, K., DIGIACOMO, R., INDELICATO, S. R., IYO, A. H., NAGABHUSHAN, T. L., PARKER, M. H. & WALTER, M. R. 2000a. Design and analysis of an engineered human interleukin-10 monomer. *J Biol Chem,* 275**,** 13552-7.

JOSEPHSON, K., DIGIACOMO, R., INDELICATO, S. R., IYO, A. H., NAGABHUSHAN, T. L., PARKER, M. H., WALTER, M. R. & AYO, A. H. 2000b. Design and analysis of an engineered human interleukin-10 monomer. *J Biol Chem,* 275**,** 13552-7.

JOSEPHSON, K., JONES, B. C., WALTER, L. J., DIGIACOMO, R., INDELICATO, S. R. & WALTER, M. R. 2002. Noncompetitive antibody neutralization of IL-10 revealed by protein engineering and x-ray crystallography. *Structure,* 10**,** 981-7.

JOSEPHSON, K., LOGSDON, N. J. & WALTER, M. R. 2001. Crystal structure of the IL-10/IL-10R1 complex reveals a shared receptor binding site. *Immunity,* 15**,** 35-46.

JOYCE, D. A., GIBBONS, D. P., GREEN, P., STEER, J. H., FELDMANN, M. & BRENNAN, F. M. 1994. Two inhibitors of pro-inflammatory cytokine release, interleukin-10 and interleukin-4, have contrasting effects on release of soluble p75 tumor necrosis factor receptor by cultured monocytes. *Eur J Immunol,* 24**,** 2699-705.

JUNG, M., SABAT, R., KRATZSCHMAR, J., SEIDEL, H., WOLK, K., SCHONBEIN, C., SCHUTT, S., FRIEDRICH, M., DOCKE, W. D., ASADULLAH, K., VOLK, H. D. & GRUTZ, G. 2004. Expression profiling of IL-10-regulated genes in human monocytes and peripheral blood mononuclear cells from psoriatic patients during IL-10 therapy. *Eur J Immunol,* 34**,** 481-93.

JUNTTILA, I. S., CREUSOT, R. J., MORAGA, I., BATES, D. L., WONG, M. T., ALONSO, M. N., SUHOSKI, M. M., LUPARDUS, P., MEIER-SCHELLERSHEIM, M., ENGLEMAN, E. G., UTZ, P. J., FATHMAN, C. G., PAUL, W. E. & GARCIA, K. C. 2012. Redirecting cell-type specific cytokine responses with engineered interleukin-4 superkines. *Nat Chem Biol,* 8**,** 990-8.

JUNTTILA, I. S., MIZUKAMI, K., DICKENSHEETS, H., MEIER-SCHELLERSHEIM, M., YAMANE, H., DONNELLY, R. P. & PAUL, W. E. 2008. Tuning sensitivity to IL-4 and IL-13: differential expression of IL-4Ralpha, IL-13Ralpha1, and gammac regulates relative cytokine sensitivity. *J Exp Med,* 205**,** 2595-608.

KALIA, V., SARKAR, S., SUBRAMANIAM, S., HAINING, W. N., SMITH, K. A. & AHMED, R. 2010. Prolonged interleukin-2Ralpha expression on virus-specific CD8+ T cells favors terminal-effector differentiation in vivo. *Immunity,* 32**,** 91-103.

KALIE, E., JAITIN, D. A., ABRAMOVICH, R. & SCHREIBER, G. 2007. An interferon alpha2 mutant optimized by phage display for IFNAR1 binding confers specifically enhanced antitumor activities. *J Biol Chem,* 282**,** 11602-11.

KALIE, E., JAITIN, D. A., PODOPLELOVA, Y., PIEHLER, J. & SCHREIBER, G. 2008. The stability of the ternary interferon-receptor complex rather than the affinity to the individual subunits dictates differential biological activities. *J Biol Chem,* 283**,** 32925-36.

KARAGHIOSOFF, M., NEUBAUER, H., LASSNIG, C., KOVARIK, P., SCHINDLER, H., PIRCHER, H., MCCOY, B., BOGDAN, C., DECKER, T., BREM, G., PFEFFER, K. & MULLER, M. 2000. Partial impairment of cytokine responses in Tyk2-deficient mice. *Immunity,* 13**,** 549-60.

KASAMA, T., STRIETER, R. M., LUKACS, N. W., BURDICK, M. D. & KUNKEL, S. L. 1994. Regulation of neutrophil-derived chemokine expression by IL-10. *J Immunol,* 152**,** 3559-69.

KESKINEN, P., RONNI, T., MATIKAINEN, S., LEHTONEN, A. & JULKUNEN, I. 1997. Regulation of HLA class I and II expression by interferons and influenza A virus in human peripheral blood mononuclear cells. *Immunology,* 91**,** 421-9.

KIRCHHOFER, A., HELMA, J., SCHMIDTHALS, K., FRAUER, C., CUI, S., KARCHER, A., PELLIS, M., MUYLDERMANS, S., CASAS-DELUCCHI, C. S., CARDOSO, M. C., LEONHARDT, H., HOPFNER, K. P. & ROTHBAUER, U. 2010. Modulation of protein properties in living cells using nanobodies. *Nature Structural & Molecular Biology,* 17**,** 133-U162.

KIRKEN, R. A., RUI, H., MALABARBA, M. G., HOWARD, O. M., KAWAMURA, M., O'SHEA, J. J. & FARRAR, W. L. 1995. Activation of JAK3, but not JAK1, is critical for IL-2-induced proliferation and STAT5 recruitment by a COOH-terminal region of the IL-2 receptor beta-chain. *Cytokine,* 7**,** 689-700.

KOPPELMAN, B., NEEFJES, J. J., DE VRIES, J. E. & DE WAAL MALEFYT, R. 1997. Interleukin-10 down-regulates MHC class II alphabeta peptide complexes at the plasma membrane of monocytes by affecting arrival and recycling. *Immunity,* 7**,** 861-71.

KOTLARZ, D., BEIER, R., MURUGAN, D., DIESTELHORST, J., JENSEN, O., BOZTUG, K., PFEIFER, D., KREIPE, H., PFISTER, E. D., BAUMANN, U., PUCHALKA, J., BOHNE, J., EGRITAS, O., DALGIC, B., KOLHO, K. L., SAUERBREY, A., BUDERUS, S., GUNGOR, T., ENNINGER, A., KODA, Y. K., GUARISO, G., WEISS, B., CORBACIOGLU, S., SOCHA, P., USLU, N., METIN, A., WAHBEH, G. T., HUSAIN, K., RAMADAN, D., AL-HERZ, W., GRIMBACHER, B., SAUER, M., SYKORA, K. W., KOLETZKO, S. & KLEIN, C. 2012. Loss of interleukin-10 signaling and infantile inflammatory bowel disease: implications for diagnosis and therapy. *Gastroenterology,* 143**,** 347-55.

KOVANEN, P. E. & LEONARD, W. J. 2004. Cytokines and immunodeficiency diseases: critical roles of the gamma(c)-dependent cytokines interleukins 2, 4, 7, 9, 15, and 21, and their signaling pathways. *Immunol Rev,* 202**,** 67-83.

KRAUSE, C. D., MEI, E., MIROCHNITCHENKO, O., LAVNIKOVA, N., XIE, J., JIA, Y., HOCHSTRASSER, R. M. & PESTKA, S. 2006. Interactions among the components of the interleukin-10 receptor complex. *Biochem Biophys Res Commun,* 340**,** 377-85.

KRUTZIK, P. O., CLUTTER, M. R., TREJO, A. & NOLAN, G. P. 2011. Fluorescent cell barcoding for multiplex flow cytometry. *Curr Protoc Cytom,* Chapter 6**,** Unit 6 31.

KUHN, R., LOHLER, J., RENNICK, D., RAJEWSKY, K. & MULLER, W. 1993. Interleukin-10-deficient mice develop chronic enterocolitis. *Cell,* 75**,** 263-74.

LAUW, F. N., PAJKRT, D., HACK, C. E., KURIMOTO, M., VAN DEVENTER, S. J. & VAN DER POLL, T. 2000. Proinflammatory effects of IL-10 during human endotoxemia. *J Immunol,* 165**,** 2783-9.

LEVIN, A. M., BATES, D. L., RING, A. M., KRIEG, C., LIN, J. T., SU, L., MORAGA, I., RAEBER, M. E., BOWMAN, G. R., NOVICK, P., PANDE, V. S., FATHMAN, C. G., BOYMAN, O. & GARCIA, K. C. 2012. Exploiting a natural conformational switch to engineer an interleukin-2 'superkine'. *Nature,* 484**,** 529-33.

LIU, Y., DE WAAL MALEFYT, R., BRIERE, F., PARHAM, C., BRIDON, J. M., BANCHEREAU, J., MOORE, K. W. & XU, J. 1997. The EBV IL-10 homologue is a selective agonist with impaired binding to the IL-10 receptor. *J Immunol,* 158**,** 604-13.

LIU, Y., WEI, S. H., HO, A. S., DE WAAL MALEFYT, R. & MOORE, K. W. 1994. Expression cloning and characterization of a human IL-10 receptor. *J Immunol,* 152**,** 1821-9.

LIVNAH, O., STURA, E. A., MIDDLETON, S. A., JOHNSON, D. L., JOLLIFFE, L. K. & WILSON, I. A. 1999. Crystallographic evidence for preformed dimers of erythropoietin receptor before ligand activation. *Science,* 283**,** 987-90.

LOGSDON, N. J., JONES, B. C., JOSEPHSON, K., COOK, J. & WALTER, M. R. 2002. Comparison of interleukin-22 and interleukin-10 soluble receptor complexes. *J Interferon Cytokine Res,* 22**,** 1099-112.

LUPARDUS, P. J., ULTSCH, M., WALLWEBER, H., BIR KOHLI, P., JOHNSON, A. R. & EIGENBROT, C. 2014. Structure of the pseudokinase-kinase domains from protein kinase TYK2 reveals a mechanism for Janus kinase (JAK) autoinhibition. *Proc Natl Acad Sci U S A,* 111**,** 8025-30.

MANGLIK, A., KOBILKA, B. K. & STEYAERT, J. 2017. Nanobodies to Study G Protein-Coupled Receptor Structure and Function. *Annu Rev Pharmacol Toxicol,* 57**,** 19-37.

MARTINEZ-FABREGAS, J., WILMES, S., WANG, L., HAFER, M., POHLER, E., LOKAU, J., GARBERS, C., COZZANI, A., FYFE, P. K., PIEHLER, J., KAZEMIAN, M., MITRA, S. & MORAGA, I. 2019. Kinetics of cytokine receptor trafficking determine signaling and functional selectivity. *Elife,* 8.

MASOPUST, D., SIVULA, C. P. & JAMESON, S. C. 2017. Of Mice, Dirty Mice, and Men: Using Mice To Understand Human Immunology. *J Immunol,* 199**,** 383-388.

MATHUPALA, S. P., KO, Y. H. & PEDERSEN, P. L. 2006. Hexokinase II: cancer's double-edged sword acting as both facilitator and gatekeeper of malignancy when bound to mitochondria. *Oncogene,* 25**,** 4777-86.

MATTHEWS, E. E., THEVENIN, D., ROGERS, J. M., GOTOW, L., LIRA, P. D., REITER, L. A., BRISSETTE, W. H. & ENGELMAN, D. M. 2011. Thrombopoietin receptor activation: transmembrane helix dimerization, rotation, and allosteric modulation. *FASEB J,* 25**,** 2234-44.

MATTHEYSES, A. L., SIMON, S. M. & RAPPOPORT, J. Z. 2010. Imaging with total internal reflection fluorescence microscopy for the cell biologist. *J Cell Sci,* 123**,** 3621-8.

MAURAS, A., CHAIN, F., FAUCHEUX, A., RUFFIE, P., GONTIER, S., RYFFEL, B., BUTEL, M. J., LANGELLA, P., BERMUDEZ-HUMARAN, L. G. & WALIGORA-DUPRIET, A. J. 2018. A New Bifidobacteria Expression SysTem (BEST) to Produce and Deliver Interleukin-10 in Bifidobacterium bifidum. *Front Microbiol,* 9**,** 3075.

MCINNES, I. B., ILLEI, G. G., DANNING, C. L., YARBORO, C. H., CRANE, M., KUROIWA, T., SCHLIMGEN, R., LEE, E., FOSTER, B., FLEMMING, D., PRUSSIN, C., FLEISHER, T. A. & BOUMPAS, D. T. 2001. IL-10 improves skin disease and modulates endothelial activation and leukocyte effector function in patients with psoriatic arthritis. *J Immunol,* 167**,** 4075-82.

MCINNES, I. B. & SCHETT, G. 2007. Cytokines in the pathogenesis of rheumatoid arthritis. *Nat Rev Immunol,* 7**,** 429-42.

MCMAHON, C., BAIER, A. S., PASCOLUTTI, R., WEGRECKI, M., ZHENG, S., ONG, J. X., ERLANDSON, S. C., HILGER, D., RASMUSSEN, S. G. F., RING, A. M., MANGLIK, A. & KRUSE, A. C. 2018. Yeast surface display platform for rapid discovery of conformationally selective nanobodies. *Nat Struct Mol Biol,* 25**,** 289-296.

MENDOZA, J. L., SCHNEIDER, W. M., HOFFMANN, H. H., VERCAUTEREN, K., JUDE, K. M., XIONG, A., MORAGA, I., HORTON, T. M., GLENN, J. S., DE JONG, Y. P., RICE, C. M. & GARCIA, K. C. 2017. The IFN-λ-IFN-λR1-IL-10Rβ Complex Reveals Structural Features Underlying Type III IFN Functional Plasticity. *Immunity,* 46**,** 379-392.

METZEMAEKERS, M., VANHEULE, V., JANSSENS, R., STRUYF, S. & PROOST, P. 2017. Overview of the Mechanisms that May Contribute to the Non-Redundant Activities of Interferon-Inducible CXC Chemokine Receptor 3 Ligands. *Front Immunol,* 8**,** 1970.

MIDDLETON, S. A., BARBONE, F. P., JOHNSON, D. L., THURMOND, R. L., YOU, Y., MCMAHON, F. J., JIN, R., LIVNAH, O., TULLAI, J., FARRELL, F. X., GOLDSMITH, M. A., WILSON, I. A. & JOLLIFFE, L. K. 1999. Shared and unique determinants of the erythropoietin (EPO) receptor are important for binding EPO and EPO mimetic peptide. *J Biol Chem,* 274**,** 14163-9.

MINSHAWI, F., LANVERMANN, S., MCKENZIE, E., JEFFERY, R., COUPER, K., PAPOUTSOPOULOU, S., ROERS, A. & MULLER, W. 2020. The Generation of an

Engineered Interleukin-10 Protein With Improved Stability and Biological Function. *Front Immunol,* 11**,** 1794.

MITTAL, S. K. & ROCHE, P. A. 2015. Suppression of antigen presentation by IL-10. *Curr Opin Immunol,* 34**,** 22-7.

MOHAN, K., UEDA, G., KIM, A. R., JUDE, K. M., FALLAS, J. A., GUO, Y., HAFER, M., MIAO, Y., SAXTON, R. A., PIEHLER, J., SANKARAN, V. G., BAKER, D. & GARCIA, K. C. 2019. Topological control of cytokine receptor signaling induces differential effects in hematopoiesis. *Science,* 364.

MOORE, K. W., DE WAAL MALEFYT, R., COFFMAN, R. L. & O'GARRA, A. 2001. Interleukin-10 and the interleukin-10 receptor. *Annu Rev Immunol,* 19**,** 683-765.

MOORE, K. W., VIEIRA, P., FIORENTINO, D. F., TROUNSTINE, M. L., KHAN, T. A. & MOSMANN, T. R. 1990. Homology of cytokine synthesis inhibitory factor (IL-10) to the Epstein-Barr virus gene BCRFI. *Science,* 248**,** 1230-4.

MORAGA, I., RICHTER, D., WILMES, S., WINKELMANN, H., JUDE, K., THOMAS, C., SUHOSKI, M. M., ENGLEMAN, E. G., PIEHLER, J. & GARCIA, K. C. 2015a. Instructive roles for cytokine-receptor binding parameters in determining signaling and functional potency. *Sci Signal,* 8**,** ra114.

MORAGA, I., SPANGLER, J., MENDOZA, J. L. & GARCIA, K. C. 2014. Multifarious determinants of cytokine receptor signaling specificity. *Adv Immunol,* 121**,** 1-39.

MORAGA, I., SPANGLER, J. B., MENDOZA, J. L., GAKOVIC, M., WEHRMAN, T. S., KRUTZIK, P. & GARCIA, K. C. 2017. Synthekines are surrogate cytokine and growth factor agonists that compel signaling through non-natural receptor dimers. *Elife,* 6.

MORAGA, I., WERNIG, G., WILMES, S., GRYSHKOVA, V., RICHTER, C. P., HONG, W. J., SINHA, R., GUO, F., FABIONAR, H., WEHRMAN, T. S., KRUTZIK, P., DEMHARTER, S., PLO, I., WEISSMAN, I. L., MINARY, P., MAJETI, R., CONSTANTINESCU, S. N., PIEHLER, J. & GARCIA, K. C. 2015b. Tuning Cytokine Receptor Signaling by Re-orienting Dimer Geometry with Surrogate Ligands. *Cell,* 160**,** 1196-208.

MORISSETTE, M. C., PARENT, J. & MILOT, J. 2007. Perforin, granzyme B, and FasL expression by peripheral blood T lymphocytes in emphysema. *Respir Res,* 8**,** 62.

MUMM, J. B., EMMERICH, J., ZHANG, X., CHAN, I., WU, L., MAUZE, S., BLAISDELL, S., BASHAM, B., DAI, J., GREIN, J., SHEPPARD, C., HONG, K., CUTLER, C., TURNER, S., LAFACE, D., KLEINSCHEK, M., JUDO, M., AYANOGLU, G., LANGOWSKI, J., GU, D., PAPORELLO, B., MURPHY, E., SRIRAM, V., NARAVULA, S., DESAI, B., MEDICHERLA, S., SEGHEZZI, W., MCCLANAHAN, T., CANNON-CARLSON, S., BEEBE, A. M. & OFT, M. 2011. IL-10 elicits IFNgamma-dependent tumor immune surveillance. *Cancer Cell,* 20**,** 781-96.

MUMM, J. B. & OFT, M. 2013. Pegylated IL-10 induces cancer immunity: the surprising role of IL-10 as a potent inducer of IFN-γ-mediated CD8(+) T cell cytotoxicity. *Bioessays,* 35**,** 623-31.

MUYLDERMANS, S. 2013. Nanobodies: natural single-domain antibodies. *Annu Rev Biochem,* 82**,** 775-97.

NAGALAKSHMI, M. L., MURPHY, E., MCCLANAHAN, T. & DE WAAL MALEFYT, R. 2004. Expression patterns of IL-10 ligand and receptor gene families provide leads for biological characterization. *Int Immunopharmacol,* 4**,** 577-92.

NAING, A., INFANTE, J. R., PAPADOPOULOS, K. P., CHAN, I. H., SHEN, C., RATTI, N. P., ROJO, B., AUTIO, K. A., WONG, D. J., PATEL, M. R., OTT, P. A., FALCHOOK, G. S., PANT, S., HUNG, A., PEKAREK, K. L., WU, V., ADAMOW, M., MCCAULEY, S., MUMM, J. B., WONG, P., VAN VLASSELAER, P., LEVEQUE, J., TANNIR, N. M. &

OFT, M. 2018. PEGylated IL-10 (Pegilodecakin) Induces Systemic Immune Activation, CD8. *Cancer Cell,* 34**,** 775-791.e3.

NAING, A., PAPADOPOULOS, K. P., AUTIO, K. A., OTT, P. A., PATEL, M. R., WONG, D. J., FALCHOOK, G. S., PANT, S., WHITESIDE, M., RASCO, D. R., MUMM, J. B., CHAN, I. H., BENDELL, J. C., BAUER, T. M., COLEN, R. R., HONG, D. S., VAN VLASSELAER, P., TANNIR, N. M., OFT, M. & INFANTE, J. R. 2016. Safety, Antitumor Activity, and Immune Activation of Pegylated Recombinant Human Interleukin-10 (AM0010) in Patients With Advanced Solid Tumors. *J Clin Oncol,* 34**,** 3562-3569.

NAING, A., WONG, D. J., INFANTE, J. R., KORN, W. M., ALJUMAILY, R., PAPADOPOULOS, K. P., AUTIO, K. A., PANT, S., BAUER, T. M., DRAKAKI, A., DAVER, N. G., HUNG, A., RATTI, N., MCCAULEY, S., VAN VLASSELAER, P., VERMA, R., FERRY, D., OFT, M., DIAB, A., GARON, E. B. & TANNIR, N. M. 2019. Pegilodecakin combined with pembrolizumab or nivolumab for patients with advanced solid tumours (IVY): a multicentre, multicohort, open-label, phase 1b trial. *Lancet Oncol,* 20**,** 1544-1555.

NETTLESHIP, J. E. 2012. *Structural Biology of Glycoproteins,* Glycosylation, IntechOpen.

NEVEN, B., MAMESSIER, E., BRUNEAU, J., KALTENBACH, S., KOTLARZ, D., SUAREZ, F., MASLIAH-PLANCHON, J., BILLOT, K., CANIONI, D., FRANGE, P., RADFORD-WEISS, I., ASNAFI, V., MURUGAN, D., BOLE, C., NITSCHKE, P., GOULET, O., CASANOVA, J. L., BLANCHE, S., PICARD, C., HERMINE, O., RIEUX-LAUCAT, F., BROUSSE, N., DAVI, F., BAUD, V., KLEIN, C., NADEL, B., RUEMMELE, F. & FISCHER, A. 2013. A Mendelian predisposition to B-cell lymphoma caused by IL-10R deficiency. *Blood,* 122**,** 3713-22.

O'FARRELL, A. M., LIU, Y., MOORE, K. W. & MUI, A. L. 1998. IL-10 inhibits macrophage activation and proliferation by distinct signaling mechanisms: evidence for Stat3-dependent and -independent pathways. *EMBO J,* 17**,** 1006-18.

O'SHEA, J. J., HOLLAND, S. M. & STAUDT, L. M. 2013. JAKs and STATs in immunity, immunodeficiency, and cancer. *N Engl J Med,* 368**,** 161-70.

OFT, M. 2014. IL-10: master switch from tumor-promoting inflammation to antitumor immunity. *Cancer Immunol Res,* 2**,** 194-9.

OHASHI, H., MARUYAMA, K., LIU, Y. C. & YOSHIMURA, A. 1994. Ligand-induced activation of chimeric receptors between the erythropoietin receptor and receptor tyrosine kinases. *Proc Natl Acad Sci U S A,* 91**,** 158-62.

OLSZYNA, D. P., PAJKRT, D., LAUW, F. N., VAN DEVENTER, S. J. & VAN DER POLL, T. 2000. Interleukin 10 inhibits the release of CC chemokines during human endotoxemia. *J Infect Dis,* 181**,** 613-20.

OUYANG, W. & O'GARRA, A. 2019. IL-10 Family Cytokines IL-10 and IL-22: from Basic Science to Clinical Translation. *Immunity,* 50**,** 871-891.

PAL, G., ULTSCH, M. H., CLARK, K. P., CURRELL, B., KOSSIAKOFF, A. A. & SIDHU, S. S. 2005. Intramolecular cooperativity in a protein binding site assessed by combinatorial shotgun scanning mutagenesis. *J Mol Biol,* 347**,** 489-94.

PEARCE, K. H., JR., CUNNINGHAM, B. C., FUH, G., TEERI, T. & WELLS, J. A. 1999. Growth hormone binding affinity for its receptor surpasses the requirements for cellular activity. *Biochemistry,* 38**,** 81-9.

PIEHLER, J., THOMAS, C., GARCIA, K. C. & SCHREIBER, G. 2012. Structural and dynamic determinants of type I interferon receptor assembly and their functional interpretation. *Immunol Rev,* 250**,** 317-34.

PILS, M. C., PISANO, F., FASNACHT, N., HEINRICH, J. M., GROEBE, L., SCHIPPERS, A., ROZELL, B., JACK, R. S. & MULLER, W. 2010. Monocytes/macrophages and/or

neutrophils are the target of IL-10 in the LPS endotoxemia model. *Eur J Immunol,* 40, 443-8.

PINO-MARTINEZ, A. M., MIRANDA, C. G., BATALLA, E. I., GONZALEZ-CAPPA, S. M. & ALBA SOTO, C. D. 2019. IL-10 participates in the expansion and functional activation of CD8(+) T cells during acute infection with Trypanosoma cruzi. *J Leukoc Biol,* 105, 163-175.

PLETNEV, S., MAGRACHEVA, E., WLODAWER, A. & ZDANOV, A. 2005. A model of the ternary complex of interleukin-10 with its soluble receptors. *BMC Struct Biol,* 5, 10.

POLUKORT, S. H., ROVATTI, J., CARLSON, L., THOMPSON, C., SER-DOLANSKY, J., KINNEY, S. R., SCHNEIDER, S. S. & MATHIAS, C. B. 2016. IL-10 Enhances IgE-Mediated Mast Cell Responses and Is Essential for the Development of Experimental Food Allergy in IL-10-Deficient Mice. *J Immunol,* 196, 4865-76.

PULLIAM, S. R., UZHACHENKO, R. V., ADUNYAH, S. E. & SHANKER, A. 2016. Common gamma chain cytokines in combinatorial immune strategies against cancer. *Immunol Lett,* 169, 61-72.

RAGIMBEAU, J., DONDI, E., ALCOVER, A., EID, P., UZE, G. & PELLEGRINI, S. 2003. The tyrosine kinase Tyk2 controls IFNAR1 cell surface expression. *EMBO J,* 22, 537-47.

REYES, R., CARDENES, B., MACHADO-PINEDA, Y. & CABANAS, C. 2018. Tetraspanin CD9: A Key Regulator of Cell Adhesion in the Immune System. *Front Immunol,* 9, 863.

RICHTER, D., MORAGA, I., WINKELMANN, H., BIRKHOLZ, O., WILMES, S., SCHULTE, M., KRAICH, M., KENNEWEG, H., BEUTEL, O., SELENSCHIK, P., PATEROK, D., GAVUTIS, M., SCHMIDT, T., GARCIA, K. C., MULLER, T. D. & PIEHLER, J. 2017. Ligand-induced type II interleukin-4 receptor dimers are sustained by rapid re-association within plasma membrane microcompartments. *Nat Commun,* 8, 15976.

RILEY, J. K., TAKEDA, K., AKIRA, S. & SCHREIBER, R. D. 1999. Interleukin-10 receptor signaling through the JAK-STAT pathway. Requirement for two distinct receptor-derived signals for anti-inflammatory action. *J Biol Chem,* 274, 16513-21.

ROCHA-PERUGINI, V., GONZALEZ-GRANADO, J. M., TEJERA, E., LOPEZ-MARTIN, S., YANEZ-MO, M. & SANCHEZ-MADRID, F. 2014. Tetraspanins CD9 and CD151 at the immune synapse support T-cell integrin signaling. *Eur J Immunol,* 44, 1967-75.

RODIG, S. J., MERAZ, M. A., WHITE, J. M., LAMPE, P. A., RILEY, J. K., ARTHUR, C. D., KING, K. L., SHEEHAN, K. C., YIN, L., PENNICA, D., JOHNSON, E. M., JR. & SCHREIBER, R. D. 1998. Disruption of the Jak1 gene demonstrates obligatory and nonredundant roles of the Jaks in cytokine-induced biologic responses. *Cell,* 93, 373-83.

ROISMAN, L. C., JAITIN, D. A., BAKER, D. P. & SCHREIBER, G. 2005. Mutational analysis of the IFNAR1 binding site on IFNalpha2 reveals the architecture of a weak ligand-receptor binding-site. *J Mol Biol,* 353, 271-81.

ROLLINGS, C. M., SINCLAIR, L. V., BRADY, H. J. M., CANTRELL, D. A. & ROSS, S. H. 2018. Interleukin-2 shapes the cytotoxic T cell proteome and immune environment-sensing programs. *Sci Signal,* 11.

ROSS, S. H., ROLLINGS, C., ANDERSON, K. E., HAWKINS, P. T., STEPHENS, L. R. & CANTRELL, D. A. 2016. Phosphoproteomic Analyses of Interleukin 2 Signaling Reveal Integrated JAK Kinase-Dependent and -Independent Networks in CD8(+) T Cells. *Immunity,* 45, 685-700.

ROWBOTTOM, A. W., LEPPER, M. A., GARLAND, R. J., COX, C. V. & CORLEY, E. G. 1999. Interleukin-10-induced CD8 cell proliferation. *Immunology,* 98, 80-9.

SABAT, R., GRUTZ, G., WARSZAWSKA, K., KIRSCH, S., WITTE, E., WOLK, K. & GEGINAT, J. 2010. Biology of interleukin-10. *Cytokine Growth Factor Rev,* 21**,** 331-44.

SAG, D., CARLING, D., STOUT, R. D. & SUTTLES, J. 2008. Adenosine 5'-monophosphate-activated protein kinase promotes macrophage polarization to an anti-inflammatory functional phenotype. *J Immunol,* 181**,** 8633-41.

SANCHO, D., GOMEZ, M. & SANCHEZ-MADRID, F. 2005. CD69 is an immunoregulatory molecule induced following activation. *Trends Immunol,* 26**,** 136-40.

SARAIVA, M., VIEIRA, P. & O'GARRA, A. 2020. Biology and therapeutic potential of interleukin-10. *J Exp Med,* 217.

SATO, T., MCCUE, P., MASUOKA, K., SALWEN, S., LATTIME, E. C., MASTRANGELO, M. J. & BERD, D. 1996. Interleukin 10 production by human melanoma. *Clin Cancer Res,* 2**,** 1383-90.

SAWANT, D. V., YANO, H., CHIKINA, M., ZHANG, Q., LIAO, M., LIU, C., CALLAHAN, D. J., SUN, Z., SUN, T., TABIB, T., PENNATHUR, A., CORRY, D. B., LUKETICH, J. D., LAFYATIS, R., CHEN, W., POHOLEK, A. C., BRUNO, T. C., WORKMAN, C. J. & VIGNALI, D. A. A. 2019. Adaptive plasticity of IL-10(+) and IL-35(+) Treg cells cooperatively promotes tumor T cell exhaustion. *Nat Immunol,* 20**,** 724-735.

SCHREIBER, G. & WALTER, M. R. 2010. Cytokine-receptor interactions as drug targets. *Curr Opin Chem Biol,* 14**,** 511-9.

SCHREIBER, S., FEDORAK, R. N., NIELSEN, O. H., WILD, G., WILLIAMS, C. N., NIKOLAUS, S., JACYNA, M., LASHNER, B. A., GANGL, A., RUTGEERTS, P., ISAACS, K., VAN DEVENTER, S. J., KONINGSBERGER, J. C., COHARD, M., LEBEAUT, A. & HANAUER, S. B. 2000. Safety and efficacy of recombinant human interleukin 10 in chronic active Crohn's disease. Crohn's Disease IL-10 Cooperative Study Group. *Gastroenterology,* 119**,** 1461-72.

SCHUETZE, N., SCHOENEBERGER, S., MUELLER, U., FREUDENBERG, M. A., ALBER, G. & STRAUBINGER, R. K. 2005. IL-12 family members: differential kinetics of their TLR4-mediated induction by Salmonella enteritidis and the impact of IL-10 in bone marrow-derived macrophages. *Int Immunol,* 17**,** 649-59.

SCHULZ, D., SEVERIN, Y., ZANOTELLI, V. R. T. & BODENMILLER, B. 2019. In-Depth Characterization of Monocyte-Derived Macrophages using a Mass Cytometry-Based Phagocytosis Assay. *Sci Rep,* 9**,** 1925.

SERGE, A., BERTAUX, N., RIGNEAULT, H. & MARGUET, D. 2008. Dynamic multiple-target tracing to probe spatiotemporal cartography of cell membranes. *Nat Methods,* 5**,** 687-94.

SEUBERT, N., ROYER, Y., STAERK, J., KUBATZKY, K. F., MOUCADEL, V., KRISHNAKUMAR, S., SMITH, S. O. & CONSTANTINESCU, S. N. 2003. Active and inactive orientations of the transmembrane and cytosolic domains of the erythropoietin receptor dimer. *Mol Cell,* 12**,** 1239-50.

SHARIF, M. N., TASSIULAS, I., HU, Y., MECKLENBRAUKER, I., TARAKHOVSKY, A. & IVASHKIV, L. B. 2004. IFN-alpha priming results in a gain of proinflammatory function by IL-10: implications for systemic lupus erythematosus pathogenesis. *J Immunol,* 172**,** 6476-81.

SHAW, M. H., FREEMAN, G. J., SCOTT, M. F., FOX, B. A., BZIK, D. J., BELKAID, Y. & YAP, G. S. 2006. Tyk2 negatively regulates adaptive Th1 immunity by mediating IL-10 signaling and promoting IFN-gamma-dependent IL-10 reactivation. *J Immunol,* 176**,** 7263-71.

SHOUVAL, D. S., BISWAS, A., GOETTEL, J. A., MCCANN, K., CONAWAY, E., REDHU, N. S., MASCANFRONI, I. D., AL ADHAM, Z., LAVOIE, S., IBOURK, M., NGUYEN, D. D.,

SAMSOM, J. N., ESCHER, J. C., SOMECH, R., WEISS, B., BEIER, R., CONKLIN, L. S., EBENS, C. L., SANTOS, F. G., FERREIRA, A. R., SHERLOCK, M., BHAN, A. K., MULLER, W., MORA, J. R., QUINTANA, F. J., KLEIN, C., MUISE, A. M., HORWITZ, B. H. & SNAPPER, S. B. 2014. Interleukin-10 receptor signaling in innate immune cells regulates mucosal immune tolerance and anti-inflammatory macrophage function. *Immunity,* 40**,** 706-19.

SILVER, J. S. & HUNTER, C. A. 2010. gp130 at the nexus of inflammation, autoimmunity, and cancer. *J Leukoc Biol,* 88**,** 1145-56.

SLEDZ, P., ZHENG, H., MURZYN, K., CHRUSZCZ, M., ZIMMERMAN, M. D., CHORDIA, M. D., JOACHIMIAK, A. & MINOR, W. 2010. New surface contacts formed upon reductive lysine methylation: improving the probability of protein crystallization. *Protein Sci,* 19**,** 1395-404.

SMITH, L. K., BOUKHALED, G. M., CONDOTTA, S. A., MAZOUZ, S., GUTHMILLER, J. J., VIJAY, R., BUTLER, N. S., BRUNEAU, J., SHOUKRY, N. H., KRAWCZYK, C. M. & RICHER, M. J. 2018. Interleukin-10 Directly Inhibits CD8(+) T Cell Function by Enhancing N-Glycan Branching to Decrease Antigen Sensitivity. *Immunity,* 48**,** 299-312 e5.

SPANGLER, J. B., MORAGA, I., JUDE, K. M., SAVVIDES, C. S. & GARCIA, K. C. 2019. A strategy for the selection of monovalent antibodies that span protein dimer interfaces. *J Biol Chem,* 294**,** 13876-13886.

SPANGLER, J. B., MORAGA, I., MENDOZA, J. L. & GARCIA, K. C. 2015. Insights into cytokine-receptor interactions from cytokine engineering. *Annu Rev Immunol,* 33**,** 139-67.

STAERK, J., DEFOUR, J. P., PECQUET, C., LEROY, E., ANTOINE-POIREL, H., BRETT, I., ITAYA, M., SMITH, S. O., VAINCHENKER, W. & CONSTANTINESCU, S. N. 2011. Orientation-specific signalling by thrombopoietin receptor dimers. *EMBO J,* 30**,** 4398-413.

STEIDLER, L., HANS, W., SCHOTTE, L., NEIRYNCK, S., OBERMEIER, F., FALK, W., FIERS, W. & REMAUT, E. 2000. Treatment of murine colitis by Lactococcus lactis secreting interleukin-10. *Science,* 289**,** 1352-5.

STEINER, E., HOLZMANN, K., PIRKER, C., ELBLING, L., MICKSCHE, M., SUTTERLUTY, H. & BERGER, W. 2006. The major vault protein is responsive to and interferes with interferon-gamma-mediated STAT1 signals. *J Cell Sci,* 119**,** 459-69.

SUKUMAR, M., LIU, J., JI, Y., SUBRAMANIAN, M., CROMPTON, J. G., YU, Z., ROYCHOUDHURI, R., PALMER, D. C., MURANSKI, P., KAROLY, E. D., MOHNEY, R. P., KLEBANOFF, C. A., LAL, A., FINKEL, T., RESTIFO, N. P. & GATTINONI, L. 2013. Inhibiting glycolytic metabolism enhances CD8+ T cell memory and antitumor function. *J Clin Invest,* 123**,** 4479-88.

SWAMY, M., PATHAK, S., GRZES, K. M., DAMEROW, S., SINCLAIR, L. V., VAN AALTEN, D. M. & CANTRELL, D. A. 2016. Glucose and glutamine fuel protein O-GlcNAcylation to control T cell self-renewal and malignancy. *Nat Immunol,* 17**,** 712-20.

SYTO, R., MURGOLO, N. J., BRASWELL, E. H., MUI, P., HUANG, E. & WINDSOR, W. T. 1998. Structural and biological stability of the human interleukin 10 homodimer. *Biochemistry,* 37**,** 16943-51.

TAGA, K., CHERNEY, B. & TOSATO, G. 1993. IL-10 inhibits apoptotic cell death in human T cells starved of IL-2. *Int Immunol,* 5**,** 1599-608.

TAGA, K. & TOSATO, G. 1992. IL-10 inhibits human T cell proliferation and IL-2 production. *J Immunol,* 148**,** 1143-8.

TAKEDA, K., CLAUSEN, B. E., KAISHO, T., TSUJIMURA, T., TERADA, N., FORSTER, I. & AKIRA, S. 1999. Enhanced Th1 activity and development of chronic enterocolitis in mice devoid of Stat3 in macrophages and neutrophils. *Immunity,* 10**,** 39-49.

TAKEDA, K., NOGUCHI, K., SHI, W., TANAKA, T., MATSUMOTO, M., YOSHIDA, N., KISHIMOTO, T. & AKIRA, S. 1997. Targeted disruption of the mouse Stat3 gene leads to early embryonic lethality. *Proc Natl Acad Sci U S A,* 94**,** 3801-4.

TAKESHITA, S., GAGE, J. R., KISHIMOTO, T., VREDEVOE, D. L. & MARTINEZ-MAZA, O. 1996. Differential regulation of IL-6 gene transcription and expression by IL-4 and IL-10 in human monocytic cell lines. *J Immunol,* 156**,** 2591-8.

TANG, Y., ZHOU, J., HOOI, S. C., JIANG, Y. M. & LU, G. D. 2018. Fatty acid activation in carcinogenesis and cancer development: Essential roles of long-chain acyl-CoA synthetases. *Oncol Lett,* 16**,** 1390-1396.

THIBODEAU, J., BOURGEOIS-DAIGNEAULT, M. C., HUPPE, G., TREMBLAY, J., AUMONT, A., HOUDE, M., BARTEE, E., BRUNET, A., GAUVREAU, M. E., DE GASSART, A., GATTI, E., BARIL, M., CLOUTIER, M., BONTRON, S., FRUH, K., LAMARRE, D. & STEIMLE, V. 2008. Interleukin-10-induced MARCH1 mediates intracellular sequestration of MHC class II in monocytes. *Eur J Immunol,* 38**,** 1225-30.

THOMAS, C., MORAGA, I., LEVIN, D., KRUTZIK, P. O., PODOPLELOVA, Y., TREJO, A., LEE, C., YARDEN, G., VLECK, S. E., GLENN, J. S., NOLAN, G. P., PIEHLER, J., SCHREIBER, G. & GARCIA, K. C. 2011. Structural linkage between ligand discrimination and receptor activation by type I interferons. *Cell,* 146**,** 621-32.

TILG, H., VAN MONTFRANS, C., VAN DEN ENDE, A., KASER, A., VAN DEVENTER, S. J., SCHREIBER, S., GREGOR, M., LUDWICZEK, O., RUTGEERTS, P., GASCHE, C., KONINGSBERGER, J. C., ABREU, L., KUHN, I., COHARD, M., LEBEAUT, A., GRINT, P. & WEISS, G. 2002. Treatment of Crohn's disease with recombinant human interleukin 10 induces the proinflammatory cytokine interferon gamma. *Gut,* 50**,** 191-5.

VALLIERES, F. & GIRARD, D. 2017. Mechanism involved in interleukin-21-induced phagocytosis in human monocytes and macrophages. *Clin Exp Immunol,* 187**,** 294-303.

VAN DER WINDT, G. J., EVERTS, B., CHANG, C. H., CURTIS, J. D., FREITAS, T. C., AMIEL, E., PEARCE, E. J. & PEARCE, E. L. 2012. Mitochondrial respiratory capacity is a critical regulator of CD8+ T cell memory development. *Immunity,* 36**,** 68-78.

VAN DER WINDT, G. J. & PEARCE, E. L. 2012. Metabolic switching and fuel choice during T-cell differentiation and memory development. *Immunol Rev,* 249**,** 27-42.

VAZIRINEJAD, R., AHMADI, Z., KAZEMI ARABABADI, M., HASSANSHAHI, G. & KENNEDY, D. 2014. The biological functions, structure and sources of CXCL10 and its outstanding part in the pathophysiology of multiple sclerosis. *Neuroimmunomodulation,* 21**,** 322-30.

VIEIRA, P., DE WAAL-MALEFYT, R., DANG, M. N., JOHNSON, K. E., KASTELEIN, R., FIORENTINO, D. F., DEVRIES, J. E., RONCAROLO, M. G., MOSMANN, T. R. & MOORE, K. W. 1991. Isolation and expression of human cytokine synthesis inhibitory factor cDNA clones: homology to Epstein-Barr virus open reading frame BCRFI. *Proc Natl Acad Sci U S A,* 88**,** 1172-6.

WALK, R. M., ELLIOTT, S. T., BLANCO, F. C., SNYDER, J. A., JACOBI, A. M., ROSE, S. D., BEHLKE, M. A., SALEM, A. K., VUKMANOVIC, S. & SANDLER, A. D. 2012. T-cell activation is enhanced by targeting IL-10 cytokine production in toll-like receptor-stimulated macrophages. *Immunotargets Ther,* 1**,** 13-23.

WALLACH, T. E. & BAYRER, J. R. 2017. Intestinal Organoids: New Frontiers in the Study of Intestinal Disease and Physiology. *J Pediatr Gastroenterol Nutr,* 64**,** 180-185.

WALTER, M. R. 2014. The molecular basis of IL-10 function: from receptor structure to the onset of signaling. *Curr Top Microbiol Immunol,* 380**,** 191-212.

WALTER, M. R. & NAGABHUSHAN, T. L. 1995. Crystal structure of interleukin 10 reveals an interferon gamma-like fold. *Biochemistry,* 34**,** 12118-25.

WALTER, T. S., MEIER, C., ASSENBERG, R., AU, K. F., REN, J., VERMA, A., NETTLESHIP, J. E., OWENS, R. J., STUART, D. I. & GRIMES, J. M. 2006. Lysine methylation as a routine rescue strategy for protein crystallization. *Structure,* 14**,** 1617-22.

WANG, X., LUPARDUS, P., LAPORTE, S. L. & GARCIA, K. C. 2009. Structural biology of shared cytokine receptors. *Annu Rev Immunol,* 27**,** 29-60.

WANG, X., WONG, K., OUYANG, W. & RUTZ, S. 2019. Targeting IL-10 Family Cytokines for the Treatment of Human Diseases. *Cold Spring Harb Perspect Biol,* 11.

WARDA, W., LAROSA, F., NETO DA ROCHA, M., TRAD, R., DECONINCK, E., FAJLOUN, Z., FAURE, C., CAILLOT, D., MOLDOVAN, M., VALMARY-DEGANO, S., BIICHLE, S., DAGUINDAU, E., GARNACHE-OTTOU, F., TABRUYN, S., ADOTEVI, O., DESCHAMPS, M. & FERRAND, C. 2019. CML Hematopoietic Stem Cells Expressing IL1RAP Can Be Targeted by Chimeric Antigen Receptor-Engineered T Cells. *Cancer Res,* 79**,** 663-675.

WEBER-NORDT, R. M., RILEY, J. K., GREENLUND, A. C., MOORE, K. W., DARNELL, J. E. & SCHREIBER, R. D. 1996. Stat3 recruitment by two distinct ligand-induced, tyrosine-phosphorylated docking sites in the interleukin-10 receptor intracellular domain. *J Biol Chem,* 271**,** 27954-61.

WEHINGER, J., GOUILLEUX, F., GRONER, B., FINKE, J., MERTELSMANN, R. & WEBER-NORDT, R. M. 1996. IL-10 induces DNA binding activity of three STAT proteins (Stat1, Stat3, and Stat5) and their distinct combinatorial assembly in the promoters of selected genes. *FEBS Lett,* 394**,** 365-70.

WESTERHOF, L. B., WILBERS, R. H., ROOSIEN, J., VAN DE VELDE, J., GOVERSE, A., BAKKER, J. & SCHOTS, A. 2012. 3D domain swapping causes extensive multimerisation of human interleukin-10 when expressed in planta. *PLoS One,* 7**,** e46460.

WHITTY, A. & BORYSENKO, C. W. 1999. Small molecule cytokine mimetics. *Chem Biol,* 6**,** R107-18.

WILBERS, R. H. P., VAN RAAIJ, D. R., WESTERHOF, L. B., BAKKER, J., SMANT, G. & SCHOTS, A. 2017. Re-evaluation of IL-10 signaling reveals novel insights on the contribution of the intracellular domain of the IL-10R2 chain. *PLoS One,* 12**,** e0186317.

WILKINS, M. R., GASTEIGER, E., BAIROCH, A., SANCHEZ, J. C., WILLIAMS, K. L., APPEL, R. D. & HOCHSTRASSER, D. F. 1999. Protein identification and analysis tools in the ExPASy server. *Methods Mol Biol,* 112**,** 531-52.

WILLIAMS, L., BRADLEY, L., SMITH, A. & FOXWELL, B. 2004. Signal transducer and activator of transcription 3 is the dominant mediator of the anti-inflammatory effects of IL-10 in human macrophages. *J Immunol,* 172**,** 567-76.

WILMES, S., BEUTEL, O., LI, Z., FRANCOIS-NEWTON, V., RICHTER, C. P., JANNING, D., KROLL, C., HANHART, P., HOTTE, K., YOU, C., UZE, G., PELLEGRINI, S. & PIEHLER, J. 2015. Receptor dimerization dynamics as a regulatory valve for plasticity of type I interferon signaling. *J Cell Biol,* 209**,** 579-93.

WILMES, S., HAFER, M., VUORIO, J., TUCKER, J. A., WINKELMANN, H., LOCHTE, S., STANLY, T. A., PULGAR PRIETO, K. D., POOJARI, C., SHARMA, V., RICHTER, C. P., KURRE, R., HUBBARD, S. R., GARCIA, K. C., MORAGA, I., VATTULAINEN, I.,

HITCHCOCK, I. S. & PIEHLER, J. 2020. Mechanism of homodimeric cytokine receptor activation and dysregulation by oncogenic mutations. *Science,* 367**,** 643-652.

WINDSOR, W. T., SYTO, R., TSARBOPOULOS, A., ZHANG, R., DURKIN, J., BALDWIN, S., PALIWAL, S., MUI, P. W., PRAMANIK, B., TROTTA, P. P. & ET AL. 1993. Disulfide bond assignments and secondary structure analysis of human and murine interleukin 10. *Biochemistry,* 32**,** 8807-15.

WYATT, E., WU, R., RABEH, W., PARK, H. W., GHANEFAR, M. & ARDEHALI, H. 2010. Regulation and cytoprotective role of hexokinase III. *PLoS One,* 5**,** e13823.

YAMAGUCHI, T., HIRAKATA, Y., IZUMIKAWA, K., MIYAZAKI, Y., MAESAKI, S., TOMONO, K., YAMADA, Y., KOHNO, S. & KAMIHIRA, S. 2000. Prolonged survival of mice with Pseudomonas aeruginosa-induced sepsis by rIL-12 modulation of IL-10 and interferon-gamma. *J Med Microbiol,* 49**,** 701-707.

YAMAOKA, K., SAHARINEN, P., PESU, M., HOLT, V. E., 3RD, SILVENNOINEN, O. & O'SHEA, J. J. 2004. The Janus kinases (Jaks). *Genome Biol,* 5**,** 253.

YASUDA, K., NAKANISHI, K. & TSUTSUI, H. 2019. Interleukin-18 in Health and Disease. *Int J Mol Sci,* 20.

YI, J. S., HOLBROOK, B. C., MICHALEK, R. D., LANIEWSKI, N. G. & GRAYSON, J. M. 2006. Electron transport complex I is required for CD8+ T cell function. *J Immunol,* 177**,** 852-62.

YOON, S. I., JONES, B. C., LOGSDON, N. J., HARRIS, B. D., DESHPANDE, A., RADAEVA, S., HALLORAN, B. A., GAO, B. & WALTER, M. R. 2010. Structure and mechanism of receptor sharing by the IL-10R2 common chain. *Structure,* 18**,** 638-48.

YOON, S. I., JONES, B. C., LOGSDON, N. J., HARRIS, B. D., KURUGANTI, S. & WALTER, M. R. 2012. Epstein-Barr virus IL-10 engages IL-10R1 by a two-step mechanism leading to altered signaling properties. *J Biol Chem,* 287**,** 26586-95.

YOON, S. I., JONES, B. C., LOGSDON, N. J. & WALTER, M. R. 2005. Same structure, different function crystal structure of the Epstein-Barr virus IL-10 bound to the soluble IL-10R1 chain. *Structure,* 13**,** 551-64.

YOON, S. I., LOGSDON, N. J., SHEIKH, F., DONNELLY, R. P. & WALTER, M. R. 2006. Conformational changes mediate interleukin-10 receptor 2 (IL-10R2) binding to IL-10 and assembly of the signaling complex. *J Biol Chem,* 281**,** 35088-96.

YOSHIMURA, T., MATSUSHIMA, K., OPPENHEIM, J. J. & LEONARD, E. J. 1987. Neutrophil chemotactic factor produced by lipopolysaccharide (LPS)-stimulated human blood mononuclear leukocytes: partial characterization and separation from interleukin 1 (IL 1). *J Immunol,* 139**,** 788-93.

YOU, C., MARQUEZ-LAGO, T. T., RICHTER, C. P., WILMES, S., MORAGA, I., GARCIA, K. C., LEIER, A. & PIEHLER, J. 2016. Receptor dimer stabilization by hierarchical plasma membrane microcompartments regulates cytokine signaling. *Sci Adv,* 2**,** e1600452.

YU, T., ROBOTHAM, J. L. & YOON, Y. 2006. Increased production of reactive oxygen species in hyperglycemic conditions requires dynamic change of mitochondrial morphology. *Proc Natl Acad Sci U S A,* 103**,** 2653-8.

ZDANOV, A., SCHALK-HIHI, C., GUSTCHINA, A., TSANG, M., WEATHERBEE, J. & WLODAWER, A. 1995. Crystal structure of interleukin-10 reveals the functional dimer with an unexpected topological similarity to interferon gamma. *Structure,* 3**,** 591-601.

ZHAO, W., LEE, C., PIGANIS, R., PLUMLEE, C., DE WEERD, N., HERTZOG, P. J. & SCHINDLER, C. 2008. A conserved IFN-alpha receptor tyrosine motif directs the biological response to type I IFNs. *J Immunol,* 180**,** 5483-9.

ZHU, L., SHI, T., ZHONG, C., WANG, Y., CHANG, M. & LIU, X. 2017. IL-10 and IL-10 Receptor Mutations in Very Early Onset Inflammatory Bowel Disease. *Gastroenterology Res,* 10**,** 65-69.

ZHU, Y. P., BROWN, J. R., SAG, D., ZHANG, L. & SUTTLES, J. 2015. Adenosine 5'-monophosphate-activated protein kinase regulates IL-10-mediated anti-inflammatory signaling pathways in macrophages. *J Immunol,* 194**,** 584-94.

Appendix

Appendix Table 1. Monocyte RNA sequencing. Log_2 fold change of genes significantly upregulated by WTD 50 nM > 0.6 log2 fold change and significantly downregulated by WTD 50 nM <-0.6 log2 fold change compared to non-IL-10 treated cells and their corresponding regulation by the IL-10 variants. Only those in the WTD 50 nM were filtered for significance, other conditions were not filtered for significance. Fold change is the average of three biological replicates. WTD50= WTD 50 nM, R5D50= R5A11D 50 nM, WTM50= WTM 50 nM, R5M50= R5A11M 50nM, WTD01= WTD 0.1 nM, R5D01= R5A11D 0.1 nM

Gene Name	WTD50/US	R5D50/US	WTM50/US	R5M50/US	WTD01/US	R5D01/US
TNIP3	9.3183	9.5838	6.5489	8.8555	8.9489	10.1695
CLEC4GP1	8.0675	8.1438	2.4937	6.1780	7.3157	7.5454
C3orf70	7.8293	8.3823	3.6545	6.9244	8.0584	9.0313
APCDD1	7.7724	7.9390	3.4811	6.2680	8.5247	9.8225
IL12RB2	7.6135	7.7576	3.6630	6.4518	7.2733	8.8677
HSD11B1	6.8381	6.7419	1.7010	5.2596	6.2260	7.2444
KIAA1199	6.8165	6.3328	1.7275	5.2549	6.4143	7.4655
HCAR3	6.3585	5.0589	0.8301	3.6943	5.6989	7.4603
RP11-439A17.9	6.3261	6.4223	3.1739	5.6263	5.8541	6.6833
CASP5	6.1590	5.9596	3.3079	5.5741	5.8825	6.5811
TNFAIP8L3	6.0959	6.0843	2.3803	5.0793	6.0726	7.6656
ENPP2	6.0856	6.2212	3.1416	5.6382	5.9516	6.7174
TNFSF18	6.0114	5.9923	1.0842	5.1666	5.8461	7.3461
TMEM163	5.9236	5.3177	2.1320	4.8964	5.0517	6.6487
RP11-79H23.3	5.8787	6.0480	1.9773	4.5763	4.8394	6.4951
PLTP	5.8744	6.1212	2.7187	5.0217	5.7811	6.3703
RP11-1080G15.1	5.8236	6.0386	3.6477	5.5361	5.4139	6.9441
KREMEN1	5.7746	6.0445	3.7986	5.1957	5.4264	6.0678
MCTP2	5.7590	5.6352	3.0199	4.7711	5.1686	5.8749
TMEM158	5.7191	6.1802	3.2222	4.7318	5.8123	6.6033
RP13-52K8.1	5.6439	6.1430	2.0000	5.8989	5.9425	6.9049
SLC16A10	5.5611	5.5941	2.3183	4.5639	5.5459	6.5773
FPR1	5.4881	5.8024	2.9345	4.7845	5.5440	6.4822
NEURL2	5.4638	6.0102	1.4054	4.8253	5.4306	5.9226
C10orf10	5.4129	5.0148	3.9124	4.6431	4.8661	5.4451
FAM20A	5.0874	5.4373	3.1406	4.8637	5.1150	5.4926
CCL18	5.0546	5.0069	3.0994	4.6885	5.3974	5.3877
DACT1	5.0305	5.6032	2.5267	4.8055	5.0076	5.7564
PDGFA	5.0290	5.6026	1.7370	3.8289	4.9117	6.0851
MAT1A	5.0285	4.2395	1.1699	4.5656	5.4127	5.4567
MUC1	4.9534	5.7313	4.3345	5.3476	4.9353	4.9001

FCGR1B	4.9361	5.4168	2.7332	4.5528	5.0247	5.7273
SLCO4A1	4.9332	5.2863	1.9203	4.1133	4.7109	5.7252
SOCS3	4.8260	4.6285	4.4777	4.5669	4.4343	4.6569
LILRA3	4.7499	4.9816	1.8649	3.7680	4.5153	5.3857
NEDD9	4.7112	4.8616	0.4131	3.5849	4.8024	6.1215
DCHS1	4.6241	4.5696	1.7465	3.9321	4.5865	4.9400
SPATA25	4.6141	4.7973	1.0377	3.7409	4.4454	4.6658
GPR85	4.5820	4.7942	2.8870	4.2399	4.6050	5.0258
FCGR1C	4.5177	4.9319	2.3644	4.0349	4.2271	4.9603
FPR2	4.4814	4.5107	1.8938	3.4606	4.0267	5.4332
FCGR1A	4.4322	4.8573	2.4980	4.2689	4.4554	5.0026
RP11-424I19.2	4.3299	5.0379	4.4883	5.0232	4.8310	4.4619
CD72	4.3081	3.9361	2.0907	3.7008	3.9980	4.1064
ABCA8	4.2864	4.5394	2.7464	4.0133	4.3264	4.4985
IL21R	4.2221	4.2279	1.8281	3.7238	4.1618	4.6767
RP1-28O10.1	4.2044	3.7460	-0.0067	3.1186	3.7142	4.0855
PIM1	4.1976	4.4413	2.5419	3.9176	4.2183	4.8779
S100A8	4.1184	4.6907	1.8752	3.7312	4.0536	4.5758
ABHD17C	4.0371	4.6872	1.8472	4.0927	4.3126	5.0796
FEZ1	4.0353	4.1452	1.1726	3.3028	4.0973	4.9691
PTX3	4.0189	4.0318	2.2953	3.5469	4.4470	5.4881
RP4-647J21.1	4.0034	4.3261	2.6194	3.7945	3.8600	4.2355
CX3CR1	3.9938	4.1170	0.8902	2.3607	4.2370	5.1960
AC079325.6	3.9499	4.1828	1.2000	3.5065	3.5334	4.7323
CCL23	3.9355	3.6236	2.7021	4.1592	3.9087	4.1661
IL7	3.9290	3.8203	0.8931	3.0352	3.2442	4.2276
AC010507.5	3.8781	4.7409	1.2116	6.0617	4.2597	4.5151
AMIGO2	3.8424	4.1488	2.4871	4.0516	4.0713	4.1974
IL7R	3.7939	3.8014	1.4057	2.9113	3.0512	4.0762
SH3PXD2B	3.7713	3.7706	1.5445	2.8339	3.3706	3.8086
GPR124	3.7620	4.0542	0.3627	2.0984	3.4935	4.8212
PROS1	3.7168	3.8829	1.9196	3.4204	3.9304	4.2650
AC008746.10	3.7057	3.8782	2.5914	3.4553	4.1571	4.1951
PCDH12	3.6961	3.9627	1.1519	2.5062	3.8513	4.6534
AC006129.4	3.6571	3.7620	3.1007	3.6987	3.6993	3.6480
ARG2	3.6278	3.4484	1.6212	2.7386	3.4891	4.3027
CLEC4G	3.5794	3.3257	1.0817	3.3004	3.4195	4.0995
SERPINA1	3.5750	3.6627	1.4848	3.3099	3.6536	3.9971
SLAMF1	3.5411	3.7655	0.7962	2.8986	3.0323	4.4449
JAK3	3.5358	3.6748	2.5663	3.5060	3.5914	3.6981
RP11-242C19.2	3.5269	2.9727	1.9572	3.0854	3.1892	2.8513
ADAMTS2	3.5106	2.9400	2.0805	3.4300	3.7536	3.6601
RP11-701P16.5	3.4583	4.0164	2.3147	3.7699	3.2159	3.7115

ABLIM3	3.4448	3.9410	1.5174	3.1700	3.5797	4.0544
ELANE	3.4363	3.7082	2.5002	3.1202	3.7676	4.4363
CH25H	3.4287	3.7350	1.3326	3.1247	3.2813	3.1684
MS4A6E	3.4190	3.0705	2.0987	3.0762	3.1691	3.4457
CTD-2006K23.1	3.3450	3.9615	1.5508	3.5547	3.3580	4.3679
DLL1	3.3220	3.3280	1.6164	2.6796	2.8232	3.2947
TUBA1A	3.3004	3.5394	1.2331	2.8597	3.3064	4.1997
CR1	3.2975	3.2881	1.4714	2.9028	3.3226	3.6777
EMR2	3.2803	3.2691	1.4608	2.6845	3.0072	3.4977
FAM129A	3.2786	2.8150	0.7534	2.3660	2.7971	3.5648
RP11-47I22.2	3.2236	3.2624	1.5398	3.0608	3.0307	3.2531
CHI3L2	3.2018	4.2329	1.4047	2.3505	2.8719	2.8726
G0S2	3.1710	3.6608	0.9700	2.7409	3.3538	4.3963
XCR1	3.1681	2.6581	2.7440	3.0538	3.1126	3.2451
VCAN	3.1623	2.9383	1.5680	2.8612	3.0557	3.4379
CDYL2	3.1472	3.2124	1.4291	2.8361	3.2143	3.7800
EPHB3	3.0565	2.9847	2.0720	2.9378	3.1638	3.2613
RP11-25K19.1	3.0473	3.8128	0.7059	2.8970	3.7427	4.8912
GK-AS1	3.0213	2.6769	1.6201	2.4601	2.7461	3.1881
GZMB	3.0066	3.2320	1.7467	2.4828	2.4852	3.1438
FFAR2	2.9820	3.2764	1.4308	2.7160	2.8446	4.1765
NFKBIZ	2.9652	2.6643	1.1738	2.2522	2.6638	3.3880
TIFA	2.9387	3.0073	1.3415	2.6384	2.8864	3.3816
GK	2.9386	2.8554	1.6911	2.5198	2.6133	2.9334
SEBOX	2.9362	2.3623	1.7656	2.0237	2.6197	2.5708
GNG2	2.9324	3.2714	0.7039	2.1376	3.1431	4.1277
MARCO	2.8538	3.5869	0.8034	1.7196	2.5277	2.9322
LAMB3	2.8317	3.2586	0.8082	2.4379	2.7950	3.5595
FCGR3A	2.8202	3.0514	1.6921	2.6775	2.9712	3.3349
C1orf21	2.8168	2.8544	1.2237	2.5836	2.7488	3.4706
FAM157A	2.7997	2.8466	-0.3313	1.7618	2.2944	3.0382
PGLYRP4	2.7863	2.7644	1.1722	2.8920	2.5501	3.0291
RP11-211G3.2	2.7810	2.6032	1.8011	2.0662	2.8462	2.3061
CHRNE	2.7685	2.7187	0.4011	2.1217	2.9532	3.5752
AFAP1	2.7284	2.7866	1.2998	2.3113	2.6824	3.0075
NAMPT	2.7207	2.8326	1.3066	2.2893	2.4315	3.3901
PCBP3	2.7161	2.6371	1.9197	1.9402	2.6274	2.8438
LILRA5	2.7109	2.7854	1.0700	2.3125	2.7934	3.7808
EHD1	2.6949	2.9295	0.9193	2.3425	2.8512	3.9328
HEG1	2.6886	3.0560	0.9154	2.3811	2.5941	3.3772
TFRC	2.6709	2.6577	1.0727	2.0263	2.2670	2.7329
RP11-430K21.2	2.6540	2.9637	2.0408	3.7923	2.7484	2.3491
MYO1G	2.6479	3.0224	1.6970	2.5667	2.6574	2.9727

FOLR3	2.6347	2.3222	2.3033	2.5830	2.1433	2.3401
SDC2	2.6170	2.6464	1.5293	2.2579	2.7497	3.2802
SH2B2	2.6165	2.8340	1.3619	2.2907	2.6743	3.1126
AC005795.2	2.6146	2.5782	2.1715	2.4898	2.6520	2.5908
PCED1B	2.6075	2.9490	1.2756	2.3086	2.7825	2.8258
NAMPTL	2.6057	2.7991	1.1397	2.0628	2.3022	3.2850
NLRP6	2.5859	2.7971	1.4946	1.5173	1.9733	2.8486
TPBGL	2.5822	2.9980	1.5576	2.2602	2.6199	3.0664
S100A9	2.5715	3.0655	1.5406	2.5667	2.6227	2.9178
ACE	2.5353	2.2976	1.2387	1.9269	2.3337	2.3741
LILRB1	2.5347	2.6229	1.1563	2.3372	2.5473	3.0932
STMN3	2.5311	2.6168	0.8835	1.8970	2.4662	2.9359
MAOA	2.5299	1.9828	1.7673	2.4065	2.3454	2.6470
KIAA0226L	2.5195	3.0320	1.2665	2.2593	2.5761	3.0998
UGCG	2.5104	2.5880	0.6545	2.0001	2.2602	2.9245
KIFC3	2.4986	2.7963	1.8234	2.5258	2.6575	2.7626
TUBB2A	2.4760	2.8858	1.2735	2.0992	2.3629	2.8585
HIVEP2	2.4755	2.3304	0.7037	1.7712	1.9947	2.8132
PDE4B	2.4729	1.9768	0.6772	1.4805	1.7760	2.5550
MAPK11	2.4697	2.2768	1.1969	2.0449	2.2265	2.5603
EDNRB	2.4488	2.5901	1.9095	2.1862	2.3226	2.3206
SHB	2.4308	2.7674	1.1793	2.1140	2.3737	2.5586
CEACAM4	2.4283	2.7605	0.9839	1.9398	2.0028	2.7953
ICAM5	2.4251	2.2412	1.1571	1.8184	2.3998	2.3404
ETS1	2.3982	2.6395	0.8622	2.1112	2.3198	3.0582
SPATA6	2.3893	2.4911	0.4117	1.4686	2.5036	3.3449
PSD3	2.3606	2.2757	0.8720	2.0151	2.1178	2.8073
AL627309.1	2.3564	2.6608	1.2901	2.2149	2.1064	2.3660
OLFML2B	2.3557	2.2400	1.6079	2.0595	2.3932	2.4060
AC074011.2	2.3417	2.2667	1.5482	2.0478	2.2292	2.3761
RP11-398A8.3	2.3368	2.5063	1.0062	2.0915	2.4098	3.0764
SLC16A7	2.3326	2.4533	0.5389	1.6091	2.3965	2.9528
LINC00085	2.3270	2.3573	1.9230	2.2305	1.9639	2.2559
EMR1	2.3226	2.7457	1.1247	2.1120	2.1973	2.5783
SRGAP1	2.3186	2.9803	0.9039	2.3318	2.7312	3.0917
MPP3	2.3184	2.6347	2.1648	2.1293	2.2811	1.7718
SLC8A1	2.3067	2.2287	0.6699	1.8730	2.1245	2.8600
LGI2	2.2996	2.7165	1.0852	2.0112	2.5787	3.5324
GRIN3B	2.2979	2.7845	0.7110	2.0349	2.4250	2.4741
HIST1H2BC	2.2928	2.1302	1.9218	2.4797	2.3026	2.3219
CBS	2.2928	2.8858	1.8115	2.6326	2.5051	2.2444
FAM157C	2.2909	2.4126	0.4975	2.1762	1.8818	2.1671
PROK2	2.2659	1.4856	2.0903	1.6837	1.3941	1.5247

Gene						
CD93	2.2624	2.8325	1.0260	1.8628	1.9988	2.5379
TUBB2B	2.2586	2.8122	1.0270	1.8883	2.3656	2.9487
TSPAN9	2.2453	2.0761	0.5626	1.3757	1.8801	2.4222
GLUL	2.2423	2.4068	1.0782	1.9629	2.0603	2.5941
ADM	2.2322	2.1354	1.1006	1.9918	2.1893	2.5894
UTF1	2.2305	2.1048	1.8499	1.6901	2.1470	2.9203
RP11-18F14.2	2.2293	2.3209	0.7002	1.7690	2.0840	2.6839
STARD8	2.2278	2.5334	0.8112	1.8876	2.2387	2.7254
PLB1	2.2147	2.4290	1.2102	2.0498	2.3073	2.4932
NFATC2	2.1774	2.2694	0.9483	1.7943	2.2817	2.6443
LILRB2	2.1672	2.2139	0.7744	1.7349	2.1053	2.7981
RP11-67C2.2	2.1633	2.7052	1.4733	1.9114	2.1658	2.8682
ANKS1A	2.1621	2.2741	0.7108	1.5779	2.1476	2.6266
DSE	2.1600	2.2705	1.2260	1.9668	2.1400	2.5458
FCGBP	2.1452	2.1921	0.3449	1.3612	2.4859	3.2458
IFITM2	2.1447	2.1848	1.0574	1.9029	2.2415	2.5819
VAMP5	2.1234	2.1417	1.2340	2.1622	2.1245	2.3239
CHPF	2.1216	1.9414	0.7943	1.5351	2.0645	2.4573
GNG12	2.1160	2.5770	0.8794	2.4396	2.8427	3.0130
LDLRAD3	2.1156	2.0190	0.5795	1.7587	1.8523	2.3867
HRH2	2.1015	2.4095	0.8419	1.8330	2.0892	2.4159
FZD5	2.0819	2.3460	1.0176	1.8888	1.9651	2.5258
SQLE	2.0804	2.1753	0.8838	1.9252	2.2476	2.8255
PRKCA	2.0700	2.3930	0.5168	1.6156	2.0278	2.8966
CDCP1	2.0560	2.1786	1.2126	1.8962	2.2946	2.3663
PDPN	2.0548	2.6470	1.0735	1.3747	1.4714	1.9206
CEACAM21	2.0262	2.1632	1.2434	1.5899	1.8512	2.2614
ADAMTS10	2.0144	1.9867	1.2634	2.0507	2.2251	1.8402
MAP3K8	2.0105	2.2345	1.1642	1.9987	2.1108	2.5063
DSC2	2.0070	1.9238	1.4496	1.7945	1.9823	1.9253
TMEM173	2.0023	2.4045	0.9477	1.6192	2.0055	2.4362
PRR5L	1.9918	2.2760	0.4848	1.7148	2.1420	2.7435
PCBP1-AS1	1.9831	2.2523	1.2493	2.0166	2.0886	2.3879
PTPN2	1.9719	2.0789	0.8720	1.6236	1.8786	2.3473
S1PR2	1.9647	2.0774	0.7527	1.3227	1.7225	2.2715
SPATA13	1.9620	2.3080	0.7472	1.6231	1.8008	2.4734
MS4A4A	1.9607	2.2141	0.9952	1.6193	1.9828	2.1824
RP11-206L10.11	1.9552	2.0542	0.5174	1.2643	1.4261	2.5613
TMEM2	1.9498	2.0622	1.1645	1.7847	1.9865	2.1924
RP11-304M2.2	1.9453	2.2829	1.1272	1.6728	1.6655	1.9068
TGFA	1.9424	2.1305	1.3789	1.9084	2.0510	2.5817
RP11-792D21.2	1.9338	1.8547	1.1438	1.6645	1.8129	2.1612
TNFRSF8	1.9294	2.1816	0.9100	1.5558	1.9274	2.2144

RP11-363E6.3	1.9260	1.4030	0.9566	0.9062	1.4930	2.3262
C1QB	1.9060	2.2271	1.2918	1.9644	2.1034	2.2251
Mar-02	1.9058	2.0220	0.7775	1.5692	1.7790	2.2092
CCR5	1.9049	1.9158	0.9015	1.6884	1.8224	2.3303
C1RL	1.8923	2.3131	1.4002	2.0266	2.1903	2.3861
VNN2	1.8894	2.0893	1.2682	1.6610	1.9716	2.1726
CHCHD7	1.8878	2.1173	0.9599	1.7683	1.8652	2.4270
LTBP2	1.8776	1.8230	1.0358	1.4047	1.8368	1.8190
GAL3ST4	1.8771	1.6163	0.7899	1.1529	1.5186	1.7153
CD209	1.8696	1.9909	0.7937	1.6079	1.8116	2.1229
RP11-400F19.18	1.8651	1.4359	1.0764	1.5189	1.2501	1.4246
PPM1N	1.8551	2.1511	0.6863	1.6001	1.7755	2.0805
ARHGAP12	1.8501	2.0069	0.3116	1.3097	1.6565	2.4521
GPR27	1.8493	1.7964	0.8768	1.4065	1.7172	2.1567
SBNO2	1.8488	2.0838	1.0220	1.7037	1.8082	2.0614
SMAGP	1.8422	2.2770	0.5323	1.1490	1.9518	2.5281
FABP5P7	1.8389	2.1081	0.4146	1.5685	2.1497	3.0625
BCL6	1.8289	1.9699	0.7680	1.7616	1.8101	2.0422
RP11-536K7.3	1.8284	1.9265	1.4583	1.9690	1.8901	2.0121
NAV1	1.8102	1.6890	0.5132	1.1368	1.5464	1.8366
FABP5	1.8095	1.9426	0.2337	1.4388	2.1759	2.9597
HFE	1.8053	1.9245	0.7920	1.5381	1.9035	2.1625
SIGLEC10	1.8041	2.1305	1.1844	1.1868	1.3174	1.5240
CD163	1.8019	1.7679	0.6880	1.4793	1.7618	2.0583
ALOX5	1.7985	1.9498	0.9009	1.5920	1.8721	2.2176
ACPP	1.7957	1.7813	0.5465	1.0894	1.8638	2.6873
PRDM8	1.7951	2.0048	0.4716	1.3875	1.7070	2.0605
GPR146	1.7945	1.5614	0.0926	0.5657	1.5863	1.9103
TLN2	1.7896	1.6150	0.7273	1.3518	1.4288	0.9491
RP11-65J3.1	1.7824	1.9881	0.7483	1.4224	1.7133	2.1301
ATP2B4	1.7809	1.7140	0.6416	1.3181	1.6672	1.7014
ASPH	1.7766	1.8967	0.8132	1.5796	1.7633	2.1192
LIMA1	1.7566	1.9930	0.9642	1.7607	2.0207	2.4618
BHLHE41	1.7511	1.7263	-0.6484	1.0107	1.8692	2.5188
SMCO4	1.7495	1.8069	0.8228	1.6437	1.9796	2.1980
RHPN1	1.7494	1.9729	0.7709	1.6720	1.7107	1.9978
S1PR1	1.7472	1.7116	1.0281	1.4600	1.7206	1.8857
F13A1	1.7419	2.1406	1.2675	1.7796	1.8546	2.0254
CDKN1A	1.7392	1.8491	1.0434	1.4516	1.6066	1.9259
DHCR7	1.7265	2.0108	0.6241	1.5718	2.0557	2.7525
CDH13	1.7259	1.7228	0.8830	1.8147	1.8834	2.1543
GLT1D1	1.7147	2.3720	1.0266	1.9329	1.8094	2.3533
CREB5	1.7095	1.7556	0.8510	1.2755	1.5851	2.0020

ALDH1A2	1.7082	1.3099	0.6201	2.0522	2.0422	1.7282
AC046143.7	1.7056	1.6456	0.4101	1.0669	1.7625	2.3296
LIMK2	1.6906	2.1739	0.4662	1.4985	1.4046	1.8353
TUBA1B	1.6903	1.9082	0.6247	1.4710	1.7995	2.2366
FCGR2B	1.6850	1.6666	1.1294	1.5949	1.6130	1.8253
PTPN1	1.6813	1.7118	0.5545	1.2767	1.5438	1.9415
HLX	1.6801	1.6322	0.8794	1.3617	1.6675	1.8704
RP11-351I24.3	1.6781	1.8726	0.3356	1.6521	1.8461	2.3904
RASSF4	1.6773	1.9245	0.4867	1.3646	1.4809	2.0190
BASP1	1.6680	1.6784	0.7563	1.3010	1.6667	1.9094
RARRES1	1.6594	1.7743	1.4919	1.8715	1.7852	1.3935
TMEM14A	1.6538	1.8481	1.7122	1.8926	2.0232	1.7584
RP11-282O18.3	1.6530	1.7601	1.4799	1.7244	1.8813	1.9008
NLGN2	1.6511	1.7232	0.8560	1.4453	1.6431	1.9361
DNAJB4	1.6498	1.5786	0.5971	1.0636	1.5240	2.2066
TNS3	1.6477	1.6883	1.0596	1.5041	1.6657	1.7457
GUCY1B3	1.6471	1.0780	0.6527	0.9068	1.4080	1.8903
SDC3	1.6409	1.6903	1.1160	1.7127	1.8380	1.9560
RHOBTB3	1.6211	1.9201	0.7854	1.2359	1.7910	2.1637
VSIG4	1.6198	1.8622	1.0628	1.6049	1.8215	2.0034
RP11-63E5.6	1.6076	1.8109	0.6355	1.1657	1.6798	2.3144
FLVCR2	1.6038	1.8000	0.8148	1.4810	1.5121	1.9379
SGMS2	1.5979	2.3058	1.0857	1.3652	1.6812	2.3457
CNTNAP1	1.5944	1.9498	0.4205	1.1633	1.1876	1.1958
CHSY1	1.5875	1.9380	1.1366	1.5409	1.6920	2.0712
TMEM26	1.5850	2.7114	0.7532	1.6583	1.6195	2.8252
FKBP5	1.5834	1.7095	0.2727	1.0739	1.3384	2.0687
TRIB1	1.5794	1.8397	0.9402	1.2391	1.6452	1.9895
SNX9	1.5792	1.8285	0.6193	1.3522	1.6692	2.2936
AK4	1.5790	1.0922	0.1848	0.6872	1.0932	1.9971
RP11-24F11.2	1.5786	1.5976	0.7613	1.4408	1.4328	1.8373
SLC2A3	1.5784	1.9302	1.3333	1.5386	1.6101	1.7560
TSPAN33	1.5782	1.7384	0.7317	1.4667	1.5714	1.7754
SPP1	1.5762	1.0064	-0.3860	0.4051	1.3270	1.8752
CMTM4	1.5599	1.8597	0.6581	1.2268	1.4981	2.1066
PTPRJ	1.5577	1.7352	0.4414	1.2585	1.5905	2.1769
HK3	1.5388	1.9656	0.6159	1.2566	1.5520	1.8040
CD55	1.5366	1.5286	0.9293	1.2162	1.5599	1.8526
CTD-2587H19.1	1.5329	1.7717	0.7208	1.4988	1.7167	1.9336
KLF6	1.5326	1.7623	0.8215	1.4777	1.5836	2.0213
XBP1	1.5285	1.6575	0.6817	1.3300	1.3423	1.7865
MTL5	1.5251	1.0490	1.1696	1.0571	1.2359	1.3714
LXN	1.5214	1.3282	1.1307	1.3960	1.6252	1.3777

TLR8	1.5053	1.4668	0.6443	1.0769	1.3455	1.8045
VMO1	1.5001	0.7461	1.1153	0.7603	1.1794	1.2469
CTD-2369P2.2	1.4914	1.7530	0.4730	1.1932	1.3762	1.9368
S100A12	1.4892	2.0803	1.0493	1.1055	0.9464	1.6468
B3GNT7	1.4851	2.3849	1.4821	1.8677	1.7565	1.7065
BCL3	1.4829	1.6853	1.2237	1.5461	1.6248	1.8018
PIK3R6	1.4812	1.5951	0.6529	1.1418	1.3386	1.5054
CDKN2D	1.4739	1.8775	1.0169	1.2180	1.5130	1.7876
TLR1	1.4722	1.6270	0.6147	1.1690	1.4532	1.9232
MAP3K6	1.4702	1.8637	1.1075	1.5804	1.5692	1.6442
AC006129.1	1.4701	2.1006	1.6682	0.6966	1.9745	1.4295
ABCA6	1.4632	0.9632	0.9271	1.6273	2.0182	1.9147
PCED1B-AS1	1.4606	1.9251	0.7976	1.4395	1.9357	1.9944
KANK2	1.4558	1.6470	0.6750	1.3948	1.5454	1.9144
GGN	1.4540	2.4519	1.5118	1.7662	2.1487	2.4513
SCD	1.4482	1.5518	0.5233	1.2567	1.5766	2.0805
RALGPS2	1.4353	1.3749	0.5086	0.9894	1.2399	1.6313
CFH	1.4339	1.1182	0.3748	1.2920	1.3288	1.5392
DERL3	1.4337	1.6234	0.7376	1.6784	1.8848	1.9779
MBOAT2	1.4337	1.7078	0.9054	1.5918	1.6693	1.8746
PVRL2	1.4291	1.5864	0.9840	1.4170	1.5045	1.7864
NRP1	1.4219	1.7963	0.8028	1.3522	1.5541	1.8253
ID3	1.4206	1.4859	0.6699	1.1432	1.1571	1.2878
LMNB1	1.4073	1.6647	0.5032	1.1193	1.2815	1.8941
AC144831.1	1.4038	1.7877	1.0038	1.3180	1.3459	1.5476
RP11-84C10.2	1.3971	1.5383	1.6649	1.4920	1.6206	1.9124
TBC1D30	1.3958	1.7803	0.4952	1.4702	1.4841	1.9308
NDUFV2P1	1.3869	0.9627	0.8990	1.0637	0.9711	1.1137
POU2F2	1.3752	1.4039	0.6660	1.1139	1.3192	1.6336
IRF2BPL	1.3685	1.4909	0.8284	1.1761	1.5405	1.5229
HIST1H1C	1.3570	1.1526	0.7836	1.1343	1.4284	1.6114
WWC3	1.3556	1.4471	0.8071	1.3004	1.4341	1.5725
GCA	1.3504	1.4956	0.8895	1.2861	1.2737	1.5779
LINC00115	1.3465	1.2402	1.4528	1.6144	1.6595	1.8522
PIK3AP1	1.3448	1.4328	0.6350	1.1728	1.3108	1.7847
AC004383.4	1.3446	1.5725	0.6742	1.3292	1.5102	1.8198
PLEKHG2	1.3404	1.6499	0.5690	1.1572	1.4677	1.7488
FZD2	1.3323	1.5077	0.8367	1.1986	1.3310	1.4481
CNN2	1.3291	1.5923	0.5894	1.0981	1.3292	1.7510
PDIA4	1.3289	1.4454	0.7269	1.3143	1.3347	1.6515
DENND3	1.3276	1.6853	0.7676	1.2664	1.3241	1.5704
ZDHHC20	1.3273	1.4563	0.6042	1.0366	1.2359	1.5179
PAM	1.3253	1.1705	0.3846	1.0654	1.3693	1.6248

TSHZ3	1.3206	1.8097	0.7178	1.1989	1.3143	1.6285
EBI3	1.3196	1.8948	0.0046	0.5545	0.6097	1.4282
PLK2	1.3148	1.0428	0.5551	0.7679	1.0889	1.8975
LRRC63	1.3145	1.4185	1.2807	1.6155	1.4493	1.3330
PPARG	1.3140	1.7660	0.4834	1.4687	1.6106	2.1663
IDI1	1.3117	1.5793	0.7587	1.2212	1.4182	2.0094
CD163L1	1.3074	1.3589	0.5112	0.8043	0.8987	1.0105
LENG9	1.3065	1.4506	0.1927	0.7120	1.4077	2.0814
CD44	1.3050	1.3239	0.5718	1.1505	1.3260	1.7874
ADAMTSL4	1.3048	1.4257	1.0127	1.2768	1.2989	1.2934
GTDC1	1.3031	1.4637	0.4124	1.1063	1.4266	1.9122
SLC22A23	1.3019	1.5909	0.2734	1.0466	1.4091	1.9491
CYTH4	1.3014	1.6228	0.5233	0.9845	1.2261	1.6808
GPR137B	1.2950	1.4747	0.6236	1.0684	1.3850	1.6853
LRRC25	1.2949	1.5279	0.8206	1.0962	1.3044	1.6187
FLOT1	1.2933	1.5276	0.8843	1.3011	1.3364	1.5389
ANO8	1.2923	1.4237	0.6398	1.0388	1.2515	1.3660
RHPN1-AS1	1.2900	1.1659	0.5902	1.5439	1.4774	1.5464
FPGS	1.2827	1.5617	0.6078	1.2395	1.3037	1.6712
HSD3B7	1.2802	1.6051	0.5534	1.1352	1.4483	1.4912
PLEKHG6	1.2761	0.7459	0.1735	0.9832	1.2096	0.9933
S1PR4	1.2739	1.4008	0.4857	0.9739	1.3042	1.3701
RP11-295G20.2	1.2681	1.6030	1.1085	1.4974	1.3495	1.6025
CTSL1	1.2640	1.6019	1.0881	1.3162	1.2705	1.2227
RHOC	1.2610	1.5256	0.6012	1.1176	1.3754	1.7685
ADAM9	1.2518	1.3278	0.6375	1.0703	1.3132	1.6316
RP11-568N6.1	1.2492	1.0711	0.7894	1.0184	0.8702	1.1290
C1orf228	1.2432	0.7208	-0.1530	1.0384	1.1794	1.5255
CTC-1337H24.1	1.2395	0.3999	0.3219	1.3847	1.0297	1.2730
PPP1R3B	1.2349	1.3387	0.6479	0.7753	1.0413	1.2198
RASGRP2	1.2316	1.4793	0.5264	1.1117	1.3558	1.7296
LILRP1	1.2302	1.1949	0.6283	0.9023	1.1895	1.1746
STEAP3	1.2254	1.2843	0.4891	1.0422	0.9614	1.5710
CD59	1.2251	1.4801	0.8972	1.1783	1.3366	1.5166
CABP4	1.2244	1.2039	0.7177	1.7267	1.6533	1.5472
BCL2L11	1.2233	0.9273	0.4318	0.8447	1.1425	0.9974
LAIR1	1.2217	1.4090	0.6269	1.1004	1.2496	1.5331
PSMC4	1.2183	1.3673	0.2970	0.9878	1.3739	1.9194
HSPA7	1.2136	1.3784	0.8892	1.2432	1.2379	1.1452
FCGR2C	1.2101	1.3641	0.8457	1.2519	1.1792	1.1313
MTSS1	1.2093	1.4539	0.7814	1.1110	1.2504	1.3124
METRNL	1.2088	1.6331	0.8637	1.0956	1.4395	1.6401
DDAH2	1.2074	1.5062	0.6129	1.1279	1.3329	1.5985

Mar-01	1.2052	1.3249	0.6414	1.0671	1.1436	1.4498
MTMR6	1.2045	1.3380	0.5616	0.9322	1.0144	1.4878
CHCHD2P9	1.1984	1.4538	0.7644	1.2158	1.0214	1.5273
TUBA1C	1.1964	1.4391	0.6077	1.0797	1.2486	1.6832
GLTPD2	1.1956	1.1006	0.6420	0.7759	1.1513	1.4803
HCK	1.1955	1.4509	0.6771	1.1026	1.2515	1.6318
SEMA3A	1.1912	1.2971	-0.4924	0.1578	0.8831	1.3906
BTBD19	1.1897	1.4789	0.7525	1.2768	1.0772	1.3200
ABI1	1.1887	1.3277	0.5832	1.0012	1.2055	1.5802
PTK2	1.1857	1.2992	0.7399	1.2246	1.3135	1.5091
LYN	1.1848	1.5440	0.6314	1.1304	1.2250	1.8944
GSDMA	1.1808	1.6845	1.4454	1.1328	1.4395	1.1961
CCR2	1.1792	1.0257	0.5621	0.6132	1.0580	1.2262
CARM1	1.1759	1.4888	0.7522	1.1795	1.2832	1.5409
RTN2	1.1713	1.4359	0.5333	1.0162	1.5019	1.8289
INPP4B	1.1639	1.2633	-0.2847	0.7741	1.3356	1.5902
EIF4G3	1.1593	1.3857	0.6005	1.1592	1.2399	1.3894
RNF149	1.1588	1.4220	0.5623	0.8475	0.9891	1.4125
RNF217	1.1553	1.1836	0.9453	1.1154	1.1505	1.1876
ARAP2	1.1522	1.5983	0.6000	1.1124	1.2154	2.0742
UBE2J1	1.1502	1.3826	0.6098	1.1423	1.1479	1.6118
IL4R	1.1442	1.4443	0.7000	1.1532	1.1935	1.4429
ACTBP11	1.1431	1.3215	0.2645	0.8365	1.2358	1.8674
TWF1	1.1370	1.4649	0.7121	1.2279	1.0879	1.5526
HIF1A	1.1308	1.1083	0.5784	0.8494	0.9856	1.3314
PDE1B	1.1298	1.2868	0.3237	0.9777	1.3819	2.0843
LDHA	1.1245	1.3979	0.7136	1.1038	1.1296	1.5625
Sep-06	1.1240	1.2591	0.3251	0.7010	1.0954	1.6555
TMEM176A	1.1212	1.2520	0.8040	1.0790	1.1173	1.0965
RFX2	1.1164	1.5428	0.6408	1.1522	1.2796	1.4401
CTSC	1.1118	1.2114	0.5801	0.9627	1.1040	1.2758
FAM213A	1.1106	1.1666	0.4475	1.1441	1.3812	1.7071
ATP13A3	1.1067	1.2061	0.5676	0.9074	1.0838	1.7197
CLTC	1.1048	1.3395	0.7080	1.0602	1.1950	1.4074
MLLT1	1.1012	1.3357	0.4529	0.8680	1.1659	1.3979
TUBB6	1.0994	1.3754	0.5568	1.0543	1.1698	1.6165
MICAL2	1.0992	1.4719	0.6246	0.9824	1.2925	1.5879
PNMA1	1.0979	1.4503	0.6597	1.1226	1.1813	1.3716
RGAG4	1.0965	1.2060	0.7183	1.0454	1.1844	1.1880
MIDN	1.0949	1.4126	0.7450	0.9525	1.1715	1.4137
HDGFRP3	1.0947	1.4239	0.7526	0.9170	0.9881	2.2043
BATF	1.0912	1.5053	0.8575	1.3647	1.2625	1.6314
RYR1	1.0907	1.0625	0.5676	0.9504	1.3823	1.3619

DDR1	1.0840	1.1502	0.7402	1.0095	1.3727	1.3170
UHRF1BP1	1.0779	1.1983	0.5401	0.9195	1.0792	1.2600
SLCO2B1	1.0762	1.3019	0.6201	0.9420	1.0649	1.1658
SLC12A9	1.0695	1.3487	0.5890	0.9176	1.0810	1.2873
PDCD1LG2	1.0690	0.9629	1.0372	1.1196	1.2286	1.4103
ACTBP2	1.0660	1.5193	0.4063	0.8084	1.4429	1.7501
CD14	1.0611	1.3351	0.7234	0.8624	1.0525	1.3292
APIP	1.0601	1.1553	0.5976	1.0152	1.1142	1.4510
SMPDL3A	1.0538	0.9254	0.3422	0.6609	0.8392	1.4090
SREBF1	1.0512	1.3519	0.5379	1.0421	1.2188	1.5436
PAG1	1.0501	1.3825	0.0734	0.7359	0.9257	1.3367
STOM	1.0493	1.2118	0.5914	0.8958	0.9916	1.3050
CIC	1.0485	1.1998	0.5393	0.9165	1.0615	1.2444
EPB41L3	1.0458	1.3386	0.6092	1.0712	1.0776	1.4003
ENPP4	1.0450	1.1754	0.4086	0.9665	1.0692	1.3720
FCGR2A	1.0394	1.2464	0.9667	1.0854	1.1106	1.1722
SLC31A1	1.0373	1.1040	0.5544	0.8952	0.9900	1.2473
GIMAP6	1.0337	1.1389	0.7702	1.0481	1.2635	1.3654
ORC6	1.0330	1.3804	0.4863	0.9017	1.2416	1.7591
NFE2	1.0251	1.2039	-0.2271	0.7144	0.5244	0.6779
ENG	1.0225	1.2148	0.4766	0.8371	1.0078	1.2064
RP11-283G6.4	1.0212	1.3287	1.0596	1.3008	1.6174	1.1282
DIRC3	1.0208	1.3019	0.7395	1.1555	1.4576	1.2025
BTG2	1.0188	1.1278	0.8438	0.6761	1.2734	1.3507
ECT2	1.0120	1.0595	0.6589	1.0693	0.9976	1.0416
RALA	1.0110	1.0776	0.4703	0.6244	0.8327	1.4990
CYP51P2	1.0022	0.5154	0.3325	0.4315	1.1618	0.9679
RUNX1	1.0014	1.2734	0.5729	0.9070	1.0755	1.4353
C3AR1	0.9989	1.0608	0.4487	0.7238	1.0090	1.2428
PLK3	0.9986	1.4012	0.3947	0.8539	1.0038	1.4929
MAPRE3	0.9977	1.1282	0.7765	0.9490	1.0442	1.1233
FYB	0.9954	0.9387	0.5563	0.8736	0.8497	1.0797
HNRNPKP4	0.9948	0.1413	0.0215	0.2039	0.7310	0.8898
ATP11C	0.9905	1.2601	0.5333	0.9103	1.0877	1.3469
CD47	0.9902	1.1538	0.5844	0.9684	1.0923	1.4781
SEMA4B	0.9902	1.4220	0.6711	0.9246	0.8859	1.0557
ACSL4	0.9897	1.1355	0.3522	0.8627	0.9980	1.7641
TBC1D2B	0.9889	0.9252	0.4424	0.6336	0.9392	1.1170
BCL9	0.9880	1.2977	0.4169	0.5137	0.4153	0.9691
ABHD3	0.9848	1.2182	0.8147	1.1782	1.1650	1.2193
CDK2AP1	0.9845	1.2977	0.5010	0.8156	1.2483	1.4426
ADA	0.9834	1.0924	0.4350	0.7860	1.1096	1.5413
CMIP	0.9806	1.1471	0.6792	0.9151	1.0623	1.1948

SLC4A7	0.9797	1.1023	0.3437	0.6273	0.8558	1.1738
CTSB	0.9781	1.1914	0.7167	1.0774	1.1277	1.1959
EFHD2	0.9746	1.2847	0.5492	0.8890	1.1033	1.3686
TM2D2	0.9731	1.0902	0.6169	0.8724	1.0641	1.3200
VASP	0.9730	1.2927	0.5783	0.9074	1.0811	1.5535
RNF145	0.9725	1.0794	0.5985	0.9943	1.0547	1.2483
NUPL1	0.9690	0.9755	0.4200	0.7097	0.7667	1.0894
LILRB3	0.9668	1.1863	0.7910	0.9676	0.9372	1.0780
CTC-503J8.6	0.9646	1.2303	0.5880	0.9143	0.9949	1.2639
PHLPP2	0.9635	0.7083	0.5184	0.6259	0.8218	1.0854
ARHGAP26	0.9628	1.1229	0.6494	1.0170	0.9781	1.0599
PIM2	0.9626	0.9350	0.6736	0.8202	0.9622	1.3604
TP53INP2	0.9589	1.3056	0.6734	1.1608	1.1968	1.5185
EHBP1L1	0.9579	1.2000	0.4593	0.8290	0.9751	1.1846
CHD7	0.9574	1.5794	0.5784	1.0488	1.1774	1.6740
DTNB	0.9567	1.2502	0.9723	1.0940	1.0690	0.8321
TNFRSF10C	0.9563	1.2001	0.0918	0.9417	0.7538	1.4018
HSPA6	0.9547	1.2166	1.0867	1.1831	1.0282	0.8763
RNF141	0.9542	1.1833	0.6533	0.9421	1.1429	1.3835
ELL2	0.9535	0.9478	0.3295	0.7989	0.9491	1.2977
SPINT2	0.9492	1.1066	0.7397	0.8214	0.9542	0.9966
ZNF319	0.9478	1.1253	0.7392	0.9849	1.0428	1.3265
TMOD2	0.9475	0.8894	0.6842	0.8168	0.9011	0.9932
KLF3	0.9447	1.1995	0.3831	0.8499	1.0235	1.5322
NONOP2	0.9442	0.7959	0.8119	0.1782	0.4730	0.6167
SIPA1L2	0.9413	1.2158	0.4973	0.7863	0.8906	0.9754
SSH2	0.9366	1.0583	0.4669	0.8154	0.9871	1.1656
RP11-1024P17.1	0.9363	1.4946	1.1537	1.2029	1.2955	1.6981
GRIN2D	0.9362	1.0916	0.3944	0.8062	0.9843	1.1150
MBOAT7	0.9334	0.9918	0.5567	0.6697	0.8704	1.0050
LRMP	0.9290	1.1123	0.4678	0.7150	0.9520	1.1170
FURIN	0.9285	1.1365	0.5098	0.6931	0.8504	1.1030
USB1	0.9271	1.1621	0.6834	0.9124	1.0331	1.2143
RHOU	0.9268	1.2415	0.7058	0.9057	0.9492	1.1711
FAM49B	0.9264	1.3064	0.4470	0.8436	1.1247	1.6918
TRIM8	0.9225	1.0950	0.5030	0.7678	0.9773	1.1598
ARL3	0.9217	1.1581	0.4822	0.7828	0.9741	1.1907
EPS8	0.9195	1.0970	0.5459	0.9574	1.2256	1.4061
CBX6	0.9126	1.0839	0.6108	0.7726	0.9111	1.0302
VMP1	0.9106	0.9682	1.0399	1.1182	0.9552	0.8723
PTPRC	0.9103	0.9458	0.4535	0.7473	0.8513	1.1464
SLC39A1	0.9075	1.0887	0.5727	0.8264	0.9313	1.1913
CTD-2620I22.7	0.9066	1.3605	1.0483	0.9847	1.2415	1.4523

ZFP36	0.9058	1.0714	1.1215	0.8478	1.0984	1.2335
SLC6A8	0.9032	1.1531	0.5963	0.8543	1.1810	1.2892
CEP85L	0.9016	0.7631	0.5304	0.5903	0.9176	0.8008
RP11-497H16.4	0.9012	1.5704	1.3283	1.1434	1.0418	0.6729
SRGAP2C	0.9004	0.8320	0.2959	0.4894	0.7619	1.2266
DEF6	0.8995	1.1880	0.4094	0.8225	1.0849	1.3564
TSC22D3	0.8961	1.1817	0.7799	0.7856	0.9482	1.1096
C1QC	0.8958	1.1739	0.7420	0.9609	1.0078	1.1182
TBC1D14	0.8949	0.9586	0.5204	0.7457	0.8450	0.8813
CSK	0.8921	1.1273	0.3896	0.7184	0.9519	1.3190
PYGL	0.8883	1.1842	0.4580	0.7392	0.8186	1.1407
MVP	0.8882	1.1580	0.7713	0.9605	0.9750	1.1726
KCNMB4	0.8880	0.9849	0.8203	0.7704	0.8425	0.9035
NUF2	0.8794	1.1171	0.5148	0.2177	0.4586	0.2100
RP13-383K5.4	0.8791	1.1870	0.4030	1.2910	0.9766	1.1813
TNFRSF1A	0.8790	1.0937	0.6512	0.8468	0.9505	1.0751
ACSS2	0.8758	1.0140	0.5210	0.8465	0.9292	1.1222
YBX3	0.8735	1.0587	0.5890	0.7589	0.9251	1.0877
PLEK	0.8731	1.0048	0.4302	0.8118	0.8446	1.1577
DUSP1	0.8729	0.8539	0.7585	0.5643	1.0991	1.1493
MGME1	0.8728	1.1183	0.7701	1.0175	1.0193	1.0771
NLRC4	0.8727	1.0705	0.2228	0.6942	0.8922	1.3648
TPTEP1	0.8659	1.0241	0.6358	0.8010	0.9906	1.4195
ARHGAP32	0.8642	1.0641	0.5045	0.7855	1.2615	1.0588
SMAD1	0.8623	0.7777	0.3681	0.2088	0.5698	0.9351
TPM4	0.8607	1.2426	0.4407	0.8556	0.9995	1.5295
SLC4A8	0.8581	1.3016	0.5539	0.6626	0.8640	1.1054
ATP6V0A1	0.8574	0.9660	0.4420	0.6657	0.8226	1.0291
CALR	0.8572	0.9695	0.6170	0.9483	0.8555	1.0737
VAV1	0.8572	1.0130	0.4735	0.8431	0.9774	1.2757
LRRC8B	0.8564	1.0698	0.4570	0.8020	1.0427	1.2356
PIGX	0.8561	1.1506	0.6036	0.8945	1.0281	1.3657
SLC39A8	0.8519	1.0980	0.8198	1.4630	1.0407	1.4582
CSGALNACT1	0.8514	0.6438	0.1143	0.9641	0.9125	0.4804
SNX5	0.8483	1.0624	0.6533	0.8237	0.9757	1.0556
HSPA5	0.8480	0.8859	0.5802	0.9585	0.7556	1.0538
LY96	0.8465	1.0466	0.7240	0.9409	0.8687	0.9556
ACTB	0.8464	1.2790	0.4565	0.8308	1.0001	1.4861
CCR1	0.8450	1.0762	0.6896	0.8392	0.8894	1.1462
EAF2	0.8442	1.0305	0.6710	0.8012	0.9216	1.0695
GTF3C6	0.8406	1.2187	0.6164	0.9879	0.9614	1.1733
GOLGA6L5	0.8372	1.3047	0.7777	1.0507	0.7899	0.6586
PPP1R13L	0.8366	0.8719	0.6802	0.7040	0.7228	0.5697

C2	0.8365	1.1286	0.9065	1.0833	1.0169	1.0808
CASP4	0.8315	0.7758	0.6365	0.7266	0.7765	1.0045
JUNB	0.8310	1.0625	1.0962	0.8838	1.0964	1.0434
MVD	0.8295	1.1618	0.5774	0.9326	0.9761	1.4544
STXBP5	0.8290	0.8819	0.3612	0.5810	0.6838	1.0110
TCEB1P2	0.8265	1.1411	0.9843	0.5710	0.5945	0.8578
STAMBPL1	0.8263	1.3619	0.7521	1.0781	0.9483	1.8757
ACSL1	0.8259	1.1011	0.6022	0.9968	0.8952	1.4053
NEDD4	0.8258	0.9721	0.7532	0.7602	1.0726	0.8758
USP32	0.8253	0.9875	0.4820	0.7542	0.7722	0.9156
AC026806.2	0.8197	1.0746	0.7682	0.8994	1.0216	1.1140
RBMS1	0.8188	1.1547	0.5890	0.8662	0.8876	1.0589
FRMD4B	0.8146	1.3153	0.5845	0.7953	0.8535	1.2201
APEX2	0.8132	0.9325	0.3870	0.7537	0.7418	0.9581
MERTK	0.8085	1.4853	0.2769	0.7172	0.7417	1.4743
DISC1	0.8083	0.9567	0.4735	0.6928	0.8647	0.9475
SLC39A13	0.8066	1.1337	0.2719	0.7517	0.9864	1.3754
RP5-1125A11.1	0.8054	0.5514	1.0448	0.5630	0.8210	0.7339
SEL1L3	0.8038	0.1680	0.3092	0.4900	0.7809	0.6739
TUBA4A	0.8003	1.1328	0.6775	0.8917	0.9023	0.9716
STAT3	0.7992	0.9304	0.6914	0.7904	0.8172	0.9310
RIMKLB	0.7975	1.0933	0.7034	0.9936	0.8800	1.0028
AQP9	0.7971	0.4875	-0.0457	0.5576	0.7253	0.5698
PAK1	0.7967	0.8644	0.4080	0.6155	0.8469	1.1371
MAD2L2	0.7960	1.1164	0.6300	0.9243	0.9270	1.1203
DNAJC25	0.7954	1.1318	0.6831	1.0252	0.8064	0.9020
AGFG1	0.7932	1.2151	0.5014	0.8434	0.9057	1.3775
LCP1	0.7931	0.9540	0.4030	0.7465	0.9489	1.2283
SGTB	0.7924	1.0889	0.6595	0.9236	0.7818	0.8617
FOXRED2	0.7917	0.9878	0.5910	0.7292	0.8874	0.8254
MIR22HG	0.7871	1.3709	0.7218	1.0660	0.8610	1.2036
TRAM2	0.7782	1.0098	0.8190	0.7875	0.9123	0.9037
SERPINB1	0.7773	1.0299	0.6169	0.7155	0.7552	0.8995
CREM	0.7744	0.6244	0.7174	0.6274	0.8239	0.7074
RAB42	0.7738	1.1592	0.6062	0.9362	0.9000	0.8463
NBEAL2	0.7738	1.0357	0.4176	0.8352	0.8764	0.9376
NABP1	0.7726	0.8298	0.4091	0.6325	0.7499	1.0140
GNA15	0.7724	1.0591	0.5892	0.7928	0.8242	1.0298
AC109826.1	0.7722	0.9182	0.6522	1.0681	0.7376	0.6405
PREX1	0.7712	1.0836	0.4592	0.6681	0.7785	1.0020
ARPC3P1	0.7708	0.5268	0.4405	0.9057	0.7529	0.6964
ZHX2	0.7694	0.9070	0.5789	0.8881	0.9275	1.1955
SARM1	0.7682	0.8442	0.3971	0.6404	0.8654	0.9480

MLXIP	0.7664	0.9319	0.3283	0.6359	0.7899	0.9744
RP11-497H16.6	0.7646	1.1684	0.7965	0.9038	0.6706	0.3681
CCDC149	0.7622	1.1750	0.7417	0.9209	0.8645	1.0162
DPP4	0.7610	-0.0707	1.2136	0.4002	0.7370	0.8126
ARHGAP33	0.7608	1.1063	0.7175	0.8372	0.7641	0.8485
VPS9D1	0.7591	1.2610	0.5309	0.8342	0.7424	1.1340
JAZF1	0.7582	0.8679	0.5564	0.8215	0.8326	0.9855
KLF16	0.7560	1.0970	0.4425	0.7000	0.9118	1.1405
PAFAH1B3	0.7553	0.9379	0.5312	0.7491	0.7666	0.8374
ITPR2	0.7546	0.9154	0.5776	0.7703	0.7907	0.9212
TUBB	0.7512	1.0557	0.3432	0.7014	0.8398	1.1135
GNB2	0.7500	1.0750	0.5226	0.6987	0.8529	1.1841
RBPJ	0.7489	1.1029	0.5410	0.9065	0.8980	1.2011
C17orf62	0.7489	0.9762	0.4196	0.7575	0.7822	0.8576
ZNF503	0.7462	1.0728	0.2297	0.4742	1.0149	1.3701
NACC2	0.7444	0.9627	0.4221	0.6122	0.7925	0.9734
TPM1	0.7422	1.0091	0.5648	0.7339	0.8547	0.9566
MS4A7	0.7417	0.8131	0.4778	0.6499	0.6918	0.9195
CCDC24	0.7414	1.0357	0.7281	0.7537	0.9838	0.9064
CTD-2382E5.3	0.7409	1.1599	0.7311	0.9102	0.8180	0.8641
SVIL	0.7400	0.5804	0.2231	0.5299	0.7234	1.2610
AGO4	0.7367	0.9272	0.5673	0.7596	0.7520	0.8521
RP11-361D15.2	0.7363	1.2962	1.5652	1.0741	-0.2959	0.4448
BACH1	0.7361	0.9138	0.4850	0.7325	0.7210	1.2043
RP11-46D6.1	0.7346	0.6172	0.3833	0.4304	0.7614	0.7750
ARNTL	0.7326	0.8895	0.4605	0.7283	0.8472	1.0031
R3HDM4	0.7325	1.0648	0.4846	0.7188	0.9033	1.2146
AC147651.4	0.7319	0.8734	-0.0784	0.4029	0.5821	0.9931
NAGS	0.7298	1.1880	0.4040	0.6220	0.8655	1.2735
OPLAH	0.7289	0.9267	0.3284	0.7039	0.9402	1.1010
KIAA1841	0.7286	0.8904	0.4159	0.8240	0.7556	1.0563
GOLPH3	0.7273	0.8120	0.5008	0.6749	0.7689	1.1290
TSPYL5	0.7273	0.5905	0.7543	0.8796	0.8175	0.9604
YTHDF1	0.7259	0.9424	0.3428	0.5750	0.6853	1.0515
FCHSD2	0.7251	0.9235	0.5289	0.7927	0.8485	0.8964
RP11-848G14.5	0.7234	1.0551	0.7132	0.8811	0.7394	0.5330
PTGR1	0.7231	0.8897	0.3527	0.4071	0.7893	0.7767
UCP2	0.7226	1.1092	0.5080	0.7836	0.9091	1.0840
PLIN3	0.7216	0.9137	0.5106	0.6445	0.7615	1.0217
HDAC4	0.7201	1.0946	0.6573	0.7875	0.7953	1.1136
CPEB4	0.7180	0.8734	0.4911	0.7607	0.7019	0.8029
NDST2	0.7170	0.9531	0.4281	0.6705	0.6181	0.8904
NRSN2	0.7168	0.9315	0.5016	1.1953	0.9815	1.4997

SAMSN1	0.7155	0.8594	0.5171	0.6889	0.7217	1.0935
YIPF1	0.7138	0.9331	0.5504	0.7626	0.7980	0.9864
NMRK1	0.7118	0.8213	0.5209	0.6945	0.7156	0.7306
GPR141	0.7109	0.6458	0.4868	0.6525	0.8715	0.5262
EMILIN2	0.7093	1.0131	0.3439	0.5138	0.8046	1.1221
HIPK2	0.7076	0.8794	0.5077	0.6802	0.8592	0.9179
SSBP2	0.7056	0.7228	0.5656	0.5802	0.8604	0.7726
PXN	0.7044	0.9293	0.6437	0.7137	0.6992	0.6593
YPEL2	0.7028	0.7867	0.2834	0.4850	0.7479	0.8034
DUSP3	0.7007	0.9841	0.8727	0.7586	0.7151	0.7432
PTPN6	0.7001	0.9143	0.3538	0.5147	0.6961	1.0802
DPH3	0.6991	1.0174	0.6051	0.9071	0.8162	1.1363
SORT1	0.6990	0.7827	0.1460	0.3596	0.6659	0.8475
FBXO4	0.6977	0.9635	0.6315	0.6765	0.8347	1.0756
KCNK6	0.6973	0.8445	0.5381	0.6301	0.7984	0.9310
SMAD7	0.6956	0.8992	0.6544	0.6978	0.7347	0.9962
TMSB4XP4	0.6951	0.9904	0.5749	0.7104	0.8488	0.8398
OTUD1	0.6951	0.6693	0.5809	0.4185	0.8293	0.8858
CBFA2T3	0.6923	0.8169	0.4992	0.6573	0.8116	0.7920
TMBIM1	0.6917	0.8244	0.4305	0.6099	0.7071	0.8038
MILR1	0.6905	0.9586	0.5497	0.8290	0.8861	0.9352
CXCL1	0.6897	0.2470	0.2820	0.1372	0.6022	0.7050
RERE	0.6871	0.8040	0.5124	0.6416	0.6812	0.7478
PLD2	0.6867	0.7493	0.3849	0.5923	0.6492	0.8021
TMCO3	0.6867	0.7907	0.4184	0.5430	0.6769	0.8630
IER3	0.6856	0.7496	0.7504	0.5953	0.8868	0.6093
NBEAL1	0.6829	0.5407	0.5654	0.7972	0.9338	0.6697
NDN	0.6807	1.1104	0.7751	0.5574	1.0341	0.9889
ZSWIM1	0.6777	1.1300	0.3387	0.7046	0.9396	1.1182
CSF1R	0.6774	0.6877	0.4496	0.4765	0.6522	0.7491
CTC-774J1.2	0.6767	0.6754	0.5727	0.8558	0.9414	0.9099
PRSS36	0.6743	0.9617	0.5468	0.7620	0.8330	0.6475
MAFB	0.6735	0.9054	0.3905	0.4351	0.7050	0.8624
PNPLA6	0.6726	0.8693	0.4274	0.6813	0.8004	1.0135
ATG3	0.6726	0.8045	0.6332	0.7615	0.6106	0.8674
SNHG15	0.6722	0.9122	0.9958	0.8348	0.8074	0.9766
ACACA	0.6715	0.8867	0.3472	0.5867	0.9071	1.2644
LPCAT3	0.6711	0.9134	0.3573	0.6380	0.7763	1.0620
MANF	0.6710	0.7302	0.5717	0.8491	0.5099	0.7842
LEPR	0.6666	0.9245	0.6839	0.6440	0.6275	0.5833
GOSR2	0.6666	1.1023	0.4312	0.6451	0.7052	1.0234
CLIC1	0.6656	1.0044	0.4666	0.6756	0.7581	1.1301
PICALM	0.6644	0.7895	0.4180	0.5703	0.6859	0.8651

RELT	0.6632	1.0289	0.5185	0.7621	0.8355	0.9859
CDK9	0.6631	0.9179	0.3784	0.6271	0.7237	0.8670
MCM5	0.6608	0.8070	0.3782	0.5648	0.7239	0.8422
CTD-2085J24.4	0.6592	0.6958	0.5479	0.7682	0.4495	0.6172
TMEM70	0.6583	1.0360	0.5283	0.6101	0.7515	1.0175
TSPAN14	0.6580	0.8836	0.3885	0.5444	0.6575	0.8369
SELT	0.6564	0.8771	0.4199	0.6724	0.6978	1.0913
BMP2K	0.6561	1.1138	0.3583	0.6075	0.7851	1.1383
ME1	0.6527	0.6900	0.8162	0.9191	0.7775	0.8455
HPS5	0.6491	0.7443	0.6108	0.6940	0.6497	0.6207
RP11-797A18.3	0.6477	0.5895	0.8732	1.3247	0.6980	0.3118
PPARD	0.6473	0.9028	0.6298	0.7614	0.7424	0.7852
RANBP9	0.6466	0.7111	0.4284	0.5544	0.6246	0.9312
MYO1C	0.6464	0.9951	0.6939	0.6802	0.6943	0.8787
CNEP1R1	0.6458	0.8708	0.4812	0.6872	0.6449	0.8747
POLE4	0.6447	1.0276	0.2984	0.6919	0.7172	1.1069
TMEM88	0.6443	0.7781	1.4797	1.4190	0.8150	1.0678
C3orf14	0.6417	0.7539	0.4322	0.5116	0.7166	0.7657
POU6F1	0.6395	0.8684	0.8003	0.7798	0.8271	0.7893
CEBPB	0.6395	1.0109	0.6231	0.6036	0.8334	0.9510
TDRKH	0.6374	0.8748	0.4267	0.6930	0.7876	1.0285
SFT2D2	0.6373	0.7238	0.1946	0.4944	0.6587	0.9689
ATN1	0.6367	0.6916	0.4962	0.5385	0.6937	0.7344
FAM89B	0.6367	1.1067	0.5286	0.8244	0.8092	1.0341
CAB39	0.6361	0.9258	0.3979	0.5494	0.7530	1.0450
RRBP1	0.6357	0.8900	0.3930	0.6250	0.6703	0.9610
TNIP2	0.6339	0.8936	0.4570	0.7309	0.7926	1.0417
TLN1	0.6334	0.8467	0.3745	0.5205	0.6607	0.8291
HSPA1B	0.6326	0.8898	0.4930	0.8626	0.7751	0.7854
RAP1B	0.6314	0.8561	0.3748	0.6062	0.7746	1.2048
TGFBR2	0.6312	0.8053	0.3228	0.3927	0.5950	1.0231
PCK2	0.6293	0.9295	0.5046	0.6298	0.6251	0.8136
NRBP2	0.6283	1.0634	0.4106	0.5922	0.7068	0.7462
CRK	0.6279	0.8950	0.4389	0.6795	0.7033	1.0758
TRPV2	0.6279	0.8224	0.3476	0.6236	0.7457	1.0395
RBM47	0.6271	0.9976	0.5939	0.6976	0.7548	0.9430
ABL2	0.6269	0.7888	0.4200	0.6489	0.6523	0.8176
SH2D3C	0.6260	0.8684	0.5555	0.5899	0.6556	0.6952
MPZL1	0.6258	0.8019	0.4347	0.6213	0.7123	0.8997
NASP	0.6245	0.8564	0.4645	0.7064	0.6133	0.8405
PRKCB	0.6237	0.8077	0.3255	0.5264	0.8112	1.2318
CTB-175E5.7	0.6235	0.8783	0.4937	0.3524	0.3269	0.3922
PHTF2	0.6218	0.6819	0.4310	0.5202	0.6506	0.7998

KIAA0895L	0.6204	0.8033	0.3601	0.7267	0.6223	0.6500
PFN1P1	0.6204	0.8764	0.3760	0.7693	0.6205	0.8337
CRADD	0.6198	0.9376	0.4307	0.7439	0.7027	0.7015
TPM3	0.6181	0.9776	0.4536	0.6865	0.6897	1.0459
MED16	0.6180	0.8443	0.4800	0.5347	0.7406	1.0608
PLK4	0.6173	0.3940	0.2828	0.3432	0.5850	0.6306
PDLIM5	0.6169	0.8768	0.3691	0.6881	0.8044	1.1041
XRN2	0.6165	0.7187	0.4376	0.5066	0.6016	0.7967
STOML1	0.6164	0.9075	0.2848	0.5561	0.8277	1.0123
GPR107	0.6157	0.7278	0.2915	0.4339	0.6554	0.8837
MYL6	0.6144	0.9583	0.4355	0.6384	0.7334	1.1326
STK3	0.6133	0.7642	0.4736	0.6225	0.7121	0.8809
TNFAIP8	0.6130	0.6930	0.5088	0.6895	0.6728	0.8118
WDR11	0.6124	0.7608	0.2273	0.4586	0.6189	1.0502
H3F3A	0.6117	0.7975	0.4563	0.5627	0.6388	0.8119
SMURF2P1	0.6116	1.1496	0.6951	0.7647	1.0065	1.0467
AIF1	0.6115	0.9148	0.5495	0.6512	0.6422	0.9111
ATP13A2	0.6094	1.0679	0.5676	0.8515	0.8694	0.9174
FKBP15	0.6083	0.7879	0.4085	0.5752	0.5996	0.6898
HYAL2	0.6075	0.8347	0.5713	0.5978	0.7249	0.9933
MESDC1	0.6074	1.0772	0.5192	0.6271	0.8628	1.1617
C1orf54	0.6009	0.8420	0.4171	0.6566	0.6220	0.7241
DDX31	-0.6001	0.1140	-0.0912	-0.2799	-0.4367	-0.1189
RRP1	-0.6003	-0.1461	-0.0577	-0.3053	-0.3912	-0.2778
61E3.4	-0.6015	-0.2218	0.0870	-0.0999	-0.3106	-0.5721
PPOX	-0.6021	-0.3129	0.0079	-0.4014	-0.5188	-0.6434
DCAF17	-0.6023	-0.1601	0.1049	-0.1405	-0.3327	-0.3965
CASP10	-0.6028	-0.5259	0.1146	-0.5006	-0.4954	-0.6982
RPP21	-0.6032	-0.4382	0.0195	-0.5152	-0.4797	-0.4739
RP1-39G22.7	-0.6058	-0.1792	0.1417	-0.2985	-0.6650	-0.3401
SLC2A11	-0.6061	-0.5179	0.1859	0.0474	-0.3809	-0.6944
QTRT1	-0.6070	-0.2218	0.1069	-0.3030	-0.3327	-0.3458
TMEM194A	-0.6074	-0.4646	0.0482	-0.3624	-0.4343	-0.8117
ZSCAN5A	-0.6075	-0.2729	0.0419	-0.2470	-0.2442	-0.7882
GPR132	-0.6082	-0.2156	0.2219	-0.2957	-0.4532	-0.6409
JMY	-0.6086	-0.3782	0.2210	-0.4891	-0.5154	-1.0467
ITGA6	-0.6095	-0.3620	-0.0997	-0.2417	-0.4254	-0.5412
RP11-288I21.1	-0.6100	-0.5370	-0.2040	0.1548	-0.6416	-0.9172
CLUH	-0.6101	-0.2515	-0.0402	-0.4229	-0.4048	-0.3083
NIPAL3	-0.6102	-0.5910	0.1063	-0.4156	-0.3427	-0.8723
ING5	-0.6115	-0.2782	0.0806	-0.4408	-0.3484	-0.3969
WDR75	-0.6117	-0.2522	0.0569	-0.3877	-0.4722	-0.4819
AC004166.7	-0.6125	0.0548	0.1400	-0.1515	-0.2011	-0.2760

MFNG	-0.6134	-0.2338	0.0098	-0.3977	-0.4994	-0.3905
TIMM9	-0.6144	-0.3006	0.0690	-0.3409	-0.3912	-0.3613
HIGD2A	-0.6144	-0.1966	0.1276	-0.1930	-0.4282	-0.4735
RPP25L	-0.6146	-0.3294	0.0602	-0.3304	-0.3578	-0.4459
PLEKHG4	-0.6151	-0.6302	-0.3748	-0.1844	-0.3760	-0.7164
PKD1P1	-0.6153	-1.2004	-0.0723	-0.1373	-0.9791	-0.4207
HMBS	-0.6161	-0.1594	0.0229	-0.1821	-0.6162	-0.3131
MAN2A2	-0.6163	-0.3292	-0.1268	-0.4227	-0.5355	-0.5872
DDX11	-0.6170	-0.5463	0.0432	-0.4719	-0.6409	-0.7371
RP11-640M9.2	-0.6178	-0.4635	0.0851	-0.3293	-0.4750	-0.6314
RP11-420L9.5	-0.6180	0.1818	0.3489	-0.1134	-0.2183	-0.1901
TTC3	-0.6181	-0.5035	-0.0403	-0.3886	-0.5279	-0.6490
SLC25A6	-0.6187	-0.3884	0.0710	-0.4959	-0.4748	-0.5741
TOMM40	-0.6193	-0.1181	0.0573	-0.3097	-0.3203	-0.1605
TMPO	-0.6196	-0.5001	0.0150	-0.4287	-0.4653	-0.7533
SLC25A5	-0.6199	-0.2291	-0.0140	-0.4053	-0.4555	-0.3797
CENPK	-0.6202	-0.0070	0.1859	-0.6049	-1.1941	-0.9339
RRP9	-0.6205	0.0277	-0.1236	-0.2196	-0.2596	-0.1921
CTB-118N6.3	-0.6211	-0.4991	-0.2323	-0.5901	-0.2299	-0.9403
WDR89	-0.6219	-0.1472	0.2099	-0.2013	-0.5065	-0.3259
RNF122	-0.6221	-0.7279	-0.3410	-0.5859	-0.4209	-0.0201
PTTG1	-0.6222	-0.2622	0.3531	-0.0019	-0.1705	-0.2164
PPP1R3E	-0.6237	-0.3865	0.2611	-0.2936	-0.5082	-0.7813
MOSPD1	-0.6242	-0.6993	0.2532	-0.3407	-0.6591	-0.8313
ARHGAP11B	-0.6247	-0.0122	0.3643	-0.0787	-0.6869	-0.6688
KIF11	-0.6248	-0.6705	0.2443	-0.2451	-0.7295	-1.1471
TRERF1	-0.6250	-0.5334	0.0261	-0.4774	-0.6513	-0.9495
LENG8-AS1	-0.6253	-0.4834	0.3974	-0.2114	-0.3748	-0.4247
SKP2	-0.6261	-0.3969	-0.0893	-0.3167	-0.4944	-0.7570
TAF6L	-0.6264	-0.1281	-0.0434	-0.3792	-0.2140	-0.3227
PTRHD1	-0.6264	-0.5273	0.1608	-0.4021	-0.6166	-0.7428
SRPRB	-0.6270	-0.2751	0.0338	-0.1846	-0.3955	-0.3084
ZNF649	-0.6273	-0.0625	-0.0425	-0.0806	-0.2072	-0.2749
RP5-1115A15.1	-0.6284	-0.0885	0.7494	0.0634	0.0289	-0.4700
SLFN12	-0.6295	-0.4526	0.0110	-0.2803	-0.3720	-0.5694
POLR3E	-0.6296	-0.0648	-0.0866	-0.4477	-0.4189	-0.2520
NOP14-AS1	-0.6297	-0.2368	-0.2095	-0.5082	-0.8867	-0.5915
CTC-788C1.1	-0.6303	-0.2918	0.3630	0.1169	-0.6280	-0.5530
TSPYL1	-0.6304	-0.6086	-0.0258	-0.5472	-0.4632	-0.6699
EVC	-0.6307	-0.6453	-0.2418	-0.5837	-0.7638	-1.0251
GK5	-0.6316	-0.4345	-0.2958	-0.5238	-0.4131	-0.6066
L3HYPDH	-0.6347	-0.2195	0.0045	-0.1514	-0.2852	-0.5218
LRIG1	-0.6362	-0.3586	0.1972	-0.0920	-0.2508	-0.6093

KIF22	-0.6369	-0.3562	-0.0012	-0.4084	-0.5863	-0.6350
INO80B	-0.6377	-0.5374	0.0150	-0.4885	-0.5994	-0.6993
MRPL2	-0.6379	-0.3042	0.1122	-0.2930	-0.4010	-0.4354
WDR85	-0.6384	-0.3955	-0.0446	-0.3534	-0.6191	-0.8442
RMND1	-0.6390	-0.3130	0.0087	-0.4285	-0.3973	-0.3008
FASTKD1	-0.6392	-0.3653	-0.0887	-0.4426	-0.6682	-0.8421
CSRP2BP	-0.6395	-0.2557	0.0436	-0.2319	-0.4281	-0.3309
NBPF1	-0.6397	-0.4729	-0.0842	-0.5121	-0.5053	-0.6771
CCDC86	-0.6404	-0.0714	-0.0307	-0.2990	-0.5168	-0.1558
NOC3L	-0.6418	-0.2329	-0.0659	-0.3799	-0.4665	-0.1989
ABHD10	-0.6429	-0.4012	0.0427	-0.3949	-0.5028	-0.5568
TRIB3	-0.6431	0.1085	0.0180	0.1116	-0.2909	-0.1785
RP11-267J23.4	-0.6433	-0.1871	0.0240	-0.2749	-0.5057	-0.2021
DLEU1	-0.6435	-0.3619	-0.0899	-0.7916	-0.2188	-0.4252
S100A13	-0.6446	-0.3786	0.1440	-0.4943	-0.6292	-0.9981
FAM35A	-0.6452	-0.1622	0.1846	-0.3210	-0.3534	-0.4848
RP11-464F9.1	-0.6454	-0.1549	-0.1397	-0.5938	-0.6307	-0.6943
PAICS	-0.6458	-0.1775	0.0582	-0.2990	-0.3567	-0.1085
CREB3L2	-0.6465	-0.4483	0.0286	-0.4754	-0.6049	-0.8834
MBP	-0.6470	-0.5072	-0.0931	-0.6302	-0.5886	-0.8459
CTD-2284J15.1	-0.6472	-0.7665	0.2710	-0.2961	-0.6679	-0.6175
FTSJ2	-0.6476	-0.2453	0.0553	-0.4281	-0.4907	-0.5430
FAM86FP	-0.6479	-0.7101	0.0338	-0.8242	-0.8282	-0.3370
NME7	-0.6492	-0.0557	0.2324	-0.4164	-0.6449	-0.5519
CLEC2D	-0.6492	-0.6214	0.1745	-0.2496	-0.4652	-0.9806
TNK2	-0.6493	-0.3820	0.0096	-0.3917	-0.4844	-0.7796
MRPL40	-0.6493	-0.1822	0.1100	-0.2310	-0.3648	-0.3336
RP11-169K16.9	-0.6497	-0.2994	0.3703	-0.1104	-0.3145	-0.5258
AP4B1	-0.6517	-0.3254	0.2048	-0.1548	-0.3861	-0.5568
RP11-304L19.11	-0.6523	0.1071	0.7646	0.4209	-0.0528	-0.1406
ZNF605	-0.6525	-0.3348	0.1743	-0.0656	-0.4235	-0.5056
CHCHD4	-0.6526	-0.3751	0.0168	-0.3161	-0.2646	-0.4024
NAP1L1	-0.6534	-0.5648	0.0831	-0.4987	-0.5449	-0.6465
AC027763.2	-0.6543	-0.0862	0.3052	-0.2333	-0.1750	-0.3133
THNSL2	-0.6545	-0.6578	0.2769	-0.2856	-0.3388	-0.6454
HDHD3	-0.6546	-0.4428	0.2195	-0.1449	-0.4241	-0.7907
HDDC3	-0.6551	-0.2523	0.0671	-0.5103	-0.3499	-0.5471
DGKD	-0.6569	-0.1608	0.1338	-0.2449	-0.3944	-0.3696
ZNF169	-0.6572	-0.0918	0.1190	-0.2062	-0.3191	-0.3721
ZNF124	-0.6572	-0.2171	-0.0329	-0.3358	-0.1328	-0.2569
GGCT	-0.6573	-0.2103	0.0459	-0.3434	-0.4690	-0.4364
NFKBIE	-0.6575	-0.4030	-0.0450	-0.2434	-0.3369	-0.3849
PEBP1	-0.6576	-0.3078	0.0864	-0.3182	-0.5598	-0.5436

FARSB	-0.6577	-0.0621	0.1017	-0.0549	-0.1603	0.0360
RSL1D1	-0.6581	-0.4116	0.0469	-0.4384	-0.4991	-0.5094
CD3EAP	-0.6589	-0.2832	0.0984	-0.2169	-0.1724	-0.1684
TMEM38A	-0.6596	-0.1196	-0.0114	-0.4892	-0.7514	-0.7595
HMGN3	-0.6611	-0.3098	0.1614	-0.3015	-0.5234	-0.5619
ERCC6	-0.6612	-0.5985	-0.0416	-0.5253	-0.7089	-1.0858
APEX1	-0.6613	-0.3136	-0.0525	-0.4834	-0.5646	-0.4863
TXLNG	-0.6624	-0.1852	0.0804	-0.2872	-0.3057	-0.3362
Sep-09	-0.6626	-0.3056	-0.0243	-0.5332	-0.6365	-0.6216
EBAG9	-0.6633	-0.4825	0.2215	-0.2935	-0.6001	-0.4007
FAM162A	-0.6638	-0.3392	0.0061	-0.3438	-0.4749	-0.4965
HSPBAP1	-0.6647	-0.4809	0.1117	-0.4034	-0.5139	-1.0248
SLC25A32	-0.6657	-0.1670	0.0070	-0.3346	-0.2972	-0.3947
GTF2IRD2B	-0.6661	-0.6723	0.1208	-0.6297	-0.9945	-0.7783
NDUFAF4	-0.6664	-0.5097	0.0581	-0.3427	-0.4550	-0.2772
TRMT10B	-0.6668	-0.2095	-0.0383	-0.2099	-0.3885	-0.5302
RRP15	-0.6677	-0.2402	-0.0346	-0.0889	-0.4685	-0.1739
SLC5A6	-0.6681	-0.2955	0.0440	-0.3007	-0.4527	-0.4611
TBC1D24	-0.6686	-0.2769	-0.0558	-0.3437	-0.3329	-0.6947
IDUA	-0.6692	-0.2867	0.0125	-0.3199	-0.4843	-0.6190
PTPN4	-0.6696	-0.9929	-0.2834	-0.6912	-0.6149	-0.7739
LBX2-AS1	-0.6700	-0.1636	0.2836	-0.1229	-0.4505	-0.6452
WDR91	-0.6703	-0.4668	0.0514	-0.4473	-0.5520	-1.0143
GEMIN8	-0.6705	-0.4741	-0.0197	-0.5199	-0.5865	-0.8011
DNAJC28	-0.6705	-0.2820	0.4202	-0.1770	-0.1809	0.0333
MTA3	-0.6709	-0.1110	-0.0244	-0.1601	-0.2198	-0.0630
ATP5G1	-0.6723	-0.1836	0.0964	-0.2060	-0.4811	-0.3873
TFB2M	-0.6725	-0.4258	0.0688	-0.1772	-0.3429	-0.2116
IL27RA	-0.6736	-0.4363	-0.2298	-0.4291	-0.4129	-0.5886
WDR4	-0.6736	-0.4011	-0.5381	-0.2365	-0.2895	0.1594
AC069282.6	-0.6740	-0.4725	0.0594	-0.4399	-0.6287	-0.8020
BPHL	-0.6741	0.1445	-0.2641	-0.1959	-0.2801	-0.4010
DNPH1	-0.6745	-0.3434	-0.0141	-0.3564	-0.4415	-0.4673
LRPPRC	-0.6747	-0.4559	0.0275	-0.4990	-0.5944	-0.5124
FAHD2A	-0.6748	-0.1930	0.1069	-0.1927	-0.3007	-0.5775
URI1	-0.6765	-0.3179	0.0410	-0.3305	-0.4067	-0.3409
CCDC41	-0.6772	-0.2734	-0.1314	-0.1848	-0.7046	-0.2928
TIMM8A	-0.6776	-0.4035	0.1757	-0.5661	-0.4494	-0.3851
FAM211B	-0.6780	-0.2849	-0.0016	-0.5594	-0.1515	-0.1999
RABL2A	-0.6787	-0.3812	0.1170	-0.4649	-0.6479	-0.8241
JMJD7-PLA2G4B	-0.6790	-0.7408	-0.0676	-0.4306	-0.5001	-1.0222
FAM98A	-0.6799	-0.1782	0.0865	-0.0950	-0.3567	-0.4256
PABPC1L	-0.6803	-0.4491	-0.2401	-0.5890	-0.4659	-0.8993

EIF2S3L	-0.6810	-0.7689	-0.0730	-0.7088	-0.2035	-0.3931
TMEM251	-0.6813	-0.4083	0.2071	-0.3969	-0.5105	-0.7561
TRAPPC6A	-0.6815	-0.3254	0.1883	-0.3850	-0.6009	-0.5815
COX10	-0.6818	-0.2186	0.1376	-0.2784	-0.2621	-0.1799
SNHG5	-0.6818	-0.5739	0.0671	-0.4543	-0.4920	-0.5607
DDX51	-0.6820	-0.1871	0.0033	-0.3505	-0.4391	-0.3367
DDX12P	-0.6820	-0.2079	0.1721	-0.2913	-0.6237	-0.7851
ZNF48	-0.6820	-0.4706	-0.1323	-0.7653	-0.4679	-0.5960
C12orf66	-0.6825	-0.2632	0.1979	-0.5057	-0.6071	-0.4236
POLR2J3	-0.6829	-0.4436	-0.0654	-0.1950	-0.5916	-0.3860
RP1-90J20.12	-0.6831	-0.5118	0.1308	-0.3107	-0.2823	-1.1267
RP11-733O18.1	-0.6841	0.0115	0.3788	-0.0039	-0.6181	-0.4739
ALG3	-0.6854	-0.3333	-0.0733	-0.3719	-0.5235	-0.5867
FKBP14	-0.6855	-0.3595	-0.0652	-0.1631	-0.4284	-0.6290
PICK1	-0.6857	-0.5389	0.0796	-0.3732	-0.5321	-0.9233
AC156455.1	-0.6860	-0.0325	0.3835	-0.8869	-0.5007	-0.2988
SELRC1	-0.6864	-0.2264	-0.0692	-0.5639	-0.3294	-0.4277
CST3	-0.6865	-0.2767	0.1654	-0.3119	-0.4034	-0.4870
ISOC1	-0.6873	-0.4211	-0.1835	-0.3915	-0.3364	-0.1226
ENDOD1	-0.6875	-0.5539	-0.1590	-0.5521	-0.5681	-0.4553
IARS	-0.6875	-0.3498	-0.0348	-0.3393	-0.3633	-0.1489
ZBTB24	-0.6887	-0.4431	0.0481	-0.4174	-0.4660	-0.6152
SLC24A4	-0.6891	-0.1086	0.5005	-0.2094	-0.4174	-0.8830
CLIP4	-0.6899	-0.3387	0.0910	-0.4036	-0.6037	-0.7302
Mar-01	-0.6903	-0.3778	0.1080	-0.0938	-0.3196	-0.3397
RAD51D	-0.6908	0.0582	-0.0342	0.0260	-0.3815	-0.1665
VAV2	-0.6926	-0.4547	-0.0515	-0.4343	-0.5400	-0.6478
FANCD2	-0.6930	-0.3408	0.0518	-0.2914	-0.5945	-0.6597
AURKA	-0.6931	-0.3321	-0.0289	-0.5281	-0.6412	-0.4795
GPX4	-0.6932	-0.4191	0.1728	-0.2767	-0.5165	-0.7113
SNX29	-0.6946	-0.4445	0.0652	-0.6230	-0.5959	-0.9172
SLC25A10	-0.6953	-0.2863	-0.1064	-0.0916	-0.2824	-0.5525
SYT1	-0.6957	-1.3456	0.2952	-0.8083	-1.2752	-1.8068
LTV1	-0.6959	-0.1538	0.1511	-0.1420	-0.3093	-0.0638
UXS1	-0.6964	-0.3609	0.0407	-0.3975	-0.3381	-0.4494
PPAN	-0.6971	-0.3105	0.0120	-0.9724	-0.8731	-0.5195
RP11-686D22.7	-0.6976	-0.0701	0.3709	-0.2167	-0.4126	-0.7962
SNHG1	-0.6978	-0.4902	0.0535	-0.3899	-0.5373	-0.5820
CTD-2270L9.4	-0.6986	-0.2627	0.5714	0.5389	-0.1608	0.4149
ATL2	-0.6987	-0.3495	-0.0916	-0.4128	-0.6110	-0.5415
LSMEM1	-0.7002	-0.6823	0.0312	-0.6029	-0.7542	-1.1908
PSMA6	-0.7006	-0.1233	0.2943	0.0514	-0.5235	-0.4136
PAPLN	-0.7006	-0.7038	-0.1388	-0.4885	-0.6374	-0.6327

BTG1	-0.7010	-0.5466	0.0562	-0.5645	-0.4675	-0.7192
RP11-568K15.1	-0.7013	-0.6431	-0.0602	-0.6024	-0.8062	-0.7637
RASSF2	-0.7013	-0.2857	-0.0374	-0.4827	-0.5198	-0.3639
TTLL11	-0.7021	-0.1062	-0.1039	-0.2236	-0.2151	-0.0851
CEP85	-0.7036	-0.2957	-0.0348	-0.3116	-0.4389	-0.4502
STK32C	-0.7038	-0.3763	0.1028	-0.3584	-0.5003	-0.4881
SPATS2	-0.7041	-0.2905	0.0322	-0.3839	-0.4275	-0.8519
EIF2D	-0.7051	-0.4428	0.1203	-0.5433	-0.5982	-0.5754
DKC1	-0.7051	-0.2794	0.0205	-0.2399	-0.4207	-0.2836
C17orf51	-0.7058	-0.3229	0.0852	-0.2289	-0.4987	-0.6397
RCC2	-0.7067	-0.4791	-0.0725	-0.4316	-0.5388	-0.5623
MAN2C1	-0.7071	-0.4166	-0.1054	-0.4383	-0.5847	-0.6437
ASF1B	-0.7079	-0.3429	0.1473	-0.4271	-0.4955	-0.8109
USP36	-0.7087	-0.2092	0.0183	-0.3824	-0.5820	-0.4163
DUT	-0.7092	-0.4911	0.0936	-0.3303	-0.5495	-0.7277
AC093391.2	-0.7093	-0.7437	0.2404	-0.2057	-0.5887	-1.4884
ZNF331	-0.7098	-0.5641	0.1481	-0.4285	-0.6033	-0.9755
SNAPC1	-0.7100	-0.7427	-0.1065	-0.8456	-0.6870	-0.7226
AL161915.1	-0.7101	-0.7902	0.2332	-0.3595	-0.5113	-1.1798
FDX1	-0.7114	-0.3556	-0.0969	-0.3925	-0.4371	-0.3140
CDK10	-0.7115	-0.4043	-0.0517	-0.4170	-0.5904	-0.6986
WDR43	-0.7123	-0.4511	-0.2463	-0.4756	-0.6476	-0.4246
E2F6	-0.7124	-0.3218	0.0023	-0.4290	-0.5456	-0.5075
NEIL1	-0.7139	-0.4078	0.0863	-0.3251	-0.8023	-0.8682
CALM2	-0.7146	-0.3627	0.0718	-0.4730	-0.5793	-0.5431
OSBP2	-0.7153	-0.6744	0.1842	-0.4545	-0.6096	-1.1140
AC008982.2	-0.7162	-0.2869	-0.1282	-0.1992	0.4923	-0.1544
HEXIM2	-0.7163	-0.9003	0.0397	-0.7410	-0.5095	-1.1143
TRAP1	-0.7165	-0.4123	-0.0918	-0.4085	-0.3721	-0.5200
TSC22D1	-0.7171	-0.9077	0.0230	-0.5180	-0.6235	-1.1372
ENGASE	-0.7179	-0.4801	0.0266	-0.3338	-0.6076	-0.9092
RP11-817O13.6	-0.7183	-0.3108	0.1542	-0.2383	-0.8430	-1.0228
MCCC2	-0.7187	-0.3377	0.0228	-0.5023	-0.5557	-0.3265
CAD	-0.7189	-0.3875	-0.0772	-0.3790	-0.4243	-0.5513
MALT1	-0.7190	-0.5035	0.0699	-0.4251	-0.4975	-0.5552
C19orf24	-0.7210	-0.2122	0.0389	-0.3316	-0.4576	-0.3299
STIM2	-0.7227	-0.5410	-0.0063	-0.3948	-0.5669	-0.5398
C3orf62	-0.7239	-0.2989	-0.0153	-0.2541	-0.4883	-0.5814
THUMPD2	-0.7244	-0.7614	0.0550	-0.4937	-0.7363	-0.8342
LILRB5	-0.7244	-0.5152	0.3571	0.0231	-0.2555	-0.4394
CCDC85B	-0.7265	-0.1706	0.0539	-0.4803	-0.6077	-0.5328
THAP9	-0.7266	-0.0497	0.4493	0.1944	-0.3189	0.0741
ZMYND19	-0.7270	-0.2074	-0.0344	-0.4953	-0.3644	-0.2340

DUS3L	-0.7275	-0.2406	-0.0556	-0.5419	-0.4310	-0.4052
ANKRD46	-0.7277	-0.6387	-0.0836	-0.4851	-0.6420	-0.6928
HMGB2	-0.7278	-0.5938	0.1167	-0.3600	-0.5832	-0.9479
PUS1	-0.7282	-0.1361	0.0109	-0.3069	-0.3719	-0.0937
PTK2B	-0.7293	-0.5357	0.0089	-0.5062	-0.6920	-0.8287
RPS26P3	-0.7294	-0.3815	-0.1257	-0.0803	-0.7987	0.2428
SESN1	-0.7301	-0.7163	0.0398	-0.6453	-0.4762	-0.8706
OPTN	-0.7308	-0.1350	0.3481	-0.1054	-0.5195	-0.8203
MRPL55	-0.7314	-0.2641	0.0448	-0.4618	-0.6438	-0.5246
CTD-2228K2.5	-0.7329	-0.4583	-0.1013	-0.7809	-1.2023	-1.1453
TIAF1	-0.7332	-0.2778	-0.1330	-0.1951	-0.2324	-0.4103
SIN3B	-0.7338	-0.3778	0.0310	-0.3736	-0.6002	-0.6543
GRWD1	-0.7344	-0.1923	0.0310	-0.3993	-0.3545	-0.0789
ZSCAN12	-0.7367	-0.1855	-0.2881	-0.6171	-0.6956	-0.7246
DTWD1	-0.7370	-0.2484	0.1063	-0.1086	-0.4224	-0.1709
AC009403.2	-0.7375	-0.0336	0.0767	-0.1753	-0.2439	-0.0266
PSMG4	-0.7387	-0.2024	0.3019	-0.1231	-0.4127	-0.2121
EARS2	-0.7389	-0.5818	-0.1128	-0.3994	-0.7155	-0.4153
UAP1L1	-0.7402	-0.2184	0.1465	-0.2390	-0.5707	-0.9175
LRRC48	-0.7403	-0.3008	0.2285	-0.2015	-0.5363	-0.3013
RNASEH2B	-0.7407	-0.4506	0.1314	-0.4415	-0.6221	-0.9712
LIPT1	-0.7419	-0.6184	0.0512	-0.3871	-0.6284	-0.8365
IL6R	-0.7425	-0.3819	-0.0601	-0.5962	-0.5747	-0.6852
ELMSAN1	-0.7428	-0.5240	-0.1264	-0.6328	-0.6541	-0.8839
POLR1B	-0.7428	-0.3667	0.0289	-0.4540	-0.4554	-0.2834
LRRC69	-0.7432	-0.6547	-0.3729	-0.2269	-0.4393	-0.9783
DAPK1	-0.7433	-0.4457	0.1171	-0.2852	-0.6015	-0.9261
SLC25A45	-0.7436	-0.5228	-0.2059	-0.4961	-0.6488	-0.6782
SLC16A5	-0.7456	-0.3047	0.0355	-0.3184	-0.5372	-0.6079
HLTF	-0.7463	-0.6460	-0.0437	-0.6394	-0.8238	-0.8647
NAT6	-0.7466	-0.4137	0.1584	-0.4476	-0.8184	-0.5801
ECSIT	-0.7466	-0.6673	-0.0068	-0.5543	-0.6466	-0.7773
TARSL2	-0.7469	-0.7541	0.2369	-0.4828	-0.6260	-0.9277
NPM1	-0.7470	-0.5192	0.0254	-0.5028	-0.5618	-0.5981
COQ9	-0.7472	-0.2888	0.1078	-0.3908	-0.4078	-0.4879
ALDH3A2	-0.7480	-0.3765	0.2293	-0.3464	-0.5321	-0.8074
ADORA3	-0.7510	-0.2682	0.0567	-0.4941	-0.8275	-1.1009
ACCS	-0.7543	-0.3835	0.0453	-0.4612	-0.6532	-0.8493
CD3E	-0.7544	-0.0761	0.0222	-0.2800	-0.1889	-0.3345
PSAP	-0.7547	-0.5166	0.0828	-0.4696	-0.6100	-0.7954
SLC25A40	-0.7547	-0.6444	0.0177	-0.5023	-0.8229	-0.9131
ZNF717	-0.7550	-0.3969	-0.0896	-0.4605	-0.4808	-0.5976
CTA-29F11.1	-0.7557	-0.1215	-0.1984	-0.3712	-0.6386	-0.6627

CTB-41I6.1	-0.7565	-0.4415	0.1274	-0.4519	-0.5181	-0.8762
CAMK1D	-0.7569	-0.5150	0.0693	-0.5557	-0.5587	-0.6920
MAGEH1	-0.7574	-0.2619	0.0481	-0.3230	-0.3773	-0.6329
RPUSD2	-0.7578	0.0107	-0.0374	0.0251	-0.0614	-0.2555
JARID2	-0.7589	-0.4591	0.0043	-0.4716	-0.5777	-0.8089
AHCY	-0.7596	-0.3608	0.0430	-0.4383	-0.6393	-0.6294
SLFN11	-0.7607	-0.5634	0.0815	-0.4811	-0.6515	-0.8622
TMEM39B	-0.7609	-0.5163	-0.0028	-0.5806	-0.4998	-0.6133
MTERFD1	-0.7626	-0.2867	0.1310	-0.1998	-0.3981	-0.3148
POGLUT1	-0.7643	-0.5149	-0.1148	-0.4466	-0.8034	-0.6384
MNF1	-0.7649	-0.2127	0.1599	-0.0802	-0.3478	-0.0926
DPH2	-0.7652	-0.3528	-0.1934	-0.5928	-0.6383	-0.3932
CCDC154	-0.7661	-0.5114	0.1098	-0.3833	-0.5664	-1.4280
HGF	-0.7665	-0.8460	0.2052	-0.5808	-0.5225	-1.4276
ZNF706	-0.7668	-0.4942	0.0534	-0.5250	-0.6957	-0.7391
SIRT4	-0.7672	-0.2847	0.2766	-0.1440	-1.4495	-2.1210
SPICE1	-0.7672	-0.5089	0.0284	-0.4899	-0.5266	-0.9304
MSI2	-0.7677	-0.7243	-0.2450	-0.7103	-0.4388	-0.7005
MPHOSPH9	-0.7677	-0.4765	0.0639	-0.6212	-0.5304	-0.7980
IGSF6	-0.7679	-0.3785	0.1542	-0.4060	-0.6087	-0.9503
C17orf76-AS1	-0.7682	-0.5886	-0.1832	-0.6969	-0.6579	-0.6380
NUDT16P	-0.7692	-0.1735	0.2157	-0.3494	-0.3444	-0.5475
FAM185A	-0.7694	-0.2374	0.0339	-0.5510	-0.4944	-0.2893
HTATSF1P2	-0.7697	-0.6269	0.0313	-0.5099	-0.6544	-1.1399
CMSS1	-0.7714	-0.7643	-0.1790	-0.6014	-0.6852	-0.3091
TTC27	-0.7716	-0.2410	-0.0816	-0.3098	-0.2285	-0.3273
PARP16	-0.7716	-0.5012	-0.0633	-0.6813	-0.5141	-1.0118
NUDT15	-0.7721	-0.4852	-0.0116	-0.5666	-0.5965	-0.5835
BAG2	-0.7721	-0.6411	-0.2450	-0.5451	-0.6053	-1.3327
RP11-154D6.1	-0.7723	-0.6253	0.0925	-0.5113	-0.6422	-0.8092
RPIA	-0.7730	-0.3930	-0.1643	-0.3686	-0.4497	-0.4193
AMT	-0.7736	-0.4295	0.1658	-0.4262	-0.6848	-1.0860
C2CD2	-0.7738	-0.7769	-0.0243	-0.5014	-0.5036	-0.9230
ILF3-AS1	-0.7764	-0.2820	0.3765	-0.1733	-0.4535	-0.4939
NUFIP1	-0.7767	-0.2642	0.0572	-0.4592	-0.7393	-0.4552
FLNA	-0.7774	-0.3441	0.0313	-0.4290	-0.6044	-0.6571
EFHC1	-0.7778	-0.6704	0.2211	-0.4111	-0.6184	-1.1501
PEX7	-0.7787	-0.1756	-0.3570	-0.7394	-0.5633	-0.2372
FBXW8	-0.7788	-0.3094	-0.0683	-0.4482	-0.3490	-0.3727
IMP3	-0.7793	-0.4849	0.0257	-0.5312	-0.5569	-0.5306
RPL36A	-0.7797	-0.4011	-0.2614	-0.3071	-0.4369	-0.8477
UTP20	-0.7798	-0.2602	0.0607	-0.4836	-0.2189	-0.1042
ZNF14	-0.7810	-0.2241	-0.1556	-0.5111	-0.5457	-0.4218

OSBPL3	-0.7814	-0.3679	0.0846	-0.3905	-0.5884	-0.9548
LIPA	-0.7820	-0.6203	-0.2564	-0.6115	-0.6069	-0.8384
RBFA	-0.7821	-0.1640	0.2782	-0.2944	-0.2313	0.0619
LIMK1	-0.7825	-0.5079	-0.2207	-0.5455	-0.6478	-0.5950
TP53	-0.7826	-0.5915	-0.0202	-0.5310	-0.6407	-0.7529
RPL23P8	-0.7833	0.3210	0.4489	0.1550	0.3545	0.0352
RP11-526I2.5	-0.7834	-0.3089	-0.1238	-0.3508	-0.3915	-0.9249
DNAJA3	-0.7839	-0.6166	-0.2207	-0.5100	-0.6059	-0.5872
RP11-452L6.5	-0.7859	-0.2718	0.2176	-0.3313	-0.3025	-0.1877
PDE7A	-0.7859	-0.6442	-0.0102	-0.4372	-0.6694	-0.9598
LINC00338	-0.7883	0.2173	0.7115	0.1904	-0.3059	-0.1625
MYADM	-0.7888	-0.7588	-0.3774	-0.9288	-0.6991	-0.7961
ZNF852	-0.7909	-0.3812	-0.1461	-0.4719	-0.3818	-0.6362
UNC5CL	-0.7919	-0.4316	-0.1298	-0.4071	-0.7164	-0.9885
GS1-124K5.4	-0.7926	-1.0514	-1.4133	-0.9951	-0.5766	-0.5170
ANKMY1	-0.7927	-0.4437	-0.0364	-0.5698	-0.6332	-0.8742
RP11-473M20.14	-0.7941	-0.5879	-0.0236	-0.4929	-0.5681	-0.6417
STARD13	-0.7957	-0.2867	0.1400	-0.4122	-0.7035	-0.9513
KBTBD6	-0.7959	-0.3331	0.0798	-0.2373	-0.4930	-0.3527
ADSSL1	-0.7960	-0.3999	0.1573	-0.6559	-0.7609	-1.2170
C2CD5	-0.7984	-0.3927	0.0241	-0.5473	-0.5829	-0.5409
ZNF519	-0.8001	-0.8250	-0.1531	-0.6747	-0.6615	-1.1273
MMD	-0.8005	-0.4099	-0.1305	-0.3211	-0.6558	-0.4885
GSE1	-0.8007	-0.6097	-0.0128	-0.5767	-0.5982	-0.7631
IRS2	-0.8009	-0.5958	0.0566	-0.5480	-0.4637	-0.9694
RCSD1	-0.8042	-0.6464	-0.0168	-0.6190	-0.6799	-0.6760
MCM4	-0.8050	-0.0887	0.0025	-0.4817	-0.4434	-0.6616
LMTK2	-0.8063	-0.4838	0.0790	-0.1952	-0.5754	-0.5948
VAV3	-0.8071	-0.2277	0.2554	-0.2534	-0.5897	-0.8072
ERMAP	-0.8076	-0.6350	-0.0572	-0.4572	-0.6203	-0.9388
AC133528.2	-0.8078	-0.3288	0.3338	0.0250	-0.2674	-0.3058
RP11-248J18.3	-0.8121	-0.2287	0.1085	-0.0035	-0.5753	-0.5941
ESPL1	-0.8123	-0.4638	0.1959	-0.3075	-0.3132	-0.4673
AC073043.2	-0.8132	-0.1624	0.5638	0.0353	-0.4790	-0.3936
ZNF566	-0.8134	-0.4598	0.0992	-0.3849	-0.4329	-0.4480
FAM78A	-0.8135	-0.4420	0.0100	-0.5324	-0.6174	-0.8796
RP11-85F14.5	-0.8146	-0.3048	0.2614	-0.3463	-0.5695	-1.1143
PPAT	-0.8153	-0.4438	-0.0002	-0.6421	-0.9321	-0.7893
NPM3	-0.8154	-0.3312	-0.2805	-0.3357	-0.4479	-0.2701
ACRC	-0.8159	-1.0824	-0.2192	-0.7806	-0.7836	-1.4332
LYRM4	-0.8169	-0.4626	0.0702	-0.6384	-0.5506	-0.5973
CKS2	-0.8176	-0.7810	0.1979	-0.3247	-0.4928	-0.9096
SLC38A6	-0.8202	-0.5026	0.1590	-0.3506	-0.6532	-1.0548

MDN1	-0.8208	-0.4453	-0.1180	-0.5466	-0.7095	-0.6986
RP11-153A23.6	-0.8219	-0.3201	-0.2258	-0.2780	-0.4646	-0.9209
PRDM1	-0.8228	-0.7682	0.0491	-0.6608	-0.7714	-1.1394
CDK4	-0.8247	-0.4155	0.0828	-0.4247	-0.5327	-0.6151
ADK	-0.8248	-0.5361	-0.0017	-0.7187	-0.8481	-0.9732
ZNF570	-0.8258	-0.1634	-0.0345	-0.4203	-0.1870	-0.4149
SCARF1	-0.8263	-0.5526	0.0410	-0.4758	-0.8028	-1.1091
ANO9	-0.8267	-0.3295	0.0357	-0.1627	-0.0729	-0.4904
MTFR2	-0.8270	0.2183	0.0681	-0.4214	0.0118	-0.5059
MXI1	-0.8271	-0.8448	0.1738	-0.6773	-0.8385	-1.2168
RPL21P28	-0.8298	-0.4157	0.0705	0.0730	-0.2382	-0.8059
DAGLA	-0.8307	-0.5518	-0.0818	-0.5253	-0.5920	-0.8894
BTN3A1	-0.8307	-0.6912	0.1038	-0.4443	-0.6811	-1.1884
CDCA7L	-0.8325	-0.2385	-0.1556	-0.7293	-0.7528	-0.7331
IL8	-0.8338	-1.3359	0.1519	-0.8609	-0.7783	-1.3517
MRTO4	-0.8348	-0.3221	0.0179	-0.3729	-0.4608	-0.0860
ANGEL1	-0.8350	-0.6113	-0.1053	-0.5310	-0.6426	-0.8163
RSG1	-0.8354	-0.5005	0.0264	-0.3277	-0.6045	-0.6632
SETDB2	-0.8367	-0.5453	0.0506	-0.4749	-0.7451	-1.1630
PRKAG2-AS1	-0.8367	-0.4124	0.1055	-0.5551	-0.6253	-0.8190
ASAH1	-0.8369	-0.5348	0.0766	-0.5246	-0.6968	-0.9524
RP11-296I10.6	-0.8380	-0.3754	0.1828	-0.3213	-0.7606	-0.7176
61E3.4	-0.8387	0.0564	0.0672	-0.0557	-0.4161	-0.4989
CAMKK2	-0.8388	-0.6204	-0.0675	-0.5260	-0.6249	-0.7188
EPB41	-0.8388	-0.7791	-0.1007	-0.7410	-0.7113	-0.9492
CTD-2349P21.9	-0.8392	-0.9891	-0.6002	-0.9645	-0.3847	-1.5159
CTPS1	-0.8393	-0.3674	-0.1622	-0.2895	-0.2619	0.5630
ZSCAN18	-0.8410	-0.6263	0.1282	-0.2069	-0.3656	-0.6018
GGT1	-0.8411	-0.6195	-0.1922	-0.6382	-0.7608	-0.7985
RP3-473L9.4	-0.8418	-0.5679	-0.0069	-1.4854	-1.8729	-2.1597
LRRN2	-0.8429	-1.2985	-0.2164	-0.3650	-0.5852	-1.6078
ZNF33B	-0.8434	-0.3362	0.0704	-0.6304	-0.7304	-0.9127
RP11-705C15.3	-0.8455	-0.5391	0.1033	-0.2784	-0.2663	-0.5387
AGAP9	-0.8477	-0.4383	0.1271	-0.3737	-0.8076	-0.8415
RP11-876N24.4	-0.8478	-0.6061	-0.2562	-0.5394	-0.5694	-1.2078
TDRD6	-0.8480	-0.6974	0.0128	-0.2647	-0.6320	-1.1661
POLR1C	-0.8516	-0.1905	0.0123	-0.4308	-0.6600	-0.5699
INO80C	-0.8520	-0.6272	0.1208	-0.4145	-0.8192	-0.4914
LTA4H	-0.8524	-0.8117	-0.0008	-0.6072	-0.7627	-1.0851
CCDC101	-0.8536	-0.4380	0.1639	-0.3501	-0.5988	-0.6440
THADA	-0.8538	-0.5950	0.0351	-0.5390	-0.6635	-0.8632
CECR5	-0.8540	-0.5053	0.0278	-0.5311	-0.7547	-0.8125
STARD10	-0.8540	-0.8638	0.2536	-0.4432	-0.5938	-1.1424

PPT2	-0.8547	-0.0835	0.0810	-0.3984	-0.4742	-0.1756
TCF7	-0.8562	-0.3205	0.0908	-0.9356	-0.5378	-0.8081
CFLAR-AS1	-0.8566	-0.7271	-0.2077	-0.3086	-0.1529	-0.9460
TP53I11	-0.8570	-0.4383	-0.2849	-0.3304	-0.8008	-0.7723
LDHB	-0.8587	-0.4561	0.0361	-0.4573	-0.6203	-0.6129
ZNF835	-0.8589	-0.7112	-0.6075	-1.2381	-1.2928	-1.5369
WBSCR27	-0.8600	-0.7747	0.2260	-0.5865	-0.6011	-1.2525
PFAS	-0.8625	-0.4738	-0.1177	-0.6280	-0.7081	-0.6897
SHMT2	-0.8627	-0.5960	-0.0548	-0.5624	-0.6982	-0.7474
PRC1	-0.8633	-0.5860	-0.1135	-0.4358	-0.9190	-0.6897
GRN	-0.8641	-0.5840	0.0180	-0.6108	-0.7315	-0.9017
FAM117B	-0.8648	-1.0298	-0.1204	-0.8216	-0.6042	-1.1627
MYBBP1A	-0.8654	-0.2435	-0.1473	-0.4078	-0.4673	-0.2847
BCL11A	-0.8659	-0.3993	-0.2675	-0.5558	-0.8812	-0.8386
CTB-41I6.2	-0.8660	-0.5527	-0.1325	-0.5954	-0.6666	-1.0982
GTF2IRD2	-0.8667	-0.5681	0.1498	-0.2466	-0.3846	-0.6776
TYSND1	-0.8675	-0.7462	-0.0986	-0.6797	-0.7532	-0.8186
DUSP28	-0.8677	-0.4660	-0.1609	-0.7588	-0.6879	-0.6784
PLD6	-0.8678	-0.3356	-0.0470	-0.2782	-0.7630	-0.9018
TBC1D8	-0.8685	-0.7819	-0.3889	-0.6058	-0.5468	-0.8451
ACVR2A	-0.8692	-0.4546	-0.0241	-0.3549	-0.4994	-0.5261
PEAK1	-0.8693	-0.7685	0.0841	-0.5110	-0.6998	-1.1437
WDR27	-0.8703	-0.8303	-0.2660	-0.6975	-0.7529	-1.0750
CYP2U1	-0.8711	-0.7926	0.1034	-0.5200	-1.0505	-0.9014
ENOSF1	-0.8728	-0.5170	0.1067	-0.3768	-0.6797	-0.9927
ATF3	-0.8754	-1.0840	-0.4833	-1.1020	-0.4946	-0.5655
RUNX3	-0.8760	-0.5070	0.0133	-0.6553	-0.7164	-0.7595
CCDC125	-0.8775	-0.5562	-0.2990	-0.6826	-0.7011	-0.7713
SLC1A4	-0.8775	-0.5475	-0.4657	-0.7243	-0.8994	-0.8471
ZNF137P	-0.8782	-0.1179	0.0245	-0.3496	-0.3563	-0.6427
DHX57	-0.8821	-0.5545	-0.0453	-0.5162	-0.8570	-0.7807
ZNF490	-0.8830	-0.5943	-0.2132	-0.5248	-0.2714	-0.8462
CD6	-0.8837	-0.7110	-0.4019	-0.2740	-0.1680	-0.4783
DCBLD1	-0.8879	-0.8121	-0.1196	-0.5318	-0.8945	-1.0818
PSPH	-0.8887	-0.6592	0.0940	-0.3214	-0.3860	-0.6860
RP11-849H4.2	-0.8889	-0.8986	-0.1141	-0.2499	-0.4910	-1.0304
RNF166	-0.8892	-0.4839	-0.0973	-0.4883	-0.5767	-0.8470
CPED1	-0.8928	-0.7372	0.0870	-0.4801	-0.6976	-0.8626
RP11-62J1.3	-0.8928	-0.1185	-0.0579	-0.8858	-0.4726	-0.0360
MICAL1	-0.8972	-0.5271	0.0843	-0.5657	-0.8136	-1.2612
MYH7B	-0.8973	-0.4276	-0.0448	-0.8673	-0.9288	-1.0589
SVIP	-0.9002	-0.6007	0.1699	-0.7769	-0.8385	-0.9410
CTC-524C5.2	-0.9014	-0.4113	-0.0095	-0.4442	-0.3955	-1.0657

PDLIM1	-0.9034	-0.3411	1.2051	0.4751	-0.9465	-0.2938
WDR92	-0.9047	-0.0840	0.4898	0.0433	-0.1797	-0.0886
ZZZ3	-0.9053	-0.6642	-0.0871	-0.6746	-0.7640	-0.8995
TMEM201	-0.9055	-0.5997	-0.1037	-0.4724	-0.5242	-0.3911
DDHD1	-0.9059	-0.6875	0.1313	-0.4445	-0.6948	-0.8590
ADAM1A	-0.9092	-0.4768	-0.1522	-0.8940	-0.7757	-0.8303
FSCN1	-0.9097	-0.0702	0.1245	-0.3895	-0.4636	-0.1197
AGAP8	-0.9113	-0.3953	0.2483	0.0083	-0.1548	-0.8608
FAM217B	-0.9123	-0.7414	-0.0665	-0.4712	-0.7899	-0.8985
SMIM4	-0.9160	-0.4011	0.1167	-0.4247	-0.7311	-0.8097
GAS5	-0.9166	-0.6127	0.1143	-0.5377	-0.5144	-0.6796
YJEFN3	-0.9172	-0.6084	-0.0345	-0.1617	-1.0496	-1.1037
COQ4	-0.9172	-0.4649	0.0107	-0.4888	-0.5809	-0.7042
ZNF10	-0.9183	-0.6827	0.1030	0.1075	-0.7371	-0.8847
HSD17B14	-0.9184	-0.4816	0.2748	-0.2097	-0.4772	-0.6079
GABPB1-AS1	-0.9200	-0.5273	-0.4210	-0.4828	-0.7365	-1.1969
ATP2A3	-0.9202	-0.8583	-0.1504	-0.8770	-0.8645	-1.2377
PLCD4	-0.9205	-0.0865	0.1948	-0.1399	-0.4996	-0.4889
NT5DC1	-0.9207	-0.8038	0.1320	-0.4577	-0.7298	-1.1838
MICALL2	-0.9217	-0.6972	-0.2786	-0.6154	-0.6791	-1.3453
GINS1	-0.9219	-0.0592	0.1273	-0.3627	-0.7652	-0.9611
RP5-864K19.4	-0.9221	-0.5963	-0.2058	-0.6307	-0.8616	-1.5992
MARVELD1	-0.9222	-0.6100	0.0071	-0.6945	-0.8134	-1.1734
DAK	-0.9244	-0.6278	-0.0947	-0.6614	-0.8383	-0.9896
NMNAT3	-0.9250	-0.7587	0.1995	-0.5728	-0.3113	-0.5100
TRGV5	-0.9259	-0.8986	-0.0601	-0.9547	-1.0995	-0.2426
FNDC3A	-0.9275	-0.8510	-0.0304	-0.6546	-0.8044	-1.0219
REPIN1	-0.9282	-0.6324	-0.0598	-0.5814	-0.6726	-0.8578
RBM38	-0.9285	-0.4963	-0.1353	-0.6313	-0.8778	-0.6863
C18orf32	-0.9296	-0.1464	-0.3007	-0.3730	-0.5374	-0.2522
PDXP	-0.9298	-0.7199	-0.7338	-1.1719	-0.7594	-0.5235
ZNF600	-0.9302	-0.4331	0.0738	-0.3920	-0.8562	-0.8658
TTC7A	-0.9309	-0.7083	0.0574	-0.7133	-0.9198	-1.1959
UBAP1L	-0.9312	-0.7443	-0.0425	-0.3674	-0.4417	-1.0783
URB2	-0.9314	-0.3009	-0.0804	-0.4250	-0.4899	-0.1897
CLDN12	-0.9325	-0.9707	-0.4693	-0.5800	-0.6243	-0.9642
PHYH	-0.9325	-0.5339	-0.0715	-0.5408	-0.5328	-0.6386
CDR2	-0.9327	-0.4108	0.0147	-0.2536	-0.6218	-1.0314
CPNE9	-0.9347	-0.1771	0.4502	-0.2728	-0.9504	-1.1556
IQGAP2	-0.9359	-0.6041	0.1660	-0.5870	-0.7778	-1.2485
RP11-395P17.3	-0.9368	-0.2732	0.2019	-0.3520	-0.6524	-0.7443
POPDC2	-0.9375	-0.4589	-0.1661	-0.7822	-0.7963	-1.3822
SRSF8	-0.9383	-0.5719	-0.1569	-0.7197	-0.7923	-0.7431

M1AP	-0.9383	-0.6766	0.2493	-0.6689	-0.6906	-1.5790
C14orf79	-0.9384	-0.1897	0.2260	-0.2510	-0.5422	-0.4495
MCM2	-0.9407	-0.4662	0.1021	-0.4952	-0.5356	-0.7111
RP11-403I13.8	-0.9425	-0.6020	0.1206	-0.2151	-0.6595	-0.4505
LRRC8D	-0.9434	-0.6956	-0.0144	-0.6157	-0.6829	-0.8427
RPS6KA5	-0.9445	-0.5895	-0.0843	-0.7791	-0.3179	-0.9541
ATG4C	-0.9445	-0.8977	0.0717	-0.5427	-0.8040	-1.2136
HMGA1	-0.9458	-0.5032	-0.1014	-0.6039	-0.6465	-0.5908
NIT2	-0.9463	-0.3724	-0.0243	-0.3802	-0.6565	-0.6325
TBC1D2	-0.9470	-0.5430	0.0959	-0.6960	-0.8901	-1.5341
DHRS3	-0.9471	-0.7120	0.0734	-0.5174	-0.7299	-1.2982
RP11-264B17.4	-0.9491	-0.9367	-0.6122	-1.5366	-1.4396	-1.6034
ATG16L2	-0.9498	-1.0100	-0.0987	-0.8215	-0.9189	-1.3935
SNHG8	-0.9507	-0.6046	-0.2599	-0.7007	-0.7543	-0.6563
UBXN11	-0.9524	-0.6873	-0.0427	-0.4771	-0.8580	-1.1769
MMP19	-0.9531	-1.1018	0.0675	-0.5328	-0.7308	-1.1716
ZNF296	-0.9533	-0.2211	-0.0728	-0.6908	-0.8703	-0.7797
BTN3A2	-0.9536	-0.8079	0.2094	-0.4475	-0.7661	-1.2367
NHSL1	-0.9540	-0.2115	0.0951	-0.0706	-0.4446	-0.4757
SH3BP5-AS1	-0.9553	-0.8024	0.1501	-0.4964	-0.8741	-1.1654
NCF2	-0.9560	-0.6622	0.0702	-0.6558	-0.9348	-1.2765
TSPAN4	-0.9560	-0.4617	0.0914	-0.5240	-0.7556	-1.1113
TTYH2	-0.9564	-0.8567	-0.1655	-0.9203	-0.9444	-1.3242
PNPLA7	-0.9565	-0.5974	0.2587	-0.7355	-0.8722	-1.6610
OSGIN1	-0.9597	-0.2353	0.1655	-0.0361	-0.5099	-0.6327
PRPF40B	-0.9602	-0.3884	0.2014	-0.4306	-0.5254	-0.5104
ACVRL1	-0.9602	-0.5509	0.1947	-0.4236	-0.6576	-0.3238
GPR35	-0.9632	-0.4267	-0.4362	-0.8506	-0.7673	-0.7244
SNRPEP4	-0.9636	-0.1826	0.1306	-0.0563	-0.0567	-0.6097
PFKM	-0.9653	-0.6475	0.0342	-0.5332	-0.7532	-0.9276
COQ10A	-0.9654	-0.8604	-0.1990	-0.7277	-1.0160	-1.6569
RP11-10K16.1	-0.9664	-0.7544	-0.2010	-0.5426	-0.5317	-1.1940
RP11-390P2.4	-0.9664	-0.3185	0.0764	-0.3643	-0.3224	-0.4621
PRR22	-0.9685	-0.6697	-0.1022	-0.4643	-1.0043	-0.7874
KLHDC8B	-0.9697	-0.6224	-0.0201	-0.7115	-0.9503	-1.5731
SMYD3	-0.9717	-0.4022	-0.0520	-0.5886	-0.4654	-0.4631
CTD-2373H9.6	-0.9722	-0.8754	-0.6919	-1.6902	-0.9181	-1.5389
TRGV4	-0.9726	-0.4827	0.3126	-0.3616	-0.7394	-0.5872
IVD	-0.9742	-0.8389	-0.1336	-0.7924	-0.9488	-0.9818
CENPP	-0.9751	-0.2626	-0.0483	-0.2664	-0.4641	-0.7129
SAMD3	-0.9758	-0.9985	-0.4727	-1.0592	-0.8833	-0.6334
RP11-496I9.1	-0.9770	-0.7234	-0.2917	-0.4860	-1.1132	-1.0794
MITF	-0.9787	-0.8915	-0.0528	-0.6057	-0.6591	-1.1653

SPR	-0.9789	-0.6692	0.2426	-0.3034	-0.4844	-0.9554
CTD-2337J16.1	-0.9801	-0.5268	0.4632	0.0122	-0.3189	-0.6027
TMEM104	-0.9811	-0.3296	-0.0396	-0.5024	-0.6778	-0.7736
RP11-350G8.5	-0.9821	-0.4998	0.3509	-0.5514	-0.8966	-1.4222
TRIM16L	-0.9823	-0.9440	0.1591	-0.5007	-0.5614	-0.9872
PLA2G7	-0.9840	-0.7011	-0.0339	-0.5003	-0.8536	-1.2435
EID2B	-0.9841	-0.5363	0.1117	-0.3777	-0.4005	-0.4102
MOK	-0.9843	-1.0415	-0.1176	-0.7609	-0.5645	-0.7790
GSTP1	-0.9844	-0.6926	0.1057	-0.5873	-0.8782	-1.0845
ZNF404	-0.9852	-0.6660	0.2250	-0.7045	-0.5492	-1.4001
DDX47	-0.9858	-1.0257	0.0262	-0.4752	-0.9840	-1.0761
THEM4	-0.9887	-0.4396	-0.0937	-0.3881	-0.7462	-0.8114
AHRR	-0.9898	-0.7304	-0.0929	-0.5773	-0.8913	-1.1129
LRRC37A4P	-0.9899	-0.8934	-0.3421	-0.7867	-0.8016	-0.9287
MAP4K1	-0.9917	-0.5855	-0.0352	-0.6055	-0.7567	-1.1117
SFXN4	-0.9937	-0.7129	-0.1349	-0.5669	-0.6749	-0.8920
FXYD5	-0.9939	-0.5566	0.1058	-0.5677	-0.8265	-0.9486
CDC42EP3	-0.9940	-0.6093	-0.0034	-0.6210	-0.8563	-1.0307
KAT2A	-0.9954	-0.6638	0.0148	-0.6494	-0.8661	-1.2311
AKAP1	-0.9959	-0.6331	-0.1529	-0.6357	-0.7204	-0.8556
FBXO36	-0.9967	0.5311	-0.0123	-0.3698	-0.2931	-0.0662
ABCA5	-0.9968	-0.5279	0.1936	-0.3797	-0.5454	-1.3049
TUBE1	-1.0009	-0.6274	-0.1058	-0.4013	-0.7855	-0.5990
XRCC6BP1	-1.0020	-1.0522	-0.1639	-0.6874	-0.8108	-1.3798
GADD45A	-1.0022	-0.8308	0.1232	-0.6697	-0.9718	-1.2107
AC005082.12	-1.0023	-0.4478	0.0816	-0.4780	-0.4411	-0.9010
OXER1	-1.0024	-0.7284	0.1855	-0.3138	-0.7656	-1.3304
DTX4	-1.0039	-1.1531	-0.3664	-1.1996	-1.2273	-1.3223
TYW1B	-1.0046	-0.4067	-0.5246	-0.9712	-0.8336	-0.7782
ZHX3	-1.0076	-0.5234	-0.0757	-0.5643	-0.8385	-0.7977
THG1L	-1.0082	-0.8710	-0.0585	-0.6153	-0.5893	-0.6432
ADCK1	-1.0085	-0.6295	-0.0526	-0.5893	-0.7306	-0.9106
LA16c-390E6.4	-1.0097	-0.6796	-0.2057	-0.4482	-0.8234	-1.8323
ALKBH2	-1.0119	-0.2124	-0.1244	-0.3606	-0.3986	-0.1866
TRIM59	-1.0128	-0.6301	0.3694	-0.3759	-0.4222	-0.5803
PABPC4	-1.0139	-0.7908	-0.0918	-0.8561	-0.8797	-1.1434
CCL4L2	-1.0165	-1.8241	-0.0171	-0.3809	-0.7773	-1.6306
C9orf41	-1.0169	-0.7989	-0.0664	-0.4373	-0.3841	-0.5234
AMICA1	-1.0185	-0.8850	0.0692	-0.7937	-1.0147	-1.6551
NFE2L3	-1.0198	-0.9848	0.2170	-0.3537	-0.5471	-0.6934
EPDR1	-1.0212	-0.7480	0.4211	-0.2291	-0.4448	-1.0474
EVL	-1.0224	-1.0599	-0.4674	-1.0264	-0.8952	-1.3231
ST7	-1.0232	-0.6497	0.1070	-0.5466	-0.6163	-0.7544

DPH1	-1.0242	-0.8383	-0.1754	-0.6634	-1.0225	-0.8603
EPB41L4A-AS1	-1.0248	-0.8453	0.1528	-0.7350	-0.9710	-1.0305
TIPARP	-1.0254	-0.7154	-0.3110	-0.8649	-0.9873	-0.9566
FAM69A	-1.0255	-1.0020	0.1805	-0.7506	-1.0808	-1.3223
SRSF7	-1.0270	-0.6192	0.0167	-0.5440	-0.8664	-0.9781
CD109	-1.0272	-1.9329	-0.3462	-1.1237	-1.0755	-1.9060
TMEM71	-1.0280	-0.9869	0.2393	-0.8567	-0.9376	-1.2193
KNSTRN	-1.0283	-0.4659	0.0377	-0.5376	-0.5719	-0.8537
URB1	-1.0293	-0.6280	-0.1020	-0.8295	-0.9964	-0.6166
RAB37	-1.0296	-1.3742	0.0217	-1.0683	-1.2545	-1.9819
MARS2	-1.0307	-0.3410	0.2271	-0.2408	-0.0806	-0.5266
MUSTN1	-1.0309	-1.3593	-0.4181	-1.3056	-0.6285	-1.5760
PKD1P1	-1.0309	-0.6480	1.2728	-0.9912	-0.7309	0.4352
NLRP1	-1.0310	-0.9888	-0.0117	-0.9789	-0.9434	-1.4916
FUCA1	-1.0329	-0.4567	0.0489	-0.5640	-0.8960	-1.2234
RP11-66N11.8	-1.0352	-0.1027	-0.0797	-0.2917	-0.8957	-1.1562
SLC19A2	-1.0362	-0.6222	-0.2256	-0.6550	-0.9298	-0.9604
HOMER2	-1.0379	-0.7231	-0.0054	-0.3928	-1.0486	-1.0033
RRP7B	-1.0382	-0.5003	-0.2864	-0.4252	-0.8312	-0.6504
TMEM120B	-1.0387	-0.7313	-0.2153	-0.6018	-0.8149	-1.0543
EPM2A	-1.0393	-0.5772	-0.1791	-0.5017	-0.6370	-0.6433
GATM	-1.0409	-0.6872	-0.1003	-0.7765	-0.9738	-1.1171
RP11-626A5.2	-1.0413	-0.4471	-0.2449	-1.5939	-0.9691	-1.7445
LFNG	-1.0427	-0.5522	-0.0686	-0.8511	-0.8111	-0.8615
CD82	-1.0429	-1.0058	-0.5605	-1.1722	-1.0036	-0.8967
MGLL	-1.0429	-0.4568	0.0608	-0.3691	-0.7977	-0.9360
PYROXD2	-1.0434	-0.6170	0.1406	-0.5612	-0.9741	-1.1875
CCNB1	-1.0443	-0.6589	0.0556	-0.7037	-1.2302	-1.0855
GOLPH3L	-1.0453	-1.0688	0.0246	-0.7352	-0.7400	-1.4614
SLC12A2	-1.0462	-0.6282	0.1137	-0.4113	-0.6468	-0.2722
CSTA	-1.0472	-0.6975	0.1988	-0.4946	-0.8413	-1.1323
AC026740.1	-1.0473	-0.0246	0.1032	-0.3295	-0.4965	-0.9931
WLS	-1.0490	-0.6425	0.1093	-0.6639	-0.7873	-1.0984
CCDC34	-1.0491	-0.9990	0.1056	-0.6828	-1.4723	-2.0351
IRF5	-1.0505	-0.4953	0.0423	-0.5819	-0.9015	-1.0769
ZRANB3	-1.0519	-0.5267	0.0259	-0.9711	-0.5382	-1.1079
XYLB	-1.0522	-0.8681	-0.3179	-1.1909	-0.6798	-0.8167
ARRDC5	-1.0542	-0.6928	-0.0393	-0.6514	-0.8645	-1.3019
RNF144A	-1.0558	-0.8845	0.2532	-0.4722	-0.8876	-0.8650
AC010980.2	-1.0573	-0.5924	0.2295	-0.2198	-0.6745	-1.4435
NBPF11	-1.0594	-0.7795	0.1450	-0.5083	-1.1033	-0.9809
CLYBL	-1.0617	-0.9425	0.1293	-0.8474	-1.1554	-1.3768
FECH	-1.0631	-0.5442	-0.1164	-0.5521	-0.8468	-0.8949

RGCC	-1.0644	-0.7305	-0.6794	-1.1771	-0.7270	-1.0210
WDR52	-1.0657	-0.9593	0.1305	-0.4947	-1.0291	-1.5095
HEXA	-1.0667	-0.6672	0.0449	-0.6893	-0.8882	-1.1071
BUB1	-1.0676	-0.6904	-0.0387	-1.1147	-0.9469	-1.1409
ARHGAP10	-1.0681	-0.8423	-0.1012	-0.6396	-0.8815	-1.2630
FGL2	-1.0683	-0.8579	-0.1987	-0.8234	-0.9554	-0.9027
RP11-229P13.20	-1.0684	-0.8309	0.2475	-0.2421	-0.7191	-1.5282
SMAD3	-1.0694	-0.9795	-0.4849	-1.1015	-1.1225	-0.4162
HCST	-1.0699	-0.9223	-0.0740	-0.8334	-1.0400	-1.1743
LINC00865	-1.0701	-0.7295	0.1475	-0.3170	-0.1764	-1.1111
PLAU	-1.0722	-0.5110	0.1059	-0.4585	-1.0185	-1.4468
ZNF607	-1.0737	-0.3158	-0.0982	-0.3742	-0.4389	-0.4571
NOB1	-1.0740	-0.7225	-0.2016	-0.6738	-0.7594	-0.6335
RPH3AL	-1.0746	-0.3379	-0.4221	-0.6825	-0.6525	-0.7050
CEBPA	-1.0749	-0.4690	-0.4501	-1.2437	-0.6382	-0.6324
ZNF132	-1.0757	-0.7045	-0.4763	-1.1427	-0.5180	-0.8212
VWF	-1.0762	-0.9204	-0.3672	-1.1550	-0.8079	-1.4205
MUC20	-1.0768	-0.8482	0.1109	-0.3981	-0.9483	-1.0160
RAB40B	-1.0780	-0.5051	-0.0570	-0.2669	-0.9680	-0.9023
SLC16A1	-1.0794	-0.6097	-0.1806	-0.5339	-0.7485	-0.6414
RP11-474P12.5	-1.0812	-0.3906	0.3366	-0.0977	-0.0763	-0.0159
EXOSC5	-1.0827	-0.8125	-0.1150	-0.7508	-1.0622	-1.0608
CTD-2020K17.1	-1.0831	-1.0421	0.0327	-0.7366	-0.9907	-1.3848
RRS1	-1.0859	-0.0758	-0.3635	-0.3367	-0.4042	-0.1224
GCLC	-1.0871	-0.8455	-0.2451	-0.8398	-0.9123	-1.1922
LGALS3	-1.0883	-0.6039	-0.0355	-0.6081	-0.9477	-1.1718
DDX10	-1.0889	-0.7581	-0.1651	-0.5337	-0.6340	-0.5839
SLC25A5-AS1	-1.0928	-0.4598	0.0064	-0.5779	-0.5537	-0.8363
ICAM3	-1.0933	-0.8572	-0.3362	-0.9100	-1.1093	-1.1863
RP11-793H13.11	-1.0939	-0.2693	-0.4291	-0.8845	-0.6866	-1.1232
PTCH2	-1.0941	-1.0835	-0.1369	-0.3641	-0.7873	-1.7945
RRN3P1	-1.0950	-0.6053	0.2219	-0.4778	-0.8541	-1.3219
EIF4EBP3	-1.0965	-1.2363	-0.3943	-1.1696	-1.0115	-1.5582
MAFF	-1.0975	-1.1054	-0.2668	-0.9433	-0.7475	-0.7117
PPFIBP2	-1.0985	-0.8362	-0.1287	-0.7902	-0.8805	-1.1366
CYB5RL	-1.1018	-0.5782	-0.0970	-0.6099	-0.7612	-0.8946
RP11-443P15.2	-1.1057	-0.8795	0.3714	-0.2683	-0.8211	-1.1127
TEX2	-1.1074	-0.8431	-0.1032	-0.6300	-0.8532	-1.1862
LA16c-316G12.2	-1.1085	0.1748	1.2074	0.2675	0.6367	-0.1831
CTD-2228K2.7	-1.1106	-1.1068	-0.1532	-0.5097	-0.9805	-1.1942
OSBPL1A	-1.1112	-0.7472	0.0450	-0.4962	-0.8573	-1.2521
SERPINF2	-1.1143	-1.0227	-0.0934	-1.0810	-1.2343	-1.7480
RGS12	-1.1154	-0.7775	-0.1105	-0.7183	-0.8572	-1.4652

LDHD	-1.1159	-0.6455	-0.1852	-0.8340	-1.0179	-0.9722
TNFSF8	-1.1195	-0.8392	0.1337	-0.5358	-0.6477	-1.0209
ADAT2	-1.1205	-0.3202	-0.2173	-0.3495	-1.1402	-0.8272
GM2A	-1.1208	-0.7748	-0.0503	-0.8233	-1.0680	-1.4199
IL11RA	-1.1222	-0.8210	0.0295	-0.4964	-0.7361	-1.3011
IL18	-1.1234	-0.7316	0.0931	-0.2864	-0.8392	-1.2476
RRN3P2	-1.1256	-0.8119	-0.2955	-0.8978	-0.8134	-1.3189
AC093627.10	-1.1257	-1.1422	-0.2173	-1.1399	-1.2254	-1.4835
RP11-329L6.1	-1.1270	-0.5643	-0.0677	-0.1783	-0.7031	-0.6278
PRKXP1	-1.1270	-0.5672	-0.2609	-1.0961	-1.1105	-0.9026
COX7A1	-1.1304	0.0028	-0.4003	0.0412	-0.0355	-0.9659
MTAP	-1.1316	-0.8207	-0.0583	-0.7556	-0.9261	-1.0307
NUSAP1	-1.1336	-0.6807	0.2620	-0.6619	-1.1593	-1.6315
MYH3	-1.1348	-0.6128	0.2726	-0.4470	-0.7441	-0.9938
GRAMD4	-1.1353	-0.7605	0.0898	-0.6707	-0.9211	-1.5493
CHCHD6	-1.1364	-0.9132	0.0442	-0.9105	-1.1298	-1.4065
MORN1	-1.1378	-1.3917	0.4651	-0.6838	-0.0933	-1.2437
RP11-111M22.3	-1.1379	-0.5461	-0.1894	-0.7835	-0.7397	-1.5389
CTD-2086O20.3	-1.1390	-0.2724	-0.2299	-0.6799	-0.5494	-0.5871
AEN	-1.1408	-0.5926	-0.1562	-0.5606	-0.5280	-0.1778
RDH13	-1.1411	-0.7503	-0.3170	-0.6451	-0.6630	-0.9732
FANCA	-1.1411	-0.7725	0.2782	-0.4903	-0.9222	-1.1178
CDK14	-1.1428	-1.4766	-0.6488	-1.0921	-0.8439	-0.8193
FABP4	-1.1440	-1.4513	-1.1015	-1.2328	-0.2173	-1.5217
CENPF	-1.1445	-1.1224	0.5193	-0.4904	-1.6098	-1.0745
CTD-2002H8.2	-1.1462	-0.4183	0.0652	-0.6056	-0.9487	-1.0818
TVP23A	-1.1466	-0.4804	-0.0392	-0.0581	-1.3783	-0.6003
CHCHD10	-1.1510	-0.5905	-0.1637	-0.8593	-0.8750	-0.9252
ACSS1	-1.1518	-0.9484	-0.0441	-0.7657	-0.9334	-1.1217
CHIT1	-1.1537	-1.6467	-1.2316	-1.5843	-1.4921	-1.5995
CTC-203F4.1	-1.1545	-0.6889	1.0393	0.2050	-1.0713	-0.9939
SNAI3	-1.1551	-0.8309	-0.0768	-0.8605	-0.8872	-1.0168
CCNB1IP1	-1.1553	-0.8354	-0.2648	-0.7597	-0.9781	-1.1117
TOB1-AS1	-1.1564	-1.7200	0.0725	-1.1699	-1.2522	-1.3806
ARL5C	-1.1578	-0.1623	0.4678	-0.7778	-0.3631	-1.9242
KB-431C1.3	-1.1596	-1.6272	-0.6746	-1.1692	-2.0286	-2.5850
AF127936.5	-1.1596	-0.6903	0.0765	-0.6310	-0.8250	-0.9366
SIGLEC14	-1.1602	-0.5146	0.0432	-0.5634	-0.8118	-1.0545
CHST13	-1.1649	-0.7365	-0.1255	-1.0279	-1.0371	-1.4045
CDKN2B	-1.1655	-0.6815	-0.6107	-0.4833	-0.3959	-0.4970
RP11-488C13.5	-1.1675	-0.6882	0.0927	-0.7461	-0.8511	-1.0883
MREG	-1.1681	-0.8886	-0.8061	-1.1783	-0.5205	-1.3528
PPFIBP1	-1.1684	-1.0539	-0.5974	-1.1661	-1.2771	-1.2826

RP11-107F6.3	-1.1690	-1.2196	-0.5805	-0.5841	-0.9652	-1.7990
TRIM6	-1.1700	-0.6471	-0.2945	-0.4820	-0.6079	-0.9300
RPS6KA2	-1.1723	-0.8792	-0.0380	-0.9652	-1.1813	-1.7245
TIGD2	-1.1739	-0.8194	-0.1486	-0.3793	-0.4764	-0.7470
ASCL2	-1.1739	-0.6465	0.1119	-0.7136	-0.7578	-1.1507
RP11-108P20.1	-1.1739	-0.6371	-0.2904	-0.3907	-0.7483	-0.6274
CTD-2639E6.9	-1.1739	-0.1580	0.2939	-0.7730	-0.3455	-0.7624
LONRF3	-1.1758	-0.3370	-0.2539	-0.4872	-0.9240	-1.0858
MAD2L1	-1.1769	-0.4640	-0.0049	-0.5172	-1.1809	-1.0946
KCNAB2	-1.1772	-0.7229	-0.0823	-0.8140	-1.0544	-1.5115
ARSG	-1.1779	-0.7663	-0.1646	-0.8622	-1.2231	-1.1475
CXorf24	-1.1806	-0.6333	0.1566	-0.4924	-0.4967	-0.5024
CD9	-1.1809	-0.9803	-0.0137	-0.9485	-1.0881	-1.7153
NCF1	-1.1814	-0.9212	0.1682	-0.7722	-0.9893	-1.5022
LSR	-1.1821	-0.8612	-0.4171	-0.8938	-1.0258	-1.5756
ZNF74	-1.1831	-0.8330	-0.2037	-0.7646	-0.8394	-1.5349
IRF2BP2	-1.1851	-0.8724	0.0441	-0.6579	-0.7906	-1.1687
FAM195A	-1.1859	-0.6690	-0.2024	-0.8183	-1.0063	-0.9723
SFMBT2	-1.1861	-0.7685	0.0538	-0.3750	-0.7894	-1.0571
NCOA7	-1.1867	-1.0972	0.1040	-0.7884	-0.8994	-1.2469
AC108488.4	-1.1888	-1.0382	-0.2779	-0.7869	-1.2051	-1.1255
NPM1P25	-1.1907	-0.7910	-0.1820	-0.4470	-1.0407	-1.1424
GALNT3	-1.1910	-0.9426	-0.0853	-0.8838	-1.5145	-1.5303
ADAL	-1.1924	-0.5509	-0.1229	-0.6267	-0.6966	-0.6308
CERS4	-1.1940	-0.8984	0.0150	-0.6968	-0.9257	-1.0678
CAPG	-1.1959	-0.7516	0.0287	-0.7178	-1.1523	-1.4100
TMEM48	-1.1964	-0.8901	-0.0504	-0.6967	-0.7932	-0.7268
AC079250.1	-1.2000	-0.1538	0.2945	-0.2102	-0.1684	-1.0814
DHODH	-1.2005	-0.6880	-0.1410	-0.5799	-0.8643	-0.9509
RP4-800G7.2	-1.2024	-0.9218	0.0097	-0.5441	-0.9369	-0.9865
COL23A1	-1.2052	-1.0448	-0.0869	-1.3571	-1.5437	-1.9048
TRAF5	-1.2064	-0.6508	-0.2181	-0.8069	-1.1020	-1.2572
SETD6	-1.2080	-0.8654	-0.4573	-0.8840	-1.0948	-1.4117
RHOBTB1	-1.2110	-0.8391	-0.2256	-0.9064	-0.8496	-0.9654
TMEM220	-1.2128	-0.8705	-0.1563	-0.5956	-1.1734	-1.6414
CC2D2A	-1.2153	-0.3943	0.3945	-0.6662	-1.1829	-1.0850
KIF17	-1.2197	-1.5109	-0.1186	-0.8600	-1.0297	-2.2671
RP11-468E2.9	-1.2222	-1.0830	-0.4124	-0.9196	-0.9848	-1.7383
SOX12	-1.2231	-1.0614	-0.2340	-1.4261	-1.0027	-1.4373
KIF27	-1.2249	-0.4008	-0.4830	-0.9910	-0.7131	-0.9826
LL22NC03-86G7.1	-1.2273	-1.0729	-0.3129	-0.6601	-0.7392	-1.5979
AGPAT5	-1.2296	-0.9794	-0.1808	-0.8504	-1.0171	-1.3153
GNRH1	-1.2302	-0.5686	-0.3676	-0.1162	-0.2971	-0.5582

ANKH	-1.2324	-0.9518	-0.1474	-1.0696	-1.1544	-1.4010
RP11-254F7.2	-1.2368	-0.8320	-0.1956	-0.9257	-1.0736	-1.3315
SNED1	-1.2382	-1.1631	-0.2006	-1.2785	-0.5304	-1.8570
OSBPL7	-1.2383	-0.9110	-0.0670	-0.7699	-1.1440	-1.0814
SLC25A38	-1.2419	-0.8260	-0.0808	-0.6416	-0.8287	-0.9044
CTD-2037K23.2	-1.2440	-0.9310	0.1168	-0.7440	-1.0340	-0.8770
FAAH	-1.2471	-0.8844	-0.1199	-0.6769	-1.0820	-1.0232
SLC9A3	-1.2490	-1.3015	-0.2315	-1.0907	-0.9520	-1.0374
NUP210	-1.2494	-1.0022	-0.3195	-0.9918	-1.2125	-1.5673
SLC25A27	-1.2494	-0.9810	-0.0737	-0.7691	-1.4228	-1.3473
FBP1	-1.2521	-1.5048	-0.6481	-1.2710	-1.0823	-1.4473
CITED4	-1.2525	-0.7184	0.2249	-0.3690	-0.6894	-0.3284
RP11-334C17.5	-1.2535	-1.0327	-0.1699	-0.8644	-1.2672	-1.7808
CTSD	-1.2550	-0.7775	-0.2089	-0.8854	-1.0850	-1.2040
ACACB	-1.2550	-1.2379	-0.2459	-0.9629	-1.1386	-1.8061
CTD-2619J13.8	-1.2562	-1.0066	-0.0651	-0.9391	-1.1688	-1.2314
RP5-1103G7.4	-1.2572	-0.9227	-0.1525	-1.0951	-1.0935	-0.8199
NR4A1	-1.2586	-1.2313	-0.1757	-0.8557	-0.4701	-0.9804
RAB11FIP4	-1.2592	-1.3751	-0.6397	-1.2250	-0.8055	-1.3833
COLQ	-1.2634	-1.4009	-0.5600	-1.0213	-1.2137	-2.5285
GPR82	-1.2658	-1.3632	-0.1707	-1.2322	-1.6054	-2.5851
CARD14	-1.2668	-1.0094	-0.2901	-1.6149	-1.6986	-2.0444
EREG	-1.2750	-3.3626	0.3865	-1.4131	-0.8937	-2.0653
RP11-368P15.3	-1.2764	-0.9413	0.0184	-0.4716	-1.0134	-1.6005
EME1	-1.2773	-0.3971	0.3330	-0.8538	-1.0016	-0.8384
FARP1	-1.2785	-1.0345	0.1909	-0.7087	-1.0602	-1.1146
BACE1	-1.2812	-1.1459	-0.3421	-0.8508	-1.1278	-1.3445
CDIP1	-1.2818	-0.9810	-0.2046	-1.0820	-1.0493	-1.1907
NCF1B	-1.2865	-1.0525	0.1706	-0.8757	-1.0765	-1.6185
IL18BP	-1.2883	-0.7193	-0.1824	-0.7370	-1.2108	-1.4776
C3orf18	-1.2909	-1.0906	-0.4669	-0.9967	-1.3218	-1.7091
C11orf1	-1.2915	-0.6032	-0.3121	-0.7708	-1.0408	-0.6412
C14orf159	-1.2928	-0.9572	0.0545	-0.8469	-1.3245	-1.7032
CCL22	-1.2932	-1.8220	-0.4359	-0.8071	-0.8785	-1.9108
AL592284.1	-1.2935	-1.0365	0.1282	-0.5174	-0.5125	-1.1093
RASL10A	-1.2946	-0.7737	-0.2817	-0.9918	-0.9352	-1.2078
GFOD1	-1.2966	-0.5673	-0.0026	-0.7274	-1.3978	-1.1003
ECE2	-1.2980	-0.3407	0.3343	-0.3318	-0.6004	-0.4723
DDO	-1.2995	-0.8193	0.0837	-0.3037	-0.6221	-0.9084
IRF4	-1.3005	-0.6771	-0.0529	-0.8147	-0.9858	-1.1881
RP11-430C7.5	-1.3049	-0.9587	-0.0951	-0.8532	-1.1323	-1.3828
SLC26A11	-1.3114	-0.9628	-0.3922	-1.0213	-1.2182	-1.4688
CLEC18B	-1.3123	-0.5711	-0.4054	-0.6495	-1.2529	-0.9969

FAH	-1.3124	-0.6569	-0.0135	-0.6216	-1.1904	-1.2967
OAF	-1.3155	-1.1020	-0.0605	-0.8948	-1.1544	-1.4206
SLC29A3	-1.3171	-0.9611	-0.3825	-0.9937	-1.0824	-1.2669
CD244	-1.3222	-1.2391	-0.3791	-0.9619	-1.5408	-1.5213
AC004840.9	-1.3223	-0.9288	-0.5478	-0.8975	-1.3360	-1.3978
RP11-472N13.3	-1.3260	-1.0185	0.2123	-0.9672	-1.5189	-2.4734
SAMD4A	-1.3287	-0.6296	-0.0326	-0.6876	-0.7550	-0.8187
RP11-196G11.2	-1.3332	-0.7308	-0.0074	-0.4824	-0.6136	-1.1249
DNAJC5B	-1.3341	-2.2156	-0.0719	-1.3027	-1.4644	-2.6696
RP3-395M20.8	-1.3355	-1.2669	-0.2547	-1.0641	-1.3013	-1.9940
IFITM10	-1.3389	-0.7630	-0.1017	-0.9829	-1.0359	-1.5196
CTC-471J1.2	-1.3431	-0.0383	0.3155	-0.5209	-0.3739	-0.2836
ABCC3	-1.3458	-1.1971	0.0802	-0.7840	-1.0184	-1.8510
SLC9A7	-1.3491	-1.5534	-0.6699	-1.2266	-1.5821	-1.8906
P2RY8	-1.3494	-1.3028	-0.1437	-0.9673	-1.2284	-1.7281
BAIAP2	-1.3498	-0.9436	-0.1010	-0.9222	-1.0204	-1.6411
TXNRD3	-1.3501	-1.1367	-0.4424	-0.5824	-1.1283	-1.1698
TNFAIP2	-1.3544	-1.0499	0.0625	-0.8368	-1.1299	-1.6275
C10orf128	-1.3550	-0.9855	0.0167	-0.7816	-1.0214	-1.5855
IQCH-AS1	-1.3566	-1.0004	-0.2840	-1.0393	-0.9630	-1.5455
PPM1H	-1.3569	-0.7118	-0.2121	-0.5951	-0.7084	-0.9762
EEPD1	-1.3602	-0.7634	-0.0555	-0.8587	-1.0301	-1.1578
AC068580.5	-1.3635	-1.3303	-1.0995	-0.6498	-1.6304	-1.4987
AP001258.4	-1.3647	-0.6243	-0.1229	-0.8584	-1.5441	-1.3179
TRABD2A	-1.3655	-0.4980	-0.1662	-0.6452	-1.0676	-1.1647
SLC16A6	-1.3682	-0.7781	0.2183	-0.8627	-1.1634	-1.1711
NREP	-1.3682	-0.8349	-0.1704	-0.9980	-1.1488	-1.4961
ALCAM	-1.3722	-1.2712	-0.4354	-0.9672	-1.0680	-1.3983
SOX13	-1.3731	-0.5725	-0.0521	-0.9819	-1.1864	-1.7809
GALM	-1.3741	-0.9551	-0.4495	-1.0523	-1.3211	-1.7426
PDK4	-1.3754	-1.4439	-0.9674	-1.2057	-1.1176	-1.5625
ST6GALNAC2	-1.3775	-1.1851	0.0830	-0.6122	-0.7612	-1.6520
CCL3L1	-1.3783	-1.4288	-0.7007	-0.9268	-0.8879	-1.8228
GRASP	-1.3794	-0.5273	0.0094	-0.6725	-0.5252	-0.8261
NUPR1	-1.3838	-0.9521	0.3108	-0.8068	-1.1687	-1.7988
RP11-278C7.1	-1.3860	-0.3736	0.6556	-0.0218	-0.1651	-0.5214
FAM177B	-1.3862	-1.0749	0.4897	-0.2567	-1.2115	-2.0571
RPL7AP10	-1.3887	-1.1423	-0.1927	-0.7653	-0.4954	-1.0942
SLC17A9	-1.3966	-0.8531	-0.1819	-0.7246	-1.1514	-1.3544
ITGAX	-1.3970	-1.2861	-0.1024	-1.0225	-1.2405	-1.8491
RP11-611D20.2	-1.3973	-0.8452	0.0234	-0.7850	-1.0371	-1.5895
MPZL2	-1.3979	-1.2981	0.0417	-1.2737	-0.9797	-1.3931
CCL24	-1.4038	-2.5567	-0.0011	-1.1482	-1.7693	-2.8008

LRFN4	-1.4049	-0.5184	-0.1188	-0.6978	-1.0629	-1.4185
ZNF704	-1.4084	-1.5405	-0.0071	-1.0321	-1.3653	-2.0493
FXN	-1.4089	-1.0661	-0.3708	-0.7079	-1.1700	-0.7334
PPM1K	-1.4093	-1.5135	-0.1642	-1.2553	-0.8348	-2.1279
CALCRL	-1.4159	-0.9815	0.4115	-0.3190	-0.7648	-0.8196
TMCC3	-1.4197	-1.1796	0.0228	-1.2442	-1.2913	-1.4733
CLEC12A	-1.4207	-1.1539	0.1015	-0.9175	-1.2125	-2.0683
KBTBD11	-1.4214	-0.8464	-0.5010	-1.2102	-1.2251	-1.1150
PDE4DIP	-1.4221	-1.3455	0.0503	-0.8105	-1.3183	-2.0383
AC025335.1	-1.4233	-0.7974	-0.0169	-1.0471	-1.0206	-1.4086
FAM86B3P	-1.4236	-0.4934	-0.4010	-0.9840	-1.1225	-1.0532
SLC7A11	-1.4243	-2.0178	0.2926	-1.0453	-0.8581	-1.9134
RP11-368J21.3	-1.4263	-0.6334	0.2577	-0.6787	-1.0959	-1.6228
APOBR	-1.4263	-0.8428	-0.3162	-1.2077	-1.5762	-1.6062
RP11-213H15.3	-1.4290	-1.1982	0.1778	-0.3135	-0.9167	-1.2437
A2M	-1.4299	-1.8694	-0.3022	-1.4953	-1.3568	-2.3976
C1orf127	-1.4382	-1.2863	0.0917	-0.7628	-1.1507	-1.8305
UBE3D	-1.4384	-1.0957	-0.4935	-1.2459	-1.2492	-0.8880
H2AFY2	-1.4432	-1.2561	-0.3666	-0.9610	-1.5092	-1.3553
DNM1	-1.4453	-0.5158	0.1023	-0.5209	-1.0893	-1.3341
HPSE	-1.4484	-1.0351	-0.0541	-1.0912	-1.3885	-1.9694
CHST7	-1.4496	-1.2106	-0.1476	-0.8202	-1.0102	-1.6489
CD83	-1.4529	-1.3090	-0.5358	-0.9299	-0.9837	-1.1111
ZC3H12C	-1.4540	-1.1970	-0.0751	-0.8504	-1.2702	-1.6544
SEMA4D	-1.4546	-1.0427	-0.1914	-0.9357	-1.1641	-1.3429
RP11-152N13.5	-1.4616	-1.6790	-0.4902	-0.1680	-1.6680	-0.1661
AC074289.1	-1.4752	-0.6106	-0.0578	-1.0050	-1.4068	-1.9657
GPNMB	-1.4754	-1.1398	-0.0913	-1.0904	-1.3566	-1.9231
TAGAP	-1.4778	-0.8771	-0.1300	-0.6292	-1.0717	-1.2520
PUS7	-1.4790	-0.8078	-0.2680	-0.9949	-1.1781	-0.6642
ICOSLG	-1.4810	-0.9770	-0.2569	-0.9739	-1.3588	-1.4907
TNFAIP3	-1.4843	-1.4616	0.0162	-0.6633	-1.0161	-1.5646
C1orf134	-1.4847	-0.3382	-0.0324	-1.0464	-1.1614	-0.8839
CECR1	-1.4874	-1.1753	-0.1158	-1.0330	-1.2949	-1.8279
AC093162.5	-1.4891	-0.2800	-0.0661	-1.1180	-0.9676	-1.3658
MATK	-1.4901	-2.1347	-1.2779	-1.8924	-1.3716	-2.0712
F11R	-1.4931	-1.1816	-0.0924	-0.9752	-1.1897	-1.6616
CCDC88B	-1.4933	-1.2421	-0.5454	-1.0674	-1.2399	-1.3677
KITLG	-1.4940	-1.0291	0.0152	-0.3359	-1.1866	-1.4399
LINC00869	-1.4978	-1.8720	-0.2741	-1.3350	-0.6359	-0.7895
CPAMD8	-1.4997	-1.1799	-0.1201	-1.0227	-1.4391	-1.9114
PMAIP1	-1.5016	-1.1148	-0.6568	-2.0084	-1.7940	-1.6038
GPT2	-1.5052	-0.9303	-0.5251	-1.1850	-0.4647	-1.6414

SSX2IP	-1.5064	-0.5507	-0.2068	-0.6188	-0.8830	-0.9041
NCF1C	-1.5188	-1.2305	0.0379	-0.8387	-1.1491	-1.8077
DIP2C	-1.5241	-1.1364	-0.2645	-1.6149	-0.9336	-2.0765
OTOA	-1.5256	-1.1714	0.0416	-0.8390	-1.3934	-1.6433
HK2	-1.5281	-1.4115	-0.3905	-1.4503	-1.6407	-1.9867
CLEC1B	-1.5286	-0.7999	-0.1460	-1.2430	-1.3425	-1.7904
EXTL2	-1.5337	-1.1346	-0.5072	-1.2870	-1.7443	-2.0236
CRTAM	-1.5363	-1.3397	-0.0571	-1.2493	-1.1847	-2.1868
COL6A1	-1.5461	-1.5868	-0.2915	-1.1542	-1.6677	-1.9727
SH3PXD2A	-1.5471	-1.4909	-0.0767	-1.3107	-1.3880	-2.1147
TARBP1	-1.5475	-1.0728	-0.2485	-0.8392	-1.3859	-1.7308
SPAG8	-1.5520	-1.5587	-0.3121	-1.0303	-1.2805	-1.8888
A2M-AS1	-1.5545	-1.0121	-0.1380	-0.3327	-1.0495	-0.9094
METTL1	-1.5644	-0.6237	-0.5455	-0.8464	-0.8485	-0.8147
SIK1	-1.5691	-1.2097	-0.5482	-0.6614	-1.2002	-1.0629
CCDC88C	-1.5692	-1.3387	-0.2948	-1.0913	-1.2641	-1.8285
FAM46A	-1.5715	-1.4229	-0.2993	-1.2863	-1.3831	-1.8314
AVPI1	-1.5786	-1.2497	-0.3181	-1.3885	-1.4386	-2.3904
RP11-264B17.3	-1.5824	-0.9640	-0.2885	-0.5513	-0.8615	-1.7133
ARHGAP22	-1.5865	-1.2187	-0.1046	-0.9730	-1.3227	-1.8531
ATP8A1	-1.5951	-1.4067	-0.1521	-1.0810	-1.2828	-2.0063
AC093620.5	-1.6045	-0.7214	-0.4802	-0.9718	-0.5340	-0.9189
RP11-212I21.2	-1.6058	-0.9098	-0.5380	-0.4925	-1.1099	-2.0788
CDH23	-1.6058	-1.1674	-0.2503	-1.1730	-1.2087	-1.9909
IL3RA	-1.6089	-2.0289	-0.0080	-1.2487	-1.2092	-1.3946
CD1D	-1.6091	-1.3297	-0.5250	-1.0547	-1.4410	-1.4837
AKR1C3	-1.6094	-1.3555	0.3238	-0.9022	-0.6371	-1.0622
RP11-120K18.3	-1.6118	-1.8682	0.2164	-1.0512	-1.1671	-2.6851
MTMR9LP	-1.6127	-1.5077	-0.0472	-1.1699	-1.6724	-2.2550
C10orf2	-1.6149	-0.4378	-0.3467	-0.7050	-0.7937	-0.1141
PPARGC1B	-1.6150	-1.1013	-0.4706	-1.1106	-1.4131	-1.6861
PHYHD1	-1.6152	-0.4395	0.4766	-0.5580	-0.9563	-1.4956
RNASEH2B-AS1	-1.6165	-0.8225	-0.8246	-0.7881	-1.3919	-1.8634
ZNF589	-1.6279	-1.2809	-0.3993	-1.1899	-1.3908	-1.7866
ZBED3	-1.6361	-0.9645	-0.3333	-1.2902	-1.4852	-1.6352
AP001056.1	-1.6401	-0.9178	0.0060	-1.3513	-1.3408	-1.3314
PDE6G	-1.6409	-0.9430	-0.4698	-1.0191	-1.4695	-1.9299
CABLES1	-1.6460	-1.3164	-0.1420	-0.7530	-1.0606	-1.4515
PIK3C2B	-1.6460	-1.1394	-0.2768	-1.1896	-1.0497	-1.4978
GRAMD1B	-1.6542	-1.3332	-0.0372	-1.0222	-1.2053	-1.8253
AC079767.4	-1.6589	-1.3065	-0.0042	-1.0233	-1.7629	-2.3994
PHLDA3	-1.6628	-2.1532	-0.8497	-1.8251	-1.7367	-1.5704
WNT5B	-1.6640	-1.6868	-0.0272	-0.9347	-1.5714	-2.1539

XYLT1	**-1.6640**	**-1.3131**	**-0.1923**	**-1.2733**	**-1.3295**	**-1.9424**
RASGRP3	**-1.6667**	**-1.3148**	**-0.1490**	**-1.0106**	**-1.4060**	**-2.1731**
RP11-54C4.1	**-1.6711**	**-1.1085**	**0.1118**	**-0.1409**	**-1.5021**	**-1.2255**
PDGFB	**-1.6733**	**-0.7407**	**0.1392**	**-0.9211**	**-1.2328**	**-1.8383**
CTD-2516F10.2	**-1.6733**	**-1.3869**	**-0.5370**	**-1.3933**	**-1.4705**	**-2.2445**
CTSF	**-1.6746**	**-1.9353**	**-0.1364**	**-1.6737**	**-1.2903**	**-2.3698**
CTC-329D1.2	**-1.6771**	**-0.0965**	**-0.3447**	**-0.6413**	**-0.4020**	**-0.8050**
AC006272.2	**-1.6800**	**-1.4537**	**0.0401**	**-0.9372**	**-1.1516**	**-1.1478**
PLA2G16	**-1.6808**	**-1.0945**	**-0.2314**	**-0.6366**	**-0.9272**	**-1.1625**
MYCL1	**-1.6840**	**-1.7164**	**-0.2369**	**-1.1515**	**-1.1895**	**-1.7713**
CTB-31N19.3	**-1.6856**	**-1.4780**	**-0.1159**	**-0.8429**	**-1.8126**	**-2.1001**
APOC1	**-1.6938**	**-2.7498**	**-1.0649**	**-1.9594**	**-1.8460**	**-2.8946**
IGF1	**-1.7126**	**-1.1229**	**0.1421**	**-0.8725**	**-1.4653**	**-2.1272**
DCSTAMP	**-1.7161**	**-2.0377**	**-1.5155**	**-2.3400**	**-1.2238**	**-2.9403**
PIK3R3	**-1.7194**	**-1.1800**	**-0.5156**	**-1.4036**	**-1.4803**	**-1.6060**
JAG1	**-1.7287**	**-0.9401**	**0.0164**	**-1.1789**	**-1.4540**	**-1.8949**
AP000783.1	**-1.7326**	**-0.5843**	**0.2662**	**-0.6480**	**-0.8688**	**-1.2774**
SMPD3	**-1.7391**	**-1.5056**	**-0.3364**	**-1.0569**	**-1.5399**	**-1.7112**
FAIM3	**-1.7414**	**-2.1860**	**-1.2557**	**-1.9233**	**-1.7494**	**-2.3963**
CDK18	**-1.7493**	**-1.6199**	**-0.1168**	**-1.2033**	**-1.3391**	**-1.6731**
Sep-03	**-1.7494**	**-1.5719**	**-0.0195**	**-0.8826**	**-1.1978**	**-2.0272**
SPTBN1	**-1.7512**	**-1.7308**	**-1.0409**	**-1.6384**	**-1.8012**	**-1.6988**
ACP5	**-1.7534**	**-1.6232**	**0.0406**	**-1.2305**	**-1.4462**	**-2.3945**
RP11-471B22.2	**-1.7593**	**-0.5665**	**0.1186**	**-0.1881**	**-0.4893**	**-0.4899**
AP001053.11	**-1.7627**	**-1.5266**	**-0.1491**	**-1.2597**	**-1.6800**	**-2.4762**
QPRT	**-1.7652**	**-1.3534**	**-0.3862**	**-1.2284**	**-1.4382**	**-1.4708**
AP001007.1	**-1.7736**	**-1.2065**	**-0.0337**	**-1.0381**	**-1.5081**	**-2.0220**
RP11-465B22.3	**-1.7764**	**-1.0537**	**0.1226**	**-0.3216**	**-1.0815**	**-2.0462**
SELL	**-1.7900**	**-1.6557**	**-0.1852**	**-1.2929**	**-1.6386**	**-1.8375**
AL353354.1	**-1.7902**	**-0.6839**	**0.2605**	**-0.0793**	**-0.0984**	**0.1013**
RP11-389C8.2	**-1.7917**	**-1.1232**	**-0.6472**	**-0.9709**	**-0.8155**	**-1.0560**
RP11-672A2.6	**-1.7977**	**-0.7559**	**0.4555**	**-1.1910**	**-2.4376**	**-1.0113**
KCNC4	**-1.7984**	**-1.4442**	**-0.2922**	**-0.8220**	**-1.5701**	**-2.0761**
CHST15	**-1.7997**	**-1.1269**	**-0.1549**	**-1.0720**	**-1.6100**	**-1.7917**
TNNI2	**-1.8027**	**-1.4753**	**-0.4566**	**-1.3946**	**-1.6203**	**-2.0397**
AC022007.5	**-1.8119**	**-1.0507**	**-0.1996**	**-1.3898**	**-1.1627**	**-1.1705**
SLC37A2	**-1.8164**	**-1.5334**	**-0.2717**	**-1.3925**	**-1.6464**	**-2.1774**
GYPC	**-1.8177**	**-1.1214**	**-0.1513**	**-0.9436**	**-1.3488**	**-1.7583**
HTRA1	**-1.8194**	**-2.2689**	**-0.1195**	**-1.3758**	**-1.6403**	**-2.0554**
RP11-356N1.2	**-1.8386**	**-0.9756**	**-0.0193**	**-0.5895**	**-1.4297**	**-1.6058**
CD52	**-1.8477**	**-1.6511**	**-1.0093**	**-1.7252**	**-1.3255**	**-2.0261**
ESCO2	**-1.8524**	**-1.1830**	**-0.0551**	**-0.6806**	**-1.5160**	**-2.1446**
KCNAB1	**-1.8576**	**-1.3479**	**-0.0193**	**-0.7136**	**-0.8121**	**-1.2359**

CENPV	-1.8638	-1.0287	-0.1948	-0.1855	-0.6200	-1.0072
JUP	-1.8681	-1.8634	-0.1990	-1.4882	-1.6532	-2.4046
PHACTR1	-1.8902	-1.4848	-0.1607	-0.9293	-1.6116	-2.3472
TNFRSF18	-1.8926	-1.1378	-0.3648	-0.7376	-0.9525	-1.1128
HBEGF	-1.8943	-2.5356	-0.2749	-1.7525	-1.5199	-2.6471
NLE1	-1.9076	-0.7335	-0.6033	-1.3953	-1.0971	-0.8577
HSH2D	-1.9353	-1.6958	-0.1674	-1.4383	-1.6342	-2.1414
MMP2	-1.9445	-1.7336	0.0651	-1.3041	-1.5222	-1.6593
U62631.5	-1.9460	-2.3963	-0.7179	-1.4358	-3.1210	-5.4429
FCN1	-1.9519	-1.5700	-0.1262	-1.2329	-1.8502	-2.4076
SOX4	-1.9641	-1.6948	-0.6093	-1.4775	-1.4311	-2.0945
DNM3	-1.9737	-1.4236	-0.2835	-1.5291	-1.5718	-2.2591
MGST1	-1.9753	-1.5946	-0.2076	-1.1174	-1.2426	-1.9296
PTPN22	-1.9776	-1.7223	-0.1778	-1.5998	-1.7486	-2.5548
TM4SF19	-1.9854	-2.4014	-1.6866	-2.2449	-2.0103	-3.0511
TFAP4	-1.9858	-1.3980	-0.4761	-1.3491	-1.6662	-2.0176
MTSS1L	-1.9889	-1.5257	-0.4164	-1.5231	-1.2776	-1.5135
PYHIN1	-2.0000	-1.5291	0.1618	-1.4258	-1.1399	-2.0428
RASAL1	-2.0004	-2.0981	-0.4983	-1.6658	-1.9433	-3.1476
CMBL	-2.0009	-1.5162	0.4486	-0.8944	-1.2904	-2.1491
NQO1	-2.0066	-1.5108	-0.1342	-1.0301	-1.5903	-1.7638
MMP23A	-2.0086	-5.8826	1.3821	0.6414	0.6415	-1.0272
ADORA2B	-2.0255	-0.8247	-0.3249	-1.2571	-1.2734	-1.8876
GRIP1	-2.0312	-1.5337	-0.0445	-1.1354	-1.6740	-1.9391
ZMIZ1-AS1	-2.0326	-2.6775	-0.5043	-1.7343	-2.2272	-2.7200
ZFP36L2	-2.0371	-1.7525	-0.3107	-1.6487	-1.6648	-2.4112
MARCKSL1	-2.0576	-1.3653	-0.4575	-1.0479	-1.3164	-1.2832
AP001055.6	-2.0684	-1.4222	-0.1864	-1.5972	-1.9359	-2.1900
LSP1	-2.0697	-1.9761	-0.6057	-1.9558	-2.0537	-2.6122
CAMKK1	-2.1018	-1.3557	-0.6533	-1.4878	-1.9825	-1.8155
RGS1	-2.1048	-2.1277	-0.7695	-1.8138	-1.8441	-2.0153
LHFP	-2.1184	-2.2477	-0.9025	-1.4729	-0.7643	-1.3606
NINL	-2.1235	-1.5901	0.2537	-1.1941	-1.5269	-2.7849
METAP1D	-2.1307	-1.0632	-0.4302	-1.2308	-1.2933	-1.2237
GCSAM	-2.1383	-0.9083	-0.4820	-1.7701	-1.6506	-1.9718
SULF2	-2.1414	-1.6080	-0.0936	-1.5486	-2.0161	-3.0181
ITGA11	-2.1549	-1.9527	-0.8161	-1.3800	-2.1702	-2.2488
OASL	-2.1618	-0.4357	0.4407	-0.5716	-1.0594	-1.2843
CTB-179K24.4	-2.1699	-0.8934	-0.4479	-0.7462	-0.9965	-1.3326
NOTCH3	-2.1711	-3.0792	-0.6103	-1.7905	-1.4514	-2.5500
CSF1	-2.1767	-2.4318	-1.3890	-2.0395	-2.1182	-2.2309
AC100830.5	-2.1791	-1.7706	-2.1470	-1.5322	-1.2354	-1.9023
ARMC9	-2.1854	-2.0008	-0.1351	-1.5507	-1.9692	-3.1066

PTPLAD2	-2.1875	-1.8747	-0.1292	-1.5082	-1.8438	-2.2304
SLC40A1	-2.2057	-2.2115	-0.0255	-1.8039	-1.9584	-3.0381
CRABP2	-2.2173	-2.0727	-1.4868	-2.6704	-2.0901	-3.0998
RP11-760H22.2	-2.2190	-1.2514	-0.0004	-1.0466	-1.6075	-1.2746
CCL5	-2.2317	-1.4890	-0.4268	-1.3292	-1.7709	-2.1781
DHDH	-2.2357	-0.5100	-0.4337	-0.7216	-2.0602	-1.4530
OLFML3	-2.2425	-2.8423	0.1947	-1.0708	-1.6433	-1.6372
C11orf21	-2.2448	-1.5823	-0.3625	-1.6555	-1.8856	-2.7427
SPARC	-2.2456	-2.4241	-0.1890	-1.6693	-1.7275	-2.4925
SPN	-2.2551	-1.6704	-1.2091	-2.1453	-1.6057	-1.8434
ZNF618	-2.2610	-2.3659	-0.3827	-1.8049	-2.2025	-2.8419
TSPAN32	-2.2778	-1.3229	-0.2805	-1.4474	-2.2090	-2.1551
SERPINB2	-2.2870	-1.5040	0.4382	-1.0071	-2.1156	-2.4707
TNFRSF21	-2.2945	-1.6464	-0.4722	-1.7350	-2.3279	-2.9423
LEPREL4	-2.2999	-1.9499	-0.1733	-1.6070	-2.0753	-3.3944
GDF15	-2.3012	-1.7687	-0.6631	-1.7131	-1.6913	-2.2542
C11orf89	-2.3062	-2.4119	-0.5612	-1.7455	-2.0550	-2.9592
ITGA3	-2.3095	-2.9016	-1.8753	-2.5354	-2.6351	-3.1889
GADD45G	-2.3312	-2.0569	-0.7070	-1.6439	-1.6988	-2.5630
CD22	-2.3494	-2.0273	-0.5244	-1.7080	-2.3287	-2.8698
LPL	-2.3678	-2.7169	-2.0010	-2.2033	-1.7561	-2.6725
TMEM255A	-2.3680	-1.7316	-0.1499	-1.3913	-1.7114	-2.4647
TREM2	-2.3812	-3.0239	-1.1318	-2.2048	-2.1961	-3.6716
CTSL2	-2.3840	-2.5168	-0.9242	-2.4816	-3.1719	-2.7831
TNFSF14	-2.3887	-1.9018	-1.6732	-2.8704	-2.0787	-1.8973
FRMD3	-2.4361	-2.3885	-0.3538	-1.5574	-2.5236	-4.0631
IFI44L	-2.4447	-1.0274	0.2750	-0.3983	-1.8559	-2.3738
RP11-1260E13.4	-2.4599	-1.6083	-0.6215	-1.2141	-2.1666	-2.5850
MYO1A	-2.4693	-2.4031	0.1355	-2.1584	-2.0512	-3.4416
USP18	-2.4915	-1.8604	-0.0600	-0.7819	-2.0219	-2.1948
ALK	-2.4973	-1.7311	-0.1673	-1.7437	-1.9432	-3.0794
SEMA3C	-2.5004	-2.1409	-0.8025	-2.0116	-2.8499	-2.9524
ATP6V0D2	-2.5295	-2.2272	-0.3822	-2.0006	-2.5508	-3.0746
CFP	-2.5776	-2.2071	-0.2516	-1.6525	-2.3815	-2.9519
ALOX5AP	-2.6213	-1.8704	-0.3174	-1.5775	-2.5151	-2.7369
IL24	-2.6257	-2.7697	-0.4186	-1.4730	-1.1473	-1.5641
CBX3P2	-2.6465	-1.5586	-0.8394	-0.8387	-0.5111	-0.6603
AL449209.1	-2.6471	-0.9398	-0.2170	-0.6195	-1.3390	-2.2053
ALDH1A1	-2.6713	-2.1661	-0.0521	-1.5844	-2.0970	-3.1700
AC007246.3	-2.7146	-2.3318	-0.5096	-1.8938	-2.6542	-2.7196
CCND1	-2.7655	-2.7012	-1.5657	-2.5212	-2.9646	-3.0416
RP11-288L9.4	-2.7886	0.0430	1.2915	-0.7266	-2.3145	-1.5499
AGPAT9	-2.8098	-2.1937	-0.5547	-1.9400	-1.9798	-2.6390

AP1S3	-2.8171	-0.8369	-0.8883	-1.7554	-1.8462	-1.8705
RP1-80N2.2	-2.8516	-2.3157	-2.1434	-2.6568	-2.2122	-2.2412
APOBEC3A	-2.8564	-2.5169	-0.4961	-1.4506	-2.0444	-4.6562
TNFRSF4	-2.8659	-2.2249	-0.0836	-1.1162	-1.4767	-2.3054
COL9A2	-2.8666	-2.0965	-1.4737	-2.4621	-2.2868	-1.9919
LY9	-2.8710	-2.4180	-0.5010	-2.3775	-2.6490	-3.6717
MRC2	-2.9054	-2.5990	-1.1321	-2.6319	-2.7152	-4.1015
KCP	-2.9120	-2.5200	-1.1729	-2.3575	-2.9433	-3.2314
RTN4R	-2.9189	-2.3038	-1.3436	-2.6451	-2.5805	-3.6773
MFSD2A	-3.0294	-2.5196	-0.5754	-1.7159	-2.6920	-2.6385
RP11-807H22.7	-3.0342	-1.0811	-0.0420	-0.9997	-0.6443	-2.8741
CXCL10	-3.0420	-2.5960	0.4020	-1.5867	-1.6642	-3.3523
FXYD6	-3.1965	-2.5918	-0.1558	-1.9298	-2.6013	-3.4171
OLR1	-3.2818	-3.2235	-1.1488	-2.4463	-2.8566	-4.1260
TMEM119	-3.3012	-2.9825	-0.4152	-2.5178	-2.8776	-3.8565
AC017104.6	-3.3012	-1.5098	-0.9882	-3.8111	-3.0958	-5.0444
CD300LB	-3.3156	-3.1967	-0.7679	-2.2065	-2.4894	-3.1478
TREML1	-3.4098	-3.3347	-1.1630	-4.0354	-2.0991	-5.4429
BTF3P7	-3.5354	-2.4433	-0.3445	-1.6150	-2.8702	-3.5178
TIMP3	-3.5392	-3.5546	-2.7013	-2.6459	-2.9676	-4.2373
F2RL3	-3.6576	-2.5196	-0.5871	-2.3784	-3.2661	-3.8013
RUFY4	-3.6764	-3.1260	-0.3640	-2.0054	-2.4985	-4.2213
SLC45A3	-3.7387	-2.2321	-0.9056	-2.5673	-2.8461	-3.6644
AFF3	-3.8015	-3.6531	-1.3869	-3.5694	-3.9496	-4.1254
CXCL11	-3.9025	-3.7815	0.8892	-1.3020	-1.6147	-3.0461
RP11-511P7.2	-4.0081	-4.4181	-2.8192	-2.2895	-3.8345	-2.4566
ALOX15B	-4.0536	-3.9283	-1.1122	-3.4972	-4.6491	-5.6333
AC104809.3	-4.1004	-7.1997	-1.2767	-3.5815	-3.1965	-4.5518
TRPC2	-4.3699	-3.8579	-0.5387	-2.4160	-2.6706	-2.6027
PADI2	-4.6922	-3.9667	-0.7430	-2.9882	-4.3534	-4.6289
HTR2B	-4.8672	-4.9254	-0.4352	-2.9329	-3.2791	-5.1917

Appendix Table 2. CD8 RNA sequencing. Log$_2$ fold change of genes significantly upregulated by WTD 50 nM > 0.6 log2 fold change and significantly downregulated by WTD 50 nM <-0.6 log2 fold change compared to non-IL-10 treated cells and their corresponding regulation by the IL-10 variants. Only those in the WTD 50 nM were filtered for significance, other conditions were not filtered for significance. Fold change is the average of three biological replicates. WTD50= WTD 50 nM, R5D50= R5A11D 50 nM, WTM50= WTM 50 nM, R5M50= R5A11M 50nM, WTD01= WTD 0.1 nM, R5D01= R5A11D 0.1 nM

Gene Name	WTD50/US	R5D50/US	WTM50/US	R5M50/US	WTD01/US	R5D01/US
S100A9	4.4094	3.2977	-1.2630	4.2730	0.5025	2.1699
SULT1B1	4.2299	3.3821	1.6337	3.7013	3.1997	3.5394
EGFL7	3.7169	2.7309	1.1376	3.3331	1.5145	1.9995
CTD-3094K11.1	3.6912	3.3808	1.1699	4.2977	2.3923	3.0732
IGJ	3.5861	4.0461	2.7624	4.0041	2.6657	3.2909
RCAN2	3.5411	2.7266	-0.0557	3.2525	1.6658	2.2109
IGKV3-20	3.4951	4.4571	3.4509	4.3973	3.8051	4.5718
ADD2	3.3725	2.8491	0.5555	2.4331	2.0101	2.5842
SOCS3	3.3709	2.8327	0.5112	3.0319	1.4259	2.2220
PAX5	3.2763	2.4840	0.3909	2.3487	0.3268	0.5540
GPR34	3.2079	2.6507	-0.0706	2.8482	1.8133	2.6033
CLU	2.7920	2.2149	0.3947	2.5114	1.3217	1.5630
ACE	2.6878	1.9319	-0.8079	1.9458	1.0810	1.2853
TDRD9	2.6821	1.4537	0.5574	2.1710	1.7762	1.3848
GREM2	2.6649	1.4546	-0.4868	2.3499	0.6581	1.0092
GZMB	2.6646	2.3496	0.6876	2.5717	1.1565	1.8722
COX6B2	2.6125	0.9366	-0.0484	2.2121	0.1468	0.4479
FES	2.5459	2.3636	0.2708	2.4099	1.2293	1.8744
GNG7	2.4761	0.5796	0.5580	1.9889	0.8346	1.0987
GSDMA	2.4736	2.0911	1.2572	1.9767	1.8279	2.2243
MIAT	2.4432	2.1121	0.0646	2.1398	0.9752	1.1958
RASL11A	2.4384	1.0710	0.3994	2.0397	1.0945	1.3859
TIAM1	2.2790	2.0540	0.2696	1.9303	1.3945	1.9266
EPHB3	2.2691	1.7559	1.0458	2.3564	2.6963	2.6132
MAPK11	2.1734	1.6714	0.1249	1.8337	0.9150	1.2469
SLC7A8	2.1413	1.5014	0.2086	2.1413	1.5611	1.7281
HKDC1	2.1287	2.1329	0.7867	1.9741	2.1126	2.2474
ZNRF1	2.1068	1.7068	0.2786	1.9822	0.7158	1.2224
AC010761.13	2.0536	1.5436	0.0849	1.3863	1.4570	1.3283
AC092566.1	2.0389	2.0219	0.3324	1.7894	1.5988	1.3415
F5	1.9924	1.9573	0.1697	1.9183	1.0600	1.3459

ITGAX	1.9691	1.7123	0.3466	1.7964	0.9428	0.9857
SBNO2	1.9673	1.5933	0.0594	1.6784	0.7011	1.2169
FUT7	1.9654	1.7857	0.3842	1.8594	1.2036	1.2750
IGKV4-1	1.9296	0.7370	-0.1444	1.1312	1.0671	0.3890
RCN3	1.8850	1.4973	0.4495	1.8546	0.6433	0.3424
NPTX1	1.8184	1.5628	0.4170	1.5842	2.1250	2.1069
RP3-324O17.4	1.7999	0.8050	0.9309	1.3542	1.0808	0.4719
FURIN	1.7736	1.5611	0.3169	1.7164	0.7967	1.1583
PRRG2	1.7488	0.7843	-0.2481	1.5509	1.1004	1.2743
PI16	1.7385	1.6099	0.1877	1.5812	1.3659	1.0925
ITGA6	1.7337	1.4634	0.1567	1.4830	1.0394	1.2745
BCL3	1.7205	1.5895	0.2036	1.5766	0.8556	1.2078
HSD3B7	1.7082	1.3484	0.4698	1.4350	0.7922	1.0456
SPEG	1.6401	1.2444	0.3490	1.4453	1.3099	1.4755
KIRREL2	1.6011	1.3146	0.2373	1.5493	0.6791	1.1171
SERF1B	1.5933	1.7310	1.5485	2.3930	2.4012	1.8457
JUN	1.5860	0.9438	-0.1648	1.2656	0.1007	0.6053
SSTR3	1.5206	1.0241	0.2898	1.2268	-0.3034	0.4940
CD9	1.5196	1.1217	0.3709	1.4080	0.9896	0.8136
NPAS2	1.5081	1.3959	0.5483	1.4661	0.9190	1.2365
KDSR	1.4818	1.1475	0.1212	1.2880	0.4423	0.7335
INPP5A	1.4810	1.3779	0.2150	1.3680	0.8126	0.9554
ROM1	1.4560	1.1574	-0.2438	1.2258	0.7410	0.7977
RP11-17G12.2	1.4448	1.2429	0.8301	1.3867	1.4389	0.5452
RP11-295G24.5	1.4301	0.0247	0.3495	0.4700	-0.0902	0.5130
LGALSL	1.3902	0.8043	0.7960	1.5675	1.0288	0.7948
INSL3	1.3900	1.2612	0.4182	1.6391	1.0651	1.1906
PDGFRB	1.3653	1.3198	0.2413	1.4025	0.8092	0.8145
IFNGR2	1.3585	0.9299	0.1628	0.9093	0.9391	1.2789
TRAJ10	1.3536	1.6630	0.9594	1.1155	0.5305	0.7370
FGFBP2	1.3482	1.2525	0.0764	1.4396	0.7234	0.8967
S100B	1.3328	1.1100	0.2813	1.0464	0.9234	1.2346
ITGA3	1.3320	1.0106	-0.1118	1.1482	0.3699	0.5161
FAM110C	1.3301	0.8398	0.2130	1.0303	-0.0086	0.5843
TCF7	1.3236	0.9537	0.1481	0.9756	0.9931	1.2439
BCL7A	1.3185	1.0474	0.1887	1.0568	1.1669	0.9897
RP11-18I14.7	1.3095	1.1202	0.2327	0.8171	1.0863	0.8439
VWA5A	1.2811	0.9487	0.3038	1.2047	0.5081	0.6113
TBXA2R	1.2783	1.1081	-0.0496	1.2509	1.3776	1.1460
AL137059.1	1.2697	0.9772	-0.0778	1.3508	1.6858	1.6430
RP11-798K23.5	1.2610	1.0886	0.1721	1.5493	0.9733	-0.6742
CXCR6	1.2531	0.8268	0.0009	1.1064	0.1322	0.6068
ALPK1	1.2479	1.0801	0.3855	1.1046	0.4757	0.7969

JAK3	1.2422	1.1410	0.2273	1.2091	0.7764	0.7726
PSD	1.2354	0.6408	0.0237	1.3282	0.4114	0.8628
SEMA4G	1.2165	0.8921	-0.3999	0.9769	0.6303	0.5201
CCR7	1.2159	0.9578	0.1922	0.9602	0.8711	1.1020
TRERF1	1.2044	0.9518	-0.0400	1.0553	0.3921	0.4744
AC108463.1	1.2002	1.1762	0.2456	1.1444	0.4986	0.1033
PARP9	1.1907	1.1381	0.2381	1.1899	0.7765	0.8959
GPR35	1.1889	0.8570	0.0915	1.0670	0.4892	0.6918
ZNF853	1.1825	0.8540	0.1145	0.9191	0.7261	0.6475
ANKRD35	1.1751	0.6902	0.0312	0.7292	0.3775	0.5045
GLDC	1.1429	0.8102	-0.0525	0.8904	-0.2524	0.3972
LL0XNC01-237H1.2	1.1349	1.0437	0.9364	1.1176	0.5531	0.6858
PLXNB2	1.1320	0.9518	0.0670	1.0217	0.5429	0.6374
IL21R	1.1315	0.6832	-0.1596	0.9011	0.1775	0.2580
TMEM150A	1.1271	0.7198	0.0730	0.9348	0.3139	0.5562
PPP1R3B	1.1219	0.8598	-0.0504	0.9462	0.1917	0.5570
AC108004.3	1.1204	1.4604	0.5452	1.5119	0.3326	0.3949
CTD-2020K17.4	1.1136	0.8301	0.2730	0.6219	1.1592	0.1806
SMARCD3	1.1096	0.9999	0.0917	1.1483	0.4083	0.4315
MVP	1.1081	0.9638	0.1467	1.0498	0.7572	0.8055
RP11-439L18.2	1.0997	0.7204	0.4360	0.9433	0.1018	0.7012
CTA-445C9.15	1.0997	1.1687	-0.0109	1.1171	0.7020	0.7955
RP13-977J11.8	1.0977	-0.2052	0.7468	0.4713	0.2910	0.3985
LINC00852	1.0954	1.3142	0.7714	1.2331	0.9939	0.3815
TMEM229B	1.0936	0.8268	-0.0570	0.9014	0.9322	0.8091
GP5	1.0919	1.1886	0.3863	1.3571	0.8863	0.8545
AC004383.4	1.0818	1.7152	0.7442	0.3785	0.8005	0.7261
CD7	1.0754	0.8389	0.0852	0.9246	0.7013	0.7083
PTGDS	1.0746	1.0545	-0.3026	1.1139	1.1691	0.9937
BATF	1.0732	0.7648	0.0719	0.9647	0.2772	0.4741
CMTM8	1.0703	0.3392	0.0520	0.9367	0.5016	0.4115
MGAT3	1.0648	0.8014	0.1747	0.7618	1.0333	0.9251
MAP3K6	1.0614	1.0319	0.0258	0.9861	0.4695	0.4677
RAB38	1.0590	0.2681	0.1010	0.9361	-0.1583	0.0160
REG4	1.0472	0.7948	-0.0298	0.9173	0.9651	1.0876
MUC1	1.0430	1.0857	0.1959	0.9253	0.8550	0.6496
AGXT2L2	1.0429	0.8361	-0.0557	0.9632	0.4062	0.4923
HRH2	1.0225	0.8887	0.1537	1.0063	0.3871	0.4707
HAPLN3	1.0124	0.9586	0.1082	0.9593	0.7764	0.8346
LRP5	1.0122	0.8306	-0.0319	0.8136	0.6776	0.7277
PMEL	1.0008	0.4556	-0.0539	0.6612	0.8659	0.3306
RP11-270C12.3	0.9985	0.4567	0.7635	0.7274	0.0744	0.4584
GLUL	0.9913	0.7646	0.0886	0.9324	0.5625	0.3648

SEMA7A	0.9841	0.8361	0.0442	0.8499	0.3841	0.5796
CCR1	0.9822	1.1451	0.2395	1.1530	0.5359	0.7528
ARHGEF4	0.9805	1.0210	0.1638	0.9219	1.1913	0.8690
RAB15	0.9735	0.9260	0.0046	0.7382	0.6742	0.6727
DLGAP4	0.9714	0.9211	0.0557	0.9864	0.6001	0.5761
ARL5B-AS1	0.9577	0.5621	0.5638	0.8333	-0.2152	-0.2855
IL17RA	0.9566	0.8755	-0.0837	0.8976	0.6165	0.5524
GIMAP7	0.9540	0.7672	0.0279	0.8782	0.4981	0.6637
IGLV2-14	0.9475	0.4004	-0.4772	0.5179	0.0944	-0.0052
GAL3ST4	0.9456	0.7478	0.1109	0.5788	0.6992	0.6382
EEPD1	0.9395	0.5194	-0.3001	0.5674	0.1944	0.2578
RIMS3	0.9209	0.8199	-0.0710	0.8422	0.3558	0.5881
TREX2	0.9204	0.8561	0.0336	0.6366	0.5743	0.3745
GIMAP8	0.9001	0.7038	-0.1031	0.7712	0.3967	0.6407
DAPK2	0.8957	0.8517	0.4130	1.2003	0.4024	0.5792
SERTAD1	0.8946	0.6558	0.1545	0.8265	0.4717	0.5013
STAT3	0.8872	0.7916	0.0883	0.8129	0.5037	0.5756
RP11-796G6.2	0.8810	0.3029	-0.1386	0.7609	-0.0116	0.4130
SH3BP5	0.8666	0.7316	-0.1544	0.8829	0.3186	0.4360
RENBP	0.8654	0.6442	0.1251	0.7790	0.5984	0.6536
ADORA2B	0.8578	0.4718	-0.1532	0.3534	0.2765	0.6638
TPST2	0.8498	0.8178	0.0406	0.8720	0.5381	0.5513
MAST4	0.8360	0.7024	-0.0829	0.8743	0.3908	0.2315
MAP3K5	0.8341	0.6513	-0.0975	0.7405	0.2332	0.4236
LAG3	0.8316	0.7183	0.0851	0.8984	-0.0010	0.3322
DENND6B	0.8315	0.5382	0.0226	0.6214	0.2287	0.2584
FLVCR2	0.8312	0.4693	0.0672	0.5335	-0.0684	-0.2824
MEMO1P1	0.8265	0.7054	0.4417	0.9349	0.2899	1.5536
RAB3A	0.8243	0.9115	0.3148	0.8929	0.5641	0.4353
PADI4	0.8233	0.8298	0.2115	0.4394	0.5919	0.7858
ROGDI	0.8217	0.6839	-0.3264	0.6528	0.4789	0.3700
GIMAP5	0.8165	0.6635	-0.0141	0.7376	0.2966	0.5281
PHOSPHO1	0.8133	0.8594	-0.2631	0.6131	0.1884	0.6288
PLEKHN1	0.8133	0.7060	0.1998	0.8718	0.0565	0.5190
IL18RAP	0.8073	0.7668	-0.0491	0.8499	0.0823	0.4445
PITPNM2	0.8024	0.7558	-0.0955	0.7925	0.4488	0.4785
UBASH3B	0.7886	0.6245	0.0755	0.7865	0.4724	0.4459
RP1-257I20.14	0.7867	0.5640	0.7124	1.0400	0.6015	0.2331
APBA2	0.7858	0.4662	-0.1082	0.4862	0.3480	0.4800
APOL1	0.7854	0.7229	0.0430	0.7996	0.4504	0.4503
IMPDH1	0.7836	0.6201	0.1028	0.7298	0.4984	0.4173
C19orf35	0.7778	0.4423	-0.0687	0.1149	0.5501	0.4732
RNF213	0.7763	0.8788	-0.0790	0.7821	0.2455	0.4086

LINC00035	0.7702	0.3306	-1.1393	0.6877	0.6345	0.2730
RP11-61L23.2	0.7699	0.5962	0.2994	0.7096	0.1793	-0.0850
RP11-289I10.2	0.7673	1.2903	-0.1993	0.7644	0.8994	0.8798
SPHK1	0.7627	0.5053	0.1780	0.7440	0.6423	0.5322
ABCA2	0.7537	0.7962	-0.0213	0.7470	0.3635	0.3267
STOM	0.7492	0.6328	-0.0334	0.7740	0.1804	0.3851
IL18R1	0.7480	0.7600	0.0816	0.7811	0.3333	0.6962
CTD-2267D19.3	0.7438	0.3207	0.1048	0.3953	0.6307	0.3137
RAB11FIP5	0.7408	0.7306	0.0436	0.8760	0.3367	0.2161
NOL3	0.7383	0.9188	0.9970	1.1162	0.4394	0.5300
NBEAL2	0.7376	0.7801	-0.1070	0.7631	0.4502	0.3562
FBXO32	0.7369	0.3694	-0.1456	0.6327	0.1839	0.1119
GOLGA7B	0.7355	0.7015	-0.0259	0.7414	0.7162	0.5613
DTNBP1	0.7265	0.5340	0.0926	0.7365	0.2363	0.2647
NECAB3	0.7254	0.6713	-0.0541	0.7291	0.5883	0.5883
LIMS2	0.7249	0.6265	0.2844	0.6005	0.8015	0.6104
WNT11	0.7245	0.5758	-0.3878	1.1123	-0.2859	0.0034
BRSK1	0.7228	0.6330	0.1429	0.6095	0.2743	0.4406
SIAE	0.7195	0.4620	-0.0030	0.6741	0.3190	-0.0753
SNX29	0.7184	0.4159	-0.1522	0.6078	-0.0237	-0.1148
MAN2A2	0.7173	0.7191	-0.1009	0.7039	0.2896	0.2257
NBPF16	0.7115	1.1618	0.0593	0.2825	0.9437	0.5372
SLC12A9	0.7069	0.6832	-0.1131	0.6717	0.2959	0.2017
PRPS1P2	0.7065	0.5003	0.3010	0.7730	0.6453	0.2265
IGSF9B	0.7052	0.8180	-0.0863	0.6767	0.7907	0.7674
DECR2	0.7028	0.2114	0.0791	0.7317	0.0955	-0.1808
SLC6A8	0.7014	0.7260	0.6051	1.0311	0.4129	0.4599
FBXO2	0.6966	0.4855	0.2254	0.7315	0.4711	0.5675
RP5-1028K7.2	0.6963	0.5563	-0.0858	0.6444	0.3452	0.3765
KLHDC8B	0.6953	0.5103	0.6644	0.3170	0.4633	-0.1097
GNPDA1	0.6874	0.4903	0.0629	0.6814	0.4065	0.4537
JUNB	0.6874	0.4737	-0.0685	0.6268	0.0128	0.1589
NARF	0.6791	0.4733	-0.1012	0.6356	0.1192	0.1483
AC002310.12	0.6786	-0.0495	0.4857	0.4757	0.5158	-0.0636
TRIB2	0.6730	0.4687	-0.2087	0.5774	0.3663	0.2908
TRAJ3	0.6695	0.6608	-0.4475	0.5804	1.0671	-0.9505
DTX3L	0.6693	0.7203	0.0700	0.7338	0.4903	0.5259
LGALS3BP	0.6606	0.6118	0.1214	0.6004	0.6319	0.6408
TTC21A	0.6596	0.5599	-0.0671	0.7725	0.2442	-0.0959
MIDN	0.6586	0.6857	0.0100	0.6526	0.4420	0.4314
NBPF15	0.6578	0.6932	-0.0770	0.6951	0.3582	0.3248
LINS	0.6541	0.5601	-0.0775	0.6282	0.2292	0.2948
HDAC4	0.6501	0.5934	-0.2316	0.6188	0.2727	0.3035

CA6	0.6499	0.5920	0.1107	0.7425	0.8401	0.4063
CLIP3	0.6466	0.1786	0.2669	0.7381	0.3148	0.2502
NOTCH2NL	0.6457	0.9326	-0.0573	0.7531	0.1313	0.4725
TXK	0.6434	0.5188	-0.1173	0.6191	0.2076	0.3067
COL6A2	0.6401	0.4132	-0.1206	0.5348	0.4651	0.5491
PGS1	0.6318	0.6094	-0.0374	0.6892	0.2195	0.1618
RHPN2	0.6312	0.3257	0.1909	0.8957	0.7089	0.2674
RP11-561C5.4	0.6300	0.4768	0.3768	0.8122	-0.1203	0.1705
APOL2	0.6299	0.5907	-0.0119	0.5485	0.3699	0.3853
NOSIP	0.6288	0.5559	0.0381	0.6767	0.6146	0.4102
NPDC1	0.6280	0.5936	-0.0225	0.6944	0.4000	0.0994
COL18A1	0.6259	0.5108	0.0294	0.6974	0.3461	0.1631
SLC24A6	0.6251	0.5131	-0.2912	0.5244	0.2108	0.2369
GRASP	0.6165	0.4547	0.0896	0.7128	0.6311	0.6218
ABLIM1	0.6154	0.5887	-0.0430	0.7321	0.4713	0.3518
SEMA4B	0.6132	0.6353	-0.0310	0.6384	0.2786	0.3122
C14orf64	0.6113	0.5473	-0.1850	0.4344	0.2833	0.3204
RPP21	0.6019	0.7528	-0.4003	0.6969	0.5090	0.5733
CPEB4	0.6015	0.6300	-0.0052	0.5740	0.3698	0.2981
SYNJ2	0.6013	0.6717	0.0408	0.6775	0.4735	0.3614
NPM1P27	-0.6005	-0.3284	-0.1394	-0.2552	-0.2794	-0.5053
ZNF286B	-0.6005	-0.1049	-0.6019	-0.7846	-0.4986	-0.8367
QPCTL	-0.6013	-0.3373	-0.0184	-0.2465	-0.2963	-0.5474
FBXO34	-0.6018	-0.3662	-0.1905	-0.3096	-0.3398	-0.5169
PPAP2A	-0.6018	-0.4165	-0.0342	-0.3823	-0.0318	-0.3230
TRMT11	-0.6025	-0.3088	-0.1153	-0.2956	-0.3635	-0.5610
STAT4	-0.6031	-0.3063	-0.0946	-0.2503	-0.1327	-0.3403
SDC4	-0.6035	-0.3336	-0.0774	-0.3245	-0.2890	-0.3849
ARHGAP10	-0.6039	-0.3067	-0.0917	-0.3968	-0.2698	-0.6143
DUSP6	-0.6049	-0.3177	-0.0928	-0.2209	-0.1804	-0.4381
FAM69A	-0.6050	-0.4698	-0.1339	-0.2992	-0.1173	-0.4665
CHEK1	-0.6055	-0.3137	-0.0867	-0.3116	-0.2078	-0.5291
SLC4A10	-0.6058	-0.3026	-0.0829	-0.0851	-0.4620	-0.4856
RP11-495P10.2	-0.6060	-0.0622	-0.1890	-0.2048	-0.1176	-0.5086
SLC25A40	-0.6073	-0.2636	-0.0766	-0.2947	-0.2404	-0.4814
RAD51B	-0.6082	-0.2603	0.0018	-0.2440	-0.3111	-0.3853
LIM2	-0.6084	-0.3503	-0.1626	-0.4638	-0.6467	-0.2217
RP11-10O17.2	-0.6086	-0.5203	-0.0472	-0.2083	-0.2705	-0.3996
AC069282.6	-0.6099	-0.0654	-0.5122	-0.5131	-0.6171	-0.8820
TEX30	-0.6101	-0.3862	-0.0539	-0.3073	-0.1756	-0.5856
TIFA	-0.6103	-0.4148	-0.2492	-0.5162	-0.3496	-0.5680
KLHDC2	-0.6105	-0.4587	-0.1817	-0.4109	-0.3760	-0.5570
AP001258.4	-0.6108	-0.2641	-0.1754	-0.1695	-0.2241	-0.6092

GPHN	-0.6109	-0.3993	-0.0809	-0.1176	-0.1871	-0.5048
HBEGF	-0.6124	-0.1363	0.2958	0.2060	-0.3876	-0.4452
AMIGO2	-0.6130	-0.2646	-0.1966	-0.2763	-0.2828	-0.4220
C17orf75	-0.6139	-0.3293	-0.1037	-0.2563	-0.1979	-0.5573
USP13	-0.6140	-0.2775	-0.1476	-0.3268	-0.2475	-0.5318
FOXO3	-0.6140	-0.3099	-0.3485	-0.3159	-0.2715	-0.5121
SNX16	-0.6154	-0.1280	-0.0137	-0.2255	-0.2241	-0.3975
TMEM154	-0.6156	-0.3784	-0.2141	-0.3859	-0.5950	-0.7775
RP11-815I9.4	-0.6164	-0.1908	-0.0735	-0.1397	-0.4794	-0.1986
CACNA2D4	-0.6183	-0.3905	-0.3534	-0.7456	-0.4601	-0.4843
PER1	-0.6187	-0.3303	-0.1992	-0.2450	-0.3088	-0.5281
BPHL	-0.6188	-0.3577	-0.3491	-0.4536	-0.2185	-0.4062
AP001877.1	-0.6189	0.5070	-0.2611	0.4020	0.1624	-0.3949
TNFRSF10B	-0.6189	-0.4588	-0.2469	-0.5245	-0.3477	-0.6097
ZNF85	-0.6190	-0.2208	-0.2001	-0.5348	-0.3269	-0.5383
TMEM116	-0.6193	-0.4096	-0.1300	-0.5089	-0.3504	-0.6693
BRPF3	-0.6205	-0.2769	-0.2255	-0.3284	-0.2505	-0.5126
AUNIP	-0.6222	-0.3117	-0.0812	-0.3376	-0.1965	-0.5169
SOX12	-0.6225	-0.8855	-0.1170	-0.4052	-0.3736	-0.8175
KB-431C1.4	-0.6226	-0.1731	-0.0950	-0.3026	-0.3140	-0.4240
ADAM9	-0.6231	-0.2597	0.0657	-0.2810	-0.4900	-0.6808
C11orf1	-0.6231	-0.4318	-0.1703	-0.3541	-0.3713	-0.7032
RP3-475N16.1	-0.6239	-0.3738	-0.3895	-0.2487	-0.3792	-0.6670
B4GALT2	-0.6241	-0.2980	-0.0615	-0.2003	-0.1935	-0.5220
ZCCHC14	-0.6241	-0.2390	-0.3660	-0.5761	-0.4081	-0.6076
DUSP1	-0.6242	-0.4222	-0.1132	-0.3658	-0.1087	-0.4848
HNRPLL	-0.6244	-0.3653	-0.2124	-0.3133	-0.3530	-0.5319
DERL3	-0.6244	-0.1555	-0.1693	-0.3015	-0.1598	-0.5889
ADAMTS1	-0.6248	-0.0799	-0.1863	-0.1312	-0.1948	-0.5145
LINC00674	-0.6252	-0.4075	-0.4368	-0.4667	-0.4048	-0.5564
TBKBP1	-0.6269	-0.2467	-0.1951	-0.1938	-0.3537	-0.7359
USP22	-0.6271	-0.3454	-0.2131	-0.3457	-0.2885	-0.5467
SPINT1	-0.6272	-0.4832	-0.1152	-0.2306	-0.2149	-0.2913
RAD50	-0.6273	-0.3046	-0.1853	-0.2737	-0.3599	-0.5948
DUSP5	-0.6279	-0.2802	-0.1857	-0.1519	-0.4475	-0.5696
DNAJC1	-0.6281	-0.4468	-0.2774	-0.4213	-0.4538	-0.4528
AL450992.2	-0.6290	-0.3518	-0.3960	-0.3978	-0.4546	-0.6456
RPL22L1	-0.6293	-0.3607	0.0025	-0.2184	-0.3688	-0.7901
ZFP69B	-0.6294	-0.4417	-0.2425	-0.3434	-0.6007	-0.6789
APP	-0.6300	-0.5119	-0.0854	-0.4666	-0.4692	-0.6249
NCF4	-0.6301	-0.3959	-0.2073	-0.3295	-0.4714	-0.6015
ITGB1P1	-0.6318	-0.3720	-0.2487	-0.2992	-0.3195	-0.6127
KDELC1	-0.6335	-0.5070	-0.1112	-0.4270	-0.2062	-0.5191

SNX9	-0.6337	-0.4079	-0.2420	-0.3706	-0.5636	-0.6176
RP5-886K2.3	-0.6343	-0.5169	-0.7513	-0.4732	-0.5804	-0.6016
ITGB1	-0.6345	-0.3392	-0.2668	-0.3563	-0.3389	-0.5364
ACYP1	-0.6348	-0.2714	-0.1412	-0.2789	-0.0256	-0.4083
MTO1	-0.6355	-0.4394	-0.1646	-0.3770	-0.4455	-0.6098
ACCS	-0.6359	-0.4921	-0.2879	-0.3176	-0.3186	-0.6076
HLA-DPA1	-0.6361	-0.3658	-0.1753	-0.2657	-0.4504	-0.6592
NAP1L1	-0.6363	-0.3663	-0.1547	-0.3225	-0.3042	-0.5770
RNF135	-0.6372	-0.4704	-0.2477	-0.3786	-0.4369	-0.6678
SIGLEC9	-0.6376	-0.4675	-0.4619	-0.6703	-0.0393	-0.8488
ADRB2	-0.6377	-0.2219	-0.2234	-0.3111	-0.2433	-0.3207
EBP	-0.6389	-0.2591	-0.0174	-0.1537	-0.1051	-0.4044
MLF1IP	-0.6397	-0.3513	-0.1734	-0.4338	-0.2694	-0.5122
DOCK7	-0.6402	-0.5990	-0.2535	-0.4607	-0.4410	-0.7508
TMEM121	-0.6402	-0.5507	-0.1876	-0.3249	-0.2299	-0.6237
FAM110A	-0.6402	-0.3290	-0.1487	-0.4918	-0.3295	-0.5220
FSTL3	-0.6405	0.0669	-0.2878	-0.2082	-0.2643	-0.2223
NETO2	-0.6406	-0.2224	0.0096	-0.2610	-0.4575	-0.6912
GTSF1	-0.6406	-0.1275	-0.0431	-0.2002	-0.3135	-0.3476
P2RX7	-0.6408	-0.2394	-0.2920	-0.2035	-0.3287	-0.5733
AHR	-0.6414	-0.3756	-0.1548	-0.3773	-0.3737	-0.4799
RTN4R	-0.6416	-0.1177	-0.1788	-0.2167	-0.1718	-0.3935
RPSAP9	-0.6418	-0.5468	0.3828	-0.1801	0.0261	-0.5871
ERBB2	-0.6425	-0.0880	-0.1522	-0.0953	-0.4416	-0.5923
SFR1	-0.6427	-0.3338	-0.1107	-0.2312	-0.2273	-0.4418
INPP4B	-0.6427	-0.3367	-0.2380	-0.4487	-0.3685	-0.6094
AC125232.1	-0.6431	-0.3144	0.0112	-0.3031	-0.4415	-0.4278
ERN1	-0.6445	-0.4341	-0.4223	-0.4248	-0.7295	-0.8623
FAM212A	-0.6452	-0.3583	-0.3852	-0.6275	0.4273	-0.6521
MNAT1	-0.6452	-0.3126	-0.0118	-0.2497	-0.2512	-0.4841
TMEM107	-0.6452	-0.3411	-0.2386	-0.4052	-0.2533	-0.5515
CENPH	-0.6453	-0.4529	-0.1242	-0.4094	-0.2753	-0.5799
FBXO43	-0.6466	-0.3659	-0.4267	-0.3341	-0.1881	-0.6638
HIBADH	-0.6469	-0.5187	-0.2860	-0.3985	-0.4971	-0.6355
SLC35F2	-0.6472	-0.2394	-0.1404	-0.2563	-0.4016	-0.4808
FAM3C	-0.6480	-0.2832	-0.2240	-0.2625	-0.5894	-0.6211
PLEKHO1	-0.6481	-0.4411	-0.2276	-0.3744	-0.1639	-0.4465
ZNF702P	-0.6487	-0.0231	0.1286	-0.0487	0.1993	0.3762
TRIM16	-0.6488	-0.3986	-0.1390	-0.2279	-0.3233	-0.8126
AP1AR	-0.6488	-0.3473	-0.1986	-0.3454	-0.4836	-0.4587
AFMID	-0.6491	-0.4783	-0.2241	-0.3366	-0.3728	-0.4686
P2RY11	-0.6496	-0.3326	-0.3369	-0.2927	-0.2645	-0.3970
HABP4	-0.6499	-0.3370	-0.3122	-0.2545	-0.3708	-0.6031

SMIM19	-0.6516	-0.3703	-0.3265	-0.4601	-0.2471	-0.4884
OXR1	-0.6523	-0.3255	-0.2397	-0.3896	-0.3499	-0.5119
C4orf33	-0.6527	-0.3408	-0.0970	-0.3212	-0.3067	-0.4421
FABP5	-0.6538	-0.3255	0.0020	-0.2863	-0.2824	-0.5234
TREML2	-0.6539	-0.1515	0.0746	-0.1612	0.0638	-0.3212
DYRK4	-0.6543	-0.3533	-0.0957	-0.2670	-0.3600	-0.4683
CCDC7	-0.6544	-0.5610	-0.0765	-0.7052	-0.6906	-0.6721
HOXC4	-0.6553	-0.4404	-0.4474	-0.2975	-0.4845	-0.7303
AC073046.25	-0.6556	-0.1696	-0.0274	-0.1909	-0.2384	-0.3054
TCTN3	-0.6557	-0.4001	-0.1454	-0.3620	-0.4492	-0.6103
SIAH2	-0.6567	-0.4300	-0.1653	-0.3193	-0.4520	-0.5854
PPM1L	-0.6570	-0.3807	-0.2636	-0.2894	-0.3353	-0.6510
IQCG	-0.6573	-0.2624	-0.0784	-0.4061	-0.2324	-0.5185
C17orf53	-0.6578	-0.4352	-0.2270	-0.3609	-0.2201	-0.5960
ECI1	-0.6579	-0.4555	-0.1342	-0.4267	-0.3983	-0.5957
LONP1	-0.6584	-0.3171	-0.1746	-0.3718	-0.4273	-0.6419
ZNF230	-0.6587	-0.3445	-0.0542	-0.3332	-0.1195	-0.5994
TTC32	-0.6588	-0.2615	-0.2733	-0.3790	-0.3569	-0.5305
GJB6	-0.6591	-0.5029	0.0071	-0.2432	-0.0373	-0.3829
PSMG1	-0.6594	-0.4423	-0.1589	-0.4074	-0.3548	-0.6420
RHOC	-0.6598	-0.5002	-0.1183	-0.3381	-0.4437	-0.5455
P4HA1	-0.6603	-0.3314	-0.0868	-0.2579	-0.2308	-0.6249
ZNF347	-0.6607	-0.1100	-0.3369	-0.2494	-0.1691	-0.2122
IMMP2L	-0.6607	-0.9340	-0.2982	-0.6911	-0.5323	-0.7784
CTC-260E6.6	-0.6612	-0.6421	-0.2175	-0.0811	-0.5058	-0.5161
GRAMD3	-0.6625	-0.4140	-0.2342	-0.1928	-0.6083	-0.5531
SAV1	-0.6627	-0.3896	-0.1783	-0.3259	-0.4703	-0.7704
ZSCAN20	-0.6632	-0.3346	-0.2194	-0.3413	-0.5799	-0.7880
ETV2	-0.6633	-0.3682	-0.2614	-0.5979	-0.1108	-0.2854
THNSL1	-0.6642	-0.5584	-0.0759	-0.4092	-0.1914	-0.6591
DHRS4	-0.6643	-0.3357	-0.1662	-0.1934	-0.1988	-0.3721
EXOC6B	-0.6645	-0.2303	-0.2671	-0.1985	-0.2089	-0.4401
SNRPEP4	-0.6645	-0.4267	0.0734	0.0462	0.0043	0.0209
RP11-809O17.1	-0.6646	0.2445	0.1407	0.1727	-0.2186	-0.1752
CDCA7	-0.6646	-0.3696	-0.2038	-0.4497	-0.1295	-0.5604
LYST	-0.6648	-0.2667	-0.2776	-0.4145	-0.4979	-0.5423
XPOT	-0.6649	-0.3649	-0.1869	-0.3947	-0.4465	-0.6862
CCNG1	-0.6650	-0.3612	-0.1973	-0.4004	-0.3042	-0.5505
RAB8B	-0.6656	-0.3579	-0.2239	-0.3741	-0.2520	-0.5173
ATP2B1	-0.6663	-0.2533	-0.2016	-0.2893	-0.1673	-0.4784
NEDD4L	-0.6676	-0.6102	-0.2113	-0.4084	-0.2792	-0.6730
AL161915.1	-0.6679	-0.0932	-0.3596	-0.0279	0.0514	-0.2122
XPNPEP2	-0.6679	-0.0011	-0.2450	-0.0777	0.0036	-0.0414

KLF11	-0.6682	-0.4796	-0.2201	-0.3009	-0.2293	-0.4393
TNFRSF10A	-0.6685	-0.4391	-0.3219	-0.3375	-0.2790	-0.5604
STAMBP	-0.6697	-0.4073	-0.2090	-0.3121	-0.3253	-0.4885
MAP4K2	-0.6698	-0.3259	-0.1242	-0.3686	-0.1840	-0.5177
IMPDH2	-0.6710	-0.3486	-0.0925	-0.3377	-0.2975	-0.5957
MUT	-0.6716	-0.3503	-0.0819	-0.2921	-0.2875	-0.5046
NCR3	-0.6718	-0.2372	-0.0378	-0.1668	0.0264	-0.3892
PAQR8	-0.6726	-0.4222	-0.1966	-0.4999	-0.0800	-0.3714
C4orf32	-0.6729	-0.5480	-0.2326	-0.4485	-0.5105	-0.5192
AC017002.1	-0.6739	-0.4770	-0.0373	-0.2080	-0.6405	-0.7914
RASA4DP	-0.6744	0.1998	0.1532	0.1430	-0.3492	-0.1934
PDE4B	-0.6750	-0.4814	-0.1927	-0.4061	-0.5281	-0.6928
FBXO48	-0.6753	-0.3104	-0.0568	-0.1627	-0.1567	-0.7108
SAMSN1	-0.6754	-0.3868	-0.1088	-0.3950	-0.4275	-0.4808
CCDC28A	-0.6764	-0.3027	-0.2721	-0.3235	-0.3730	-0.5408
ARNTL2	-0.6779	-0.3014	-0.0404	-0.3557	-0.3204	-0.4640
HSPD1P1	-0.6782	-0.3704	-0.1250	-0.4048	-0.2363	-0.6639
PDCD4-AS1	-0.6798	-0.4845	-0.3684	-0.5708	-0.3353	-0.6234
ZNF616	-0.6800	-0.2345	-0.1559	-0.1995	-0.3092	-0.4534
AP000640.10	-0.6805	-0.1871	-0.2469	-0.9437	-0.2270	-0.1582
GLCE	-0.6812	-0.3512	-0.2342	-0.2133	-0.2304	-0.5509
SCML2	-0.6814	-0.5047	-0.0939	-0.4141	-0.2312	-0.4049
JMY	-0.6817	-0.5208	-0.4596	-0.5876	-0.8291	-0.9346
ACSF2	-0.6821	-0.4736	-0.1296	-0.3289	-0.1970	-0.5709
RP11-463M16.4	-0.6824	-0.4773	-0.3709	-0.3540	-0.1935	-0.2793
CHIC2	-0.6825	-0.2759	-0.2517	-0.2310	-0.5770	-0.5735
C17orf76-AS1	-0.6843	-0.5296	-0.1583	-0.3766	-0.5005	-0.6846
GADD45A	-0.6845	-0.5284	-0.1562	-0.4878	-0.3601	-0.5901
DPYD	-0.6849	-0.4811	-0.3246	-0.4217	-0.2466	-0.5979
SLC29A2	-0.6855	0.0185	-0.1453	-0.1057	-0.2270	-0.4177
CCNG2	-0.6856	-0.5143	-0.3768	-0.4772	-0.4178	-0.7773
CITED2	-0.6864	-0.4686	-0.2759	-0.3771	-0.4226	-0.7749
MAPK13	-0.6866	-0.3469	-0.1392	-0.3027	-0.2908	-0.5859
MAP2K6	-0.6872	-0.3219	-0.1220	-0.3641	-0.2485	-0.6300
TBXAS1	-0.6874	-0.6185	-0.1588	-0.6461	-0.7131	-0.7170
ZCCHC7	-0.6880	-0.4289	-0.2157	-0.4702	-0.3858	-0.5580
AC018816.3	-0.6883	-0.1823	-0.5968	-0.4769	-0.1455	-0.2965
NT5DC1	-0.6884	-0.3769	-0.2799	-0.3590	-0.3030	-0.5763
FANCL	-0.6884	-0.3772	-0.1028	-0.3757	-0.1872	-0.6488
RP11-764K9.2	-0.6891	-0.4244	-0.3774	-0.3738	-0.6898	-0.7808
TATDN1	-0.6893	-0.4348	-0.2450	-0.2789	-0.3245	-0.7252
ZFAS1	-0.6895	-0.5692	-0.1727	-0.3641	-0.4595	-0.7572
AC004152.5	-0.6897	-0.0709	-0.5139	-0.0798	-0.3560	-0.4627

RNF32	-0.6901	-0.3049	-0.6299	-0.0987	-0.6253	-0.4233
TLE1	-0.6907	-0.5717	-0.5561	-0.8906	-0.6938	-0.6202
ZSCAN16	-0.6909	-0.2192	-0.1865	-0.2437	-0.2325	-0.3855
PYHIN1	-0.6919	-0.4547	-0.2356	-0.5157	-0.5017	-0.6030
WDR41	-0.6924	-0.3005	-0.0449	-0.2677	-0.2390	-0.6807
SGK1	-0.6925	-0.3623	-0.1391	-0.3827	-0.6561	-0.6322
AAED1	-0.6939	-0.1942	-0.1185	-0.0722	-0.2556	-0.4795
GALM	-0.6942	-0.4573	-0.1855	-0.3942	-0.6287	-0.7466
MEOX1	-0.6954	-0.4838	-0.4562	-0.6354	0.1091	-0.4001
PIK3AP1	-0.6971	-0.4302	-0.3836	-0.4663	-0.6934	-0.5770
TNK2	-0.6975	-0.3453	-0.1957	-0.3782	-0.3635	-0.6319
XRCC6BP1	-0.6977	-0.5053	-0.1088	-0.3636	-0.3899	-0.5950
NBR2	-0.6983	-0.5269	-0.4064	-0.5332	-0.5562	-0.8459
NFE2L3	-0.6988	-0.4027	-0.0945	-0.4115	-0.4855	-0.5093
CCDC28B	-0.6991	-0.3845	-0.0693	-0.3392	-0.0779	-0.4432
CCR4	-0.6997	-0.7026	-0.3974	-0.7690	-0.6743	-0.8237
C19orf48	-0.7000	-0.4271	-0.1863	-0.4840	-0.3562	-0.6265
EIF4BP6	-0.7009	-0.4598	-0.1153	-0.2595	-0.2517	-0.6837
TMEM44	-0.7010	-0.2979	-0.0045	-0.4684	-0.1347	-0.6419
FBXO4	-0.7017	-0.4118	-0.1943	-0.4314	-0.4760	-0.6214
MYO6	-0.7018	-0.4140	-0.1887	-0.3680	-0.8596	-0.6595
ZNF219	-0.7026	-0.6278	0.0068	-0.4614	-0.6246	-0.6730
KLF9	-0.7026	-0.3712	-0.1228	-0.3086	-0.4787	-0.7832
CTC-788C1.1	-0.7031	-0.7488	0.0233	-0.4459	0.0273	-0.4852
MRPL45P2	-0.7034	-0.3651	-0.2189	-0.4857	-0.1632	-0.8444
KIF3C	-0.7035	-0.4124	-0.1960	-0.4248	-0.2760	-0.6009
GNAQ	-0.7036	-0.3021	-0.1652	-0.3599	-0.3116	-0.5116
AIF1	-0.7044	-0.5273	-0.0091	-0.3405	-0.3041	-0.5753
AKAP3	-0.7047	-0.5223	-0.2970	-0.1873	-0.2613	-0.8586
CDK6	-0.7049	-0.1508	-0.1529	-0.3110	-0.3196	-0.5516
CRIM1	-0.7052	-0.3592	-0.2402	-0.3285	-0.3489	-0.5545
C2CD4D	-0.7061	-0.3442	-0.1815	-0.3058	-0.3069	-0.8121
FOXN3	-0.7066	-0.3633	-0.3283	-0.4226	-0.3913	-0.5393
FADS3	-0.7073	-0.4480	-0.2559	-0.5254	-0.3708	-0.4360
NEIL3	-0.7076	-0.4319	-0.1714	-0.4021	-0.2791	-0.5210
RP11-521C20.4	-0.7080	-0.4415	-0.2838	-0.3811	-0.8167	-0.1656
DMC1	-0.7082	-0.3134	-0.0659	-0.3210	-0.2769	-0.4259
AP3M2	-0.7084	-0.4306	-0.1353	-0.4211	-0.3604	-0.6508
CDCA7L	-0.7090	-0.4392	-0.1021	-0.3760	-0.2845	-0.5223
VAV3	-0.7092	-0.3694	-0.1962	-0.2954	-0.2402	-0.4948
PARVB	-0.7095	-0.3661	-0.0586	-0.3525	-0.3648	-0.5856
POC1B	-0.7099	-0.3650	-0.1096	-0.3311	-0.3866	-0.6327
SUOX	-0.7105	-0.7028	-0.0987	-0.5965	-0.4736	-1.0908

HYLS1	-0.7115	-0.5159	-0.1872	-0.5014	-0.1913	-0.6019
AC010733.5	-0.7115	-0.4173	-0.7363	-0.3483	-0.7247	-0.4187
ZNF607	-0.7125	-0.6541	-0.1081	-0.4284	-0.5657	-0.7203
ZNF90	-0.7133	-0.4176	0.0013	-0.5774	-0.4735	-0.7236
PGBD1	-0.7137	-0.2597	-0.0740	-0.3527	-0.2424	-0.4636
EOMES	-0.7137	-0.4351	-0.2651	-0.4825	-0.4695	-0.4701
AP1S2	-0.7137	-0.5165	-0.2280	-0.4334	-0.3263	-0.5716
USP44	-0.7139	-0.4331	-0.1187	-0.3266	-0.3877	-0.7838
NR4A2	-0.7150	-0.5650	-0.3288	-0.8140	-0.9180	-1.0218
AC009299.3	-0.7162	-0.4967	-0.3212	-0.6126	-0.5665	-0.6036
DOK4	-0.7163	-0.3548	-0.0455	0.0136	-0.1807	-0.6812
BBS12	-0.7189	-0.2186	-0.2649	-0.4467	-0.3940	-0.7485
FAM216A	-0.7200	-0.4426	-0.1624	-0.3710	-0.4135	-0.7831
LINC00484	-0.7206	-0.0637	-0.1412	-0.5501	-0.5005	-0.4319
MYO1E	-0.7212	-0.2567	-0.0343	-0.2569	-0.1047	-0.4877
CCDC171	-0.7212	-0.0500	0.1919	-0.4002	-0.0195	-0.3118
RHBDL3	-0.7214	-0.6416	-0.3063	-0.8031	-0.2294	-0.3819
CHST2	-0.7248	-0.6702	-0.2879	-0.6250	-0.4880	-0.8685
KLRB1	-0.7249	-0.5851	-0.4052	-0.6570	-0.5834	-0.5657
CTBP2	-0.7259	-0.2061	-0.1264	-0.5858	-0.2768	-0.3513
FBLN5	-0.7269	-0.4960	-0.2964	-0.3636	-0.6026	-0.7661
CDC14A	-0.7271	-0.4082	-0.3044	-0.4574	-0.3629	-0.5745
KHDC1	-0.7277	-0.6905	-0.4245	-0.5804	-0.3660	-0.7562
RP3-527F8.2	-0.7284	-0.2799	-0.0728	-0.1317	-0.2597	-0.4304
ITGA4	-0.7287	-0.3227	-0.2340	-0.3851	-0.2403	-0.5619
ARHGEF39	-0.7291	-0.2536	-0.1596	-0.4329	-0.3679	-0.5959
KIAA0101	-0.7300	-0.3858	-0.1829	-0.4246	-0.2232	-0.5501
AGAP3	-0.7302	-0.4243	0.0042	-0.4391	-0.4639	-0.6756
MRPL10	-0.7306	-0.4393	-0.2711	-0.4339	-0.4522	-0.6350
SH2B3	-0.7308	-0.4391	-0.3155	-0.6009	-0.1317	-0.3749
PPIAP29	-0.7316	-0.4213	-0.2762	-0.3612	-0.2760	-0.7335
EFCAB2	-0.7320	0.1259	-0.0038	0.2333	-0.2299	-0.1649
RNLS	-0.7344	-0.5390	-0.0683	-0.4350	-0.3015	-0.4334
GJB2	-0.7351	-0.3226	-0.1586	-0.4447	-0.4765	-0.8220
CBX7	-0.7355	-0.6523	-0.4076	-0.5406	-0.6024	-0.8359
PRIM1	-0.7358	-0.3897	-0.0786	-0.4353	-0.2297	-0.5609
MVK	-0.7360	-0.4182	-0.2060	-0.4560	-0.2857	-0.6198
IL2RA	-0.7382	-0.3740	-0.0544	-0.2981	-0.5842	-0.7033
TNC	-0.7384	0.1451	-0.3269	-0.3742	-0.1964	-0.5707
C9orf66	-0.7388	-0.0567	-0.1797	-0.1465	-0.2430	-0.3315
PLAUR	-0.7394	-0.0358	-0.0883	-0.2987	-0.4153	-0.4803
PDCD4	-0.7401	-0.6375	-0.3937	-0.5668	-0.5732	-0.7304
ADAP1	-0.7404	-0.4094	-0.3930	-0.4880	-0.3180	-0.4488

PDE4A	-0.7412	-0.3937	-0.2268	-0.4668	-0.3731	-0.5334
SCCPDH	-0.7426	-0.4783	-0.1711	-0.4193	-0.4084	-0.4918
SLC1A4	-0.7433	-0.4775	-0.3161	-0.5218	-0.4642	-0.6881
RP11-214C8.5	-0.7435	-0.4328	-0.4519	-0.4568	-0.7564	-0.8173
CCNB1IP1	-0.7439	-0.5304	-0.1939	-0.5205	-0.4123	-0.7054
ENC1	-0.7455	-0.3395	-0.2809	-0.3974	-0.5735	-0.5864
C12orf57	-0.7459	-0.5555	-0.2186	-0.4600	-0.2955	-0.5879
LIMA1	-0.7463	-0.3958	-0.1344	-0.4454	-0.4620	-0.6486
RPL4P1	-0.7481	-0.0036	-0.0864	-0.1120	-0.3299	-0.7626
IFI27L1	-0.7484	-0.4533	-0.2748	-0.5729	-0.2704	-0.6496
LINC00623	-0.7487	-0.4834	-0.5578	-0.7745	0.6437	-0.6364
CARD17	-0.7509	-0.4017	0.0074	-0.5227	-0.5013	-0.2501
SPATA7	-0.7513	-0.2255	-0.2782	-0.2170	-0.5344	-0.6160
ZNF391	-0.7514	-0.2945	-0.2720	-0.5938	-0.2804	-0.3696
AMZ2P1	-0.7514	-0.4155	-0.3278	-0.5755	-0.2863	-0.5125
DGCR6	-0.7517	-0.2246	-0.4147	-0.3432	-0.5933	-0.7298
ICAM2	-0.7529	-0.3725	-0.2364	-0.3733	-0.0967	-0.6207
LRRCC1	-0.7534	-0.3171	-0.0900	-0.2847	-0.2893	-0.4976
GPD2	-0.7548	-0.4074	-0.2865	-0.4055	-0.5104	-0.6270
DAK	-0.7561	-0.5791	-0.3769	-0.4166	-0.3904	-0.7467
C17orf51	-0.7561	-0.3676	-0.0666	-0.4470	-0.5799	-0.7074
RP11-24B19.3	-0.7562	-0.3626	-0.3548	-0.2075	-0.3774	-0.7185
ZC3HAV1L	-0.7564	-0.4274	-0.2046	-0.3000	-0.4472	-0.7491
AKIP1	-0.7578	-0.5343	-0.0589	-0.4713	-0.2167	-0.5847
PATL2	-0.7584	-0.5994	-0.3702	-0.6367	-0.6260	-1.1634
SPRY4	-0.7610	-0.5089	0.0299	0.1652	-0.3169	-0.4453
CERKL	-0.7613	-0.3565	-0.2285	-0.3712	-0.3018	-0.5500
RP11-430B1.2	-0.7613	-0.6401	-0.6011	-1.0001	-0.5891	-1.5799
RP4-659J6.2	-0.7615	-0.5276	-0.4910	-0.4314	-0.6148	-0.6779
SSBP2	-0.7619	-0.4395	-0.1660	-0.5024	-0.0709	-0.5052
TBC1D19	-0.7634	-0.5089	-0.4514	-0.4322	-0.5347	-0.4924
PIGV	-0.7643	-0.5085	-0.2648	-0.4526	-0.5011	-0.7929
ARL4A	-0.7645	-0.5268	-0.3268	-0.3608	-0.2564	-0.6125
MAPK8	-0.7646	-0.3970	-0.0941	-0.3348	-0.5693	-0.6869
CTB-131B5.4	-0.7648	-0.6494	-0.6064	-0.0884	-0.2746	-0.5350
ACP6	-0.7653	-0.3959	-0.0524	-0.3378	-0.3318	-0.5902
PRELID2	-0.7654	-0.4667	-0.0299	-0.8992	-0.8436	-1.4027
AC004381.6	-0.7655	-0.4190	-0.0994	-0.5011	-0.6161	-0.4405
AP001816.1	-0.7663	-0.4832	-0.2596	-0.5872	-0.5224	-0.7859
RAB31	-0.7676	-0.0322	-0.1034	-1.0908	-0.5548	-1.5476
MCOLN2	-0.7678	-0.3822	-0.2757	-0.4141	-0.5265	-0.6906
SPIN1	-0.7682	-0.3612	-0.1325	-0.3460	-0.2576	-0.6004
ALDH6A1	-0.7691	-0.3914	-0.1728	-0.3388	-0.3264	-0.6131

DUSP4	-0.7707	-0.4500	-0.2435	-0.4293	-0.6223	-0.8291
CDKN2A	-0.7709	-0.5445	-0.2289	-0.5231	-0.2176	-0.5698
SH3TC1	-0.7716	-0.3702	-0.2916	-0.8297	-0.4670	-0.6563
TMEM2	-0.7717	-0.3134	-0.2275	-0.3468	-0.4648	-0.5704
PALD1	-0.7726	-0.5606	-0.1397	-0.5142	-0.2211	-0.6287
MYO5C	-0.7744	-0.4250	-0.1331	-0.3951	-0.0847	-0.8338
RTN2	-0.7745	-0.1911	-0.4218	0.0219	0.0444	-0.1879
PBLD	-0.7750	-0.6399	-0.4525	-0.5249	-0.6066	-0.8082
FXYD7	-0.7752	-0.6290	-0.1885	-0.7642	-0.4138	-0.5400
AC016747.3	-0.7764	-0.4996	-0.2509	-0.4273	-0.4436	-0.6624
NAT6	-0.7766	-0.3226	-0.1713	-0.3117	-0.0973	-0.7372
CTSH	-0.7773	-0.3854	-0.0341	-0.2801	-0.1293	-0.5390
KLRG1	-0.7774	-0.5350	-0.4106	-0.5308	-0.4591	-0.5550
NR1H3	-0.7775	-0.3557	-0.3172	-0.3498	-0.1959	-0.3985
RP11-393B14.1	-0.7783	-0.3744	-0.2388	-0.4024	-0.7723	-0.6718
DHRS4L2	-0.7795	-0.4337	-0.1033	-0.3533	-0.3772	-0.5971
RP11-89M16.1	-0.7799	-1.0826	-0.3773	-1.1140	-1.3245	-1.3427
NFIL3	-0.7801	-0.4521	-0.2007	-0.3542	-0.4998	-0.7679
RP11-968A15.2	-0.7804	-0.3887	-0.3700	-0.7244	-0.2368	-1.5351
AC092295.7	-0.7819	-0.3492	-1.2658	-0.9178	-0.4843	-1.1167
MAP3K7CL	-0.7823	-0.2382	0.0205	0.0666	-0.1311	-0.7211
CCPG1	-0.7831	-0.5127	-0.2429	-0.5254	-0.4169	-0.7109
CTB-186H2.2	-0.7831	0.1166	0.1234	0.2330	-0.0384	-0.0638
AC104820.2	-0.7832	-0.1122	-0.1230	-0.5070	-0.5089	-0.5646
TP53I11	-0.7860	-0.6454	-0.2368	-0.8101	-0.5578	-0.8066
SIRPG	-0.7870	-0.4074	-0.1829	-0.3868	-0.1951	-0.5335
AIM2	-0.7875	-0.5760	-0.1282	-0.5270	-0.8941	-0.7022
CREB3L4	-0.7883	-0.4244	-0.1764	-0.3699	-0.4190	-0.6801
NEDD9	-0.7892	-0.4348	-0.2572	-0.4531	-0.3759	-0.5761
SLC43A1	-0.7895	-0.5570	-0.3346	-0.5460	-0.4245	-0.8257
PPP1R15A	-0.7915	-0.5669	-0.2636	-0.5156	-0.6927	-0.7775
CPNE7	-0.7921	-0.7660	-0.4275	-0.5892	-0.3557	-0.9372
BTG1	-0.7923	-0.5804	-0.2802	-0.5684	-0.5134	-0.7209
FAR2	-0.7946	-0.3868	-0.1523	-0.4992	-0.3396	-0.4536
PAM	-0.7953	-0.5278	-0.3226	-0.5602	-0.6642	-0.6753
CPNE8	-0.7958	-0.5449	-0.0555	-0.3647	-0.3436	-0.5526
ZNF35	-0.7959	-0.6881	-0.0712	-0.4742	-0.6803	-0.5547
GPR15	-0.7981	-0.4614	-0.3387	-0.4103	-0.4520	-0.6981
RPL12P4	-0.7984	-0.5104	-0.0579	-0.2216	-0.6517	-0.4798
MBNL2	-0.8009	-0.5886	-0.2684	-0.4815	-0.5115	-0.7373
RP1-152L7.5	-0.8010	-0.5774	-0.2840	-0.5176	-0.3726	-0.7809
NAMPT	-0.8013	-0.4707	-0.1094	-0.3956	-0.5625	-0.7501
ANKRD6	-0.8033	-0.5330	-0.2550	-0.8223	-0.4153	-0.6808

ZC3H6	-0.8036	-0.4883	-0.4323	-0.3720	-0.6074	-0.5852
SLC38A2	-0.8038	-0.4670	-0.1945	-0.4564	-0.4492	-0.7751
ATP6AP1L	-0.8044	-0.3579	-0.3777	-0.5927	-0.6107	-0.9665
AKT3	-0.8051	-0.5179	-0.3009	-0.4371	-0.6430	-0.8416
TGFBR3	-0.8057	-0.4314	-0.3378	-0.4340	-0.4253	-0.6499
TIMD4	-0.8059	-0.2562	0.2607	-0.2154	-0.0601	-0.3241
KIF3A	-0.8061	-0.4245	-0.1265	-0.3487	-0.5586	-0.7360
EAF2	-0.8068	-0.3033	-0.2143	-0.5005	-0.6501	-0.7009
RAVER2	-0.8071	-0.6162	-0.1026	-0.5316	-0.6322	-1.0362
AVPI1	-0.8101	-0.7288	0.0960	-0.5016	0.0322	-0.1572
SLC26A4-AS1	-0.8139	-0.5379	0.2678	0.1963	-0.8044	-1.5368
PPIAP11	-0.8139	-0.3723	-0.2621	-0.2192	-0.3728	-0.8088
CEP128	-0.8155	-0.4375	-0.2799	-0.6185	-0.3509	-0.7188
C20orf197	-0.8157	-0.2322	-0.3456	-0.3518	-0.3168	-0.5347
RMI2	-0.8161	-0.4927	-0.1545	-0.5513	-0.3292	-0.5556
HVCN1	-0.8166	-0.4907	-0.1521	-0.5550	-0.2256	-0.5379
RBM38	-0.8186	-0.3608	-0.1070	-0.2654	-0.1971	-0.5735
ADAM22	-0.8194	-0.5477	-0.3135	-0.6504	-0.3417	-0.9658
RND1	-0.8209	-0.4539	-0.0466	-0.2141	-0.0409	-0.1222
NAMPTL	-0.8212	-0.3781	-0.1660	-0.3240	-0.5121	-0.6206
EGR1	-0.8214	-0.5560	-0.2627	-0.5895	-0.7285	-0.7813
EFCAB4A	-0.8220	-0.4903	-0.1158	-0.5857	-0.0813	-0.9611
LRRC1	-0.8224	-0.4899	-0.1055	-0.4318	-0.5562	-0.6802
GAB2	-0.8227	-0.5131	-0.1487	-0.6614	-0.5042	-0.7244
TMEM55A	-0.8231	-0.7792	-0.2625	-0.6690	-0.4018	-0.7965
APOBEC3H	-0.8238	-0.3602	-0.1224	-0.4450	-0.3206	-0.5225
HSPB1	-0.8250	-0.5465	-0.1438	-0.4302	-0.2857	-0.7317
EPS8	-0.8256	-0.5450	-0.2568	-0.2965	-0.1913	-0.8268
HSPA6	-0.8261	-0.5022	-0.2913	-0.8466	-0.6404	-0.7189
ABHD17C	-0.8272	-0.7127	-0.2331	-0.5831	-0.8461	-0.7847
SMS	-0.8273	-0.4632	-0.0950	-0.4589	-0.3086	-0.5631
EDARADD	-0.8279	-0.7005	-0.1804	-0.6956	-0.7125	-0.9128
C7orf41	-0.8292	-0.4673	-0.3301	-0.4210	-0.5937	-0.6106
RP11-1415C14.4	-0.8302	-0.2722	-0.5480	0.2961	-0.0291	0.4501
SLC18B1	-0.8315	-0.5777	-0.2292	-0.4626	-0.3982	-0.7149
TPM2	-0.8315	-0.5347	-0.4177	-0.4153	-0.0832	-0.6761
ATXN1	-0.8328	-0.4229	-0.3823	-0.5704	-0.6122	-0.7585
C5orf34	-0.8339	-0.4980	-0.3756	-0.5199	-0.3108	-0.6027
NAB2	-0.8347	-0.4328	-0.1760	-0.5530	-0.3755	-0.6470
C12orf60	-0.8350	-0.5324	-0.1162	-0.1369	-0.3128	-0.6661
AUH	-0.8357	-0.5027	-0.1948	-0.5293	-0.4901	-0.8328
IFT81	-0.8358	-0.4737	-0.2553	-0.2701	-0.5318	-0.4553
KLRD1	-0.8358	-0.5179	-0.3092	-0.4424	-0.6392	-0.7054

SLC22A18	-0.8361	-0.3665	-0.4786	-0.5079	-0.2888	-0.5903
TFAP2E	-0.8361	-0.5261	-0.2024	-0.3389	-0.6936	-0.6372
CCDC141	-0.8372	-0.4041	-0.3017	-0.4128	-0.4380	-0.7231
INPP5F	-0.8385	-0.3670	-0.2521	-0.3976	-0.4212	-0.5841
CDT1	-0.8396	-0.5181	-0.2434	-0.6112	-0.3258	-0.7066
H1FX	-0.8413	-0.6276	-0.2806	-0.4958	-0.4779	-0.7535
CXCR4	-0.8420	-0.4735	-0.1130	-0.5027	-0.2344	-0.4810
GEM	-0.8436	-0.3158	-0.4811	-0.5428	-0.5837	-0.4158
TESK2	-0.8455	-0.5514	-0.3282	-0.4464	-0.5460	-0.7920
RIPK2	-0.8474	-0.6212	-0.3898	-0.6322	-0.5641	-0.7325
CTPS2	-0.8485	-0.5142	-0.2806	-0.5026	-0.4952	-0.8051
S100A5	-0.8487	-0.4524	-0.4435	-0.2411	-0.5825	-0.5387
ABCA3	-0.8491	-0.5033	-0.2616	-0.7012	-0.5539	-0.8074
RP4-575N6.4	-0.8499	-0.3689	-0.4154	-0.4452	-0.4504	-0.9311
RAB39B	-0.8549	-0.6355	-0.2118	-0.4334	-0.6681	-0.8706
CTA-292E10.6	-0.8553	0.1707	0.1752	0.1598	-0.0360	-0.4979
FGR	-0.8571	-0.4598	-0.0825	-0.4947	-0.5497	-0.7305
ZFP69	-0.8597	-0.3928	-0.1808	-0.3298	-0.5187	-0.5702
SNX10	-0.8609	-0.3541	-0.0576	-0.3795	-0.3082	-0.5845
BCAR3	-0.8613	-0.8805	-0.6167	-0.4414	-0.6660	-1.0523
NFKBIL1	-0.8623	-0.4575	-0.3299	-0.3586	-0.4395	-0.7019
COCH	-0.8638	-1.4347	-0.1387	-0.3514	-0.5329	-0.6007
AC147651.4	-0.8643	-0.4067	-0.2093	-0.4271	-0.5260	-0.7323
RBMS2	-0.8674	-0.5899	-0.3437	-0.4328	-0.7181	-1.0053
APOLD1	-0.8684	-0.4777	-0.3605	-0.5978	-0.3261	-0.7151
MAFG-AS1	-0.8698	-0.8036	-0.3719	-0.3903	-0.3347	-1.0930
CTC-303L1.1	-0.8709	-0.6170	-0.4106	-0.6054	-0.7060	-1.0080
BACE1	-0.8714	-0.5563	-0.2624	-0.3658	-0.7073	-0.5603
FAM84B	-0.8715	-0.5622	-0.2553	-0.5243	-0.5901	-0.9045
CMAHP	-0.8726	-0.5426	-0.2420	-0.6533	-0.7171	-0.8602
SAP30	-0.8733	-0.5627	-0.2141	-0.4051	-0.6118	-0.7014
GPR174	-0.8738	-0.4463	-0.2398	-0.5716	-0.5082	-0.5766
KIR3DX1	-0.8741	-0.1782	-0.2312	-0.4542	-0.8321	-0.7872
LRMP	-0.8744	-0.6414	-0.2733	-0.7296	-0.4875	-0.7170
CCDC50	-0.8745	-0.5271	-0.1040	-0.3027	-0.7359	-0.7658
KB-1027C11.4	-0.8750	-0.2722	-0.2190	0.0489	-0.6059	-0.1858
COLQ	-0.8759	-0.6474	-0.6087	-0.3856	-0.4579	-0.8351
HIST1H2BG	-0.8762	-1.0740	-0.1232	0.0802	-0.9426	-1.1353
SLC27A5	-0.8798	-0.5768	-0.0473	-0.2109	-0.7008	-0.9311
EVA1B	-0.8802	-0.5681	-0.3383	-0.6043	-0.4459	-0.6882
ZBTB16	-0.8806	-0.6783	-0.2606	-0.6582	-0.3841	-0.5178
CREM	-0.8811	-0.5621	-0.1694	-0.4536	-0.6270	-0.6240
FUCA2	-0.8812	-0.5136	-0.2195	-0.5165	-0.4546	-0.7151

CCDC74A	-0.8819	-0.4690	-0.2838	-0.6084	-0.5469	-0.7396
FAM172BP	-0.8821	-0.4965	-0.2318	-0.7078	-1.1834	-0.6844
EVC	-0.8833	-0.8110	-0.4485	-0.7745	-1.0277	-0.7340
IRF4	-0.8846	-0.4151	-0.1993	-0.4592	-0.5333	-0.7893
HOMER2	-0.8853	-0.4893	-0.0748	-0.4735	-0.2268	-0.5401
THG1L	-0.8911	-0.6268	-0.1432	-0.5090	-0.5311	-0.7338
GPX4	-0.8920	-0.6471	-0.1082	-0.5920	-0.2479	-0.7389
MICALCL	-0.8922	-0.3605	-0.2466	-0.3817	-0.5645	-1.2432
LEPR	-0.8993	-0.4603	0.0335	-0.1865	-0.7849	-0.9532
SPEF2	-0.9020	-0.3941	-0.3541	-0.3660	-0.5550	-0.6534
LST1	-0.9021	-0.3602	-0.1197	-0.2938	-0.0333	-0.2939
RP11-620J15.3	-0.9023	-0.8771	-0.3587	-0.5671	-0.6632	-0.8325
TCEAL1	-0.9028	-0.4249	-0.0919	-0.5233	-0.4661	-0.6313
CTD-2162K18.5	-0.9030	-0.8043	-0.4625	-0.5403	-0.3135	-0.5042
CMC1	-0.9051	-0.6116	-0.2784	-0.6061	-0.5552	-0.7701
LYN	-0.9056	-0.4974	-0.3280	-0.6531	-0.8132	-0.8586
NUDT6	-0.9061	-0.5311	-0.2294	-0.4939	-0.4036	-0.7963
PMAIP1	-0.9063	-0.6012	-0.0856	-0.4637	-0.5451	-0.7891
TRGC1	-0.9067	-0.5681	-0.2697	-0.6339	-0.5367	-0.6942
IQGAP3	-0.9069	-0.5916	-0.1962	-0.5388	-0.1729	-0.6383
ZCCHC18	-0.9080	-0.5295	-0.3473	-0.5342	-0.5006	-0.7132
PLD1	-0.9093	-0.0854	-0.4081	-0.2204	-0.5622	-0.7748
MYO18B	-0.9109	-0.4138	-0.9072	-0.4960	-1.0174	-0.9636
PLK1S1	-0.9122	-0.5810	-0.3517	-0.5688	-0.5768	-0.8378
COQ2	-0.9125	-0.4566	-0.3079	-0.5567	-0.4037	-0.5951
FCGR3A	-0.9132	-0.5681	-0.3295	-0.6285	-0.7699	-0.6382
JUP	-0.9153	-0.4640	-0.2382	-0.5149	0.0354	-0.3939
RP11-25K19.1	-0.9164	-0.5636	-0.0315	-0.8897	-0.5866	-0.7286
NMB	-0.9172	-0.9074	-0.4767	-0.7348	-0.4856	-0.7217
GZMK	-0.9201	-0.5918	-0.2826	-0.6436	-0.7210	-0.5687
CTD-2006C1.2	-0.9204	-0.6425	-0.2946	-0.3606	-0.4409	-0.5317
FCRLB	-0.9204	-0.7073	-0.2205	-1.1962	-0.3160	-0.8529
RP11-254F7.2	-0.9220	-1.1516	-0.4992	-0.5492	-1.0510	-1.2625
MND1	-0.9222	-0.5315	-0.1943	-0.4083	-0.2561	-0.6835
PTGER4	-0.9240	-0.5178	-0.2317	-0.5527	-0.3262	-0.6191
FAM115B	-0.9264	-0.2257	-0.8110	-0.6854	-1.0138	-0.5671
NCALD	-0.9266	-0.4916	-0.1528	-0.4428	-0.4273	-0.6286
PAQR7	-0.9268	-0.5630	-0.0390	-0.6168	-0.4993	-0.5250
RP11-104G3.2	-0.9275	-0.5485	-0.3732	-0.6449	-0.9893	-1.3363
C18orf56	-0.9276	-0.7060	-0.2293	-0.9650	-0.6788	-0.6163
RP11-446H18.3	-0.9298	-1.1454	-0.9266	-0.7006	-0.9697	-1.0216
TRGV8	-0.9300	-1.0936	-0.2737	-0.7293	-0.4317	-0.7185
NEK3	-0.9306	-0.5725	-0.2033	-0.2392	-0.6447	-0.6833

MYO1D	-0.9316	-0.6886	-0.2296	-0.3484	-0.7290	-0.6064
ACTN1	-0.9321	-0.4716	0.0180	-0.4833	-0.1409	-0.6898
TRIB3	-0.9337	-0.6691	-0.1741	-0.5911	-0.6781	-0.9640
RP11-458F8.2	-0.9343	-0.5280	-0.0206	-0.1419	-0.2363	-0.7826
NDFIP2	-0.9362	-0.5855	-0.0385	-0.5749	-0.5824	-0.5354
TNFSF9	-0.9364	-0.5480	-0.1547	-0.5441	-0.6143	-0.7173
CTB-55O6.8	-0.9378	-0.4216	-0.0774	-0.3106	-0.3752	-0.7528
CLECL1	-0.9381	-0.4265	-0.2485	-0.4802	-0.6887	-0.5657
TNFSF4	-0.9382	-0.8270	-0.2027	-0.7933	-0.6523	-0.7179
GPR63	-0.9402	-0.3556	-0.2684	-0.7307	-0.5422	-0.6840
PYROXD2	-0.9412	-0.3788	-0.2142	-0.3858	-0.2965	-0.8041
PDE8A	-0.9423	-0.4406	-0.2166	-0.4623	-0.5661	-0.7992
DUSP10	-0.9429	-0.5739	-0.2905	-0.5573	-0.5322	-0.7487
IRF5	-0.9431	-0.7214	-0.1472	-0.5792	-0.7666	-0.8129
NECAB1	-0.9444	-0.4302	-0.4356	0.0520	-0.5317	-0.8986
GFOD1	-0.9464	-0.4273	-0.1468	-0.6230	-0.5980	-0.7276
ZNF821	-0.9465	-0.6686	-0.4442	-0.6040	-0.5812	-1.0079
AVIL	-0.9470	-0.4383	-0.4751	-0.3081	-0.4628	-1.4419
MGLL	-0.9493	-0.6771	-0.1920	-0.1405	-0.1928	-0.8726
CCL5	-0.9557	-0.6420	-0.3520	-0.6026	-0.5856	-0.7732
RP5-995J12.2	-0.9565	-0.7685	-0.3685	-0.6405	-0.3966	-0.6606
SMAD7	-0.9565	-0.4744	-0.2194	-0.6134	-0.5402	-0.6791
EXD2	-0.9571	-0.5975	-0.1643	-0.5421	-0.4992	-0.5184
AC009948.5	-0.9599	-0.6574	-0.3231	-0.6232	-0.7392	-0.9683
TRAV25	-0.9610	-0.5150	-0.2701	-0.2676	-0.0365	-0.4953
SHMT2	-0.9642	-0.6055	-0.2165	-0.6524	-0.5508	-0.8768
TGIF1	-0.9659	-0.6468	-0.3321	-0.7322	-0.7915	-0.9344
PLCB1	-0.9666	-0.3503	-0.1421	-0.4534	-0.4987	-0.3778
AC006369.2	-0.9669	-0.1211	-0.3534	-0.4607	-0.3796	-0.7545
TRGV10	-0.9678	-0.5530	-0.2307	-0.6486	-0.4569	-0.8422
NPM2	-0.9712	-0.2593	-0.3907	-0.2468	-0.8279	-0.4682
LINC00426	-0.9713	-0.5463	-0.4298	-0.4631	-0.5140	-0.8789
RHBDD2	-0.9717	-0.6062	-0.2596	-0.6938	-0.5934	-0.7780
C1orf21	-0.9722	-0.8076	-0.4620	-0.6379	-0.6587	-0.7751
CTD-2325M2.1	-0.9722	-0.8064	-0.3854	-1.4249	-0.5444	-0.2551
CXCL16	-0.9737	-0.5764	-0.2141	-0.5264	-0.6948	-0.6658
SLC41A2	-0.9744	-0.5745	-0.3402	-0.5362	-1.1079	-0.7856
SLC4A4	-0.9755	-0.5056	-0.1983	-0.6021	-0.6348	-0.6444
ARSD	-0.9771	-0.5369	-0.4066	-0.9709	-0.5211	-0.8333
ALCAM	-0.9780	-0.5863	-0.0177	-0.4858	-0.4868	-0.9364
TIAM2	-0.9786	-0.4754	-0.2541	-0.5481	-0.5405	-0.7345
MAF	-0.9797	-0.6097	-0.2933	-0.4744	-0.6436	-0.7000
PANK1	-0.9799	-0.4843	-0.1444	-0.8985	-0.3742	-0.6785

DNAJC18	-0.9800	-0.5756	-0.4065	-0.5753	-0.5918	-0.9241
ATP5G2P4	-0.9812	-0.5403	0.0773	-0.6230	0.1596	-0.6759
AHI1	-0.9831	-0.4610	-0.2201	-0.5875	-0.5833	-0.9250
FAM43A	-0.9841	-0.8798	-0.4553	-0.9699	-0.7356	-1.0938
GMPR	-0.9849	-0.7963	0.1461	-0.4972	-0.2998	-0.9514
CDKN2B-AS1	-0.9856	-0.5220	-0.3670	-0.4698	-0.6043	-0.7888
GAS2L1	-0.9862	-0.3901	-0.0522	-0.3336	-0.1682	-0.3810
IFI44	-0.9881	-0.4294	0.0709	-0.3195	-0.4615	-0.7131
C5	-0.9898	-0.7143	-0.3097	-0.6163	-0.1599	-0.9160
IVNS1ABP	-0.9917	-0.5307	-0.1718	-0.6263	-0.5960	-0.7710
SCPEP1	-0.9953	-0.8215	-0.3789	-0.6033	-0.8020	-0.9362
AP001055.6	-0.9959	0.0977	-0.7847	-0.7449	-0.0111	-0.8712
PLEKHA5	-0.9981	-0.6318	-0.2077	-0.4782	-0.5780	-0.8378
SLC44A1	-1.0003	-0.7311	-0.1992	-0.7601	-0.5821	-0.7734
ABCG2	-1.0007	-0.3029	-0.4403	-0.6980	-0.3525	-0.2088
ELL2	-1.0026	-0.6028	-0.3241	-0.6452	-0.9214	-0.9849
CTC-378H22.2	-1.0041	-0.3913	0.1260	-0.7653	-0.2882	-0.8084
GSTA4	-1.0044	-0.4236	-0.1256	-0.2516	-0.7353	-0.9220
ROCK1P1	-1.0086	-0.8959	0.0079	-0.3740	-0.8033	-1.5254
LAYN	-1.0103	-0.9362	0.1232	-0.8808	-0.8750	-0.9945
RP11-312J18.5	-1.0105	-0.6714	-0.0057	-0.6012	-0.5192	-0.5228
ZEB2	-1.0141	-0.5024	-0.2687	-0.5271	-0.8771	-0.8445
ZSCAN9	-1.0149	-0.7543	-0.4578	-0.9910	-0.9921	-1.0940
GPR27	-1.0235	-0.4687	-0.3065	-0.4527	-1.2466	-1.3917
FEZ1	-1.0256	-0.4195	-0.2393	-0.8741	-0.8579	-0.6344
PRSS30P	-1.0284	-0.8800	-0.2088	-0.6710	-0.8427	-1.1550
MDFIC	-1.0286	-0.6026	-0.2788	-0.5917	-0.4223	-0.7279
GK	-1.0336	-0.6271	-0.2429	-0.7017	-0.5852	-0.9126
NEO1	-1.0339	-0.5443	-0.2311	-0.5271	-0.7643	-0.8842
AMOTL1	-1.0357	-0.9210	-0.6758	-0.9175	-0.5355	-0.8182
CRNDE	-1.0379	-0.5973	-0.1459	-0.7977	-0.5565	-0.9504
IFNLR1	-1.0388	-0.5116	-0.2582	-0.5525	-0.5823	-0.8901
PRSS16	-1.0426	-0.1514	-0.4317	-0.3436	-0.0555	-0.1969
RP3-340N1.5	-1.0433	-0.1770	-0.1271	0.0673	-0.3393	-0.6190
CCDC112	-1.0464	-0.6134	-0.2200	-0.6547	-0.5482	-0.8734
BTN2A3P	-1.0466	-0.2804	-0.1146	-0.1575	-0.3198	-0.9183
B4GALNT3	-1.0483	-0.2175	0.0136	-0.1085	-0.1590	-0.2537
IL12RB2	-1.0507	-0.4447	-0.0840	-0.5394	-0.7227	-0.7008
HLA-DQB1	-1.0511	-0.7634	-0.2574	-0.5127	-0.5267	-0.9206
SLC11A1	-1.0528	-0.3796	-1.1520	-0.8886	-0.1580	-0.9550
PEG10	-1.0542	-0.6568	0.0264	-0.7809	-1.1749	-1.4651
EIF4EBP1	-1.0562	-0.7315	-0.2616	-0.7275	-0.7070	-0.9068
ATXN7L1	-1.0578	-0.5849	-0.5659	-0.5645	-0.7221	-0.8973

CCNI2	-1.0579	-0.9104	-0.1259	-0.7655	-0.5149	-0.8695
HMGN5	-1.0608	-0.6344	-0.1075	-0.7109	-0.6457	-1.1629
CTD-3014M21.4	-1.0611	-0.7625	-0.4665	-0.4141	-0.1890	-0.7369
SLMO1	-1.0614	-0.0169	-0.3981	-0.4299	-0.9964	-0.9884
VSIG10	-1.0644	-0.6429	-0.2427	-0.7972	-0.7642	-0.9924
APLF	-1.0663	-0.2987	-0.5085	-0.4753	-0.4917	-0.7576
MAMLD1	-1.0671	-0.5699	-0.4218	-0.8691	-1.0127	-0.9957
METTL7A	-1.0746	-0.6642	-0.3026	-0.6540	-0.3991	-0.9733
RHEBL1	-1.0748	-0.4985	-0.0766	-0.4364	-0.5815	-0.8242
AC012146.7	-1.0762	-0.4181	-0.1742	-0.5631	-0.3710	-0.6749
B3GALNT1	-1.0797	-0.6729	-0.1062	-0.8096	-0.3738	-0.7048
RP11-383H13.1	-1.0815	-0.8411	-0.3852	-0.9540	-1.0578	-1.3062
PLA2G4C	-1.0866	-0.1445	-1.8614	-1.1831	-1.6059	-1.6937
PTGES3P2	-1.0907	-0.9132	-0.4234	-0.5791	-0.6904	-0.8822
SYK	-1.0920	-0.5639	-0.7501	-1.0299	-0.5618	-0.5277
CAMK1D	-1.0949	-0.7536	-0.5449	-0.7717	-0.5324	-0.7810
TMEM170B	-1.0955	-0.1976	-0.1873	-0.2790	-0.5129	-0.5990
PIR	-1.0966	-0.3337	0.2857	-0.1327	-0.4002	-0.9907
HIST1H1E	-1.0978	-0.5031	-0.4598	-0.3013	-0.7480	-0.7303
RP11-472B18.2	-1.0981	-0.8205	-0.0602	-0.8755	-0.9035	-0.3129
ADPRH	-1.0987	-0.7638	-0.1888	-0.8312	-0.6739	-1.0050
DUSP2	-1.1025	-0.8431	-0.3562	-0.7326	-0.5906	-0.8281
TRGV9	-1.1029	-0.8260	-0.0780	-0.5666	-0.7259	-0.7346
TRGC2	-1.1055	-0.6691	-0.3648	-0.6690	-0.6726	-0.7584
METRNL	-1.1094	-0.8312	-0.3241	-0.6128	-1.2386	-1.1003
HIST3H2BA	-1.1127	-0.2065	-0.8114	-0.5850	-0.6993	-1.3392
NCKAP1	-1.1225	-0.8584	-0.3796	-1.1250	-1.0039	-1.0680
CD70	-1.1229	-0.7910	-0.2550	-0.7290	-0.7603	-0.8095
RAB37	-1.1235	-0.6439	-0.2755	-0.7974	-0.4106	-0.8551
TNFRSF11A	-1.1286	-0.7345	-0.0967	-0.5766	-0.9100	-0.7714
SESN2	-1.1301	-0.8452	-0.2605	-0.8592	-0.9971	-1.1113
TNFRSF4	-1.1310	-0.6405	0.0517	-0.6151	-0.7874	-0.9308
IFIT2	-1.1353	-0.4056	0.0935	0.2264	-0.3918	-0.7373
DYNC2H1	-1.1385	-0.6396	-0.4455	-0.6617	-1.0524	-0.8315
SH2D1B	-1.1396	-0.4223	-0.0895	-0.6172	-0.5718	-0.6650
CCR2	-1.1401	-0.5956	-0.1507	-0.4739	-0.4071	-0.7041
MYBL1	-1.1467	-0.5758	-0.3581	-0.7437	-0.4385	-0.6751
INSR	-1.1506	-0.3107	-0.3851	-0.2592	-0.1701	-0.6426
ACTA2	-1.1552	-1.0147	-0.5222	-1.1455	-0.9442	-1.1134
MLLT4	-1.1594	-0.7544	-0.2912	-0.6205	-0.7758	-0.9440
MAN1C1	-1.1604	-0.8965	-0.4237	-0.8476	-0.8399	-1.0815
AJUBA	-1.1606	-0.8321	-0.6456	-0.8861	-0.2594	-0.8358
MGC20647	-1.1621	-0.3798	0.0237	-0.6612	0.0073	-0.6373

MRC2	-1.1636	-1.2592	-0.6949	-1.1983	-1.0344	-1.5590
BSPRY	-1.1642	-0.7079	-0.0991	-0.6830	-0.6264	-0.8745
TNFAIP3	-1.1680	-0.8008	-0.4336	-0.7914	-0.8607	-0.9098
FHL1	-1.1688	-0.8842	-0.3027	-0.7966	-0.5378	-0.6743
B3GALT2	-1.1698	-0.5224	-0.3698	-0.7097	-0.5100	-0.7114
EPDR1	-1.1714	-0.6064	-0.2063	-0.5862	-0.6270	-0.7953
GAS7	-1.1735	-1.0006	-0.4346	-1.1916	-0.9122	-0.8443
CDKN2B	-1.1774	-0.7044	-0.3784	-0.6718	-0.3166	-0.6060
SLC9A7	-1.1822	-0.7845	-0.3137	-0.6391	-0.6823	-0.9232
ENTPD1	-1.1849	-0.7830	-0.2690	-0.7225	-0.9330	-0.9457
SETD7	-1.1874	-0.9758	-0.2889	-0.8475	-1.0544	-1.1214
BATF3	-1.1905	-0.7254	-0.0767	-0.6541	-0.9180	-0.9594
TCEAL4	-1.1923	-0.8481	-0.1607	-0.8418	-0.6098	-0.7595
AC018642.1	-1.1947	-0.6848	-0.3360	-0.6299	-0.9548	-0.7109
NR4A1	-1.1957	-0.4924	-0.1192	-0.5678	-0.7738	-1.0409
TOX	-1.1960	-0.7130	-0.3825	-0.8689	-0.7264	-0.9312
APOBEC3B	-1.1998	-0.6485	-0.3663	-0.9088	-0.6058	-0.9727
CDCP1	-1.2034	-0.3278	-0.0201	-0.4705	0.2930	-0.2924
AXIN2	-1.2053	-0.5088	-0.3546	-0.5048	0.0154	-0.2117
KCNQ5	-1.2056	-0.6473	-0.2311	-0.7453	-0.4424	-0.8083
AC016708.2	-1.2065	-1.1699	-0.2566	-0.6590	-0.1284	0.0369
RP11-693N9.2	-1.2123	-0.6090	-0.3256	-0.4206	-0.5817	-0.7506
RP11-132A1.4	-1.2144	-0.6970	-0.0462	-0.5017	-0.5079	-0.6012
POU2AF1	-1.2151	-0.1676	-0.1263	-0.4787	-0.4801	-0.9110
MIR155HG	-1.2226	-0.7508	-0.0078	-0.7125	-0.8550	-1.2320
EPHX4	-1.2226	-0.5465	-0.1635	-0.2820	-0.5292	-0.8859
CKAP4	-1.2299	-1.0042	-0.2771	-0.8272	-0.5996	-1.1564
IL17RB	-1.2360	-0.9601	-0.2853	-0.7889	-0.7148	-1.2235
RASGEF1B	-1.2474	-0.4596	-0.3368	-0.8874	-0.6419	-0.6810
EGFL6	-1.2528	-0.8208	-0.2479	-0.9859	-0.7659	-1.0421
SPRED2	-1.2541	-0.8151	-0.2059	-0.6399	-0.4009	-0.7513
RP11-474B16.1	-1.2559	-0.7732	-0.0763	-0.9169	-0.9811	-1.0703
F8	-1.2581	-0.8077	-0.3116	-0.8486	-0.8033	-0.8952
BCAT1	-1.2584	-0.8829	-0.3051	-0.7956	-1.1441	-1.3593
RP4-781K5.8	-1.2659	-0.5769	-0.1520	-0.5102	-0.4046	-0.9734
KRT7	-1.2725	-1.3567	-0.0896	-1.0814	-0.5743	-0.6434
TPRG1	-1.2748	-0.6175	-0.2617	-0.8114	-1.0183	-1.1460
HDAC5	-1.2779	-0.8205	-0.4643	-0.8380	-0.7123	-1.0872
IFIT3	-1.2846	-0.4207	0.2119	0.3346	-0.4909	-0.7948
XCL2	-1.2881	-1.2481	-0.3500	-1.0923	-1.0899	-0.8851
FAM49A	-1.2907	-0.7672	-0.4102	-0.8472	-0.9915	-0.8734
RP11-162J8.3	-1.2919	-0.9105	-0.1054	-0.6311	-1.2332	-0.9083
AC105344.2	-1.2941	-1.0355	-0.3442	-0.8103	-0.7389	-0.9128

CTC-378H22.1	**-1.2976**	**-1.1284**	**-0.5269**	**-0.4786**	-0.0996	-0.5273
WWTR1	**-1.2983**	**-0.3122**	**-0.4057**	**-0.3543**	-0.8637	-1.5122
CYBRD1	**-1.2986**	**-0.5258**	**-0.5521**	**-1.3167**	-0.8889	-2.1404
VNN2	**-1.2993**	**-0.9042**	**-0.5054**	**-1.0233**	-0.7790	-0.9869
RP1-43E13.2	**-1.3020**	**-0.0881**	**-0.5299**	**-0.2630**	-1.2251	-0.5454
ETV1	**-1.3043**	**-0.8577**	**-1.0352**	**-0.8344**	-1.4861	-1.4161
LAIR2	**-1.3086**	**-1.1228**	**-0.3466**	**-1.3713**	-1.0570	-0.3454
LINC00263	**-1.3105**	**-0.7779**	**-0.1188**	**-0.5981**	-0.6977	-1.2534
NUDT7	**-1.3166**	**-0.3268**	**-0.5024**	**-0.3364**	-0.0286	-0.6730
PHLPP1	**-1.3170**	**-0.7770**	**-0.3778**	**-0.7446**	-1.0504	-1.2423
PLXNC1	**-1.3174**	**-0.7495**	**-0.3946**	**-1.0818**	-0.6087	-0.7583
AK4	**-1.3187**	**-0.4917**	**0.2902**	**-0.3425**	-0.6017	-1.0114
GYLTL1B	**-1.3215**	**-1.2056**	**-0.8919**	**-0.4455**	-0.3223	-1.1960
C10orf128	**-1.3238**	**-0.8586**	**-0.2400**	**-0.7988**	-0.8268	-1.0190
Sep-03	**-1.3265**	**-0.7457**	**-0.2100**	**-0.6143**	-0.8005	-0.7949
KB-1460A1.1	**-1.3343**	**-0.4657**	**-0.4271**	**-1.2162**	-1.2185	-1.4870
SIGLEC12	**-1.3405**	**0.0038**	**0.1870**	**-0.5491**	-0.3251	-0.3957
FAM174B	**-1.3406**	**-0.1719**	**-0.8388**	**-0.8115**	-0.1979	-0.7510
CCL3	**-1.3421**	**-0.6336**	**-0.1543**	**-0.5365**	-1.2904	-0.9831
GCSAM	**-1.3424**	**-0.9424**	**-0.4625**	**-0.9965**	-0.8708	-1.1202
CLIC4	**-1.3437**	**-0.8821**	**-0.2122**	**-1.0044**	-1.0370	-1.1768
ANGPTL6	**-1.3482**	**-1.0289**	**-0.4290**	**-0.9754**	-0.9246	-0.8690
MYB	**-1.3484**	**-0.8321**	**-0.2097**	**-0.8881**	-0.9349	-1.2411
RP4-728D4.2	**-1.3526**	**-0.9781**	**-0.2101**	**-1.0290**	-0.7171	-1.1584
RP1-111D6.3	**-1.3596**	**-0.7157**	**-0.1849**	**-0.9442**	-1.2849	-0.7554
CCBP2	**-1.3687**	**-1.2006**	**-0.5823**	**-0.9972**	-1.3576	-1.4388
SMIM14	**-1.3723**	**-1.0382**	**-0.4189**	**-0.8210**	-0.9167	-1.1369
EGR2	**-1.3762**	**-0.9219**	**-0.3495**	**-1.0966**	-1.1224	-1.2070
TSC22D3	**-1.3818**	**-1.0942**	**-0.4126**	**-0.9601**	-0.9773	-1.2869
ELOVL4	**-1.3835**	**-0.9316**	**-0.3317**	**-0.7515**	-1.1304	-1.2774
AC092580.3	**-1.3886**	**-1.0533**	**-0.3070**	**-2.0557**	-1.5760	-1.4657
RHOB	**-1.3921**	**-1.1356**	**-0.1555**	**-0.8726**	-1.3802	-1.3018
ATF3	**-1.3931**	**-0.9571**	**-0.0327**	**-0.6744**	-1.0521	-1.2321
CFH	**-1.4026**	**-0.8837**	**-0.3753**	**-0.5734**	-1.1187	-1.4285
HLA-DQA1	**-1.4066**	**-0.9560**	**-0.4891**	**-0.8221**	-1.2236	-1.1190
CD109	**-1.4124**	**-0.8244**	**-0.3425**	**-1.1258**	-0.5692	-1.0603
FGFR1	**-1.4153**	**-0.8627**	**-0.2346**	**-1.0570**	-0.6093	-0.9869
TRGV7	**-1.4158**	**-0.7115**	**-0.3514**	**-1.2096**	-0.5730	-0.8149
hsa-mir-146a	**-1.4170**	**-0.8152**	**-0.8279**	**-1.4166**	-1.2540	-1.2757
AC069363.1	**-1.4228**	**-0.2498**	**-0.5210**	**-0.6996**	-0.5588	-0.4213
FBP1	**-1.4244**	**-1.8977**	**-0.9626**	**-1.2072**	-1.7289	-0.8864
TRAJ44	**-1.4258**	**0.3090**	**-0.5261**	**0.5525**	-1.1168	0.4797
AFAP1	**-1.4308**	**-0.9291**	**-0.7423**	**-1.0206**	-1.1551	-0.8618

SOCS2	-1.4314	-0.9425	-0.2548	-0.9190	-0.8299	-1.0778
MLK4	-1.4352	-1.1642	-0.0814	-1.0524	-1.1240	-1.5616
CD160	-1.4444	-0.7051	-0.3348	-0.5844	-0.5431	-0.5951
CTD-2514K5.2	-1.4564	-1.1785	-0.9946	-1.2828	-1.5298	-1.3325
PRSS57	-1.4624	-0.8750	-0.2270	-0.6563	-0.3216	-1.1403
RP11-227H4.4	-1.4779	-0.3095	0.1755	-0.5343	-1.0964	-0.7870
DTHD1	-1.4800	-1.0326	-0.9152	-1.0638	-1.4542	-0.9688
ZC2HC1A	-1.4801	-0.7638	-0.4372	-0.7825	-0.9992	-1.0169
PTPRM	-1.4840	-1.0722	-0.8763	-1.4519	-1.3766	-1.1615
MCAM	-1.4860	-1.3015	-0.0471	-1.0263	-0.5455	-1.0635
RDH10	-1.4878	-1.0086	-0.2603	-1.1148	-1.1887	-1.2586
IL4I1	-1.4938	-1.3972	-0.4019	-0.8572	-1.1717	-1.2718
TRAJ47	-1.5015	-0.7294	-2.1444	-3.5850	-1.9773	-2.4854
PROK2	-1.5040	-0.6492	-0.1082	-0.5634	-1.1225	-1.2357
EXTL2	-1.5140	-1.1609	-0.3020	-0.8646	-0.7777	-1.4891
GNA11	-1.5237	-0.5081	-0.3320	-0.6979	-0.9607	-1.5614
CACNA1I	-1.5238	-1.3133	-0.7530	-1.1700	-0.8889	-1.2881
RGS2	-1.5298	-1.1999	-0.5421	-1.1337	-1.1262	-1.5239
ABCG1	-1.5307	-0.9766	-0.2904	-1.0410	-0.7223	-1.1715
AC002331.1	-1.5390	-1.9962	-0.3282	-1.2615	-1.7754	-1.1028
MLF1	-1.5421	-0.3104	-0.1943	-0.4154	-0.6614	-0.3751
HLA-DQA2	-1.5455	-0.8591	-0.6125	-0.6288	-1.2978	-1.3029
ST8SIA6	-1.5505	-1.1986	-0.5889	-1.2688	-1.5947	-1.3733
VLDLR	-1.5589	-0.9198	-0.2018	-1.1129	-0.9962	-1.4626
COLGALT2	-1.5613	-0.7899	-0.9097	-1.3545	-1.4156	-1.7317
SHC4	-1.5633	-0.5787	0.0376	-0.7634	-1.4710	-1.1053
CD86	-1.5659	-0.9087	-0.3431	-0.9812	-1.2651	-1.3400
SMOX	-1.5689	-1.2219	-0.2226	-1.0511	-1.2073	-1.7268
AC013460.1	-1.5733	-0.9653	-0.6377	-0.0345	-0.2147	-1.4282
TNFRSF9	-1.5843	-0.9899	-0.3567	-0.9718	-1.2482	-0.9954
LIF	-1.5955	-0.9217	0.0394	-0.9779	-0.4472	-0.9116
FILIP1L	-1.5965	-1.1477	-0.3689	-0.9775	-0.6716	-0.8103
ZDHHC14	-1.6029	-1.0677	-0.4594	-1.1336	-0.9652	-1.1009
COL9A2	-1.6112	-0.7269	-0.2882	-0.9545	-0.8801	-0.8838
SMKR1	-1.6173	-1.1514	0.0641	-1.0061	-0.7246	-0.8368
ZNF826P	-1.6206	-0.5070	0.0502	-0.3824	-0.8595	-0.8104
NXPH4	-1.6431	-1.3705	-0.3764	-1.5653	-1.5850	-1.2930
SHROOM1	-1.6453	-0.6577	-0.0887	-0.9376	-0.9913	-0.8844
PTGIR	-1.6482	-0.8085	-0.4503	-1.1422	-0.3349	-1.5684
SOCS2-AS1	-1.6518	-1.0139	-0.4065	-1.2032	-0.6335	-1.1046
PLAU	-1.6676	-1.0243	0.1098	-0.8621	-0.7045	-1.3599
NEK6	-1.6741	-1.0744	-0.3981	-1.2551	-0.5816	-1.0958
PPFIBP1	-1.6746	-1.2446	-0.3056	-1.2789	-1.0951	-1.3486

CADM1	-1.6789	-1.2384	-0.4143	-1.0012	-1.3205	-1.2550
SLC35F3	-1.6899	-1.1424	-0.1352	-1.0789	-0.6915	-1.1864
HECW2	-1.7053	-0.9592	-0.5627	-0.8310	-1.5299	-1.3848
RP3-395M20.9	-1.7061	-1.5222	-1.4009	-0.5006	-0.0910	-0.3793
EPAS1	-1.7120	-0.9578	-0.1830	-0.9356	-1.1528	-1.2467
EEF1A2	-1.7120	-1.6435	-0.4626	-1.7315	-1.4138	-1.4783
GNAO1	-1.7165	-1.1909	-0.7546	-1.5552	-1.0881	-1.2471
HDAC9	-1.7167	-0.9668	-0.6865	-0.8029	-0.9934	-1.0500
CD83	-1.7176	-1.3224	-0.2412	-1.5508	-0.8559	-1.0636
SLC14A1	-1.7269	-1.1190	-0.8137	-0.9786	-0.7623	-0.7589
SGCE	-1.7364	-0.7304	0.0607	-0.3269	-1.2241	-1.1203
CD80	-1.7406	-1.1692	-0.1166	-1.0225	-0.4186	-0.9834
ZSCAN31	-1.7793	-1.3082	-0.1915	-0.8850	-1.0263	-1.0563
CCR8	-1.7985	-1.2059	-0.1731	-1.3214	-0.7736	-1.1042
AKR1C3	-1.7994	-1.4972	-0.4658	-1.1240	-0.8013	-1.1070
AARD	-1.8024	-1.2760	-0.5285	-1.3027	-1.2862	-1.2029
FTH1P22	-1.8028	-1.0590	-0.1801	-1.5404	-1.0945	-1.4604
TRPC1	-1.8035	-1.1752	-0.2691	-1.1442	-0.8229	-1.4157
RNASE6	-1.8080	-1.7054	-0.3879	-1.3982	-0.8195	-1.9551
CHN2	-1.8207	-1.0994	-0.5884	-1.1232	-1.1580	-1.2906
LMCD1	-1.8385	-0.6898	-0.0995	-0.8901	-0.8362	-0.7263
PRKCE	-1.8409	-1.3543	-0.3779	-1.0875	-1.6272	-1.6496
SERPINE2	-1.8535	-1.0326	-0.3384	-1.3788	-1.1319	-1.5569
PTPLA	-1.8588	-1.7630	-0.2154	-0.7628	-1.2143	-1.7761
RP11-316P17.2	-1.8651	-1.2230	-0.6473	-1.0875	-1.2775	-1.7980
HNRNPA1P21	-1.8785	-1.4646	-0.4509	-1.4415	-0.9763	-1.6186
H1F0	-1.8977	-1.2063	-0.3541	-1.2197	-1.1443	-1.5898
ISL2	-1.9011	-1.2745	-0.2716	-1.0804	-1.8711	-1.0231
EVI5	-1.9022	-1.5972	-0.2422	-0.6511	-1.6150	-1.6371
CLDN12	-1.9152	-0.9874	-0.4896	-1.3885	-1.3741	-1.5814
GPT2	-1.9171	-1.2710	-0.3134	-1.4451	-1.4411	-1.7199
TMEM63C	-1.9202	-1.1188	-0.2807	-0.9474	-0.8550	-1.3003
APBA1	-1.9345	-1.0309	-0.4154	-1.2701	-1.4183	-1.4878
SH3RF2	-1.9535	-1.8396	-0.9633	-0.7729	-1.0455	-1.8322
ETV5	-1.9557	-1.9587	-0.2133	-1.5994	-1.5368	-1.8280
HHLA2	-1.9611	-1.0700	-0.1601	-1.0144	-1.2236	-1.5596
FAM211B	-1.9646	-1.2337	-0.3112	-1.0984	-1.1872	-1.2321
TIGIT	-1.9650	-1.3866	-0.4877	-1.4175	-1.5224	-1.4713
CCR3	-1.9676	-0.9073	-0.5284	-0.7120	-1.0178	-1.0756
RAMP1	-1.9946	-1.0380	-0.2428	-1.0469	-0.4671	-0.7803
UST	-2.0027	-1.2015	-0.3294	-1.5175	-0.9537	-1.2755
SBF2-AS1	-2.0080	-1.1594	-0.3368	-1.2521	-1.1931	-1.3161
B9D1	-2.0182	-1.6344	-0.1457	-0.6799	-2.0909	-2.1102

RP11-305L7.1	-2.0231	-0.9927	-0.3709	-0.8816	-1.1277	-1.3266
PDGFD	-2.0343	-1.6644	-0.6563	-1.1761	-1.4919	-1.3524
ILDR1	-2.0503	-1.4728	-0.3440	-1.5307	-1.3562	-2.2420
MARVELD1	-2.0643	-1.5342	-0.3659	-1.3757	-1.0159	-1.0925
ETV4	-2.0689	-1.0382	-0.1188	-0.8342	-1.1752	-1.1530
TRIB1	-2.0731	-1.2947	-0.4780	-1.2525	-1.3242	-1.6648
RGS16	-2.0775	-1.6428	-0.5862	-1.4204	-1.8280	-1.9300
PACSIN1	-2.0970	-1.2859	-0.2482	-1.4204	-1.3939	-1.6956
CDC14B	-2.1269	-1.4621	-0.3226	-1.0596	-1.7175	-1.8913
S100P	-2.1550	-1.1307	-0.6680	-1.6559	-1.2599	-1.0507
RGS1	-2.1847	-1.6731	-0.5279	-1.5413	-1.8283	-1.6738
CCL23	-2.1963	-2.0948	-0.8879	-0.7789	-1.9587	-1.3470
RP11-324I22.3	-2.2246	-1.2847	-0.7059	-0.6587	-1.4423	-0.3626
CTH	-2.2264	-1.6956	-0.4262	-1.5990	-2.0658	-1.9254
EBI3	-2.2566	-2.2613	-0.0471	-2.2934	-1.8330	-1.8334
GNG8	-2.2662	-1.5955	-0.2884	-1.5850	-0.6521	-1.3395
BCAS2P2	-2.4106	-1.5035	-0.4204	-1.4667	-1.2065	-1.9103
NKD2	-2.4574	-1.4123	-0.7114	-1.6986	-0.9969	-1.1621
COL5A2	-2.5477	-1.5462	-0.5162	-1.6741	-1.1936	-1.7579
CHDH	-2.5647	-1.6016	-0.4837	-1.3150	-1.8133	-2.7518
PTK2	-2.5670	0.1284	-0.4194	-1.2568	-2.4050	-2.0315
FAM167A	-2.6891	-1.8819	-0.5494	-1.4746	-1.1248	-2.2974
IL13	-2.7009	-1.5728	-0.0258	-1.6228	-1.5817	-1.2959
COX20P2	-2.8300	-1.8444	0.1314	-2.0255	-1.7658	-2.2441
STC2	-2.8577	-1.9295	-0.1391	-1.5322	-2.0535	-2.4257
DAPK1	-2.9233	-1.2684	0.0361	-2.6856	-0.7090	-1.9053
AKR1C7P	-3.0840	-1.9061	-0.5085	-1.8559	-0.7414	-2.1831
AC099552.4	-3.0950	-1.3288	-0.1326	-1.5604	-1.7862	-2.4010
DNAJC12	-3.2696	-2.2876	-0.4569	-2.0108	-2.0944	-2.5067
ATP12A	-3.5788	-2.9808	-1.0160	-2.2669	-2.9570	-2.7930

Appendix Table 3. Genes associated with an exhausted CD8 T cell phenotype. List of genes previously identified as upregulated (1) or downregulated (-1) in exhausted CD8 T cells (Bengsch et al., 2018). Their corresponding $\log_2$ fold change induced by WTD at 50 nM in this study is shown in column three.

Gene Name	Previously reported	WTD50 log2 fold change
S100A9	1	4.409391
ACE	1	2.687795
LGALSL	1	1.390236
CD7	1	1.07537
DAPK2	1	0.895695
STAT3	1	0.887183
RENBP	1	0.865449
LAG3	1	0.831617
UBASH3B	1	0.788562
LIM2	1	-0.608384
TIFA	1	-0.61033
ADAM9	1	-0.62308
DERL3	1	-0.624422
NCF4	1	-0.630144
DOCK7	1	-0.640155
AFMID	1	-0.649064
OXR1	1	-0.65231
SAMSN1	1	-0.675389
SGK1	1	-0.69247
CDK6	1	-0.704876
SUOX	1	-0.710546
EOMES	1	-0.713721
NR4A2	1	-0.715028
MYO1E	1	-0.721196
CHST2	1	-0.724764
KLRB1	1	-0.724909
CDC14A	1	-0.727093
GJB2	1	-0.735064
GPD2	1	-0.754813
PRELID2	1	-0.765364
DUSP4	1	-0.770669
TMEM2	1	-0.771667
EAF2	1	-0.806805

CEP128	1	-0.815531
EGR1	1	-0.821417
ATXN1	1	-0.832809
RAB39B	1	-0.854936
FGR	1	-0.857058
MYO18B	1	-0.910937
GZMK	1	-0.920116
PTGER4	1	-0.923961
NDFIP2	1	-0.936174
TNFSF4	1	-0.938183
ALCAM	1	-0.978035
AHI1	1	-0.983066
IFI44	1	-0.988114
GSTA4	1	-1.004397
MDFIC	1	-1.02861
CCDC112	1	-1.046438
HLA-DQB1	1	-1.051093
SUV39H2	1	-1.091967
SYK	1	-1.091967
TMEM170B	1	-1.095479
METRNL	1	-1.109433
SH2D1B	1	-1.139647
MYBL1	1	-1.146663
GAS7	1	-1.173454
ENTPD1	1	-1.184866
TOX	1	-1.196013
POU2AF1	1	-1.215056
CKAP4	1	-1.229929
IFIT3	1	-1.284612
C10orf128	1	-1.323768
ZC2HC1A	1	-1.480093
CD86	1	-1.565925
PPFIBP1	1	-1.674597
CD83	1	-1.717614
CD80	1	-1.74058
TRPC1	1	-1.8035
RNASE6	1	-1.807966
CHN2	1	-1.820656
TIGIT	1	-1.965003
ILDR1	1	-2.050287
TRIB1	1	-2.073117
RGS16	1	-2.077546
RGS1	1	-2.184661

RCN3	-1	1.884982
TCF7	-1	1.323565
CCR7	-1	1.215875
IL17RA	-1	0.956607
FAM69A	-1	-0.604967
ACYP1	-1	-0.634779
HIBADH	-1	-0.646926
PPM1L	-1	-0.657046
PSMG1	-1	-0.659389
NEDD4L	-1	-0.667623
GLCE	-1	-0.681181
TLE1	-1	-0.690656
AAED1	-1	-0.693927
C12orf57	-1	-0.74589
MAPK8	-1	-0.764629
THG1L	-1	-0.891135
SPEF2	-1	-0.901969
SMAD7	-1	-0.956494
RAB37	-1	-1.123516
AXIN2	-1	-1.205297
EEF1A2	-1	-1.711985